Université de Montréal

Relevé spectroscopique et étude des propriétés physiques des étoiles naines blanches à moins de 40 parsecs du Soleil

par

Marie-Michèle Limoges

Département de physique

Faculté des arts et des sciences

Thèse présentée à la Faculté des études supérieures

en vue de l'obtention du grade de

Philosophiae Doctor (Ph.D.)

en physique

Avril, 2014

Université de Montréal

Faculté des études supérieures

Cette thèse intitulée:

Relevé spectroscopique et étude des propriétés physiques des étoiles naines blanches à moins de 40 parsecs du Soleil

présentée par:

Marie-Michèle Limoges

a été évaluée par un jury composé des personnes suivantes:

Gilles Fontaine,	président-rapporteur
Pierre Bergeron,	directeur de recherche
Sébastien Lépine,	codirecteur de recherche
René Doyon,	membre du jury
Matthew A. Wood,	examinateur externe

Thèse acceptée le: _____

Remerciements

Bien qu'il n'y ait qu'un seul nom sur la page couverture, il faut une armée de gens pour qu'un tel projet puisse se réaliser, et tous devraient avoir leur nom en première page. Tout d'abord, j'aimerais remercier mon directeur de recherche depuis 7 ans, Pierre Bergeron, pour avoir cru en moi depuis le début. Jamais je n'aurai pensé, lorsque nous avons commencé à travailler ensemble en 2007 avec un petit projet de fin d'études, me retrouver en 2014 avec une thèse de 300 pages, en ayant passé par une quinzaine de missions d'observations en Arizona! Je veux également remercier mon codirecteur de recherche Sébastien Lépine, pour son précieux catalogue SUPERBLINK et ses non moins précieux conseils. Je vous dois beaucoup, ainsi qu'à Gilles Fontaine, Patrick Dufour et tous les professeurs en astrophysique, car je crois bien avoir demandé un conseil, une information ou un service à presque chacun, et ce fut un honneur d'apprendre de vous tous. Sur la page couverture de ma thèse devrait également apparaître le nom de mes collègues et amis au département, dont plusieurs sont déjà partis continuer leur carrière ailleurs, et en particulier Alexandros, Amélie, Cassandra, Julie, Kim, Lison, Marilyn, Marie-Eve, Noemi et Pier-Emmanuel. Avec vous, j'ai adoré échanger des trucs de programmation, étudier le prédoc, échanger des conseils, rire, se changer les idées, faire du sport, boire une bière, participer à des conférences, aller à l'observatoire, et célébrer les petites victoires, une à la fois. Il faut également souligner l'importance de l'équipe de soutien à la maison qui, si j'étais une athlète, serait toujours présente dans les gradins en train de brandir une immense affiche avec mon nom écrit en grosses lettres. On y retrouve mes parents Rita et Michel, ainsi que ma soeur Geneviève, qui en plus d'être admirables, me supportent dans tous les sens du terme! Il y a aussi mes amies Andréane, Geneviève et Véronique, ainsi que Victor qui me gardent les pieds sur Terre, ma belle-famille Thibault qui est toujours, toujours

présente, prête à aider et à encourager, et mon ami Sylvain, qui me pousse à réaliser mes rêves. Finalement, un immense merci à mon collaborateur principal et coauteur de ma vie, le merveilleux Jean-Philippe.

Pour terminer, j'aimerais mentionner les organismes qui m'ont soutenue financièrement. J'ai donc pu me consacrer aux étoiles naines blanches à temps plein grâce au Fonds de recherche du Québec − Nature et technologies, au Conseil de recherches en sciences naturelles et génie du Canada, à la Faculté des études supérieures et postdoctorales de l'Université de Montréal, et aux bourses venant de la Banque Nationale et de la fondation J. Armand Bombardier.

Sommaire

Les étoiles naines blanches représentent la fin de l'évolution de 97% des étoiles de notre galaxie, dont notre Soleil. L'étude des propriétés globales de ces étoiles (distribution en température, distribution de masse, fonction de luminosité, etc.) requiert l'élaboration d'ensembles statistiquement complets et bien définis. Bien que plusieurs relevés d'étoiles naines blanches existent dans la littérature, la plupart de ceux-ci souffrent de biais statistiques importants pour ce genre d'analyse. L'échantillon le plus représentatif de la population d'étoiles naines blanches demeure à ce jour celui défini dans un volume complet, restreint à l'environnement immédiat du Soleil, soit à une distance de 20 pc ($\sim$ 65 années-lumière) de celui-ci. Malheureusement, comme les naines blanches sont des étoiles intrinsèquement peu lumineuses, cet échantillon ne contient que $\sim$ 130 objets, compromettant ainsi toute étude statistique significative. Le but de notre étude est de recenser la population d'étoiles naines blanches dans le voisinage solaire à une distance de 40 pc, soit un volume huit fois plus grand.

Nous avons ainsi entrepris de répertorier toutes les étoiles naines blanches à moins de 40 pc du Soleil à partir de SUPERBLINK, un vaste catalogue contenant le mouvement propre et les données photométriques de plus de 2 millions d'étoiles. Notre approche est basée sur la méthode des mouvements propres réduits qui permet d'isoler les étoiles naines blanches des autres populations stellaires. Les distances de toutes les candidates naines blanches sont estimées à l'aide de relations couleur-magnitude théoriques afin d'identifier les objets se situant à moins de 40 pc du Soleil, dans l'hémisphère nord. La confirmation spectroscopique du statut de naine blanche de nos $\sim$ 1100 candidates a ensuite requis 15 missions d'observations astronomiques sur trois grands télescopes à Kitt Peak en Arizona, ainsi qu'une soixantaine d'heures allouées sur les télescopes de 8 m des observatoires Gemini Nord et Sud. Nous avons

ainsi découvert 322 nouvelles étoiles naines blanches de plusieurs types spectraux différents, dont 173 sont à moins de 40 pc, soit une augmentation de 40% du nombre de naines blanches connues à l'intérieur de ce volume. Parmi ces nouvelles naines blanches, 4 se trouvent probablement à moins de 20 pc du Soleil. De plus, nous démontrons que notre technique est très efficace pour identifier les étoiles naines blanches dans la région peuplée du plan de la Galaxie.

Nous présentons ensuite une analyse spectroscopique et photométrique détaillée de notre échantillon à l'aide de modèles d'atmosphère afin de déterminer les propriétés physiques de ces étoiles, notamment la température, la gravité de surface et la composition chimique. Notre analyse statistique de ces propriétés, basée sur un échantillon presque trois fois plus grand que celui à 20 pc, révèle que nous avons identifié avec succès les étoiles les plus massives, et donc les moins lumineuses, de cette population qui sont souvent absentes de la plupart des relevés publiés. Nous avons également identifié plusieurs naines blanches très froides, et donc potentiellement très vieilles, qui nous permettent de mieux définir le côté froid de la fonction de luminosité, et éventuellement l'âge du disque de la Galaxie. Finalement, nous avons aussi découvert plusieurs objets d'intérêt astrophysique, dont deux nouvelles étoiles naines blanches variables de type ZZ Ceti, plusieurs naines blanches magnétiques, ainsi que de nombreux systèmes binaires non résolus.

Mots clés: voisinage solaire - étoiles: naines blanches - relevés - mouvements propres - distances - atmosphères - paramètres fondamentaux - technique: spectroscopie

Abstract

White dwarf stars represent the endpoint of stellar evolution for 97% of stars in the Galaxy. Our own Sun, in particular, will lose its external gas layers in about 5 billion years, and end up as an Earth-sized white dwarf. The study of their global properties (temperature distribution, mass distribution, luminosity function, etc.) requires statistically complete samples, free from any selection bias, and thus the best strategy to adopt when surveying these low-luminosity objects is to restrict the search to a given volume such as the immediate vicinity of the Sun. However, the current census of white dwarfs in the solar neighborhood suffers from significant statistical biases, since the most representative sample of the local white dwarf population, i.e. the stars within a sphere with a radius of 20 pc from the Sun ($\sim$ 65 light-years), contains only $\sim$ 130 objects, and is thus dominated by large uncertainties due to small-number statistics. In order to perform a statistical analysis of the local white dwarf population which is more statistically significant, we present a study aimed at obtaining a complete sample of white dwarfs in the solar neighborhood within 40 pc of the Sun, thus increasing the sampled volume by a factor of 8.

To identify every white dwarf within 40 pc of the Sun, we rely on SUPERBLINK, a large catalog containing proper motions and photometric information for over 2 million stars. Our approach is based on reduced proper motion diagrams, which are efficient at separating white dwarfs from other stellar populations. The distances for all white dwarf candidates in the northern hemisphere are determined from theoretical color-magnitude relations, in order to identify the stars that lie within 40 pc of the Sun. The spectral confirmation of the resulting $\sim$ 1100 candidates required 15 observing runs with 3 large telescopes at Kitt Peak, Arizona, as well as $\sim$ 60 hours of allocated time on the 8-m telescopes of Gemini North and South

Observatories. From these spectroscopic observations, we identified 322 new white dwarf stars, among which 173 lie within 40 pc the Sun, thus increasing the current census of white dwarfs in this volume of space by 40%. Among the new white dwarf identifications, 4 could even belong to the 20 pc sample. We also show that our method is efficient at recovering white dwarfs in the densely populated area of the Galactic plane.

We then present a spectroscopic and photometric analysis of our sample with state-of-the-art model atmospheres in order to determine their physical properties, in particular the effective temperature, surface gravity, and chemical composition of each star. Our statistical analysis of these properties — based on a sample almost three times larger than the 20 pc sample — reveals that we are successfully uncovering the most massive, and thus less luminous stars of this population, which are often missing in most surveys reported in the literature. We also identify a significant number of very cool, and thus potentially old white dwarfs, which are useful to sample the cool end of the luminosity function used to constrain the age of the Galactic disk. Finally, we report the discovery of several objects of astrophysical interest, including two new ZZ Ceti variable stars, several magnetic white dwarfs, and a few unresolved double degenerate binaries.

Subject headings: solar neighborhood - stars: white dwarfs - surveys - proper motions - distances - atmospheres - fundamental parameters - technique: spectroscopy

Table des matières

Table des figures

Liste des tableaux

Liste des abréviations

2MASS	Two Micron All-Sky Survey
CPAPIR	Camera PAnoramique Proche InfraRouge
DENSE	Discovery and Evaluation of Nearby Stellar Embers
DR	Data Release
ESO	European Southern Observatory
EUV	Ultraviolet extrême
EUVE	Extreme Ultraviolet Explorer
FUV	UV lointain (far-UV)
GALEX	Galaxy Evolution Explorer
KPNO	Kitt Peak National Observatory
KUV	KISO Ultraviolet Excess Survey
LHS	Luyten Half-Second Catalog
LSPM	Lépine-Shara Proper Motion Survey
MACHOs	Massive astrophysical compact halo object
NLTT	New Luyten Two-Tenths Catalog
NOAO	National Optical Astronomy Observatory
NUV	proche UV (near UV)
OMM	Observatoire du Mont-Mégantic
PG	Palomar Green Survey
POSS	Palomar Observatory Sky Survey

ROSAT	ROentgen SATellite
RPMD	diagramme de mouvement propre réduit (reduced proper motion diagram)
SDSS	Sloan Digital Sky Survey
SERC	Southern ESO Schmidt Survey
SSS	SuperCOSMOS Sky Surveys
SSSWDS	SOAR + SOAR + SMARTS Southern White Dwarf SURVEY
STScI	Space Telescope Science Institute
UCAC2	Second U.S. Naval Observatory CCD Astrograph Catalog
USNO	United States Naval Observatory
WD	naine blanche (white dwarf)

Chapitre 1

Introduction

À la toute fin de leur évolution, les étoiles qui ont des masses entre 0.07 et 8 $M_{\odot}$ perdent leurs couches externes. Au centre de la nébuleuse planétaire ainsi formée se trouve le coeur de l'étoile à découvert, qui se refroidira à rayon constant pendant plusieurs milliards d'années. Les naines blanches sont des objets stellaires dégénérés de petite taille ($\sim$0.01 $R_{\odot}$), initialement chauds, qui se refroidissent avec le temps, et représentent la fin de l'évolution de 97% des étoiles de la Galaxie. Une panoplie de relevés et d'études se complètent en variant les méthodes et les critères de sélection dans le but de détecter le plus grand nombre de naines blanches possible et de relever le défi d'en obtenir un échantillon complet, mais une telle entreprise est difficile, à cause de la faible luminosité des naines blanches. Les premiers à identifier un grand nombre de naines blanches furent les relevés d'étoiles à grand mouvement propre. Afin de les compléter, des études colorimétriques furent aussi menées. Parmi celles-ci, on compte le fameux relevé Palomar Green, tel que publié dans Green et al. (1986), et le grand *Sloan Digitial Sky Survey* (SDSS), qui, dès la publication de son premier catalogue, avait déjà doublé le nombre de naines blanches connues. Des diagrammes de mouvement propre réduit, qui combinent les critères sur la couleur et sur le mouvement propre ont aussi prouvé leur efficacité. Le récent catalogue SUPERBLINK a permis de détecter des mouvements propres si petits, que plus de 2 millions d'étoiles ont été détectées, dont environ 1200 candidates naines blanches.

La population de naines blanches du voisinage solaire est étudiée à l'aide d'outils statistiques tels que la fonction de luminosité et la distribution de masse, ainsi qu'à l'aide de la

densité et de la composition chimique de sous-échantillons donnés. Ces outils permettent de comprendre l'évolution des populations de la Galaxie, et d'évaluer leur âge. Par contre, afin que les résultats soient significatifs, ils doivent être basés sur des échantillons statistiquement complets. Parmi les types d'échantillon, on retrouve d'une part ceux qui sont limités par la magnitude, qui, la plupart du temps, proviennent de relevés basés sur la couleur, et contiennent d'importants biais en ce qui concerne la sélection. D'autre part, un échantillon limité par le volume permet d'obtenir un échantillon d'un rayon relativement petit, à l'intérieur duquel il serait possible de détecter toutes les naines blanches, même les plus froides. Le meilleur volume qu'on puisse sonder est celui centré sur le Soleil. Dans un tel échantillon, la détermination de la distance des objets joue un rôle important. Les déterminations de distances les plus précises proviennent de la mesure de la parallaxe trigonométrique. Par contre, de telles mesures impliquent beaucoup de temps d'observation, et par conséquent un faible pourcentage des naines blanches ont une mesure de leur parallaxe. En attendant d'obtenir ces informations, les distances peuvent être estimées soit à l'aide de calibrations empiriques, ou à l'aide d'ajustement de modèles d'atmosphère avec la photométrie ou la spectroscopie disponible.

Les naines blanches les plus chaudes, soit celles qui sont visibles à plus grande distance, ont des spectres très simples. Le type spectral DA représente les étoiles qui montrent seulement des raies d'hydrogène, tandis que les types DO et DB montrent uniquement des raies d'hélium. Dans le cas d'une DO, il s'agit d'hélium He II, et la DB est composée d'He I. Chez les naines blanches les plus froides, c'est-à-dire celles qui ont une température effective sous 12 000 K, se trouvent les DZ et les DQ, dans lesquelles les raies d'hélium sont invisibles. Les DZ ont des traces de métaux (Mg, Ca, Fe) dans leur spectre, et chez les DQ, les traces de carbone sont visibles sous forme de bandes moléculaires de C_2, et parfois, de carbone atomique. Sous les 5000 K, l'hydrogène devient spectroscopiquement invisible et les étoiles qui ne montrent pas de raies spectrales portent l'étiquette de DC. L'atmosphère de ces étoiles peut être dominée par l'hydrogène ou par l'hélium.

Les naines blanches les plus froides sont les moins brillantes, et sont ainsi les plus difficiles à observer. Par conséquent, la fonction de luminosité des naines blanches est incomplète du côté froid, et il est alors difficile d'obtenir à la fois une bonne estimation de la densité spatiale des

naines blanches, et de comparer de manière précise la fonction de luminosité avec des modèles théoriques. Compléter le côté froid de la fonction de luminosité des naines blanches permettrait de déterminer avec précision l'âge de la Galaxie et de vérifier la théorie de refroidissement des naines blanches. De plus, l'échantillon local est le seul qui permette d'obtenir un relevé complet de naines blanches froides. On peut aussi espérer y trouver des objets de transition qui permettraient de faire le lien entre les différents types spectraux et de mieux comprendre la séquence d'évolution et la structure des naines blanches.

Dans cette thèse, nous nous efforcerons d'obtenir un échantillon complet d'étoiles naines blanches du ciel de l'hémisphère nord dans une demi-sphère définie par un rayon de 40 parsecs (pc) autour du Soleil. Afin de bien justifier l'intérêt d'un tel effort et les technique utilisées pour arriver à nos fins, nous débuterons par une revue des principaux relevés qui ont permis la découverte des naines blanches que nous connaissons aujourd'hui. Nous découvrirons les effets de sélection associés aux différentes stratégies utilisées, et nous pourrons ainsi mieux comprendre comment s'en affranchir afin d'arriver à assembler notre propre échantillon statistiquement représentatif de la population des naines blanches du voisinage solaire.

1.1 La recherche d'étoiles naines blanches

1.1.1 Les grands relevés d'étoiles: les catalogues de Giclas et Luyten

La technique la plus répandue pour la détection d'étoiles proches est certainement celle qui se base sur le mouvement propre. Le mouvement propre d'une étoile, tel que vu par un observateur sur Terre, est la somme d'une composante radiale et d'une composante tangentielle. Cette dernière est responsable du changement angulaire dans les coordonnées de l'étoile. Afin de détecter le mouvement propre d'une étoile, on utilise des images du ciel prises à deux époques. En comparant les images qui correspondent à la même portion du ciel, certaines étoiles se déplacent par rapport aux étoiles de fond plus lointaines. Puisque ces étoiles bougent aussi, les mouvement propres ainsi déterminés sont relatifs. Il est donc nécessaire de les transformer en mouvements propres absolus en utilisant, par exemple, la position de galaxies lointaines et de quasars. Les relevés de W.J. Luyten, de l'Université du Minnesota, et

de H.L. Giclas au *Lowell Observatory* ont grandement augmenté le nombre d'étoiles connues.

Les catalogues de Giclas et al. (1971, 1978) contiennent ∼11 800 étoiles, dont les mouvements propres sont plus élevés que $0''.20$ par année pour environ 10 300 objets, et 1 500 objets ont $\mu \geq 0''.10$ par année (la limite de détection). Les images ont été prises à partir des années 1930 sur des plaques photographiques à l'aide d'un télescope de 13 pouces. Les objets, qui ont des magnitudes entre 8 et 17, ont été séparés en 6 classes de couleurs, et comparés avec les indices de couleur $U - B$ et $B - V$ de naines blanches connues (Giclas 1971). Les objets qui montraient les mouvements propres réduits les plus grands et qui étaient les plus bleus devenaient des candidates naines blanches. Dans le catalogue de naines blanches confirmées spectroscopiquement de McCook & Sion (2006), 590 objets proviennent des catalogues de Giclas.

Les étoiles détectées par Luyten se trouvent dans deux catalogues: *A Catalogue of Stars with Proper Motions Exceeding 0".5 Annually* (LHS, Luyten 1979a), qui contient 4470 objets et le *New Luyten Catalogue of Stars with Proper Motions Larger than Two Tenths of an Arcsecond* (NLTT, Luyten 1979b), avec 58 845 étoiles. Luyten avait accès aux données du *National Geographic-Palomar Observatory Sky Survey*, qui consiste en 936 paires de plaques photographiques rouges et bleues, prises avec le télescope Palomar Schmidt au début des années 1950. Elles couvrent 77% du ciel, du Pôle Nord jusqu'à une déclinaison de $-33°$ (Luyten 1974). En 1962 a débuté le relevé Palomar Proper Motion, qui avait pour but d'obtenir des observations d'une deuxième époque, afin d'identifier les étoiles ayant un grand mouvement propre. Ainsi, 153 paires de plaques de deux époques différentes ont été inspectées visuellement. À partir de 1972, le numériseur microdensitomètre développé par Luyten a permis d'augmenter la cadence des détections, et d'en améliorer la précision. Les *Luyten's White Dwarf Catalogues* (Luyten, 1970-1977) contiennent 3035 candidates naines blanches qui ont un grand mouvement propre réduit, soit $H = m + 5 + 5 \log \mu > 20$ (Luyten 1979a), et qui sont des objets bleus.

Les relevés de Giclas et Luyten se basent sur des mouvements propres assez élevés, et comportent donc d'importants biais cinématiques. De plus, ils ne sont composés que d'objets brillants. Ils représentent néanmoins un effort de pionnier, et une précieuse référence. Les catalogues de Giclas et de Luyten sont une importante source d'objets pour beaucoup d'études

visant à découvrir, par exemple, des naines blanches par suivi photométrique ou spectroscopique. Par contre, malgré tous les suivis des étoiles de Luyten, il reste encore dans le LHS et le NLTT des objets sans classification spectrale (Lépine & Shara 2005).

1.1.2 Les relevés photométriques

1.1.2.1 L'excès dans l'ultraviolet

L'objectif premier des relevés d'objets à excès dans l'ultraviolet est la détection de quasars, mais on découvrit très rapidement que ces relevés arrivent également à repérer des naines blanches. On en identifia plus de 300 dans le relevé Palomar Green, destiné à la découverte de nouveaux quasars. Une naine blanche chaude, dont la température effective est, par exemple, de 15 000 K, aura son maximum d'intensité d'émission à $\sim$2000 Å, ce qui permet de la détecter lorsqu'on recherche des objets à excès dans l'UV.

Les relevés d'excès dans l'ultraviolet ont en commun la prise successive d'images dans les bandes U et B, sur la même plaque, séparées par quelques secondes d'arc. Les images sont ensuite comparées, et les étoiles qui ont, par exemple, un excès UV de $U - B < -0.46$ sont sélectionnées en tant que candidates naines blanches.

1.1.2.2 Le Sandage two-color survey of the Galactic plane

En 1973, Howard Lanning rapportait la fin d'un programme qui avait permis de photographier la partie nord du plan galactique. L'objectif premier était la recherche d'objets à excès dans l'ultraviolet, susceptibles d'être des candidates de sources de rayons-X (Lanning 1973). Ce relevé allait plus tard devenir le *Sandage two-color survey of the Galactic plane*. Le relevé contenait un grand nombre d'objets plus faibles que la 10^e magnitude, qui en faisait des candidates d'étoiles à faible luminosité. Plusieurs catalogues furent donc publiés pour permettre à d'autres observateurs de les découvrir.

Même si 754 objets ont été détectés, moins d'une dizaine de naines blanches étaient confirmées jusqu'à ce que Lanning & Lépine (2006) déterminent qu'une fraction significative du relevé Sandage serait composée de naines blanches. Sur 46 candidates observées, Lépine et al. (2011) publient la classification spectrale pour 41 nouvelles naines blanches.

1.1.2.3 Le relevé Palomar Green

Le relevé Palomar Green (PG, Green et al. 1986) est un relevé photographique couvrant 10 714 degrés carrés, effectué à l'aide du télescope Schmidt Palomar de 46 cm. Des spectres pour toutes les candidates avec $U-B<-0.46$ mag furent obtenus, afin de séparer les quasars des étoiles, et de procéder à la classification spectrale. L'échantillon statistique complet de 1715 objets compte 348 naines blanches de type DA, chaudes pour la plupart dû à l'effet de sélection basé sur la couleur.

Une fonction de luminosité a été réalisée par Fleming et al. (1986), à partir de magnitudes absolues calculées avec des calibrations photométriques. Plus tard, Liebert et al. (1988) ont étudié un échantillon de 43 naines blanches froides tirées du LHS, et pour compléter le côté chaud de la fonction de luminosité, ils ont utilisé les données de Fleming et al. (1986). Cette étude, qui doit combiner les naines blanches de deux relevés différents, est un bon exemple d'échantillon mal défini du point de vue statistique. Les deux types de relevés utilisés pour rassembler une fonction de luminosité entière sont incomplets et mutuellement exclusifs. Cette étude reflète également l'incomplétude des échantillons limités par la magnitude.

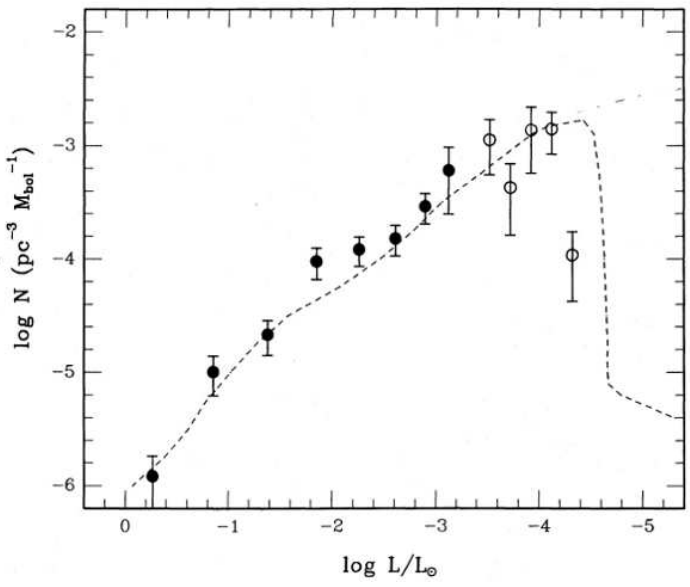

FIGURE 1.1 – Fonction de luminosité des naines blanches. Les cercles pleins (naines blanches chaudes) proviennent de Fleming et al. (1986). Les cercles vides (naines blanches froides) viennent de Liebert et al. (1988). La courbe est une fonction de luminosité théorique, de Winget et al. (1987). La figure est tirée de Liebert et al. (1988).

La fonction de luminosité doit toujours être dérivée à partir d'un échantillon complet d'étoiles naines blanches. Dans le cas contraire, les résultats dérivés à l'aide de l'étude statistique que représente la fonction de luminosité ne sont pas significatifs. La fonction de lumino-

sité est une mesure de la densité spatiale d'étoiles en fonction de leur luminosité intrinsèque. Elle permet d'estimer la contribution des naines blanches à la densité de matière dans la Galaxie, de mesurer le taux de mort stellaire et de se renseigner sur l'historique de la formation stellaire dans le disque local. La partie descendante de la fonction de luminosité est très sensible à l'âge du système stellaire. Elle est aussi peuplée par les étoiles naines blanches les plus massives, les moins nombreuses et les plus vieilles (et froides) d'une population donnée. La comparaison de modèles avec des fonctions de luminosité expérimentales permet de valider ou de contraindre le calcul théorique du taux de refroidissement des naines blanches et de poser une limite inférieure sur l'âge de la Galaxie. En effet, les naines blanches les plus vieilles ont un âge total (temps de vie sur la séquence principale + temps de refroidissement) égal à l'âge du système stellaire auquel elles appartiennent.

Liebert et al. (2005) ont recalculé la fonction de luminosité du relevé PG à l'aide d'une méthode développée dans Bergeron et al. (1992), qui permet de déterminer les paramètres atmosphériques des naines blanches DA en utilisant les raies de la série de Balmer pour l'hydrogène. Les magnitudes absolues pouvaient donc être déterminées de manière beaucoup plus précise, ce qui a permis d'améliorer l'étude statistique de l'échantillon PG. Selon leur étude, la complétude de l'échantillon est évaluée à 84%.

1.1.2.4 Le relevé Kiso

Le relevé Kiso fut mené au Japon à partir de 1977, à l'aide du télescope Kiso Schmidt de 105 cm. Ce relevé a permis de recenser 1186 objets à excès dans l'ultraviolet, publiés dans Noguchi et al. (1980) et Kondo et al. (1984). Les objets se trouvent pour la plupart à une longitude galactique de 180°, dans une superficie d'environ 1400 degrés carrés. Le relevé Kiso contient 234 naines blanches, dont 175 de type DA et 23 de type DB.

La première fonction de luminosité des naines blanches du relevé Kiso fut publiée par Darling (1994). Celle-ci était basée sur des calibrations photométriques, comme dans Fleming et al. (1986), et l'auteur affirmait une complétude de 74% jusqu'à $M_B \sim 15 - 16$. Limoges et al. (2010) ont refait l'analyse spectroscopique du relevé Kiso, montrant que le relevé est complet à 84.4% en ce qui concerne les naines blanches. Le fait que le relevé Kiso n'est pas

plus complet que le relevé PG n'a rien d'étonnant, puisque les deux études partagent la même méthode de détection et les mêmes effets de sélection.

1.1.2.5 Les sources d'incertitude dans les relevés à excès dans l'ultraviolet

Les relevés à excès dans l'ultraviolet ne permettent que de détecter les objets les plus chauds. Par exemple, dans Limoges et al. (2010), seulement 10 naines blanches ont une température sous 10 000 K. Il est donc impossible, à l'aide de ces relevés, d'espérer compléter le côté froid de la fonction de luminosité. De plus, la transformation des magnitudes photographiques en système standard introduit une incertitude. Pour le relevé PG, les erreurs sur les mesures sont de 0.29 mag sur la magnitude B et 0.38 sur l'indice de couleur $U - B$. Ces incertitudes peuvent empêcher la détection d'un bon nombre d'objets si elles ne sont pas considérées lors de l'application des critères sur la couleur. Une image très brillante en bande B trop près d'une image en bande U rendra celle-ci inutilisable. Il arrive également que des étoiles soient à quelques millimètres du bord d'une plaque, que des images soient très faibles, ou que l'image en bande B soit correcte, mais que l'image correspondante en bande U soit faible et floue. Les images sont alors rejetées. De plus, les étoiles très bleues et très brillantes ($B \leq 8$) sont presque impossibles à calibrer avec précision. Finalement, chaque plaque photographique possède une magnitude limite différente, en raison de l'état de chacune, et il est difficile d'évaluer une magnitude près de la magnitude limite de la plaque, ce qui peut introduire des incertitudes. Pour le relevé KUV, la magnitude limite moyenne est de $V = 17.7$.

1.1.2.6 La détection grâce à l'émission dans l'ultraviolet extrême

Selon Burleigh et al. (1997), il est estimé que 50 à 80% des naines blanches appartiendraient à des systèmes binaires, et plusieurs de ces naines blanches seraient cachées dans des systèmes non résolus. Si le compagnon de la naine blanche est une naine rouge, les deux composantes seront discernables dans le spectre en lumière visible du système. Dans les systèmes de type Sirius, le compagnon, de type K ou plus précoce, domine complètement le spectre visible, masquant la présence de la naine blanche. Par contre, une naine blanche chaude sera détectable

par son flux ultraviolet si son compagnon est une étoile de type plus tardif que A6.

Les satellites ROSAT (*ROentgen SATellite*) et EUVE (*Extreme Ultraviolet Explorer*) ont permis, grâce à leurs relevés dans les rayons-X et l'ultraviolet extrême, de découvrir environ 120 naines blanches chaudes. La plupart (70%) des naines blanches étaient isolées, mais certaines faisaient partie de systèmes naine blanche-naine rouge, et d'autres étaient dans des systèmes binaires résolus (Burleigh et al. 1997). L'étude de Burleigh et al. avait pour but de trouver les naines blanches cachées dans des systèmes binaires où le spectre visible de la naine blanche est masqué par la présence du compagnon. Cette étude devait servir de complément aux études colorimétriques qui favorisent la détection de naines blanches isolées.

Les candidates naines blanches ont été identifiées à l'aide de ROSAT grâce à leur émission dans l'UV extrême ou dans les rayons-X mous. Par contre, les spectres visibles (*Steward Observatory*) et ultraviolet (*International Ultraviolet Explorer*) obtenus n'ont révélé que trois naines blanches, ce qui est beaucoup moins que le nombre prévu (Burleigh et al. 1997).

Une minorité d'étoiles seulement qui ont une absorption interstellaire assez faible ont les caractéristiques citées plus haut. Aussi, pour détecter ces objets, il faut trouver des objets brillants dans l'EUV, mais qui ne sont pas actifs (puisque l'excès UV est dû à la naine blanche). Or, la plupart des sources EUV détectées sont des étoiles de type tardif très actives. Les naines blanches sont donc difficiles à trouver de cette manière. Finalement, cette méthode ne permet que de détecter les naines blanches les plus chaudes.

1.1.3 Le mouvement propre réduit

Le mouvement propre réduit se définit ainsi, $H_V = V + 5\log\mu + 5$, où le mouvement propre μ est mesuré en seconde d'arc par année. Il est analogue à la magnitude absolue, $M_V = V + 5\log\pi + 5$, où la parallaxe π est remplacée par le mouvement propre de l'objet. Avec v_T en km s^{-1}, on obtient $H_V = M_V + 5\log v_T - 3.38$.

Le diagramme de mouvement propre réduit est donc analogue à un diagramme couleur-magnitude et les naines blanches y occupent le même endroit, soit la partie inférieure gauche. Par contre, les différentes populations ont différentes valeurs de v_T, ce qui permet de les séparer dans le diagramme de mouvement propre réduit. Les étoiles du disque ont une vitesse

transversale moyenne de 50 km s^{-1}, et donc $\langle H_V \rangle_{\rm disque} = M_V + 5.1$. Les étoiles du halo, quant à elles, ont des valeurs de v_T plus grandes, $\langle v_T \rangle = 300$ km s^{-1}, alors $\langle H_V \rangle_{\rm halo} = M_V + 9.0$ (Lépine & Shara 2005). De courbes de refroidissement à une vitesse transversale donnée pour les naines blanches du Data Release 2 (DR2) du SDSS sont tracées dans la Figure 1.2 dans un diagramme de mouvement propre réduit. On y remarque que les populations stellaires sont séparées: les points individuels montrent les étoiles qui se trouvent dans la partie allouée aux naines blanches tandis que les contours représentent les autres objets du relevé. On remarque également que les naines blanches (triangles foncés) sont séparées des sous-naines (carrés) par la courbe à $v_T = 20$ km s^{-1}. Les courbes de refroidissement des naines blanches à v_T constante tournent abruptement à cause de l'absorption induite par collisions due à l'hydrogène moléculaire dans les naines blanches les plus froides qui ont une atmosphère d'hydrogène (Kilic et al. 2006). Cette opacité diminue le flux dans la bande i, ce qui rend les étoiles plus bleues.

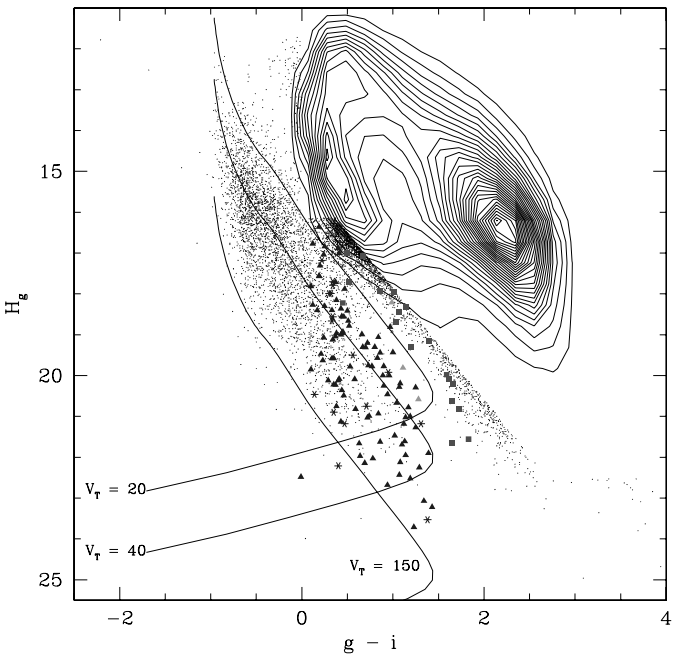

FIGURE 1.2 – Diagramme de mouvement propre réduit des étoiles du relevé SDSS. Les triangles foncés présentent les naines blanches confirmées spectroscopiquement par leur étude, les triangles pâles les systèmes binaires naine blanche+sous-naine de type tardif et les carrés indiquent les sous-naines. Les astérisques représentent les naines blanches qui ont des mouvements propres incertains selon les auteurs et les contours représentent les étoiles qui ont des mouvements propres réduits incompatibles à ceux des naines blanches. La figure est tirée de Kilic et al. (2006).

1.1.3.1 Le Lépine-Shara Proper Motion Survey (LSPM)

Le relevé de mouvement propre Lépine-Shara s'étend sur tout le ciel. L'hémisphère nord est analysé dans Lépine & Shara (2005a), et l'hémisphère sud dans Lépine & Shara (2005b).

Le relevé est basé sur une analyse des plaques Oschin Schmidt POSS-I et POSS-II, faites au *Space Telescope Science Institute* (STScI). La limite de détection est de $0\farcs15$ par année, ce qui est inférieur à tous les relevés d'étoiles à grand mouvement propre précédents. Dans l'hémisphère nord seulement, 61 977 étoiles ont été identifiées. Parmi celles-ci, on retrouve 40 843 étoiles avec $\mu > 0\farcs18$ an^{-1}, dont 28 486 font partie du catalogue NLTT. Le relevé LSPM contient aussi 21 133 étoiles avec $0\farcs15$ an^{-1} $< \mu <$ $0\farcs18$ an^{-1}, dont seulement 2875 appartiennent au NLTT (la limite de détection du NLTT est plus élevée, avec $0\farcs2$ par année). La complétude du relevé, basée sur les étoiles du LHS, est estimée à 89.1%. Le catalogue serait complet à plus de 99% à haute latitude galactique ($b > 15°$) jusqu'à une magnitude de $V = 19$ et la magnitude limite est de $V = 21$. Un grand nombre de nouveaux objets (naines rouges, sous-naines, naines blanches) ont pu être identifiés à partir du relevé LSPM grâce à la faible limite de détection du relevé, au fait que les régions densément peuplées telles que le centre galactique sont inclues et grâce au programme d'analyse digitale des images.

L'analyse des plaques a été faite grâce au programme SUPERBLINK, un logiciel extracteur et comparateur d'image. Il dégrade d'abord la qualité des plaques POSS-II pour qu'elles se comparent aux plaques POSS-I plus anciennes. Les plaques sont ensuite alignées et comparées pour identifier les objets qui se déplacent par rapport aux étoiles de fond. SUPERBLINK permet ainsi l'identification d'étoiles dans le plan galactique, une région souvent abandonnée en raison du risque élevé d'erreur. Grâce à toutes ces caractéristiques, le catalogue SUPERBLINK possède un grand potentiel pour la détection d'étoiles du voisinage solaire.

Des diagrammes de mouvement propre réduit ont permis d'isoler près de 1200 candidates naines blanches. Les relevés basés sur le mouvement propre permettent d'obtenir un relevé de tous les objets stellaires les plus près, jusqu'à la magnitude limite donnée. Ici, la faible limite de détection due à l'informatisation de la technique de détection permet d'obtenir plus d'objets très peu brillants, ou à très faible mouvement propre. Cette technique permet non seulement de détecter un grand nombre de naines blanches, mais également de détecter même les objets froids, en éliminant les effets de sélection reliés à la couleur. De plus, tel qu'expliqué dans Lépine & Shara (2005), les étoiles à grande vitesse transversale, comme celles du halo et du disque mince, sont sur-représentées dans les relevés actuels puisqu'on peut les détecter

à plus grande distance que les étoiles du disque mince. Afin de se débarrasser de ce biais cinématique, il est important de réduire la limite de détection des mouvements propres.

Lépine & Shara (2005) ont remarqué qu'une fraction importante des étoiles manquées par les relevés précédents est située dans des champs densément peuplés, à basse latitude galactique. Parmi les étoiles ayant été identifiées, certaines ont des erreurs importantes concernant l'estimation de leur mouvement propre. En ce qui concerne les autres sources d'erreur des relevés de mouvement propre, une étoile très brillante ($V < 15$) située à proximité d'une autre étoile peut induire une fausse détection et il arrive également que sur une des plaques, l'étoile faible soit mélangée à l'image de l'objet le plus brillant. Par contre, Lépine & Shara (2005) affirment que SUPERBLINK arrive à détecter l'étoile quand même, même si les magnitudes des objets sont alors certainement faussées. L'image d'un objet brillant qui montre des anneaux de diffraction est aussi source d'erreur, et le mouvement propre doit alors être confirmé par inspection visuelle.

1.1.4 Les naines blanches froides du Guide Star Catalog II

Carollo et al. (2006) ont fouillé la base de données du *Guide Star Catalogue II* (McLean et al. 2000) pour présenter un catalogue de naines blanches confirmées spectroscopiquement. Leur relevé devait contraindre la densité spatiale de naines blanches du halo dans le cadre de la recherche de MACHOs (MAssive Compact Halo Objets). Les naines blanches ont été cherchées dans une surface de 1150 degrés carrés concentrés vers le pôle nord galactique, afin d'éviter les régions densément peuplées de la Galaxie. Tout comme pour le relevé LSPM, ils utilisent principalement les plaques POSS-I et POSS-I afin d'identifier les objets et d'évaluer leur mouvement propre.

Afin de séparer les naines blanches des autres populations stellaires, les objets faibles ($R_F \geq 16$) avec un grand mouvement propre ($0.28 < \mu < 2.5''$ par année) furent sélectionnés. Un diagramme de mouvement propre réduit a ensuite permis de raffiner la sélection. Pour déterminer la frontière entre les naines blanches et les sous-naines, ils ont utilisé la séquence de refroidissement pour les naines blanches de $0.6\,M_{\odot}$ à atmosphère d'hydrogène pur, avec la vitesse tangentielle moyenne des étoiles du disque mince. Le suivi spectroscopique a révélé que

parmi les 59 candidates, 41 sont des naines blanches, et 24 sont des nouvelles identifications.

Carollo et al. (2006) ont pris soin d'éviter les régions densément peuplées pour éviter les fausses détections, malgré le fait que ces régions soient souvent évitées dans ce type d'étude et que le potentiel de détection de nouvelles naines blanches y est très élevé. Finalement, la limite de détection des objets ($\mu > 2''.5$ par année) est plus grande que celle du NLTT.

1.1.5 Combinaison mouvement propre réduit−couleur

Kawka et al. (2004) ont sélectionné 545 candidates naines blanches à partir du catalogue NLTT révisé de Salim & Gould (2003) et d'un diagramme de mouvement propre réduit. Par contre, Vennes & Kawka (2003) ont trouvé que les sous-naines peuvent contaminer jusqu'à 2/3 de l'échantillon de candidates. À l'aide d'un diagramme couleur-couleur, un critère supplémentaire en $V - J > 3.28(J - H) - 0.75$ fut alors appliqué, réduisant le nombre de candidates à 417. Parmi celles-ci, 217 sont des naines blanches confirmées. Par contre, ces critères visible-infrarouge peuvent éliminer accidentellement les candidates WD+dM. De plus, leur échantillon de candidates ne peut être complet, puisqu'ils ne tiennent pas compte des naines blanches avec $\delta < 17°$ (où l'échantillon n'est pas homogène).

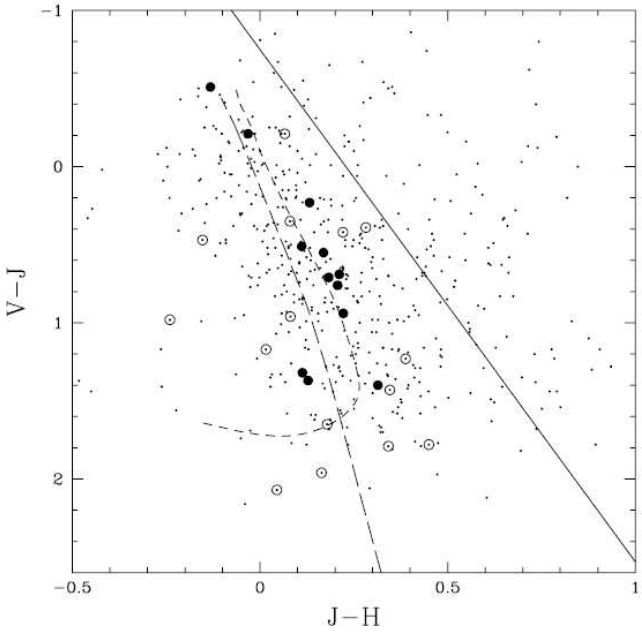

FIGURE 1.3 – Diagramme couleur-couleur des naines blanches qui ont été sélectionnées à l'aide du diagramme de mouvement propre réduit. Les candidates naines blanches se trouvent sous la droite. Elles sont comparées aux séquences de refroidissement des naines blanches pour $\log g = 8$ pour des atmosphères d'hydrogène (petits traits) et d'hélium (grands traits). Les cercles pleins montrent les nouvelles naines blanches tirées du NLTT révisé de Salim & Gould (2003), et les cercles vides montrent les naines blanches à grande vitesse. Figure tirée de Kawka et al. (2004).

1.1.6 Les naines blanches tirées du Sloan Digital Sky Survey

L'ancêtre du relevé Sloan est le *Two-Degree Field (2dF) QSO Redshift Survey*. Il s'agit d'un relevé spectroscopique (Boyle et al. 2000), qui a permis de produire un catalogue de naines blanches (Vennes et al. 2002). Il est un peu plus profond que SDSS ($18.4 \leq B \leq 21.0$), mais il couvre un angle solide plus petit (740 degrés carrés). Près de 950 naines blanches de type DA y ont été spectroscopiquement identifiées.

Le relevé du Sloan Digital Sky Survey (SDSS) représente certainement la source de données d'observation des naines blanches la plus importante depuis le relevé PG. Il s'agit d'un relevé qui couvre le tiers du ciel à l'aide d'image dans 5 bandes passantes (*ugriz*), à partir desquelles des galaxies, des quasars et des étoiles sont choisis afin d'en faire le suivi spectroscopique. Le but premier du SDSS est d'obtenir les décalages vers le rouge de galaxies lointaines et de quasars, et l'étude des naines blanches est un des projets secondaires. Si les 640 fibres par plaque ne sont pas toutes utilisées pour le projet principal, les fibres qui restent sont assignées à d'autres projets, selon leur ordre de priorité.

Il existe donc plusieurs catégories d'objets à observer [1]. La priorité accordée à l'obtention des spectres de naines blanches à l'aide de la catégorie « STAR WHITE DWARF » est faible, et elle est utilisée pour observer des naines blanches très froides. Kleinman et al. (2004) ont trouvé 2551 naines blanches dans le premier catalogue (Data Release 1; DR1). Ils ont ainsi presque doublé le nombre de naines blanches contenues dans McCook & Sion (1999), mais une petite partie seulement des naines blanches identifiées furent observées dans la catégorie « STAR WHITE DWARF ». La plupart ont été observées dans les catégories qui cherchent des objets bleus. Les candidates naines blanches sont choisies en fonction de plusieurs critères sur la couleur et le mouvement propre réduit, qu'on retrouve dans le tableau 2 de Kleinman et al. (2004). Ces cibles seront ensuite l'objet d'un suivi spectroscopique.

Kilic et al. (2006) ont identifié les candidates naines blanches du DR2. Les objets qui ont une magnitude entre $15 < g < 20$ et dont le mouvement propre est plus grand que $0\farcs2$ par année sont placés dans un diagramme de mouvement propre réduit en H_g en fonction de $g - i$. Celui-ci utilise les données photométriques du SDSS et les données astrométriques qui

1. Voir le tableau 1 de Kleinman et al. (2004).

proviennent du USNO-B. Les étoiles sont tracées dans le diagramme seulement si $g-i>0$ et si $H_g > 15.136 + 2.727(g-i)$. Ils arrivent ainsi à séparer les naines blanches froides du disque et du halo des étoiles de la séquence principales de population II, qui ont de plus grandes vitesses tangentielles. Selon les auteurs, ce critère devrait inclure toutes les naines blanches.

La figure 6 de Kilic et al. (2006) (voir figure 1.2) montre leurs résultats dans un diagramme de mouvement propre réduit. En tenant compte de la fiabilité des valeurs de mouvement propre réduit, les auteurs remarquent que la contamination de la portion des naines blanches par les sous-naines serait due à des mouvements propres incertains. Si les étoiles ont des mouvements propres fiables (les étoiles sont détectées dans les cinq époques du USNO-B et n'ont pas de voisin trop brillant, trop près) les naines blanches (triangles) sont clairement séparées des sous-naines (carrés). Des 95 candidates qui sont plus bleues que $g-i=1.5$ et qui ont $v_T < 20$ km s^{-1}, 91 sont des naines blanches. Ils ont également trouvé 16 naines blanches parmi les étoiles à mouvement propre incertain (astérisques). Finalement, les 37 sous-naines qui ont été trouvées à la frontière entre les naines blanches et les sous-naines avaient des mouvement propres incorrects. La méthode du diagramme de mouvement propre réduit est donc efficace pour détecter des naines blanches, lorsque les mouvements propres mesurés sont précis.

1.1.6.1 Effets systématiques

Dans le relevé Sloan, les effets de sélection sont très importants, tel que discuté dans Kleinman et al. (2004) et Eisenstein et al. (2006). À cause des critères de sélection pour l'identification des naines blanches, et du fait que l'observation des naines blanches n'est pas prioritaire, le SDSS n'est pas fait pour être statistiquement complet. En effet, DeGennaro et al. (2008) évaluent la complétude de l'échantillon de naines blanches du SDSS à 51%.

Pour les spectres SDSS, le rapport signal sur bruit dépend de la magnitude de l'étoile. En effet, puisque le temps d'intégration est fixe, le rapport signal sur bruit est plus élevé pour les étoiles les plus brillantes. Les objets les moins brillants ont donc un faible rapport signal sur bruit, ce qui cause problème pour la classification spectrale. Ainsi, des objets ont un statut de naine blanche incertain. Toujours en conséquence du temps d'intégration fixe et par souci de ne pas saturer les images, le relevé Sloan ne contient pas d'objet plus brillant que les magnitudes

$u = 13$, $g = 14$, $r = 14$, $i = 14$ et $z = 12$ (York et al. 2000). Finalement, les objets passent automatiquement à travers un critère de sélection en couleur, qui élimine systématiquement les naines blanches avec $T_{\rm eff} \lesssim 8000$ K, et le système de détection automatique échoue souvent à détecter les naines blanches magnétiques.

1.2 Identifier les naines blanches dans le voisinage solaire

Les étoiles les plus près du Soleil sont sans doute celles qui nous apportent le plus d'information. Les mesures directes de luminosité, de couleur, de température, et de masse des étoiles proches nous permettent de mieux comprendre les objets locaux, et d'étendre ce savoir aux objets plus éloignés. Les étoiles du voisinage solaire permettent aussi des études statistiques, telles les fonctions de luminosité et de masse, ainsi que l'étude de la multiplicité stellaire et des types spectraux. Ces études permettent de déterminer la nature des composants de la Galaxie (Henry et al. 1997).

Le premier registre des étoiles à moins de 25 pc du Soleil était le *Third Catalogue of Nearby Stars* de Gliese & Jahreiss (1991). Cette étude et les recherches qui suivirent ont révélé que la population du voisinage solaire est majoritairement composée d'étoiles de faible luminosité difficiles à détecter à grande distance et que beaucoup de ces étoiles seraient des naines blanches (Holberg et al. 2002). Selon Henry et al. (1997), si on suppose que la densité d'étoiles à 5 pc peut s'extrapoler à 10 pc, 130 systèmes n'auraient pas été détectés (voir figure 1.4). Les absents seraient surtout des naines M de faible luminosité, et le manque serait plus grand dans l'hémisphère sud, où peu de suivis spectroscopiques ont été faits.

Par le fait même, un grand nombre de naines blanches du voisinage solaire sont aussi passées inaperçues. Ces dernières nous renseignent sur l'histoire, la formation et l'évolution stellaire dans le plan galactique. La fonction de luminosité des naines blanches permet de poser une limite inférieure sur l'âge de la Galaxie, tandis que la densité locale de naines blanches permet d'améliorer notre compréhension de la densité de masse dans la Galaxie. Finalement, plusieurs études recherchent des planètes autour des naines blanches les plus près du Soleil, puisque la signature astrométrique due à la présence d'une planète sera plus grande que pour une naine blanche plus éloignée (Subasavage et al. 2007). Il est donc primordial d'obtenir un

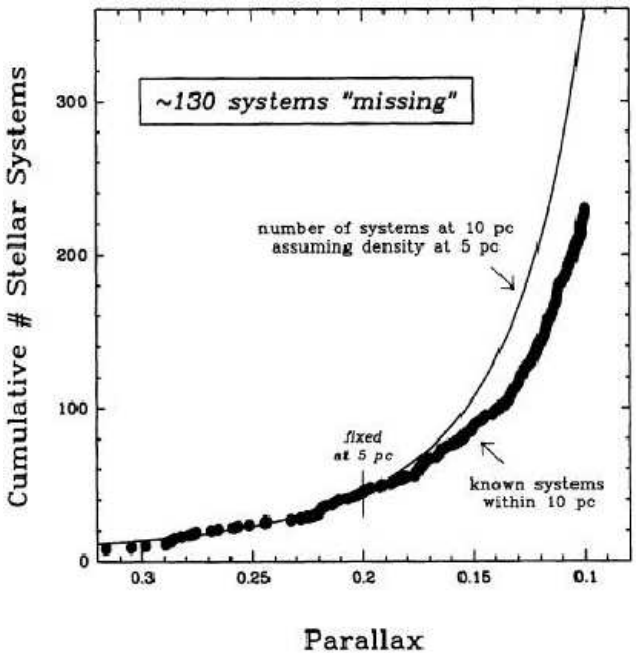

FIGURE 1.4 – Nombre cumulatif de systèmes stellaires en fonction de la distance. Le nombre de systèmes connus à moins de 10 pc est indiqué par les points. Le trait représente le nombre d'étoiles attendues en supposant que la densité d'étoiles à 5 pc peut s'extrapoler à 10 pc. Il manquerait 130 systèmes stellaires dans les catalogues, en date de 1997. Figure tirée de Henry et al. (1997).

recensement précis et complet des étoiles du voisinage solaire.

1.2.1 La mesure des parallaxes trigonométriques

La recherche de naines blanches du voisinage solaire s'effectue selon deux volets. Le premier constitue l'identification d'étoiles naines blanches parmi les étoiles du champ, dont les principales techniques ont été discutées précédemment. Ensuite, il est nécessaire d'obtenir des mesures de distance robustes pour les naines blanches les plus susceptibles de se trouver dans l'univers local. Or, la distance géométrique donnée par la parallaxe trigonométrique est la plus fiable puisqu'elle est la seule qui ne dépend pas des modèles, mais de telles mesures ne sont disponibles que pour environ 300 naines blanches.

Les mesures de parallaxes des étoiles de l'échantillon local proviennent pour la plupart du *Yale Parallax Catalog* (van Altena et al. 1995), qui contient des parallaxes pour 8112 étoiles, et quelques-unes proviennent du catalogue Hipparcos (van Leeuwen 2007). Le satellite Hipparcos de l'Agence spatiale européenne a permis d'obtenir des mesures de position pour 118 218 étoiles, entre 1989 et 1993. Par contre, très peu de ces étoiles sont des naines blanches (~ 20), d'où le besoin prendre des mesures de parallaxe pour des naines blanches locales à partir du sol (on en retouve par exemple dans le catalogue UCAC2 du *US Naval Observatory*; USNO).

Finalement, certaines ont été mesurées grâce à la recherche de compagnons d'étoiles naines blanches (Subasavage et al. 2009). Cette méthode nécessitait de mesurer la position exacte des naines blanches afin de déceler un mouvement induit par la présence d'un compagnon. On retrouve aussi des mesures de parallaxes trigonométriques de naines blanches mesurées à l'aide du satellite Hipparcos dans le catalogue *Tycho-2*, qui est le fruit d'une collaboration entre le *Copenhagen University Observatory* et le USNO, et contient 2.5 millions d'étoiles.

Le projet *Discovery and Evaluation of Nearby Stellar Embers* (DENSE) (voir, par exemple, Subasavage et al. 2009) a pour but de compléter l'échantillon local à moins de 25 pc. En effet, 112 naines blanches seulement avaient des parallaxes les plaçant à moins de 20 pc. On retrouvait également deux fois plus de naines blanches à 25 pc avec des mesures de parallaxes dans l'hémisphère nord que dans le sud. Des parallaxes ont été obtenues pour 25 naines blanches de l'hémisphère sud, et grâce aux 20 naines blanches à moins de 25 pc trouvées dans l'hémisphère sud (dont 7 sont des nouvelles identifications), ils ont augmenté l'échantillon de 20% et ont réduit l'asymétrie nord-sud (Subasavage et al. 2007, 2008).

1.2.2 Le biais cinématique

L'étude de Subasavage et al. (2007) avait pour but de réduire l'effet de sélection qui semble favoriser la détection de naines blanches à grand mouvement propre dans le voisinage solaire. En effet, une seule naine blanche a un mouvement propre inférieur à $1\farcs0$ an^{-1} parmi les 18 naines blanches avec des parallaxes qui les placent à moins de 10 pc. Par opposition, 50% des étoiles de la séquence principale à 10 pc et moins ont $\mu > 1\farcs0$ an^{-1}.

Cette étude est basée sur des relevés de mouvement propre récents dans l'hémisphère sud. Les objets à grands mouvements propres ont été sélectionnés, et leurs magnitudes photographiques sont extraites du SuperCOSMO Sky Survey (SSS). Après avoir sélectionné leurs candidates à l'aide de diagrammes de mouvement propre réduit, l'obtention de spectres et leur analyse a permis d'identifier 20 naines blanches (8 nouvelles et 12 connues) dont les distances estimées les placent à moins de 25 pc. Ces objets ont été ajoutés au *Cerro Tololo Inter-American Observatory Parallax Investigation* afin de déterminer leur distance avec précision. Ces 20 objets constituent une augmentation de 18% du nombre de naines blanches avec des

parallaxes trigonométriques $\geq 0''.04$ par année, qui était de 109. De plus, dans cet échantillon, on a presque le double de systèmes avec $\mu < 1''.0$ an^{-1} (13) qu'avec $\mu > 1''.0$ an^{-1} (7). C'est un pas important vers l'élimination du biais cinématique.

1.2.3 Un catalogue de naines blanches à moins de 20 pc du Soleil

Un des premiers relevés de la population de naines blanches locales fut mené par Jahreiss (1987), et comptait 96 naines blanches à moins de 20 pc du Soleil. Plus tard, Tat & Terzian (1999) ont également catalogué 121 naines blanches à moins de 20 pc, à partir du *Catalog of Spectroscopically Identified White Dwarfs* de McCook & Sion (1987) et du *Catalogue of Nearby Stars* (Gliese & Jahreiss 1991), dans le but de déterminer la distribution de l'ionisation dans le milieu interstellaire local. L'étude fut reprise par Holberg et al. (2002) afin d'évaluer la complétude de l'échantillon et de calculer la densité spatiale de naines blanches dans le voisinage solaire. Ils utilisent les 2249 objets du catalogue de McCook & Sion (1999) pour identifier les objets avec une parallaxe $\pi \geq 0''.05$ et des distances photométriques qui correspondent à $V - M_V \leq 1.505$, où les magnitudes absolues proviennent de relations couleur-magnitude empiriques. Les distances parallactiques et photométriques sont toutes deux considérées afin de déterminer la distance finale adoptée. L'échantillon final compte 109 naines blanches, ce qui représente 6% du catalogue de McCook & Sion (1999). Parmi celles-ci, on retrouve 3 systèmes de naines blanches binaires, dont 2 sont non résolus.

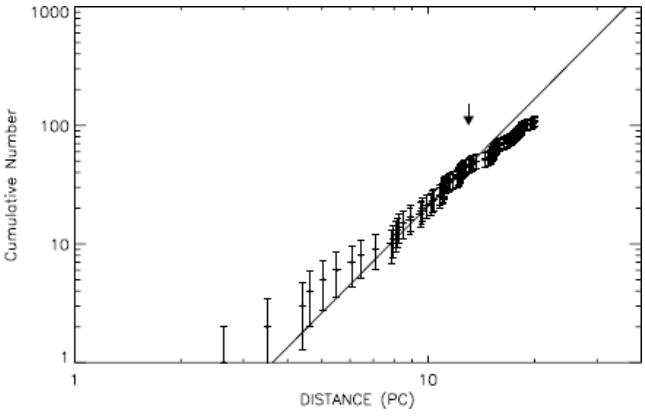

FIGURE 1.5 – Nombre cumulatif de naines blanches en fonction de la distance pour l'échantillon local. La droite représente le nombre attendu de naines blanches en supposant une densité spatiale moyenne de 5.0×10^{-3} pc^{-3}. La distribution est compatible avec une densité spatiale constante jusqu'à 13 pc. Figure tirée de Holberg et al. (2002).

La distribution des naines blanches de Holberg et al. (2002) est représentée à la figure 1.5

par un graphique de la distribution cumulative en fonction de la distance. La droite représente le nombre attendu de naines blanches en supposant une densité spatiale moyenne constante. La distribution est compatible avec une densité spatiale constante de 5.0×10^{-3} pc^{-3}, jusqu'à 13 pc. La complétude de leur échantillon est estimée à 65% à moins de 20 pc.

Holberg et al. (2008) reprennent l'étude de Holberg et al. (2002), en ajoutant les étoiles pouvant se trouver à moins de 20 pc identifiées par Vennes & Kawka (2003), Kawka et al. (2004) et Kawka & Vennes (2006) à partir du catalogue NLTT révisé de Salim et Gould (2003). L'échantillon local contient maintenant 126 naines blanches. Certains objets se trouvent désormais à moins de 20 pc grâce aux nouvelles valeurs de parallaxes trigonométriques publiées entre la parution des deux articles. Les autres nouveaux membres de la population locale proviennent des listes de naines blanches potentielles de Farihi et al. (2005), Kawka & Vennes (2006), Kawka et al. (2007) et Subasavage et al. (2007, 2008). En plus de ces sources publiées, 2 DA ont été trouvées, 12 étoiles ont été retirées, et certaines ont été reclassées comme des étoiles non dégénérées (par exemple, par Kawka et al. 2004). Parmi les 126 étoiles, 26 n'ont pas de mesures de parallaxe, et 36 ont des distances qui les placent à moins de 20 pc, mais les auteurs considèrent que les distances ne sont pas déterminées de manière assez précise pour les inclure dans leur échantillon. Des observations de parallaxe trigonométrique ou de photométrie pourraient donc améliorer les estimés de distances et les incertitudes, et faire varier le nombre total d'objets à l'intérieur de 20 pc du Soleil.

Finalement, les étoiles à moins de 20 pc du Soleil ont été recensées avec minutie dans l'étude de Giammichele et al. (2012). Cette étude tient compte de nouvelles mesures de parallaxes, détaille la photométrie disponible pour chaque objet, et surtout, fournit la première analyse homogène des propriétés physiques des naines blanches locales. La complétude de l'échantillon est évaluée à 90%, et bien qu'il y reste encore des étoiles pour lesquelles nous ne serons certains de leur distance que lorsque des mesures de parallaxes seront disponibles, son biais majeur n'est dû qu'au petit nombre d'objets qu'il comporte. En effet, avec 130 objets, les études statistiques menées sont encore affectées par les incertitudes de petit nombre.

1.3 Objectifs de la présente étude

Le premier pas vers l'obtention d'un échantillon statistiquement significatif serait de compléter le catalogue des naines blanches à moins de 20 pc du Soleil, afin qu'il soit aussi complet que celui à 13 pc, notamment par l'obtention de mesures de parallaxes. Ensuite, il faut obtenir un échantillon complet à plus grande distance, et c'est ici que nous intervenons, avec l'objectif de nous servir du relevé de mouvements propres de Lépine-Shara (Lépine & Shara 2005) afin de constituer un échantillon complet des naines blanches jusqu'à 40 pc du Soleil.

Afin d'arriver à dresser un portrait des naines blanches à moins de 40 pc du Soleil qui s'apparente à celui des naines blanches à 20 pc, il a fallu d'abord chercher à identifier les naines blanches déjà connues dans la littérature. Ensuite, nous avons pu déterminer les critères de sélection à appliquer aux étoiles de SUPERBLINK afin d'assembler une liste de candidates naines blanches, et trouver une manière d'estimer leur distance. La stratégie adoptée pour arriver à nos fins est expliquée dans un article publié dans l'*Astronomical Journal* et présentée dans le Chapitre 2. Il s'en est suivi la rédaction de nombreuses demandes de temps, car pas moins de 15 missions d'observations classiques ont été nécessaires, sur 3 télescopes à Kitt Peak en Arizona totalisant plus de 70 nuits, afin d'observer plus de 500 étoiles pour confirmer le type spectral des candidates. Nous avons également obtenu du temps à distance pour 3 programmes d'observation en 2011 et 2012 à l'aide des télescopes Gemini Nord (Hawaii) et Sud (Chili). Par la suite, nous avons classifié tous les objets, et fait une analyse de leurs propriétés physiques à l'aide des spectres et de toute la photométrie disponible, ainsi qu'avec les modèles d'atmosphère calculés au fil des années au sein du groupe de recherche des naines blanches de l'Université de Montréal. Nous avons également amélioré la manière de mesurer les distances aux étoiles pour lesquelles nous déterminons les paramètres atmosphériques par ajustement des raies spectrales. Nous avons finalement étudié les propriétés cinématiques et physiques des nouvelles étoiles trouvées, ainsi que de toutes les naines blanches à moins de 40 pc.

Dans le Chapitre 2, nous détaillons les critères de sélection et expliquons comment les distances des candidates naines blanches ont pu être estimées à partir de calibrations couleur-

magnitudes. Nous y présentons également les premières 193 nouvelles naines blanches identifiées après 8 missions d'observations. Dans le Chapitre 3, nous retrouvons un article qui sera soumis à l'*Astrophysical Journal*. Les progrès dans le grand relevé spectroscopique effectués depuis la publication des premiers résultats sont détaillés, et nous y présentons chaque nouvelle naine blanche, ainsi que les solutions adoptées en ce qui concerne leurs paramètres atmosphériques. Puisque le relevé est suffisamment complet, nous procédons à l'analyse des propriétés physiques des étoiles naines blanches qu'il contient, et pouvons conclure quant à la complétude à la fois du relevé et de l'échantillon des naines blanches à moins de 40 pc du Soleil.

1.4 Déclaration de l'étudiante

Les articles présentés aux Chapitres 2 et 3, ainsi que dans le contenu des annexes, sont le résultat de mes travaux réalisés dans le cadre de ce doctorat, pour lesquels j'ai pu bénéficier de l'aide de deux directeurs de recherche complémentaires. En effet, le début du projet a fait appel à l'expertise de Sébastien Lépine pour l'extraction de données et les calibrations empiriques afin de débusquer les naines blanches cachées dans SUPERBLINK, tandis que Pierre Bergeron a apporté son expertise théorique pour l'analyse des naines blanches trouvées par le relevé.

En ce qui concerne l'article présenté au Chapitre 2, à partir du grand catalogue d'étoiles assemblé par Sébastien Lépine, j'ai d'abord cherché à identifier les naines blanches déjà connues dans la littérature, pour ensuite déterminer les critères de sélection qui m'ont permis d'établir une liste de candidates naines blanches sous la supervision de Sébastien Lépine. Ensuite, nous avons trouvé une manière d'estimer leur distance à l'aide de relations couleur-magnitude théoriques. Pendant toute la durée du travail sur le premier article, j'ai obtenu du temps pour 8 missions d'observations, ce qui m'a permis d'observer plus de 500 étoiles afin de confirmer le type spectral des candidates. Pour les deux premières demandes de temps, j'ai collaboré étoitement avec Sébastien Lépine, qui avait l'expérience des observations avec les télescopes du NOAO. J'ai planifié et effectué la collecte de données, aidée au télescope par plusieurs membres de notre groupe de recherche. J'ai ensuite classifié tous les objets, et fait une analyse

préliminaire de leurs propriétés physiques à l'aide des modèles de Pierre Bergeron.

Pour l'article présenté au Chapitre 3, j'ai continué mon relevé spectroscopique lors de 7 autres missions d'observations pour lesquelles j'ai obtenu du temps, et j'ai planifié et effectué la collecte des données. Encore une fois, un membre du groupe de recherche m'accompagnait chaque fois, et j'ai ainsi pu initier 3 étudiants à la maîtrise à l'observation en spectroscopie. J'ai classifié les objets, et fait leur analyse détaillée toujours à partir des modèles de Pierre Bergeron. Ensemble, nous avons amélioré la manière de déterminer les distances aux étoiles pour lesquelles nous déterminons les paramètres atmosphériques par ajustement des raies spectrales, et avons également étendu l'ajustement des raies spectrales à Hα. Les modèles d'atmosphère développés par Patrick Dufour m'ont également permis d'obtenir les paramètres atmosphériques pour les étoiles DQ et DZ de mon échantillon. J'ai finalement étudié les propriétés cinématiques et physiques des nouvelles étoiles trouvées, et de toutes les naines blanches à moins de 40 pc, en collaboration avec mes deux directeurs de recherche.

Chapitre 2

Toward a Spectroscopic Census of White Dwarfs Within 40 parsecs of the Sun

M.-M. Limoges [1 2], S. Lépine [3], and P. Bergeron[1]

Published in *The Astronomical Journal*

Published 2013 April 4

1. Visiting Astronomer, Kitt Peak National Observatory, National Optical Astronomy Observatory, which is operated by the Association of Universities for Research in Astronomy (AURA) under cooperative agreement with the National Science Foundation.

2. Département de Physique, Université de Montréal, C.P. 6128, Succ. Centre-Ville, Montréal, Québec H3C 3J7, Canada

3. Department of Astrophysics, Division of Physical Sciences, American Museum of Natural History, Central Park West at 79th Street, New York, NY 1002

2.1 Abstract

We present the preliminary results of a survey aimed at significantly increasing the range and completeness of the local census of spectroscopically confirmed white dwarfs. The current census of nearby white dwarfs is reasonably complete only to about 20 pc of the Sun, a volume that includes around 130 white dwarfs, a sample too small for detailed statistical analyses. This census is largely based on follow-up investigations of stars with very large proper motions. We describe here the basis of a method that will lead to a catalog of white dwarfs within 40 pc of the Sun and north of the celestial equator, thus increasing by a factor of 8 the extent of the northern sky census. White dwarf candidates are identified from the SUPERBLINK proper motion database, allowing us to investigate stars down to a proper motion limit $\mu > 40$ mas yr^{-1}, while minimizing the kinematic bias for nearby objects. The selection criteria and distance estimates are based on a combination of color-magnitude and reduced proper motion diagrams. Our follow-up spectroscopic observation campaign has so far uncovered 193 new white dwarfs, among which we identify 127 DA (including 9 DA+dM and 4 magnetic), 1 DB, 56 DC, 3 DQ, and 6 DZ stars. We perform a spectroscopic analysis on a subsample of 84 DAs, and provide their atmospheric parameters. In particular, we identify 11 new white dwarfs with spectroscopic distances within 25 pc of the Sun, including 5 candidates to the $D < 20$ pc subset.

2.2 Introduction

Statistics of the local white dwarf population, such as the space density, luminosity function, and mass distribution, are fundamental tools for understanding the evolution of the Galactic stellar populations and quantifying their ages (Oswalt et al. 1996, Leggett et al. 1998). Because of their low luminosities, obtaining a large and complete census of white dwarfs within a well-defined volume remains a challenge. The best volume that can be defined for a census of low-luminosity objects is the solar neighborhood, which alleviates the need for deep surveys, and also allows one to map out the sample in velocity space using readily available proper motions.

A catalog and analysis of the sample of white dwarfs within 20 pc of the Sun were presented by Holberg et al. (2002), and later refined by Holberg et al. (2008) and Sion et al. (2009). In light of these studies, the current census of nearby white dwarfs is believed to be 80% complete, and contains 127 white dwarfs (Sion et al. 2009). Every white dwarf suspected to lie within 20 pc of the Sun was analyzed in greater detail by Giammichele et al. (2012), and 130 members ended up in their sample of local white dwarfs. Even if one assumes that the local sample is complete, the size of the sample is too small for detailed statistical analyses, and there is a need to extend the census and obtain a complete sample of white dwarfs from a larger volume. Such an effort was undertaken by Subasavage et al. (2009, and earlier references within) by measuring trigonometric parallaxes for new white dwarfs that are candidates of the 25 pc sample, as part of their DENSE project focused on objects in the southern hemisphere. Holberg et al. (2011) also announced that the complete sample of white dwarfs will be extended to 25 pc, thus doubling the volume of the local sample. Based on the space density of white dwarfs known within 10 pc of the Sun, Subasavage et al. (2009) estimated that the census of white dwarfs within 25 pc *and* with accurate trigonometric parallaxes is only ∼40% complete, and if we extend this horizon a little further — to 40 pc for instance — the census of white dwarfs remains largely incomplete.

Nearby white dwarfs have been traditionally discovered in catalogs of stars with high proper motions. Major contributions have been made, for instance, by Luyten (1979a,b), Giclas (1971), and Giclas et al. (1978), who identified a significant number of faint, blue, high proper motion stars, and their pioneer work is still useful to today's astronomers. Indeed, in the first study dedicated to building a complete census of the local sample of white dwarfs by Holberg et al. (2002), LHS, G, and GD objects form an important fraction of the 109 objects reported in that sample. Major contributions to the completeness of the local white dwarf sample also come from the work of Vennes & Kawka (2003), Kawka et al. (2004), and Kawka & Vennes (2006), who surveyed the revised NLTT catalog of Salim & Gould (2003), and in particular, identified eight new white dwarfs lying within 20 pc of the Sun. The contribution of Farihi et al. (2005) is also worth mentioning in this effort, as well as those of Subasavage et al. (2007, 2008, 2009), and Sayres et al. (2012), aimed at completing the 25 pc sample.

But in order to extend the volume of our complete sample of white dwarfs, the first step is to identify nearby stars with smaller proper motions, the coolest ($T_{\rm eff}$ ∼3500 K) of which are extremely faint due to the intrinsic small radius of white dwarfs. With the goal to improve the statistics of the local white dwarf population, we have been hunting for white dwarfs in the SUPERBLINK catalog. This catalog, which is based on a re-analysis of the Digitized Sky Surveys — with its 20-45 yr baseline — is at least 95% complete for the entire northern sky down to $V = 19.0$, with a very low rate of spurious detection. It thus constitutes an ideal database from which to search for faint, high proper motion objects such as nearby white dwarfs. Also, because of its low proper motion limit ($\mu > 0\farcs04$ yr^{-1}), the SUPERBLINK sample effectively eliminates the kinematic bias for stars in the immediate vicinity of the Sun, which is a known limitation of traditional catalogues such as the LHS catalog ($\mu > 0\farcs5$ yr^{-1}; Luyten 1979a) and the NLTT catalog ($\mu > 0\farcs18$ yr^{-1}; Luyten 1979b). Hence, the SUPERBLINK catalog also represents a powerful tool for the study of the solar neighborhood. Searching this database should provide a complete sample of white dwarfs to a much larger distance limit.

Also, the high completeness and deep magnitude limit of SUPERBLINK allows the detection of all white dwarfs down to the luminosity function turnoff, which occurs at $L/L_{\odot} \simeq 10^{-4}$ (Fontaine et al. 2001), up to a relatively large distance. For a 0.6 $M_{\odot}$ white dwarf with a pure hydrogen atmosphere, for instance, this corresponds to $T_{\rm eff} = 5000$ K, or M_V=15.23. The limiting magnitude of $V = 19$ implies that SUPERBLINK should be detecting all white dwarfs down to the luminosity function turnoff to a distance of 56.7 pc from the Sun. The main question is what fraction of these stars are expected to have proper motions above the SUPERBLINK limit of $\mu > 0\farcs04$ yr^{-1}. Assuming that the distribution of velocities for white dwarfs to be the same as that of main-sequence stars in the vicinity of the Sun, we can use Figure 1 of Lépine & Gaidos (2011), which shows the kinematic selection effects of SUPERBLINK by illustrating the fraction of stars in the *Hipparcos* catalog that would be selected with a proper motion cut of $\mu > 0\farcs04$ yr^{-1} up to a given distance. At 56.7 pc, more than 90% of the stars are detected. This minimal kinematic bias therefore allows one to detect most white dwarfs down to the luminosity function turnoff, and to perform a complete statistical

analysis on a sample ∼10 times larger than the current 20 pc census.

The interest in the local population of white dwarf stars is not only statistical, but also astrophysical. Indeed, probing the solar neighborhood allows the detection of faint, cool stars that would remain undetected at larger distances. Since the cool end of the white dwarf luminosity function is incomplete, obtaining a reliable estimate of the space density of white dwarf stars and comparing the luminosity function to models remains a challenge. The completion of the cool end of the white dwarf luminosity function would allow the accurate determination of the Galactic age and the verification of the white dwarf cooling theory. Furthermore, many cool white dwarfs are peculiar (Giammichele et al. 2012), and it is among them that we can expect to find transition objects that would allow us to establish the link between the different spectral types and to achieve a better understanding of the white dwarf spectral evolution. The catalog of Holberg et al. (2008) contains a large number of stars of particular astrophysical interest. For a detailed description of these stars, see Giammichele et al. (2012) and references therein. It is expected that surveys at 25 and 40 pc will unveil an even larger number of such key objects.

In this paper, we search the SUPERBLINK catalog to extend significantly the census of white dwarfs in the solar neighborhood. Lépine & Shara (2005) have shown how reduced proper motion diagrams constructed from the SUPERBLINK catalog can produce a large number of white dwarf candidates. We present here a more detailed search and identification of these white dwarfs through a large spectroscopic follow-up program. Our specific goal is to obtain spectral confirmation of all suspected white dwarfs within 40 pc of the Sun. Given the enormous amount of data and limited telescope access, we restrict ourselves to the northern part of the sky. The first step of this spectroscopic survey consists in the identification, observation, and classification of the white dwarf candidates. In Section 2.3, we present the catalog from which the candidates are obtained. We detail our selection method in Section 2.4, as well as distance estimates and candidate list in Section 2.5. Section 2.6 describes the results of our spectroscopic observation campaign, while a preliminary spectroscopic analysis, including the determination of atmospheric parameters, is provided in Section 2.7. Finally, a discussion follows in Section 2.8. A more thorough model atmosphere analysis of the atmospheric para-

meters of our complete survey of new white dwarfs within 40 pc will be reported in subsequent papers.

2.3 Proper Motion and Photometric Database

Our white dwarf candidates are identified from the SUPERBLINK catalog of stars with proper motions $\mu > 40$ mas yr^{-1}. This catalog, based on a re-analysis of the Digitized Sky Surveys (which include POSS-I and POSS-II plate scans), is estimated to be $> 95\%$ complete in the northern hemisphere down to a visual magnitude of $V = 19$, but extends to $V \sim 20$ in many areas of higher Galactic latitudes. The current version of the catalog comprises 2,283,540 objects, all designated by the letters "PM I" followed by 10 characters based on the right ascension (α) and declination (δ) of the object. The basic search algorithm is described in Lépine et al. (2002), while quality control procedures, including cross-correlation with other catalogs and the compilation of astrometric and photometric results, are discussed at length in Lépine & Shara (2005) and Lépine & Gaidos (2011). A complete list of 61,977 northern stars with $\mu > 150$ mas yr^{-1} has already been published in Lépine & Shara (2005). We provide below a brief summary of the astrometric and photometric entries given in the current SUPERBLINK catalog.

2.3.1 Astrometry

SUPERBLINK provides coordinates on the International Celestial Reference System for the 2000.0 epoch. For stars catalogued in *Hipparcos*, the positions are extrapolated to the 2000.0 epoch from the values given in van Leeuwen (2007), which are listed for the 1991.25 epoch. Likewise, those not in *Hipparcos* but listed in Tycho-2 have their positions extrapolated from the proper motions listed in Tycho-2, and if a star has a counterpart in 2MASS (Cutri et al. 2003), its position is extrapolated from the position of the 2MASS counterpart. Finally, coordinates for stars without a *Hipparcos* or 2MASS counterparts are calculated by SUPERBLINK from the position of the stars on the POSS-II scans. The coordinates of those stars are thus less accurate but are generally within a few arcseconds (see Lépine & Shara 2005 for details).

SUPERBLINK also lists proper motions for each entry, tabulated from three sources. When available, proper motions are taken from the *Hipparcos* catalog (van Leeuwen 2007) or from the *Tycho-2* catalog (Høg et al. 2000). Otherwise, the proper motions listed are those measured in the SUPERBLINK proper motion survey, based on the Digitized Sky Survey images. SUPERBLINK ends up providing proper motions for more than 2 million stellar objects, and in particular, a total of 1,567,461 stars with $\delta > 0$. From now on, when we mention the SUPERBLINK database, we refer to the northern part of the catalog.

2.3.2 Photometric Data

TABLE 2.1 – Available Photometric Data

Catalog	Version	Bands	Counterparts	Reference
2MASS	–	JHK_S	1,472,665	Skrutskie et al. (2006)
SDSS	DR6	$ugriz$	345,958	Adelman-McCarthy et al. (2008)
Hipparcos, *Tycho-2*	–	B_T, V_T	118,475	van Leeuwen (2007) Høg et al. (2000)
USNO-B1.0	–	B_J, R_F, I_N	1,567,461	Monet et al. (2003)
GALEX	GR6	FUV, NUV	147,096	Gil de Paz et al. (2009)

The construction of reduced proper motion diagrams requires, in addition to proper motion measurements, a set of photometric data in order to estimate the color of each star. Fortunately, the cross-correlation of SUPERBLINK with other catalogs not only allows coordinates and proper motions to be measured with more accuracy, but it also provides a useful set of photometric data covering a large portion of the electromagnetic spectrum. We describe these data in turn, and a summary is provided in Table 2.1.

The Two Micron All Sky Survey (2MASS) Point Source Catalog (Skrutskie et al. 2006) represents an excellent source of near-infrared magnitudes for our targets in SUPERBLINK since the 2MASS survey covers the whole sky and is complete down to $J \sim$16.5. Lépine & Shara (2005, see their Figure 30) successfully showed that white dwarfs in SUPERBLINK could easily be separated from other stellar populations in a H_V vs. $V - J$ reduced proper motion diagram. For the present study, we used a version of the SUPERBLINK catalog in

which 2MASS counterparts had already been found and assigned to 1,472,665 of the stars ($\sim 94\%$), with the remainder having no detectable counterpart in 2MASS. These infrared J, H, and K_S magnitudes have a 0.02-0.03 mag accuracy down to 13th magnitude, and point sources are detected with S/N better than 10 for stars brighter than $J = 15.9$, $H = 15.0$, and $K_S = 14.3$ (Skrutskie et al. 2006).

The Sloan Digital Sky Survey (SDSS) also represents a useful source of photometric data, with *ugriz* photometry from the Data Release 6 (Adelman-McCarthy et al. 2008) for 345,958 counterparts in the SUPERBLINK catalog. The SDSS magnitudes have photometric uncertainties of roughly 1% in the *griz* bands and 2% in u (Padmanabhan et al. 2008). This is by far the most accurate optical photometry available in our study, and will be especially useful to identify white dwarfs in the SUPERBLINK catalog.

Optical photometry in the blue (B_T) and in the visual (V_T) range are also extracted for 118,475 stars with counterparts in the *Hipparcos* and *Tycho-2* catalogs. Additional optical photometry was also obtained from the USNO-B1.0 database (Monet et al. 2003), providing photographic magnitudes for the totality of the catalog, i.e. 1,567,461 objects. However, for some entries, the photometry is available only for one or two bands. More specifically, B_J magnitudes are available for 1,390,471 objects, R_F magnitudes for 1,405,840, and I_N magnitudes for 912,550 objects. The blue B_J magnitudes are extracted mostly from scans of IIIaJ plates from the Palomar Sky Surveys (POSS-I, POSS-II) and the Southern ESO Schmidt (SERC) Survey, the red R_F magnitudes are extracted from scans of IIIaF plates from POSS-I and POSS-II and also from the Anglo-Australian Observatory red survey (AAO-red), while the near-infrared I_N magnitudes are extracted from the IVn plates from POSS-II and SERC. The B_T and V_T magnitudes are more accurate (0.1 mag or better) than the photographic magnitudes (typically 0.5 mag), but they are available only for the brightest stars in SUPERBLINK, while photographic magnitudes are available for every object.

Finally, we also searched the sixth data release (GR6) of the *GALEX* database (Gil de Paz et al. 2009) and identified 147,096 counterparts to the SUPERBLINK objects (for a $5\farcs0$ search radius). The corresponding far-ultraviolet (FUV, 1350-1780 Å) and near-ultraviolet (NUV, 1770-2730 Å) magnitudes are particularly useful for the identification of blue objects,

and in particular white dwarf stars.

2.4 Selection of the Candidates Based on Reduced Proper Motion Diagrams

Reduced proper motion diagrams (RPMD) are a particularly efficient tool to identify white dwarf candidates with known proper motions (see, for instance, Knox et al. 1999, Oppenheimer et al. 2001, Vennes & Kawka 2003, Carollo et al. 2006, Kilic et al. 2006). The reduced proper motion of an object is defined as $H_m = m+5\log\mu+5$, where m is the apparent magnitude in some bandpass and μ is the proper motion measured in arcseconds per year. The reduced proper motion is analogous to the absolute magnitude $M_m = m + 5\log\pi + 5$, where the trigonometric parallax π is replaced with the proper motion μ of the object. A reduced proper motion diagram is thus similar to a color-magnitude diagram, and white dwarfs occupy a similar location in the diagram, i.e. the bottom-left region. Furthermore, using the tangential velocity $v_{\rm tan} = 4.74\,\mu\pi^{-1}$ in units of km s^{-1} instead of the proper motion, we obtain $H_m = M_m + 5\log v_{\rm tan} - 3.38$, and each star population can be isolated based on the mean value of its tangential velocity.

One major problem with the identification of white dwarf candidates using reduced proper motion diagrams is the contamination of the white dwarf region by other stellar populations, and by high-velocity subdwarfs in particular. Vennes & Kawka (2003) showed, however, that this contamination can be substantially reduced by the inclusion of a criterion based on $V-J$. Similarly, Kilic et al. (2006) demonstrated that reduced proper motion diagrams are efficient for detecting cool white dwarfs only when the measured proper motions of all stellar populations are reliable, since subdwarfs with inaccurate proper motions can contaminate the other stellar populations, and notably the white dwarf region of the diagram. SUPERBLINK has an estimated false detection level of less than 1% down to $V = 19$, but the false detection rate increases significantly for fainter sources. In our selection criteria, we thus restrict our search to that stars with $V < 19$. Fortunately, SUPERBLINK has a very high level of completeness for $V < 19$, exceeding 98% for most of the sky. We are thus confident that we can easily iden-

tify a significant fraction of the nearby white dwarfs using this technique. The next sections describe the four reduced proper motion diagrams we used to identify white dwarf candidates in SUPERBLINK, in an effort to take advantage of the whole set of photometric information available. The order in which these are presented follows the order of their estimated efficiency at isolating the white dwarf population, starting with the most efficient one.

2.4.1 RPMD Using *ugriz* Photometry

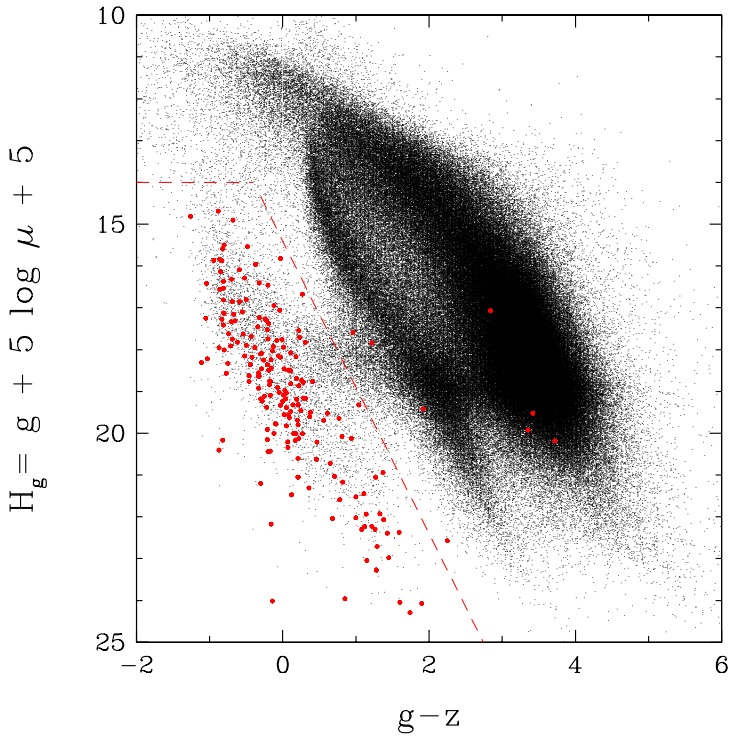

FIGURE 2.1 – Reduced proper motions diagram $(H_g, g-z)$ for the 345,958 stars in the SUPERBLINK catalog ($\mu > 40$ mas yr^{-1}) with counterparts in the SDSS 6th Data Release. The red dashed lines show the limits used to define the location of the white dwarfs. These limits include 4929 white dwarf candidates, i.e. 1.4% of the sample of SUPERBLINK stars with SDSS photometry. The spectroscopically confirmed white dwarfs from the WD Catalog are shown as large red dots.

We present in Figure 2.1 the H_g vs. $g-z$ reduced proper motion diagram constructed from the 345,958 SUPERBLINK objects in the northern hemisphere with *ugriz* photometry

available from the 6th Data Release of the Sloan Digital Sky Survey. As a result of the relatively high accuracy of the SDSS magnitudes, the white dwarf population is particularly well separated from the other populations in this diagram.

To verify the accuracy of our procedure, we also display as red dots in Figure 2.1 the sample of white dwarfs taken from the 2008 May electronic version of the Catalogue of Spectroscopically Identified White Dwarfs [4] (McCook & Sion 1999, hereafter WD Catalog) with $\delta > 0$ also found in SUPERBLINK and with g and z photometry available. We first note that 191 spectroscopically confirmed white dwarfs lie in the expected region near the bottom left of the diagram, and that a small number of white dwarfs are color outliers. More precisely, 3 white dwarfs overlap the subdwarf region, and 4 are found in the redder, main sequence portion of the diagram. Two of these are actually binary systems: 0855+604.1 is a DBQ (Greenstein 1969) and 0855+604.2 is a DCE? (Eggen & Greenstein 1965), while 1133+358 is an unresolved DC+dM (Greenstein 1976).

Fortunately, there are enough spectroscopically identified white dwarfs that are well separated from the other populations to allow us to define selection criteria for the white dwarf area. These criteria are defined by the need to include as many white dwarf candidates as possible, while trying to keep the contamination from subdwarfs to a minimum. As a general criterion, the area occupied by the white dwarfs must include *at least* 80% of the spectroscopically confirmed white dwarfs. In the present case, this limit between the halo subdwarfs and the white dwarf area is defined by the following linear equation $H_g = 3.5(g - z) + 16.5$. The slope and y-intercept are chosen in a very conservative manner, and include 96% of the WD Catalog sample with measured *ugriz* photometry. The reason why we recover almost all white dwarfs from the WD Catalog is that the known white dwarf population is well separated in this reduced proper motion diagram, and only a few objects are color outliers. However, in the upper part of the diagram ($H_g \lesssim 14$) there is again some confusion between the different stellar populations defined by our linear equation, so we simply apply an additional cutoff at $H_g = 14$ based on the known white dwarf population, in order to keep the contamination to a minimum. These adopted selection criteria for the H_g vs. $g - z$ diagram are displayed

4. http://www.astronomy.villanova.edu/WDCatalog/index.html

in Figure 2.1. Out of the 345,958 SUPERBLINK stars with a counterpart in the 6th Data Release of the SDSS, 4929 fall within the white dwarf selection limits. This number represents 1.4% of the stars in the catalog with SDSS photometry, or 0.5% of the total number of objects in SUPERBLINK.

2.4.2 RPMD Using *GALEX* Photometry

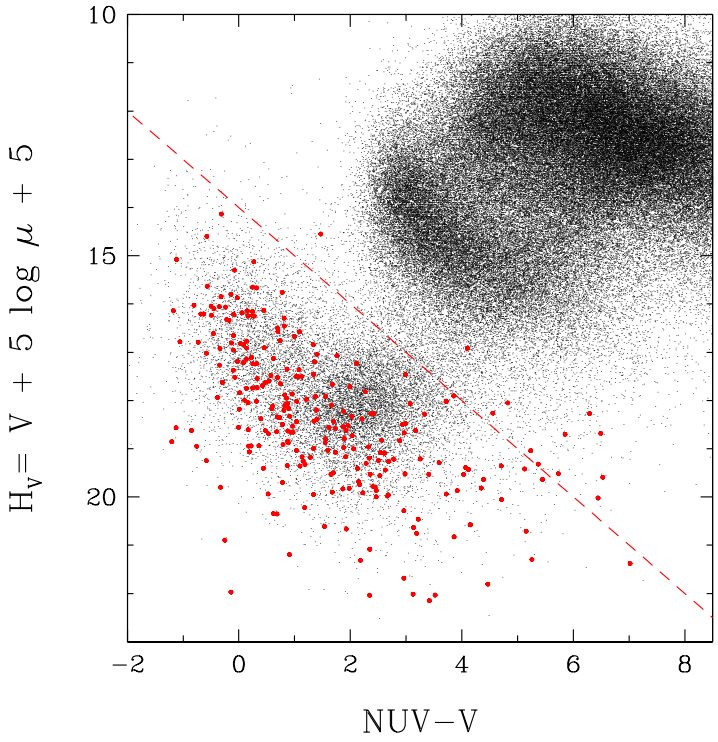

FIGURE 2.2 – Reduced proper motions diagram (H_V, NUV $- V$) for the 147,096 stars in the SUPERBLINK catalog ($\mu > 40$ mas yr^{-1}) with counterparts in the 6th Data Release of the *GALEX* survey. The red dashed line shows the limits used to define the location of the white dwarfs. This limit includes 19,150 white dwarf candidates, i.e. 12.7% of the sample of SUPERBLINK stars with *GALEX* photometry. The spectroscopically confirmed white dwarfs from the WD Catalog are shown as large red dots.

White dwarf stars are generally hotter than main sequence or subdwarf stars, and since their atmospheres are usually devoid of heavy elements that could absorb the UV flux, they are moderately strong UV emitters and can easily be distinguished from non-degenerate stars in a

reduced proper motion diagram built from *GALEX* photometry. We present in Figure 2.2 the H_V vs. NUV $- V$ diagram containing 147,096 stars in SUPERBLINK with NUV magnitudes measured by *GALEX*. NUV magnitudes are used in this diagram since they are available for a much larger number of stars than the FUV magnitudes. No corrections are applied for interstellar reddening, since according to the characterization of the Local Bubble of Reis et al. (2011), the smallest distance to the wall of dust that causes extinction ($E(b-y) \geq 0.040$) is $\sim$80 pc. The reddening should thus not affect the white dwarf candidates of the local sample.

Here and in the following diagrams, the V magnitudes are estimated from the relation

$$V = B_J - 0.46(B_J - R_F) \tag{2.1}$$

as recommended by Lépine & Shara (2005), where B_J and R_F are photographic magnitudes taken from the USNO-B1.0 catalog. These estimated V magnitudes are believed to be accurate to $\pm$0.5 mag (Lépine & Shara 2005). As mentioned earlier, while V_T magnitudes from the *Tycho-2* catalog are more accurate than photographic magnitudes, they are only available for a small number of SUPERBLINK objects, whereas B_J and R_F exist for the majority of our targets. Hence, despite the relatively large uncertainties of the V magnitudes employed here, they have the advantage of being available for most of the entries in SUPERBLINK.

As in Figure 2.1, the spectroscopically confirmed white dwarfs from the WD Catalog are also shown in red. Here, a total of 13 spectroscopically confirmed white dwarfs are scattered in areas normally occupied by other stellar populations. Most of these objects are cool degenerates, including 9 DA, 2 DC, 1 DZ (1705+030, Greenstein 1984) and 1 DQ star (1105+412, Koester & Knist 2006). Most likely, these have very little UV flux and thus inaccurate NUV magnitudes.

We define the slope and y-intercept of the line that characterizes the white dwarf region with the same criteria as before. Also, since the halo subdwarfs and main sequence stars are generally not as bright in the UV as white dwarfs are, there is no need to apply any further cutoff in H_V. Therefore, to be considered a white dwarf candidate, a star must have a reduced proper motion larger than $H_V = (\text{NUV} - V) + 14$. With this limit, 94% of the white dwarfs from the WD Catalog with measured NUV photometry are recovered. Finally, if this criterion

is applied to the 147,096 SUPERBLINK objects with both NUV and V magnitudes, we obtain a sample of 19,150 white dwarf candidates, which represent 12.7% of the stars with *GALEX* photometry in SUPERBLINK, or 2.0% of the complete catalog.

2.4.3 RPMD Using 2MASS Photometry

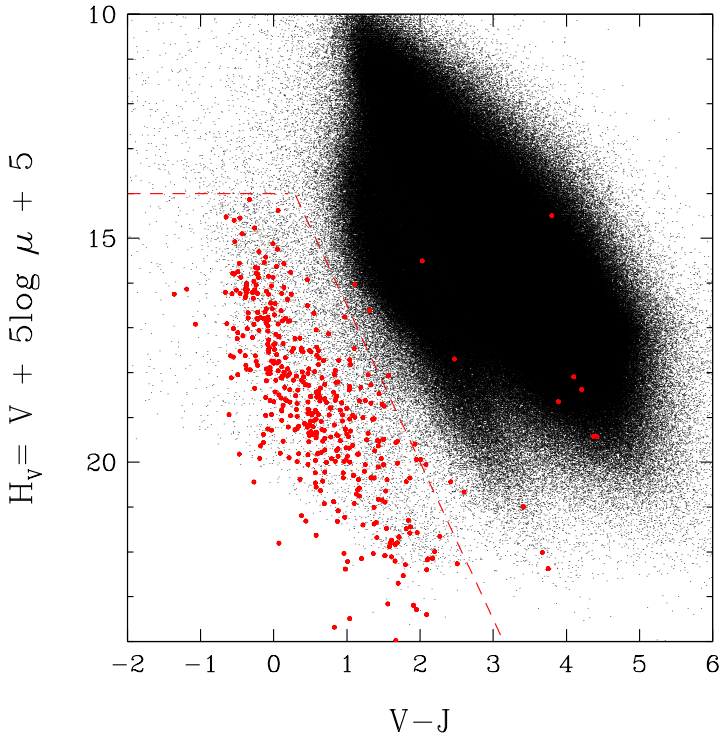

FIGURE 2.3 – Reduced proper motions diagram ($H_V, V-J$) for the 1,265,733 stars in the SUPERBLINK catalog ($\mu > 40$ mas yr^{-1}) with counterparts in the 2MASS catalog and for which an estimation of the V magnitude was possible. The red dashed lines show the limits used to define the location of the white dwarfs. These limits include 16,977 white dwarf candidates, i.e. 1.3% of the initial sample. The spectroscopically confirmed white dwarfs from the WD Catalog are shown as large red dots.

As discussed above, the reduced proper motion diagram in H_V vs. $V-J$, displayed in Figure 30 of Lépine & Shara (2005), showed that nearly 2000 white dwarfs could be identified in the SUPERBLINK catalog of stars with proper motions $\mu > 150$ mas yr^{-1}. Since the SUPERBLINK catalog now includes stars with $\mu > 40$ mas yr^{-1}, and because a significant

fraction of its entries has a counterpart in the 2MASS catalog, such a diagram has an even greater potential for identifying white dwarf stars. The resulting H_V vs. $V - J$ diagram is shown in Figure 2.3, and contains 1,265,733 stars from SUPERBLINK with J magnitudes taken from 2MASS as well as B_J and R_F magnitudes from the USNO-B1.0 catalog. Here again, the V magnitudes are obtained from the empirical calibration given by Equation (2.1).

The comparison with the spectroscopically confirmed white dwarfs from the WD Catalog reveals 20 objects that fall in a region to the right of that occupied by the bulk of white dwarfs. Among them, there are 9 DA, 4 DC, 1 DQ, and 1 DZ star. This diagram also includes the largest number of multiple-star systems identified so far. Indeed, we find four WD+dM systems, a DB+DC binary (2058+342, Farihi 2004), and 0023+388, the triple star system discussed earlier.

Applying similar criteria as before, the white dwarf candidates are selected from Figure 2.3 if their reduced proper motion is larger than $H_V = 3.5(V - J) + 13$, with a cutoff of $H_V > 14$. These limits, displayed in Figure 2.3, recover 86% of the white dwarfs from the WD Catalog listed in SUPERBLINK and for which 2MASS and photographic magnitudes are available. This defines a sample of 16,977 white dwarf candidates out of the 1,265,733 objects in the initial SUPERBLINK sample with 2MASS photometry, or a fraction of 1.3% (0.23% of the total initial sample).

2.4.4 RPMD Using Photographic Magnitudes

Even if USNO-B1.0 photographic magnitudes are less accurate than CCD photometry obtained in recent large surveys such as SDSS, they have the advantage of covering the whole sky, and are thus available for all 1.6 million SUPERBLINK objects. We present in Figure 2.4 the reduced proper motion diagram in H_V vs. $V - I_N$ constructed with V as defined by Equation (2.1). To be included in this diagram, photographic B_J, R_F, and I_N magnitudes must all be available for each object. However, as discussed by Lépine & Shara (2005), not all USNO-B1.0 entries have magnitude information in all three bands. Whenever possible, Lépine & Shara tried to combine data if a USNO-B1.0 star appeared as more than one entry, but some sources remained without information for one or more bands. As a result, Figure 2.4 includes

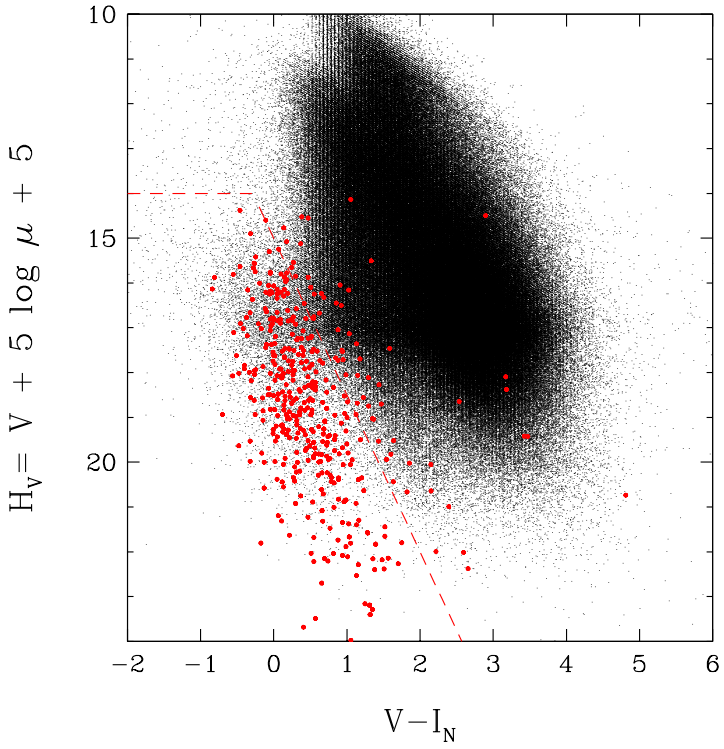

FIGURE 2.4 – Reduced proper motions diagram $(H_V, V - I_N)$ for the 878,847 stars in the SUPERBLINK catalog ($\mu > 40$ mas yr^{-1}) with counterparts in the USNO-B1.0 catalog for all three B_J, R_F and I_N photographic magnitudes. The red dashed lines show the limits used to define the location of the white dwarfs. These limits include 20,862 white dwarf candidates, i.e. 2.4% of the initial sample. The spectroscopically confirmed white dwarfs from the WD Catalog are shown as large red dots.

878, 847 stars out of the 1, 567, 461 entries in SUPERBLINK with at least one photographic magnitude in USNO-B1.0.

In Figure 2.4, the separation between the white dwarf and subdwarf populations is not as well defined as in the other reduced proper motion diagrams. The V and I_N filters are indeed too close in wavelength to allow an efficient separation of the two populations, as was the case with $V - J$ or $g - z$, for instance. We also have to consider the fact that there is an uncertainty of ± 0.5 mag in both V and I_N, which adds to the dispersion in $V - I_N$. The comparison of the white dwarfs in the WD Catalog displayed in Figure 2.4 with those in Figure 2.3 using $V - J$ reveals that most of the 55 outliers in $V - I_N$ are also outliers in $V - J$, the difference

between the two diagrams being that there is a larger concentration of outliers in $V - I_N$ near the white dwarf locus. Once again, the measurement uncertainty in $V - I_N$ is to blame. All of the interesting outliers have been discussed in the preceding sections and will not be repeated here.

Despite this large contamination, we must still define some selection criteria, and as before, the slope and y-intercept of the limit between white dwarfs and halo subdwarfs is chosen to include 80% of the white dwarfs from the WD Catalog; a lower limit in H_V is also defined. Using these criteria, the white dwarf candidates are selected from Figure 2.4 if their reduced proper motion is larger than $H_V = 3.5(V - I_N) + 13$, with a cutoff of $H_V > 14$. This time, since the contamination is much larger than in previous reduced proper motion diagrams, a more conservative cut must be used, and no more than 80% of the white dwarfs from the WD Catalog are recovered. We finally end up with 20,862 white dwarf candidates out of the $878,847$ SUPERBLINK objects in the original sample with USNO photometry, or a fraction of 2.2% of the total catalog.

Combining the results from all four reduced proper motion diagrams, we obtain a total of 20,862 white dwarf candidates, since all of them have USNO photographic magnitudes, but only a fraction of them have data available in other photometric systems. Some of these candidates, however, can be found in up to four reduced proper motion diagrams. At this point, each candidate can be assigned an order of priority depending on the quality of the photometry used for its identification.

2.4.5 A Priority Approach

For each given star, data can be available for up to four photometric systems and their corresponding reduced proper motion diagrams. Thus, it is possible that a star could be within the white dwarf region defined by our selection criteria in one diagram and outside in another diagram. We must therefore decide which photometric system should be prioritized to decide whether or not a star should be included in our final list of $\sim 21,000$ white dwarf candidates. For instance, *ugriz* magnitudes should take precedence over photographic magnitudes, since the former are much more accurate. In the following, we establish the order of priority for our

four photometric systems, based on their degree of photometric accuracy.

SDSS magnitudes have a relatively high degree of accuracy and cover a wavelength range that allows an efficient separation of the white dwarfs from the other stellar populations, as discussed above. The reduced proper motion diagram based on *ugriz* magnitudes is arguably the most accurate, and it is therefore given the highest priority. However, a comparison of our preliminary list of white dwarf candidates based on *ugriz* data with those found in the literature shows a significant contamination from subdwarfs. Kawka et al. (2004) successfully reduce this contamination by including a color-color criterion to their reduced proper motion cut, namely $(V-J) < 3.28(J-H)-0.75$. But such limits also get rid of the white dwarfs with red, main-sequence companions, which we would like to include. Also, as observed by Kilic et al. (2006) and Sayres et al. (2012), any uncertainty in the proper motion measurements can lead to contamination. Also, spurious proper motions are possible for stars near the faint magnitude limit of the SUPERBLINK. With all these considerations in mind, we apply on top of the criteria in $(H_g, g-z)$, a criterion inspired by Kawka et al. (2004), but based on Figure 2.3. It is defined as follows: stars with $V < 14$ must also have $H_V = 3.5(V-J)+13$. This limit on V removes the largest number of known main sequence stars from our list of candidates, while keeping all the known white dwarfs. Applying the criterion in $(H_V, V-J)$ to fainter candidates results in the elimination of spectroscopically confirmed white dwarfs, so it is not applied to those fainter stars. Finally, using the criteria defined in Section 2.4.1, combined with those defined in Section 2.4.3 when $V < 14$, we retain a total of 4823 white dwarf candidates. Unfortunately, the SDSS survey, at the epoch of the DR6, only covered about a quarter of the northern sky. Bright stars also tend to be saturated in SDSS, and we need to limit our selection to stars with $u > 13$, $g > 14$, $r > 14$, $i > 14$, and $z > 12$ (York et al. 2000). Consequently, there is no SDSS counterpart for every star in the SUPERBLINK catalog, and we must therefore rely on other photometric systems to select our targets.

In the absence of SDSS photometric data, *GALEX* UV photometry is used instead for the selection, whenever it is available. It is our second choice because of the corresponding photometric accuracy as well as the efficiency of the criteria in NUV $-$ V to separate white dwarfs from other stellar populations. Here, we also apply the $(H_V, V-J)$ criterion for stars

with $V < 14.0$ in an effort to decontaminate our sample of candidates. The criteria and the method described in Section 2.4.2 led to the identification of 8092 additional white dwarf candidates. The *GALEX* survey covers 80% of the sky, with special care taken to avoid the Galactic plane and Magellanic clouds, which could provide excess background flux in the UV [5].

In the absence of SDSS and *GALEX* data, 2MASS photometry combined with the criteria defined in Section 2.4.3 are used to identify 1132 additional white dwarf candidates with $\delta > 0$ and $V > 14.0$. The 2MASS survey is a precious source of photometric information since it covers practically the whole sky. However, since it is only complete down to $J \sim$16.5, our fainter targets do not have a 2MASS counterpart. Finally, if there is no SDSS, *GALEX*, or 2MASS photometry available for a given target, we must rely on photographic magnitudes obtained from the USNO-B1.0 catalog. With the criteria defined in Section 3.4 and the $(H_V, V - J)$ criterion for stars with $V < 14.0$, we identify an additional list of 6688 white dwarf candidates.

All in all, a total of 20,735 white dwarf candidates are identified with the help of the four reduced proper motion diagrams described in this section. This large number of candidates amply justifies our decision to restrict our search to the northern hemisphere. Moreover, given our interest in establishing a census of white dwarfs in the solar neighborhood within 40 pc of the Sun, we must further restrain our list of candidates by evaluating photometric distances for each object on our target list.

2.5 A Sample of White Dwarf Candidates within 40 pc of the Sun

2.5.1 Distances from Color-Magnitude Relations

In the absence of trigonometric parallax measurements for most white dwarf candidates in our sample, we must rely on distances estimated using the only information available, which are the apparent magnitudes of each star in a set of bandpasses covering the ultraviolet to the near-infrared. In this section, we estimate *photometric distances* from the distance modulus, $m - M_m = 5 \log D - 5$, where the absolute magnitude M_m is determined from theoretical

5. http://galex.stsci.edu/GR6/

color-magnitude relations combined with a measured color index in some specified photometric system. To do so, we rely on synthetic colors obtained using the procedure outlined in Holberg & Bergeron (2006) based on the improved Vega fluxes taken from Bohlin & Gilliland (2004). These color-magnitude relations are available on our Web site [6], or upon request on any photometric system. They cover a range of effective temperature between $T_{\rm eff} = 1500$ K and 110,000 K and surface gravities between $\log g = 6.5$ and 9.5 for hydrogen-rich atmospheres, and between $T_{\rm eff} = 3500$ K and 40,000 K and $\log g = 7.0$ and 9.0 for helium-rich atmospheres. Note that we now include in our hydrogen models the opacity from the red wing of Lyα calculated by Kowalski & Saumon (2006) and kindly provided to us by P. Kowalski, which is known to affect the flux in the ultraviolet region of the energy distribution. The calculations of absolute magnitudes also require the use of mass-radius relations for white dwarfs, which are based on evolutionary models similar to those described in Fontaine et al. (2001) but with C/O cores, $q({\rm He}) \equiv \log M_{\rm He}/M_\star = 10^{-2}$ and $q({\rm H}) = 10^{-4}$, which are representative of hydrogen-atmosphere white dwarfs, and $q({\rm He}) = 10^{-2}$ and $q({\rm H}) = 10^{-10}$, which are representative of a helium-atmosphere. From these color-magnitude relations at constant $\log g$ values, we can obtain the corresponding relations at constant *mass* values using the same evolutionary models as described above.

We present below our results on the SDSS, *GALEX*, and 2MASS photometric systems, as well as on the USNO-B1.0 photographic system. Synthetic colors were calculated from the bandpasses available from the SDSS website [7] and discussed in Fukugita et al. (1996), while the 2MASS filters are described in Cohen et al. (2003) and the transmission functions were taken from the survey website [8]. Similarly, *GALEX* synthetic colors were calculated from the bandpasses available from the *GALEX* website [9] and described in Morrissey & GALEX Science Team (2004), and information about the filters for the USNO-B1.0 are given in Monet et al. (2003), and transmission curves are available from the Digitized Sky Survey website [10].

6. See http://www.astro.umontreal.ca/~bergeron/CoolingModels
7. http://www.sdss.org/dr6/instruments/imager/#filters
8. http://www.ipac.caltech.edu/2mass/releases/allsky/doc/sec6_4a.html
9. http://galexgi.gsfc.nasa.gov/docs/galex/Documents/PostLaunchResponseCurveData.html
10. http://www3.cadc-ccda.hia-iha.nrc-cnrc.gc.ca/dss/

2.5.1.1 M_g vs. $g-z$ Calibration

We show in Figure 2.5 the theoretical M_g vs. $g-z$ color-magnitude relation for hydrogen-atmosphere white dwarfs at 0.6 $M_\odot$ together with similar sequences at 0.4 $M_\odot$ and 0.8 $M_\odot$, which are representative of the intrinsic mass distribution for DA stars (see, e.g., Gianninas et al. 2011). These are used below to evaluate the accuracy of our color-magnitude calibration. Also shown in Figure 2.5 is a single 0.6 $M_\odot$ helium-atmosphere sequence used to evaluate the influence of the unknown atmospheric composition on the color-magnitude relations. As can be seen, the 0.6 $M_\odot$ helium sequence follows closely the corresponding hydrogen sequence in this particular diagram, and it is thus perfectly justified to rely on the hydrogen-rich sequence only to evaluate the photometric distances to our objects.

As an external verification of our color-magnitude relations, we also plot in Figure 2.5 the 50 spectroscopically confirmed white dwarfs from the WD Catalog that also have trigonometric parallax measurements published in the Yale Parallax Catalog (van Altena et al. 1995) and with SDSS photometry available; we consider here only stars with parallax uncertainties less than 30%. We also distinguish DA and non-DA stars. The absolute magnitudes M_g are directly obtained from the distance modulus $M_g = g + 5\log\pi + 5$. Our results show that the observed scatter with respect to the 0.6 $M_\odot$ theoretical sequence is entirely consistent with that expected from the intrinsic white dwarf mass distribution, as indicated by the theoretical sequences at 0.4 and 0.8 $M_\odot$. This can be tested more quantitatively by measuring the mass of each star directly from the color-magnitude diagram using our theoretical sequences and a simple interpolation scheme. We obtain a mean mass of $\langle M\rangle = 0.63$ $M_\odot$, with a dispersion of $\sigma(M) = 0.20$ $M_\odot$, entirely consistent with the photometric mass distribution obtained by Bergeron et al. (2001, see their section 5.3) for the sample of cool white dwarfs with trigonometric parallaxes from the Yale Parallax Catalog, $\langle M\rangle = 0.65$ $M_\odot$, $\sigma(M) = 0.20$ $M_\odot$. As also discussed by Bergeron et al., however, the dispersion expected from spectroscopic mass distributions are considerably smaller, typically $\sigma(M)$ $\sim$0.15 $M_\odot$ (see, e.g., Gianninas et al. 2011) due to the increased sensitivity to $\log g$ of the spectroscopic technique over the photometric method based on trigonometric parallax measurements. We thus conclude from this comparison that our M_g vs. $g-z$ color-magnitude relation is well calibrated.

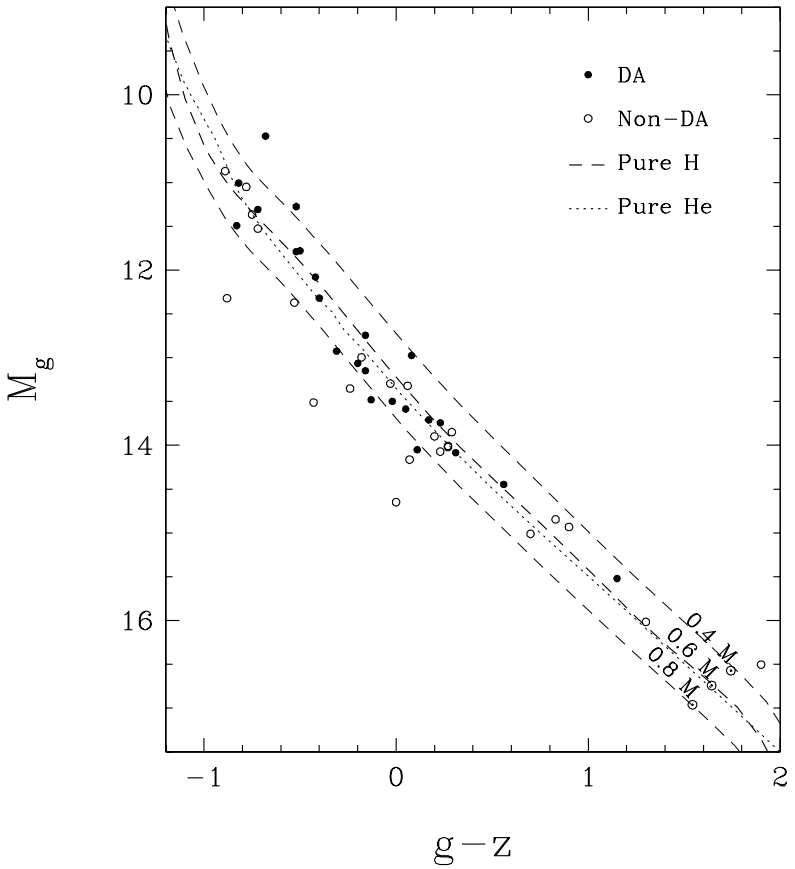

FIGURE 2.5 – Theoretical color-magnitude relations for pure hydrogen-atmosphere white dwarfs at 0.4, 0.6, and 0.8 $M_{\odot}$ (dashed lines) and for pure helium-atmosphere white dwarfs at 0.6 $M_{\odot}$ (dotted line). The pure hydrogen sequence at 0.6 $M_{\odot}$ is used to determine absolute M_g magnitudes for stars with SDSS photometry. Also shown are the 50 white dwarfs from the WD Catalog with available *ugriz* photometry and trigonometric parallaxes from the Yale Parallax Catalog.

Finally, we use the M_g vs. $g-z$ theoretical relation for all white dwarf candidates in our sample with observed *ugriz* photometry to estimate a photometric distance for each object assuming a hydrogen-atmosphere and a mass of 0.6 $M_{\odot}$, the average mass for white dwarfs. The photometric distances for 4823 white dwarf candidates in our sample, identified from the $(H_g, g-z)$ reduced proper motion diagram, are estimated in this manner.

2.5.1.2 M_V vs. NUV $- V$ Calibration

In an approach similar to that described in the previous section, we use the theoretical relation between the absolute magnitude M_V and the color index NUV $- V$ to determine an

absolute magnitude for every object with observed *GALEX* photometry, assuming a hydrogen atmosphere at 0.6 $M_{\odot}$. We show in Figure 2.6 the theoretical M_V vs. NUV$-V$ color-magnitude relations for the same mass values and atmospheric compositions as above. In contrast with the results from the previous section, the helium sequence starts to differ from the hydrogen sequence at 0.6 $M_{\odot}$ for NUV $- V > 2$, or $T_{\rm eff} < 8000$ K, and becomes significantly different for NUV $- V > 4$, or $T_{\rm eff} < 6000$ K. However, since we do not expect to identify many white dwarfs cooler than ∼6000 K on the basis of their UV magnitudes, it is justified to rely solely on the pure hydrogen sequence.

Figure 2.6 also shows the 82 white dwarfs from the WD Catalog observed by *GALEX*,

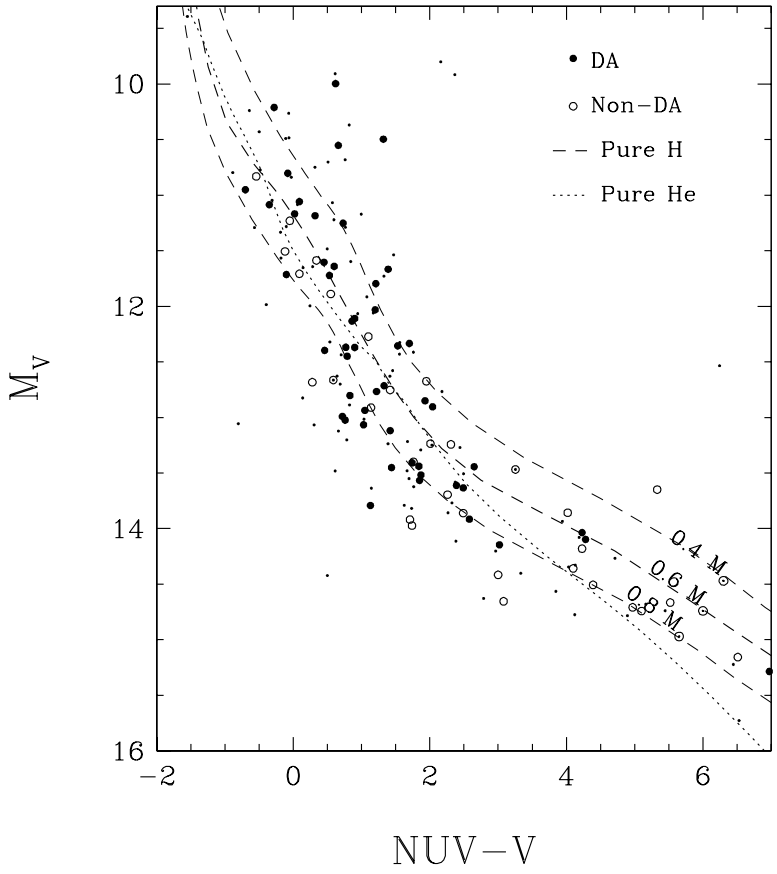

FIGURE 2.6 – Same as Figure 2.5 but for the determination of absolute M_V magnitudes for stars with *GALEX* photometry. Also shown are the 82 white dwarfs from the WD Catalog with available *GALEX* photometry and trigonometric parallaxes from the Yale Parallax Catalog. The small dots correspond to USNO photographic magnitudes while the larger symbols make use of Johnson V magnitudes.

with trigonometric parallax measurements available in the Yale Parallax Catalog. Since we are mostly interested here in verifying the validity of our color-magnitude relations, we want to use the best photometry available for each star in order to reduce the scatter related to the uncertainty of photographic magnitudes. Hence, in addition to V magnitudes estimated from USNO photographic magnitudes (small dots in Figure 2.6), we also show the results obtained using apparent V magnitudes measured on the Johnson photometric system, and taken from the literature (larger symbols in Figure 2.6). This comparison is thus analogous to that shown in Figure 2.5, and we see once again that the bulk of white dwarfs is well contained between the 0.4 $M_{\odot}$ and 0.8 $M_{\odot}$ theoretical sequences. Performing the same calculations as before, we find a mean mass of $\langle M \rangle = 0.67\ M_{\odot}$ and a dispersion of $\sigma(M) = 0.22\ M_{\odot}$, still consistent with the values obtained by Bergeron et al. (2001).

We finally apply this calibration to all white dwarf candidates identified from the (H_V, NUV−V) reduced proper motion diagram, and estimate photometric distances for 8092 stars with *GALEX* photometry (but with no SDSS counterparts).

2.5.1.3 M_V vs. $V - J$ Calibration

The theoretical relations between the absolute M_V magnitude and color index $V - J$ are shown in Figure 2.7. Also displayed are the 167 white dwarfs from the WD Catalog for which a trigonometric parallax measurement in the Yale Parallax Catalog and a $V - J$ color index are available (both Johnson V and USNO photographic magnitudes are displayed, as explained in the previous section).

We note again in this figure that most of the points are contained between the 0.4 $M_{\odot}$ and 0.8 $M_{\odot}$ theoretical sequences, with $\langle M \rangle = 0.67\ M_{\odot}$ and $\sigma(M) = 0.21\ M_{\odot}$, and that the hydrogen- and helium-atmosphere sequences agree sufficiently enough to assume a hydrogen-rich composition for all objects in our sample. We obtain the absolute magnitudes and photometric distances for all 1132 white dwarf candidates having counterparts in the 2MASS catalog (but with no SDSS or *GALEX* counterparts), assuming a hydrogen-atmosphere and a mass of 0.6 $M_{\odot}$.

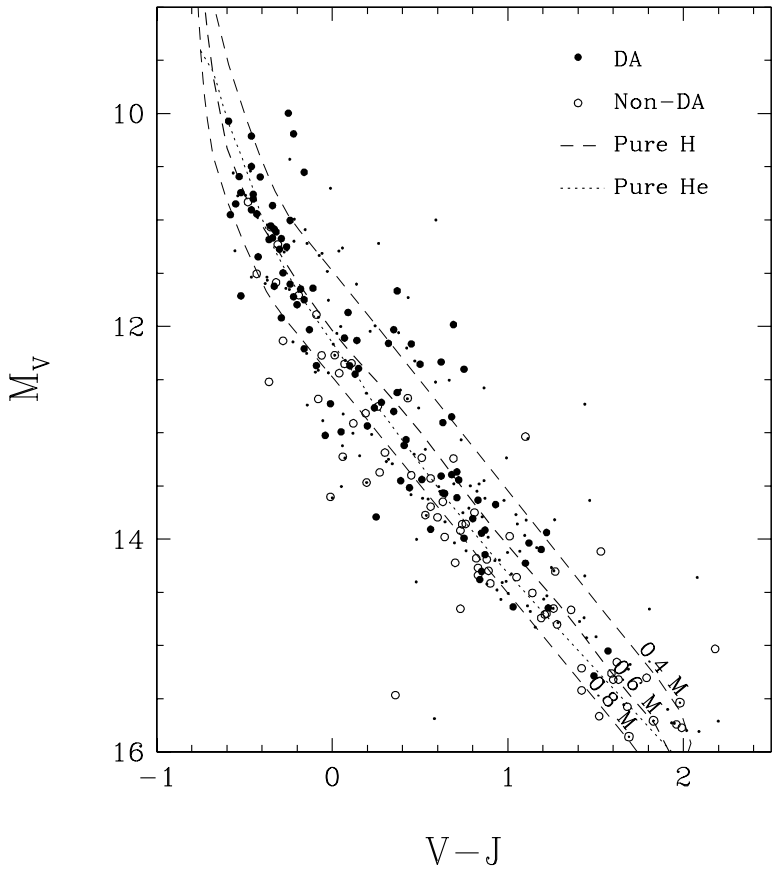

FIGURE 2.7 – Same as Figure 2.5 but for the determination of absolute M_V magnitudes for stars with 2MASS photometry. Also shown are the 167 white dwarfs from the WD Catalog with available 2MASS photometry and trigonometric parallaxes from the Yale Parallax Catalog. The small dots correspond to USNO photographic magnitudes while the larger symbols make use of Johnson V magnitudes.

2.5.1.4 M_V vs. $V - I_N$ Calibration

Figure 2.8 displays our last color-magnitude relation, that between M_V and the photographic color index $V - I_N$. Also shown are the 151 white dwarfs from the WD Catalog with trigonometric parallax measurements in the Yale Parallax Catalog and $V - I_N$ color indices available. Again, both Johnson V and USNO photographic magnitudes are used in this plot. Not unexpectedly, the comparison between the observed M_V values and the theoretical sequences reveals a much larger scatter, larger than that expected from the intrinsic mass distribution alone. Indeed, we measure a mean mass of $\langle M \rangle = 0.58\ M_\odot$, which is 0.07 $M_\odot$ lower than the value of Bergeron et al. (2001) for a similar sample, but more importantly, we

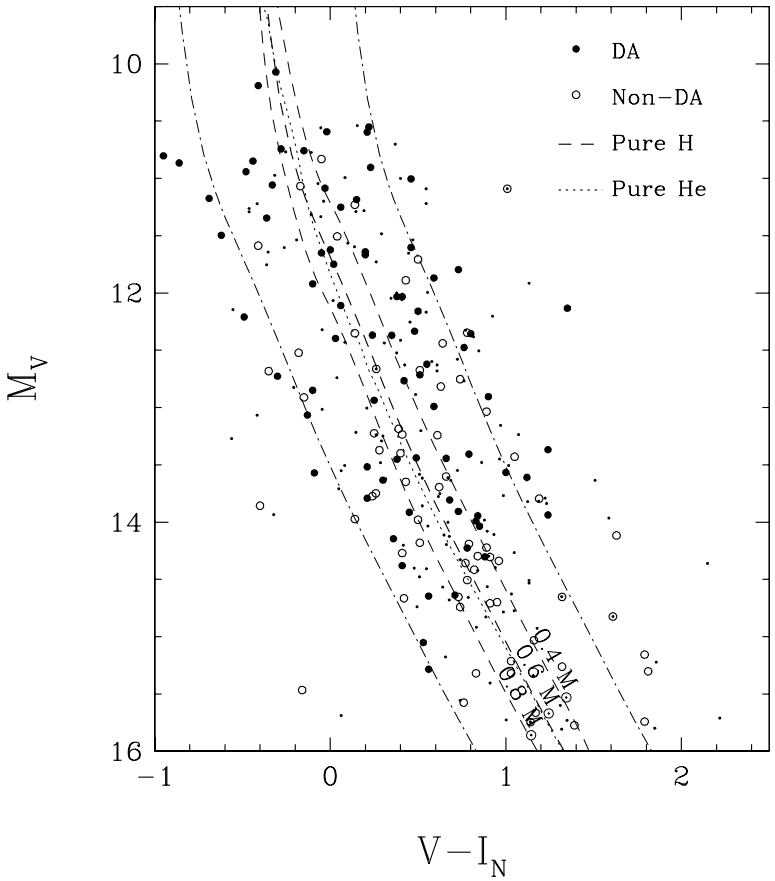

FIGURE 2.8 – Same as Figure 2.5 but for the determination of absolute M_V magnitudes for stars with USNO-B1.0 photographic magnitudes. Also shown are the 151 white dwarfs from the WD Catalog with available USNO photographic magnitudes and trigonometric parallaxes from the Yale Parallax Catalog; the small dots correspond to USNO photographic magnitudes while the larger symbols make use of Johnson V magnitudes. The dot-dashed lines represent the 0.5 mag dispersion around the pure hydrogen sequence at 0.6 $M_{\odot}$ estimated from the accuracy of the B_J, R_F, and I_N magnitudes.

find a significantly larger dispersion of $\sigma(M) = 0.26$ $M_{\odot}$, compared to the value of 0.20 $M_{\odot}$ obtained by Bergeron et al. This is a direct consequence of the lesser accuracy of photographic magnitudes. Indeed, most of the scatter observed here is likely due to the 0.5 mag uncertainty in photographic I_N magnitudes (Monet et al. 2003). For instance, we also illustrate in Figure 2.8 the effect of a 0.5 mag error on the $V - I_N$ color-index for the theoretical hydrogen sequence at 0.6 $M_{\odot}$. Most of the points are then contained within these boundaries. The reliability of the color-magnitude relation is therefore limited by the accuracy of the photographic magnitudes. Unfortunately, these photographic magnitudes are the only information available

to estimate photometric distances for the 6688 candidates with no SDSS, *GALEX*, or 2MASS counterparts.

We finally conclude from the figures above that the color-magnitude relations derived from SDSS, *GALEX*, and 2MASS photometry are comparable in their level of accuracy, and that the least accurate photometric distances, as one might expect, are those estimated from photographic magnitudes.

2.5.2 Error on Photometric Distances

There are 70 spectroscopically confirmed white dwarfs with measured trigonometric parallaxes recovered by our four reduced proper motion diagrams. For these 70 white dwarfs, we can estimate photometric distances using the photometric system corresponding to the reduced proper motion diagram where each object was identified. For instance, 19 objects were identified on the basis of their SDSS photometry, that is, they were selected from the $(H_g, g-z)$ reduced proper motion diagram while their photometric distance was estimated using the M_g vs. $(g-z)$ color-magnitude calibration. Similarly, 8 objects were identified with the help of *GALEX* photometry, 35 from 2MASS photometry, and 8 from photographic magnitudes. We finally end up with a sample of 70 confirmed white dwarfs with distances measured from trigonometric parallax measurements, where each star has also been identified in at least one of the reduced proper motion diagrams, and with a corresponding photometric distance estimate.

The distances obtained from parallax measurements are compared to photometric distances in Figure 2.9. The dashed lines represent the average 8.5 pc (rms) dispersion relative to the 1:1 relation estimated using the white dwarfs displayed in Figures 2.5 to 2.8 for all four sets of color-magnitude relations. Given the observed dispersion in Figure 2.9 and the fact that this dispersion appears to increase with distance, we choose to include in our list of white dwarf candidates within 40 pc of the Sun all objects with an estimated photometric distance less than 55 pc. We believe that this conservative buffer of 15 pc (dotted line in Figure 2.9) is enough to include all white dwarfs that could potentially lie within 40 pc of the Sun. Of course, we keep in mind that the main purpose of this calibration is purely to identify

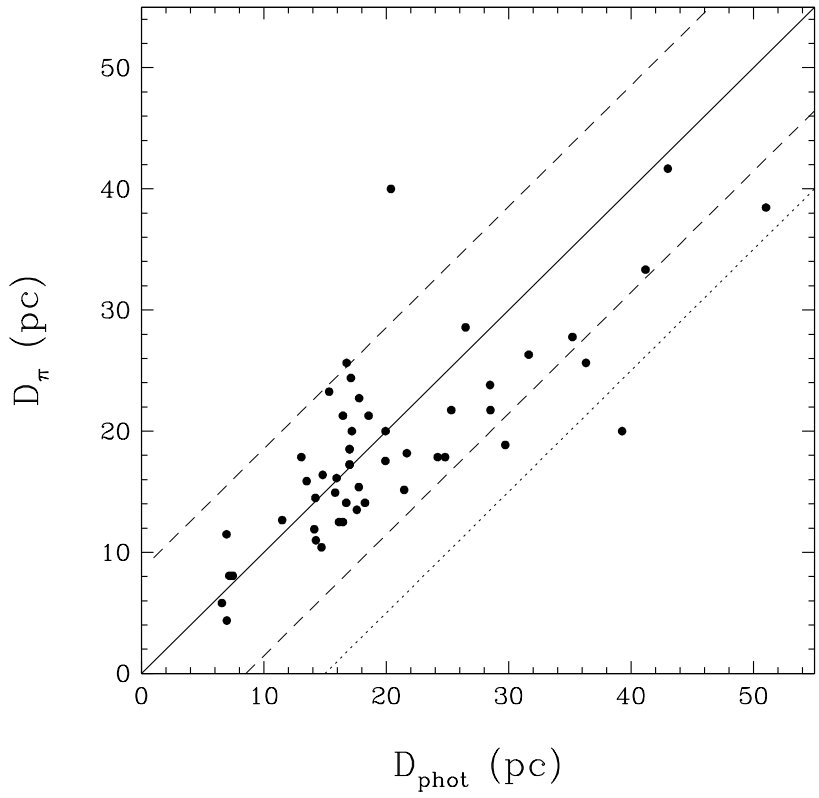

FIGURE 2.9 – Distances obtained from trigonometric parallaxes compared with photometric distances estimated from theoretical color-magnitude relations. The dots represent the 70 spectroscopically confirmed white dwarfs with parallax uncertainties less than 30% and also selected from our reduced proper motion diagrams. The solid line represents the 1:1 relation, while the dashed lines represent the 1σ dispersion of 8.5 pc resulting from the combined errors of the 4 color-magnitude relations. The dotted line indicates the +15 pc error adopted in our analysis to ensure all white dwarf candidates within 40 pc of the Sun are included in our sample.

the nearest objects. Subsequent spectroscopic analyses are expected to provide more accurate distances, and lead to an independent estimation of the error on the photometric distances.

2.5.3 List of White Dwarf Candidates

We are now able to determine photometric distances for each object on our list of white dwarf candidates following the method described in the previous sections. If the estimated distance places it within 55 pc of the Sun, the object becomes part of our list of candidates for follow-up spectroscopy. This process leaves us with a list of 1978 spectroscopic targets. The

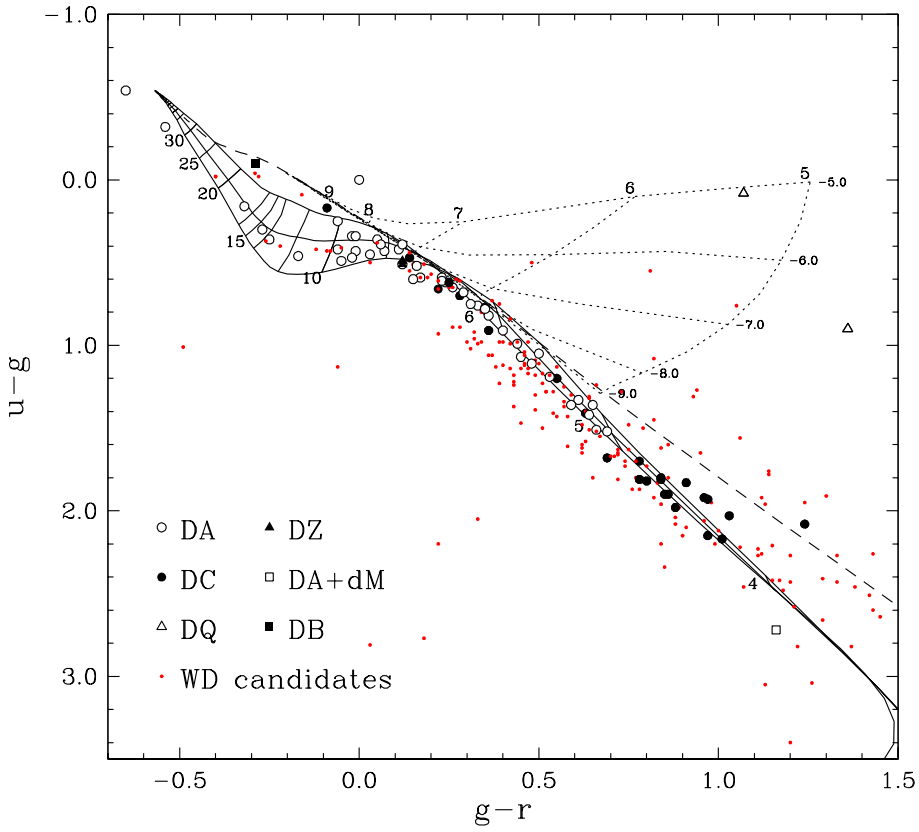

FIGURE 2.10 – $(u-g,\, g-r)$ color-color diagram showing the 268 white dwarf candidates with *ugriz* photometry available. The 76 white dwarfs spectroscopically confirmed in Section 2.6 are shown with various symbols explained in the legend, while those without spectroscopic data are shown with red dots. The solid curves represent pure hydrogen model atmospheres at $\log g = 7.0$, 8.0, and 9.0 (from bottom to top); effective temperatures are indicated in units of 10^3 K. The dashed curve corresponds to pure helium atmospheres at $\log g = 8.0$, and the dotted lines represent DQ models for 5 different compositions, from $\log \mathrm{C/He} = -9.0$ to -5.0.

sample can be further reduced by eliminating all previously known white dwarfs. To do so, the coordinates of each candidate are compared to those listed in the WD Catalog, and then with every star in the Simbad Astronomical Database [11] within a 1 arcmin radius. This way, we found 499 white dwarfs in our candidate list that were previously known, and an additional 35 objects with a known spectral type that identifies them either as a main sequence star or a background galaxy. The presence of these 9 galaxies in our candidate list indicates that there are apparently some spurious objects with false proper motions in the SUPERBLINK catalog. From all these objects with a known spectral type, we can evaluate the contamination of our

11. http://simweb.u-strasbg.fr/

sample of white dwarf candidates to be ∼8%.

With the objects with a known spectral type removed from our candidate list, we finally end up with a list of 1341 targets for follow-up spectroscopy. This sample divides into 268 candidates identified on the basis of SDSS photometry, 130 from *GALEX* photometry, 731 from 2MASS photometry, and 212 from USNO-B1.0 photographic magnitudes. The candidates identified with SDSS and *GALEX* colors are given first priority for follow-up spectroscopy, followed by stars with 2MASS photometry. Finally, objects with only photographic magnitudes available are given the lowest priority.

The 268 white dwarf candidates with available SDSS photometry are shown in Figure 2.10 in a $(u - g,\ g - r)$ color-color diagram, together with theoretical predictions for our pure hydrogen, pure helium, and DQ models. This two-color diagram reveals that our sample is dominated by cool white dwarfs. We also expect that an important fraction of these cool objects will have a hydrogen-dominated atmosphere, and that some candidates are most likely DQ stars.

The 1341 white dwarf candidates identified in SUPERBLINK are also displayed in Figure 2.11. The upper panel shows their space distribution using a cylindrical equal-area projection of the equatorial coordinates, while in the lower panel, the same distribution is binned into a histogram to illustrate more clearly the space density as a function of right ascension. This figure shows that our white dwarf candidates are distributed uniformly on the sky, without any drop in surface density near the galactic plane. The spectroscopically confirmed white dwarfs from the WD Catalog are also shown for comparison. Given this characteristic of our survey, we hope to increase significantly the completeness of the local white dwarf sample in this region, which has often been neglected in the past due to field crowding near the Galactic plane.

2.6 Spectroscopic follow-up of the candidates

We provide in this section a status report of our ongoing spectroscopic survey, and present results for a first set of 422 objects from our target list, or nearly a third of our complete sample.

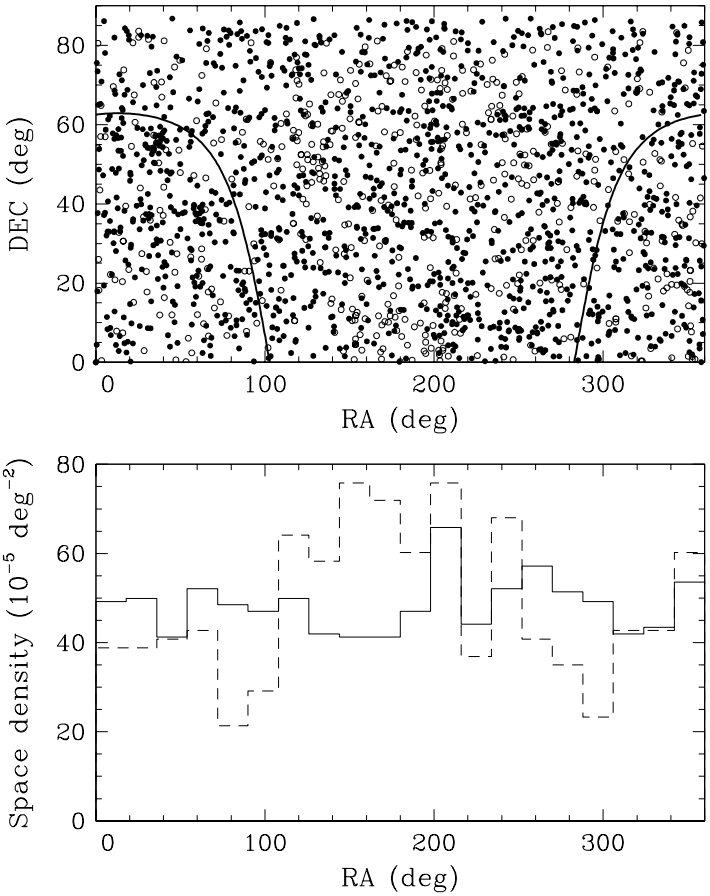

FIGURE 2.11 – Upper panel: Equal cylindrical projection of the equatorial coordinates for the sample of 1341 white dwarf candidates identified from SUPERBLINK (solid circles) compared with the sample of 499 stars from the WD Catalog recovered by our selection criteria (open circles). Also shown by the bold solid line is the region of the galactic plane. Lower panel: Space density as a function of right ascension, normalized to the total number of stars in each bin (both lines are thus on a comparable scale). The solid line represents the 1341 white dwarf candidates, while the dashed line corresponds to the white dwarfs from the WD Catalog.

2.6.1 Spectroscopic Observations

Optical spectra have been obtained with the Steward Observatory 2.3-m telescope, and the NOAO Mayall 4-m and 2.1-m telescopes, during 8 different observing runs between 2009 May and 2010 October. The adopted configurations allow a spectral coverage of $\lambda\lambda$3800–5600 and $\lambda\lambda$3800–6700, at an intermediate resolution of $\sim$6 Å FWHM. Spectra were first obtained at low signal-to-noise ratio (S/N $\sim$25), which is sufficient to identify main sequence objects, but also represents the lower limit required to obtain reliable model fits to the spectral lines. Table 2.2 summarizes our spectroscopic observing runs and observational setups.

TABLE 2.2 – Spectroscopic Observing Runs

Date	Telescope	Spectrograph	Grating (l mm^{-1})	Blaze (Å)	Coverage (Å)	Slit ($''$)
2009 May	Steward Observatory Bok 2.3 m	B&C	600	3568	3800-5600	4.5
2009 August	NOAO Mayall 4 m	RC	527	5540	3800-6800	2
2009 November	Steward Observatory Bok 2.3 m	B&C	600	3568	3800-5600	4.5
2009 December	NOAO 2.1 m	Goldcam	600	4900	3800-6700	2
2010 March	NOAO Mayall 4 m	RC	316	4000	3900-6700	2
2010 May	NOAO 2.1 m	Goldcam	500	5500	3800-6700	2
2010 July	Steward Observatory Bok 2.3 m	B&C	400	4800	3800-6700	4.5
2010 October	NOAO Mayall 4 m	RC	316	4000	3900-6700	2

As a result of our spectroscopic observations, 193 newly identified white dwarfs have been spectroscopically confirmed. Among these, 68 were identified on the basis of SDSS photometry, 18 from *GALEX*, 70 from 2MASS, and 12 from USNO photographic magnitudes. The remaining 25 objects were discovered using an earlier version of our selection method, based on criteria different from those adopted in the final version. These objects have revised photometric distance estimates beyond 55 pc, and are thus not included in our final list of 1341 candidates.

2.6.2 Spectroscopic Content

Our spectroscopic follow-up observations identify 193 new white dwarfs, listed in Tables 2.3 and 2.4. Table 2.3 provides astrometric data as well as NLTT and SDSS designations, when available, while Table 2.4 lists the same objects but with the available photometry and adopted spectral types. In the earlier presentation of our results (Limoges et al. 2010), the 'LSPM J' notation was used for the object names, as in Lépine & Shara (2005), but the the proper motion limit for stars in SUPERBLINK has lowered to $\mu > 0.04$"yr^{-1}, and the entries were homogenized with a 'PM I' designation. In summary, this subsample contains 127 DA (among which 9 DA+dM and 4 magnetic), 1 DB, 56 DC, 3 DQ, and 6 DZ white dwarfs.

Once we have a confirmed white dwarf, it is possible to improve upon our preliminary distance estimates, which were based on approximate V magnitudes and color-magnitude relations, by making use of the full set of photometric data. Here we rely on the so-called photometric method described at length in Giammichele et al. (2012, and references therein) where the available photometry for each star is fitted with theoretical fluxes, properly averaged

over each bandpass. Both $T_{\rm eff}$ and the solid angle $\pi(R/D)^2$ are considered free parameters, where R is the radius of the star and D its distance from Earth. We assume a value of $\log g = 8$ and corresponding radius R, and obtain directly the distance D. These improved photometric distances are given in Table 2.4.

When this survey was undertaken in 2009 May, none of these objects had a white dwarf classification or a spectral type available in the literature. But since then, white dwarf identifications have been reported in Kilic et al. (2010), Vennes et al. (2011), Tonry et al. (2012), and Sayres et al. (2012). We identified these stars in Table 2.3 and chose to leave these objects in our sample since they have been discovered independently. We also want to point out that even though Table 2.3 contains 25 stars with existing SDSS spectra, all our targets have been identified using our own spectroscopic data.

Optical spectra from our subsample of DA stars covering H8 to Hβ — or Hα when available — are shown in Figure 2.12. Note that 14106+0245 (right panel of Figure 2.12b, second object from the top) is a DAZ, and that our subsample of 4 magnetic DA white dwarfs (05158+2839, 06019+3726, 06513+6242, and 15164+2803) is displayed in Figure 2.13. Our survey also detected 9 new DA white dwarfs with an M dwarf companion; these are plotted separately in Figure 2.14. This was quite unexpected, since the cuts in the reduced proper motion diagrams were chosen in order to avoid main sequence stars. As a consequence, we avoided all objects that are bright in the infrared portion of the spectrum. As discussed earlier, however, this is true for our criteria in $g-z$, $V-J$, and $V-I_N$, but not for our criteria in NUV $-\,V$, which is efficient for detecting blue objects. And indeed, all 9 DA+dM systems were detected using this last reduced proper motion diagram.

The DB, DQ, and DZ stars in our sample are plotted together in Figure 2.15. Unfortunately, the observational setup with the NOAO telescopes does not allow the coverage of wavelengths shorter than ∼3900 Å, while covering Hα simultaneously. Calcium lines can still be easily identified, however, but additional spectroscopic observations near the ∼3700 Å region are currently being obtained in order to perform a proper model atmosphere analysis of these DZ stars. In the case of DQ white dwarfs, one particular object, 12476+0646, exhibits the pressure-shifted carbon lines characteristic of DQpec stars (Kowalski 2010). Finally, we

display our featureless DC spectra in Figure 2.16 in order of their Right Ascension.

Some of the results of our spectroscopic observations are summarized in the color-color diagram shown in Figure 2.10, where we identify the various spectral types of the 76 confirmed white dwarfs with available SDSS colors. As expected, the DQ stars are located in the appropriate region of the $(u-g,\, g-r)$ diagram, and in the next phase of the survey, we plan to use this characteristic to identify all possible DQ stars in SUPERBLINK. We also note the presence of a DA + dM system at $(u-g, g-r) \sim (2.8, 1.2)$, in the redder part of the diagram. Finally, the sample of DC stars follows the theoretical, pure hydrogen sequence, with only one outlier near $u-g = 2.0$, giving us a preliminary indication of the atmospheric composition even before performing a full analysis of their energy distribution.

In the following section, we present a preliminary spectroscopic analysis of the DA component of our survey.

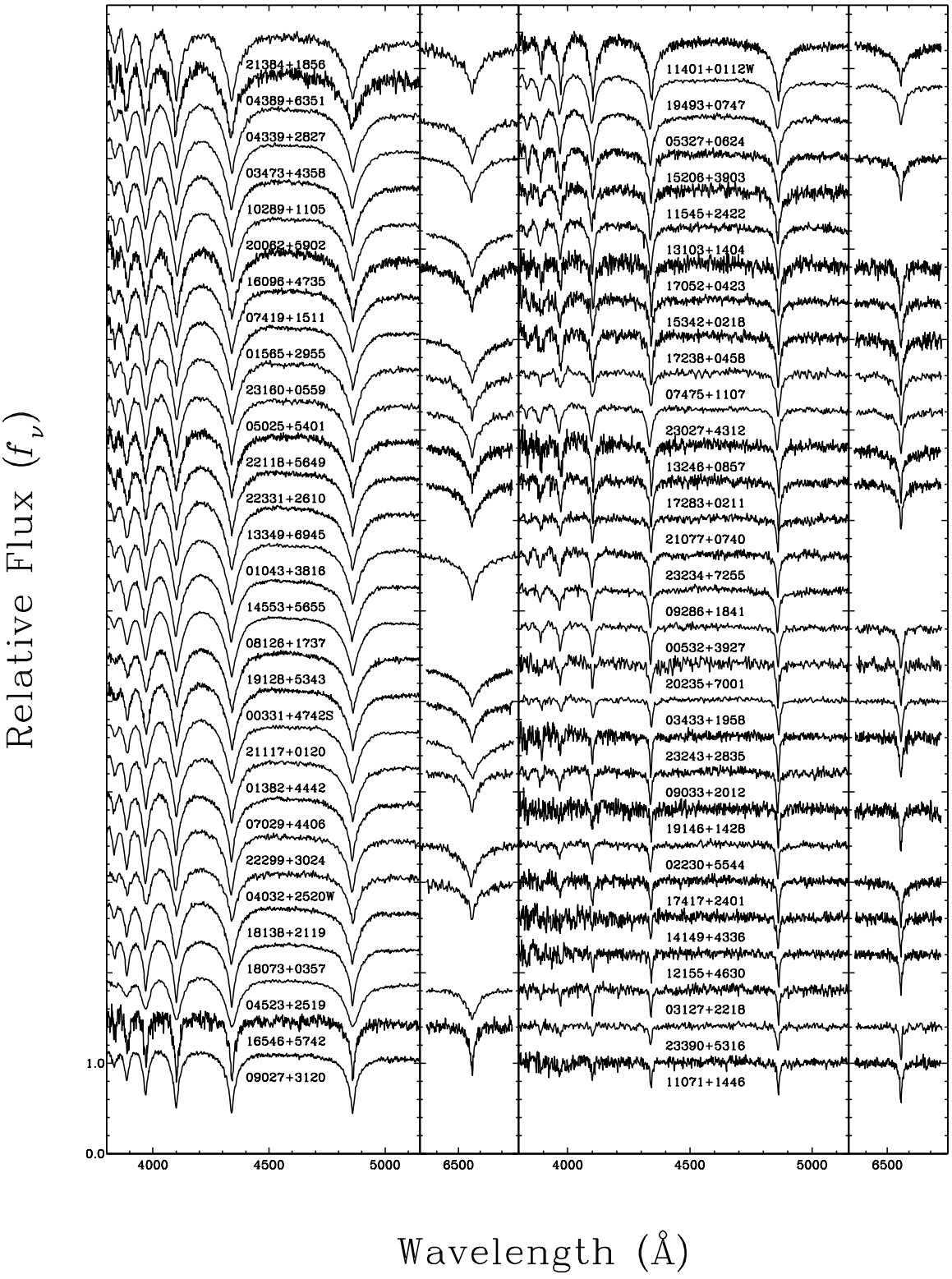

FIGURE 2.12 – (a) - Optical spectra for our sample of DA white dwarfs from SUPERBLINK. The spectra are displayed in order of decreasing equivalent width of Hβ, from upper left to bottom right, and shifted vertically for clarity. The Hα line is also shown, when available, and normalized to a continuum set to unity.

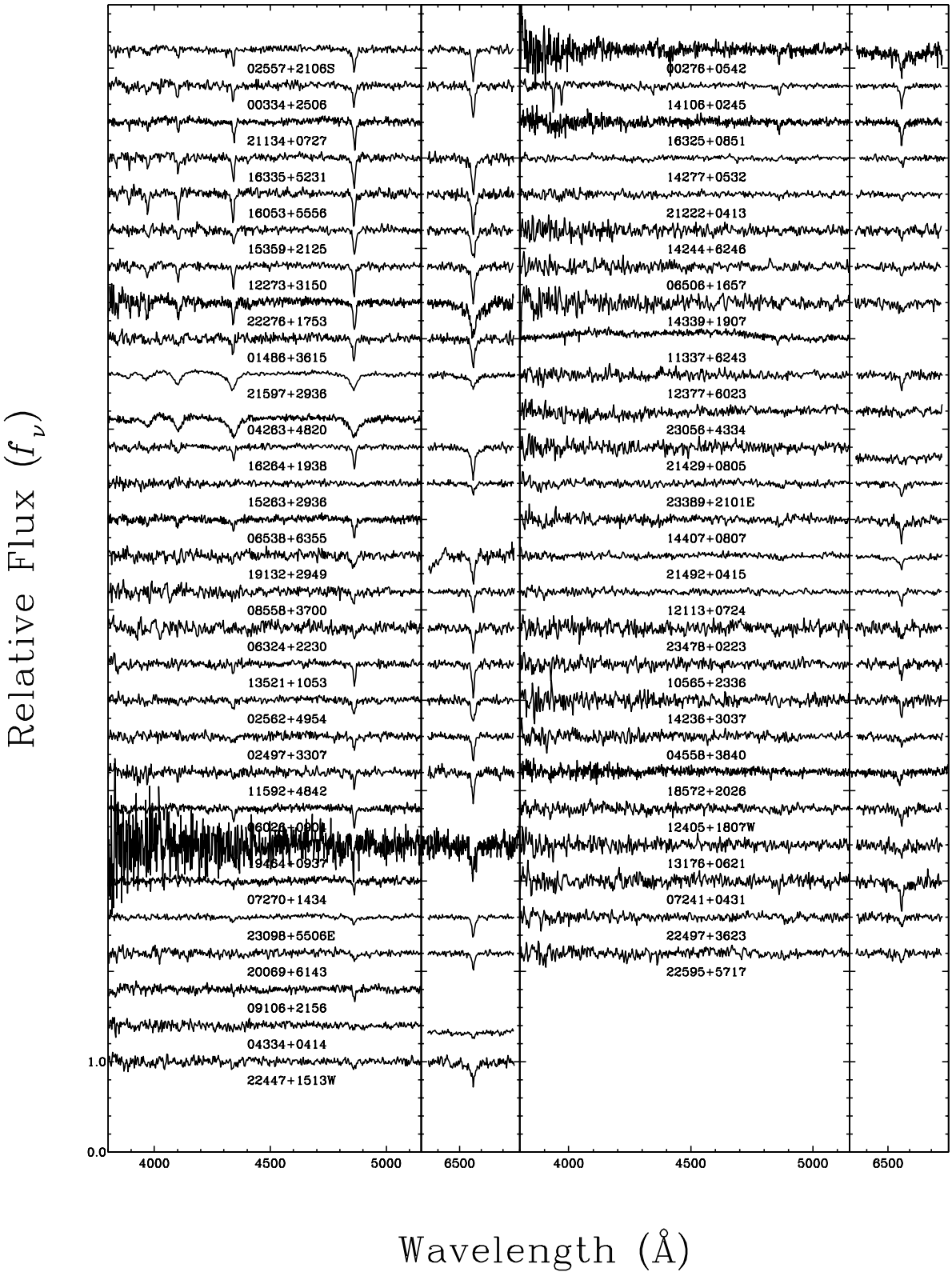

FIGURE 2.12 – (b) - continued.

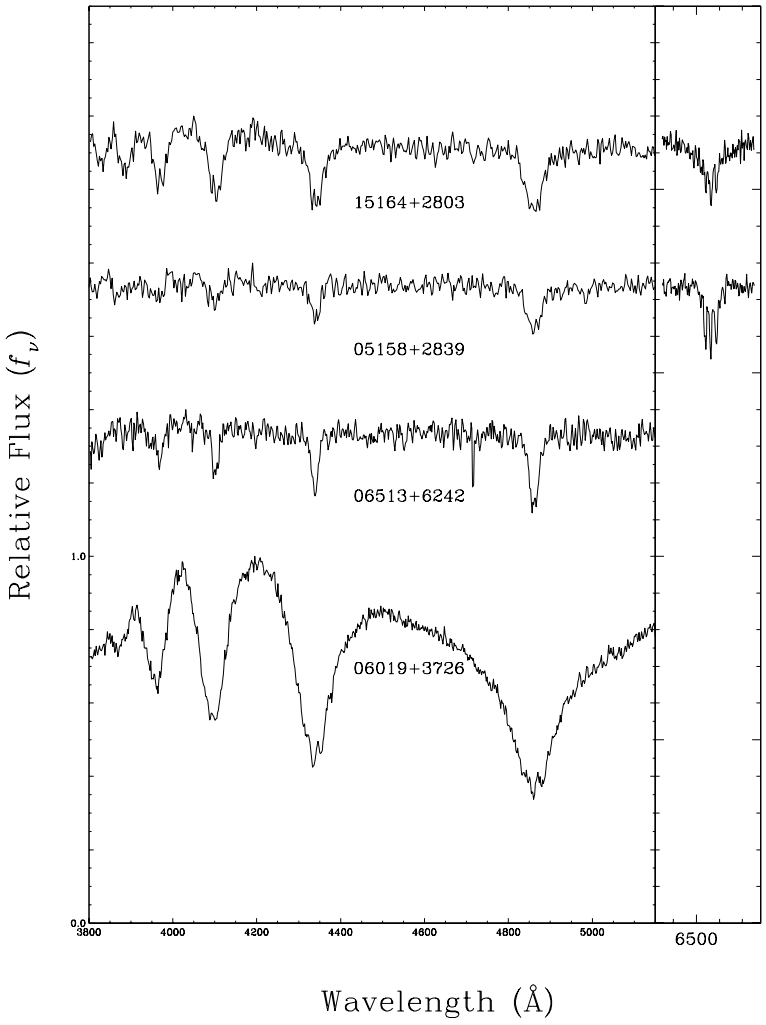

FIGURE 2.13 – Our subsample of magnetic DA white dwarfs, shifted vertically for clarity.

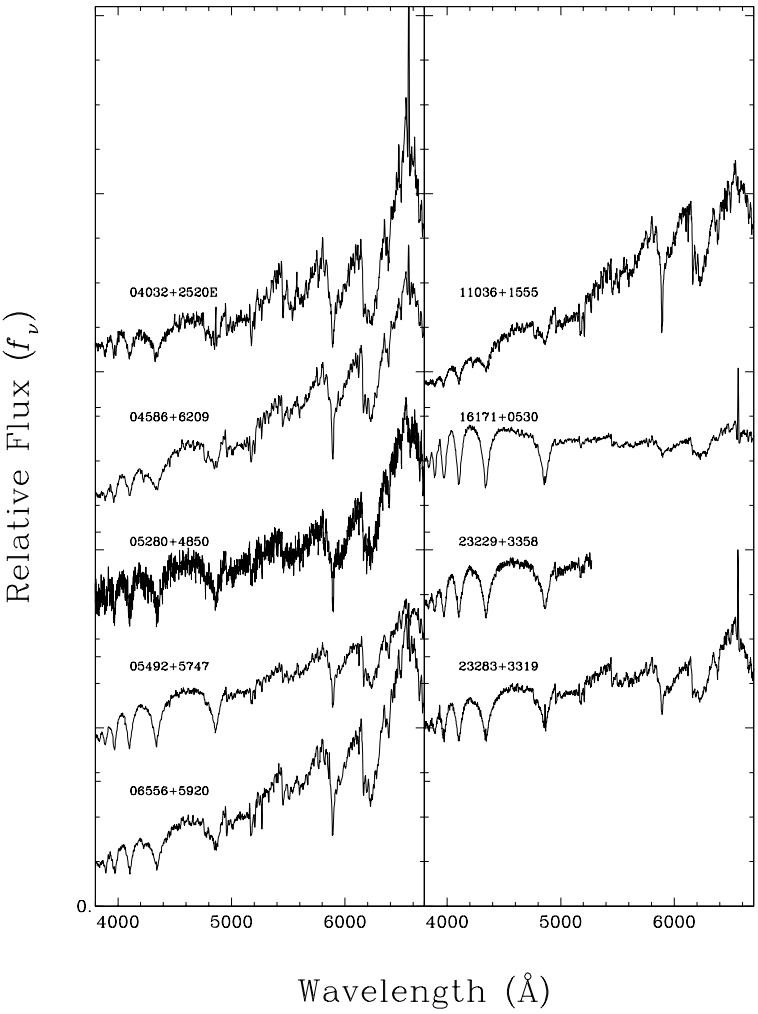

FIGURE 2.14 – Our sample of binary systems composed of a DA white dwarf and a M dwarf companion. The spectra are shifted vertically for clarity. The Hα and Hβ line cores of 04032+2520E (not to be confused with the DA 04032+2520W), 06556+5920, 16171+0530, and 23283+3319 are contaminated by emission from the M dwarf.

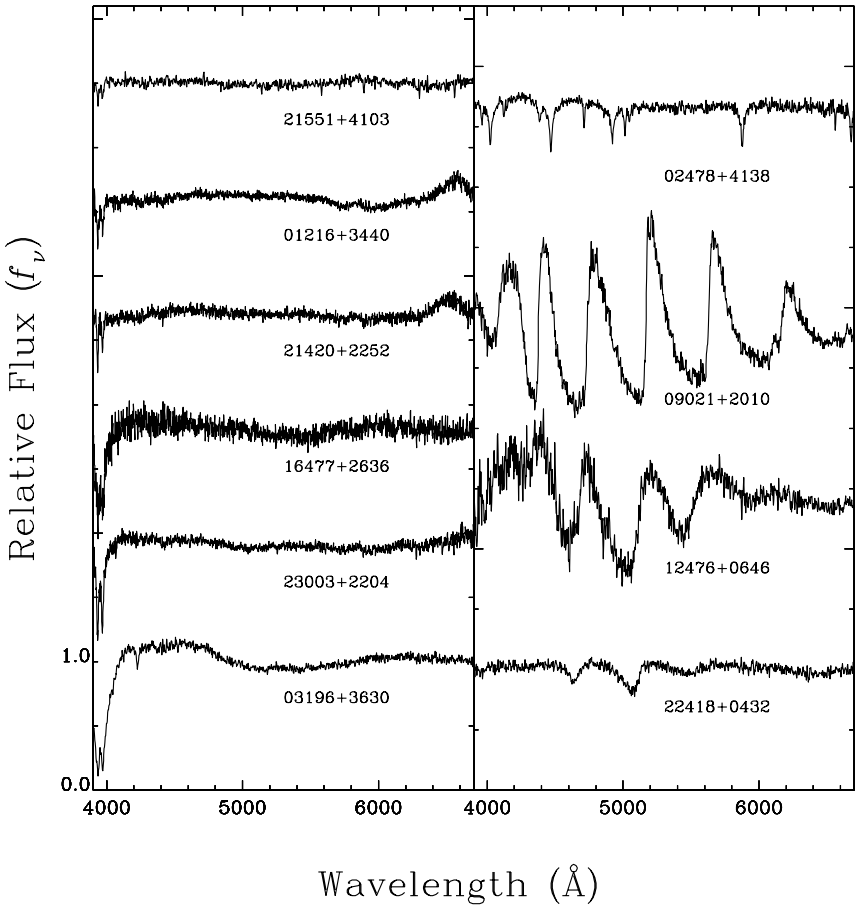

FIGURE 2.15 – Spectra of white dwarfs in our sample with helium-rich atmospheres. The panel on the left displays the DZ stars, while the panel on the right shows our only DB star, as well as 3 DQ stars.

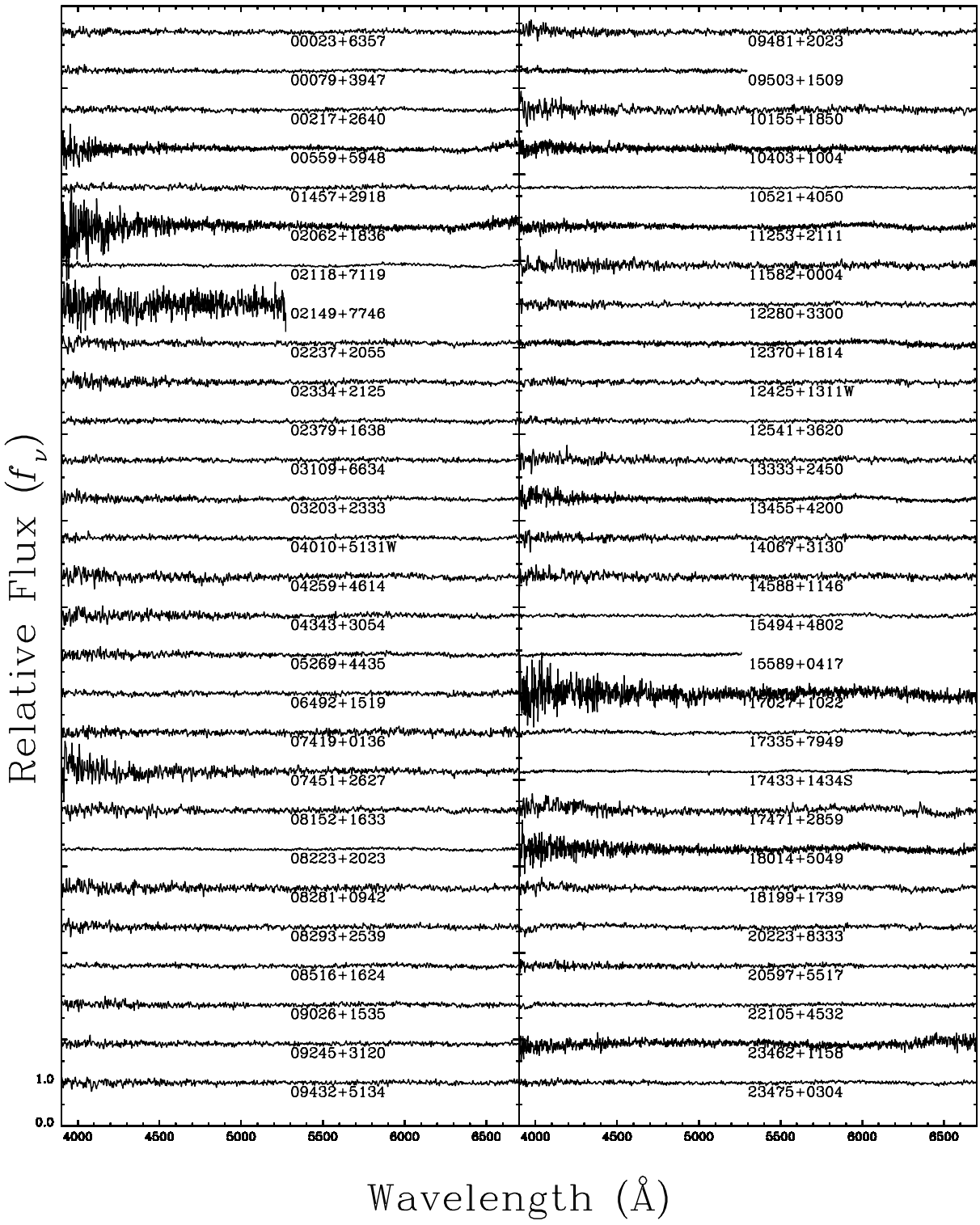

FIGURE 2.16 – Our sample of featureless DC stars. All spectra are normalized to a continuum set to unity and are offset from each other by a factor of 0.9.

TABLE 2.3 – Spectroscopically Confirmed White Dwarfs from SUPERBLINK − Astrometry

PM I	**NLTT**	**SDSS**	**RA** J_{2000}	**DEC** J_{2000}	$\mu_{\rm tot}$ ($''{\rm yr}^{-1}$)	μ**RA** ($''{\rm yr}^{-1}$)	μ**DE** ($''{\rm yr}^{-1}$)	**Notes**
00023+6357			00:02:22.61	+63:57:44.3	0.911	0.906	0.092	
00079+3947	317		00:07:54.11	+39:47:32.2	0.370	0.362	−0.075	
00217+2640	1119		00:21:47.32	+26:40:36.3	0.330	−0.074	−0.322	
00276+0542			00:27:36.63	+05:42:03.2	0.381	0.266	−0.273	
00331+4742S			00:33:10.51	+47:42:12.4	0.079	−0.060	0.052	
00334+2506	1783	J003325.44+25061	00:33:25.28	+25:06:14.1	0.499	0.477	0.146	
00532+3927			00:53:13.75	+39:27:06.1	0.209	−0.152	−0.143	
00559+5948			00:55:58.28	+59:48:02.4	0.458	0.454	−0.061	
01043+3816			01:04:19.32	+38:16:55.0	0.070	−0.054	−0.046	
01216+3440		J012137.74+34404	01:21:37.80	+34:40:43.2	0.132	−0.131	0.017	
01382+4442			01:38:12.93	+44:42:52.2	0.049	−0.014	−0.047	
01457+2918	5850		01:45:44.62	+29:18:23.8	0.529	0.529	0.008	
01486+3615	6026		01:48:40.45	+36:15:31.0	0.231	0.000	−0.231	
01565+2955			01:56:29.90	+29:55:35.9	0.104	0.054	−0.089	
02062+1836	6996		02:06:14.67	+18:36:24.1	0.789	0.784	0.093	
02118+7119		J021148.35+71191	02:11:48.17	+71:19:13.3	0.252	0.166	−0.190	
02149+7746			02:14:56.99	+77:46:00.0	0.469	0.265	−0.387	
02230+5544			02:23:00.30	+55:44:27.2	0.172	0.126	−0.117	
02237+2055		J022348.96+20555	02:23:48.93	+20:55:53.8	0.477	0.014	−0.476	
02334+2125		J023339.00+21251	02:33:38.98	+21:25:13.2	0.234	0.062	−0.226	
02379+1638	8525		02:37:59.15	+16:38:13.0	0.321	−0.036	−0.319	
02478+4138			02:47:51.80	+41:38:29.6	0.074	−0.018	−0.072	
02497+3307		J024944.28+33072	02:49:44.20	+33:07:25.6	0.303	0.175	0.247	
02557+2106S		J025545.70+21062	02:55:45.60	+21:06:21.7	0.257	0.225	−0.125	
02562+4954	9314		02:56:17.18	+49:54:41.9	0.193	0.032	−0.191	
03109+6634			03:10:57.60	+66:34:02.1	0.812	0.691	−0.426	
03127+2218	10206		03:12:42.85	+22:18:28.5	0.277	0.202	−0.189	
03196+3630			03:19:38.25	+36:30:29.5	0.107	0.105	0.016	
03203+2333	10606		03:20:20.30	+23:33:31.7	0.366	0.077	−0.358	
03433+1958			03:43:23.11	+19:58:13.5	0.177	0.081	0.157	
03473+4358			03:47:22.43	+43:58:57.2	0.176	−0.160	0.074	
04010+5131W		J040101.58+51313	04:01:01.50	+51:31:30.2	0.890	0.365	−0.812	
04032+2520E			04:03:16.51	+25:20:19.2	0.051	−0.045	−0.025	
04032+2520W			04:03:16.51	+25:20:19.2	0.051	−0.045	−0.025	
04259+4614			04:25:57.00	+46:14:17.6	0.174	0.157	−0.075	

TABLE 2.3 – Continued

PM I	NLTT	SDSS	RA J_{2000}	DEC J_{2000}	$\mu_{\rm tot}$ ($''$yr^{-1})	μRA ($''$yr^{-1})	μDE ($''$yr^{-1})	Notes
04263+4820			04:26:23.59	+48:20:09.7	0.128	0.039	−0.122	
04334+0414			04:33:29.80	+04:14:47.7	0.463	0.092	−0.453	
04339+2827			04:33:54.42	+28:27:31.1	0.060	0.047	−0.038	
04343+3054			04:34:20.55	+30:54:22.4	0.307	−0.040	−0.305	
04389+6351			04:38:56.94	+63:51:34.2	0.184	0.145	−0.113	
04523+2519			04:52:19.36	+25:19:34.0	0.104	0.004	−0.104	1
04558+3840			04:55:51.38	+38:40:50.4	0.220	0.210	−0.069	
04586+6209			04:58:39.26	+62:09:07.9	0.144	0.112	−0.092	
05025+5401			05:02:34.18	+54:01:08.5	0.190	−0.040	−0.185	
05158+2839			05:15:53.53	+28:39:16.6	0.200	0.160	−0.109	
05269+4435			05:26:56.11	+44:35:39.1	0.450	0.250	−0.381	
05280+4850			05:28:03.21	+48:50:47.5	0.130	0.029	−0.126	
05327+0624			05:32:42.87	+06:24:28.6	0.066	−0.059	−0.030	
05492+5747			05:49:14.55	+57:47:57.3	0.090	0.063	0.064	
06019+3726			06:01:58.71	+37:26:02.1	0.074	0.009	−0.073	
06026+0904			06:02:36.72	+09:04:23.6	0.268	0.098	−0.250	
06324+2230			06:32:29.37	+22:30:04.6	0.210	−0.140	−0.157	
06492+1519			06:49:17.30	+15:19:30.9	0.346	0.246	−0.243	
06506+1657			06:50:36.80	+16:57:53.7	0.268	−0.175	−0.202	
06513+6242			06:51:22.90	+62:42:54.9	0.143	−0.075	−0.122	
06538+6355			06:53:50.41	+63:55:58.1	0.432	−0.142	−0.407	
06556+5920			06:55:38.50	+59:20:27.4	0.150	0.000	−0.159	
07029+4406			07:02:58.93	+44:06:53.8	0.093	0.092	−0.001	
07241+0431			07:24:06.16	+04:31:30.2	0.417	0.076	−0.410	
07270+1434	17874	J072704.21+14343	07:27:04.15	+14:34:40.3	0.192	0.150	−0.119	
07419+0136			07:41:54.02	+01:36:45.0	0.267	0.143	−0.226	
07419+1511		J074156.42+15111	07:41:56.44	+15:11:17.0	0.119	0.004	−0.119	
07451+2627		J074509.02+26270	07:45:08.94	+26:27:06.6	0.890	0.490	−0.744	
07475+1107		J074730.12+11073	07:47:30.09	+11:07:35.0	0.190	0.060	−0.181	
08126+1737		J081237.82+17370	08:12:37.80	+17:37:01.4	0.114	0.077	−0.084	1
08152+1633		J081516.84+16331	08:15:16.79	+16:33:17.0	0.266	0.244	−0.106	2
08223+2023		J082219.23+20232	08:22:19.23	+20:23:26.2	0.100	0.040	−0.100	2
08281+0942		J082808.04+09421	08:28:07.93	+09:42:17.8	0.460	0.440	−0.142	
08293+2539		J082922.05+25393	08:29:22.84	+25:39:39.9	0.563	0.227	−0.515	
08516+1624	20389	J085140.35+16245	08:51:40.48	+16:24:54.4	0.430	−0.410	−0.156	

TABLE 2.3 – Continued

PM I	**NLTT**	**SDSS**	**RA** J_{2000}	**DEC** J_{2000}	$\mu_{\rm tot}$ ($''{\rm yr}^{-1}$)	μ**RA** ($''{\rm yr}^{-1}$)	μ**DE** ($''{\rm yr}^{-1}$)	**Notes**
08558+3700		J085549.88+37001	08:55:49.86	+37:00:16.8	0.160	0.130	−0.094	3
09021+2010		J090208.40+20104	09:02:08.31	+20:10:51.6	0.345	0.098	−0.330	2
09026+1535	20824	J090240.47+15355	09:02:40.60	+15:35:57.8	0.382	−0.309	−0.224	2
09027+3120		J090242.66+31204	09:02:42.67	+31:20:43.9	0.087	−0.087	−0.002	
09033+2012	20852	J090318.54+20124	09:03:18.57	+20:12:46.7	0.204	−0.009	−0.204	2,4
09106+2156	21118	J091037.29+21561	09:10:37.21	+21:56:16.1	0.303	0.225	−0.203	4
09245+3120	21660	J092430.80+31203	09:24:30.85	+31:20:33.5	0.424	−0.193	−0.378	2,4
09286+1841	21844	J092840.28+18411	09:28:40.22	+18:41:14.9	0.295	0.165	−0.245	2
09432+5134		J094316.62+51344	09:43:16.59	+51:34:41.3	0.292	0.127	−0.263	3
09481+2023	22620	J094806.09+20231	09:48:06.15	+20:23:15.4	0.203	−0.202	0.019	2
09503+1509		J095021.77+15090	09:50:21.80	+15:09:10.1	0.323	−0.069	−0.310	
10155+1850	23818	J101535.36+18502	10:15:35.40	+18:50:22.9	0.212	−0.079	−0.197	2
10289+1105		J102854.91+11055	10:28:54.88	+11:05:51.3	0.091	0.067	−0.062	
10403+1004		J104019.68+10040	10:40:19.70	+10:04:00.4	0.147	−0.098	−0.110	
10521+4050	25548	J105211.67+40500	10:52:11.73	+40:50:04.2	0.276	−0.200	−0.190	
10565+2336	25771	J105630.01+23361	10:56:30.08	+23:36:19.0	0.282	−0.181	−0.216	4
11036+1555		J110338.81+15551	11:03:38.85	+15:55:14.6	0.097	−0.092	0.030	
11071+1446	26335	J110709.66+14465	11:07:09.72	+14:46:54.4	0.281	−0.264	0.097	4
11253+2111	27340	J112521.29+21111	11:25:21.41	+21:11:15.2	0.398	−0.267	−0.295	
11337+6243		J113347.79+62431	11:33:47.81	+62:43:13.3	0.122	−0.063	0.104	
11401+0112W		J114009.11+01122	11:40:09.12	+01:12:23.0	0.166	−0.165	−0.014	
11545+2422		J115434.57+24223	11:54:34.57	+24:22:39.5	0.110	0.016	−0.109	2,4
11582+0004		J115814.51+00045	11:58:14.51	+00:04:58.4	0.180	−0.038	0.176	3
11592+4842	29180	J115916.47+48423	11:59:16.51	+48:42:38.9	0.236	−0.226	−0.067	
11598+0007		J115952.04+00075	11:59:52.03	+00:07:51.7	0.090	0.079	−0.044	
12113+0724		J121118.80+07244	12:11:18.82	+07:24:48.2	0.227	−0.065	−0.218	3,4
12155+4630	30149	J121531.63+46301	12:15:31.71	+46:30:14.0	0.269	−0.269	0.016	5
12273+3150		J122724.30+31502	12:27:24.27	+31:50:24.0	0.204	0.084	−0.186	2,4
12280+3300		J122801.59+33003	12:28:01.57	+33:00:36.3	0.187	0.048	−0.181	2
12370+1814		J123700.74+18145	12:37:00.77	+18:14:59.1	0.229	−0.181	−0.139	2
12377+6023		J123743.15+60232	12:37:43.16	+60:23:20.4	0.159	−0.064	0.146	
12405+1807W	31483	J124030.27+18072	12:40:30.48	+18:07:28.8	0.571	−0.565	−0.085	
12425+1311W		J124234.43+13114	12:42:34.49	+13:11:42.1	0.343	−0.274	−0.207	
12476+0646		J124739.04+06460	12:47:39.12	+06:46:04.3	0.389	−0.383	0.065	2,3
12541+3620	32251	J125411.37+36205	12:54:11.51	+36:20:58.4	0.407	−0.406	−0.028	

TABLE 2.3 – Continued

PM I	NLTT	SDSS	RA J_{2000}	DEC J_{2000}	$\mu_{\rm tot}$ ($''{\rm yr}^{-1}$)	μRA ($''{\rm yr}^{-1}$)	μDE ($''{\rm yr}^{-1}$)	Notes
13103+1404		J131023.76+14041	13:10:23.77	+14:04:20.5	0.134	−0.037	−0.129	2,4
13176+0621		J131737.45+06212	13:17:37.40	+06:21:21.5	0.304	0.262	−0.154	3
13246+0857		J132436.88+08575	13:24:36.87	+08:57:54.6	0.219	0.088	−0.201	2,4
13333+2450		J133319.26+24504	13:33:19.22	+24:50:49.6	0.209	−0.072	−0.196	2
13349+6945			13:34:59.90	+69:45:29.4	0.048	−0.019	0.044	
13455+4200	35148	J134532.91+42004	13:45:32.97	+42:00:43.7	0.238	−0.203	0.123	
13521+1053		J135211.73+10535	13:52:11.79	+10:53:51.8	0.309	−0.242	−0.192	
14067+3130	36284	J140644.53+31302	14:06:44.61	+31:30:22.7	0.301	−0.214	0.212	
14106+0245		J141039.97+02451	14:10:39.97	+02:45:13.1	0.247	−0.038	−0.244	4
14149+4336	36723	J141454.73+43365	14:14:54.79	+43:36:58.4	0.243	−0.205	−0.131	2
14236+3037		J142336.65+30374	14:23:36.64	+30:37:42.5	0.203	0.023	−0.201	2
14244+6246		J142429.52+62461	14:24:29.52	+62:46:17.0	0.272	−0.269	−0.041	
14277+0532		J142748.11+05323	14:27:48.13	+05:32:32.5	0.250	−0.179	−0.174	2,4
14339+1907		J143358.19+19073	14:33:58.20	+19:07:38.3	0.210	−0.137	−0.160	
14407+0807		J144045.12+08072	14:40:45.06	+08:07:29.3	0.294	0.229	−0.186	
14553+5655		J145521.34+56554	14:55:21.35	+56:55:44.2	0.076	−0.075	0.015	
14588+1146		J145848.51+11465	14:58:48.54	+11:46:56.2	0.168	−0.129	−0.107	3,4
15164+2803		J151625.07+28032	15:16:25.10	+28:03:22.2	0.107	−0.106	−0.010	2
15206+3903		J152038.34+39034	15:20:38.36	+39:03:49.3	0.169	−0.095	0.139	
15263+2936		J152621.08+29362	15:26:21.06	+29:36:22.7	0.188	0.086	0.167	
15342+0218		J153417.49+02184	15:34:17.50	+02:18:48.0	0.143	−0.118	−0.080	2,4
15359+2125		J153554.02+21250	15:35:54.06	+21:25:06.6	0.248	−0.142	0.203	
15494+4802		J154927.19+48022	15:49:27.20	+48:02:29.0	0.176	0.108	−0.139	2,4
15589+0417		J155857.68+04170	15:58:57.69	+04:17:05.1	0.071	−0.025	−0.066	2
16053+5556		J160520.60+55564	16:05:20.69	+55:56:45.4	0.274	−0.222	0.160	
16096+4735		J160939.78+47350	16:09:39.74	+47:35:10.7	0.062	0.043	−0.044	
16171+0530		J161710.56+05303	16:17:10.56	+05:30:38.2	0.097	0.011	−0.096	
16264+1938		J162626.28+19384	16:26:26.33	+19:38:39.3	0.275	−0.174	0.213	
16325+0851		J163233.27+08512	16:32:33.17	+08:51:22.6	0.375	0.271	−0.259	4
16335+5231	43101	J163332.24+52314	16:33:32.14	+52:31:50.0	0.265	0.103	−0.244	
16477+2636		J164744.70+26364	16:47:44.74	+26:36:46.3	0.204	−0.151	0.137	2
16546+5742			16:54:41.01	+57:42:16.3	0.066	−0.058	0.031	
17027+1022		J170246.29+10224	17:02:46.29	+10:22:41.2	0.255	0.077	0.243	
17052+0423			17:05:13.25	+04:23:45.3	0.168	0.009	−0.167	
17238+0458			17:23:49.57	+04:58:49.1	0.149	−0.041	−0.143	

TABLE 2.3 – Continued

PM I	NLTT	SDSS	RA J_{2000}	DEC J_{2000}	$\mu_{\rm tot}$ ($''$yr^{-1})	μRA ($''$yr^{-1})	μDE ($''$yr^{-1})	Notes
17283+0211			17:28:18.47	+02:11:10.2	0.224	−0.029	−0.223	
17335+7949			17:33:34.29	+79:49:16.3	0.397	0.394	−0.045	
17417+2401			17:41:46.23	+24:01:49.6	0.360	−0.030	−0.359	
17433+1434S			17:43:22.97	+14:34:52.4	0.386	−0.252	0.293	
17471+2859			17:47:08.30	+28:59:09.8	0.198	−0.121	−0.157	
18014+5049		J180127.50+50495	18:01:27.49	+50:49:58.2	0.288	−0.108	0.267	
18073+0357			18:07:23.37	+03:57:01.7	0.121	−0.012	−0.121	
18138+2119			18:13:48.55	+21:19:20.6	0.050	0.019	0.046	
18199+1739			18:19:59.23	+17:39:19.0	0.230	0.216	0.080	
18572+2026			18:57:13.95	+20:26:28.4	0.316	−0.013	−0.316	
19128+5343			19:12:48.56	+53:43:13.5	0.205	0.148	0.142	
19132+2949			19:13:16.53	+29:49:28.2	0.287	−0.056	0.281	
19146+1428			19:14:36.11	+14:28:25.4	0.422	−0.114	−0.406	
19464+0937			19:46:29.80	+09:37:14.9	0.574	0.060	−0.571	
19493+0747			19:49:23.51	+07:47:31.7	0.184	0.137	−0.122	
20062+5902		J200616.93+59022	20:06:16.96	+59:02:27.3	0.108	−0.019	−0.106	
20069+6143		J200655.03+61430	20:06:54.89	+61:43:10.3	0.238	0.168	−0.168	
20223+8333			20:22:21.50	+83:33:55.6	0.208	−0.127	0.166	
20235+7001			20:23:29.87	+70:01:55.5	0.320	−0.260	−0.186	
20597+5517		J205945.11+55173	20:59:44.91	+55:17:29.9	0.498	0.274	0.417	
21077+0740			21:07:45.05	+07:40:44.3	0.116	−0.019	−0.114	
21117+0120			21:11:46.37	+01:20:54.4	0.068	0.058	−0.035	
21134+0727			21:13:28.92	+07:27:04.2	0.341	0.321	0.115	
21222+0413		J212212.31+04135	21:22:12.35	+04:13:56.7	0.425	−0.089	−0.415	4
21384+1856		J213827.28+18564	21:38:27.28	+18:56:41.9	0.169	−0.141	−0.093	
21420+2252			21:42:03.90	+22:52:29.0	0.186	0.118	−0.144	
21429+0805			21:42:54.49	+08:05:27.4	0.218	−0.098	−0.195	
21492+0415			21:49:13.60	+04:15:50.2	0.227	0.011	−0.226	
21551+4103			21:55:06.36	+41:03:06.6	0.193	0.172	0.087	
21597+2936			21:59:46.94	+29:36:41.7	0.097	0.097	0.005	1
22105+4532			22:10:34.53	+45:32:40.0	0.361	−0.122	−0.340	
22118+5649			22:11:53.64	+56:49:46.4	0.250	0.249	0.022	
22276+1753	53908		22:27:40.36	+17:53:21.4	0.219	0.203	−0.081	
22299+3024			22:29:58.03	+30:24:10.6	0.122	0.050	−0.111	
22331+2610			22:33:11.59	+26:10:14.9	0.089	0.085	0.026	

TABLE 2.3 – Continued

PM I	NLTT	SDSS	RA J_{2000}	DEC J_{2000}	$\mu_{\rm tot}$ ($''$yr^{-1})	μRA ($''$yr^{-1})	μDE ($''$yr^{-1})	Notes
22418+0432			22:41:53.18	+04:33:00.2	0.226	0.115	−0.194	
22447+1513W			22:44:43.02	+15:13:46.3	0.291	0.162	0.241	
22497+3623	54984		22:49:46.43	+36:23:22.8	0.370	0.330	−0.167	
22595+5717			22:59:33.81	+57:17:57.3	0.334	−0.316	−0.109	
23003+2204			23:00:21.96	+22:04:16.0	0.225	0.201	0.102	
23027+4312			23:02:44.89	+43:12:47.7	0.181	−0.174	−0.051	
23056+4334			23:05:39.06	+43:34:03.8	0.270	−0.120	−0.230	
23098+5506E			23:09:58.53	+55:06:49.1	0.408	0.406	0.040	
23160+0559		J231605.60+05594	23:16:05.46	+05:59:46.6	0.178	0.175	0.034	
23229+3358			23:22:59.82	+33:58:47.1	0.179	0.128	0.125	
23234+7255			23:23:28.24	+72:55:07.4	0.088	0.069	0.055	
23243+2835			23:24:18.85	+28:35:55.5	0.134	−0.050	−0.124	
23283+3319			23:28:18.03	+33:19:31.1	0.147	0.053	−0.137	
23389+2101E			23:38:56.29	+21:01:18.2	0.338	0.290	0.174	
23390+5316			23:39:00.48	+53:16:00.0	0.467	0.466	0.033	
23462+1158			23:46:12.50	+11:58:49.7	0.136	−0.107	−0.084	
23475+0304		J234735.20+03043	23:47:35.11	+03:04:31.9	0.278	0.177	0.215	
23478+0223		J234753.64+02234	23:47:53.76	+02:23:40.8	0.224	−0.183	−0.129	

(1) Also in Vennes et al. (2011); (2) Classified using our own data, but SDSS spectrum exists; (3) Also in Kilic et al. (2010); (4) Also in Sayres et al. (2012); (5) Also in Tonry et al. (2012).

TABLE 2.4 – Spectroscopically Confirmed White Dwarfs from SUPERBLINK – Photometry

PM I	**FUV**	**NUV**	B_F	R_I	I_N	J	H	K_S	u	g	r	i	z	D_{phot} **(pc)**	**ST**	**Notes**
00023+6357	–	–	–	16.2	17.3	15.80	15.57	15.51	–	–	–	–	–	25.9	DC	
00079+3947	–	–	17.4	16.2	15.8	15.18	14.85	14.65	–	–	–	–	–	20.2	DC	
00217+2640	–	–	17.9	17.2	16.9	16.18	15.91	15.81	–	–	–	–	–	35.2	DC	
00276+0542	–	–	17.2	15.6	15.4	14.97	14.67	14.57	–	–	–	–	–	18.2	DA	
00331+4742S	14.55	14.63	14.9	14.9	–	15.16	15.02	15.14	–	–	–	–	–	50.8	DA	
00334+2506	–	20.36	16.6	16.6	16.1	15.96	15.70	15.45	17.88	17.12	16.79	16.69	16.68	37.0	DA	
00532+3927	–	18.45	17.9	16.4	16.8	16.03	15.84	15.40	–	–	–	–	–	54.4	DA	
00559+5948	–	–	15.2	16.0	15.8	15.44	15.21	15.03	–	–	–	–	–	32.1	DC:	
01043+3816	14.70	14.80	15.6	15.4	–	15.29	15.32	15.14	–	–	–	–	–	55.7	DA	
01216+3440	–	19.61	17.9	16.3	15.9	16.13	16.15	15.88	17.27	16.76	16.64	16.64	16.74	43.6	DZ	
01382+4442	–	–	15.5	16.0	15.2	15.62	15.61	15.71	–	–	–	–	–	60.5	DA	
01457+2918	–	–	18.4	18.0	17.7	16.56	16.09	15.51	–	–	–	–	–	31.1	DC	
01486+3615	–	20.64	17.6	16.5	16.3	15.85	15.48	15.42	–	–	–	–	–	37.0	DA	
01565+2955	14.56	14.68	14.7	14.9	–	14.96	15.04	15.18	–	–	–	–	–	46.8	DA	
02062+1836	–	–	19.2	17.8	17.1	16.50	16.38	15.63	–	–	–	–	–	31.0	DC:	
02118+7119	–	–	17.8	16.4	16.6	15.78	15.42	15.32	19.04	17.57	16.94	16.67	16.57	28.1	DC	
02149+7746	–	–	19.2	18.0	18.1	16.48	17.50	15.89	–	–	–	–	–	67.9	DC:	1
02230+5544	–	–	17.2	16.6	16.8	16.07	15.77	15.68	–	–	–	–	–	39.6	DA	
02237+2055	–	–	17.0	14.9	–	12.28	11.65	11.45	19.26	16.60	15.17	14.12	13.56	58.6	DC	
02334+2125	–	–	18.4	16.5	–	14.32	13.63	13.44	21.11	18.53	16.99	16.11	15.61	25.9	DC	
02379+1638	–	–	17.6	16.8	16.7	15.97	15.83	14.88	–	–	–	–	–	24.3	DC	
02478+4138	16.81	16.41	15.1	16.3	16.4	16.95	17.86	17.19	–	–	–	–	–	79.7	DB	
02497+3307	–	–	18.0	16.7	16.4	16.01	15.49	15.39	18.48	17.43	16.97	16.79	16.73	34.9	DA	
02557+2106S	–	–	17.7	17.1	16.5	16.48	16.04	16.06	18.47	17.68	17.36	17.25	17.20	41.3	DA	
02562+4954	–	–	17.5	17.1	16.4	16.17	15.79	15.45	–	–	–	–	–	30.1	DA	

TABLE 2.4 – Continued

PM I	**FUV**	**NUV**	B_F	R_I	I_N	J	H	K_S	u	g	r	i	z	D_{phot} **(pc)**	**ST**	**Notes**
03109+6634	–	–	18.8	17.7	17.4	16.55	16.30	15.31	–	–	–	–	–	29.4	DC	
03127+2218	–	19.86	17.8	16.4	16.8	16.13	15.85	15.88	–	–	–	–	–	46.8	DA	
03196+3630	–	20.96	17.3	16.2	16.1	15.84	15.84	15.38	–	–	–	–	–	36.7	DZ	
03203+2333	–	–	18.9	17.0	17.0	16.21	15.65	15.76	–	–	–	–	–	29.2	DC	
03433+1958	–	–	16.6	15.2	15.2	14.95	14.96	15.04	–	–	–	–	–	27.6	DA	
03473+4358	–	–	14.3	14.3	14.3	14.23	14.30	14.36	–	–	–	–	–	29.9	DA	
04010+5131W	–	–	17.5	16.8	16.4	15.93	15.74	15.20	19.33	17.78	17.08	16.83	16.72	141.5	DC	
04032+2520E	–	–	15.4	14.6	13.0	12.36	11.77	11.51	–	–	–	–	–	112.8	DA+dM	
04032+2520W	–	–	15.4	14.6	13.0	12.36	11.77	11.51	–	–	–	–	–	112.8	DA	
04259+4614	–	–	19.0	17.2	17.0	16.46	16.00	16.08	–	–	–	–	–	32.4	DC	
04263+4820	16.92	16.97	16.0	15.9	15.9	15.64	15.65	15.30	–	–	–	–	–	44.6	DA	2
04334+0414	–	–	17.4	16.3	16.1	15.55	15.26	15.18	–	–	–	–	–	27.5	DA	
04339+2827	–	–	16.0	15.8	–	15.48	14.79	14.56	–	–	–	–	–	56.5	DA	
04343+3054	–	–	18.8	17.6	17.5	16.49	16.35	15.83	–	–	–	–	–	36.3	DC:	
04389+6351	–	–	17.2	16.8	16.1	15.39	14.72	14.24	–	–	–	–	–	39.5	DA	
04523+2519	–	–	15.2	14.8	14.6	15.08	15.15	15.17	–	–	–	–	–	55.8	DA	3
04558+3840	–	–	18.1	16.9	16.8	16.14	15.85	15.32	–	–	–	–	–	32.5	DA	
04586+6209	–	–	15.5	14.1	–	11.31	10.76	10.55	–	–	–	–	–	78.7	DA+dM	
05025+5401	–	–	15.3	15.4	15.3	15.27	15.30	15.08	–	–	–	–	–	42.3	DA	
05158+2839	–	19.58	16.5	16.0	15.9	15.66	15.31	15.27	–	–	–	–	–	35.2	DAH	
05269+4435	–	–	18.8	17.4	17.5	16.50	16.42	15.85	–	–	–	–	–	36.7	DC	
05280+4850	18.18	17.53	17.2	15.0	13.1	12.60	12.00	11.73	–	–	–	–	–	124.2	DA+dM	
05327+0624	–	–	16.5	16.1	16.1	–	–	–	–	–	–	–	–	59.5	DA	4
05492+5747	–	–	15.8	14.7	13.6	12.76	12.21	12.00	–	–	–	–	–	86.9	DA+dM	
06019+3726	–	–	16.4	17.0	16.3	–	–	–	–	–	–	–	–	35.5	DAH	

TABLE 2.4 – Continued

PM I	**FUV**	**NUV**	B_F	R_I	I_N	J	H	K_S	u	g	r	i	z	D_{phot} **(pc)**	**ST**	**Notes**
06026+0904	–	–	17.4	16.5	16.0	15.95	15.54	15.25	–	–	–	–	–	27.9	DA	
06324+2230	–	–	–	17.1	16.5	16.12	15.81	15.76	–	–	–	–	–	35.5	DA	
06492+1519	–	–	18.1	17.3	16.6	–	–	–	–	–	–	–	–	35.8	DC	
06506+1657	–	–	17.9	16.9	16.6	16.14	15.73	15.31	–	–	–	–	–	32.7	DA	
06513+6242	–	20.38	17.5	17.6	16.8	–	–	–	–	–	–	–	–	62.2	DAH	
06538+6355	–	20.47	16.7	15.8	–	15.28	15.10	14.91	–	–	–	–	–	28.0	DA	
06556+5920	–	–	15.9	14.7	13.2	12.05	11.41	11.17	–	–	–	–	–	79.4	DA+dM	
07029+4406	18.08	16.04	15.2	15.4	15.3	15.30	15.31	15.48	–	–	–	–	–	46.5	DA	
07241+0431	–	–	19.1	17.5	17.2	–	–	–	–	–	–	–	–	31.5	DA	
07270+1434	–	–	17.2	16.2	16.2	15.71	15.27	15.18	18.21	17.14	16.69	16.51	16.45	30.9	DA	
07419+0136	–	21.57	18.6	18.4	17.3	–	–	–	–	–	–	–	–	90.2	DC	
07419+1511	15.75	15.88	15.2	15.5	–	16.06	16.12	15.91	16.01	15.73	16.02	16.19	16.53	76.3	DA	
07451+2627	–	–	20.1	18.6	17.9	–	–	–	22.06	19.98	18.74	18.18	17.98	32.6	DC	
07475+1107	–	–	16.6	16.4	16.5	16.10	15.77	15.64	17.13	16.74	16.68	16.69	16.78	53.4	DA	
08126+1737	13.17	13.76	13.5	13.8	–	13.76	13.84	13.94	14.01	14.55	15.20	14.23	14.26	27.7	DA	
08152+1633	–	–	18.9	17.9	17.7	16.78	16.14	15.67	20.80	19.00	18.16	17.84	17.69	41.1	DC:	5
08223+2023	–	18.38	16.4	15.6	–	15.62	15.48	15.39	16.73	16.26	16.12	16.13	16.22	37.6	DC	5
08281+0942	–	–	19.0	17.8	17.7	–	–	–	21.09	19.16	18.19	17.82	17.63	29.4	DC	
08293+2539	–	–	20.1	18.4	17.9	16.83	16.93	17.10	21.45	19.21	18.29	17.97	17.86	80.5	DC	
08516+1624	–	21.72	16.9	16.4	16.0	15.75	15.69	15.70	17.87	16.96	16.60	16.46	16.43	33.4	DC	
08558+3700	–	–	17.9	17.1	16.5	16.51	16.17	15.85	19.07	17.96	17.48	17.28	17.25	43.7	DA	
09021+2010	–	21.74	18.9	17.4	17.3	–	–	–	18.94	18.86	17.79	17.25	17.29	27.5	DQ	5
09026+1535	–	–	18.6	17.4	–	16.23	16.08	15.20	20.41	18.51	17.65	17.32	17.18	31.0	DC	5
09027+3120	–	–	14.9	14.9	–	15.05	14.90	15.07	15.62	15.28	15.30	15.39	15.56	36.7	DA	
09033+2012	–	19.26	17.5	16.8	16.7	16.27	16.19	15.86	17.59	17.07	16.91	16.88	16.96	52.5	DA	5

TABLE 2.4 – Continued

PM I	**FUV**	**NUV**	B_F	R_I	I_N	J	H	K_S	u	g	r	i	z	D_{phot} **(pc)**	**ST**	**Notes**
09106+2156	–	–	17.7	17.1	16.6	16.31	16.11	16.03	18.65	17.66	17.22	17.06	17.00	42.1	DA	
09245+3120	–	–	18.1	17.4	17.5	16.47	15.97	16.91	20.53	18.73	17.94	17.63	17.52	57.7	DC	5
09286+1841	–	18.28	16.9	16.4	–	15.99	16.27	15.68	17.09	16.70	16.58	16.57	16.68	51.8	DA	5
09432+5134	–	–	19.1	17.5	17.5	16.68	16.60	16.07	20.77	18.92	18.13	17.83	17.69	39.9	DC	
09481+2023	–	–	18.7	17.3	17.3	16.62	16.26	15.74	20.32	18.53	17.76	17.46	17.34	36.6	DC	5
09503+1509	–	–	18.5	17.2	–	16.16	15.95	15.36	19.14	17.94	17.39	17.17	17.10	32.8	DC	1
10155+1850	–	–	19.2	18.4	–	16.73	16.97	16.50	21.32	19.40	18.44	18.14	18.01	45.7	DC	5
10289+1105	15.75	15.68	15.3	15.4	–	15.99	15.95	15.40	15.86	15.49	15.77	16.01	16.26	65.9	DA	
10403+1004	–	21.12	17.7	16.7	–	16.01	16.33	16.10	18.19	17.42	17.07	16.96	16.95	46.1	DC	
10521+4050	–	–	17.7	16.6	16.5	16.11	15.53	15.21	17.67	17.00	16.69	16.60	16.61	34.0	DC	
10565+2336	–	–	19.0	17.6	17.5	16.52	16.57	16.25	19.83	18.41	17.77	17.55	17.41	43.2	DA	
11036+1555	–	–	15.6	13.8	–	11.57	11.16	10.76	18.60	15.88	14.72	17.14	12.86	107.7	DA+dM	
11071+1446	–	19.38	17.4	16.6	15.9	15.75	15.47	15.42	17.39	16.77	16.53	16.45	16.48	39.1	DA	
11253+2111	–	19.83	16.8	16.7	16.6	16.24	16.18	15.65	17.88	17.18	16.90	16.79	16.79	45.4	DC	
11337+6243	–	19.52	16.5	15.9	15.4	15.57	15.39	15.56	17.09	16.50	16.27	16.20	16.23	33.8	DA	
11401+0112W	19.48	16.73	15.2	14.2	13.5	–	–	–	16.19	15.77	15.83	15.89	16.08	54.2	DA	
11545+2422	21.23	16.95	15.6	15.2	15.4	15.24	15.11	15.40	15.94	15.60	15.61	15.66	15.80	37.8	DA	5
11582+0004	–	–	18.7	17.9	17.5	16.72	15.99	17.20	20.92	18.89	17.86	17.52	17.34	65.8	DC	
11592+4842	–	21.62	18.5	17.5	16.9	16.47	15.96	16.08	18.65	17.74	17.34	17.17	17.15	44.5	DA(Z?)	
11598+0007	–	17.29	15.5	16.0	–	15.62	15.37	15.54	16.00	15.75	15.81	15.87	16.01	41.1	DA	
12113+0724	–	–	17.2	16.1	16.4	15.37	15.09	15.10	18.51	17.14	16.52	16.30	16.20	24.8	DA	
12155+4630	–	19.83	17.1	16.7	16.4	16.18	16.07	15.74	17.85	17.24	17.01	16.95	16.98	48.4	DA	
12273+3150	–	21.69	16.2	15.4	–	14.47	14.09	14.08	17.51	16.23	15.69	15.50	15.44	39.7	DA	5
12280+3300	–	–	18.6	17.7	17.3	16.70	16.16	16.01	20.71	18.88	17.97	17.61	17.46	34.8	DC	5
12370+1814	19.47	17.79	17.8	16.8	16.6	–	–	–	16.96	16.78	16.88	17.02	17.16	78.2	DC	5

TABLE 2.4 – Continued

PM I	**FUV**	**NUV**	B_F	R_I	I_N	J	H	K_S	u	g	r	i	z	D_{phot} **(pc)**	**ST**	**Notes**
12377+6023	–	–	18.4	17.5	17.6	16.65	15.99	15.60	19.81	18.48	17.87	17.67	17.57	39.8	DA	
12405+1807W	–	–	19.1	17.3	16.9	16.59	15.93	15.79	19.20	17.99	17.41	17.19	17.11	38.0	DA	
12425+1311W	–	–	19.5	18.0	17.6	–	–	–	20.42	18.74	18.05	17.80	17.69	38.7	DC	
12476+0646	–	–	20.2	18.5	18.0	–	–	–	20.93	20.03	18.67	18.37	18.22	39.4	DQpec	5
12541+3620	–	–	18.1	16.7	16.1	15.90	15.72	15.40	19.74	17.93	17.15	16.83	16.66	26.9	DC	
13103+1404	22.12	17.71	16.2	16.3	–	15.84	15.89	15.67	16.79	16.33	16.34	16.40	16.51	49.7	DA	5
13176+0621	–	–	19.3	17.5	16.1	–	–	–	19.98	18.62	17.97	17.74	17.67	46.3	DA:	
13246+0857	–	18.10	17.4	16.3	15.1	16.17	16.17	15.81	17.08	16.63	16.60	16.62	16.73	55.9	DA	5
13333+2450	–	–	20.2	19.0	18.0	–	–	–	21.42	19.44	18.55	18.21	18.03	45.0	DC	5
13349+6945	15.61	15.76	15.9	15.6	15.2	15.93	16.23	15.58	–	–	–	–	–	61.8	DA	
13455+4200	–	–	17.9	16.4	16.3	15.61	15.43	14.99	19.76	17.86	17.01	16.71	16.55	23.4	DC	
13521+1053	–	–	17.1	16.0	16.0	15.74	15.59	15.06	17.92	17.10	16.74	16.57	16.55	30.7	DA	
14067+3130	–	–	19.4	17.3	17.3	16.61	15.88	16.12	20.54	18.72	17.92	17.64	17.52	35.8	DC	
14106+0245	–	–	16.9	16.2	16.0	15.48	15.14	15.02	18.05	17.00	16.50	16.33	16.27	27.6	DAZ	
14149+4336	–	–	18.2	17.3	16.8	16.46	15.76	15.67	18.22	17.54	17.25	17.19	17.16	46.4	DA	5
14236+3037	–	–	18.8	17.3	16.8	16.44	16.18	15.67	19.51	18.15	17.56	17.36	17.28	40.3	DA	5
14244+6246	–	–	19.4	17.8	17.7	–	–	–	20.35	18.83	18.14	17.86	17.70	45.0	DA	
14277+0532	–	–	20.6	19.2	17.3	15.31	14.59	14.29	17.61	17.02	16.86	16.82	16.86	50.0	DA	5
14339+1907	–	–	19.1	18.1	17.5	16.88	16.07	15.33	20.42	18.76	18.10	17.82	17.74	39.7	DA	
14407+0807	–	–	19.3	17.6	17.0	16.54	15.94	16.30	19.20	18.01	17.48	17.30	17.20	46.8	DA	
14553+5655	14.65	14.85	15.4	14.7	14.1	15.13	15.15	15.40	14.96	14.67	14.98	15.24	15.52	50.9	DA	
14588+1146	–	–	18.9	17.5	17.6	–	–	–	20.67	18.86	18.02	17.71	17.66	36.5	DC	
15164+2803	–	18.24	17.6	16.3	–	15.98	16.26	15.70	17.01	16.59	16.52	16.52	16.62	50.3	DAH	5
15206+3903	–	–	16.9	16.9	16.7	16.35	16.52	15.83	17.44	16.95	17.00	16.82	16.79	60.6	DA	
15263+2936	–	–	18.4	16.1	15.8	15.30	14.97	14.80	18.64	17.12	16.46	16.20	16.11	11.7	DA	

TABLE 2.4 – Continued

PM I	**FUV**	**NUV**	B_F	R_I	I_N	J	H	K_S	u	g	r	i	z	D_{phot} **(pc)**	**ST**	**Notes**
15342+0218	–	17.73	16.5	16.7	–	15.78	15.79	15.56	16.68	16.31	16.27	16.30	16.41	46.5	DA	5
15359+2125	–	–	17.4	16.6	16.7	16.29	16.08	16.98	18.28	17.53	17.22	17.12	17.12	67.9	DA	
15494+4802	–	–	17.0	16.9	16.8	16.63	15.85	16.75	18.03	17.41	17.16	17.09	17.11	60.5	DC	5
15589+0417	22.95	18.80	16.6	–	15.8	15.46	15.27	14.82	16.86	16.26	15.97	15.96	16.09	32.9	DC	5
16053+5556	–	–	17.5	17.4	16.6	15.98	15.53	15.57	18.28	17.68	17.49	18.74	17.29	28.9	DA	
16096+4735	–	–	16.3	16.3	16.1	–	–	–	16.74	16.37	16.63	16.86	17.17	106.7	DA	
16171+0530	15.01	15.14	15.1	14.6	13.6	11.53	10.96	10.67	15.11	14.62	14.60	13.81	13.06	44.5	DA+dM	
16264+1938	–	–	17.0	16.2	15.8	15.64	15.33	15.41	17.61	16.83	16.48	16.35	16.36	33.1	DA	
16325+0851	–	–	15.7	14.6	14.4	13.85	13.61	13.49	16.44	15.34	14.88	14.69	14.64	13.4	DA	
16335+5231	–	–	18.1	17.5	16.8	16.37	16.19	15.70	18.10	17.49	17.23	17.15	17.13	42.0	DA	
16477+2636	–	–	17.4	17.0	16.7	16.10	17.33	14.33	17.51	17.02	16.90	16.95	17.09	63.5	DZ	5
16546+5742	20.81	17.19	16.0	16.0	15.3	15.65	15.95	15.20	–	–	–	–	–	40.4	DA	
17027+1022	–	–	18.4	17.3	16.8	16.41	16.05	17.04	19.81	18.27	17.61	17.38	17.25	68.7	DC:	
17052+0423	–	–	16.2	16.0	15.5	15.70	15.65	15.40	–	–	–	–	–	46.0	DA	
17238+0458	–	18.29	17.0	16.7	16.4	16.40	16.05	15.86	–	–	–	–	–	51.1	DA	
17283+0211	–	–	16.1	15.6	15.7	15.67	15.95	15.94	–	–	–	–	–	45.9	DA	
17335+7949	–	–	18.0	16.0	15.8	16.06	16.05	15.48	–	–	–	–	–	31.7	DC	
17417+2401	–	–	16.8	16.5	15.9	15.99	15.57	15.70	–	–	–	–	–	41.2	DA	
17433+1434S	–	–	14.9	14.2	13.7	14.89	14.83	15.05	–	–	–	–	–	43.6	DC	
17471+2859	–	–	18.1	17.1	16.8	16.23	16.17	16.16	–	–	–	–	–	46.8	DC	
18014+5049	–	–	18.2	17.1	16.5	16.00	16.20	15.94	19.87	18.15	17.33	17.05	16.91	28.5	DC	
18073+0357	–	–	15.6	14.8	14.4	14.57	14.51	14.46	–	–	–	–	–	25.4	DA	
18138+2119	–	–	15.9	15.8	–	15.70	15.63	15.55	–	–	–	–	–	49.4	DA	
18199+1739	–	–	18.4	17.5	17.3	16.39	16.02	15.96	–	–	–	–	–	34.1	DC	
18572+2026	–	–	16.3	16.5	16.3	15.87	15.61	16.11	–	–	–	–	–	61.9	DA	

TABLE 2.4 – Continued

PM I	**FUV**	**NUV**	B_F	R_I	I_N	J	H	K_S	u	g	r	i	z	D_{phot} **(pc)**	**ST**	**Notes**
19128+5343	–	–	13.2	13.2	12.9	13.62	13.73	13.82	–	–	–	–	–	33.1	DA	
19132+2949	–	–	17.4	17.0	15.9	16.12	15.67	15.48	–	–	–	–	–	30.8	DA	
19146+1428	–	–	16.5	15.1	15.6	15.26	14.92	14.78	–	–	–	–	–	26.0	DA	
19464+0937	–	–	17.1	16.9	16.2	–	–	–	–	–	–	–	–	39.4	DA	
19493+0747	–	–	15.1	15.6	15.2	15.21	15.27	15.17	–	–	–	–	–	41.8	DA	
20062+5902	15.58	15.61	16.2	16.3	15.8	15.70	15.87	15.10	15.75	15.36	15.64	15.87	16.15	55.9	DA	
20069+6143	–	–	17.5	16.2	16.0	15.17	14.90	14.68	18.16	16.91	16.34	16.12	16.06	22.9	DA	
20223+8333	–	–	17.5	16.8	16.7	16.17	16.40	15.99	–	–	–	–	–	46.0	DC	
20235+7001	–	–	19.1	17.9	17.4	–	–	–	–	–	–	–	–	107.0	DA	
20597+5517	–	–	18.7	17.0	16.4	15.66	15.45	15.49	19.97	17.97	17.02	16.66	16.49	21.5	DC	
21077+0740	–	18.63	16.3	15.8	–	15.77	15.79	15.14	–	–	–	–	–	34.7	DA	
21117+0120	15.01	15.12	15.2	15.1	–	15.52	15.69	15.32	–	–	–	–	–	60.5	DA	
21134+0727	–	–	16.0	15.6	15.8	15.21	14.95	14.81	–	–	–	–	–	28.7	DA	
21222+0413	–	–	17.5	16.2	15.7	15.24	15.01	14.88	18.86	17.20	16.49	16.23	16.12	20.7	DA	
21384+1856	–	–	17.5	16.7	16.3	15.96	15.38	15.45	19.72	18.10	17.59	17.52	17.45	31.5	DA	
21420+2252	–	–	15.9	16.1	15.6	15.98	15.74	15.54	–	–	–	–	–	47.7	DZ	
21429+0805	–	–	18.0	15.6	15.5	15.77	15.27	15.18	–	–	–	–	–	25.7	DA	
21492+0415	–	–	17.4	15.5	15.3	15.38	15.21	15.10	–	–	–	–	–	25.2	DA	
21551+4103	–	–	17.9	16.4	16.3	16.18	15.80	15.80	–	–	–	–	–	36.8	DZA	
21597+2936	13.47	13.94	14.7	15.5	–	15.83	15.90	15.36	–	–	–	–	–	74.6	DA	
22105+4532	–	–	18.1	17.1	16.5	16.20	15.97	15.74	–	–	–	–	–	33.6	DC	
22118+5649	–	–	13.9	13.6	13.4	13.19	12.99	12.86	–	–	–	–	–	11.4	DA	
22276+1753	–	–	16.8	16.0	15.2	15.85	15.57	15.47	–	–	–	–	–	39.4	DA	
22299+3024	18.61	17.02	16.1	16.0	–	15.55	15.22	15.02	–	–	–	–	–	79.7	DA	
22331+2610	15.63	15.72	15.6	15.3	–	15.94	15.65	16.01	–	–	–	–	–	71.1	DA	

TABLE 2.4 – Continued

PM I	FUV	NUV	B_F	R_I	I_N	J	H	K_S	u	g	r	i	z	D_{phot} (pc)	ST	Notes
22418+0432	–	–	18.7	17.6	17.2	–	–	–	–	–	–	–	–	81.1	DQ	
22447+1513W	–	–	19.0	17.8	17.3	–	–	–	–	–	–	–	–	65.6	DA	
22497+3623	–	–	19.1	17.7	16.9	16.58	16.22	17.12	–	–	–	–	–	73.3	DA	
22595+5717	–	–	19.1	17.2	16.0	16.18	15.93	15.20	–	–	–	–	–	26.9	DA	
23003+2204	–	–	17.8	17.0	16.6	–	–	–	–	–	–	–	–	54.2	DZ	
23027+4312	–	–	17.7	16.2	16.4	15.96	15.97	17.03	–	–	–	–	–	95.0	DA	
23056+4334	–	–	19.4	18.1	17.5	16.76	16.04	16.47	–	–	–	–	–	33.5	DA	
23098+5506E	–	–	20.9	18.9	17.2	15.77	15.26	14.82	–	–	–	–	–	4.9	DA	
23160+0559	–	–	17.1	17.1	16.5	–	–	–	16.95	16.63	16.91	17.14	17.39	69.7	DA	
23229+3358	–	–	16.2	15.4	13.2	13.14	12.59	12.28	–	–	–	–	–	114.9	DA+dM	
23234+7255	–	18.33	16.8	16.0	16.1	15.83	15.77	16.16	–	–	–	–	–	56.6	DA	
23243+2835	–	18.53	16.3	15.9	–	15.60	15.24	15.41	–	–	–	–	–	37.5	DA	
23283+3319	15.85	15.91	15.1	14.9	–	12.14	11.62	11.42	–	–	–	–	–	81.2	DA+dM	
23389+2101E	–	–	18.2	16.8	17.2	16.32	16.18	15.14	–	–	–	–	–	51.6	DA	
23390+5316	–	–	17.0	16.9	16.2	16.10	15.48	15.63	–	–	–	–	–	29.7	DA	
23462+1158	–	21.57	18.1	17.0	16.6	16.33	15.93	15.62	–	–	–	–	–	39.1	DC	
23475+0304	–	–	17.8	16.2	15.5	15.61	15.60	15.87	19.13	17.24	16.52	16.25	16.16	38.3	DC	
23478+0223	–	–	18.8	17.5	16.5	16.44	16.28	16.30	20.00	18.55	17.91	17.64	17.59	44.2	DA	

(1) Spectral range of $\lambda\lambda 3200 - 5300$; H$\alpha$ data will be obtained to confirm DC status; (2) DA+DC candidate; (3) Magnetic candidate; (4) DA+DA candidate; (5) Classified using our own data, but SDSS spectrum exists.

2.7 Atmospheric Parameter Determination of DA Stars

The coolest white dwarfs in our sample are either featureless, or present too few spectral lines for a proper spectroscopic analysis, and the determination of their atmospheric parameters ($T_{\rm eff}$, $\log g$) can only be achieved from an analysis of their photometric energy distribution (see, e.g., Bergeron et al. 1997). At the moment, not enough photometric information is available to proceed with a homogeneous analysis of the coolest objects in our sample, and we are still securing the appropriate optical and infrared photometry for cool DA, DC, DQ, and DZ stars, the results of which will be reported in subsequent papers. We thus restrict our determination of the atmospheric parameters to the subsample of 84 spectroscopically confirmed DA stars for which the spectroscopic technique can be successfully applied.

2.7.1 Theoretical Framework

Our model atmospheres and synthetic spectra for DA stars are built from the model atmosphere code originally described in Bergeron et al. (1995) and references therein, with recent improvements discussed in Tremblay & Bergeron (2009). These are pure hydrogen, plane-parallel model atmospheres, with non-local thermodynamic equilibrium effects explicitly taken into account above $T_{\rm eff} = 30,000$ K, and energy transport by convection is included in cooler models following the ML2/$\alpha = 0.7$ prescription of the mixing-length theory. The theoretical spectra are calculated within the occupation formalism of Hummer & Mihalas (1988), which provides a detailed treatment of the level populations as well as a consistent description of bound-bound and bound-free opacities. We also rely on the improved calculations for the Stark broadening of hydrogen lines from Tremblay & Bergeron (2009), which include nonideal perturbations from protons and electrons directly inside the line profile calculations. Our model grid covers a range of effective temperature between $T_{\rm eff} = 1500$ K and 120,000 K, and $\log g$ values between 6.0 and 9.5.

Our fitting technique is based on the approach pioneered by Bergeron et al. (1992, see also Liebert et al. 2005), which relies on the nonlinear least-squares method of Levenberg-Marquardt (Press et al. 1986). The optical spectrum of each star, as well as the model spectra (convolved with a Gaussian instrumental profile), are first normalized to a continuum set

to unity. The calculation of χ^2 is then carried out in terms of these normalized line profiles only. The atmospheric parameters – $T_{\rm eff}$, $\log g$ – are considered free parameters in the fitting procedure.

Special care needs to be taken in the case of DA stars with an unresolved M dwarf companion in order to reduce the contamination of the white dwarf spectrum by the companion. When the contamination affects only Hβ, and sometimes Hγ as well, we simply exclude these lines from the fit (e.g., 05280+4820 and 23229+3358). At other times, emission lines from the M dwarf are also observed in the center of the Balmer lines, in which case the line centers are also simply excluded from our fitting procedure (e.g., 04586+6209). A similar approach was also adopted if the flux contribution from the M dwarf is too important and "fills up" the Balmer line cores, resulting in predicted lines that are too deep (06556+5920, 16171+0530, and 23283+3319). In some cases, however, the white dwarf spectrum is too contaminated by the M dwarf companion to be fitted with the simple approach described above (e.g., 04032+2325E — not to be confused with the DA star 04032+2325W — and 11036+1555 [12]), and a more robust fitting procedure using M dwarf templates will be required (Gianninas et al. 2011). These results will be presented elsewhere.

2.7.2 Spectroscopic Results

Even though the spectroscopic technique is arguably the most accurate method for measuring the atmospheric parameters of DA stars, it has an important drawback at low effective temperatures ($T_{\rm eff} \lesssim 13,000$ K) where spectroscopic values of $\log g$ are significantly larger than those of hotter DA stars, the so-called high-$\log g$ problem (see Tremblay et al. 2010 and references therein). Tremblay et al. (2011b) showed that this high-$\log g$ problem is actually related to the limitations of the mixing-length theory used to describe the convective energy transport in DA stars, and that more realistic, 3D hydrodynamical model atmospheres are required in order to obtain a surface gravity distribution that resembles that of hotter radiative-atmosphere DA stars. Since these spurious high-$\log g$ values affect directly the estimated distances, Giammichele et al. (2012) derived an empirical procedure (see their Section

12. In the case of 11036+1555, we even detect the 4226 Å line from the M dwarf in the white dwarf spectrum.

5 and Figure 2.16) to correct the $\log g$ values based on the DA stars in the Data Release 4 of the Sloan Digital Sky Survey, analyzed by Tremblay et al. (2011a). We adopt a similar approach here and apply their $\log g$ correction to all DA stars between $T_{\rm eff}$ = 7000 K and 14,000 K.

The spectroscopic fits for our subsample of 84 DA stars are displayed in Figure 2.17. The corresponding atmospheric parameters ($T_{\rm eff}$ and $\log g$) are reported in Table 2.5 together with the stellar mass ($M/M_{\odot}$), absolute absolute visual magnitude (M_V), luminosity ($L/L_{\odot}$), estimated visual magnitude (V), spectroscopic distance (D), and white dwarf cooling time (τ). Whenever necessary, we rely on the same evolutionary models as those described above to derive these quantities. In principle, the spectroscopic distance can be obtained directly from the distance modulus, by combining the theoretical absolute magnitude in a single given bandpass with the observed magnitude in the same bandpass. However, since the photometric errors can be large in some systems we used — the USNO photographic magnitudes in particular —, we estimated the spectroscopic distances by using the full set of photometry available for each star, and calculated an average spectroscopic distance, properly weighted by the photometric uncertainties in each bandpass. This is equivalent to using the photometric method described above but by forcing the effective temperature at the spectroscopic value, thus fitting only the solid angle $\pi(R/D)^2$, where R is the radius of the star determined from the spectroscopic $\log g$ value. In doing so, we also fold in the uncertainty of the spectroscopic $\log g$ measurement.

The mass distribution for the DA stars in our sample is displayed in Figure 2.18 as a function of effective temperature. This figure clearly illustrates the efficiency of our survey to identify white dwarfs using reduced proper motion diagrams even at very low effective temperatures. We also distinguish with various color codes the criteria used in our survey to discover each white dwarf, allowing us to study the impact of one particular photometric system on the selection process as a function of temperature. For instance, white dwarfs identified on the basis of *GALEX* photometry extend down to relatively low effective temperatures. Indeed, the observed photometric sequence allows us to apply our selection criteria down to NUV $- V = 6.5$ (see Figure 2.6), or $T_{\rm eff} \sim 5300$ K. Similarly, white dwarfs identified on the basis of *ugriz* photometry are mostly found at the low end of the temperature distri-

bution. Most SDSS targets are intrinsically faint, and thus include an impressive amount of cool white dwarfs that can only only be identified through the use of reduced proper motion diagrams. Surprisingly, white dwarfs identified on the basis of 2MASS photometry are found at all temperatures. This is due to the fact that our photometric sequences allow us to apply our color criteria as blue as $V - J = -0.5$ (see Figure 2.7), or $T_{\rm eff}$ $\sim$20,000 K. Finally, only a few white dwarfs in this subsample were identified on the basis of USNO photographic magnitudes. From these results, we can conclude that even though SDSS represents the most reliable photometric data set, *GALEX*, 2MASS, and even photometric magnitudes are also required to identify white dwarfs over the complete range of effective temperature.

The mass distribution of DA white dwarfs in our subsample, regardless of their temperature, is displayed in Figure 2.19. The mean mass of these 84 DA stars is 0.689 $M_{\odot}$ with a standard deviation of $\sigma = 0.172$ $M_{\odot}$, a value significantly larger than the value obtained by Giammichele et al. (2012) for the DA white dwarfs within 20 pc of the Sun (0.647 $M_{\odot}$ with $\sigma = 0.171$ $M_{\odot}$). One obvious difference is that we do not include here the white dwarfs already known in the literature. Most likely these are brighter, intrinsically more luminous, and probably have larger radii and thus lower masses. The mass distribution of the 37 DA white dwarfs within 40 pc of the Sun displayed in Figure 2.19 (shaded histogram) actually shows an important high-mass component (see also Figure 2.18). These high-mass white dwarfs, with their small stellar radii, are intrinsically less luminous than their normal-mass counterparts, and they are thus more abundant in a volume-limited sample, such as the local neighborhood, than in a magnitude-limited sample. Our results indicate that we are successfully recovering these high-mass white dwarfs in our survey, often missing in magnitude-limited surveys (see, e.g., Liebert et al. 2005 in the case of the PG survey).

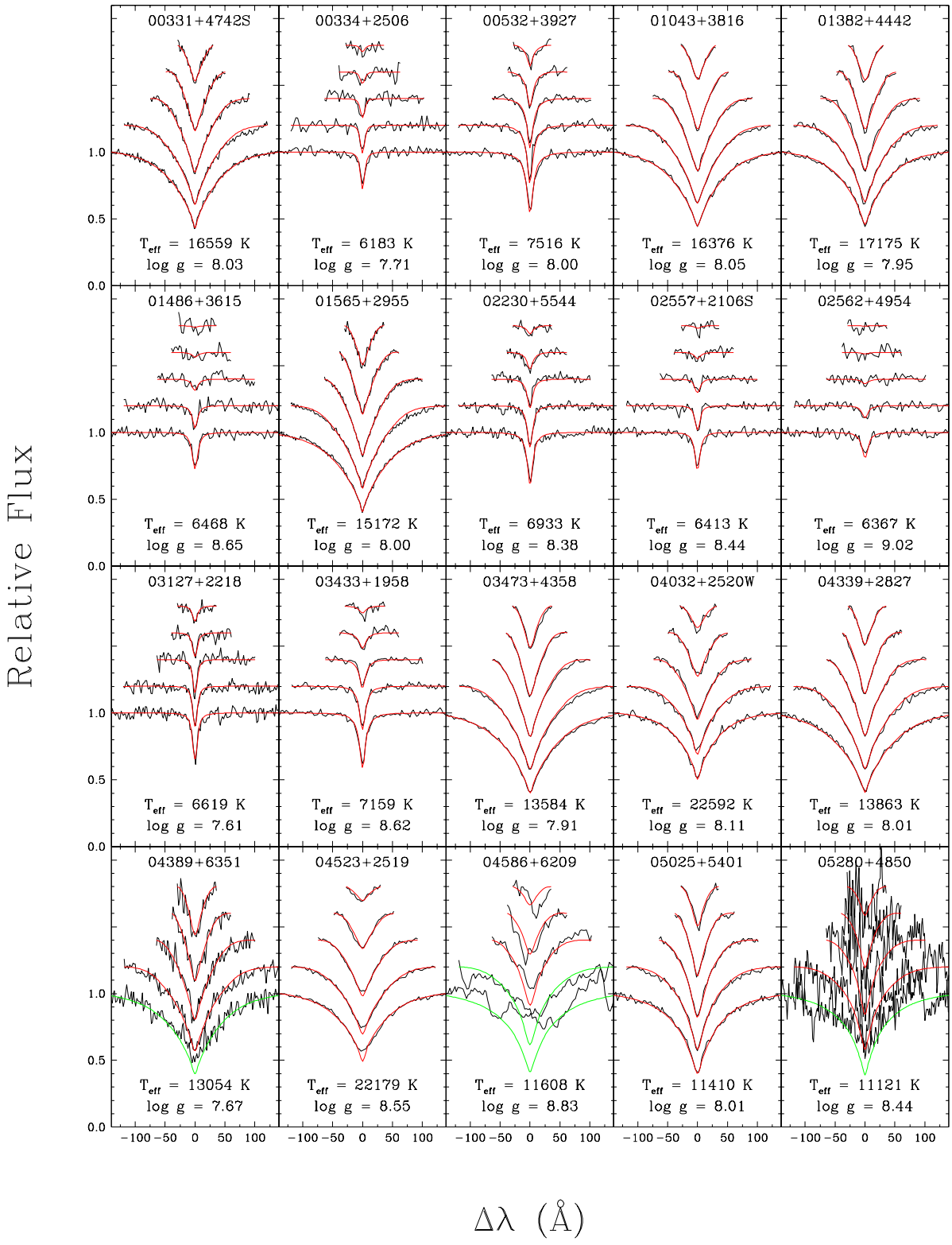

FIGURE 2.17 – (a) - Fits to the optical spectra of the DA stars in our sample. The lines range from Hβ (bottom) to H8 (top), each offset vertically by a factor of 0.2. Theoretical line profiles shown in green are not used in the fitting procedure.

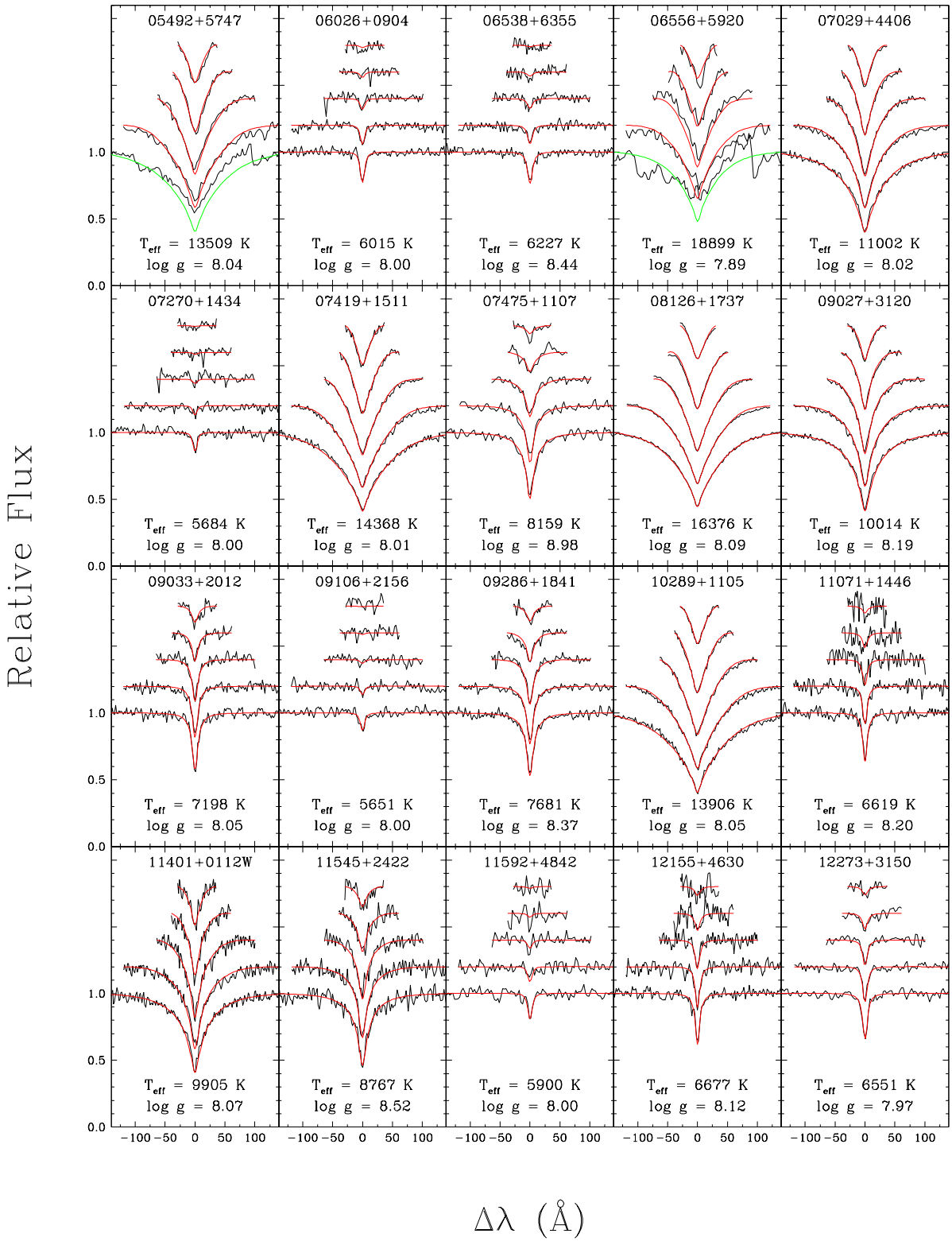

FIGURE 2.17 – (b) -continued.

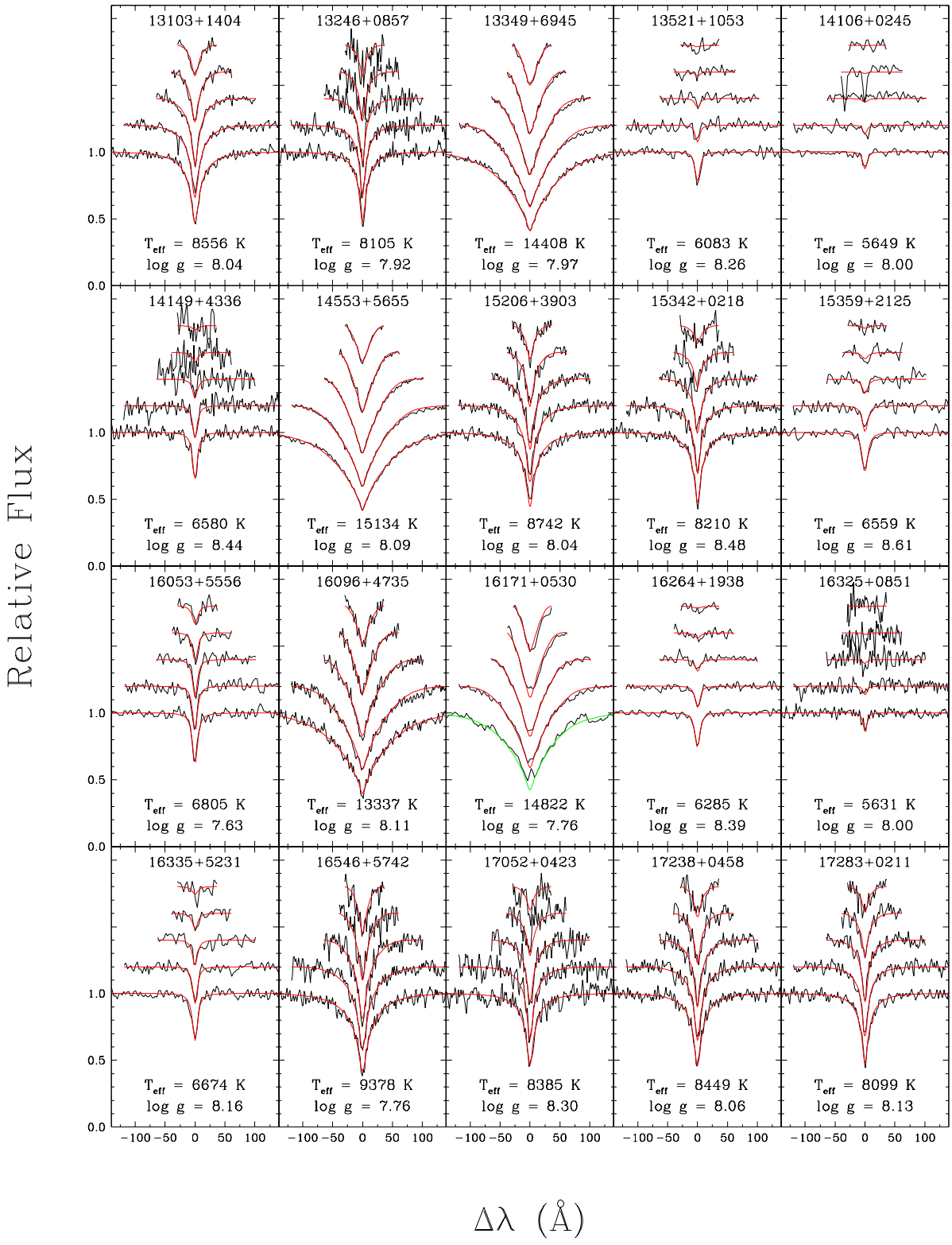

FIGURE 2.17 – (c) - continued

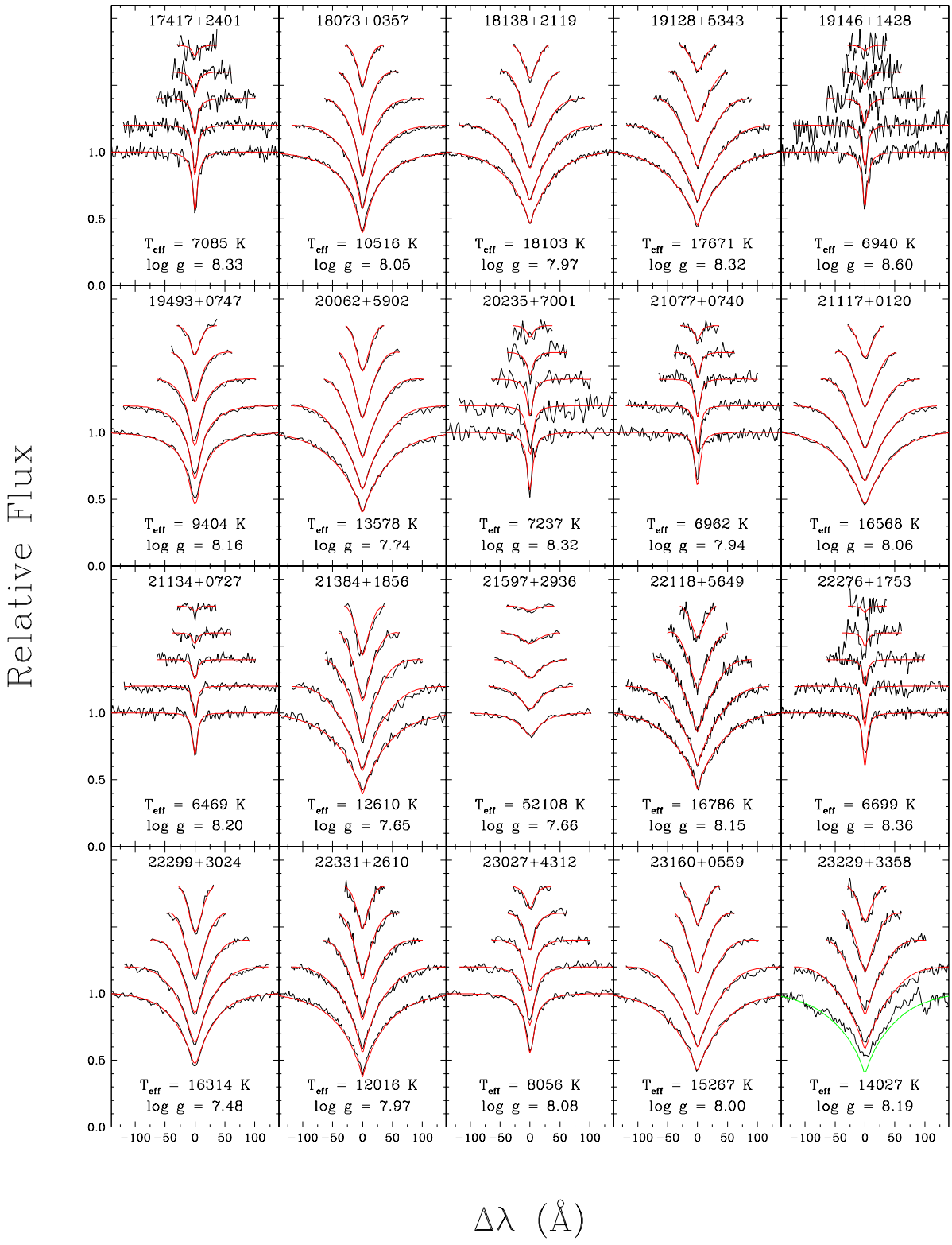

FIGURE 2.17 – (d) - continued

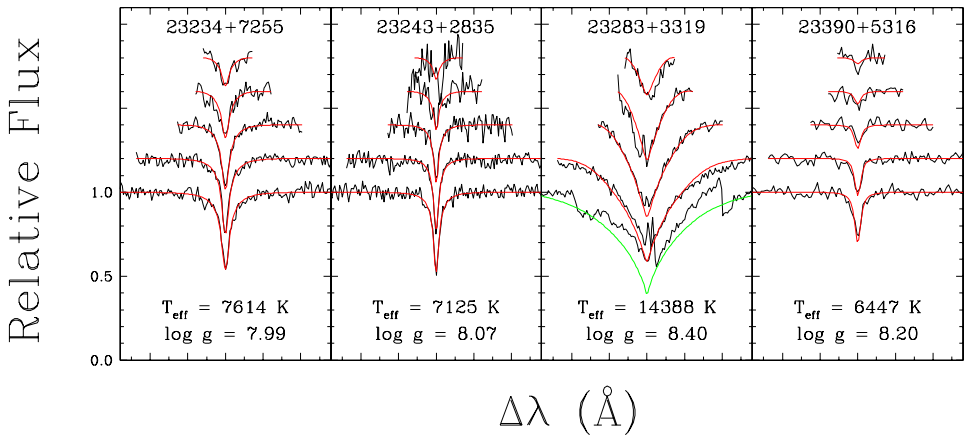

FIGURE 2.17 – (e) - continued

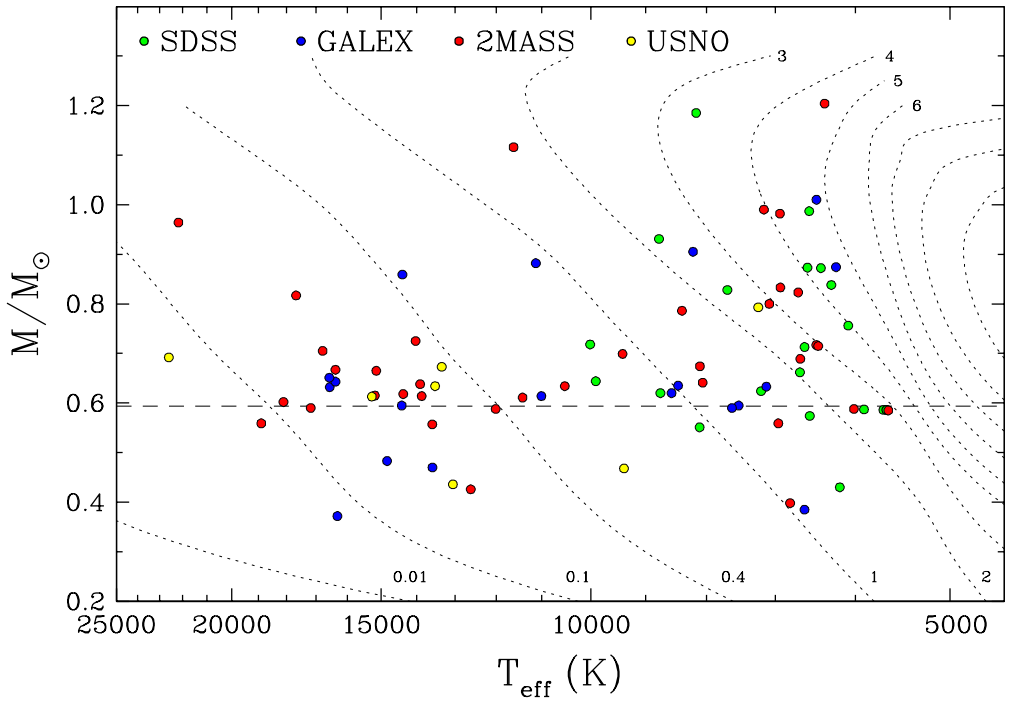

FIGURE 2.18 – Mass as a function of effective temperature for a subsample of 84 DA white dwarfs with spectroscopic mass determinations. All stars are identified with a different color based on the photometric system from which they were discovered. The dotted lines represent the theoretical isochrones for our C/O core evolutionary models with thick hydrogen layers, corresponding to the white dwarf cooling age in units of Gyr. The dashed line indicates the median mass of DA white dwarfs, 0.594 $M_{\odot}$, as determined by Tremblay et al. (2011a).

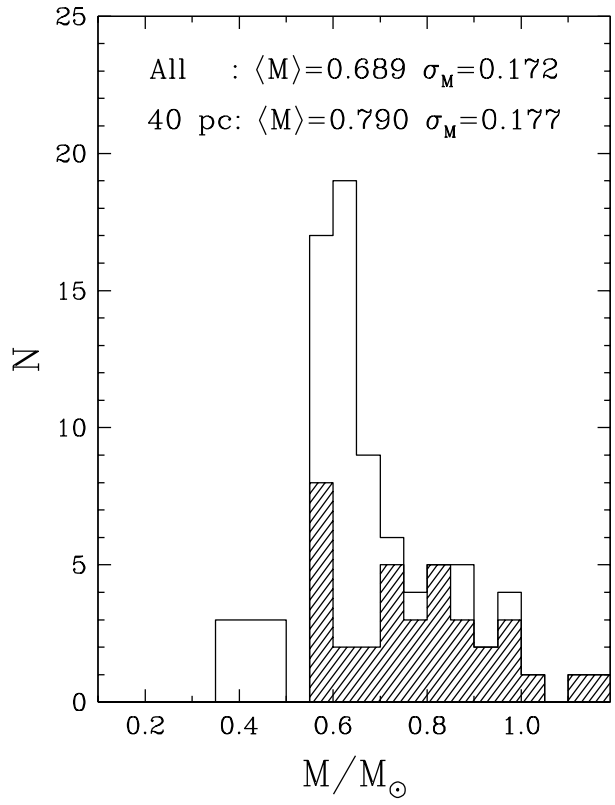

FIGURE 2.19 – Mass distribution for the DA white dwarfs in our sample. The solid line histogram shows the distribution for the 84 DA stars with spectroscopic masses available, while the shaded histogram corresponds to the subsample of 37 objects with spectroscopic distances less than 40 pc from the Sun. The mean values and standard deviations are given in the figure.

TABLE 2.5 – Atmospheric Parameters of DA White Dwarfs from SUPERBLINK

PM I	$T_{\rm eff}$ **(K)**	**log** g	$M/M_\odot$	M_V	**log** $L/L_\odot$	V^a	D(pc)	**log** τ	**Notes**
00331+4742S	16560 (125)	8.03 (0.05)	0.63 (0.03)	11.14	−1.96	14.75	55.5 (1.5)	8.18	
00334+2506	6180 (100)	7.71 (0.27)	0.43 (0.13)	13.67	−3.52	16.43	44.6 (1.1)	9.15	
00532+3927	7520 (44)	8.00 (0.09)	0.60 (0.05)	13.26	−3.33	17.05	45.2 (1.3)	9.10	1
01043+3816	16380 (102)	8.05 (0.05)	0.64 (0.03)	11.19	−1.99	15.35	58.3 (1.6)	8.21	
01382+4442	17180 (157)	7.95 (0.05)	0.59 (0.03)	10.96	−1.85	15.57	69.3 (2.0)	8.06	
01486+3615	6470 (138)	8.65 (0.28)	1.01 (0.17)	14.87	−4.01	16.93	24.2 (0.9)	9.68	
01565+2955	15170 (121)	8.00 (0.05)	0.62 (0.03)	11.25	−2.10	14.64	48.3 (1.3)	8.28	
02230+5544	6930 (49)	8.38 (0.10)	0.83 (0.07)	14.13	−3.70	16.76	35.8 (1.1)	9.53	
02557+2106S	6410 (93)	8.44 (0.20)	0.87 (0.13)	14.54	−3.88	17.25	37.5 (1.2)	9.64	
02562+4954	6370 (166)	9.02 (0.31)	1.20 (0.13)	15.65	−4.33	17.14	16.7 (0.7)	9.65	
03127+2218	6620 (63)	7.61 (0.16)	0.38 (0.07)	13.25	−3.34	16.99	56.9 (1.5)	9.03	
03433+1958	7160 (47)	8.62 (0.09)	0.99 (0.06)	14.41	−3.81	15.80	18.4 (0.7)	9.60	
03473+4358	13580 (290)	7.91 (0.05)	0.56 (0.03)	11.32	−2.24	14.16	33.9 (1.0)	8.37	
04032+2520W	22590 (246)	8.11 (0.05)	0.69 (0.03)	10.72	−1.46	14.89	98.1 (2.9)	7.72	2
04339+2827	13860 (318)	8.01 (0.05)	0.61 (0.03)	11.42	−2.26	15.75	75.9 (2.2)	8.40	
04389+6351	13050 (626)	7.67 (0.10)	0.44 (0.05)	11.06	−2.17	16.85	83.5 (2.3)	8.28	3
04523+2519	22180 (195)	8.55 (0.05)	0.96 (0.03)	11.48	−1.79	14.87	47.7 (1.6)	8.20	
04586+6209	11610 (967)	8.83 (0.12)	1.12 (0.06)	13.14	−3.13	14.71	24.9 (0.9)	9.23	4
05025+5401	11410 (70)	8.01 (0.05)	0.61 (0.03)	11.79	−2.60	15.19	46.9 (1.4)	8.64	
05280+4850	11120 (380)	8.44 (0.14)	0.88 (0.09)	12.53	−2.92	16.04	75.0 (2.4)	8.95	4
05492+5747	13510 (410)	8.04 (0.07)	0.63 (0.04)	11.52	−2.33	15.15	75.5 (2.1)	8.46	4
06026+0904	6020 (42)	8.00 (0.04)	0.59 (0.03)	14.17	−3.72	16.82	32.6 (0.9)	9.35	
06538+6355	6230 (104)	8.44 (0.23)	0.87 (0.15)	14.67	−3.93	16.13	21.1 (0.7)	9.67	
06556+5920	18900 (618)	7.89 (0.12)	0.56 (0.06)	10.70	−1.64	15.20	267.7 (7.3)	7.82	4
07029+4406	11000 (46)	8.02 (0.05)	0.61 (0.03)	11.89	−2.67	15.14	49.1 (1.4)	8.68	
07270+1434	5680 (55)	8.00 (0.04)	0.59 (0.03)	14.44	−3.82	16.58	30.7 (0.8)	9.43	
07419+1511	14370 (163)	8.01 (0.05)	0.62 (0.03)	11.36	−2.20	15.18	75.7 (2.2)	8.36	
07475+1107	8160 (60)	8.98 (0.09)	1.18 (0.04)	14.62	−3.86	15.84	25.7 (1.1)	9.52	
08126+1737	16380 (80)	8.09 (0.05)	0.67 (0.03)	11.25	−2.01	13.50	29.4 (0.8)	8.24	
09027+3120	10010 (28)	8.19 (0.05)	0.72 (0.03)	12.46	−2.94	14.75	35.3 (1.1)	8.90	
09033+2012	7200 (51)	8.05 (0.11)	0.62 (0.06)	13.49	−3.44	17.01	49.5 (1.5)	9.18	
09106+2156	5650 (59)	8.00 (0.04)	0.59 (0.03)	14.47	−3.83	17.25	39.0 (1.0)	9.44	
09286+1841	7680 (39)	8.37 (0.07)	0.83 (0.05)	13.72	−3.51	16.51	37.6 (1.2)	9.39	
10289+1105	13910 (290)	8.05 (0.05)	0.64 (0.03)	11.47	−2.28	15.19	64.9 (1.9)	8.42	
11071+1446	6620 (87)	8.20 (0.19)	0.71 (0.12)	14.04	−3.67	16.87	33.0 (1.0)	9.42	

TABLE 2.5 – Continued

PM I	$T_{\rm eff}$ **(K)**	**log** g	$M/M_{\odot}$	M_V	**log** $L/L_{\odot}$	V^a	D(pc)	**log** τ	**Notes**
11401+0112W	9910 (51)	8.07 (0.06)	0.64 (0.04)	12.32	−2.89	14.60	49.2 (1.4)	8.84	
11545+2422	8770 (67)	8.52 (0.09)	0.93 (0.06)	13.49	−3.39	15.26	26.3 (0.9)	9.35	
11592+4842	5900 (78)	8.00 (0.04)	0.59 (0.03)	14.26	−3.76	17.86	44.7 (1.2)	9.37	
12155+4630	6680 (78)	8.12 (0.17)	0.66 (0.11)	13.88	−3.60	16.75	43.0 (1.2)	9.33	
12273+3150	6550 (67)	7.97 (0.16)	0.57 (0.09)	13.76	−3.56	16.25	37.9 (1.1)	9.23	
13103+1404	8560 (37)	8.04 (0.07)	0.62 (0.04)	12.82	−3.12	16.08	49.7 (1.4)	8.98	
13246+0857	8110 (64)	7.92 (0.11)	0.55 (0.06)	12.86	−3.15	16.73	56.1 (1.6)	8.97	
13349+6945	14410 (155)	7.97 (0.05)	0.60 (0.03)	11.30	−2.17	15.61	70.3 (2.0)	8.33	
13521+1053	6080 (159)	8.26 (0.37)	0.76 (0.24)	14.50	−3.86	16.43	29.2 (0.9)	9.60	
14106+0245	5650 (61)	8.00 (0.04)	0.59 (0.03)	14.47	−3.83	16.42	28.1 (0.8)	9.44	
14149+4336	6580 (125)	8.44 (0.25)	0.87 (0.17)	14.43	−3.83	17.61	37.0 (1.2)	9.61	
14553+5655	15130 (106)	8.09 (0.05)	0.67 (0.03)	11.38	−2.15	14.93	48.3 (1.4)	8.34	
15206+3903	8740 (44)	8.04 (0.07)	0.62 (0.05)	12.73	−3.09	16.73	65.8 (1.9)	8.96	
15342+0218	8210 (56)	8.48 (0.09)	0.90 (0.06)	13.67	−3.47	16.43	32.9 (1.1)	9.40	
15359+2125	6560 (109)	8.61 (0.22)	0.99 (0.14)	14.75	−3.96	16.87	38.2 (1.4)	9.67	
16053+5556	6810 (72)	7.63 (0.18)	0.40 (0.08)	13.16	−3.31	17.28	57.5 (1.5)	9.01	
16096+4735	13340 (237)	8.11 (0.06)	0.67 (0.04)	11.63	−2.39	16.14	92.6 (2.7)	8.51	3
16171+0530	14820 (260)	7.76 (0.06)	0.48 (0.03)	10.95	−2.00	14.72	63.6 (1.7)	8.14	4
16264+1938	6290 (93)	8.39 (0.21)	0.84 (0.14)	14.54	−3.88	16.47	26.0 (0.8)	9.63	
16325+0851	5630 (79)	8.00 (0.04)	0.58 (0.03)	14.48	−3.84	15.05	13.2 (0.4)	9.45	
16335+5231	6670 (83)	8.16 (0.18)	0.69 (0.12)	13.95	−3.63	17.65	46.2 (1.3)	9.37	
16546+5742	9380 (63)	7.76 (0.09)	0.47 (0.05)	12.07	−2.81	15.84	58.5 (1.5)	8.73	
17052+0423	8390 (79)	8.30 (0.12)	0.79 (0.08)	13.29	−3.32	15.95	35.5 (1.1)	9.19	
17238+0458	8450 (52)	8.06 (0.09)	0.63 (0.05)	12.90	−3.16	16.70	57.2 (1.7)	9.01	
17283+0211	8100 (47)	8.13 (0.08)	0.67 (0.05)	13.15	−3.27	15.71	40.0 (1.2)	9.10	
17417+2401	7090 (61)	8.33 (0.12)	0.80 (0.08)	13.96	−3.63	16.50	34.6 (1.1)	9.46	
18073+0357	10520 (29)	8.06 (0.05)	0.63 (0.03)	12.08	−2.77	15.08	31.6 (0.9)	8.76	
18138+2119	18100 (112)	7.97 (0.05)	0.60 (0.03)	10.90	−1.77	15.70	76.8 (2.2)	7.99	
19128+5343	17670 (100)	8.32 (0.05)	0.82 (0.03)	11.48	−2.03	13.07	22.1 (0.7)	8.31	
19146+1428	6940 (113)	8.60 (0.21)	0.98 (0.13)	14.51	−3.85	15.71	19.4 (0.7)	9.62	
19493+0747	9410 (34)	8.16 (0.06)	0.70 (0.04)	12.65	−3.03	15.17	36.3 (1.1)	8.95	
20062+5902	13580 (231)	7.74 (0.05)	0.47 (0.02)	11.08	−2.14	16.08	69.3 (1.8)	8.26	
20235+7001	7240 (102)	8.32 (0.19)	0.79 (0.12)	13.86	−3.59	18.37	88.0 (3.0)	9.42	
21077+0740	6960 (56)	7.94 (0.13)	0.56 (0.07)	13.48	−3.43	15.91	34.7 (1.0)	9.15	
21117+0120	16570 (102)	8.06 (0.05)	0.65 (0.03)	11.19	−1.98	15.00	67.5 (1.9)	8.20	

TABLE 2.5 – Continued

PM I	$T_{\rm eff}$ (K)	log g	$M/M_{\odot}$	M_V	log $L/L_{\odot}$	V^a	D(pc)	log τ	Notes
21134+0727	6470 (66)	8.20 (0.15)	0.72 (0.10)	14.14	−3.71	15.66	24.1 (0.8)	9.46	
21384+1856	12610 (225)	7.65 (0.08)	0.43 (0.04)	11.10	−2.22	16.96	115.8 (3.2)	8.31	3
21597+2936	52110 (839)	7.66 (0.08)	0.56 (0.03)	8.54	+0.34	14.91	258.0 (9.5)	6.29	3
22118+5649	16790 (166)	8.15 (0.05)	0.70 (0.03)	11.30	−2.01	12.87	18.1 (0.6)	8.25	
22276+1753	6700 (90)	8.36 (0.18)	0.82 (0.12)	14.24	−3.75	15.84	28.8 (1.0)	9.56	
22299+3024	16310 (157)	7.48 (0.05)	0.37 (0.02)	10.38	−1.66	15.89	129.8 (3.8)	7.86	1
22331+2610	12020 (91)	7.97 (0.05)	0.59 (0.03)	11.61	−2.49	15.31	52.4 (1.4)	8.55	
23027+4312	8060 (37)	8.08 (0.08)	0.64 (0.05)	13.10	−3.25	16.85	79.9 (2.3)	9.07	
23160+0559	15270 (155)	8.00 (0.05)	0.61 (0.03)	11.24	−2.08	16.93	138.9 (4.1)	8.27	3
23229+3358	14030 (558)	8.19 (0.06)	0.73 (0.04)	11.67	−2.35	15.68	101.8 (3.0)	8.51	4
23234+7255	7620 (47)	7.99 (0.09)	0.59 (0.05)	13.19	−3.30	16.27	53.2 (1.5)	9.08	
23243+2835	7130 (75)	8.07 (0.15)	0.63 (0.09)	13.56	−3.46	15.96	33.4 (1.0)	9.20	
23283+3319	14390 (724)	8.40 (0.07)	0.86 (0.05)	11.95	−2.44	14.86	58.9 (1.9)	8.62	4
23390+5316	6450 (88)	8.20 (0.20)	0.71 (0.13)	14.15	−3.71	16.79	32.6 (0.9)	9.46	

(1) Bad GALEX photometry; (2) Binary but only one set of magnitudes; (3) Not in our new selection; (4) DA+dM.
(a) Estimated from USNO photographic magnitudes.

2.8 Discussion

2.8.1 Comparison of Spectroscopic and Photometric Distances

During the target selection process, distances were estimated using approximate V magnitudes together with various color-magnitude relations, displayed in Figures 2.5 to 2.8. These distance estimates were later improved by comparing theoretical average fluxes to the set of available photometry, properly weighted by their uncertainty. At that point, we simply assumed a surface gravity of $\log g = 8.0$, and considered both $T_{\rm eff}$ and the solid angle as free parameters. These estimates are referred to as *photometric distances*. The spectroscopic analysis, on the other hand, provides *spectroscopic distances*, where for a given star, theoretical absolute magnitudes are computed from the spectroscopic values of $T_{\rm eff}$ and $\log g$, and compared to the set of available photometry. In both cases, if only the V photographic magnitude is available, the 0.5 magnitude error will introduce a 23% uncertainty on the estimated spectroscopic distance. If additional photometry is available, however, this distance uncertainty can be significantly reduced (see Table 2.5).

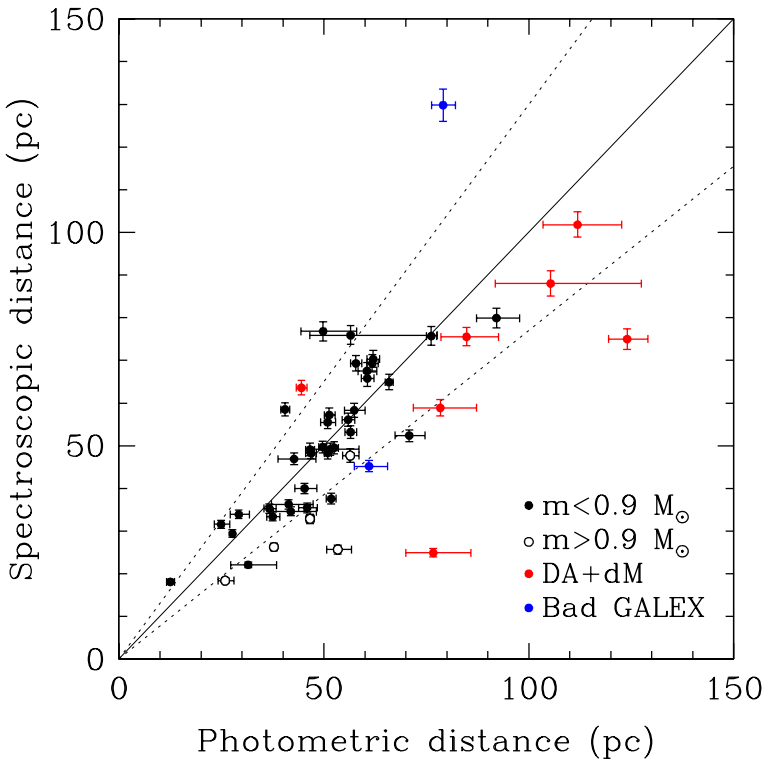

FIGURE 2.20 – Comparison of photometric and spectroscopic distances for white dwarfs with $T_{\rm eff} > 7000$ K, as defined in the text. The solid line represents the 1:1 correspondence, while the dotted lines represent a $\pm 23\%$ dispersion.

The comparison between photometric and spectroscopic distances for the DA white dwarfs in our sample is displayed in Figure 2.20. We restrict this comparison to $T_{\rm eff} > 7000$ K since the Balmer lines in cooler objects become too weak to be fitted properly with the spectroscopic method, yielding spurious $\log g$ values at low temperatures (see Figure 2.18) and corresponding distances. The dotted lines in Figure 2.20 represent a $\pm 23\%$ difference between both estimates (i.e., the maximum error on spectroscopic distances obtained from photographic magnitudes, as discussed in the previous paragraph). The bulk of stars is generally found within these limits. Part of the observed dispersion in Figure 2.20 can be attributed to the intrinsic mass distribution of our sample. Indeed, all our color-magnitude calibrations assumed a typical mass of 0.6 $M_{\odot}$, but as shown in Figures 2.5 to 2.8, there is an intrinsic dispersion in absolute

magnitude due to the mass (or radius) distribution of white dwarfs. In particular, white dwarfs with very high ($M > 0.9\ M_{\odot}$) spectroscopic masses yield photometric distances that are overestimated; these are identified with a different symbol in Figure 2.20.

Another source of scatter is due to the presence of M dwarf companions, which make the system brighter at visual and infrared magnitudes compared with single DA stars. Since these magnitudes were used to estimate their photometric distance (M_V vs. $V - J$), this can easily account for the large discrepancies with spectroscopic distances. Indeed, in the spectroscopic distance calculation, the less accurate magnitudes weigh less, and the more accurate JHK photometry dominates the distance solution. Finally, as noted in Table 2.5, we have certain doubts about the cross-correlation with the *GALEX* database for a handful of stars in our sample. For these objects, the *GALEX* photometry is inconsistent with the rest of the spectral energy distribution, and they had to be omitted from the fits used to estimate the spectroscopic distances. However, as in the previous cases, these colors were used to obtain our initial distance estimate.

To summarize, most objects in Figure 2.20 are found between the ±23% dispersion in distance, and the stars falling outside these limits can be separated into three categories: DA stars with M dwarf companions, high-mass white dwarfs, and stars with large photometric uncertainties (see the corresponding error bars in Figure 2.20). The previously estimated 15 pc error is thus enough to identify white dwarfs with reasonably accurate photometry, and we thus conclude that searching at 55 pc in order to find all white dwarfs within 40 pc is realistic, especially when photometry such as SDSS, *GALEX*, or 2MASS is available.

Our preliminary spectroscopic analysis of DA stars presented in Table 2.5 yields 11 white dwarf candidates within 25 pc of the Sun, including 5 candidates within the 20 pc sample. Incidentally, a few of these objects already have a parallax measurement available. Indeed, 21134+0727 (G25-20) has a parallax from Dahn et al. (1988), $\pi = 0\farcs0411 \pm 0\farcs0038$ yr^{-1}, placing it within 25 pc. Also, if 22118+5649 is a common proper motion companion to LTT 16500, as it is suspected to be (Subasavage et al. 2012, private communication), then it has a parallax of $\pi = 0\farcs02677 \pm 0\farcs00018$ yr^{-1} (or $D = 37.4$ pc), and thus not a member of the 20 pc sample, while still within 40 pc of the Sun. Finally, a private communication from

J. Subasavage confirms that 16325+0851 is indeed within 25 pc of the Sun. So even though spectroscopic distances are more accurate than the previous photometric estimates, the only way to confirm the membership of white dwarfs to the local sample is through trigonometric parallax measurements. Such measurements would not only provide reliable distances, but would also yield mass determinations for the coolest objects in our sample analyzed with the photometric technique.

2.8.2 Success Rate of Discovery

The absolute visual magnitudes (estimated from the calculated V magnitudes and photometric distances) for the 193 new white dwarfs identified in our survey are plotted in the upper panel of Figure 2.21 as a function of photometric distance. Also shown are the 499 white dwarfs in SUPERBLINK already known in the literature. The candidates still without spectroscopic confirmation are displayed separately in the lower panel; the objects selected on the basis of their USNO photographic magnitudes are considered second priority targets because of their higher probability of being contaminants from the main sequence. In each panel, the dashed lines represent lines of constant apparent V magnitude. We note that the white dwarfs identified in our survey are dominated by objects fainter than $V = 16$, and that most of them are found at photometric distances larger than 20 pc. This is not surprising since the census of white dwarfs within 20 pc of the Sun is believed to be at least 90% complete (Giammichele et al. 2012). There are still a few white dwarf candidates on our target list within 20 pc that have no spectroscopic data, due to observational constraints, but these stars are currently on our high priority list.

From the results shown in the upper panel of Figure 2.21, we can determine that the ratio of new to known white dwarfs is 193/499 ∼39%. Also, out of the 286 candidates observed, 220 are confirmed white dwarfs (27 in the literature [13] and 193 in our survey), for a success rate of 77%. This number is close to the 80% expected from our selection criteria, and we conclude that our survey is quite efficient for recovering the missing fraction of white dwarfs in the solar neighborhood.

13. Some spectra of spectroscopically confirmed white dwarfs were secured by us and will be used in our next paper as part of a study of the total white dwarf content of SUPERBLINK within 40 pc of the Sun.

The lower panel of Figure 2.21 reveals that a significant fraction of our remaining white dwarf candidates are fainter than $V = 17$ (590 objects fainter versus 329 objects brighter). The spectroscopic identification of these stars with 2 to 4-m telescopes requires integration times on the order of an hour under excellent weather conditions. The candidates deserving spectroscopic follow-up must then be carefully chosen, and our high-priority list now includes 89 of these faint candidates and 186 "bright" targets, for a total of 275 high-priority targets, excluding 120 objects we already observed after 2010 October and that are still being reduced.

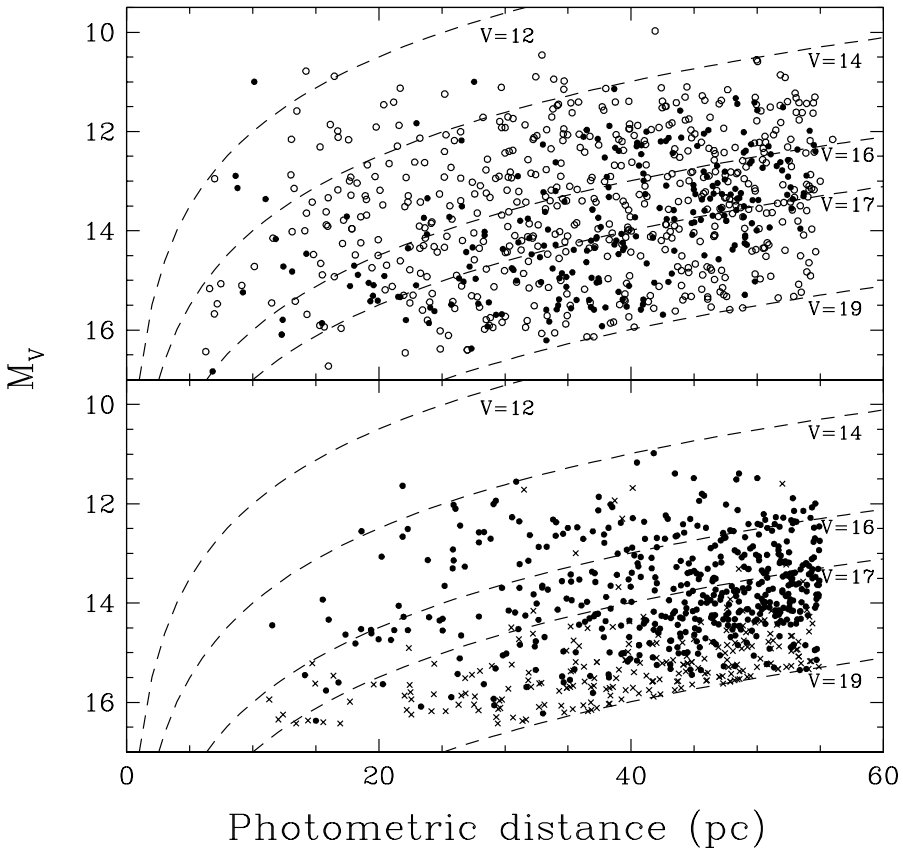

FIGURE 2.21 – Absolute magnitude as a function of photometric distance. In the upper panel, the filled circles represent the 193 new white dwarfs identified in our survey, while the open circles correspond to the 499 white dwarfs already known in the literature. Also shown by dashed lines in the figure are lines of constant apparent V magnitudes. The white dwarf candidates in our survey without spectroscopic confirmation are shown in the lower panel. The lower-priority candidates (those identified on the basis USNO photographic magnitudes) are shown with cross symbols.

Future observations will be dedicated to the follow-up of these high-priority white dwarf candidates, in particular those identified on the basis of SDSS or *GALEX* photometry.

2.8.3 Increasing the completeness of the current census

We have already established the success rate of our spectroscopic survey, and we are now interested in its completeness. First of all, our white dwarf sample is directly affected by the completeness of the SUPERBLINK catalog, which is high because of its low proper motion limit ($\mu > 0\farcs04$ yr^{-1}) which minimizes the kinematics bias. To illustrate the effect of proper motion on kinematics, we plot in Figure 2.22 the transverse motions v_t (i.e. the projected motions on the plane of the sky, where $v_t = 4.74\mu d$) for all stars in our sample as a function of the photometric distance D, as calculated in Section 2.5.1. As explained in Lépine & Gaidos (2011), a star at 50 pc from the Sun with $\mu > 0\farcs04$ yr^{-1} has a transverse velocity $v_t < 9.48$ km s^{-1}, which will occur with a probability of about 10% for stars in the solar neighborhood (see their Section 2.2 and Figure 1). Their diagram shows that operating with a proper motion limit of $\mu > 0\farcs150$ yr^{-1} will only detect half of the stars at 40 pc and very few stars (only those with very large components of motion) at 100 pc. However, a sample with a proper motion limit $\mu > 0\farcs04$ yr^{-1} will include $\sim$95% of the stars at 40 pc and $\sim$70% of the stars at 100 pc.

Hence, in terms of new white dwarf identification as a function of proper motion, we find that for $\mu > 0\farcs5$ yr^{-1} (see corresponding dashed line in Figure 2.22), which corresponds to the limit of the LHS survey, the ratio of new to known white dwarfs is 8.8%, while this ratio reaches 43.5% for $0\farcs5 > \mu > 0\farcs18$ yr^{-1} (where the lower proper motion limit is that of the NLTT survey), and it then drops slightly to 41.3% for $0\farcs18 < \mu < 0\farcs04$ yr^{-1}. Our survey is thus more efficient for proper motions lower than the LHS limit, but our results also demonstrate that the sample of white dwarfs with $\mu > 0\farcs5$ yr^{-1} could host up to 7 more white dwarfs. Previous searches for white dwarfs within the NLTT limit were also incomplete, since 33 of our new identifications have an NLTT designation. Note also that the NLTT and LHS appear to be $\gtrsim$ 80% complete down to the 19th magnitude, but only in the Completed Palomar Region (CPR), i.e. for $\delta > -32.5^\circ$ and outside a band $\pm 10^\circ$ of the Galactic plane

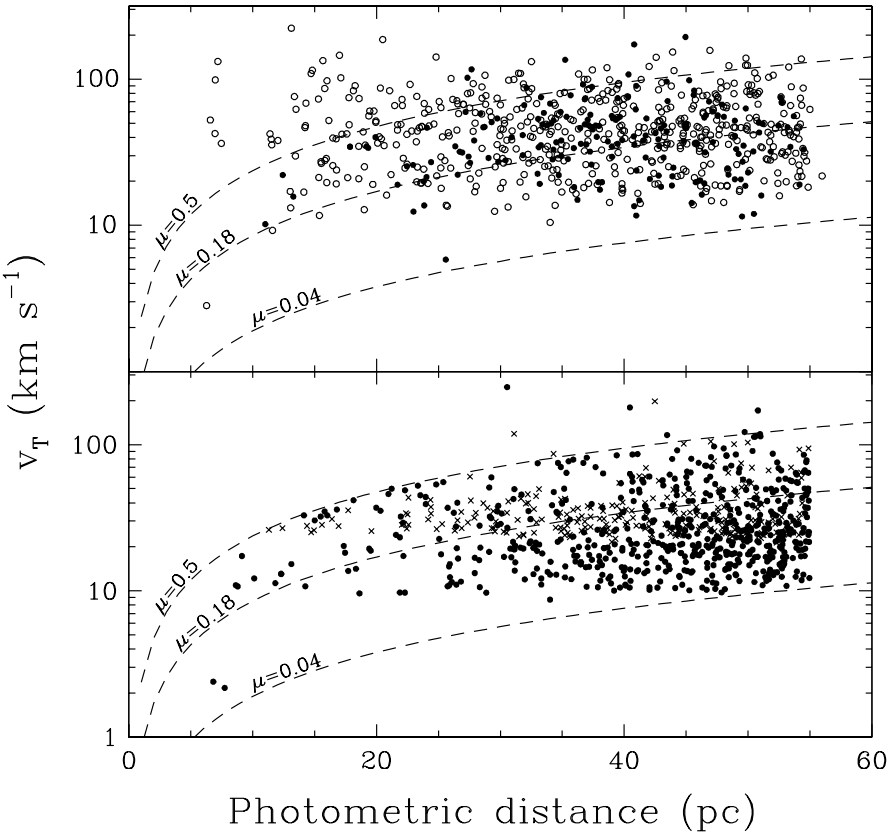

FIGURE 2.22 – Transverse velocity as a function of distance, showing the kinematic bias due to the proper motion limit of the SUPERBLINK catalog ($\mu > 40$ mas yr^{-1}). In the upper panel, the filled circles represent the 193 new white dwarfs identified in our survey, while the open circles correspond to the 499 white dwarfs already known in the literature. Also shown by dashed lines in the figure are lines of constant apparent proper motion (in units of arcsec yr^{-1}). The white dwarf candidates in our survey without spectroscopic confirmation are shown in the lower panel. The lower-priority candidates (those identified on the basis USNO photographic magnitudes) are shown with cross symbols.

(Lépine & Shara 2005).

Spectroscopic distances were obtained for 84 out of the 193 newly identified white dwarfs, while a preliminary photometric analysis (not presented here) of a subsample of the coolest objects was performed for another 78 white dwarfs. From this combined analysis of 162 white dwarfs, we find that 126 objects are within 55 pc of the Sun, and 93 within 40 pc. The spectroscopic analysis of 1151 DA stars by Gianninas et al. (2011) contains 223 white dwarfs from the WD Catalog located in the northern hemisphere whose spectroscopic distances are

within 55 pc from the Sun, and 121 within 40 pc. Using this latter survey, our ratio of new to known white dwarfs is estimated at 56% within 55 pc, and 77% within 40 pc. This difference in ratio will most likely be reduced when all candidates between 40 and 55 pc are observed. It was also mentioned in Section 2.8.2 that the ratio of new to known white dwarfs from the literature was 39%, while our success rate in detecting white dwarfs (both new and known) is 77%. Our survey is thus efficient for recovering white dwarfs that are already found in the literature as well as new identifications.

In spite of the success of our survey, the first sample of newly identified white dwarfs presented in this paper is far from complete, but the survey has not reached its limit yet. Our analysis represents the first results of an ongoing effort, and more data are still being collected and analyzed. Moreover, SUPERBLINK is currently being cross-correlated with the SDSS DR7 and *GALEX* GR7, providing additional high-quality photometric information to replace USNO magnitudes in our selection process. This will eventually result in more high-priority candidates, and will also help in the identification of DQ and DZ stars, which separate well in color-color diagrams, as we showed earlier, but only when such color information is available. Finally, these new magnitudes may also complete the set of photometry for white dwarfs in the SUPERBLINK catalog, allowing fits to the energy distribution of the cool white dwarfs that cannot be analyzed spectroscopically. Our future catalog will provide more candidates for parallax measurements, as well as more cool, massive, magnetic, and astrophysically challenging white dwarfs, while being at least 80% complete within 40 pc of the Sun. We will also be able to provide statistics on the Solar Neighborhood based on a sample of white dwarfs large enough to reduce the uncertainties related to small number statistics.

Acknowledgements

We would like to thank the director and staff of Steward Observatory and Kitt Peak National Observatory for the use of their facilities. This work was supported in part by the NSERC Canada and by the Fund FRQ-NT (Québec). S.L. was supported in this research by NSF grants AST-0607757 and AST-0908406. S.L also acknowledges support for this work from the

GALEX Guest Investigator program under NASA grant NNX09AF88G. This research has made use of the SIMBAD database, and the VizieR catalog access tool, operated at CDS, Strasbourg, France. This publication also makes use of data products from the Two Micron All Sky Survey, which is a joint project of the University of Massachusetts and the Infrared Processing and Analysis Center/California Institute of Technology, funded by the National Aeronautics and Space Administration and the National Science Foundation.

Bibliographie

Adelman-McCarthy, J. K., Agüeros, M. A., Allam, S. S., et al. 2008, ApJS, 175, 297

Bergeron, P., Ruiz, M. T., & Leggett, S. K. 1997, ApJS, 108, 339

Bergeron, P., Saffer, R., & Liebert, J. 1992, ApJ, 394, 228

Bergeron, P., Saumon, D., & Wesemael, F. 1995, ApJ, 443, 764

Bohlin, R. C. & Gilliland, R. L. 2004, AJ, 127, 3508

Carollo, D., Bucciarelli, B., Hodgkin, S. T., Lattanzi, M. G., McLean, B., Morbidelli, R., Smart, R. L., Spagna, A., & Terranegra, L. 2006, A&A, 448, 579

Cohen, M., Wheaton, W. A., & Megeath, S. T. 2003, AJ, 126, 1090

Cutri, R. M., Skrutskie, M. F., van Dyk, S., Beichman, C. A., Carpenter, J. M., Chester, T., Cambresy, L., Evans, T., Fowler, J., Gizis, J., Howard, E., Huchra, J., Jarrett, T., Kopan, E. L., Kirkpatrick, J. D., Light, R. M., Marsh, K. A., McCallon, H., Schneider, S., Stiening, R., Sykes, M., Weinberg, M., Wheaton, W. A., Wheelock, S., & Zacarias, N. 2003, VizieR Online Data Catalog, 2246, 0

Dahn, C. C., Harrington, R. S., Kallarakal, V. V., Guetter, H. H., Luginbuhl, C. B., Riepe, B. Y., Walker, R. L., Pier, J. R., Vrba, F. J., Monet, D. G., & Ables, H. D. 1988, AJ, 95, 237

Eggen, O. J. & Greenstein, J. L. 1965, ApJ, 142, 925

Farihi, J. 2004, ApJ, 610, 1013

Fontaine, G., Brassard, P., & Bergeron, P. 2001, PASP, 113, 409

Fukugita, M., Ichikawa, T., Gunn, J. E., Doi, M., Shimasaku, K., & Schneider, D. P. 1996, AJ, 111, 1748

Giammichele, N., Bergeron, P., & Dufour, P. 2012, ApJS, 199, 29

Gianninas, A., Bergeron, P., & Ruiz, M. T. 2011, ApJ, 743, 138

Giclas, H. L. 1971, in IAU Symposium, Vol. 42, White Dwarfs, ed. W. J. Luyten, 24

Giclas, H. L., Burnham, Jr., R., & Thomas, N. G. 1978, Lowell Observatory Bulletin, 8, 89

Gil de Paz, A., Boissier, S., Madore, B. F., Seibert, M., Joe, Y. H., Boselli, A., Wyder, T. K., Thilker, D., Bianchi, L., Rey, S.-C., Rich, R. M., Barlow, T. A., Conrow, T., Forster, K., Friedman, P. G., Martin, D. C., Morrissey, P., Neff, S. G., Schiminovich, D., Small, T., Donas, J., Heckman, T. M., Lee, Y.-W., Milliard, B., Szalay, A. S., & Yi, S. 2009, VizieR Online Data Catalog, 217, 30185

Greenstein, J. L. 1969, ApJ, 158, 281

—. 1976, ApJ, 207, L119

Høg, E., Fabricius, C., Makarov, V. V., Urban, S., Corbin, T., Wycoff, G., Bastian, U., Schwekendiek, P., & Wicenec, A. 2000, A&A, 355, L27

Holberg, J. B. & Bergeron, P. 2006, AJ, 132, 1221

Holberg, J. B., Oswalt, T. D., & Sion, E. M. 2002, ApJ, 571, 512

Holberg, J. B., Sion, E. M., Oswalt, T., McCook, G. P., Foran, S., & Subasavage, J. P. 2008, AJ, 135, 1225

Holberg, J. B., Sion, E. M., & Oswalt, T. D. 2011, in Bulletin of the American Astronomical Society, Vol. 43, American Astronomical Society Meeting Abstracts no.217, no.341.02

Hummer, D. G. & Mihalas, D. 1988, ApJ, 331, 794

Kawka, A., Vennes, S., & Thorstensen, J. R. 2004, AJ, 127, 1702

Kilic, M., Leggett, S. K., Tremblay, P.-E., von Hippel, T., Bergeron, P., Harris, H. C., Munn, J. A., Williams, K. A., Gates, E., & Farihi, J. 2010, ApJS, 190, 77

Kilic, M., Munn, J. A., Harris, H. C., Liebert, J., von Hippel, T., Williams, K. A., Metcalfe, T. S., Winget, D. E., & Levine, S. E. 2006, AJ, 131, 582

Knox, R. A., Hawkins, M. R. S., & Hambly, N. C. 1999, MNRAS, 306, 736

Kowalski, P. M. 2010, A&A, 519, L8

Kowalski, P. M. & Saumon, D. 2006, ApJ, 651, L137

Leggett, S. K., Ruiz, M. T., & Bergeron, P. 1998, ApJ, 497, 294

Lépine, S. & Gaidos, E. 2011, AJ, 142, 138

Lépine, S. & Shara, M. M. 2005, AJ, 129, 1483

Lépine, S., Shara, M. M., & Rich, R. M. 2002, AJ, 124, 1190

Liebert, J., Bergeron, P., & Holberg, J. 2005, ApJS, 156, 47

Limoges, M.-M., Bergeron, P., & Lépine, S. 2010, in American Institute of Physics Conference Series, Vol. 1273, American Institute of Physics Conference Series, ed. K. Werner & T. Rauch, 193–196

Luyten, W. J. 1979a, LHS catalogue. A catalogue of stars with proper motions exceeding 0”5 annually

—. 1979b, New Luyten Catalogue of Stars with Proper Motions Larger than Two Tenths of an Arcsecond, ed. Luyten, W. J.

McCook, G. P. & Sion, E. M. 1999, ApJS, 121, 1

Monet, D. G., Levine, S. E., Canzian, B., Ables, H. D., Bird, A. R., Dahn, C. C., Guetter, H. H., Harris, H. C., Henden, A. A., Leggett, S. K., Levison, H. F., Luginbuhl, C. B.,

Martini, J., Monet, A. K. B., Munn, J. A., Pier, J. R., Rhodes, A. R., Riepe, B., Sell, S., Stone, R. C., Vrba, F. J., Walker, R. L., Westerhout, G., Brucato, R. J., Reid, I. N., Schoening, W., Hartley, M., Read, M. A., & Tritton, S. B. 2003, AJ, 125, 984

Morrissey, P. & GALEX Science Team. 2004, in Bulletin of the American Astronomical Society, Vol. 36, American Astronomical Society Meeting Abstracts, 1385

Oppenheimer, B. R., Hambly, N. C., Digby, A. P., Hodgkin, S. T., & Saumon, D. 2001, Science, 292, 698

Oswalt, T. D., Smith, J. A., Wood, M. A., & Hintzen, P. 1996, Nature, 382, 692

Padmanabhan, N., Schlegel, D. J., Finkbeiner, D. P., Barentine, J. C., Blanton, M. R., Brewington, H. J., Gunn, J. E., Harvanek, M., Hogg, D. W., Ivezić, Ž., Johnston, D., Kent, S. M., Kleinman, S. J., Knapp, G. R., Krzesinski, J., Long, D., Neilsen, Jr., E. H., Nitta, A., Loomis, C., Lupton, R. H., Roweis, S., Snedden, S. A., Strauss, M. A., & Tucker, D. L. 2008, ApJ, 674, 1217

Press, W. H., Flannery, B. P., & Teukolsky, S. A. 1986, Numerical recipes. The art of scientific computing, ed. Press, W. H., Flannery, B. P., & Teukolsky, S. A.

Sayres, C., Subasavage, J. P., Bergeron, P., Dufour, P., Davenport, J. R. A., AlSayyad, Y., & Tofflemire, B. M. 2012, AJ, 143, 103

Sion, E. M., Holberg, J. B., Oswalt, T. D., McCook, G. P., & Wasatonic, R. 2009, AJ, 138, 1681

Skrutskie, M. F., Cutri, R. M., Stiening, R., Weinberg, M. D., Schneider, S., Carpenter, J. M., Beichman, C., Capps, R., Chester, T., Elias, J., Huchra, J., Liebert, J., Lonsdale, C., Monet, D. G., Price, S., Seitzer, P., Jarrett, T., Kirkpatrick, J. D., Gizis, J. E., Howard, E., Evans, T., Fowler, J., Fullmer, L., Hurt, R., Light, R., Kopan, E. L., Marsh, K. A., McCallon, H. L., Tam, R., Van Dyk, S., & Wheelock, S. 2006, AJ, 131, 1163

Subasavage, J. P., Jao, W.-C., Henry, T. J., Bergeron, P., Dufour, P., Ianna, P. A., Costa, E., & Méndez, R. A. 2009, AJ, 137, 4547

Tremblay, P.-E. & Bergeron, P. 2009, ApJ, 696, 1755

Tremblay, P.-E., Bergeron, P., & Gianninas, A. 2011a, ApJ, 730, 128

Tremblay, P.-E., Bergeron, P., Kalirai, J. S., & Gianninas, A. 2010, ApJ, 712, 1345

Tremblay, P.-E., Ludwig, H.-G., Steffen, M., Bergeron, P., & Freytag, B. 2011b, A&A, 531, L19

van Altena, W. F., Lee, J. T., & Hoffleit, E. D. 1995, The general catalogue of trigonometric [stellar] parallaxes

van Leeuwen, F. 2007, A&A, 474, 653

Vennes, S. & Kawka, A. 2003, ApJ, 586, L95

York, D. G., Adelman, J., Anderson, Jr., J. E., Anderson, S. F., et al. 2000, AJ, 120, 1579

Chapitre 3

Physical Properties of the Current Census of White Dwarfs Within 40 pc of the Sun

M.-M. Limoges [1 2], P. Bergeron[1], and S. Lépine [3]

To be submitted to *The Astrophysical Journal*

1. Visiting Astronomer, Kitt Peak National Observatory, National Optical Astronomy Observatory, which is operated by the Association of Universities for Research in Astronomy (AURA) under cooperative agreement with the National Science Foundation.

2. Département de Physique, Université de Montréal, C.P. 6128, Succ. Centre-Ville, Montréal, Québec H3C 3J7, Canada

3. Department of Physics and Astronomy, Georgia State University, Atlanta, GA 30302-4106; Department of Astrophysics, American Museum of Natural History, New York, NY 10024

3.1 Abstract

We present a detailed description of the physical properties of our current census of white dwarfs within 40 pc of the Sun, based on an exhaustive spectroscopic survey of northern hemisphere candidates from the SUPERBLINK proper motion database. This survey, undertaken several years ago, was aimed at significantly increasing the range and completeness of the local census of spectroscopically confirmed white dwarfs. Our method for selecting white dwarf candidates from the SUPERBLINK catalog is based on a combination of theoretical color-magnitude relations and reduced proper motion diagrams. Preliminary results of our endeavor were reported in an earlier publication, where we discussed the discovery of nearly 200 new white dwarfs. We present here the discovery of an additional 130 new white dwarfs, among which we identify 96 DA, 3 DB, 22 DC, 2 DQ, and 7 DZ stars, for a grand total of 322 new white dwarf identifications including our earlier work. We further identify 173 white dwarfs that lie within 40 pc of the Sun, representing a 40% increase of the current census, which now includes 460 objects. We estimate the completeness of our survey at between 63 and 73%, allowing for uncertainties in the distance estimates. We also perform a homogeneous model atmosphere analysis of this 40 pc sample and find a large fraction of massive white dwarfs, indicating that we are successfully recovering the more massive, and less luminous objects often missed in other surveys. We also show that the 40 pc sample is dominated by cool and old white dwarfs, which populate the faint end of the luminosity function, although trigonometric parallaxes will be needed to shape this part of the luminosity function more accurately. Finally, we identify 4 probable members of the 20 pc sample, 4 suspected double degenerate binaries, and we also report the discovery of a new ZZ Ceti pulsator.

3.2 Introduction

The determination of the atmospheric parameters of individual white dwarf stars — effective temperature ($T_{\rm eff}$), surface gravity ($\log g$), and atmospheric composition — has now reached an unprecedented level of accuracy, thanks to significant progress on both the observational and theoretical fronts. On the observational side, large samples of high signal-to-noise optical spectra can now be routinely obtained and analyzed using the so-called *spectroscopic technique* where observed line profiles are compared to the predictions of model atmospheres (see, e.g., Bergeron et al. 1992), reaching a precision as high as 1.2% in $T_{\rm eff}$ measurements and 0.038 dex in $\log g$ for the DA stars (Liebert et al. 2005). This technique has been applied successfully to large samples of various spectral types including DA stars from the ESO SN Ia Progenitor Survey (Koester et al. 2009), from the Villanova Catalogue of Spectroscopically Identified White Dwarfs (Gianninas et al. 2011), and in particular from the Sloan Digital Sky Survey (SDSS; Kepler et al. 2007, Tremblay et al. 2011a). The same spectroscopic technique has also been used for DB stars (Voss et al. 2007; Kepler et al. 2007; Bergeron et al. 2011). Similarly, optical and infrared photometry can be combined and compared with synthetic photometry to measure effective temperatures, as well as stellar radii when trigonometric parallaxes are available. This *photometric technique*, first applied to large photometric data sets by Bergeron et al. (1997, 2001), is particularly useful to study cool white dwarfs that lack the presence of strong absorption lines required by the spectroscopic method. Particularly interesting in this context is the large set of optical *ugriz* photometry available for white dwarfs in the SDSS, combined with independent JHK photometry (see, e.g., Kilic et al. 2010). The photometric approach, however, is more sensitive to issues related to the calibration of the synthetic photometry (Holberg & Bergeron 2006), unlike the spectroscopic approach.

Several independent model atmosphere grids have been widely used for the analysis of white dwarf stars (e.g., Bergeron et al. 1992, Vennes 1992, Koester et al. 2001), and the results obtained from these models are reassuringly comparable (see Figure 9 of Liebert et al. 2005). Despite this agreement between models, significant improvements on the theoretical front are still being achieved. For instance, new calculations for the Stark broadening of hydrogen lines that include nonideal effects directly inside the line profile calculations have recently become

available (Tremblay & Bergeron 2009). These models yield systematically higher $T_{\rm eff}$ (up to 1000 K) and $\log g$ (up to 0.1 dex) values, and a mean mass for DA stars shifted by $+0.034\ M_{\odot}$. Similarly, Kowalski & Saumon (2006) have successfully modeled the opacity from the red wing of Lyα, an important absorption process that affects the flux in the ultraviolet region of the energy distribution of cool, hydrogen-atmosphere white dwarfs. More importantly perhaps, Tremblay et al. (2013b, see also Tremblay et al. 2011a, 2013a) have produced realistic 3D hydrodynamical model atmospheres of hydrogen-rich white dwarfs and successfully showed that the so-called high-$\log g$ problem — the apparent increase of spectroscopic $\log g$ values below $T_{\rm eff}$ $\sim$13,000 K (see Tremblay et al. 2010 and references therein) — was related to the limitations of the mixing-length theory used to describe the convective energy transport in previous model atmosphere calculations.

With the availability of large data sets and improved model atmospheres, the statistical properties of white dwarf stars can now be studied in greater detail, including the luminosity function, space density, mass distribution, age distribution, and space kinematics. This can be achieved not only for the local population of white dwarfs, but also for various components of the Galaxy, including open and globular clusters (see, e.g., Tremblay et al. 2012, Woodley et al. 2012). Since white dwarfs represent the endpoint of over 97% of the stars in the Galaxy, they are a powerful tool to study the overall evolutionary history of the Galaxy. However, the determinations of these global properties are always confronted with the problem of defining statistically complete samples, minimally affected by selection biases. For instance, ultraviolet color excess surveys such as the Palomar-Green (PG) survey (Green et al. 1986) or the Kiso Schmidt (KUV) ultraviolet excess survey (Kondo et al. 1984) are restricted to the detection of blue and thus hot white dwarfs. Consequently, the luminosity functions derived from these surveys (Liebert et al. 2005; Limoges et al. 2010; Bergeron et al. 2011) do not sample the faint end of the distribution where the majority of white dwarf stars are located. Even the luminosity function determined by Harris et al. (2006) using the magnitude-limited SDSS sample, which covers the entire range of bolometric magnitudes ($7 \lesssim M_{\rm bol} \lesssim 16$), includes *several* corrections for completeness and contamination to counterbalance important selection effects, and these corrections critically determine the faint end of the luminosity function.

It is however possible, as shown by Kilic et al. (2006), to refine the selection criteria by combining the SDSS photometry and astrometry with the USNO-B plate astrometry to build a reduced proper motion diagram, which helps to identify cool white dwarf candidates in the SDSS imaging area and thus recover the faint end of the luminosity function. White dwarfs identified in proper motion surveys are indeed much better suited to identify cool white dwarfs at the faint end of the luminosity function. For many years, one of the most commonly used observational luminosity function had been that published by Liebert, Dahn, & Monet (1988), and revised by Leggett et al. (1998), based on the Luyten Half-Second Catalog (Luyten 1979), but the major drawback is that the sample contains only 43 spectroscopically confirmed white dwarfs.

Other types of statistical biases occur in determining the distribution of mass as a function of effective temperature (M versus $T_{\rm eff}$), or the cumulative mass distribution (N versus M). For instance, color excess surveys (PG, KUV, and even SDSS) are also magnitude-limited, and as such the samples drawn from these surveys suffer from a bias in mass where low-mass white dwarfs with their large radii and high luminosities are over represented, while high-mass white dwarfs are undersampled (see, e.g., Section 3.2 of Liebert et al. 2005). Another important issue is that, until recently, spectroscopic masses at low effective temperatures could not be trusted due to the high-$\log g$ problem discussed above. Thus, most analyses restricted their determination of the mass distribution of DA stars to temperatures higher than 13,000 K. Alternatively, Giammichele et al. (2012) applied an empirical correction to the $\log g$ distribution, based on the DA white dwarfs from the Data Release 4 of the SDSS analyzed by Tremblay et al. (2011a). More recently, Tremblay et al. (2013b) produced a more accurate set of $T_{\rm eff}$ and $\log g$ corrections to be applied to spectroscopic determinations, based on a comparison of detailed 3D hydrodynamical simulations with 1D model atmospheres calculated within the mixing length theory. Another problem arises at low effective temperatures when spectroscopic lines can no longer be used efficiently. This occurs below $T_{\rm eff}$ $\sim$13,000 K and $\sim$6500 K for helium- and hydrogen-atmosphere white dwarfs, respectively, i.e. near the peak of the luminosity function, in which cases one must rely on the photometric technique to measure the atmospheric parameters. With the photometric technique, unfortunately, stellar radii or

masses can only be determined for white dwarfs with trigonometric parallax measurements, which are only available for 200 stars or so. This situation will of course change dramatically when the Gaia mission is completed.

Also of interest is the study of the spectral evolution, which describes the various physical mechanisms (gravitational settling, convective mixing, convective dredge-up from the core, accretion from the interstellar medium or circumstellar material, radiative acceleration, stellar winds, etc.) that affect the surface composition of white dwarfs as they evolve along the cooling sequence. Of particular interest is the spectral evolution of white dwarfs at low $T_{\rm eff}$, where convective mixing of a thin superficial hydrogen convective layer with the deeper helium convection zone is believed to occur (see Tremblay & Bergeron 2008 and references therein). Bergeron et al. (1997, 2001) also suggested the presence of a non-DA gap (or deficiency) between $T_{\rm eff}$ ∼5000 K and 6000 K where most stars appear to have hydrogen-rich compositions, while helium-atmosphere white dwarfs exist above and below this temperature range. On the other hand, Kowalski & Saumon (2006, see also Giammichele et al. 2012) suggested that most, if not all, cool DC stars probably have hydrogen-rich atmospheres, based on a reanalysis of the Bergeron et al. (1997, 2001) photometry with their improved atmospheric model, which includes the previously missing red wing opacity from Lyα. Unfortunately, the white dwarf samples analyzed by Bergeron et al. (1997, 2001) are not complete in any statistical sense. For instance, Kilic et al. (2010) analyzed 126 cool white dwarfs identified in the SDSS and uncovered several helium-atmosphere white dwarfs in the $T_{\rm eff}$ range of the gap. To complicate matters, Chen & Hansen (2011, 2012) showed that the evolution of cool white dwarfs cannot be interpreted monotonically as a function of $T_{\rm eff}$, and that upon mixing the $T_{\rm eff}$ of a white dwarf can actually *increase*. Hence our understanding of the spectral evolution of cool white dwarfs is at best sketchy, a situation that can only be improved by studying better-defined, large, statistically complete samples.

The best way around the completeness problems discussed above is the use of a volume-limited sample. Efforts to identify white dwarfs in the immediate solar neighborhood, within 20 or 25 pc of the Sun, have been summarized in Limoges et al. (2013, hereafter Paper I) [4].

4. Paper I is Chapter 2 of the thesis.

Giammichele et al. (2012) performed a detailed photometric and/or spectroscopic analysis of every white dwarf suspected to lie within 20 parsecs of the Sun. Although Holberg et al. (2008) and Giammichele et al. (2012) have established the completeness of the 20 parsec sample at 80% and 90%, respectively, one is confronted with small number statistics since this sample contains only 130 objects or so. Hence some results reported by Giammichele et al. may not be statistically significant. For example, while the luminosity function shown in their Figure 22 agrees well with previous investigations at low temperatures and luminosities, space densities in the brighter luminosity bins (above $T_{\rm eff}$ $\sim$12,000 K) are larger by a factor of $\sim$2. As mentioned by the authors, one likely explanation for this apparent overdensity is the small number of white dwarfs in the brightest luminosity bins, which contain only a few objects ($\sim$2 to 8). The only way out of this situation is to significantly increase the volume sampled by these surveys. For instance, Holberg et al. (2011) are working on defining the sample of white dwarfs to 25 parsecs of the Sun, nearly doubling the number of objects analyzed by Giammichele et al. (2012).

It is with this idea in mind that we embarked in a large effort (see Paper I) to increase the census of white dwarfs to the larger distance range of 40 pc from the Sun (corresponding to a volume *8 times* that of the 20 pc sample). Given the space density of 4.39×10^{-3} pc^{-3} derived by Giammichele et al. (2012), the expected number of white dwarfs within 40 pc is $\sim$1200, or $\sim$600 if we restrict our search to the northern hemisphere, a sample size that would markedly improve the statistical significance of previous analyses. The SUPERBLINK survey is an all-sky search for high proper motion stars ($\mu > 40$ mas yr^{-1}) based on a re-analysis of the Digitized Sky Surveys, with its 20-45 yr baseline (Lépine & Shara 2005; Lépine & Gaidos 2011). The SUPERBLINK catalog is at least 95% complete for the entire northern sky down to $V = 19.0$, with a very low rate of spurious detection. As discussed in Paper I, the SUPERBLINK catalog should contain all white dwarfs down to the luminosity function turnoff (which occurs at $L/L_{\odot} \simeq 10^{-4}$) to a distance of 56.7 pc from the Sun. Our method for selecting white dwarf candidates, described in detail in Paper I, is based on reduced proper motion diagrams of the 1.6 million stars in SUPERBLINK with $\delta > 0$, combined with distances estimated from theoretical color-magnitude relations. A list of 1341 candidates with

photometric distance estimates of $D < 40$ pc, to within the uncertainties, was established for follow-up spectroscopic observations, excluding the objects with an already known spectral type. We successfully confirmed 193 new white dwarfs, among which 93 had *spectroscopic distances* placing them within 40 pc. Only DA stars with strong enough Balmer lines were analyzed in Paper I, using the spectroscopic method described above.

The specific goal of this work is to obtain a complete sample of white dwarfs within 40 pc of the Sun in the northern hemisphere. We report in this paper the outcome of our survey, and present a detailed photometric and spectroscopic model atmosphere analysis of all the new white dwarfs that were identified. We also provide a comprehensive analysis of the mass distribution and the chemical distribution of white dwarf stars in this volume-limited sample. In particular, since only a few white dwarfs in our sample have trigonometric parallax measurements available, we develop a robust method to derive distances from spectroscopic and photometric data alone.

We first present in Section 3.3 an update of our census of white dwarfs within 40 pc of the Sun, which includes a summary of our earlier work as well as a detailed description of the follow-up spectroscopic observations of our list of white dwarf candidates. We then perform in Section 3.4 a detailed photometric and spectroscopic analysis of all objects in our sample with state-of-the-art model atmospheres, where we also include all known white dwarfs in the SUPERBLINK catalog and from the literature, suspected to belong to the 40 pc sample. The resulting distance estimates are then used to build a complete sample of white dwarfs within 40 pc of the Sun, which we analyze in further detail in Section 3.5. In particular, we discuss several physical properties of this sample, including its completeness, kinematics, mass distribution, spectral evolution, and luminosity function. We then offer some concluding remarks in Section 3.6.

3.3 Update on our Census of White Dwarfs Within 40 pc of the Sun

3.3.1 Selection of the Candidates Based on Reduced Proper Motion Diagrams

Our method for selecting white dwarf candidates from the SUPERBLINK catalog using reduced proper motion diagrams is discussed at length in Paper I. We briefly summarize here, for completeness, the various steps involved.

The white dwarf candidates are identified from the SUPERBLINK catalog of stars with proper motions $\mu > 40$ mas yr^{-1} (Lépine et al. 2002; Lépine & Shara 2005; Lépine & Gaidos 2011). Our selection method takes advantage of the coordinates and proper motions provided by SUPERBLINK for 1,567,461 stars in the northern hemisphere ($\delta > 0$). White dwarf candidates are selected on the basis of their particular location at the bottom left of reduced proper motion diagrams. Since the construction of such diagrams requires, in addition to proper motion measurements, a set of photometric color indices for each star, we cross-correlate SUPERBLINK with other catalogs to obtain photometric data covering a large portion of the electromagnetic spectrum, and in some cases, we also obtain improved coordinates and proper motion measurements. Our version of SUPERBLINK used in Paper I includes — in the northern hemisphere only — 1,472,666 counterparts in the Two Micron All Sky Survey (2MASS) Point Source Catalog (Skrutskie et al. 2006), 345,958 in the Sloan Digital Sky Survey (SDSS, Adelman-McCarthy et al. 2008), 118,475 in the *Hipparcos* and *Tycho-2* catalogs (Høg et al. 2000), 1,567,461 in the USNO-B1.0 database (Monet et al. 2003), and 143,096 in the sixth data release (GR6) of the *GALEX* database (Gil de Paz et al. 2009). Each object in SUPERBLINK with $\delta > 0$ is then placed in all corresponding (H_m, color-index) diagrams, depending on the available photometry, where H_m represents the reduced proper motion defined as $H_m = m + 5\log\mu + 5$, m is the apparent magnitude in some bandpass, and μ is the proper motion measured in arcseconds per year. More specifically, we rely on (H_g, $g-z$) based on *ugriz* photometry, (H_V, $NUV-V$) based on UV *GALEX* photometry, (H_V, $V-J$) based on 2MASS JHK_S photometry, and (H_V, $V-I_N$) based on USNO-B1 photographic

magnitudes. We also restrict our search to stars with $V < 19$, since SUPERBLINK has an estimated false detection level of less than 1% down to $V = 19$, but the false detection rate increases significantly for fainter sources.

The limit that defines the white dwarf region in each diagram is determined from the location of SUPERBLINK objects with known white dwarf counterparts in the 2008 May electronic version of the Catalogue of Spectroscopically Identified White Dwarfs [5] (McCook & Sion 1999, hereafter WD Catalog). To be selected as a white dwarf candidate, a SUPERBLINK object must be identified in the expected white dwarf region of the diagram with the most accurate photometry. The highest priority is thus given to the reduced proper motion diagram based on SDSS magnitudes. If *ugriz* photometry is not available, the second priority is given to UV *GALEX* photometry, the third priority to 2MASS JHK_S photometry, and if no other photometric system is available, we use USNO-B1 photographic magnitudes. Finally, a criterion in $V - J$ is applied to the stars identified in (H_V, $V - J$) diagrams to exclude bright, red, main sequence contaminants.

Since we want to restrain our survey to a distance less than $D = 40$ pc from the Sun, and in the absence of trigonometric parallax measurements for most white dwarf candidates in our sample, we must rely on *photometric distances* estimated from the distance modulus, $m - M = 5 \log d - 5$, where the absolute magnitude M of each object is determined from theoretical color-magnitude relations combined with a measured color index in some specified photometric system. These theoretical relations at constant mass values (see Figures 5 to 8 of Paper I) are based on synthetic photometry from white dwarf model atmospheres, following the procedure described in Holberg & Bergeron (2006). Hence, absolute magnitudes for each white dwarf candidate are determined from color-magnitude relations in (M_g, $g - z$), (M_V, $NUV - V$), (M_V, $V - J$) or (M_V, $V - I_N$), for a 0.6 $M_\odot$ hydrogen-atmosphere sequence, and for a helium-atmosphere sequence at the same mass in order to evaluate the distance uncertainty resulting from the unknown atmospheric composition of our candidates. A comparison of these photometric distances with those obtained from parallax measurements show a 1σ dispersion of 8.5 pc (see Figure 9 of Paper I), and we thus adopt in our survey a conservative buffer of

5. http://www.astronomy.villanova.edu/WDCatalog/index.html

15 pc to include all white dwarfs that could potentially lie within 40 pc of the Sun, that is with $D_{\rm phot} < 55$ pc.

The method described above led to the identification of 193 new spectroscopically identified white dwarfs in Paper I. However, even though 14594+3618 (we omit here and below the letters "PM I" from the designation) was identified as a white dwarf in Paper I, a new spectrum at a significantly improved S/N shows that the star is a main sequence F star, hence reducing the total of new white dwarfs identified to 192. We also established that our survey is efficient at identifying nearby white dwarfs distributed uniformly across the northern sky, and estimated the ratio of new to known white dwarfs to be around 77% within 40 pc. More importantly, our survey has identified a large amount of cool white dwarfs that could possibly refine the determination of the faint end of the luminosity function. We describe in the next section the update of our spectroscopic survey.

3.3.2 Spectroscopic Follow-up of White Dwarf Candidates Within 40 pc of the Sun

In Paper I, we compiled a list of 1341 white dwarf candidates within 40 pc of the Sun — but likely extending to 55 pc given the uncertainties — and reported spectroscopic observations for 422 objects from this target list, including 192 new white dwarf identifications. We also reported that our selection criteria recovered 499 known nearby white dwarfs from the literature (see Figure 11 of Paper I). However, a thorough search indicated that while several of these objects have a WD spectral classification in Simbad, they have never been *confirmed spectroscopically* (and indeed, some of these turned out not to be white dwarfs after all). We also improved the cross-correlation of objects in our target list with known white dwarfs from the literature, and discovered several improper matches. Hence the number of previously known, actual white dwarfs identified from our selection criteria is 416. Finally, we have recently determined that our criterion based on $V - J$ color used to exclude bright, red, main sequence contaminants (see above) had not in fact been applied to our list of white dwarf candidates. Taking all these changes into account, our list of white dwarf candidates now numbers 1180 objects.

The spectroscopic observing log of our earlier survey is presented in Table 2 of Paper I. Since then, additional optical spectra have been obtained with the Steward Observatory 2.3-m telescope and the NOAO Mayall 4-m and 2.1-m telescopes during 7 different observing campaigns between 2011 January and 2013 October. A few of the brightest candidates were also observed in spectroscopy with the 1.6-m Mont-Mégantic Observatory (OMM), while ∼60 hours with the Gemini North and South 8-m telescopes were used to observe our faintest candidates ($V \simeq 17-18$). The adopted configurations allow a spectral coverage of λ ∼3200 − 5300 Å and ∼3800 − 6700 Å, at an intermediate resolution of ∼ 6 Å FWHM. Spectra were first

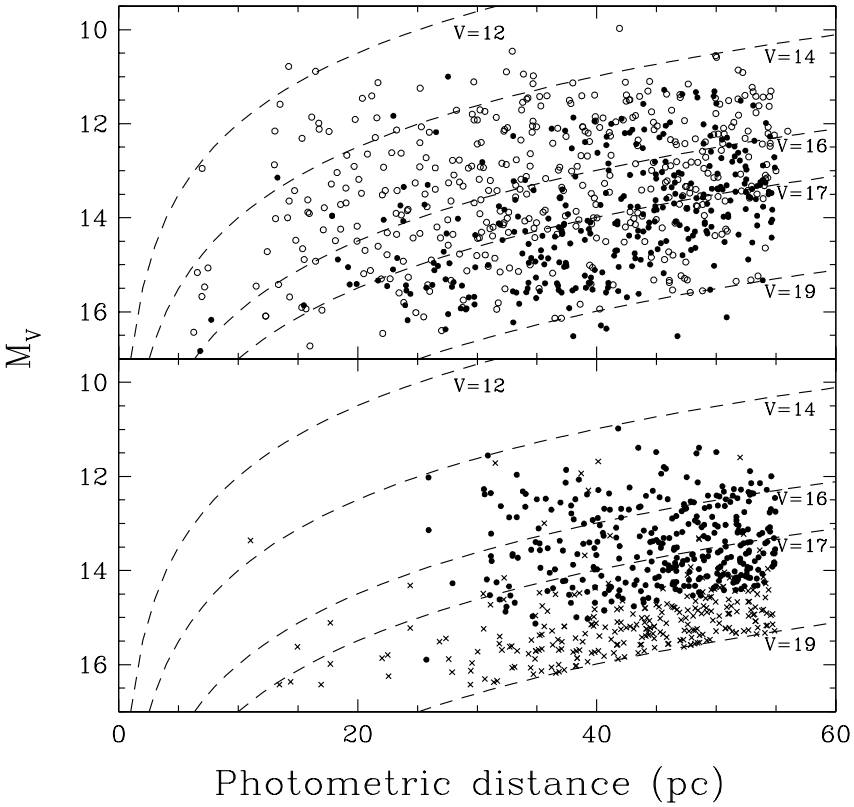

FIGURE 3.1 – Absolute visual magnitude as a function of photometric distance for spectroscopically confirmed white dwarfs (top) and our remaining candidates (bottom). In the upper panel, the filled circles represent the 322 new white dwarfs identified in our survey, while the open circles correspond to the 416 white dwarfs already known in the literature. Dashed lines in the figure are lines of constant apparent V magnitudes. The 595 remaining white dwarf candidates in our survey, still awaiting spectroscopic confirmation, are shown in the lower panel. Lower-priority candidates (those identified on the basis USNO photographic magnitudes and those with $V > 18$) are shown with cross symbols.

obtained at low signal-to-noise ratio (S/N ∼25), which is sufficient to identify main sequence objects, but also represents the lower limit required to obtain reliable model fits to the spectral lines. Some stars were however reobserved at higher S/N and resolution, whenever required. Table 3.1 summarizes our spectroscopic observation campaigns carried out since Paper I, along with their instrumental setups.

We have now secured spectra for 583 objects from our list of 1180 candidates, thus adding 163 spectra to the list of 422 objects reported in Paper I. The content of our complete spectroscopic data set, described in the next subsection, includes 322 new white dwarf identifications (192 reported in Paper I), and 261 spectra from contaminants, mainly main sequence stars and quasars. We note that 3 of the newly identified white dwarfs are included in the SDSS Data Release 7 but were not classified as such; we rely on the corresponding SDSS spectra for these stars.

The current state of our survey is summarized in Figure 3.1 (upper panel), which plots the estimated absolute visual magnitudes (from the calculated V magnitudes and photometric distances — see Paper I) as a function of the photometric distance for the 322 new white dwarfs (filled symbols) and the 416 previously known white dwarfs (open symbols). We note that the subset of new white dwarfs is dominated by objects fainter than $V = 16$, and that most of them are found at photometric distances larger than 20 pc. The 595 white dwarf candidates on our list still without spectroscopic confirmation are displayed separately in the lower panel of Figure 3.1; objects selected on the basis of the less reliable USNO photographic magnitudes (crosses) are considered second priority targets because of their higher probability of being main-sequence contaminants. If we exclude these second priority targets, we are left with ∼330 first-priority candidates for the spectroscopic follow-up survey. However, only 4 candidates with $D < 30$ pc and $V < 18$ remain to be observed, and every candidate with a high probability of being a white dwarf with an estimated distance less than 20 pc has been observed.

TABLE 3.1 – Spectroscopic Observing Runs

Date	Telescope	Spectrograph	Grating (l mm^{-1})	Blaze (Å)	Coverage (Å)	Slit ($''$)
2011 Jan	NOAO 2.1 m	Goldcam	500	5500	3800–6700	2
2011 Mar	NOAO Mayall 4 m	RC	316	5500	3900–6700	2
2011 Apr	Steward Observatory Bok 2.3 m	B&C	600	3568	3800–5600	4.5
2011 Apr	NOAO 2.1 m	Goldcam	500	5500	3800–6700	2
2012 Sep	NOAO Mayall 4 m	RC	316	5500	3900–6700	2
2011B	Gemini North	GMOS-N	600	4610	3800–6700	1
2011B	Gemini South	GMOS-S	600	4610	3800–6700	1
2012B	Gemini North	GMOS-N	600	4610	3800–6700	1
2013 Jan	Observatoire du Mont Mégantic 1.6 m	B&C	400	3568	3800–6700	4.5
2013 Jun	Steward Observatory Bok 2.3 m	B&C	600	3568	3800–5600	4.5
2013 Oct	Steward Observatory Bok 2.3 m	B&C	600	3568	3800–5600	4.5

3.3.3 Spectroscopic Content of our Updated Survey

Our spectroscopic follow-up observations from 2011 January to 2013 October (Table 3.1) have led to the identification of the 130 new white dwarfs listed in Tables 3.2 and 3.3 (including the 3 SDSS white dwarfs discussed above). Table 3.2 provides astrometric data as well as NLTT and SDSS designations, when available, while Table 3.3 lists the available photometry and adopted spectral types for the same objects. Since Paper I, the SUPERBLINK catalog has been updated with optical magnitudes from the 7th Data Release of the SDSS catalog, and ultraviolet magnitudes from the DR4-5 data release of *GALEX*. In particular, the number of stars with *GALEX* counterparts has increased to 258,076 objects, while the number of stars with SDSS counterparts now reaches 740,826. This improved photometry is essential for the analysis of the energy distribution of the SUPERBLINK white dwarfs, as well as for the estimation of their distances. For this reason, we also include in Table 3.3 revised photometry for the 192 new white dwarfs identified in Paper I. In summary, the new white dwarfs reported in this paper comprise 96 DA (including 1 DAZ, 3 DA+dM, and 4 magnetics), 3 DB, 22 DC, 2 DQ, and 7 DZ (including 1 DZA) stars.

Our new DA spectra are displayed in Figures 3.2 and 3.3, in order of decreasing $T_{\rm eff}$; only Hα is displayed in Figure 3.3 since the bluer portion of the spectrum is either featureless or too noisy to be of any use in the coolest DA stars. We also show at the bottom of the last panel of Figure 3.2, 3 new spectra of stars already presented in Paper I (see Table 2.4), that are double degenerate binary candidates and are further analyzed below. Note that 05431+3637, shown

at the bottom left panel in Figure 3.2, is actually a DAZ star. Two of the DA stars discovered in our survey — 06018+2751 (GD 258) and 18435+2740 (GD 381) — were flagged as WD candidates in Giclas et al. (1980), but to our knowledge these had not been spectroscopically confirmed, suggesting that many of the Giclas objects may still be white dwarfs awaiting spectroscopic confirmation. The magnetic DA white dwarfs, or magnetic candidates, in our updated sample are displayed in Figure 3.4. The bottom four objects are new identifications, with the Zeeman triplets clearly visible despite their low S/N. The top object, 04523+2519, was initially classified non-magnetic in Paper I, but the flat bottom line cores observed in our spectroscopic fit (see Figure 17 of Paper I) led us to reobserve this star at Hα, where the weak Zeeman splitting is now just barely detected, making us believe this star is magnetic as well. Finally, our survey also led to the discovery of 3 new DA + M dwarf binary systems, shown separately in Figure 3.5.

Our subsample of new DZ (DZA), DB (DBZ), and DQ stars are displayed together in Figure 3.6. The first object in the figure, 00050+4003, is the star GD 1, another WD candidate listed in Giclas et al. (1980). Also shown are 5 DZ stars already identified in Paper I but for which new optical spectra in the blue have been secured: 01216+3440, 03196+3630, 16477+2636, 21420+2252, and 23003+2204. Indeed, the observational setup used with the 2.1-m and 4-m NOAO telescopes does not allow simultaneous coverage of wavelengths shorter than $\sim$3900 Å and of Hα in the red. In order to better constrain the metal abundances in these objects, additional spectra covering the blue portion of the spectral energy distribution were thus obtained with the Steward Observatory 2.3-m Bok telescope. The 3 new DB white dwarfs displayed in Figure 3.6 also include 02236+4816, also known as GD 27, another WD candidate from Giclas et al. (1980) that was also lacking spectroscopic confirmation to this date. Finally, our 2 DQ spectra, easily recognizable from their strong C_2 Swan bands, are shown in the bottom right section of Figure 3.6; 16142+1729 is actually one of those peculiar DQ stars with shifted C_2 Swan bands referred to as DQpec white dwarfs, a phenomenon explained by Kowalski (2010) as a result of pressure shifts of the carbon bands that occur in very cool, helium-dominated atmospheres.

Finally, our featureless DC spectra are displayed in Figure 3.7 in order of increasing right

ascension. All spectra cover the $\lambda \sim 3900 - 6700$ Å range, and we notice a few cases where the blue portion of the spectrum is particularly noisy, preventing us from detecting the possible presence of calcium lines. These noisier spectra actually come from Gemini North and South, where the integration times were calculated for the central wavelengths near 5000 Å, but the gratings used with the GMOS-N and -S instruments (B600 G5307), chosen for their spectral coverage, have a quantum efficiency that falls below 43% blueward of 3397 Å, compared with 83% at 4983 Å.

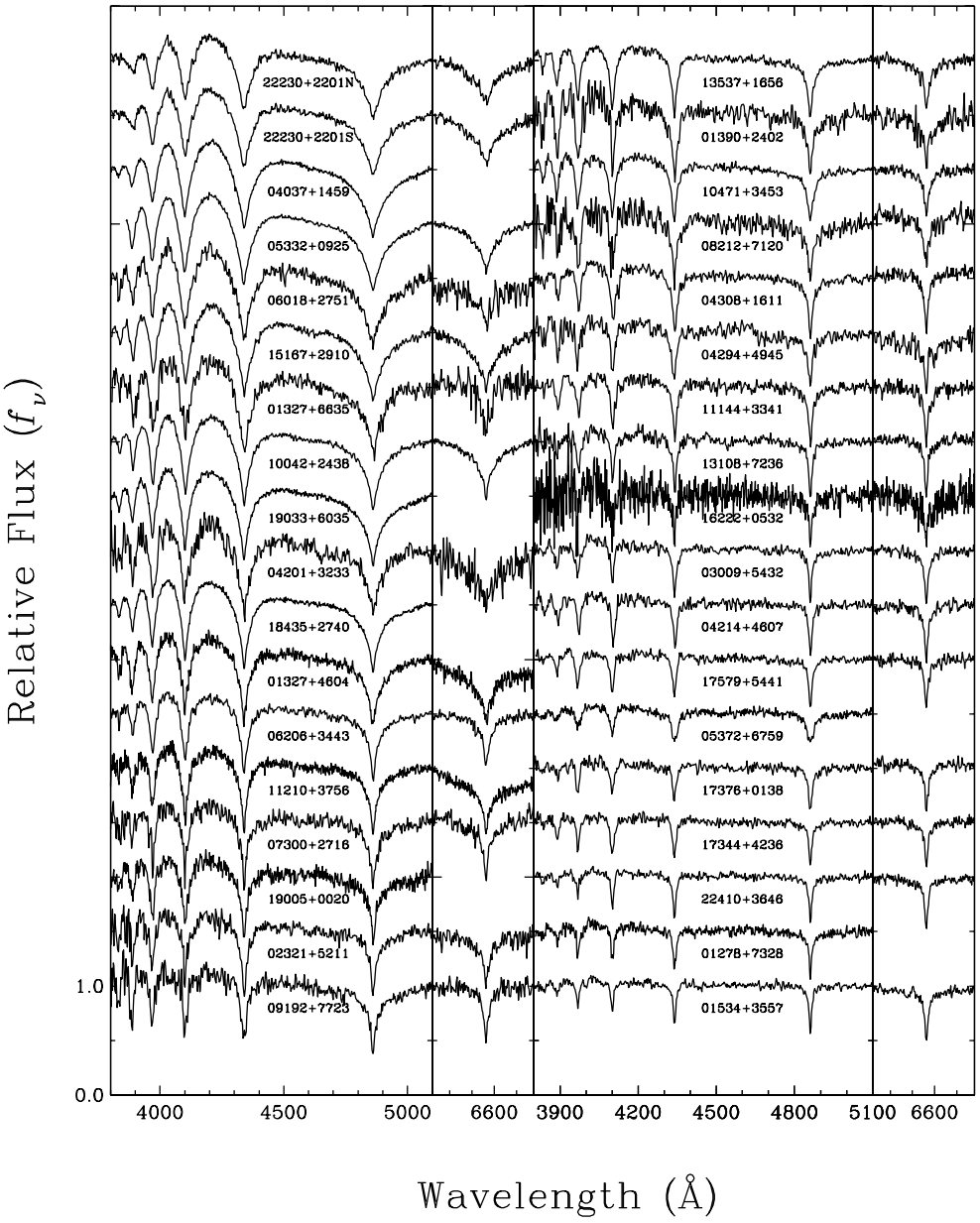

FIGURE 3.2 – (a) Optical spectra for our new, spectroscopically confirmed DA white dwarfs, displayed in order of decreasing effective temperature (upper left to bottom right) and shifted vertically for clarity; 05431+3637 is a DAZ star. The Hα line is also shown when available, and normalized to a continuum set to unity. The last 3 spectra at the bottom of the right panel are new observations of stars already presented in Paper I that are double degenerate binary candidates.

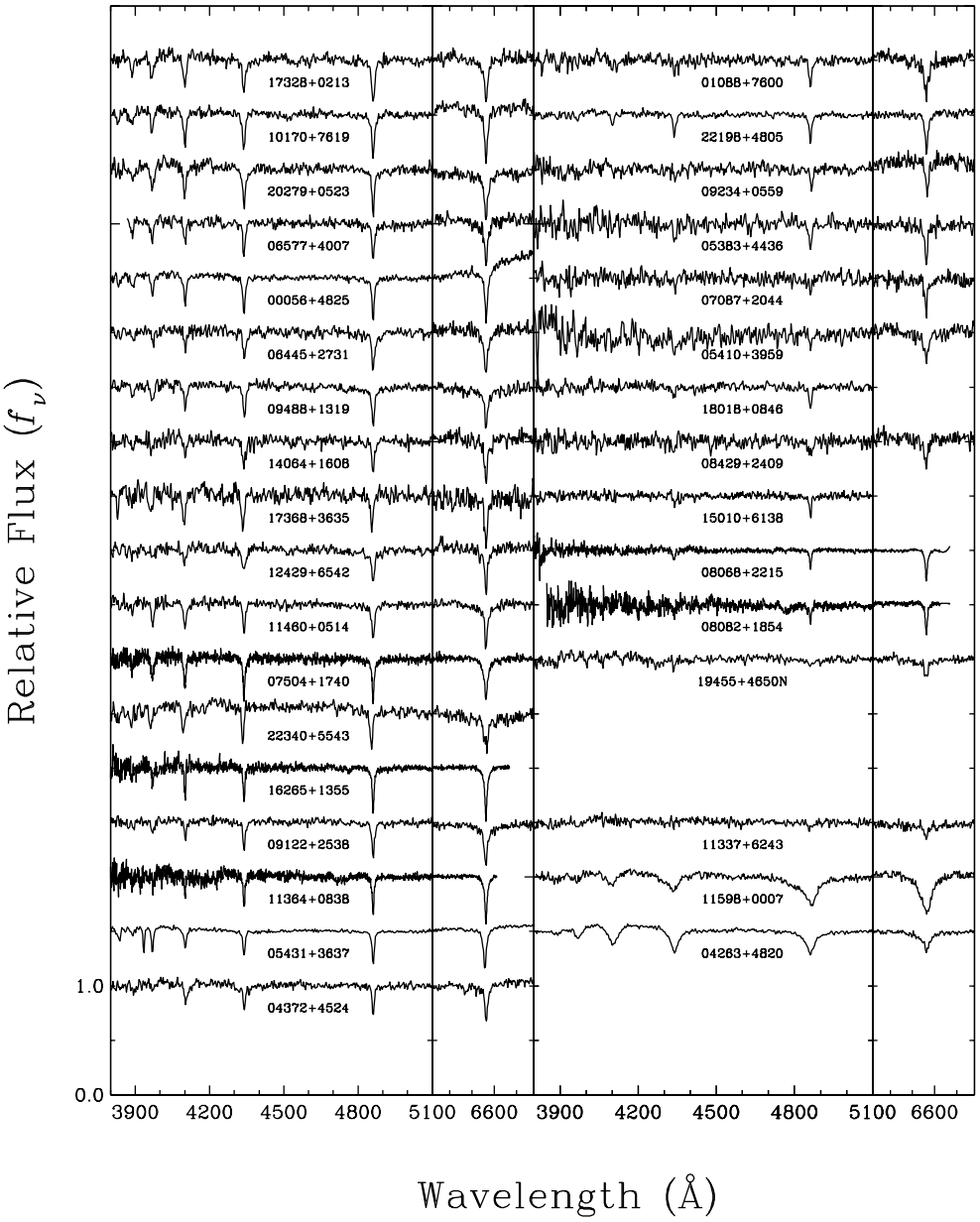

FIGURE 3.2 – (b) - continued.

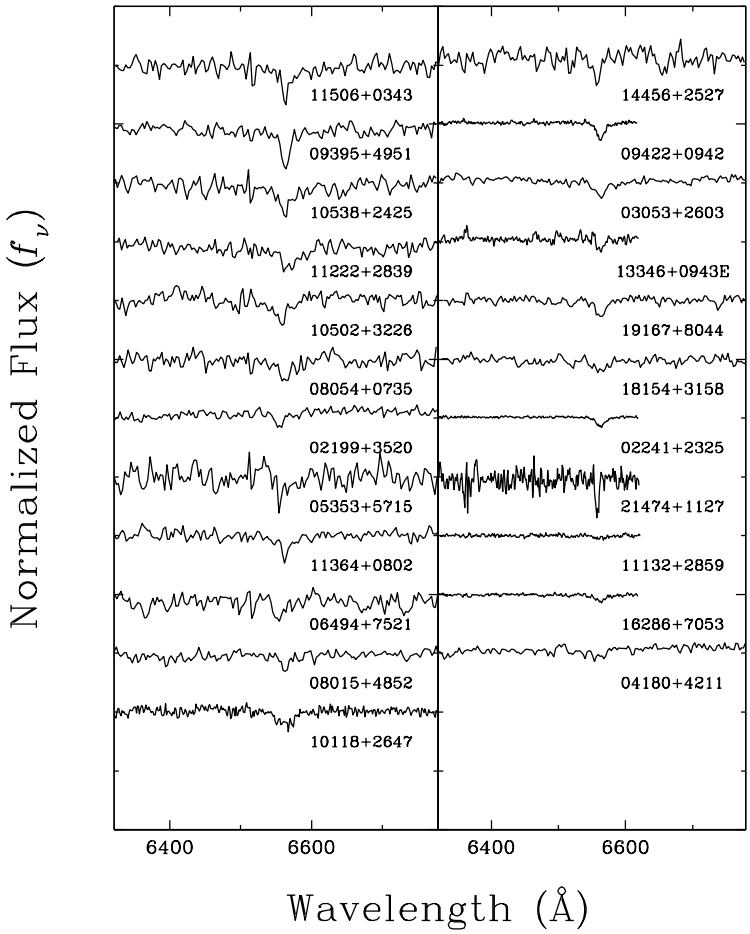

FIGURE 3.3 – Hα line for our new, spectroscopically confirmed DA stars, too cool to exhibit the rest of the Balmer series. Spectra are displayed in order of decreasing temperature from upper left to bottom right, are normalized to a continuum set to unity, and shifted vertically for clarity.

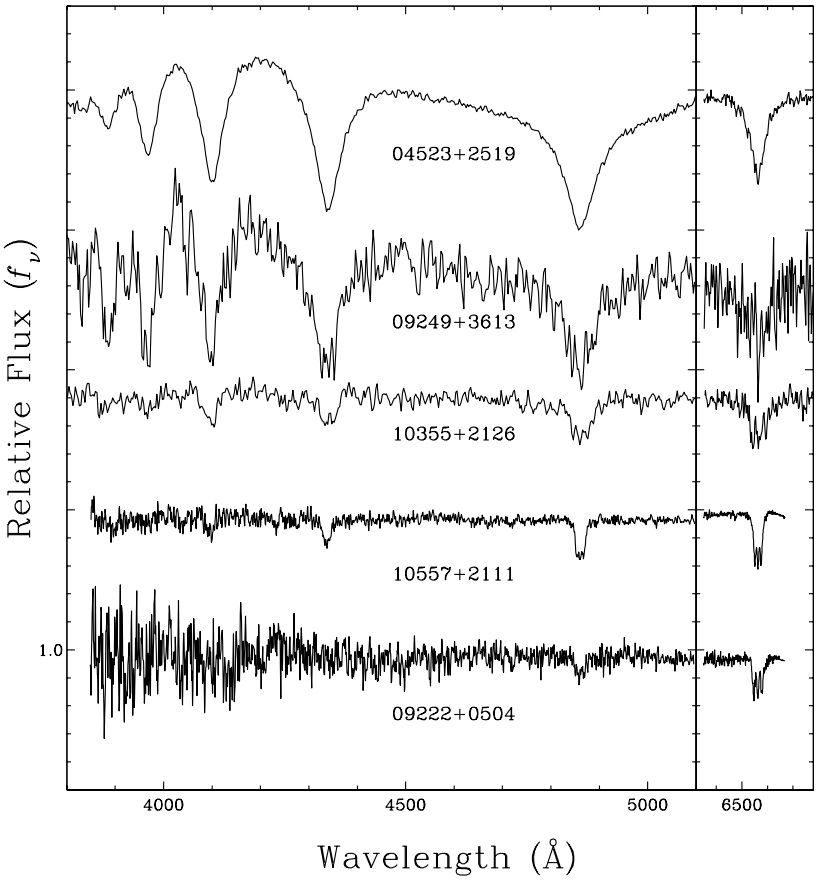

FIGURE 3.4 – Spectra of our newly identified, magnetic DA white dwarfs, shifted vertically for clarity. 04523 + 2519 was classified as non-magnetic in Paper I. All others are new white dwarf discoveries.

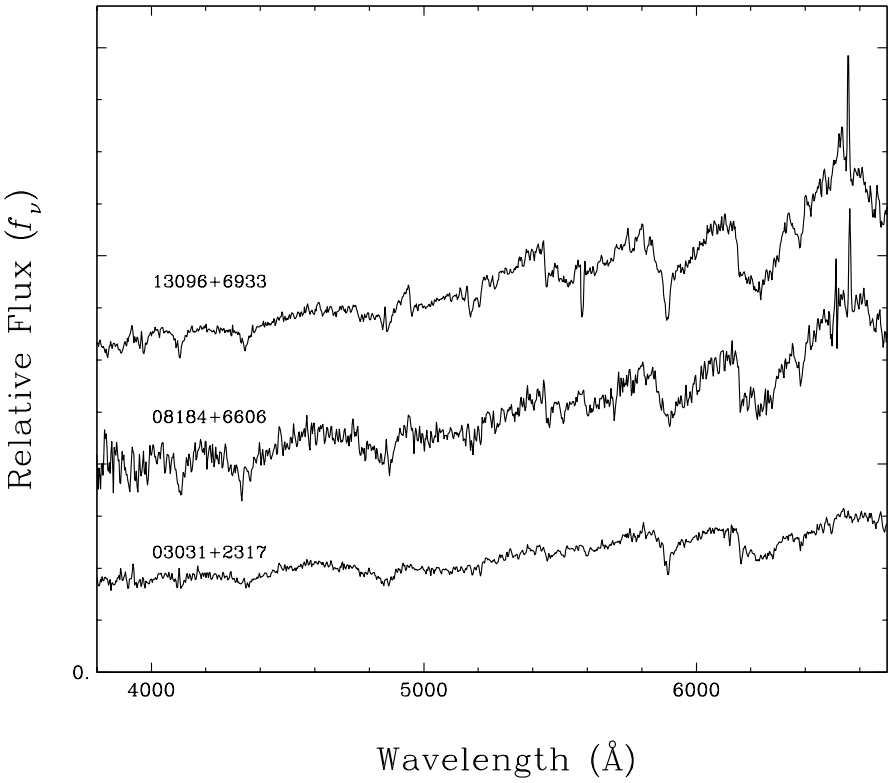

FIGURE 3.5 – Spectra of our newly identified binary systems composed of a DA white dwarf and an M dwarf companion. Spectra are shifted vertically for clarity. The Hα and Hβ line cores of 13096+6933 and 08184+6606 are contaminated by line emission from the chromospherically active M dwarf.

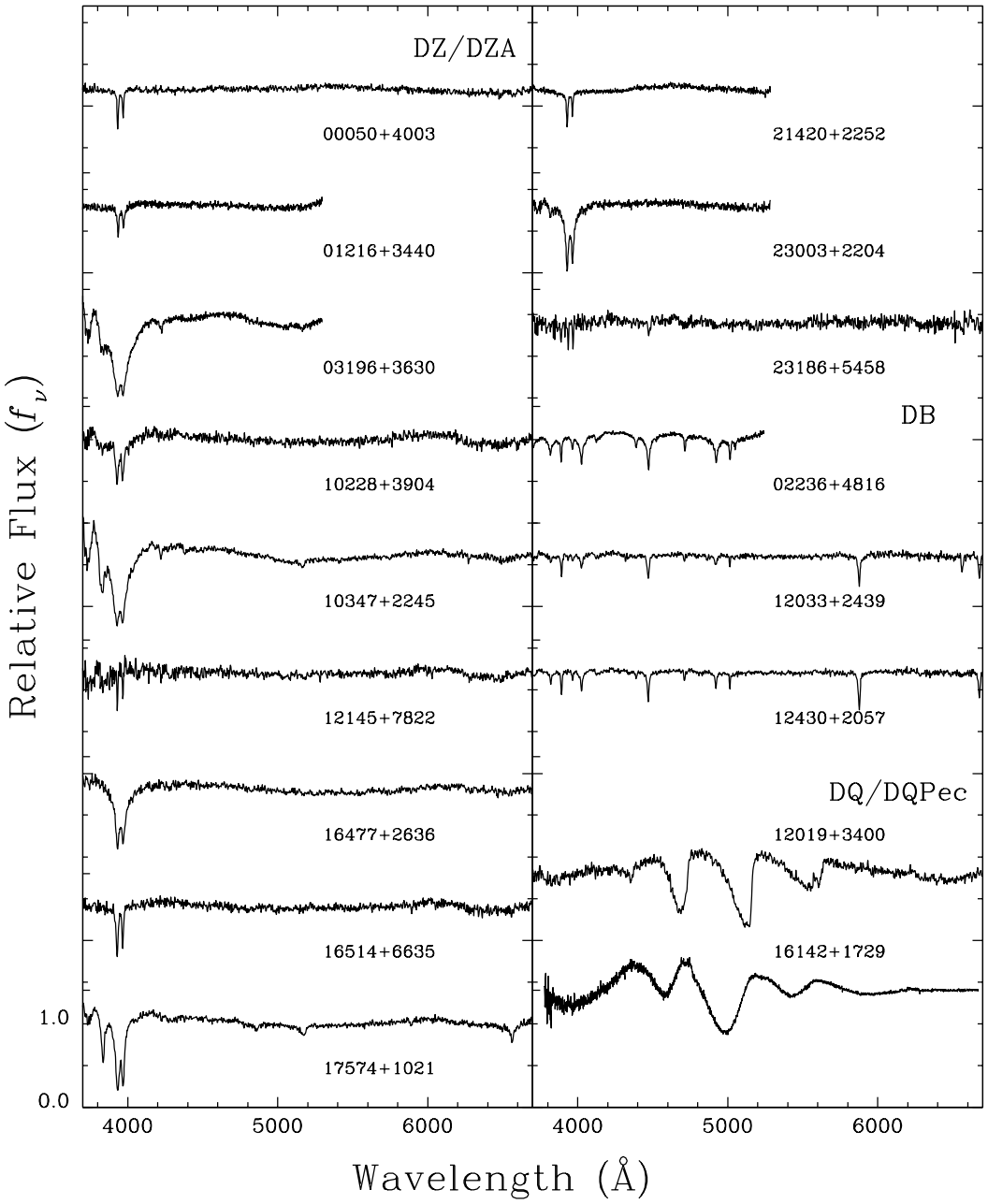

FIGURE 3.6 – New spectra of DZ (DZA), DB (DBZ), and DQ stars. Spectra for the DZ stars 01216+3440, 03196+3630, 16477+2636, 21420+2252, and 23003+2204 represent new higher S/N observations of stars reported in Paper I, used to better constrain the metal abundances.

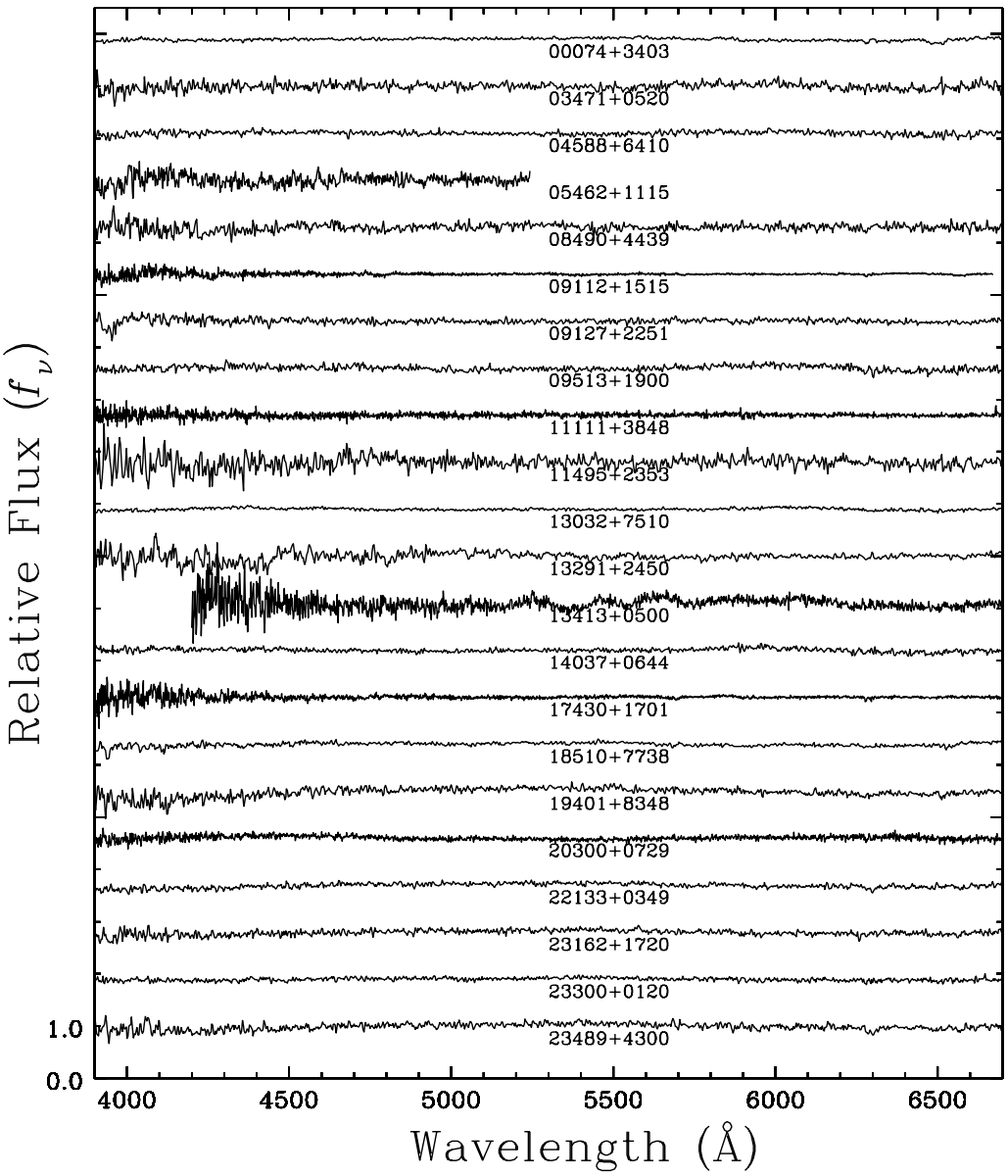

FIGURE 3.7 – Optical spectra for our new, spectroscopically confirmed DC stars. All spectra are normalized to a continuum set to unity and are offset from each other by a factor of 0.9.

The progress of our spectroscopic survey can also be summarized in the color-color diagram shown in Figure 3.8, where we display the subset of 150 spectroscopically confirmed white dwarfs in our sample that also have available *ugriz* photometry from SDSS. White dwarf candidates without spectroscopic confirmation are shown in red, and most of these have estimated distances larger than 30 pc, as can be seen from Figure 3.1. This figure reveals that our sample of new white dwarfs is composed mainly of DA stars, but also contains a significant number of cool ($T_{\rm eff} < 5000$ K) white dwarfs, with objects as cool as $T_{\rm eff} \sim$4000 K.

Finally, the entire white dwarf population detected in SUPERBLINK is presented in Figure 3.9, where we display its distribution on the sky. In the upper panel, the 322 new identifications

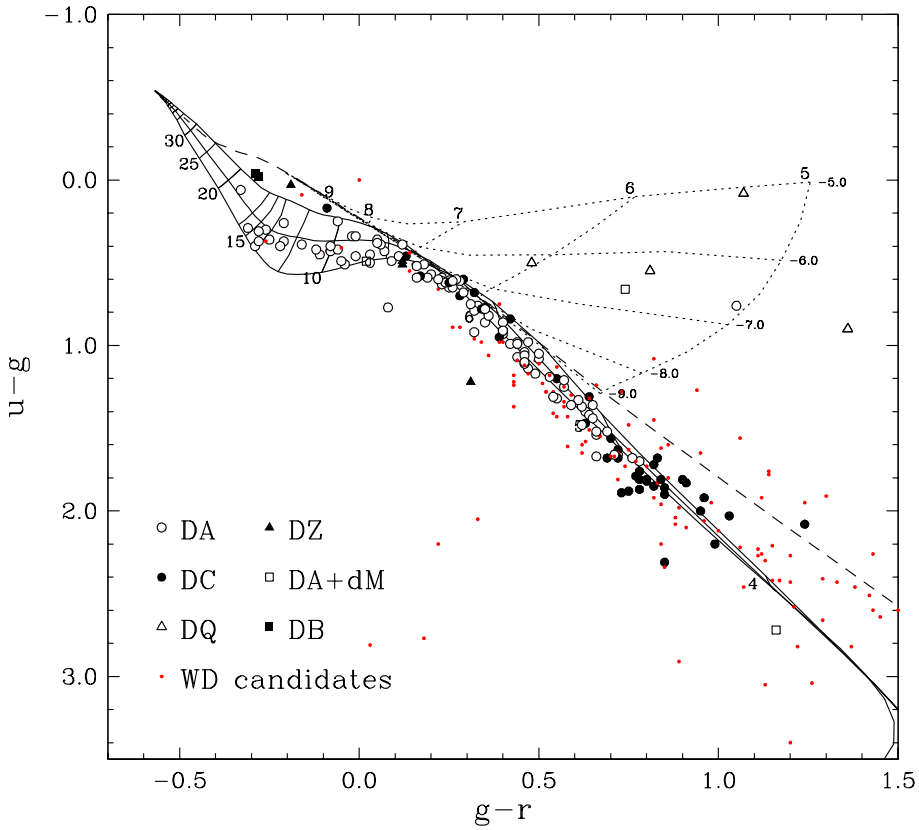

FIGURE 3.8 – $(u-g,\ g-r)$ color-color diagram showing all stars in our survey for which *ugriz* photometry is available. The 150 spectroscopically confirmed white dwarfs are shown with various black symbols explained in the legend, while the 128 white dwarf candidates still lacking spectroscopic data are shown with red dots. The solid curves represent pure hydrogen model atmospheres at $\log g = 7.0$, 8.0, and 9.0 (from bottom to top); effective temperatures are indicated in units of 10^3 K. The dashed curve corresponds to pure helium atmospheres at $\log g = 8.0$, and the dotted lines represent DQ models for 5 different compositions, from $\log {\rm C/He} = -9.0$ to -5.0.

are shown with solid dots, while the white dwarfs from the literature are represented with open circles. In the bottom panel, we plot the sky density as a function of right ascension for the 'old' white dwarf population (dotted line), and compare it to that of the 322 new identifications (dashed line) and to the sum of the old and new white dwarfs (solid line). In Paper I, Figure 11 showed that the white dwarf candidates in our survey had the potential to fill the void left in the galactic plane by earlier surveys. Here we notice that the density of new identifications, especially near RA = 100, suggests we are on our way to identify the missing white dwarfs in this particular region of the sky.

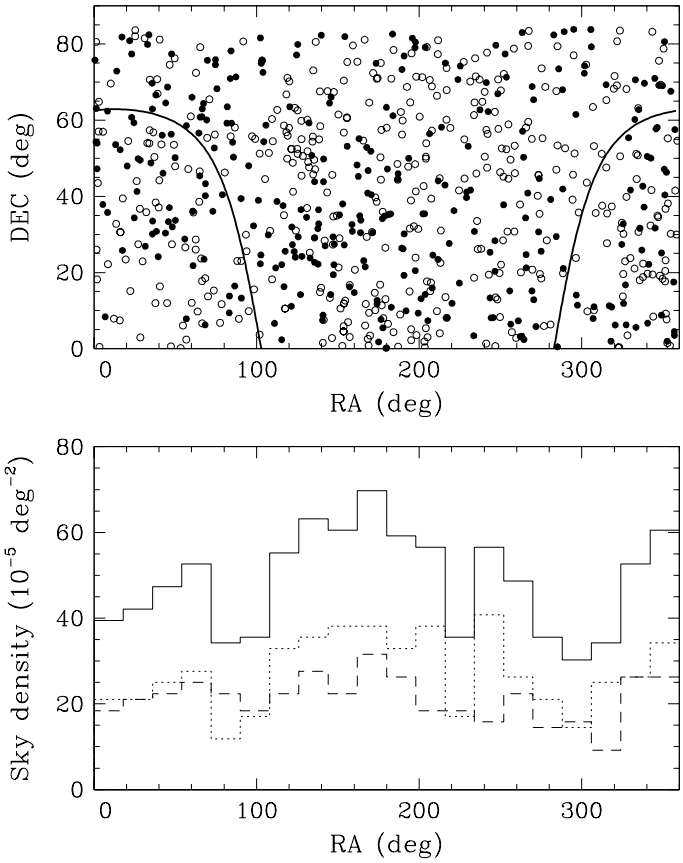

FIGURE 3.9 – Upper panel: Equal cylindrical projection of the equatorial coordinates for the sample of white dwarfs identified from SUPERBLINK. The 416 previously known stars from the WD Catalog recovered by our selection criteria (open circles) are compared to the 322 new WD identifications (solid circles). Also shown by the bold solid line is the region of the galactic plane. Lower panel: Sky density as a function of right ascension, normalized to the total number of white dwarf stars (all lines are thus on a comparable scale). The dotted line represents the 416 stars from the WD Catalog recovered by our selection criteria, while the dashed line corresponds to the 322 new identifications only. Finally, the solid line represents the sum of the contributions of the new and known white dwarfs.

TABLE 3.2 – Spectroscopically Confirmed White Dwarfs from SUPERBLINK − Astrometry

PM I	NLTT	SDSS	RA J_{2000}	DEC J_{2000}	$\mu_{\rm tot}$ ($''{\rm yr}^{-1}$)	μRA ($''{\rm yr}^{-1}$)	μDE ($''{\rm yr}^{-1}$)
00050+4003	133		00:05:01.08	+40:03:34.6	0.229	0.206	0.101
00056+4825			00:05:40.41	+48:25:05.9	0.153	0.152	−0.013
00074+3403	301		00:07:28.87	+34:03:39.9	0.199	0.021	0.197
01088+7600			01:08:49.61	+76:00:18.4	0.242	0.237	0.050
01278+7328	4799		01:27:49.09	+73:28:47.7	0.177	−0.160	0.076
01327+4604	5100		01:32:46.67	+46:04:58.8	0.211	−0.211	−0.002
01327+6635			01:32:42.90	+66:35:46.0	0.051	0.039	−0.033
01390+2402		J013900.25+24025	01:39:00.18	+24:02:58.8	0.096	0.094	−0.021
01534+3557			01:53:28.98	+35:57:29.2	0.175	0.174	−0.020
02199+3520			02:19:59.83	+35:20:18.0	0.135	0.133	0.024
02236+4816			02:23:40.36	+48:16:47.5	0.116	0.112	−0.028
02241+2325		J022411.67+23251	02:24:11.70	+23:25:18.8	0.111	−0.086	−0.070
02321+5211			02:32:10.24	+52:11:51.0	0.113	0.085	−0.075
03009+5432			03:00:59.53	+54:32:37.5	0.232	0.162	−0.166
03031+2317			03:03:07.50	+23:17:40.7	0.059	0.058	−0.012
03053+2603	9826		03:05:21.02	+26:03:12.2	0.194	−0.176	−0.081
03471+0520W			03:47:06.63	+05:20:14.5	0.167	0.161	−0.045
04037+1459		J040342.15+14592	04:03:42.08	+14:59:28.7	0.140	0.139	−0.015
04180+4211	12934		04:18:05.53	+42:11:02.2	0.214	−0.046	−0.209
04201+3233			04:20:06.31	+32:33:05.2	0.083	0.046	−0.069
04214+4607			04:21:29.34	+46:07:57.7	0.120	0.059	−0.104
04294+4945			04:29:26.36	+49:45:54.0	0.190	0.021	−0.188
04308+1611			04:30:49.87	+16:11:06.5	0.150	0.045	−0.143
04372+4524			04:37:15.48	+45:24:33.1	0.113	−0.113	−0.001
04588+6410			04:58:53.28	+64:10:44.0	0.074	−0.018	−0.072
05332+0925			05:33:14.80	+09:25:59.8	0.090	−0.067	−0.061
05353+5715	15285		05:35:23.06	+57:15:56.1	0.275	0.173	−0.214
05372+6759			05:37:14.89	+67:59:50.4	0.065	−0.029	−0.058
05383+4436			05:38:18.31	+44:36:47.8	0.080	0.011	−0.078
05410+3959			05:41:03.85	+39:59:45.4	0.566	0.335	−0.448
05431+3637			05:43:07.37	+36:37:01.2	0.163	−0.155	−0.050
05462+1115			05:46:15.59	+11:15:58.7	0.198	−0.127	−0.152
06018+2751			06:01:53.51	+27:51:35.7	0.064	0.012	−0.062
06206+3443		J062038.90+34430	06:20:38.85	+34:43:05.6	0.077	−0.023	−0.073
06445+2731		J064430.09+27311	06:44:30.18	+27:31:11.4	0.153	−0.146	−0.046

TABLE 3.2 – Continued

PM I	NLTT	SDSS	RA J_{2000}	DEC J_{2000}	$\mu_{\rm tot}$ ($''{\rm yr}^{-1}$)	μRA ($''{\rm yr}^{-1}$)	μDE ($''{\rm yr}^{-1}$)
06494+7521	16943		06:49:26.50	+75:21:24.9	0.089	0.088	−0.013
06577+4007			06:57:45.12	+40:07:25.7	0.109	0.093	−0.054
07087+2044			07:08:45.79	+20:44:51.6	0.122	0.082	−0.090
07300+2716W		J072959.99+27164	07:30:00.01	+27:16:41.2	0.162	−0.136	−0.089
07504+1740		J075026.30+17402	07:50:26.28	+17:40:30.1	0.127	0.059	−0.112
08015+4852		J080131.82+48525	08:01:31.88	+48:52:52.3	0.117	−0.116	0.014
08054+0735	18922		08:05:27.55	+07:35:35.6	0.378	−0.075	−0.370
08068+2215		J080648.04+22155	08:06:48.05	+22:15:51.6	0.169	−0.008	−0.169
08082+1854	18981		08:08:12.78	+18:54:21.6	0.202	−0.143	−0.143
08184+6606		J081825.96+66064	08:18:26.02	+66:06:45.2	0.074	−0.016	−0.073
08212+7120			08:21:12.39	+71:20:09.3	0.069	−0.068	−0.015
08429+2409		J084257.57+24093	08:42:57.59	+24:09:30.8	0.110	−0.100	−0.046
08490+4439	20277	J084901.61+44393	08:49:01.65	+44:39:35.6	0.223	−0.194	−0.110
09112+1515		J091112.15+15154	09:11:12.21	+15:15:49.2	0.144	0.063	−0.129
09122+2538		J091216.43+25382	09:12:16.40	+25:38:22.3	0.115	0.049	−0.104
09127+2251	21205	J091247.92+22515	09:12:47.95	+22:51:55.3	0.169	−0.097	−0.138
09192+7723			09:19:14.81	+77:23:50.9	0.109	−0.040	−0.101
09222+0504	21580		09:22:13.54	+05:04:37.4	0.251	−0.248	−0.043
09234+0559		J092326.91+05590	09:23:26.92	+05:59:06.3	0.146	0.066	−0.130
09249+3613		J092455.63+36130	09:24:55.42	+36:13:09.7	0.080	−0.061	−0.052
09395+4951		J093931.66+49514	09:39:31.74	+49:51:48.3	0.379	−0.379	−0.010
09422+0942		J094213.02+09424	09:42:13.07	+09:42:45.4	0.142	−0.141	−0.018
09488+1319		J094850.12+13192	09:48:50.08	+13:19:27.4	0.144	0.082	−0.118
09513+1900	22762	J095120.16+19001	09:51:20.08	+19:00:11.9	0.274	0.173	−0.213
10042+2438		J100412.46+24384	10:04:12.44	+24:38:50.2	0.054	0.005	−0.054
10118+2647			10:11:50.99	+26:47:45.3	0.142	0.133	0.049
10170+7619	23808		10:17:04.19	+76:19:02.9	0.212	0.190	−0.094
10228+3904	24170	J102251.63+39041	10:22:51.75	+39:04:14.8	0.464	−0.428	−0.180
10347+2245	24727		10:34:43.40	+22:45:48.3	0.223	−0.221	−0.025
10355+2126	24770	J103532.53+21260	10:35:32.62	+21:26:04.5	0.164	−0.077	−0.145
10471+3453		J104709.16+34534	10:47:09.20	+34:53:46.3	0.063	−0.056	−0.029
10502+3226		J105016.31+32260	10:50:16.32	+32:26:02.1	0.140	0.040	−0.134
10538+2425	25646	J105349.49+24253	10:53:49.64	+24:25:32.6	0.361	−0.355	−0.063
10557+2111		J105544.90+21110	10:55:44.95	+21:11:05.6	0.191	−0.153	−0.114
11111+3848			11:11:09.14	+38:48:57.3	0.128	0.120	−0.044

TABLE 3.2 – Continued

PM I	NLTT	SDSS	RA J_{2000}	DEC J_{2000}	$\mu_{\rm tot}$ ($''{\rm yr}^{-1}$)	μRA ($''{\rm yr}^{-1}$)	μDE ($''{\rm yr}^{-1}$)
11132+2859	26653		11:13:16.58	+28:59:07.8	0.381	−0.187	−0.332
11144+3341	26706	J111424.65+33412	11:14:24.67	+33:41:24.3	0.152	−0.031	−0.149
11210+3756		J112105.79+37561	11:21:05.81	+37:56:15.3	0.077	−0.050	−0.059
11222+2839	27173	J112215.84+28394	11:22:15.93	+28:39:42.6	0.265	−0.257	−0.065
11364+0802S			11:36:24.33	+08:02:15.7	0.214	−0.179	−0.118
11364+0838			11:36:27.59	+08:38:37.9	0.084	−0.057	−0.062
11460+0514		J114604.36+05140	11:46:04.39	+05:14:01.7	0.092	−0.090	0.017
11495+2353	28667	J114935.69+23532	11:49:35.72	+23:53:21.0	0.184	−0.183	−0.017
11506+0343	28735	J115038.73+03430	11:50:38.74	+03:43:01.6	0.258	−0.143	−0.215
12019+3400		J120154.69+34005	12:01:54.70	+34:00:55.5	0.130	−0.027	0.127
12033+2439		J120319.77+24395	12:03:19.80	+24:39:54.0	0.110	−0.109	0.012
12145+7822	30084		12:14:31.79	+78:22:56.1	0.290	0.135	−0.256
12429+6542		J124258.39+65421	12:42:58.41	+65:42:20.2	0.161	−0.106	−0.121
12430+2057		J124306.04+20570	12:43:05.99	+20:57:10.6	0.088	0.076	−0.044
13032+7510			13:03:14.16	+75:10:04.1	0.117	0.061	0.100
13096+6933			13:09:38.03	+69:33:15.6	0.084	−0.079	0.029
13108+7236			13:10:50.73	+72:36:33.8	0.088	−0.061	0.064
13291+2450		J132906.08+24502	13:29:06.19	+24:50:25.7	0.405	−0.404	−0.024
13346+0943E			13:34:38.82	+09:43:18.5	0.201	−0.200	0.021
13413+0500			13:41:21.80	+05:00:45.8	0.429	−0.428	0.020
13537+1656		J135342.38+16565	13:53:42.35	+16:56:51.7	0.103	0.072	−0.074
14037+0644		J140346.10+06444	14:03:46.08	+06:44:43.0	0.127	0.057	−0.114
14064+1608		J140625.56+16082	14:06:25.59	+16:08:27.7	0.121	−0.112	−0.045
14456+2527		J144539.44+25271	14:45:39.46	+25:27:15.9	0.155	−0.033	−0.152
15010+6138		J150105.31+61385	15:01:05.31	+61:38:54.6	0.100	−0.050	−0.087
15167+2910		J151644.70+29102	15:16:44.73	+29:10:21.4	0.086	−0.036	0.078
16142+1729	42302	J161414.12+17290	16:14:14.23	+17:29:00.3	0.260	−0.194	−0.173
16222+0532	42621	J162216.16+05325	16:22:16.19	+05:32:52.2	0.135	−0.130	−0.038
16265+1355		J162632.08+13555	16:26:32.04	+13:55:54.5	0.167	0.132	0.103
16286+7053	42988		16:28:38.60	+70:53:21.6	0.462	−0.002	−0.462
16514+6635			16:51:26.02	+66:35:06.3	0.109	−0.059	0.092
17328+0213			17:32:48.41	+02:13:08.8	0.089	0.072	−0.053
17344+4236			17:34:26.42	+42:36:40.5	0.126	−0.079	−0.098
17368+3635			17:36:52.13	+36:35:44.6	0.103	−0.096	−0.038
17376+0138			17:37:41.38	+01:38:49.8	0.093	−0.037	−0.085

TABLE 3.2 – Continued

PM I	NLTT	SDSS	RA J_{2000}	DEC J_{2000}	$\mu_{\rm tot}$ ($''{\rm yr}^{-1}$)	μRA ($''{\rm yr}^{-1}$)	μDE ($''{\rm yr}^{-1}$)
17430+1701	45332		17:43:00.76	+17:01:45.9	0.364	−0.248	−0.266
17574+1021			17:57:25.79	+10:21:24.9	0.091	−0.020	−0.088
17579+5441		J175759.50+54412	17:57:59.45	+54:41:21.8	0.074	−0.061	−0.041
18018+0846			18:01:51.35	+08:46:06.9	0.190	0.115	0.151
18154+3158	46186		18:15:27.40	+31:58:49.2	0.210	0.124	0.170
18435+2740			18:43:35.47	+27:40:26.8	0.095	0.043	−0.085
18510+7738	47202	J185106.01+77383	18:51:05.66	+77:38:37.2	0.270	0.261	−0.069
19005+0020			19:00:34.98	+00:20:17.4	0.270	−0.143	−0.229
19033+6035			19:03:19.56	+60:35:52.7	0.194	0.174	0.088
19167+8044			19:16:47.18	+80:44:30.1	0.183	0.073	0.167
19401+8348			19:40:08.67	+83:48:57.7	0.936	−0.838	−0.417
19455+4650N			19:45:30.37	+46:50:15.5	0.612	−0.455	−0.409
20279+0523			20:27:58.78	+05:23:53.8	0.120	0.072	−0.096
20300+0729	49350		20:30:04.10	+07:29:43.7	0.250	0.171	−0.182
21474+1127			21:47:25.20	+11:27:55.3	0.273	0.103	−0.252
22133+0349	53229		22:13:21.32	+03:49:11.1	0.465	0.322	−0.334
22198+4805			22:19:53.89	+48:05:34.3	0.271	0.188	0.196
22230+2201N			22:23:01.60	+22:01:31.8	0.082	0.054	−0.062
22230+2201S			22:23:01.69	+22:01:25.3	0.082	0.054	−0.062
22340+5543			22:34:02.03	+55:43:26.1	0.218	0.202	0.080
22410+3646			22:41:04.63	+36:46:38.8	0.169	0.162	0.047
23162+1720	56301	J231612.68+17204	23:16:12.53	+17:20:45.6	0.287	0.286	−0.014
23186+5458		J231838.29+54581	23:18:38.33	+54:58:16.8	0.099	0.019	−0.097
23300+0120	57056		23:30:05.52	+01:20:46.1	0.247	0.209	−0.132
23489+4300	58060	J234857.96+43003	23:48:57.89	+43:00:39.7	0.295	0.162	−0.247

TABLE 3.3 – Spectroscopically Confirmed White Dwarfs from SUPERBLINK − Photometry

PM I	FUV	NUV	B_F	R_I	I_N	J	H	K_S	u	g	r	i	z	ST	Notes
00023+6357	–	–	17.8	16.2	17.3	15.80	15.57	15.51	–	–	–	–	–	DC	
00050+4003	–	18.14	16.3	16.2	16.5	–	–	–	–	–	–	–	–	DZA:	
00056+4825	–	19.38	17.1	16.9	16.5	16.25	15.60	15.89	–	–	–	–	–	DA	
00074+3403	–	21.07	17.7	17.3	16.8	16.39	16.25	15.83	–	–	–	–	–	DC:	
00079+3947	–	–	17.4	16.2	15.8	15.18	14.85	14.65	–	–	–	–	–	DC	
00217+2640	–	–	17.9	17.2	16.9	16.18	15.91	15.81	–	–	–	–	–	DC	
00276+0542	–	–	17.2	15.6	15.4	14.97	14.67	14.57	–	–	–	–	–	DA	
00331+4742S	14.55	14.63	14.9	14.9	–	15.16	15.02	15.14	–	–	–	–	–	DA	
00334+2506	–	20.36	16.6	16.6	16.1	15.96	15.70	15.45	17.88	17.12	16.79	16.69	16.68	DA	
00532+3927	–	18.45	17.9	16.4	16.8	16.03	15.84	15.40	–	–	–	–	–	DA	
00559+5948	–	–	15.2	16.0	15.8	15.44	15.21	15.03	–	–	–	–	–	DC:	
01043+3816	14.70	14.80	15.6	15.4	–	15.29	15.32	15.14	–	–	–	–	–	DA	
01088+7600	–	20.76	17.9	17.4	16.9	16.60	16.40	16.84	–	–	–	–	–	DA	
01216+3440	–	19.64	17.9	16.3	15.9	16.13	16.15	15.88	17.27	16.76	16.64	16.64	16.74	DZ	
01278+7328	–	–	16.2	14.9	14.5	14.76	10.17	9.79	–	–	–	–	–	DA	
01327+4604	18.19	15.94	16.0	15.2	14.3	14.90	15.09	15.23	15.42	14.97	15.08	15.23	15.45	DA	1
01327+6635	16.67	16.56	17.1	16.1	16.4	–	–	–	–	–	–	–	–	DA	
01382+4442	15.79	15.84	15.5	16.0	15.2	15.62	15.61	15.71	–	–	–	–	–	DA	
01390+2402	–	19.66	17.6	16.7	16.7	–	–	–	18.69	17.92	17.84	17.84	17.90	DA	
01457+2918	–	–	18.4	18.0	17.7	16.56	16.09	15.51	–	–	–	–	–	DC	
01486+3615	–	20.64	17.6	16.5	16.3	15.85	15.48	15.42	–	–	–	–	–	DA	
01534+3557	–	19.30	17.1	16.7	16.4	16.53	16.01	15.74	–	–	–	–	–	DA	
01565+2955	14.56	14.68	14.7	14.9	–	14.96	15.04	15.18	–	–	–	–	–	DA	
02062+1836	–	–	19.2	17.8	17.1	16.50	16.38	15.63	–	–	–	–	–	DC	
02118+7119	–	–	17.8	16.4	16.6	15.78	15.42	15.32	19.04	17.57	16.94	16.67	16.57	DC	

TABLE 3.3 – Continued

PM I	FUV	NUV	B_F	R_I	I_N	J	H	K_S	u	g	r	i	z	ST	Notes
02149+7746	–	–	19.2	18.0	18.1	16.48	17.50	15.89	–	–	–	–	–	DC	
02199+3520	–	–	17.9	17.3	16.7	16.53	15.87	16.02	–	–	–	–	–	DA	
02230+5544	–	–	17.2	16.6	16.8	16.07	15.77	15.68	–	–	–	–	–	DA	
02236+4816	–	–	15.1	15.4	14.5	15.42	15.67	15.34	–	–	–	–	–	DB	
02238+2055	–	–	19.6	17.9	17.4	16.77	16.72	17.15	21.30	19.10	18.11	17.77	17.57	DC	
02241+2325	–	–	19.4	18.5	18.4	–	–	–	21.02	19.36	18.64	18.39	18.24	DA	
02321+5211	21.78	18.16	16.9	16.9	16.5	–	–	–	–	–	–	–	–	DA	
02334+2125	–	–	18.2	16.5	–	15.95	15.39	15.74	19.85	18.04	17.14	16.88	16.73	DC	
02379+1638	–	–	17.6	16.8	16.7	15.97	15.83	14.88	–	–	–	–	–	DC	
02478+4138	16.81	16.41	15.1	16.3	16.4	16.95	17.86	17.19	–	–	–	–	–	DB	
02497+3307	–	21.05	18.0	16.7	16.4	16.01	15.49	15.39	18.47	17.43	16.97	16.79	16.73	DA	
02557+2106S	–	–	17.7	17.1	16.5	16.48	16.04	16.06	18.47	17.68	17.36	17.25	17.20	DA	
02562+4954	–	–	17.5	17.1	16.4	16.17	15.79	15.45	–	–	–	–	–	DA	
03009+5432	–	18.55	17.2	16.5	16.0	16.07	15.92	15.75	–	–	–	–	–	DA	
03031+2317	15.11	15.73	15.8	15.4	14.1	13.00	12.32	12.07	–	–	–	–	–	DA+dM	
03053+2603	–	–	18.5	17.6	17.3	16.76	16.30	15.77	–	–	–	–	–	DA	
03109+6634	–	–	18.8	17.7	17.4	16.55	16.30	15.31	–	–	–	–	–	DC	
03127+2218	–	19.86	17.8	16.4	16.8	16.13	15.85	15.88	–	–	–	–	–	DA	
03196+3630	–	20.74	17.3	16.2	16.1	15.84	15.84	15.38	–	–	–	–	–	DZ	
03203+2333	–	–	18.9	17.0	17.0	16.21	15.65	15.76	–	–	–	–	–	DC	
03433+1958	–	–	16.6	15.2	15.2	14.95	14.96	15.04	–	–	–	–	–	DA	
03471+0520W	–	21.07	18.8	17.3	17.2	–	–	–	18.63	18.20	18.04	18.06	18.12	DC	
03473+4358	–	–	14.3	14.3	14.3	14.23	14.30	14.36	–	–	–	–	–	DA	
04010+5131W	–	–	17.5	16.8	16.4	15.93	15.74	15.20	19.34	17.78	17.08	16.83	16.72	DC	
04032+2520E	14.42	14.91	15.4	14.6	13.0	12.36	11.77	11.51	–	–	–	–	–	DA+dM	

TABLE 3.3 – Continued

PM I	FUV	NUV	B_F	R_I	I_N	J	H	K_S	u	g	r	i	z	ST	Notes
04032+2520W	14.42	14.91	15.4	14.6	13.0	12.36	11.77	11.51	–	–	–	–	–	DA	
04037+1459	15.07	15.07	15.0	15.2	15.0	15.42	15.70	15.33	15.18	14.88	15.14	15.39	15.65	DA	2
04180+4211	–	–	17.5	16.9	16.4	15.70	15.36	15.61	–	–	–	–	–	DA	
04201+3233	15.68	15.86	16.0	16.1	–	16.38	16.01	16.36	–	–	–	–	–	DA	
04214+4607	–	–	15.5	15.2	15.3	14.72	14.51	14.44	–	–	–	–	–	DA	
04259+4614	–	–	19.0	17.2	17.0	16.46	16.00	16.08	–	–	–	–	–	DC	
04263+4820	16.95	17.00	16.0	15.9	15.9	15.64	15.65	15.30	–	–	–	–	–	DA+DC	
04294+4945	–	17.91	16.5	16.3	16.4	15.97	15.75	15.98	–	–	–	–	–	DA	
04308+1611	–	–	17.0	16.2	16.2	16.16	16.07	14.98	–	–	–	–	–	DA	
04334+0414	–	–	17.4	16.3	16.1	15.55	15.26	15.18	–	–	–	–	–	DA	
04339+2827	–	–	16.0	15.8	–	15.48	14.79	14.56	–	–	–	–	–	DA	
04343+3054	–	–	18.8	17.6	17.5	16.49	16.35	15.83	–	–	–	–	–	DC:	
04372+4524	–	–	17.2	17.0	16.6	16.00	15.85	15.52	–	–	–	–	–	DA	
04389+6351	–	–	17.2	16.8	16.1	15.39	14.72	14.24	–	–	–	–	–	DA+dM	
04523+2519	–	–	15.2	14.8	14.6	15.08	15.15	15.17	–	–	–	–	–	DAH	3
04558+3840	–	–	18.1	16.9	16.8	16.14	15.85	15.32	–	–	–	–	–	DA	
04586+6209	15.68	15.77	15.5	14.1	–	11.31	10.76	10.55	–	–	–	–	–	DA+dM	
04588+6410	–	–	17.4	16.8	16.7	–	–	–	–	–	–	–	–	DC	
05025+5401	–	–	15.3	15.4	15.3	15.27	15.30	15.08	–	–	–	–	–	DA	
05158+2839	–	19.58	16.5	16.0	15.9	15.66	15.31	15.27	–	–	–	–	–	DAH	
05269+4435	–	–	18.8	17.4	17.5	16.50	16.42	15.85	–	–	–	–	–	DC	
05280+4850	18.42	17.63	17.2	15.0	13.1	12.60	12.00	11.73	–	–	–	–	–	DA+dM	
05327+0624	–	–	16.5	16.1	16.1	–	–	–	–	–	–	–	–	DA	
05332+0925	–	–	15.8	15.3	15.5	15.55	15.60	15.61	–	–	–	–	–	DA	
05353+5715	–	–	18.3	17.2	17.0	16.46	16.18	16.29	–	–	–	–	–	DC	

TABLE 3.3 – Continued

PM I	FUV	NUV	B_F	R_I	I_N	J	H	K_S	u	g	r	i	z	ST	Notes
05372+6759	21.23	18.08	16.3	16.2	15.7	15.89	15.89	15.55	–	–	–	–	–	DAH:	
05383+4436	–	21.13	17.3	16.8	16.8	16.21	15.77	15.85	–	–	–	–	–	DA	
05410+3959	–	–	17.6	17.3	18.2	16.35	16.20	15.73	–	–	–	–	–	DA	
05431+3637	–	–	16.0	15.5	15.3	14.78	14.60	14.51	–	–	–	–	–	DAZ	
05462+1115	–	–	18.9	17.4	16.8	16.33	16.08	15.63	–	–	–	–	–	DC:	
05492+5747	16.16	16.18	15.8	14.7	13.6	12.76	12.21	12.00	–	–	–	–	–	DA+dM	
06018+2751	–	–	15.6	15.4	–	15.42	15.35	15.28	–	–	–	–	–	DA	1
06019+3726	–	–	16.4	17.0	16.3	–	–	–	–	–	–	–	–	DAH	
06026+0904	–	–	17.4	16.5	16.0	15.95	15.54	15.25	–	–	–	–	–	DA	
06206+3443	20.50	17.48	16.5	16.6	16.4	–	–	–	16.91	16.51	16.59	16.69	16.86	DA	
06324+2230	–	–	–	17.1	16.5	16.12	15.81	15.76	–	–	–	–	–	DA	
06445+2731	–	19.60	18.2	17.2	16.5	16.23	16.75	16.38	17.72	17.15	16.95	16.91	16.97	DA	
06492+1519	–	–	18.1	17.3	16.6	–	–	–	–	–	–	–	–	DC	
06494+7521	–	20.00	17.1	16.6	–	16.13	15.80	15.46	–	–	–	–	–	DA	
06506+1657	–	–	17.9	16.9	16.6	16.14	15.73	15.31	–	–	–	–	–	DA	
06513+6242	–	20.38	17.5	17.6	16.8	–	–	–	–	–	–	–	–	DAH	
06538+6355	–	–	16.7	15.8	–	15.28	15.10	14.91	–	–	–	–	–	DA	
06556+5920	17.37	16.60	15.9	14.7	13.2	12.05	11.41	11.17	–	–	–	–	–	DA+dM	
06577+4007	–	19.78	17.2	16.8	16.4	16.36	15.90	17.11	–	–	–	–	–	DA	
07029+4406	18.08	16.04	15.2	15.4	15.3	15.30	15.31	15.48	–	–	–	–	–	DA	
07087+2044	–	22.99	17.3	16.4	16.3	15.92	15.73	15.39	–	–	–	–	–	DA	
07241+0431	–	–	19.1	17.5	17.2	–	–	–	–	–	–	–	–	DA	
07270+1434	–	–	17.2	16.2	16.2	15.71	15.27	15.18	18.20	17.13	16.69	16.51	16.45	DA	
07300+2716W	20.64	17.36	16.4	15.9	16.0	15.97	15.90	15.97	16.71	16.24	16.28	16.37	16.53	DA	
07419+0136	–	21.57	18.6	18.4	17.3	–	–	–	–	–	–	–	–	DC	

TABLE 3.3 – Continued

PM I	FUV	NUV	B_F	R_I	I_N	J	H	K_S	u	g	r	i	z	ST	Notes
07419+1511	15.75	15.88	15.2	15.5	–	16.06	16.12	15.91	16.02	15.76	15.97	16.22	16.51	DA	
07451+2627	–	–	20.1	18.6	17.9	–	–	–	22.06	19.98	18.74	18.18	17.98	DC	
07475+1107	–	–	16.6	16.4	16.5	16.10	15.77	15.64	17.13	16.74	16.68	16.69	16.78	DA	
07504+1740	–	19.55	17.1	16.8	–	16.84	16.32	15.74	17.77	17.26	17.08	17.04	17.11	DA	4
08015+4852	–	22.57	18.4	16.9	16.9	16.31	15.78	15.68	19.47	17.99	17.37	17.12	17.03	DA	
08054+0735	–	22.27	17.8	17.0	16.7	16.24	15.95	15.59	19.21	17.89	17.34	17.11	17.02	DA:	
08068+2215	–	–	18.5	17.5	17.2	16.73	16.56	16.85	19.23	18.25	17.78	17.64	17.58	DA	
08082+1854	–	23.18	18.3	17.3	17.0	16.82	16.36	16.24	19.28	18.22	17.76	17.57	17.50	DA	
08126+1737	13.48	13.76	13.5	13.8	–	13.76	13.84	13.94	14.01	14.55	15.20	14.23	14.26	DA	3
08152+1633	–	–	18.9	17.9	17.7	16.78	16.14	15.67	20.83	18.98	18.16	17.88	17.68	DC:	
08184+6606	16.82	17.06	16.6	15.3	14.1	12.96	12.37	12.13	17.20	16.54	15.80	15.11	14.31	DA+dM	
08212+7120	21.28	18.05	16.5	16.2	16.0	15.94	15.56	15.18	–	–	–	–	–	DA	
08223+2023	–	18.42	16.4	15.6	–	15.62	15.48	15.39	16.73	16.27	16.14	16.14	16.20	DC	
08281+0942	–	–	19.0	17.8	17.7	–	–	–	–	–	–	–	–	DC	
08293+2539	–	–	20.1	18.4	17.9	16.83	16.93	17.10	21.45	19.14	18.29	17.96	17.76	DC	
08429+2409	23.91	20.87	17.4	16.9	16.5	15.99	15.92	15.60	18.36	17.43	17.03	16.86	16.83	DA	5
08490+4439	–	21.83	18.7	17.5	17.7	16.28	16.03	16.18	18.76	17.98	17.64	17.51	17.47	DC	
08516+1624	–	21.99	16.9	16.4	16.0	15.75	15.69	15.70	17.92	16.97	16.58	16.46	16.47	DC	
08558+3700	–	–	17.9	17.1	16.5	16.51	16.17	15.85	19.06	17.98	17.48	17.29	17.25	DA	6
09021+2010	–	21.46	18.9	17.4	17.3	–	–	–	18.94	18.86	17.79	17.25	17.29	DQ	
09026+1535	–	–	18.6	17.4	–	16.23	16.08	15.20	20.37	18.51	17.66	17.34	17.19	DC	
09027+3120	–	–	14.9	14.9	–	15.05	14.90	15.07	15.62	15.28	15.30	15.39	15.56	DA	
09033+2012	–	19.26	17.5	16.8	16.7	16.27	16.19	15.86	17.59	17.07	16.91	16.88	16.96	DA	
09106+2156	–	21.64	17.7	17.1	16.6	16.31	16.11	16.03	18.65	17.66	17.22	17.06	17.00	DA	5
09112+1515	–	–	19.6	18.3	–	–	–	–	21.24	19.37	18.59	18.32	18.16	DC	

TABLE 3.3 – Continued

PM I	FUV	NUV	B_F	R_I	I_N	J	H	K_S	u	g	r	i	z	ST	Notes
09122+2538	–	19.60	16.8	16.8	16.2	15.90	15.44	15.08	17.53	16.88	16.63	16.55	16.56	DA	
09127+2251	–	–	18.2	18.1	17.4	16.75	16.55	15.99	20.44	18.81	18.09	17.83	17.69	DC	
09192+7723	19.62	16.30	15.7	14.9	14.4	14.91	14.91	14.92	–	–	–	–	–	DA	
09222+0504	–	22.66	18.1	17.4	16.5	–	–	–	19.37	18.39	17.95	17.79	17.73	DAH	
09234+0559	–	22.21	17.8	16.8	–	16.53	16.04	16.43	18.91	17.92	17.50	17.30	17.27	DA	
09245+3120	–	–	18.1	17.4	17.5	16.47	15.97	16.91	20.56	18.75	17.95	17.64	17.55	DC	5
09249+3613	20.20	19.16	16.3	17.5	–	–	–	–	–	–	–	–	–	DAH	
09286+1841	–	18.28	16.9	16.4	–	15.99	16.27	15.68	17.09	16.70	16.58	16.57	16.68	DA	
09395+4951	–	–	17.5	16.7	16.8	16.20	16.28	15.53	18.45	17.59	17.24	17.10	17.09	DA	
09422+0942	–	–	18.1	17.5	–	16.76	16.14	15.44	19.92	18.52	17.89	17.69	17.61	DA	
09432+5134	–	–	19.1	17.5	17.5	16.68	16.60	16.07	20.77	18.89	18.14	17.83	17.72	DC	6
09481+2023	–	–	18.7	17.3	17.3	16.62	16.26	15.74	20.32	18.53	17.76	17.46	17.34	DC	
09488+1319	–	19.95	17.3	17.0	–	16.47	16.09	16.51	18.06	17.47	17.28	17.21	17.25	DA	
09503+1509	–	–	18.5	17.2	–	16.16	15.95	15.36	19.14	17.94	17.39	17.17	17.10	DC	
09513+1900	–	–	17.6	17.2	17.3	16.70	16.36	17.33	18.94	18.10	17.68	17.55	17.54	DC	5
10042+2438	18.37	17.10	17.4	16.4	16.1	–	–	–	16.85	16.43	16.55	16.74	16.94	DA	
10118+2647	–	–	18.3	17.5	–	16.61	16.19	15.62	19.57	18.26	17.72	17.51	17.42	DA	7
10155+1850	–	–	19.2	18.4	–	16.73	16.97	16.50	21.32	19.40	18.44	18.14	18.01	DC	
10170+7619	–	19.04	16.8	16.2	16.2	16.09	15.65	15.47	–	–	–	–	–	DA	
10228+3904	–	23.76	17.5	17.5	17.1	16.69	16.28	16.45	18.81	17.59	17.28	17.22	17.24	DZ	
10289+1105	15.75	15.68	15.3	15.4	–	15.99	15.95	15.40	15.86	15.49	15.77	16.01	16.26	DA	
10347+2245	–	19.96	16.6	16.1	16.4	16.24	16.41	15.75	–	–	–	–	–	DZ	5
10355+2126	–	19.56	17.7	16.2	16.7	16.50	16.83	15.60	–	–	–	–	–	DAH	
10403+1004	–	21.12	17.7	16.7	–	16.01	16.33	16.10	18.19	17.42	17.07	16.96	16.95	DC	
10471+3453	–	–	16.7	16.4	16.2	16.01	15.96	15.73	16.98	16.48	16.45	16.49	16.58	DA	

TABLE 3.3 – Continued

PM I	FUV	NUV	B_F	R_I	I_N	J	H	K_S	u	g	r	i	z	ST	Notes
10502+3226	–	–	17.9	16.9	17.1	16.55	16.49	16.09	19.14	18.00	17.53	17.36	17.31	DA:	
10521+4050	–	20.29	17.7	16.6	16.5	16.11	15.53	15.21	17.68	17.00	16.68	16.60	16.63	DC	
10538+2425	–	–	18.7	17.3	17.4	16.76	16.34	16.12	18.93	18.02	17.62	17.47	17.41	DA	
10557+2111	–	21.26	18.3	17.5	–	16.62	17.09	15.80	18.73	17.81	17.49	17.40	17.38	DAH	
10565+2336	–	–	19.0	17.6	17.5	16.52	16.57	16.25	19.83	18.41	17.77	17.55	17.41	DA	5
11036+1555	–	–	15.6	13.8	–	11.57	11.16	10.76	18.60	15.88	14.72	17.14	12.86	DA+dM	
11071+1446	–	19.38	17.4	16.6	15.9	15.75	15.47	15.42	17.37	16.75	16.52	16.45	16.49	DA	5
11111+3848	–	–	18.6	17.8	18.0	–	–	–	20.12	18.81	18.17	17.87	17.75	DC	8
11132+2859	–	–	18.8	17.4	17.2	16.33	15.81	15.87	20.21	18.51	17.73	17.44	17.29	DA	5
11144+3341	–	–	17.8	17.8	17.7	16.27	15.65	15.20	18.25	17.87	17.82	17.76	17.63	DA	9
11210+3756	–	–	15.8	15.4	15.5	15.33	15.15	15.14	15.88	15.45	15.53	15.65	15.81	DA	
11222+2839	–	–	18.3	17.2	17.3	16.52	16.99	16.18	19.38	18.27	17.81	17.64	17.56	DA	5
11253+2111	–	19.83	16.8	16.7	16.6	16.24	16.18	15.65	17.88	17.18	16.90	16.79	16.79	DC	
11337+6243	–	19.55	16.5	15.9	15.4	15.57	15.39	15.56	17.09	16.50	16.27	16.20	16.23	DA+DC	
11364+0802S	–	–	18.4	17.4	–	–	–	–	19.46	18.29	17.80	17.60	17.48	DA	
11364+0838	–	20.79	18.1	17.3	–	–	–	–	18.41	17.80	17.52	17.43	17.43	DA	
11401+0112W	19.48	16.73	15.2	14.2	13.5	–	–	–	16.19	15.77	15.83	15.89	16.08	DA	
11460+0514	–	–	16.9	16.5	16.1	16.02	16.01	16.78	17.68	17.08	16.81	16.73	16.78	DA	5
11495+2353	–	–	18.3	17.2	17.7	16.42	15.99	17.03	20.35	18.67	17.95	17.70	17.61	DC	
11506+0343	–	21.64	17.7	17.3	17.4	16.50	17.18	16.51	18.81	17.95	17.55	17.37	17.39	DA	
11545+2422	21.23	16.95	15.6	15.2	15.4	15.24	15.11	15.40	15.94	15.60	15.61	15.66	15.80	DA	5
11582+0004	–	–	18.7	18.1	17.5	16.72	15.99	17.20	20.93	18.90	17.87	17.51	17.33	DC	6
11592+4842	–	21.91	18.5	17.5	16.9	16.47	15.96	16.08	18.65	17.74	17.34	17.17	17.15	DA	
11598+0007	23.40	17.32	15.5	16.0	–	15.62	15.37	15.54	16.00	15.75	15.81	15.87	16.01	DA	
12019+3400	–	20.68	17.2	16.4	16.5	16.76	15.95	15.53	18.24	17.74	17.26	17.18	17.23	DQ	

TABLE 3.3 – Continued

PM I	FUV	NUV	B_F	R_I	I_N	J	H	K_S	u	g	r	i	z	ST	Notes
12033+2439	17.45	16.76	21.0	16.9	16.9	–	–	–	16.50	16.54	16.83	17.05	17.31	DB	
12113+0724	–	–	17.2	16.1	16.4	15.37	15.09	15.10	18.51	17.14	16.52	16.30	16.20	DA	5
12145+7822	–	–	18.0	17.2	16.8	16.18	15.65	15.64	–	–	–	–	–	DZ	
12155+4630	–	19.83	17.1	16.7	16.4	16.18	16.07	15.74	17.85	17.24	17.01	16.95	16.98	DA	10
12274+3150	–	19.59	16.5	16.3	15.8	15.89	15.50	15.49	17.47	16.82	16.56	16.49	16.51	DA	5, 11
12280+3300	–	–	18.6	17.7	17.3	16.70	16.16	16.01	20.71	18.88	17.97	17.61	17.46	DC	
12370+1814	19.82	17.79	17.8	16.8	16.6	–	–	–	16.96	16.79	16.88	17.03	17.17	DC	
12377+6023	–	–	18.4	17.5	17.6	16.65	15.99	15.60	19.81	18.48	17.87	17.67	17.57	DA	
12405+1807W	–	–	19.1	17.3	16.9	16.59	15.93	15.79	19.20	17.99	17.42	17.19	17.11	DA	
12425+1311W	–	–	19.5	18.0	17.6	–	–	–	20.42	18.74	18.05	17.80	17.69	DC	
12429+6542	–	20.46	17.5	16.8	–	16.55	17.14	16.10	18.29	17.66	17.43	17.34	17.35	DA	
12430+2057	17.62	16.95	18.0	17.0	16.1	–	–	–	16.72	16.74	17.02	17.25	17.43	DB	
12476+0646	–	–	20.2	18.5	18.0	–	–	–	20.93	20.03	18.67	18.37	18.22	DQpec	
12541+3620	–	–	18.1	16.7	16.1	15.90	15.72	15.40	19.74	17.93	17.15	16.83	16.66	DC	
13032+7510	–	18.36	16.9	16.2	16.2	16.16	15.79	15.27	–	–	–	–	–	DC	
13096+6933	–	18.94	17.5	16.1	14.2	13.14	12.55	12.26	–	–	–	–	–	DA+dM	
13103+1404	21.82	17.71	16.2	16.3	–	15.84	15.89	15.67	16.79	16.33	16.34	16.40	16.51	DA	5
13108+7236	–	–	17.4	16.6	17.1	16.03	16.00	15.24	–	–	–	–	–	DA	
13176+0621	–	–	19.3	17.5	16.1	–	–	–	19.98	18.62	17.97	17.74	17.67	DA	6
13246+0857	–	18.10	17.4	16.3	15.1	16.17	16.17	15.81	17.08	16.63	16.60	16.62	16.73	DA	5
13291+2450	–	–	20.6	19.0	18.1	–	–	–	22.35	19.93	18.76	18.26	18.13	DC	
13333+2450	–	–	20.2	19.0	18.0	–	–	–	–	–	–	–	–	DC	
13346+0943E	–	–	18.4	18.1	18.3	–	–	–	19.19	18.43	17.38	18.42	16.90	DA	
13349+6945	15.61	15.76	15.9	15.6	15.2	15.93	16.23	15.58	–	–	–	–	–	DA	
13413+0500	–	–	17.5	16.0	15.5	14.70	14.59	14.48	19.67	17.41	16.29	15.85	15.68	DC	5

TABLE 3.3 – Continued

PM I	FUV	NUV	B_F	R_I	I_N	J	H	K_S	u	g	r	i	z	ST	Notes
13455+4200	–	–	17.9	16.4	16.3	15.61	15.43	14.99	19.76	17.86	17.01	16.71	16.55	DC	
13521+1053	–	20.76	17.1	16.0	16.0	15.74	15.59	15.06	17.92	17.10	16.74	16.57	16.55	DA	
13537+1656	–	17.91	16.5	16.2	16.0	16.39	15.84	15.76	17.11	16.60	16.64	16.70	16.81	DA	
14037+0644	–	20.44	17.3	17.0	17.0	16.58	16.62	16.36	18.02	17.44	17.27	17.25	17.33	DC	5
14064+1608	–	20.45	17.2	16.8	16.6	16.60	16.31	17.28	18.23	17.61	17.37	17.31	17.34	DA	5
14067+3130	–	–	19.4	17.3	17.3	16.61	15.88	16.12	20.54	18.72	17.92	17.64	17.52	DC	
14106+0245	–	–	16.9	16.2	16.0	15.48	15.14	15.02	18.05	17.00	16.50	16.33	16.27	DAZ	5
14149+4336	–	20.65	18.2	17.3	16.8	16.46	15.76	15.67	18.22	17.54	17.25	17.19	17.16	DA	
14236+3037	–	–	18.8	17.3	16.8	16.44	16.18	15.67	19.51	18.15	17.56	17.36	17.28	DA	
14244+6246	–	–	19.4	17.8	17.7	–	–	–	20.35	18.83	18.14	17.86	17.70	DA	
14278+0532	23.10	19.25	17.6	16.7	16.6	16.30	16.03	15.93	17.61	17.02	16.86	16.82	16.86	DA+DC	5
14339+1907	–	–	19.1	18.1	17.5	16.88	16.07	15.33	20.43	18.76	18.10	17.82	17.75	DA	
14407+0807	–	–	19.3	17.6	17.0	16.54	15.94	16.30	19.20	18.01	17.48	17.30	17.20	DA	
14456+2527	–	21.63	16.8	15.5	15.3	14.68	14.13	14.21	17.97	16.66	16.00	15.73	15.56	DA	
14553+5655	14.87	14.85	15.4	14.7	14.1	15.13	15.15	15.40	14.96	14.67	14.98	15.24	15.52	DA	
14588+1146	–	–	18.9	17.5	17.6	–	–	–	20.67	18.86	18.02	17.71	17.66	DC	5, 6
15010+6138	–	21.56	18.0	17.1	16.7	16.29	16.05	16.13	18.83	17.84	17.40	17.22	17.18	DA	
15164+2803	–	18.25	17.6	16.3	–	15.98	16.27	15.70	17.02	16.59	16.52	16.53	16.62	DAH	
15167+2910	17.33	17.24	17.6	17.0	–	–	–	–	17.25	16.85	17.07	17.29	17.56	DA	
15206+3903	22.29	18.32	16.9	16.9	16.7	16.35	16.52	15.83	17.44	16.95	17.00	16.82	16.79	DA	
15263+2936	–	–	18.4	16.1	15.8	15.30	14.97	14.80	18.64	17.12	16.46	16.20	16.11	DA	
15342+0218	21.86	17.73	16.5	16.7	–	15.78	15.79	15.56	16.68	16.32	16.27	16.30	16.42	DA	5
15359+2125	–	20.46	17.4	16.6	16.7	16.29	16.08	16.98	18.28	17.53	17.22	17.12	17.12	DA	
15494+4802	–	19.92	17.0	16.9	16.8	16.63	15.85	16.75	18.03	17.41	17.16	17.09	17.11	DC	5
15589+0417	–	18.78	16.6	–	15.8	15.46	15.27	14.82	16.86	16.26	15.97	15.97	16.09	DC	

TABLE 3.3 – Continued

PM I	FUV	NUV	B_F	R_I	I_N	J	H	K_S	u	g	r	i	z	ST	Notes
16053+5556	–	19.99	17.5	17.4	16.6	15.98	15.53	15.57	18.28	17.68	17.49	18.74	17.29	DA	
16096+4735	–	–	16.3	16.3	16.1	–	–	–	16.74	16.38	16.63	16.86	17.17	DA	
16142+1729	–	22.44	19.0	17.9	18.0	–	–	–	19.22	18.67	17.86	17.74	17.84	DQpec	
16171+0530	15.07	15.01	15.1	14.6	13.6	11.53	10.96	10.67	15.12	14.63	14.61	14.09	13.06	DA+dM	
16222+0532	–	18.52	16.9	16.4	16.7	15.92	15.85	15.22	17.31	16.82	16.73	16.71	16.80	DA	
16264+1938	–	20.48	17.0	16.2	15.8	15.64	15.33	15.41	17.61	16.83	16.48	16.35	16.36	DA	
16265+1355	–	–	18.4	17.1	16.9	16.49	16.16	15.85	18.08	17.48	17.26	17.21	17.24	DA	
16286+7053	–	–	18.8	17.6	16.9	16.10	15.85	15.63	–	–	–	–	–	DA	
16325+0851	–	20.16	15.7	14.6	14.4	13.85	13.61	13.49	16.44	15.34	14.88	14.69	14.64	DA	5
16335+5231	–	–	18.1	17.5	16.8	16.37	16.19	15.70	18.11	17.50	17.24	17.14	17.14	DA	
16477+2636	–	19.22	17.4	17.0	16.7	16.10	17.33	14.33	17.51	17.02	16.90	16.95	17.09	DZ	
16514+6635	20.55	18.04	16.6	16.1	16.3	16.33	15.93	14.81	–	–	–	–	–	DZ	
16546+5742	–	–	16.0	16.0	15.3	15.65	15.95	15.20	–	–	–	–	–	DA	
17027+1022	–	–	18.4	17.3	16.8	16.41	16.05	17.04	19.81	18.27	17.61	17.38	17.26	DA	
17052+0423	–	17.49	16.2	16.0	15.5	15.70	15.65	15.40	–	–	–	–	–	DA	
17238+0458	–	18.29	17.0	16.7	16.4	16.40	16.05	15.86	–	–	–	–	–	DA	
17283+0211	–	17.77	16.1	15.6	15.7	15.67	15.95	15.94	–	–	–	–	–	DA	
17328+0213	–	19.09	17.3	16.3	–	16.14	16.15	15.51	–	–	–	–	–	DA	
17335+7949	–	22.64	18.0	16.0	15.8	16.06	16.05	15.48	–	–	–	–	–	DC	
17344+4236	22.32	18.66	16.2	16.3	16.6	15.95	15.91	15.39	–	–	–	–	–	DA	
17368+3635	–	20.09	17.1	17.4	17.3	–	–	–	–	–	–	–	–	DA	
17376+0138	–	18.86	17.2	16.3	–	16.18	15.76	15.07	–	–	–	–	–	DA	
17417+2401	–	–	16.8	16.5	15.9	15.99	15.57	15.70	–	–	–	–	–	DA	
17433+1434S	17.41	15.74	14.9	14.2	13.7	14.89	14.83	15.05	–	–	–	–	–	DC	
17430+1701	–	–	18.8	17.6	17.3	16.34	15.70	15.78	–	–	–	–	–	DC	

TABLE 3.3 – Continued

PM I	FUV	NUV	B_F	R_I	I_N	J	H	K_S	u	g	r	i	z	ST	Notes
17471+2859	–	–	18.1	17.1	16.8	16.23	16.17	16.16	–	–	–	–	–	DC	
17574+1021	21.60	18.36	16.8	16.0	–	15.92	15.97	15.35	–	–	–	–	–	DZA	
17579+5441	–	19.04	17.1	16.7	–	–	–	–	17.71	17.25	17.14	17.15	17.24	DA	
18014+5049	–	–	18.2	17.1	16.5	16.00	16.20	15.94	19.87	18.15	17.33	17.05	16.91	DC	
18018+0846	–	–	18.1	16.8	16.8	16.38	16.01	15.53	–	–	–	–	–	DA	
18073+0357	–	–	15.6	14.8	14.4	14.57	14.51	14.46	–	–	–	–	–	DA	
18138+2119	–	–	15.9	15.8	–	15.70	15.63	15.55	–	–	–	–	–	DA	
18154+3158	–	–	19.1	17.6	17.5	16.70	16.31	16.07	–	–	–	–	–	DA	
18199+1739	–	–	18.4	17.5	17.3	16.39	16.02	15.96	–	–	–	–	–	DC	
18435+2740	17.39	15.67	14.9	15.0	–	13.98	13.34	13.14	–	–	–	–	–	DA	1
18510+7738	–	22.70	18.3	16.4	15.7	15.93	15.80	14.93	19.07	17.60	16.97	16.72	16.64	DC:	
18572+2026	–	–	16.3	16.5	16.3	15.87	15.61	16.11	–	–	–	–	–	DA	
19005+0020	–	–	17.8	17.2	17.2	15.85	14.60	13.99	–	–	–	–	–	DA	
19033+6035	16.84	15.78	14.8	14.8	14.3	15.10	15.16	14.84	–	–	–	–	–	DA	
19128+5343	–	–	13.2	13.2	12.9	13.62	13.73	13.82	–	–	–	–	–	DA	
19132+2949	–	–	17.4	17.0	15.9	16.12	15.67	15.48	–	–	–	–	–	DA	
19146+1428	–	–	16.5	15.1	15.6	15.26	14.92	14.78	–	–	–	–	–	DA	
19167+8044	–	–	18.3	17.1	16.6	16.28	16.07	15.21	–	–	–	–	–	DA	
19401+8348	–	–	18.7	17.6	17.3	16.65	16.24	16.96	–	–	–	–	–	DC	
19493+0747	–	–	15.1	15.6	15.2	15.21	15.27	15.17	–	–	–	–	–	DA	
19455+4650N	–	–	18.0	16.9	16.4	15.88	15.56	15.48	–	–	–	–	–	DAH:	
20062+5902	15.58	15.61	16.2	16.3	15.8	15.70	15.87	15.10	15.76	15.36	15.65	15.88	16.16	DA	
20069+6143	–	22.08	17.5	16.2	16.0	15.17	14.90	14.68	18.16	16.91	16.34	16.13	16.06	DA	
20223+8333	–	–	17.5	16.8	16.7	16.17	16.40	15.99	–	–	–	–	–	DC	
20235+7001	–	20.94	19.1	17.9	17.4	–	–	–	–	–	–	–	–	DA	

TABLE 3.3 – Continued

PM I	FUV	NUV	B_F	R_I	I_N	J	H	K_S	u	g	r	i	z	ST	Notes
20279+0523	–	19.57	17.1	17.0	–	16.31	15.90	15.46	–	–	–	–	–	DA	
20300+0729	–	17.77	16.3	15.8	15.6	15.66	16.08	15.60	–	–	–	–	–	DC	
20597+5517	–	–	18.7	17.0	16.4	15.66	15.45	15.49	19.97	17.97	17.02	16.67	16.49	DC	
21077+0740	–	18.63	16.3	15.8	–	15.77	15.79	15.14	–	–	–	–	–	DA	
21117+0120	15.01	15.12	15.2	15.1	–	15.52	15.69	15.32	–	–	–	–	–	DA	
21134+0727	–	19.30	16.0	15.6	15.8	15.21	14.95	14.81	–	–	–	–	–	DA	
21222+0413	–	–	17.5	16.2	15.7	15.24	15.01	14.88	18.86	17.20	16.49	16.23	16.12	DA	5
21384+1856	–	–	17.5	16.7	16.3	15.96	15.38	15.45	17.55	17.16	17.32	17.54	17.76	DA	
21420+2252	19.81	17.17	15.9	16.1	15.6	15.98	15.74	15.54	–	–	–	–	–	DZ	
21429+0805	–	–	18.0	15.6	15.5	15.77	15.27	15.18	–	–	–	–	–	DA	
21474+1127	–	–	19.5	16.6	17.4	–	–	–	20.86	19.18	18.42	18.14	18.01	DA	6
21492+0415	–	22.32	17.4	15.5	15.3	15.38	15.21	15.10	–	–	–	–	–	DA	
21551+4103	–	–	17.9	16.4	16.3	16.18	15.80	15.80	–	–	–	–	–	DZA	
21597+2936	13.47	13.94	14.7	15.5	–	15.83	15.90	15.36	–	–	–	–	–	DA	3
22105+4532	–	–	18.1	17.1	16.5	16.20	15.97	15.74	–	–	–	–	–	DC	
22118+5649	–	–	13.9	13.6	13.4	13.19	12.99	12.86	–	–	–	–	–	DA	
22133+0349	–	–	18.9	15.9	16.2	16.56	16.38	16.55	–	–	–	–	–	DC	
22198+4805	–	–	18.6	17.5	16.7	–	–	–	–	–	–	–	–	DA	
22230+2201N	14.78	14.90	14.7	14.8	–	16.05	16.19	15.66	15.64	15.58	15.91	16.22	16.50	DA	
22230+2201S	–	–	15.3	15.0	–	16.42	15.71	16.10	16.36	15.99	16.20	16.45	16.69	DA	
22276+1753	–	19.41	16.8	16.0	15.2	15.85	15.57	15.47	–	–	–	–	–	DAZ	
22299+3024	18.61	17.02	16.1	16.0	–	15.55	15.22	15.02	–	–	–	–	–	DA	
22331+2610	15.63	15.72	15.6	15.3	–	15.94	15.65	16.01	–	–	–	–	–	DA	
22340+5543	–	–	17.7	17.1	16.6	16.57	15.70	15.99	–	–	–	–	–	DA	
22410+3646	–	19.14	17.6	16.9	16.5	16.38	16.17	16.98	–	–	–	–	–	DA	

TABLE 3.3 – Continued

PM I	FUV	NUV	B_F	R_I	I_N	J	H	K_S	u	g	r	i	z	ST	Notes
22418+0432	–	21.07	18.7	17.6	17.2	–	–	–	–	–	–	–	–	DQpec	
22447+1513W	–	22.83	19.0	17.8	17.3	–	–	–	–	–	–	–	–	DA	
22497+3623	–	–	19.1	17.7	16.9	16.58	16.22	17.12	–	–	–	–	–	DA	
22595+5717	–	–	19.1	17.2	16.0	16.18	15.93	15.20	–	–	–	–	–	DA	
23003+2204	–	20.55	17.8	17.0	16.6	–	–	–	–	–	–	–	–	DZ	
23027+4312	–	–	17.7	16.2	16.4	15.96	15.97	17.03	–	–	–	–	–	DA	
23056+4334	–	–	19.4	18.1	17.5	16.76	16.04	16.47	–	–	–	–	–	DC	
23098+5506E	–	–	16.0	14.3	11.4	14.27	13.94	13.93	–	–	–	–	–	DA	
23160+0559	16.71	16.85	17.1	17.1	16.5	–	–	–	16.95	16.64	16.92	17.15	17.40	DA	
23162+1720	–	–	18.4	17.3	17.1	16.51	16.57	15.57	20.30	18.54	17.76	17.44	17.31	DC	
23186+5458	–	–	17.0	16.9	16.6	–	–	–	16.76	16.73	16.92	17.12	17.30	DZ	
23229+3358	16.84	16.84	16.2	15.4	13.2	13.14	12.59	12.28	–	–	–	–	–	DA+dM	
23234+7255	–	18.33	16.8	16.0	16.1	15.83	15.77	16.16	–	–	–	–	–	DA	
23243+2835	–	18.53	16.3	15.9	–	15.60	15.24	15.41	–	–	–	–	–	DA	
23283+3319	15.81	15.89	15.1	14.9	–	12.14	11.62	11.42	–	–	–	–	–	DA+dM	
23300+0120	–	20.73	17.7	17.5	16.5	–	–	–	–	–	–	–	–	DC	
23389+2101E	–	–	18.2	16.8	17.2	16.32	16.18	15.14	–	–	–	–	–	DA	
23390+5316	–	–	17.0	16.9	16.2	16.10	15.48	15.63	–	–	–	–	–	DA	
23462+1158	–	21.93	18.1	17.0	16.6	16.33	15.93	15.62	–	–	–	–	–	DC	
23475+0304	–	–	17.8	16.2	15.5	15.61	15.60	15.87	19.14	17.25	16.52	16.25	16.16	DC	
23478+0223	–	–	18.8	17.5	16.5	16.44	16.28	16.30	20.00	18.56	17.91	17.65	17.60	DA	
23489+4300	–	–	18.6	17.5	17.1	16.67	15.95	15.74	20.32	18.64	17.81	17.50	17.36	DC:	

(1) WD in McCook and Sion; (2) also in Schilbach & Röser (2012); (3) Also in Vennes et al. (2011); (4) SDSS spectrum 53314-1920-168;
(5) Also in Sayres et al. (2012); (6) Also in Kilic et al. (2010); (7) SDSS spectrum 54064-2386-563; (8) SDSS spectrum 54536-2871-559;
(9) DA+dM in Rebassa-Mansergas et al. (2010); (10) Also in Tonry et al. (2012);
(11) LSPM J1227+3150 wrongly identified as PM I12273+3150 in Limoges et al. (2013).

TABLE 3.4 – Known White Dwarfs from SUPERBLINK and from the literature with $D \lesssim 40$ pc

WD name	**FUV**	**NUV**	B_F	R_I	I_N	J	H	K_S	u	g	r	i	z	**ST**	**Source**	**PM I**	**Notes**
0002+729	15.27	14.63	14.3	14.4	14.7	14.61	14.60	14.76	–	–	–	–	–	DB	Archives	00051+7313	
0004+122	–	21.67	16.8	15.9	15.5	15.08	15.10	14.90	–	–	–	–	–	DC	–	00073+1230	
0008+424	–	17.62	15.3	15.0	14.9	14.54	14.35	14.39	–	–	–	–	–	DA	Archives	00113+4240	
0009+501	–	17.36	14.6	14.2	14.0	13.49	13.25	13.19	–	–	–	–	–	DAP	Archives	00122+5025	
0011+000	19.70	16.42	15.8	15.4	15.1	15.15	15.21	15.10	15.79	15.34	15.40	15.49	15.65	DA	Archives	00136+0019	
0017+136	–	–	15.2	15.5	15.6	15.73	15.86	15.80	15.04	14.15	15.52	15.80	16.07	DB	Archives		
0019+423	–	–	15.2	14.1	–	14.01	13.42	13.34	–	–	–	–	–	DA	–	00222+4236	
0031+150	–	19.36	17.9	16.6	16.3	16.08	15.94	15.52	17.56	16.98	16.79	16.74	16.79	DA	Archives	00344+1518	
0033+016	–	–	15.7	15.6	–	15.65	15.52	16.12	–	–	–	–	–	DA	Archives		
0033+771	–	–	16.1	–	16.6	–	–	–	–	–	–	–	–	DA	Archives		
0038+555	–	–	13.9	14.3	–	14.07	13.98	13.97	–	–	–	–	–	DC	Archives	00413+5550E	
0046+051	–	18.19	12.4	11.9	11.5	11.69	11.57	11.50	–	–	–	–	–	DZ	Archives	00491+0523	
0052+226	20.58	17.09	15.8	16.1	15.8	16.02	16.11	15.52	–	–	–	–	–	DA	Archives	00547+2256	
0101+048	19.54	15.49	14.4	13.7	13.2	13.50	13.40	13.42	–	–	–	–	–	DA	Archives	01038+0504	
0102+210A	–	–	18.6	17.8	17.2	16.52	16.50	15.55	–	–	–	–	–	DA	Archives	01049+2119	
0102+210B	–	–	18.9	17.8	17.0	16.73	16.27	15.59	–	–	–	–	–	DC	Archives	01049+2120	
0108+277	–	19.96	15.7	14.9	–	15.22	15.04	14.87	–	–	–	–	–	DA	Archives	01107+2758	
0115+159	18.82	15.02	14.0	13.9	14.0	13.73	13.68	13.73	–	–	–	–	–	DQ	Archives	01180+1610	
0121+401	–	–	18.7	16.2	15.8	15.86	15.51	15.28	18.85	17.48	16.88	16.66	16.56	DA	Archives	01243+4023	
0126+101	19.67	15.79	14.5	14.3	14.2	14.03	13.95	13.96	–	–	–	–	–	DA	Archives	01294+1023	
0134+833	–	–	13.3	13.2	12.2	13.58	13.81	13.70	–	–	–	–	–	DA	Archives	01414+8334	
0136+152	–	–	–	–	–	–	–	–	–	–	–	–	–	DA	Archives		
0142+312	18.92	15.98	14.9	14.7	14.4	14.43	14.32	14.43	–	–	–	–	–	DA	Archives	01451+3132	
0143+216	–	–	16.0	15.1	14.5	14.78	14.81	14.68	–	–	–	–	–	DA	Archives		
0145+234	–	–	14.5	13.9	13.9	14.21	14.24	14.23	–	–	–	–	–	DA	Archives		

TABLE 3.4 – Continued

WD name	FUV	NUV	B_F	R_I	I_N	J	H	K_S	u	g	r	i	z	ST	Source	PM I	Notes
0146+187	–	–	16.3	15.4	15.4	15.80	15.53	15.36	–	–	–	–	–	DAZB	2m	01489+1902	1
0148+467	–	–	–	–	–	12.77	12.83	12.85	–	–	–	–	–	DA	Archives		
0148+641	–	–	13.6	12.8	11.9	–	–	–	–	–	–	–	–	DA	Archives		
0150+256	21.98	17.48	16.1	15.5	15.3	15.07	15.07	15.15	–	–	–	–	–	DA	OMM	01528+2553	
0156+155	20.96	16.97	16.4	15.4	–	15.74	15.44	15.51	–	–	–	–	–	DC	2m	01596+1548	
0205+250	–	–	13.0	13.1	13.0	13.62	13.67	13.73	–	–	–	–	–	DA	Archives	02087+2514	
0208+396	–	–	14.8	14.4	–	13.83	13.67	13.60	–	–	–	–	–	DAZ	Archives	02113+3955	
0213+396	–	–	13.8	14.6	13.9	14.30	14.22	14.14	–	–	–	–	–	DA	Archives	02162+3951	
0213+427	–	–	16.6	16.3	–	14.65	13.73	15.18	–	–	–	–	–	DA	Archives	02169+4258	
0214+568	–	–	14.4	14.6	13.7	14.18	14.32	14.20	–	–	–	–	–	DA	Archives	02175+5706	
0221+399	–	–	16.2	16.7	16.1	16.15	16.06	15.41	–	–	–	–	–	DA	Archives		
0222+422.2	–	21.01	16.0	16.7	16.8	16.50	16.26	16.17	–	–	–	–	–	DA	Archives	02258+4228W	
0222+648	–	–	–	18.0	–	16.35	16.06	15.98	–	–	–	–	–	DC	Archives		
0227+050	–	–	–	–	–	–	–	–	–	–	–	–	–	DA	Archives		
0228+269	–	–	17.6	16.7	16.2	15.84	15.44	15.31	19.57	17.84	17.06	16.77	16.62	DA	–	02316+2709	
0231+570	–	–	14.7	14.0	14.2	13.92	13.93	13.89	–	–	–	–	–	DA	Archives	02355+5715	
0232+525	–	–	14.5	14.3	14.7	14.22	14.26	14.50	–	–	–	–	–	DA	Archives	02363+5244	
0236+259	–	21.50	17.0	15.4	14.9	14.91	14.61	14.47	17.55	16.42	15.92	15.73	15.69	DA	4m	02393+2609	
0236+745	20.47	17.10	16.5	15.9	15.8	15.65	15.54	15.61	16.41	15.97	15.99	16.06	16.19	DA	Bok	02415+7442	
0237+315	–	18.22	16.1	15.7	15.4	15.49	15.22	14.90	16.72	16.18	16.04	15.99	16.05	DA	OMM	02408+3142	
0239+109	21.23	17.70	16.2	16.1	15.8	15.58	15.91	15.43	–	–	–	–	–	DAH	Bok	02421+1112	
0245+541	–	–	–	15.1	14.8	13.87	13.54	13.47	–	–	–	–	–	DAZ	Archives		
0249+346	–	–	17.4	17.0	16.8	–	–	–	–	–	–	–	–	DBA	Archives		
0257+080	–	–	15.9	15.3	–	14.97	14.75	14.85	–	–	–	–	–	DAP	Archives	02599+0811	
0302+621	–	–	15.0	15.3	15.2	15.02	14.99	14.75	–	–	–	–	–	DA	Archives	03062+6222	

TABLE 3.4 – Continued

WD name	FUV	NUV	B_F	R_I	I_N	J	H	K_S	u	g	r	i	z	ST	Source	PM I	Notes
0304+154	–	–	20.2	18.2	18.0	–	–	–	–	–	–	–	–	DC:	–	03070+1540N	
0314+648	–	–	16.4	16.4	16.8	15.92	15.65	15.55	–	–	–	–	–	DA	Archives	03185+6500	
0316+345	14.16	14.22	14.5	14.5	14.2	14.57	14.68	14.57	–	–	–	–	–	DA	Archives	03197+3442	
0324+738	–	–	–	–	–	16.47	16.18	–	–	–	–	–	–	DC	Archives		
0336+040	–	17.97	17.5	16.7	16.6	16.25	15.52	16.44	17.10	16.67	16.69	16.74	16.87	DA	2m	03389+0409	
0341+182	–	17.45	15.6	14.8	14.0	14.59	14.35	14.23	–	–	–	–	–	DQ	Archives	03445+1826	
0344+014	–	–	16.7	15.8	–	15.00	14.87	14.70	–	–	–	–	–	DQ	Archives	03471+0138	
0349+495	–	–	16.7	16.3	16.5	–	–	–	17.88	17.41	17.26	17.22	17.27	DA	Archives		
0352+096	–	–	14.8	14.8	14.8	14.83	14.87	15.06	–	–	–	–	–	DA	Archives		
0354+463	21.61	17.11	15.7	15.6	15.1	13.59	13.08	12.73	–	–	–	–	–	DA+dM	Archives	03582+4628	
0357+081	–	21.57	16.5	15.4	15.5	14.56	14.34	14.12	–	–	–	–	–	DA	Archives	04004+0814	
0401+250	14.76	14.44	14.2	14.1	13.6	13.91	13.97	14.00	–	–	–	–	–	DA	Archives	04045+2508	
0406+592	13.43	13.82	14.4	14.7	15.0	14.84	14.66	14.67	–	–	–	–	–	DA	Archives	04108+5925	
0407+179	14.81	14.89	14.3	14.5	–	14.42	14.51	14.46	–	–	–	–	–	DA	Archives	04101+1802	
0407+197	–	–	17.9	17.4	16.9	16.13	15.96	15.18	–	–	–	–	–	DC	Archives	04102+1954	
0415+271	–	–	16.0	15.1	–	15.13	15.36	15.06	–	–	–	–	–	DA	Archives	04189+2717	
0421+162	13.72	13.89	14.5	15.1	–	14.74	14.81	15.09	14.22	14.95	14.49	14.79	15.08	DA	Archives	04239+1621	
0423+044.2	–	–	17.4	16.7	16.2	15.47	15.18	15.17	–	–	–	–	–	DA	Archives	04263+0432	
0423+120	–	19.16	16.6	15.4	14.9	14.48	14.35	14.25	–	–	–	–	–	DC	Archives	04258+1211	
0426+588	–	–	–	–	–	11.84	11.73	11.68	–	–	–	–	–	DC	Archives		
0429+176	–	–	15.3	14.1	13.2	10.75	10.16	–	–	–	–	–	–	DA+dM	Archives		
0431+126	–	–	14.6	15.0	15.4	14.77	14.80	14.80	–	–	–	–	–	DA	Archives	04337+1242	
0433+270	–	–	16.3	15.4	14.9	14.61	14.32	14.22	–	–	–	–	–	DA	Archives		
0435+410	–	–	14.9	15.1	14.9	15.12	15.25	14.90	–	–	–	–	–	DB	Archives	04386+4109	
0437+093	–	20.48	17.9	16.7	16.8	15.94	15.58	15.58	–	–	–	–	–	DA	Archives	04404+0923	

TABLE 3.4 – Continued

WD name	FUV	NUV	B_F	R_I	I_N	J	H	K_S	u	g	r	i	z	ST	Source	PM I	Notes
0440+510	–	–	16.6	15.9	–	15.58	15.50	15.55	–	–	–	–	–	DA	Archives	04439+5106	
0452+103	–	–	17.1	16.6	17.0	16.15	15.95	15.30	–	–	–	–	–	DA	Archives	04549+1027	
0453+418	–	–	14.1	14.3	15.0	14.40	14.36	14.55	–	–	–	–	–	DA	Archives	04573+4155	
0503+147	–	–	–	–	–	–	–	–	–	–	–	–	–	DBA	Archives		
0511+079	–	18.94	16.3	15.7	15.5	15.11	14.92	14.86	–	–	–	–	–	DA	Archives	05140+0800	
0518+333	–	–	16.9	16.7	–	15.37	15.12	14.81	–	–	–	–	–	DA	Archives	05217+3321	
0525+526	–	–	15.9	15.5	15.1	16.19	16.03	16.43	–	–	–	–	–	DA	Archives		
0532+414	–	–	14.9	14.6	14.4	14.09	13.94	13.82	–	–	–	–	–	DA	Archives	05363+4129	
0551+468	–	–	17.6	16.8	16.7	15.71	15.46	15.51	–	–	–	–	–	DA	Archives	05557+4650S	
0553+053	–	–	14.8	14.0	13.6	12.93	12.72	12.65	–	–	–	–	–	DAH	Archives	05564+0521	
0559+158	–	–	16.9	16.5	16.2	16.06	15.93	15.85	–	–	–	–	–	DA	Archives	06025+1553	
0612+177	–	–	13.5	13.4	13.4	13.91	13.99	13.89	–	–	–	–	–	DA	Archives	06153+1743	
0618+067	–	–	16.8	15.8	15.7	15.38	15.02	14.96	17.56	16.63	16.19	16.07	16.01	DA	Archives	06207+0645	
0631+107	–	–	13.9	14.5	–	14.44	14.48	14.68	–	–	–	–	–	DA	Archives	06338+1041	
0632+409	22.23	18.47	16.7	16.7	16.2	16.06	16.11	15.76	–	–	–	–	–	DA	Archives	06364+4054	
0637+477	–	–	–	14.9	15.0	15.05	15.14	15.23	–	–	–	–	–	DAP	Archives		
0644+025	–	–	15.9	15.7	15.3	14.87	14.76	14.58	–	–	–	–	–	DA	Archives	06473+0231	
0644+375	11.99	12.53	12.1	12.4	12.6	12.66	12.66	12.76	–	–	–	–	–	DA	Archives	06476+3730	
0648+641	–	20.91	17.2	16.1	15.8	15.53	15.41	15.33	–	–	–	–	–	DA	Archives	06534+6403	
0654+027	–	–	–	16.0	15.9	16.09	15.82	15.40	–	–	–	–	–	DC	Archives	06573+0241	
0657+320	–	–	16.6	15.7	15.3	15.03	14.67	14.66	–	–	–	–	–	DA	Archives	07008+3157	
0706+377	–	17.91	15.6	15.4	15.0	15.06	14.78	14.83	–	–	–	–	–	DQ	Archives	07102+3740N	
0714+458	19.08	16.11	14.8	15.2	15.1	15.08	15.20	15.03	–	–	–	–	–	DC	Archives	07180+4547	
0715+125	–	18.35	16.1	15.6	15.7	15.44	15.22	15.07	–	–	–	–	–	DA	Archives	07181+1229	
0727+482A	–	–	15.3	14.4	14.1	13.08	12.84	12.76	–	–	–	–	–	DA	Archives	07307+4810	

TABLE 3.4 – Continued

WD name	FUV	NUV	B_F	R_I	I_N	J	H	K_S	u	g	r	i	z	ST	Source	PM I	Notes
0727+482B	–	–	–	–	–	13.96	13.72	13.63	–	–	–	–	–	DA	Archives		
0728+642	–	–	16.4	15.6	14.7	14.81	14.52	14.38	–	–	–	–	–	DAP	Archives		
0730+487	–	–	15.2	14.9	15.1	15.14	15.19	15.39	–	–	–	–	–	DA	Archives		
0736+053	–	–	–	–	–	–	–	–	–	–	–	–	–	DQZ	Archives		
0743+442	–	–	14.9	15.0	14.9	15.23	15.40	15.18	15.02	14.79	15.06	15.30	15.56	DA	Archives	07474+4408W	
0747+073.1	–	–	17.9	16.2	15.8	15.03	14.90	14.75	–	–	–	–	–	DC	Archives	07502+0711N	
0747+073.2	–	–	17.6	16.1	15.6	15.00	14.71	14.63	–	–	–	–	–	DC	Archives	07502+0711S	
0749+426	–	–	18.0	16.8	16.5	15.72	15.80	14.83	20.03	18.09	17.19	16.87	16.71	DC	Archives	07532+4230	
0749+526	–	18.34	15.4	15.3	15.2	15.08	15.25	15.08	16.13	15.67	15.58	15.59	15.67	DC	SDSS	07534+5229	
0751+578	18.52	15.98	15.3	14.9	14.3	14.97	14.97	14.97	–	–	–	–	–	DC	Archives	07560+5741	
0752+365	–	17.78	15.9	15.9	15.6	15.58	15.44	15.88	16.59	16.14	16.06	16.06	16.14	DA	Archives	07554+3621	
0753+417	–	19.34	17.0	16.4	16.2	15.99	15.84	15.89	17.47	16.88	16.68	16.60	16.62	DA	Bok	07565+4139	
0756+437	–	–	16.3	16.0	15.7	15.39	15.23	15.34	16.75	16.19	16.22	16.20	16.08	DC	SDSS	07599+4335	
0756+566	–	–	16.5	16.8	17.1	16.07	15.49	15.31	–	–	–	–	–	DA	–	08005+5633	
0802+387	–	22.77	17.2	16.2	15.8	15.34	15.19	14.90	19.02	17.32	16.57	16.29	16.20	DA	Archives	08059+3833	
0805+356	19.91	16.30	15.3	15.2	14.7	14.88	14.78	14.69	15.54	15.14	15.14	15.19	15.31	DA	SDSS	08091+3527	2
0806+294	–	18.44	17.0	15.8	15.5	15.41	15.39	15.34	16.78	16.26	16.09	16.04	16.08	DA	SDSS	08097+2920	3
0810+489	–	17.67	15.4	14.7	14.0	14.32	14.13	14.06	15.76	15.18	14.95	14.92	14.96	DC	Archives	08141+4845	
0813+217	–	20.71	17.1	16.5	16.1	15.94	15.84	15.96	17.91	17.16	16.84	16.72	16.70	DA	Archives	08167+2137	
0816+387	–	18.35	–	16.4	16.3	16.07	15.83	15.58	17.04	16.61	16.49	16.47	16.53	DA	Archives	08200+3834W	
0826+455	18.24	15.98	15.1	15.1	15.0	15.01	15.04	14.84	15.51	15.03	15.13	15.27	15.49	DA	Archives	08301+4520	
0827+328	–	–	15.7	15.3	14.9	14.98	14.96	14.86	16.24	15.80	15.66	15.67	15.69	DA	Archives	08306+3241	
0842+382	22.70	17.62	18.1	15.7	15.7	15.49	15.45	15.43	16.49	16.03	15.99	16.02	16.11	DA	Archives	08454+3801	
0843+358	–	16.65	14.9	14.4	14.2	14.68	14.63	14.59	15.08	14.76	14.80	14.93	15.14	DZ	Archives	08467+3538	
0846+346	–	17.47	15.7	14.9	15.1	15.04	14.83	14.90	16.16	15.74	15.63	15.61	15.64	DA	4m	08491+3429	

TABLE 3.4 – Continued

WD name	FUV	NUV	B_F	R_I	I_N	J	H	K_S	u	g	r	i	z	ST	Source	PM I	Notes
0852+630	–	–	16.3	15.0	14.1	12.83	12.12	11.95	–	–	–	–	–	DA+dM	Archives		
0855+416	–	19.22	17.0	16.6	16.5	16.17	16.18	15.73	17.63	17.04	16.89	16.83	16.89	DAH	Bok	08585+4126	
0856+331	–	–	15.4	14.9	14.5	15.17	15.16	15.31	15.10	15.08	15.15	15.29	15.50	DQ	Archives	08592+3257	
0858+363	–	–	14.5	14.2	14.2	14.63	14.77	14.70	14.87	14.48	14.65	14.84	15.05	DA	Archives	09018+3607	
0900+734	–	–	17.4	16.5	16.1	15.56	15.27	15.13	–	–	–	–	–	DC	–	09055+7314	
0909+200	–	–	18.0	17.1	17.0	16.06	15.90	15.80	19.68	18.14	17.48	17.21	17.10	DA	Bok	09127+1951	4
0912+536	18.99	16.10	14.4	14.1	13.6	13.31	13.21	13.13	14.83	14.24	13.93	14.06	14.18	DCP	Archives	09159+5325	
0913+442	20.86	16.61	16.2	15.3	15.5	14.95	14.86	14.91	15.77	15.37	15.36	15.42	15.57	DA	Archives	09166+4359	
0920+012	–	20.51	17.2	16.1	15.3	15.02	14.77	14.88	17.64	16.84	16.50	16.37	16.34	DAZ	Bok	09229+0103	
0930+294	–	–	–	15.8	15.6	15.59	15.40	15.28	16.42	16.04	15.97	16.01	16.13	DA	Archives	09336+2911	
0930+394	22.06	17.42	15.7	15.8	15.6	15.59	15.40	15.28	16.40	16.00	15.97	16.00	16.12	DA	Archives	09336+2911	
0937+093	–	–	18.5	17.6	13.9	16.70	16.30	16.03	19.98	18.56	17.94	17.71	17.62	DC	Bok	09402+0907W	
0943+330	–	19.95	18.1	16.7	–	16.39	15.97	15.85	17.88	17.28	17.04	16.99	16.99	DA	Archives	09463+3251N	
0943+441	–	–	13.1	13.8	13.7	13.64	13.71	13.72	–	–	–	–	–	DA	Archives		
0944+192	14.31	14.36	14.6	14.9	–	14.96	15.10	15.11	14.55	14.39	14.71	14.98	15.27	DA	Bok	09475+1859	
0945+245	14.52	14.00	14.8	14.4	14.1	14.68	14.72	14.73	14.03	14.08	14.44	14.69	15.01	DAXP+DA	Archives	09487+2421	
0946+534	–	16.59	15.7	15.1	14.9	14.91	14.89	14.92	15.44	15.15	15.15	15.26	15.39	DC	Archives	09502+5315	
0955+247	20.48	16.48	15.6	14.4	–	14.65	14.66	14.66	15.37	15.09	15.08	15.13	15.25	DA	Archives	09578+2432	
0958+471	–	–	19.5	18.3	17.9	–	–	–	21.38	19.30	18.26	17.91	17.78	DC	–	10013+4656	
0958+613	–	–	19.6	18.6	17.8	–	–	–	21.82	19.42	18.43	18.04	17.85	DC	–	10024+6108	
1008+290	–	–	17.7	16.1	15.8	15.01	14.72	14.54	–	–	–	–	–	DQpecP	Archives		
1011+033	–	23.50	19.2	18.0	17.6	–	–	–	20.08	18.62	17.98	17.76	17.68	DA	GS	10140+0305N	
1011+426	–	–	16.8	16.2	16.1	15.67	15.50	15.28	16.77	16.34	16.26	16.26	16.33	DA	SDSS	10145+4226	5
1012+083.1	–	18.85	16.0	15.7	15.8	15.25	15.13	14.95	16.80	16.16	15.93	15.84	15.87	DA	Archives	10150+0806N	
1012+083.2	–	–	17.9	17.0	17.2	16.06	15.98	15.22	20.29	18.32	17.42	17.08	16.93	DC	–	10150+0806S	

TABLE 3.4 – Continued

WD name	FUV	NUV	B_F	R_I	I_N	J	H	K_S	u	g	r	i	z	ST	Source	PM I	Notes
1019+462	–	18.85	17.2	16.7	16.4	16.12	16.15	15.77	17.17	16.71	16.61	16.62	16.70	DA	Archives	10225+4600	
1019+637	–	17.25	15.2	14.6	14.4	13.87	13.73	13.69	15.44	14.82	14.63	14.56	14.59	DA	Archives	10231+6327	
1022+050	15.41	14.92	14.4	14.2	–	14.19	14.24	14.19	14.68	14.15	14.34	15.07	14.71	DA	Archives	10249+0446	
1022+461	–	18.66	17.0	16.2	15.9	15.55	15.46	15.56	16.91	16.42	16.24	16.20	16.25	DA	SDSS	10221+4612	6
1026+023	14.95	14.61	14.1	14.2	–	14.46	14.48	14.42	14.53	14.14	14.37	14.58	14.83	DA	Archives	10291+0205	
1026+117	–	19.18	16.7	16.2	16.0	15.90	15.55	15.30	17.34	16.70	16.50	16.45	16.51	DAP	Archives	10291+1127	
1033+714	–	–	17.3	16.1	15.5	15.19	14.84	14.98	–	–	–	–	–	DC	Archives	10370+7110	
1034+077	–	–	20.4	19.0	18.7	–	–	–	22.26	20.07	18.92	18.54	18.33	DC	GS	10369+0732	
1039+145	–	18.78	17.5	16.6	15.9	15.82	–	–	17.05	16.59	16.48	16.47	16.53	DQ	Archives	10418+1415	
1044+638	–	24.04	18.1	17.1	16.9	16.13	15.80	15.50	19.39	17.92	17.28	17.04	16.96	DA	–	10480+6334	
1052+273	13.17	13.54	14.0	13.8	–	14.62	14.67	14.78	13.81	14.46	14.27	14.59	14.92	DA	Archives	10547+2706	
1100+602	–	–	13.7	13.7	13.6	14.24	14.29	14.38	–	–	–	–	–	DA	Archives		
1102+005	–	–	–	15.3	15.0	15.45	15.28	15.04	15.51	15.18	15.40	15.62	15.88	DA	Archives		
1102+748	14.27	14.46	15.3	15.8	15.5	15.56	15.49	15.55	–	–	–	–	–	DA	2m	11059+7436	
1104+491	–	–	20.8	18.7	18.0	–	–	–	21.55	19.47	18.55	18.22	18.08	DC	–	11075+4855	
1106+082	–	18.04	16.3	15.5	–	15.63	15.36	15.24	16.65	16.19	16.07	16.08	16.12	DA	SDSS	11087+0801	7
1108+207	–	–	18.1	17.1	16.9	15.98	15.53	15.56	19.97	18.14	17.30	16.99	16.85	DC	Archives	11109+2026	
1113+008	–	23.24	17.9	17.0	15.9	15.80	15.65	15.59	19.48	17.91	17.24	16.99	16.90	DA	–	11156+0033	
1114+067	–	–	17.4	16.9	16.4	15.70	15.60	15.52	17.61	16.87	16.62	16.52	16.53	DA	Archives	11166+0627	
1116+026	15.68	15.08	14.9	14.8	14.6	14.75	14.73	14.61	14.96	14.52	14.70	14.94	15.19	DA	Archives	11192+0220	
1120+073	–	21.63	18.5	17.4	16.9	15.96	15.55	16.31	20.41	18.29	17.29	16.94	16.66	DC	4m	11235+0701	
1121+216	21.24	16.21	14.9	13.7	14.3	13.57	13.42	13.40	–	–	–	–	–	DA	Archives	11242+2121	
1124+595	18.45	15.91	15.2	14.8	14.3	15.05	15.18	15.10	15.45	15.11	15.20	15.33	15.51	DA	2m	11268+5919	
1129+155	–	–	14.3	14.5	14.5	14.44	14.49	14.56	–	–	–	–	–	DA	Archives		
1129+284	–	18.89	17.2	16.8	–	16.46	16.12	16.02	17.52	17.01	16.89	16.89	16.94	DAH	Bok	11322+2809	

TABLE 3.4 – Continued

WD name	FUV	NUV	B_F	R_I	I_N	J	H	K_S	u	g	r	i	z	ST	Source	PM I	Notes
1132+275	–	–	19.6	18.0	17.7	–	–	–	–	–	–	–	–	DC	4m	11354+2717	
1134+300	–	–	12.4	11.6	11.4	12.93	13.10	–	–	–	–	–	–	DA	Archives		
1135+321	–	–	–	–	–	–	–	–	–	–	–	–	–	DA	Archives		
1143+321	–	–	12.9	13.7	10.7	–	–	–	17.49	14.95	13.48	15.16	11.73	DA	Archives	11459+3149W	
1143+633	–	22.57	17.0	16.0	14.9	15.12	14.85	14.68	17.81	16.69	16.18	15.98	15.92	DC	–	11457+6305	
1149+057	–	15.70	14.9	15.0	14.7	15.02	14.85	14.92	15.39	14.96	15.08	15.23	15.44	DA	Archives	11519+0528	
1153+135	–	–	18.8	17.2	16.5	15.89	15.50	15.57	19.90	18.13	17.37	17.05	16.94	DC	Archives	11562+1315	
1154+186	–	17.58	16.2	15.6	15.2	15.10	15.22	15.09	16.09	15.67	15.57	15.60	15.70	DC	Archives	11567+1822	
1157+359	–	–	17.5	16.9	17.2	16.55	16.06	15.94	18.01	17.51	17.37	17.35	17.44	DA	Archives		
1157+438	22.94	17.41	16.0	15.6	–	15.20	15.20	15.32	16.29	15.83	15.76	15.77	15.85	DA	SDSS	12000+4335	8
1208+576	–	–	16.0	15.3	15.0	14.68	14.36	14.46	16.95	16.00	15.60	15.46	15.44	DA	Archives	12114+5724	
1213+528	–	–	14.0	13.0	10.9	–	–	–	14.67	13.69	13.13	12.17	11.65	DA+dM	Archives		
1215+323	–	–	–	–	–	17.00	16.67	16.44	–	–	–	–	–	DC	Archives		
1224+354	–	24.24	17.5	16.9	16.2	15.85	16.15	15.25	19.38	17.87	17.21	16.97	16.87	DA	4m	12265+3513	
1225+006	–	–	15.6	15.1	–	14.78	14.66	14.58	15.38	14.96	15.02	15.10	15.26	DA	Bok	12281+0022	
1235+422	–	–	17.5	16.7	17.0	16.55	16.50	15.48	17.83	17.73	17.10	16.84	16.92	DQ	SDSS	12378+4156	9
1236+457	–	19.88	16.8	16.3	16.1	15.60	15.20	15.73	17.35	16.65	16.37	16.28	16.29	DA	Archives	12392+4525	
1247+550	–	–	18.3	17.1	16.4	15.80	15.66	15.40	21.24	18.52	17.69	16.84	16.62	DC	Archives	12501+5447	
1254+223	–	12.37	13.2	13.8	13.3	14.01	14.21	14.31	13.31	13.21	13.75	14.59	14.47	DA	Archives	12570+2201	
1257+017	–	23.11	18.1	17.2	16.4	16.23	15.97	15.36	19.09	17.79	17.25	17.06	16.94	DA	–	13003+0130	
1257+037	–	20.95	16.1	15.4	15.1	14.65	14.32	14.22	17.20	16.11	15.63	15.45	15.41	DA	Archives	13001+0328	
1257+278	20.78	16.75	15.6	15.0	14.9	15.13	14.98	14.99	15.84	15.44	15.41	15.46	15.60	DA	Archives	12597+2734	
1259+674	–	19.29	16.6	15.4	15.9	15.62	15.32	15.34	17.31	16.72	16.45	16.36	16.39	DA	Bok	13013+6713	
1300+263	–	–	–	18.6	17.8	16.80	16.40	16.44	–	–	–	–	–	DC	Archives		
1309+853	–	–	16.4	15.9	14.7	14.67	14.46	14.34	–	–	–	–	–	DAP	Archives		

TABLE 3.4 – Continued

WD name	FUV	NUV	B_F	R_I	I_N	J	H	K_S	u	g	r	i	z	ST	Source	PM I	Notes
1310+583	16.16	15.00	14.3	14.2	14.3	14.02	14.00	14.08	14.46	14.04	14.20	14.33	14.52	DA	Archives	13129+5805	
1315+222	–	20.36	17.0	17.2	15.5	16.03	15.79	15.96	17.63	16.95	16.69	16.63	16.67	DC	–	13178+2157	
1319+466	14.53	14.64	14.6	14.7	14.6	14.87	14.86	14.77	14.66	14.36	14.65	14.91	15.17	DA	Archives	13212+4623	
1325+581	–	19.45	17.1	16.4	17.1	15.94	15.70	15.72	17.41	16.81	16.58	16.53	16.54	DA	Archives	13277+5755	
1328+307	–	21.44	17.2	16.0	15.6	15.40	15.28	15.41	18.29	16.30	15.89	15.91	16.09	DZ	Archives	13309+3029	
1331+021	–	–	17.0	16.3	15.4	15.99	15.81	15.26	17.99	17.10	16.81	16.72	16.70	DA	SDSS	13309+0204	10
1333+487	–	–	13.9	13.7	12.7	11.79	11.20	10.92	–	–	–	–	–	DB+dM+dM	Archives		
1334+039	–	–	15.4	14.0	14.1	13.06	12.82	12.69	16.79	15.10	14.35	14.06	13.95	DA	Archives	13365+0340	
1334+366	–	–	16.3	16.0	15.8	15.55	15.34	15.31	17.06	16.48	16.27	16.23	16.24	DA	Archives	13365+3623	
1336+613	–	–	17.9	17.2	17.1	16.48	16.35	15.62	19.30	18.16	17.66	17.46	17.40	DA	SDSS	13379+6110N	
1337+705	–	–	13.1	12.9	12.1	13.25	13.36	13.45	–	–	–	–	–	DA	Archives	13388+7017	
1344+106	–	17.51	15.2	14.8	14.0	14.41	14.14	14.23	15.72	15.35	15.05	14.99	15.02	DA	Archives	13474+1021W	
1344+572	13.71	13.73	13.4	13.5	13.2	13.70	13.82	13.76	13.92	14.49	13.74	13.94	14.22	DA	Archives	13460+5700	
1345+238	–	–	16.9	15.2	13.9	13.92	13.67	13.59	–	–	–	–	–	DA	Archives		
1346+121	–	–	18.6	17.4	17.0	16.46	16.19	15.81	20.59	18.65	17.84	17.42	17.21	DC	Archives	13490+1155	
1347+281	–	18.55	16.9	16.2	16.1	15.74	15.68	15.60	16.95	16.45	16.30	16.28	16.37	DA	Archives	13497+2755	
1349+552	17.15	16.37	15.9	15.9	16.2	15.84	16.31	16.55	16.20	15.74	15.91	16.12	16.36	DA	Bok	13513+5457	
1401+523	–	–	16.5	16.1	16.3	15.71	15.67	15.06	17.03	16.54	16.41	16.40	16.44	DA	Archives	14037+5206	
1404+670	–	–	19.9	17.9	17.6	–	–	–	–	–	–	–	–	G:ouDC	–	14059+6648	
1407+425	–	–	14.6	14.9	–	15.00	14.87	14.89	15.47	15.06	15.15	15.28	15.43	DA	Archives		
1408+323	13.43	13.72	13.8	14.3	14.1	14.40	14.48	14.43	13.94	14.26	14.17	14.46	14.78	DA	Archives	14104+3208	
1411+218	15.11	14.45	14.4	13.8	14.3	14.70	14.81	14.85	14.20	14.25	14.56	14.81	15.08	DB	Archives	14134+2137N	
1422+095	15.42	14.78	14.7	14.6	14.4	14.53	14.50	14.61	15.03	14.86	14.58	14.93	14.91	DA	Bok	14246+0917	
1434+437	–	–	18.1	17.2	16.4	15.83	15.61	15.60	19.89	18.03	17.18	16.86	16.70	DC	–	14367+4332	
1455+298	–	17.64	15.6	15.3	14.7	14.97	14.61	14.74	16.16	15.68	15.55	15.51	15.59	DA	Archives	14581+2937	

TABLE 3.4 – Continued

WD name	FUV	NUV	B_F	R_I	I_N	J	H	K_S	u	g	r	i	z	ST	Source	PM I	Notes
1508+637	17.98	15.62	15.1	14.7	14.3	14.72	14.57	14.81	–	–	–	–	–	DA	Archives	15096+6332	
1509+322	14.17	14.21	14.1	14.4	14.3	14.44	14.57	14.57	14.72	14.75	16.34	14.82	14.78	DA	Archives	15114+3204	
1509+409	20.25	17.17	16.0	15.6	15.5	15.23	15.13	14.85	16.17	15.70	15.72	15.75	15.84	DA	Bok	15111+4048	
1524+566	–	22.26	17.2	16.3	16.2	15.51	15.21	15.10	18.38	17.24	16.74	16.53	16.48	DC	–	15257+5629	
1529+141	–	–	16.2	16.4	16.2	16.12	15.92	16.44	16.87	16.55	16.58	16.64	16.77	DA+DQ	Archives		
1532+129	–	22.73	16.4	15.7	15.1	14.94	14.73	14.71	18.04	15.99	15.50	15.44	15.51	DZ	SDSS	15350+1247	
1533+469	–	–	19.2	17.8	17.2	16.45	16.14	15.48	20.94	18.76	17.76	17.34	17.17	DC	4m	15348+4649	
1534+503	21.32	17.08	16.4	15.6	15.1	15.42	15.27	15.11	16.28	15.83	15.84	15.91	16.03	DA	Archives	15362+5013	
1537+583	–	20.01	17.1	17.3	17.5	16.75	17.64	15.73	18.42	17.89	17.70	17.63	17.70	DA	–	15390+5811	
1537+651	18.60	15.66	15.2	14.6	14.0	14.46	14.45	14.47	15.23	14.76	13.24	14.91	14.96	DA	Archives	15377+6501	
1538+333	20.64	16.36	15.6	15.0	14.7	14.77	14.70	14.49	15.52	15.11	15.11	15.17	15.30	DA	Archives	15405+3308N	
1540+236	–	21.27	17.0	16.3	15.8	15.76	15.48	15.76	17.93	16.98	16.58	16.43	16.42	DA	Bok	15425+2329	
1550+183	14.93	14.81	14.6	15.2	14.9	15.17	15.31	15.28	15.24	15.06	16.66	15.36	15.37	DA	Archives	15524+1810	
1554+505	–	20.42	16.9	16.5	15.6	15.51	15.04	15.03	17.55	16.77	16.41	16.29	16.28	DA	Bok	15555+5025	
1559+369	16.27	15.09	14.6	14.7	14.3	14.43	14.32	14.39	14.82	14.39	14.50	14.72	14.91	DA	Bok	16013+3648	
1559+534	–	19.16	16.6	16.6	15.9	15.66	15.59	15.35	17.29	16.68	16.48	16.42	16.40	DA	SDSS	16012+5316	11
1602+010	–	–	19.1	17.1	16.7	16.08	15.97	15.53	19.91	18.15	17.38	17.11	16.98	DC	Archives	16048+0055	
1603+432	13.01	13.61	15.1	14.9	14.9	15.59	15.54	17.00	14.20	14.52	15.06	15.42	15.77	DA	Bok	16053+4304	
1605+345	–	21.87	17.2	16.5	16.3	15.87	15.73	15.63	18.60	17.48	16.96	16.78	16.72	DA	–	16072+3423	
1606+422	14.54	–	14.2	13.7	13.6	13.98	14.03	14.05	14.20	13.78	13.96	14.16	14.40	DA	Archives	16083+4205	
1609+135	19.80	16.16	16.2	15.2	14.9	14.86	14.78	14.86	15.45	15.10	15.13	15.23	15.38	DA	Archives	16114+1322	
1625+093	–	18.87	16.7	15.7	15.3	15.25	15.19	15.04	16.84	16.26	16.06	15.99	16.02	DA	Archives	16278+0912	
1626+368	20.17	15.70	14.4	13.9	13.2	13.64	13.65	13.57	14.25	14.02	14.03	14.18	14.17	DZA	Archives	16284+3646	
1632+177	–	–	13.4	13.5	13.5	–	–	–	–	–	–	–	–	DA	Archives		
1633+433	–	–	15.2	14.5	14.0	13.99	13.77	13.61	15.64	14.98	14.73	14.66	14.68	DAZ	Archives	16350+4317	

TABLE 3.4 – Continued

WD name	FUV	NUV	B_F	R_I	I_N	J	H	K_S	u	g	r	i	z	ST	Source	PM I	Notes
1633+572	–	18.11	15.7	14.9	14.2	14.11	14.08	14.14	–	–	–	–	–	DQpec	Archives	16343+5710	
1637+335	18.18	15.53	15.0	14.6	14.1	14.55	14.47	14.42	15.04	14.60	14.69	14.81	15.00	DA	Archives	16394+3325	
1639+153	–	17.83	15.9	15.4	15.1	15.07	14.98	15.06	–	–	–	–	–	DA	Archives	16416+1512	
1639+537	20.32	16.89	16.0	15.1	14.0	14.49	14.48	14.37	15.55	15.10	14.99	15.01	15.11	DAH	Archives	16409+5341	
1644+198	15.67	15.04	15.4	15.1	15.0	15.39	15.45	15.32	14.82	14.92	15.21	15.46	15.70	DB	Bok	16463+1946	
1645+325	12.99	13.23	13.5	13.7	13.7	14.13	14.21	14.41	14.05	13.69	15.65	14.57	14.58	DB	Archives	16473+3228	
1647+591	–	–	12.2	11.7	11.5	12.43	12.46	12.52	–	–	–	–	–	DA	Archives	16484+5903	
1653+385	–	21.39	17.1	16.5	–	15.53	15.35	15.27	17.97	16.99	16.57	16.41	16.38	DAZ	Archives	16547+3829	
1655+215	18.75	15.25	14.9	14.1	14.0	13.89	13.82	13.86	14.59	14.33	14.12	14.44	14.40	DA	Archives	16571+2126	
1657+321	–	–	17.3	17.0	17.1	16.46	16.61	15.73	18.34	17.66	17.36	17.28	17.24	DA	Archives	16596+3203	
1658+445	–	21.70	17.0	16.1	15.2	15.43	15.19	15.01	18.23	17.06	16.57	16.39	16.29	DA	Bok	16595+4425	
1703+362	–	–	18.3	17.6	17.4	16.55	16.35	17.17	20.56	18.73	17.94	17.64	17.51	DC	–	17047+3608	
1705+030	–	19.84	15.9	14.5	14.7	14.56	14.50	14.51	–	–	–	–	–	DZ	Archives	17081+0257	
1713+393	–	18.93	17.1	16.5	16.4	15.63	15.38	15.41	17.17	16.56	16.32	16.25	16.26	DAP	Bok	17148+3918	
1713+695	13.29	13.61	13.5	13.6	13.6	13.62	13.72	13.74	13.43	13.22	13.48	13.74	14.05	DA	Archives	17131+6931	
1716+020	15.06	14.87	14.0	14.1	13.9	14.60	14.53	14.56	–	–	–	–	–	DA	Archives	17185+0156N	
1729+371	–	–	16.3	16.4	16.2	16.16	16.07	15.60	–	–	–	–	–	DAZB	Archives		
1736+052	–	–	15.4	15.8	15.5	15.73	15.60	15.42	–	–	–	–	–	DA 1	Archives	17386+0516	
1741+436	–	–	17.1	16.5	16.3	15.80	15.67	15.41	18.68	17.42	16.89	16.68	16.60	DA	–	17428+4338	
1747+450	–	17.04	15.7	15.6	15.6	15.43	15.19	15.17	15.82	15.56	15.60	15.69	15.83	DC	Archives	17484+4503	
1748+708	–	18.58	14.9	13.5	13.1	12.71	12.53	12.51	–	–	–	–	–	DXP	Archives	17481+7052	
1755+408	–	21.69	17.2	16.8	16.5	15.92	15.88	15.82	18.48	17.47	16.97	16.77	16.69	DC	–	17570+4052	
1756+143	–	–	17.2	16.4	15.6	14.93	14.66	14.66	–	–	–	–	–	DA	Archives	17583+1417	
1756+827	–	16.48	14.7	14.5	13.1	13.63	13.47	13.43	–	–	–	–	–	DA	Archives	17498+8246	
1811+327.1	–	–	16.7	16.4	16.4	15.72	15.67	15.76	–	–	–	–	–	DA	Archives	18135+3248.1	

TABLE 3.4 – Continued

WD name	FUV	NUV	B_F	R_I	I_N	J	H	K_S	u	g	r	i	z	ST	Source	PM I	Notes
1811+327.2	–	19.96	17.6	16.7	16.5	16.21	15.95	15.81	–	–	–	–	–	DA	Archives	18135+3248.2	
1814+134	–	–	16.6	15.4	15.1	14.38	14.10	14.07	–	–	–	–	–	DA	Archives	18171+1328	
1814+248	–	19.61	17.3	16.9	16.5	16.08	16.11	15.51	–	–	–	–	–	DAP	Archives	18161+2454	
1818+126	–	–	15.9	15.2	15.2	14.99	14.89	14.88	–	–	–	–	–	DAH	Archives	18205+1239	
1820+609	–	22.60	16.4	15.0	13.9	14.07	13.81	13.80	–	–	–	–	–	DA	Archives	18213+6101	
1822+410	–	–	14.2	14.6	14.4	14.61	14.66	14.70	14.01	14.09	14.41	14.66	14.91	DB	Archives	18236+4104	
1824+040	–	–	14.7	14.7	14.3	14.11	14.11	14.23	–	–	–	–	–	DA	Archives	18272+0403	
1829+547	–	18.65	15.6	14.9	14.8	14.80	14.48	14.51	–	–	–	–	–	DXP	Archives	18303+5447	
1831+197	–	18.36	17.8	16.0	15.9	15.98	16.04	15.61	16.89	16.48	16.38	16.40	16.47	DQ	Archives	18339+1945	
1840+042	–	–	14.5	14.2	13.6	14.44	14.37	14.65	–	–	–	–	–	DA	Archives	18434+0420	
1855+338	–	–	14.7	14.8	14.2	14.74	14.77	14.80	–	–	–	–	–	DA	Bok	18575+3357	
1856+534	–	–	17.6	16.4	15.7	15.68	15.43	15.55	–	–	–	–	–	DC	–	18576+5330	
1858+393	–	–	16.7	15.6	14.9	15.53	15.44	15.25	16.07	15.64	15.68	15.78	15.92	DA	Archives	19002+3922	
1900+705	14.03	13.56	13.3	13.5	13.6	13.33	13.44	13.42	–	–	–	–	–	DAP	Archives	19001+7039	
1911+135	–	–	14.2	14.1	14.4	14.26	14.51	14.54	–	–	–	–	–	DA	Archives	19136+1336	
1917+386	–	–	15.3	14.1	14.2	13.78	13.67	13.52	15.41	14.73	14.51	14.37	14.38	DC	Archives	19189+3843	
1919+145	–	–	13.4	13.4	13.6	–	13.45	13.55	–	–	–	–	–	DA	Archives		
1935+276	–	–	12.9	12.7	13.0	13.18	13.21	13.33	–	–	–	–	–	DA	Bok	19372+2743	
1936+327	–	–	13.5	13.9	14.0	14.11	14.23	14.36	–	–	–	–	–	DA	Archives	19384+3253	
1939+662	–	–	18.4	17.5	17.0	16.51	16.49	15.74	–	–	–	–	–	DC	Bok	19399+6618	
1943+163	–	–	14.3	14.4	13.8	14.49	14.63	14.63	–	–	–	–	–	DA	Archives	19455+1627	
2009+622	–	–	15.5	15.7	15.4	14.28	13.91	13.58	–	–	–	–	–	DA	4m	20107+6225	
2010+310	–	–	14.9	15.2	–	15.18	15.16	14.95	14.26	14.62	14.85	15.23	15.50	DBP	Archives	20123+3113	
2011+065	–	18.53	15.4	15.0	–	15.02	14.88	15.09	16.47	15.87	15.66	15.62	15.64	DC	Archives	20139+0642	
2028+390	–	–	13.6	14.4	13.9	13.92	14.01	14.35	–	–	–	–	–	DA	Archives	20299+3913E	

TABLE 3.4 – Continued

WD name	FUV	NUV	B_F	R_I	I_N	J	H	K_S	u	g	r	i	z	ST	Source	PM I	Notes
2032+248	–	–	11.5	11.6	11.8	12.04	12.07	12.19	–	–	–	–	–	DA	Archives	20343+2503	
2047+372	–	–	12.9	13.2	12.9	13.30	13.37	13.43	–	–	–	–	–	DA	Archives	20491+3728	
2048+263	–	–	15.7	14.1	14.0	14.10	13.91	13.60	17.72	16.04	15.34	15.06	14.95	DC	Archives	20503+2630	
2048+809	–	–	–	–	–	16.15	16.14	–	–	–	–	–	–	DA	Archives		
2058+342	18.38	16.39	16.4	15.6	15.7	15.74	15.85	15.57	–	–	–	–	–	DB(+DC?)	Archives	21003+3426	
2058+506	–	–	16.0	15.0	14.9	14.81	14.96	14.94	–	–	–	–	–	DA	Archives	21005+5051	
2059+190	–	19.01	17.1	16.2	15.7	15.64	15.56	15.40	–	–	–	–	–	DA	Archives	21020+1912	
2059+247	–	20.67	17.0	16.0	15.8	15.52	15.20	15.06	17.61	16.77	16.41	16.29	16.26	DA	Archives	21022+2457	
2059+316	–	–	–	19.1	14.9	14.97	14.93	14.98	–	–	–	–	–	DQ	Archives		
2111+261	19.86	16.16	15.2	14.9	14.8	14.23	14.12	14.10	–	–	–	–	–	DA	Archives	21137+2621	
2117+539	–	–	12.6	12.9	13.2	12.68	12.78	12.85	14.22	15.32	12.59	15.13	13.81	DA	Archives	21189+5412	
2119+581	–	–	16.5	16.1	15.8	15.39	15.26	14.99	–	–	–	–	–	DA	Archives	21207+5819	
2124+550	–	–	15.7	15.0	14.8	14.99	14.96	14.90	–	–	–	–	–	DA	4m	21264+5513	
2126+734	13.05	13.06	13.1	13.4	13.5	13.10	13.16	13.17	13.36	14.27	14.22	13.50	13.57	DA	Archives	21269+7338	
2136+229	18.65	16.14	15.4	14.6	13.9	15.11	15.06	14.82	–	–	–	–	–	DA	Archives	21387+2309	
2136+828	–	–	13.3	13.5	13.5	13.45	13.49	13.50	–	–	–	–	–	DA	Archives	21337+8303	
2138+091	20.27	16.96	16.3	15.3	–	15.55	15.40	15.39	–	–	–	–	–	DA	Bok	21410+0923	
2140+207	19.59	14.88	12.9	12.9	12.5	12.98	12.93	12.92	–	–	–	–	–	DQ	Archives	21426+2059	
2144+156	21.66	18.15	16.3	16.0	16.1	15.93	15.72	15.53	17.14	16.60	16.52	16.51	16.55	DA	Bok	21465+1550	
2147+280	16.39	15.18	14.2	14.5	14.2	14.72	14.84	14.88	–	–	–	–	–	DB	Archives	21499+2816	
2148+539	–	–	18.6	16.1	15.3	15.92	15.42	15.00	–	–	–	–	–	DA	Archives	21499+5408	
2149+021	12.97	12.68	13.1	13.4	13.7	13.20	13.29	13.40	–	–	–	–	–	DA	Archives	21524+0223	
2207+142	–	17.45	16.1	15.5	14.6	14.97	14.78	14.77	–	–	–	–	–	DA	Archives	22097+1429	
2211+372	–	20.08	17.1	16.5	16.0	16.25	16.06	15.62	–	–	–	–	–	DC	Archives	22141+3727	
2213+317	–	–	17.5	16.8	16.5	16.33	16.05	15.71	–	–	–	–	–	DA	Archives	22151+3158	

TABLE 3.4 – Continued

WD name	FUV	NUV	B_F	R_I	I_N	J	H	K_S	u	g	r	i	z	ST	Source	PM I	Notes
2215+368	–	–	17.7	16.2	16.1	15.40	15.20	14.97	–	–	–	–	–	DC	Bok	22177+3707	
2216+484	–	–	16.7	16.0	15.4	15.48	15.30	15.32	–	–	–	–	–	DA	Archives	22188+4839	
2217+211	–	–	19.1	17.4	16.8	16.45	15.65	16.02	–	–	–	–	–	DC	–	22194+2122	
2220+121	–	–	20.1	16.5	17.5	–	–	–	21.54	19.45	18.34	17.92	17.70	DC	–	22225+1221	
2228+151	–	–	18.7	17.3	16.8	16.34	16.01	15.47	–	–	–	–	–	DA	–	22309+1523	
2239+132	–	21.42	17.9	16.9	16.5	16.17	15.91	15.63	18.44	17.55	17.15	17.00	16.97	DA	–	22419+1332	
2246+223	17.76	15.15	14.7	13.8	13.8	14.34	14.32	14.36	14.74	14.32	14.47	14.59	14.82	DA	Archives	22490+2236	
2248+293	–	20.07	15.7	15.1	14.3	14.32	13.98	13.94	–	–	–	–	–	DA	Archives	22513+2939	
2251+131	–	–	19.7	18.1	18.2	–	–	–	21.78	19.53	18.50	18.13	18.00	DC	–	22541+1323	
2253+812	–	–	17.6	16.0	–	15.69	12.70	12.68	–	–	–	–	–	DC:	–	22536+8130	
2258+406	–	–	16.9	16.7	16.0	–	–	–	–	–	–	–	–	DA	Archives		
2305+239	–	–	18.6	17.4	17.1	16.55	16.15	15.62	20.45	18.55	17.82	17.51	17.39	DC	–	23082+2414	
2309+129	–	–	17.6	16.7	17.0	15.91	15.47	15.27	19.23	17.73	17.10	16.87	16.77	DA	–	23121+1310	
2319+095	–	–	19.6	18.3	17.8	–	–	–	–	–	–	–	–	DC:	–	23220+0946E	
2322+137	–	22.43	16.3	15.3	14.7	14.51	14.37	14.36	18.05	16.46	15.87	15.57	15.40	DA	Archives	23253+1403	
2323+157.1	–	16.01	14.8	14.8	14.6	15.05	14.94	14.88	15.17	15.04	15.14	15.28	15.44	DC	Archives	23261+1600	
2323+256	–	–	17.2	16.6	16.2	15.84	15.43	15.46	–	–	–	–	–	DA	Archives	23259+2552	
2326+049	15.14	13.85	13.2	13.0	12.8	13.13	13.07	12.69	–	–	–	–	–	DA	Archives	23287+0514	
2329+267	18.94	15.80	15.3	15.2	15.3	15.18	15.10	15.03	–	–	–	–	–	DAH	Archives	23320+2658	
2329+407	–	–	13.8	13.9	13.7	14.21	14.32	14.25	–	–	–	–	–	DA	Archives	23315+4101	
2341+322	–	–	14.1	14.5	14.7	13.17	13.19	13.18	–	–	–	–	–	DA	Archives		
2347+292	–	–	16.1	15.9	–	14.57	14.35	14.16	–	–	–	–	–	DA	Archives	23499+2934	
2350+205	–	18.73	16.8	16.2	16.2	15.92	15.85	15.58	–	–	–	–	–	DA	–	23532+2051	
2352+401	–	–	15.1	15.0	15.1	14.58	14.45	14.51	–	–	–	–	–	DQ	Archives	23549+4027	

(1) $T_{\rm eff}$ and $\log g$ from Koester et al. (2005); (2) SDSS spectrum 52378-0892-194; (3) SDSS spectrum 52618-0930-475; (4) Also in Sayres et al. (2012); (5) SDSS spectrum 52709-1218-159; (6) SDSS spectrum 52614-0944-584; (7) SDSS spectrum 52723-1004-418; (8) SDSS spectrum 53089-1369-224; (9) SDSS spectrum 52319-0789-391; (10) SDSS spectrum 52022-0528-278; (11) SDSS spectrum 52055-0621-253.

3.3.4 Additional White Dwarfs within 40 pc of the Sun

In addition to our list of 1180 white dwarf candidates, our selection criteria applied to the SUPERBLINK catalog also recovered a total of 416 known white dwarfs with $D_{\rm phot} < 55$ pc. We reexamine this subset to exclude from the lot the known white dwarfs with distances well beyond 40 pc. This we do based on (1) a more robust photometric distance estimate described in Section 3.4.6, and (2) reliable spectroscopic distances found in the literature. We find 121 relatively distant white dwarfs, which leaves 295 white dwarfs that need to be included in our model atmosphere analysis, and for which optical spectra are thus required. Fortunately we already had spectra for 204 objects in this list, acquired over the years for various independent projects. Spectra for another 12 stars were directly available from the SDSS database. Also, optical spectra for 45 additional white dwarfs hot enough to be analyzed with the spectroscopic technique were secured during the spectroscopic observation campaigns listed in Table 3.1. Among these, GD 338 listed as a WD candidate by Giclas et al. (1980), turned out to be a main sequence star, thus reducing the number of known nearby white dwarfs to 294. Finally, 34 white dwarfs on our list are classified in the literature as DC or very cool DA stars, subtypes that can only be analyzed using the photometric technique, and for which we did not obtain new optical spectra because only a spectral type is sufficient for our present purposes.

To our analysis of white dwarfs located within ∼40 pc of the Sun, we also need to include all known white dwarfs suspected to lie within this distance range but that were missed in our search of the SUPERBLINK catalog, either because they failed our selection criteria or are missing from the SUPERBLINK catalog itself for any reason. As discussed in Paper I, about 20% of the nearby white dwarfs are likely to be missed in our search because of their unusual photometry; in particular Sirius-like systems of white dwarfs companions to main-sequence stars. With this limitation in mind, we searched the following papers for objects with spectroscopic distances less than 40 pc of the Sun: Kawka & Vennes (2006), Kilic et al. (2012), Sayres et al. (2012), Giammichele et al. (2012) as well as the large spectroscopic samples of Bergeron et al. (2011) and Gianninas et al. (2011) for DA and DB stars, respectively, and also Holberg et al. (2013) for Sirius-like systems. In all, we identified 45 nearby white dwarfs

missing from our original list, all of which had optical spectra available to us.

The 294 known white dwarfs in SUPERBLINK plus the 45 found in the literature, all suspected to lie within 40 pc of the Sun, are listed in Table 3.4 for a total of 349 entries. We provide for each object the WD designation, the photometric measurements, the spectral type, the origin of the spectrum used in our analysis, and the PM I designation if the white dwarf is a SUPERBLINK object. Combining this sample of 349 *known* with the 322 *new* white dwarfs identified in our survey of SUPERBLINK, we thus end up with a current census of 661 white dwarfs, which represents the basis of the detailed model atmosphere analysis presented in the next section.

3.4 Atmospheric Parameter Determination

3.4.1 Theoretical Framework

Our model atmospheres and synthetic spectra for hydrogen-atmosphere white dwarfs are built from the model atmosphere code originally described in Bergeron et al. (1995) and references therein, with recent improvements discussed in Tremblay & Bergeron (2009). These are pure hydrogen, plane-parallel model atmospheres, with non-local thermodynamic equilibrium effects explicitly taken into account above $T_{\rm eff} = 30,000$ K, and energy transport by convection included in cooler models following the ML2/$\alpha = 0.7$ prescription of the mixing-length theory. The theoretical spectra are calculated within the occupation formalism of Hummer & Mihalas (1988), which provides a detailed treatment of the level populations as well as a consistent description of bound-bound and bound-free opacities. We also include the improved calculations for the Stark broadening of hydrogen lines from Tremblay & Bergeron (2009), which take into account nonideal perturbations from protons and electrons directly inside the line profile calculations, as well as the opacity from the red wing of Lyα calculated by Kowalski & Saumon (2006), which is known to affect the flux in the ultraviolet region of the energy distribution, and in particular the FUV, NUV, and u magnitudes used in our analysis. Our model grid covers a range of effective temperatures between $T_{\rm eff} = 1500$ K and 120,000 K in steps of 250 K for $T_{\rm eff} < 5500$ K, 500 K up to $T_{\rm eff} = 17,000$ K, and 5000 K above. The

$\log g$ ranges from 6.0 to 9.5 by steps of 0.25 dex.

Our model atmospheres and synthetic spectra for helium-atmosphere stars are described at length in Bergeron et al. (2011). These include the Stark profiles of neutral helium from Beauchamp et al. (1997) as well as van der Waals broadening. The synthetic spectra are calculated using the occupation probability formalism of Hummer & Mihalas (1988) for helium populations and corresponding bound-bound, bound-free, and pseudo-continuum opacities. Our model grid covers a range of effective temperatures between $T_{\rm eff}$ = 3000 K and 40,000 K in steps of 1000 K, while the $\log g$ ranges from 7.0 to 9.0 in steps of 0.5 dex. In addition to pure helium models, we also calculated models above 11,000 K with $\log {\rm H/He} = -6.5$ to -2.0 by steps of 0.5 dex.

The photometric analyses of DQ and DZ white dwarfs rely on the LTE model atmosphere calculations developed by Dufour et al. (2005, 2007) for the study of DQ and DZ stars, respectively. Both are based on a modified version of the code described in Bergeron et al. (1995). The main addition to the models is the inclusion of metals and molecules in the equation of state and opacity calculations. These heavier elements provide enough free electrons to affect the atmospheric structures and predicted energy distributions of cool, helium-rich white dwarfs.

3.4.2 Photometric Analysis

3.4.2.1 General Procedure

The photometric technique developed by Bergeron et al. (1997) makes use of the apparent magnitudes in any photometric system in order to measure the atmospheric parameters ($T_{\rm eff}$ and $\log g$) and the chemical composition. This method is particularly useful for the analysis of cool white dwarfs when spectral features are either too weak or completely absent. The magnitudes in each bandpass are first converted into a set of average fluxes f_λ^m following the procedure described in Holberg & Bergeron (2006), which is mainly based on the Vega fluxes from Bohlin & Gilliland (2004), but also includes *ugriz* photometry in the AB magnitude system. In particular here, we make use of the transmission functions described in Morrissey

& GALEX Science Team (2004) and available from the *GALEX* Web site [6] for the FUV and NUV filters, while the bandpasses for the *ugriz* system (Fukugita et al. 1996) are taken from the SDSS Web site [7]. Similarly, for the 2MASS filters described in Cohen et al. (2003), we use the transmission functions from the 2MASS survey Web site [8]. Finally, the USNO-B1.0 B_J, R_F, and I_N magnitudes are described in Monet et al. (2003), and the transmission functions are taken from the Digitized Sky Survey website [9].

These observed average fluxes can be compared to the average model fluxes H_λ^m by the relation

$$f_\lambda^m = 4\pi(R/D)^2 H_\lambda^m \tag{3.1}$$

where R/D defines the ratio of the radius of the star to its distance from Earth. The model fluxes H_λ^m — which depend on $T_{\rm eff}$, $\log g$, and chemical composition — are obtained from averages over the transmission function of the corresponding bandpass [10]. We then minimize the χ^2 value defined in terms of the difference between observed and model fluxes over all bandpasses, properly weighted by the photometric uncertainties. Our minimization procedure relies on the nonlinear least-squares method of Levenberg-Marquardt (Press et al. 1986), which is based on a steepest descent method. Only $T_{\rm eff}$ and the solid angle $\pi(R/D)^2$ are considered free parameters (for an assumed chemical composition), while the error of both parameters are obtained directly from the covariance matrix of the fit. For stars with known trigonometric parallax measurements, we first assume a value of $\log g = 8$ and determine $T_{\rm eff}$ and the solid angle, which combined with the distance D obtained from the trigonometric parallax measurement, yields directly the radius of the star R. The radius is then converted into mass using evolutionary models similar to those described in Fontaine et al. (2001) but with C/O cores, $q({\rm He}) \equiv \log M_{\rm He}/M_\star = 10^{-2}$ and $q({\rm H}) = 10^{-4}$, which are representative of hydrogen-atmosphere white dwarfs, and $q({\rm He}) = 10^{-2}$ and $q({\rm H}) = 10^{-10}$, which are representative of helium-atmosphere white dwarfs. In general, the $\log g$ value obtained from the inferred mass and radius ($g = GM/R^2$) will be different from our initial assumption of $\log g = 8$,

6. http://*GALEX*gi.gsfc.nasa.gov/docs/*GALEX*/Documents/PostLaunchResponseCurveData.html
7. http://www.sdss.org/dr6/instruments/imager/#filters
8. http://www.ipac.caltech.edu/2mass/releases/allsky/doc/sec6_4a.html
9. http://www3.cadc-ccda.hia-iha.nrc-cnrc.gc.ca/dss/
10. This synthetic photometry is available at http://www.astro.umontreal.ca/~bergeron/CoolingModels

and the fitting procedure is thus repeated until an internal consistency in $\log g$ is reached. For white dwarfs with no parallax measurement, we simply assume a value of $\log g = 8$ and an uncertainty of 0.25 dex, which corresponds to the 1σ dispersion of the surface gravity distribution of hot DA stars (Gianninas et al. 2011).

3.4.2.2 Analysis with Hydrogen- and Helium-atmosphere Models

We first perform a photometric analysis of all featureless DC stars in our sample, and of all DA stars for which the Balmer lines are too weak to be analyzed with the spectroscopic method. Sample fits are shown in Figure 3.10 for a subsample of 5 newly identified white dwarfs. Average observed fluxes are represented by error bars in the left panels (with the photometric bandpasses used in the fitting procedure indicated at the top of each panel), while our best fits with pure hydrogen and pure helium models are shown as filled or open circles, respectively. The corresponding atmospheric parameters are given at the bottom of each panel. The USNO-B1.0 photographic magnitudes have an error of 0.5 mag, which explains the large error bars associated with their photometry. However, since the fit is weighted by the photometric uncertainty, these less accurate magnitudes will have little impact on the solution but they are still useful when no other photometric information is available. Also, some bandpasses had to be removed from the fitting procedure (shown in red in the left panels) either because they are obviously incorrect, or because they are contaminated by the presence of a red companion. In the right panels we compare the spectroscopic observations near Hα with the model predictions *assuming the pure hydrogen solution*; these only serve as an internal check of our photometric solutions and are not used in the fitting procedure. When Hα is observed spectroscopically, we adopt the pure hydrogen solution, as is the case for two objects in Figure 3.10, and even for magnetic DA stars (one shown in Figure 3.10). When Hα is predicted by the pure hydrogen solution but is not observed spectroscopically, we adopt the pure helium solution instead (see, e.g., second object from the top in Figure 3.10). In cases where the star is too cool to show Hα ($T_{\rm eff} \leq 5000$ K), one has to rely on the predicted energy distributions to decide which atmospheric composition best fit the photometric data. However, according to Kowalski & Saumon (2006) based on their analysis of cool white dwarfs

with models including the Lyα opacity, almost all cool DC stars appear to have hydrogen-rich atmospheres, a conclusion also reached by Giammichele et al. (2012, see their Figure 9 and their Section 4.2). We thus assume here the pure hydrogen solution for all cool DC stars in our sample (bottom object in Figure 3.10 for instance). Based on a close inspection of these photometric fits and predicted Hα features, we adopt the solution shown in red in the left panels.

The photometric fits for all 143 DC and cool DA stars in our sample are displayed in Figure 3.11 and in Appendix A (Figure A.1). Also included here are the photometric fits to 3 DA + M dwarf systems (03031+2317, 04032+2520E, and 08184+6606) hot enough to be analyzed with the spectroscopic method, but for which the optical spectra are so heavily contaminated by the presence of the companion that the spectroscopic technique cannot be used reliably. In those cases, we also had to omit from our photometric fits the I_N and JHK_s magnitudes for 03031+2317, the R_F, I_N, and JHK_s for 04032+2520E, and we kept only the B_J, R_F, and ugr magnitudes for 08184+6606. Figure 3.11 also includes the fits to 11 new magnetic white dwarfs identified in our survey. For these, the photometric technique is adopted since the presence of such small magnetic fields are not likely to affect the predicted energy distributions.

A closer inspection of all the photometric fits shown in Figure 3.11 reveals that most solutions for the DA stars predict an Hα feature that agrees remarkably well with observations (with the glaring exception of 04263+4820, 11337+6243, 11598+0007, and 14278+0532, discussed further in Section 3.4.4), giving us confidence in our photometric temperature scale, even for non-DA stars. Since we are often forced in our survey to rely on magnitudes with large uncertainties, we need to worry about the overall accuracy of the photometric method. But our results indicate that the lack of accurate photometric measurements for some objects is compensated to some extent by the large number of data points, and also by the fact that the fit is weighted by the error on the photometry.

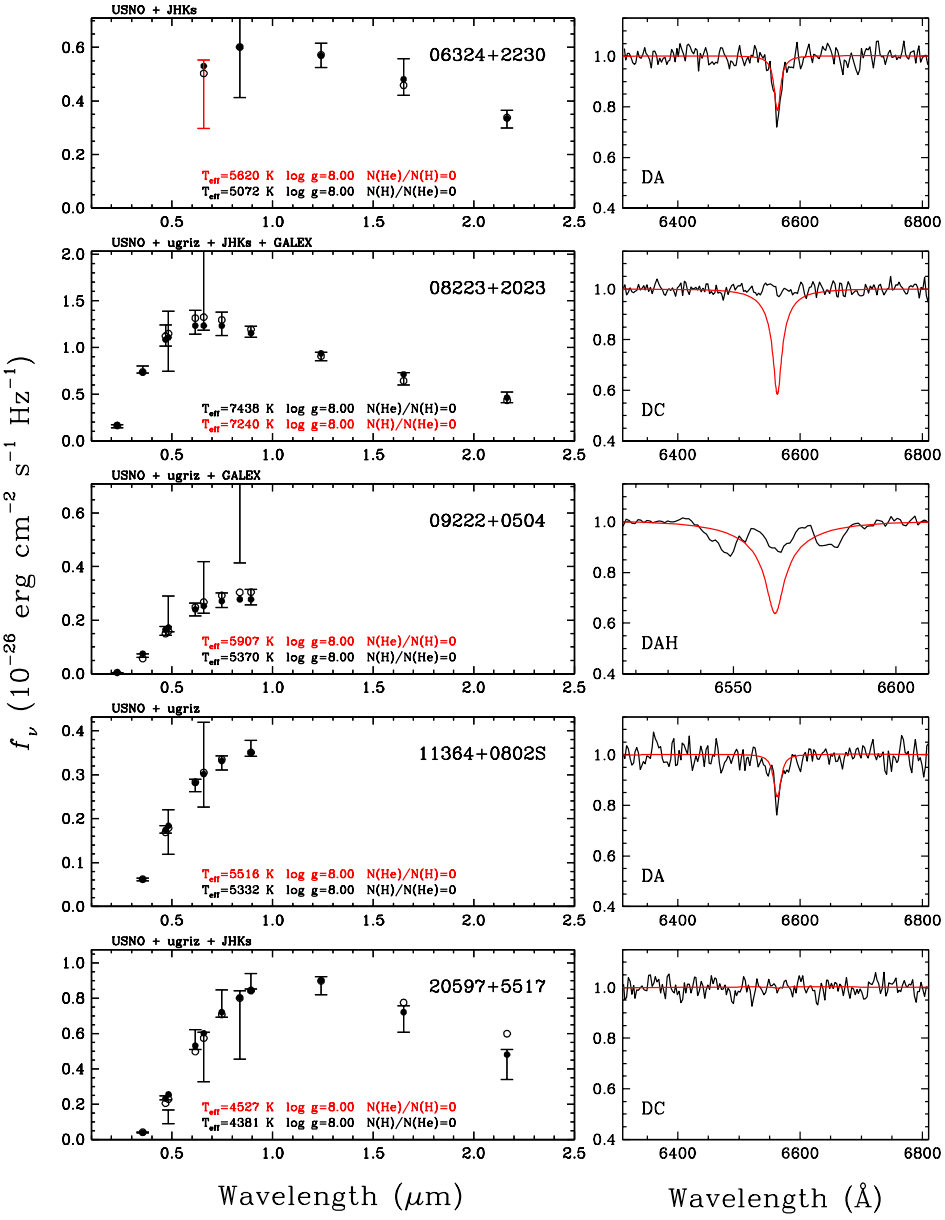

FIGURE 3.10 – Sample fits to the photometric energy distributions (represented by error bars) of 5 new white dwarf identifications with pure hydrogen models (filled circles) and with pure helium models (open circles). The adopted solution is indicated in red. In the right panels are shown the observed normalized spectra together with the synthetic line profiles calculated with the atmospheric parameters corresponding to the pure hydrogen solutions.

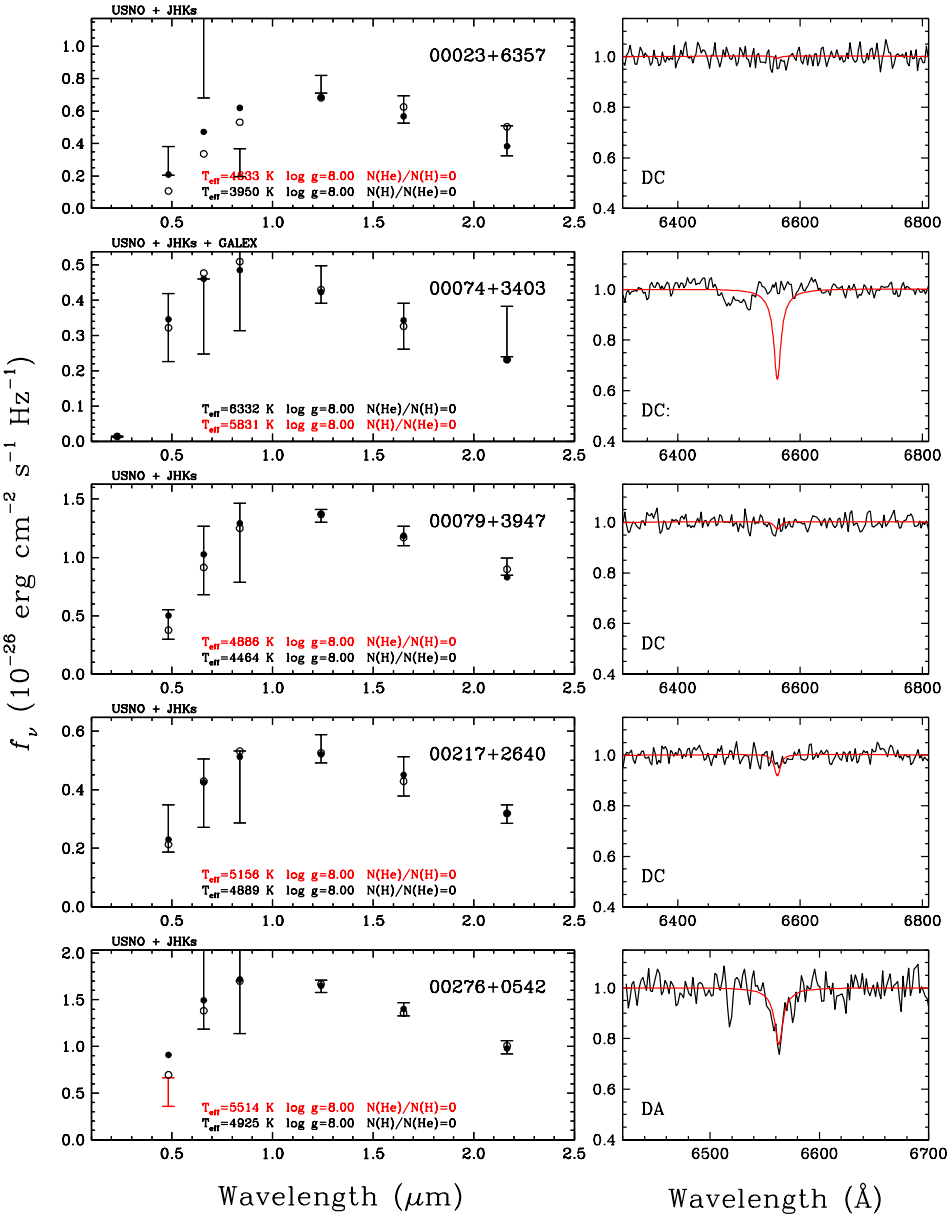

FIGURE 3.11 – Same as Figure 3.10 but for all DC and cool DA stars in our sample. The complete figure is available in Appendix A (Figure A.1).

3.4.2.3 Photometric Analysis of DQ and DZ Stars

The photometric technique used to fit the energy distributions of DQ and DZ stars is similar to that described above for the cool DA and DC stars in our sample, with the exception that the abundance of heavy elements (carbon or metals) is determined from fits to the optical spectra (see also Giammichele et al. 2012). Briefly, the energy distribution is first fitted for an arbitrary abundance of heavy elements to obtain an initial estimate of the effective temperature ($\log g$ is assumed or constrained from trigonometric parallax measurements). The spectroscopic observations are then used to determine the carbon abundance in the case of DQ stars — fitting the C_2 Swan bands — or the metal abundances in the case of DZ stars — fitting the Ca II H & K doublet — at these initial values of $T_{\rm eff}$ and $\log g$. This improved determination of heavy element abundances is then used to obtain new estimates of the atmospheric parameters, and this procedure is repeated until a consistent photometric and spectroscopic solution is reached.

Results for the 5 new DQ stars in our sample (3 from Paper I and 2 from this work) are presented in Figure 3.12, where we display in the left panels the observed and model fluxes, as well as the adopted $T_{\rm eff}$, $\log g$, and carbon abundance, and in the right panels, the observed and model spectra. The predicted energy distributions and spectra agree well for the two normal DQ stars shown at the top. The three other objects are DQpec white dwarfs, with characteristic pressure-shifted C_2 Swan bands (Kowalski 2010). Since these pressure shifts are not included in our models, the line strengths and shifts are not properly reproduced. For these DQpec stars, we simply fit/force the carbon abundance to reproduce the overall strength of the C_2 molecular bands, which is sufficient for our purposes.

The results for the 13 new DZ stars in our sample (6 from Paper I and 7 from this work) are presented in Figure 3.13, where the spectroscopic observations used to determine the calcium abundances in the fitting procedure are shown in the right panels. As mentioned above, the calcium abundances are determined from the strength of the Ca II H & K doublet (see also Dufour et al. 2007), while the abundance of other heavy elements, whether or not they are spectroscopically detected, are assumed to have solar ratios. Because hydrogen is often present in some of these DZ stars (DZA stars), we rely on model grids calculated with

hydrogen abundances of $\log \mathrm{H/He} = -3$, -4, and -5. The insert in the right panels shows the Hα absorption line used to measure or constrain the hydrogen abundance in these stars. The Hα line is particularly strong in 17574+1021, a new DZA star identified in our survey. For stars without Hα or in the absence of spectroscopic data in this region sample, the fits are performed at a fixed hydrogen abundance, determined from the quality of the fit to the H & K doublet, since the amount of hydrogen present in the atmosphere influences the strength of these lines. The predicted energy distributions and spectra agree well with the observations for all 13 stars, except for 12145+7822, for which it is impossible to reproduce the narrow calcium lines with helium-atmosphere models at the low inferred temperature of $T_{\rm eff}$ $\sim$4200 K. This suggests that this star has a hydrogen-rich atmosphere instead, which should produce much narrower absorption lines due to lower atmospheric pressures. Because we do not have model atmospheres that cover the appropriate range of parameters to fit this star, we adopt a photometric solution based on pure hydrogen models, since the presence of metals are not expected to affect the atmospheric structures of hydrogen-rich models.

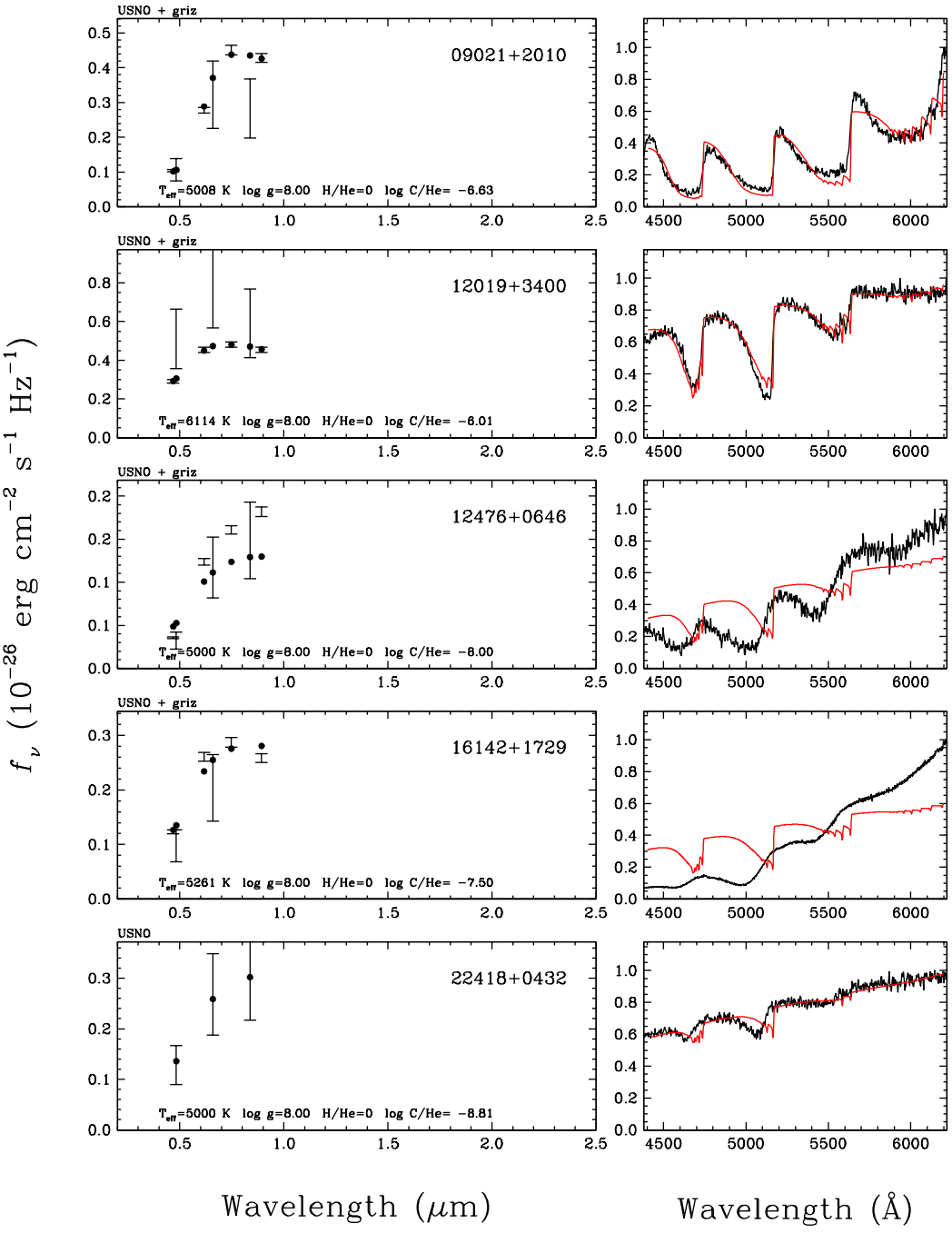

FIGURE 3.12 – Fits to the observed energy distributions for the new DQ identifications. The filled circles correspond to our best fit to the photometry, and the atmospheric parameters and carbon abundances are given in each panel. In the right panels are shown the observed spectra together with the predicted model fit (in red).

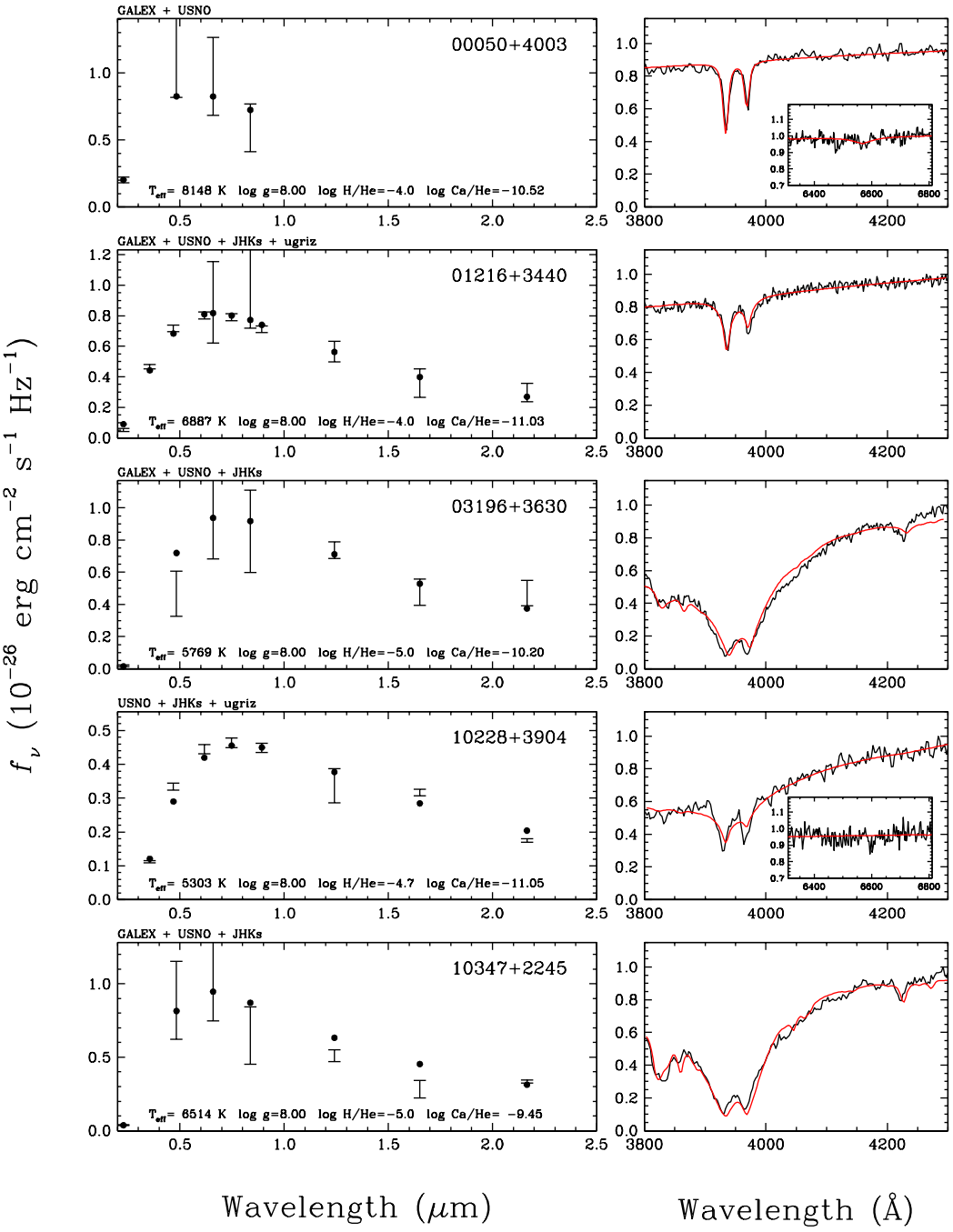

FIGURE 3.13 – (a) - Fits to the energy distributions for the new DZ identifications. The filled circles correspond to our best fit with the atmospheric parameters given in each panel. In the right panels are shown the observed spectra together with the predicted model fit (in red); the insert shows our fit to Hα, when detected.

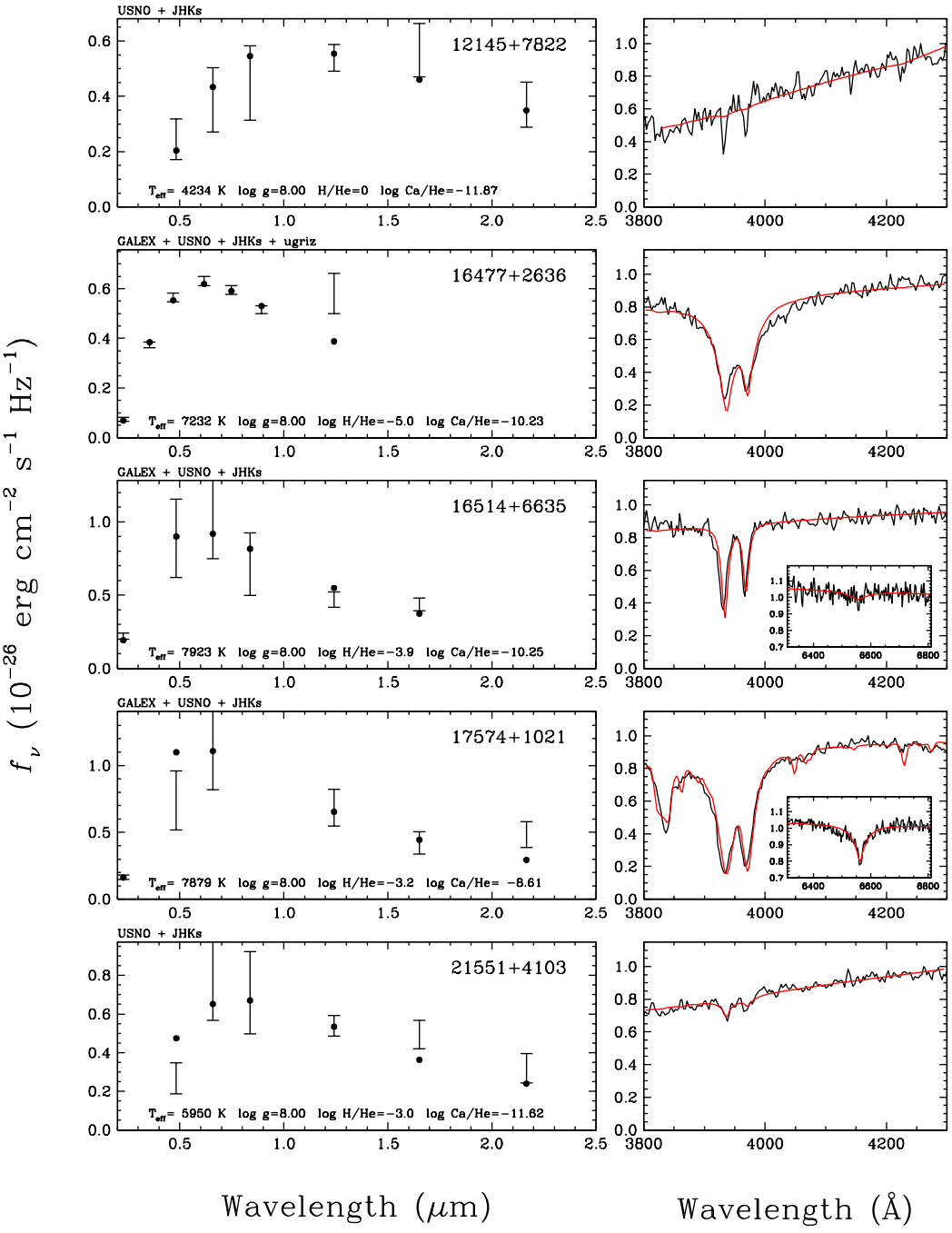

FIGURE 3.13 – (b) - Continued

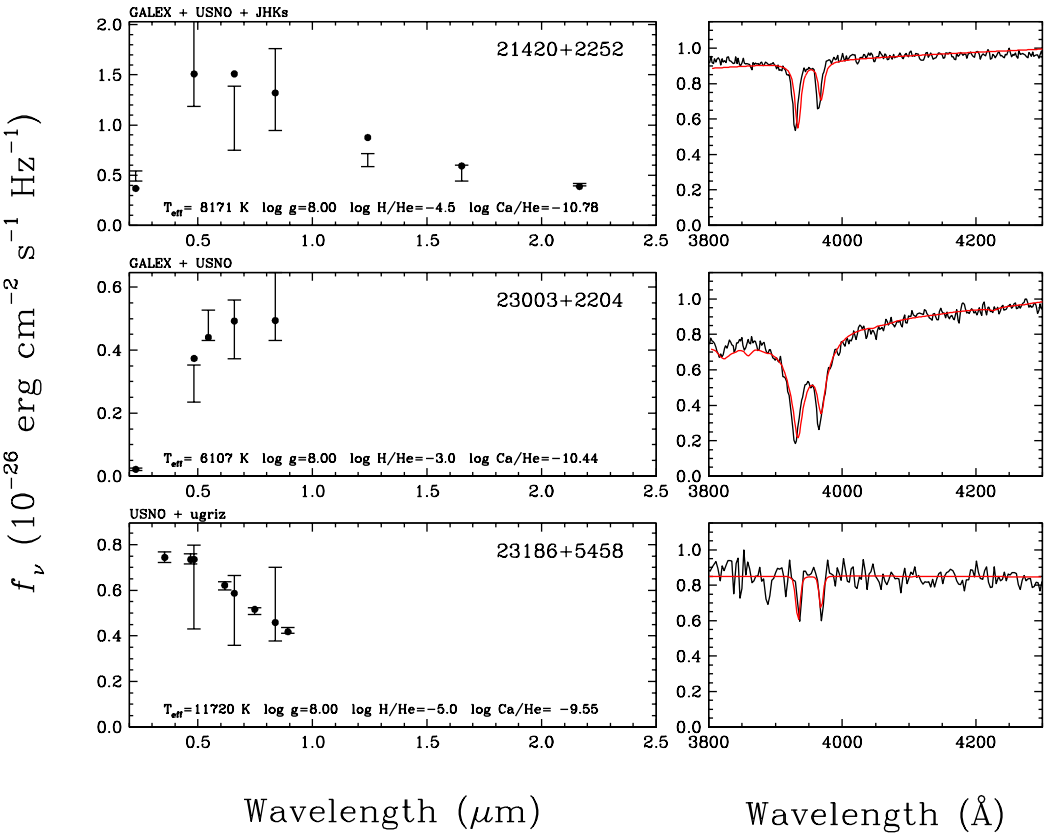

FIGURE 3.13 – (c) - Continued

3.4.3 Spectroscopic Analysis

3.4.3.1 Spectroscopic Analysis of DA Stars

The atmospheric parameters of DA stars with well-defined Balmer lines ($T_{\rm eff} \gtrsim 6500$ K) can be accurately determined from the optical spectra using the so-called spectroscopic technique pioneered by Bergeron et al. (1992, see also Liebert et al. 2005). The optical spectrum of each star, as well as all model spectra (convolved with a Gaussian instrumental profile), are first normalized to a continuum set to unity. The calculation of χ^2 is then carried out in terms of these normalized line profiles only. The atmospheric parameters – $T_{\rm eff}$ and $\log g$ – are considered free parameters in the fitting procedure. Since two solutions exist for a given star, one on each side of the maxium strength of the Balmer lines, we take advantage of our photometry to resolve the ambiguity. Also, since most of our spectra cover Hα, we include this

line in our fitting procedure, allowing us to extend our spectroscopic fits down to $T_{\rm eff}$ ∼6100 K, when Hα is available. We however find that the internal errors on $\log g$ increase significantly for stars cooler than $T_{\rm eff} < 6300$ K — and in particular for spectra with low signal-to-noise ratios (S/N < 40) — reaching a spread of values as large as $\sigma_{\log g}$ ∼0.3 dex, while for the best spectra $\sigma_{\log g}$ can be as low as 0.04. In such cases where the internal errors become too large, $\log g$ is fixed at 8.0 and the uncertainty is set at 0.25 dex, which corresponds to the 1σ dispersion of the surface gravity distribution of hot DA stars (Gianninas et al. 2011).

Spectroscopic fits for the 158 new DA stars identified in our survey are presented in Figure 3.14 and in Appendix A (Figure A.2). It is worth mentioning that 05025+5401 has atmospheric parameters placing it within the ZZ Ceti instability strip, and that periodic light variations are confirmed by observations that will be presented elsewhere. Special care needs to be taken in the case of DA stars with unresolved M dwarf components, in order to reduce the contamination from the companion. When the contamination affects only Hβ and/or Hγ, we simply exclude these lines from the fit, as indicated in Figure 3.14 by the green lines. At other times, emission lines from the M dwarf are also observed in the center of some Balmer lines (see, e.g., 13096+6933), in which case we simply exclude the line centers from our fitting procedure. A similar approach is adopted when the contribution from the M dwarf is large enough to fill up the Balmer line cores, resulting in predicted lines that are too deep (see, e.g., 04586+6209). However, as discussed in Section 3.4.2.2, the white dwarf spectrum is sometimes too contaminated by the M dwarf companion to be fitted with the spectroscopic technique (03031+2317, 04032+2520E, and 08184+6606), and we must therefore rely on the photometric technique alone for these stars. Note that 04389+6351 was classified as a single DA star in Paper I, but we now find from our fits that the predicted Hβ is too deep, suggesting that a red dwarf companion is filling the line (Hβ is actually excluded from our fit here). Our photometric fit for this star (not shown here) shows a significant infrared excess at I_N and JHK_S, also suggesting the presence of a companion. We thus reclassify this star as a DA + M dwarf binary system.

There are also a few DAZ stars in our sample (including our new DAZ identifications 05431+3637, 14106+0245 and 22276+1753; see Figure 3.14b, e, and h), for which the calcium

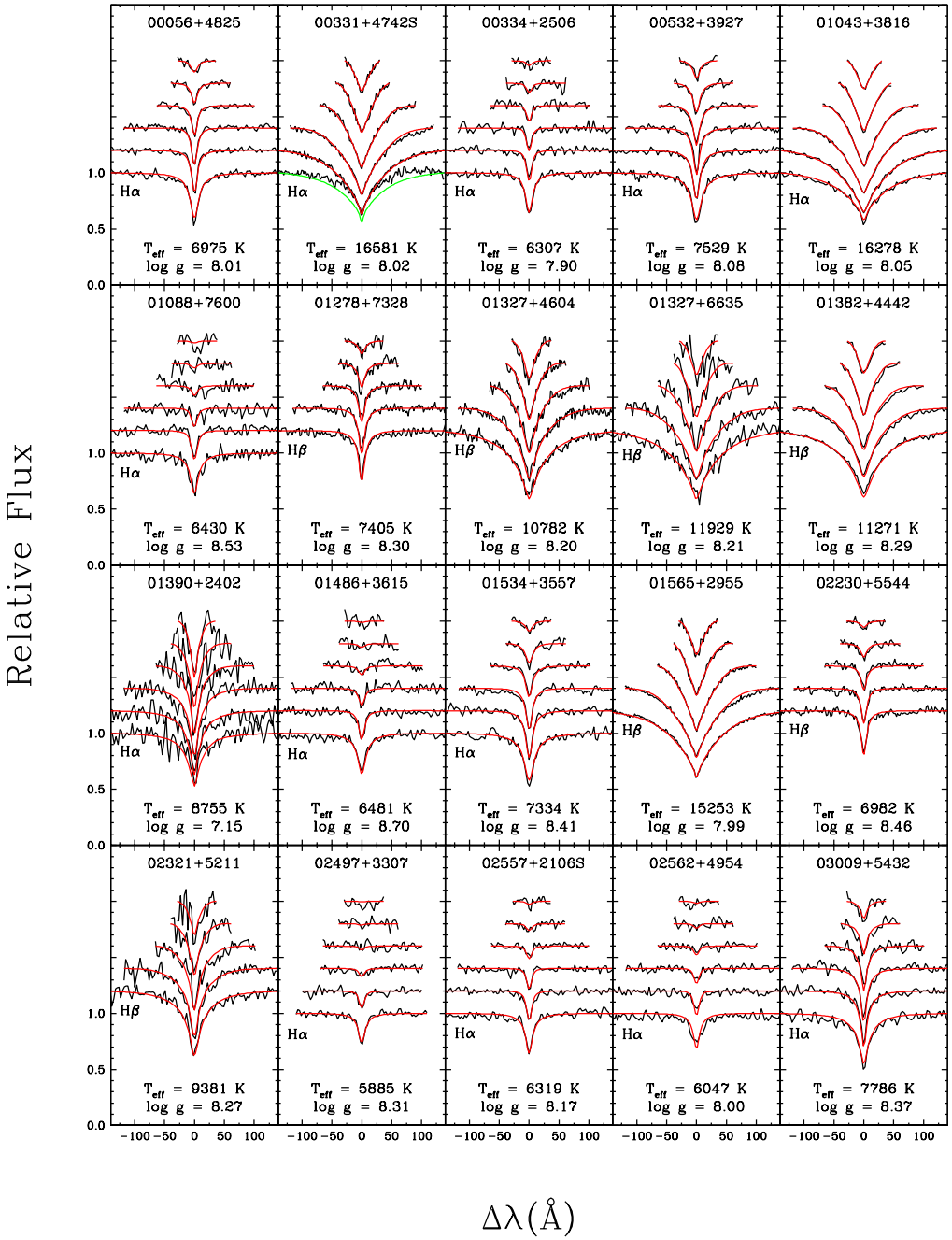

FIGURE 3.14 – Fits to the optical spectra of the DA stars in our sample. The lines range from either Hα (when available) or Hβ (bottom) to H8 (top), each offset vertically by a factor of 0.2. Theoretical line profiles shown in green are not used in the fitting procedure. The complete figure is available in Appendix A (Figure A.2).

H line (at 3968 Å) is blended with Hϵ. Since the upper Balmer lines are particularly sensitive to surface gravity, it is important to model properly the calcium lines for these stars. To do so, we rely on a small grid of synthetic spectra, based on our grid of pure hydrogen models, where calcium lines have been included in the calculation of the synthetic spectrum only (see Gianninas et al. 2011 and references therein). This grid covers a range in $T_{\rm eff}$ from 6000 to 9000 K in steps of 500 K, $\log g$ from 7.0 to 9.5 in steps of 0.5 dex, and log Ca/H from -7.0 to -9.5 in steps of 0.5 dex.

3.4.3.2 Spectroscopic Analysis of DB Stars

For the analysis of the DB and DBA white dwarfs in our sample, we rely on the spectroscopic technique described at length in Bergeron et al. (2011), which is similar to that used for DA stars but modified to fit simultaneously $T_{\rm eff}$, $\log g$, and H/He. The first step is to normalize the flux from individual predefined wavelength segments, in both observed and model spectra, to a continuum set to unity. The comparison with model spectra, which are convolved with the appropriate Gaussian instrumental profile, is then carried out in terms of this normalized spectrum only. However, as for DA stars, two solutions exist for a given DB spectrum, one on each side of the maximum strength of the neutral helium lines. Fortunately, all DB stars in our sample are relatively cool and it is easy to distinguish the cool and hot solutions from an examination of our best fits. Furthermore, the hydrogen abundance in DBA stars is better constrained if spectroscopic data near Hα are available, which is the case for most of our DB stars. The spectroscopic fits for the 4 DB white dwarfs identified in our survey, of which 2 are DBA stars, are presented in Figure 3.15. Note that the hydrogen abundances in 12430+2057 represent only upper limits based on the absence of Hα.

3.4.4 Unresolved Double Degenerate Binaries

Four objects in Figure 3.11 — 04263+4820, 11337+6243, 11598+0007, and 14278+0532 — show a predicted Hα absorption feature significantly deeper than the observed profile; these are plotted separately in Figure 3.16 for clarity. Note that 14278+0532 (1425+057) was fitted as a helium-rich DC white dwarf in Sayres et al. (2012) based on a noisy SDSS spectrum,

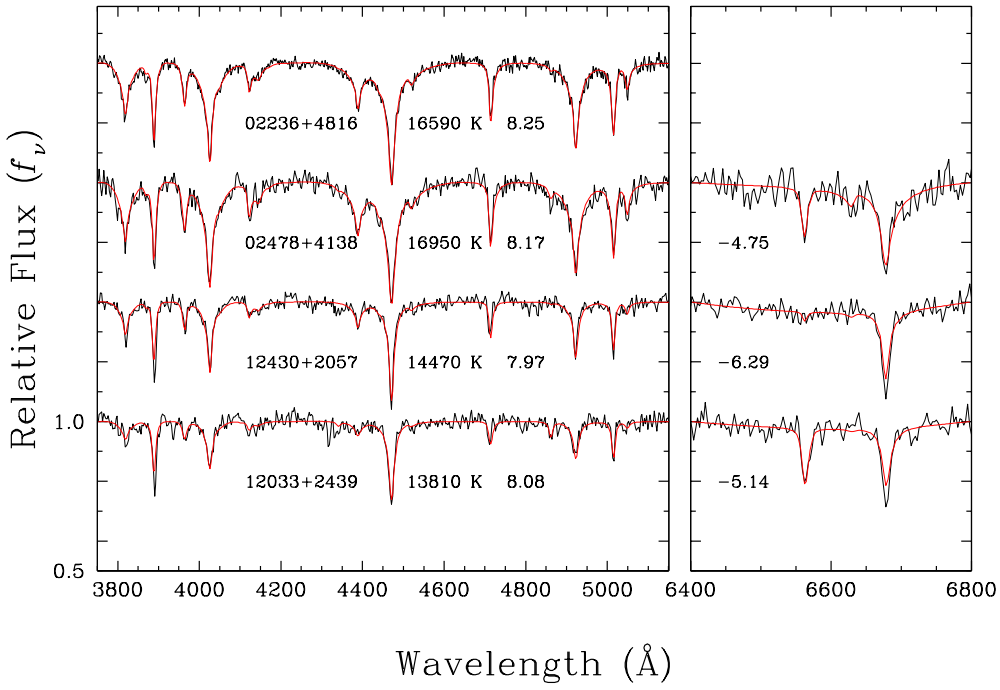

FIGURE 3.15 – Fits to the optical spectra for the 4 new DB stars in our sample; the atmospheric parameters ($T_{\rm eff}$, $\log g$, and $\log {\rm H/He}$) of each object are given in the figure. When available, the region near Hα is used to measure the hydrogen abundance.

but we clearly detect the Hα feature in our spectrum (see also Limoges et al. 2010). For all stars, we achieve excellent fits of the model spectral energy distributions to the photometry, but the fits to the observed spectra are weak. We experimented with helium-rich models containing traces of hydrogen instead of pure hydrogen models — see, e.g., L745-46A and Ross 640 shown in Figure 14 of Giammichele et al. (2012). For 11337+6243 and 14278+0532, our best fits to these models (not shown here) predict Hα profiles that are much broader than the observed profiles due to van der Waals broadening of hydrogen lines by neutral helium. The sharp features observed here rather suggest that these correspond to DA stars whose Hα absorption lines are diluted by the presence of an unresolved DC white dwarf companion. While it was possible to reproduce the Hα profile for 04263+4820 using helium-rich models, our best solution predicts a steep Balmer decrement due to the destruction of the high atomic levels of hydrogen, in sharp contrast with the optical spectrum which shows the whole Balmer series all the way to Hϵ. Here again we suggest that we are rather dealing with an unresolved

DA+DC degenerate binary.

For 11598+0007, although the discrepancy observed in Figure 3.16 is not as extreme as for the other three objects, further evidence that we are also dealing with an unresolved binary is provided by the spectroscopic fit, displayed in Figure 3.17. Also shown for comparison is our best spectroscopic fit to 04263+4820, discussed above, and SDSS 1257+5428, a double white dwarf binary (DA + DA) discussed in Badenes et al. (2009), Kulkarni & van Kerkwijk (2010), and Marsh et al. (2011), of which the optical spectrum has been kindly provided

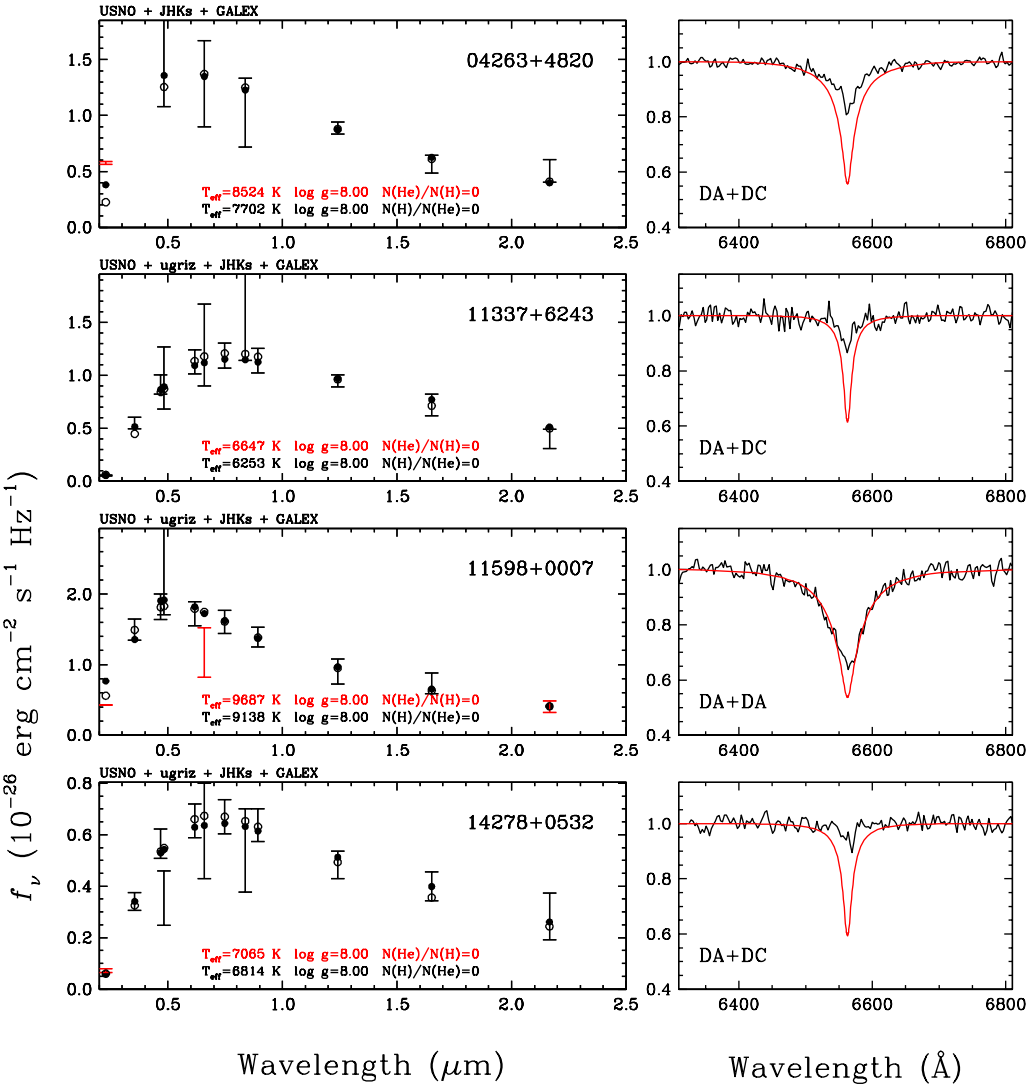

FIGURE 3.16 – Same as Figure 3.10 but for 4 double degenerate binary candidates in our sample.

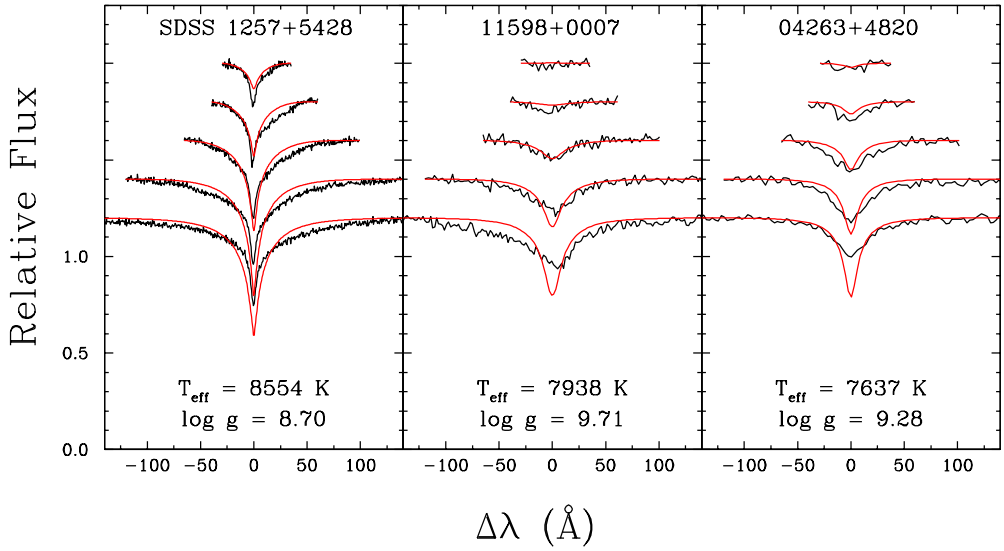

FIGURE 3.17 – Spectroscopic fits to 2 of our double degenerate binary candidates (04263+4820 and 11598+0007) and to the DA + DA white dwarf binary SDSS 1257+5428 (see text).

to us by M. H. van Kerkwijk and S. R. Kulkarni. Not only is the spectroscopic temperature for 11598+0007 ($T_{\rm eff}$ ∼7900 K) significantly different from the photometric temperature (∼9700 K), but the quality of the fit is poor, not unlike our best fit to SDSS 1257+5428 under the assumption of a single DA star. In addition, the hydrogen lines in 11598+0007 exhibit a strong asymmetry similar to that observed in Figure 1 of Kulkarni & van Kerkwijk (2010) for SDSS 1257+5428, attributed in this case to orbital motion and differences in gravitational redshift from both components of the binary system. Kulkarni & van Kerkwijk obtained $T_{\rm eff} = 6250$ K and $\log g = 6.0$ for the primary, and $T_{\rm eff} = 13,000$ K and $\log g = 8.5$ for the secondary; Marsh et al. obtained slightly different parameters but the basic suggestion of a cool, low-mass primary with a hotter, high-mass secondary remains the same. We thus suggest that 11598+0007 also represents an unresolved DA + DA double degenerate system. As demonstrated by Liebert et al. (1991), it is normally impossible to infer the presence of such DA + DA binary systems using the spectroscopic technique alone since the coaddition of synthetic spectra of two DA stars with different values of $T_{\rm eff}$ and $\log g$ can be reproduced almost perfectly by a single DA spectrum *unless the surface gravities of both components differ significantly*, which is certainly the case for SDSS 1257+5428, and it is thus most probably

the case for 11598+0007 as well. Finally, the similarity between our best spectroscopic fits to 11598+0007 and 04263+4820, both displayed in Figure 3.17, clearly suggests the same interpretation, although in the latter case, there is no obvious asymmetry in the line profiles, either because there is no velocity difference between both components of the system, or perhaps 04263+4820 is composed of a DA + DC system.

We do not attempt here to deconvolve the individual components of these double white dwarf binary candidates, and we simply adopt the effective temperatures from the photometric fits, which are more reliable than those derived from the line profiles. We further assume that both components have identical effective temperatures and surface gravities, and thus that they contribute equally to the total luminosity of the system, thus resulting in distances that are a factor of $\sqrt{2}$ larger than the values obtained under the assumption of a single white dwarf. These binaries will also contribute as two objects for the calculations of the luminosity function and the space density. A more detailed analysis of these double degenerate binaries will be presented elsewhere.

3.4.5 Known White Dwarfs within 40 pc of the Sun

In order to get a full picture of the physical properties of white dwarfs within 40 pc of the Sun, we must also include, in addition to the new white dwarfs identified in our survey, all previously known white dwarfs suspected to lie within 40 pc of the Sun; these are listed in Table 3.4 and discussed in Section 3.3.4. We perform a spectroscopic or photometric analysis of each white dwarf in this table following the same fitting procedures described above. Since most of these stars have already been analyzed elsewhere in the literature, we do not provide here the detailed fits for individual stars, although our atmospheric parameters may reflect improved data sets and/or model spectra.

As pointed out in Bergeron et al. (2011), several DB stars cooler than $T_{\rm eff}$ $\sim$15,000 K show masses in excess of 1 $M_{\odot}$, most likely because these cool objects, with their weak and shallow line profiles, lie at the limit of reliability for the spectroscopic technique. Three of these DB stars (KUV 02499+3442, 21003+3426 and 21499+2816) are in Table 3.4 and analyzed here. Since the spectroscopic $\log g$ values and inferred distances are uncertain, we adopt $\log g = 8.0$

for these 3 white dwarfs. Doing so, we obtain for 21499+2816 a distance of 37.7 ± 1.5 pc, in better agreement with the value of 35.3 ± 3.8 pc suggested by the trigonometric parallax. As mentioned in Bergeron et al., a value of $\log g = 8.2$ would actually reconcile both distance estimates perfectly, which suggests that the spectroscopic $\log g$ values for these stars are likely overestimated.

An interesting object in Table 3.4 is 09487+2421 (0945+245, LB 11146), an unresolved binary system composed of a DA star and a magnetic white dwarf (DA + DAXP). We use here the values from Liebert et al. (1993) obtained by the deconvolution of both spectra: $T_{\rm eff} = 14,500 \pm 1000$ K, $\log g = 8.4 \pm 0.1$ for the DA component, and $T_{\rm eff} = 16,000 \pm 2000$ K and $\log g = 8.5 \pm 0.2$ for the magnetic component. Based on their distance estimate of 40 ± 5 pc, this binary system is included in the 40 pc sample, and will count as 2 white dwarfs in the luminosity function.

Another interesting object in Table 3.4 is 01489+1902 (GD 16), a helium-rich DAZB star analyzed in detail by Koester et al. (2005). They obtained $T_{\rm eff} = 11,500 \pm 300$ K, $\log {\rm H/He} = -2.89 \pm 0.3$, and $\log {\rm Ca/He} = -8.7 \pm 0.2$ under the assumption of $\log g = 8.0$. Since this last assumption will affect the spectroscopic distance estimate, we analyzed this star ourselves using the same spectroscopic technique for DB stars outlined in Section 3.4.3.2, with mixed H/He model atmospheres that also include the opacity from Ca II H & K; the additional lines of Mg and Fe visible in the spectrum are not included in our models. Our best fit is displayed in Figure 3.18 where we find $T_{\rm eff} = 10,420$ K and $\log g = 7.71$; these are the only two free parameters in our fit. The helium abundance is set according to the depth of the HeI 5875 line reported by Koester et al. (2005), while the calcium abundance is fixed at a value that reproduces the observed strength of the calcium lines in our spectrum. The values we obtain for the helium abundance ($\log {\rm H/He} = -2.70$), and for the calcium abundance ($\log {\rm Ca/He} = -8.5$), are in good agreement with the values derived by Koester et al. (2005), while the effective temperature is $\sim$1100 K lower, a difference that may be explained by the fact that we do fit for $\log g$ instead of simply assuming a value of 8.0. The corresponding distance of $D = 63.7 \pm 2.9$ pc is 13.7 pc further away than the distance obtained by Koester et al., and significantly outside our limit of 40 pc. Finally, we notice that our spectrum displayed

in Figure 3.18 shows what appears to be a blue component in the wings of Hβ, Hγ, and Hδ, which could indicate that this object is in fact an unresolved double degenerate binary.

3.4.6 Adopted atmospheric parameters

As discussed in the Introduction, the spectroscopic $\log g$ values of DA stars show a significant increase at low temperatures ($T_{\rm eff} \lesssim 13,000$ K) — the so-called high-$\log g$ problem — with respect to the $\log g$ distribution of hotter DA stars. Hydrodynamical 3D models (Tremblay et al. 2013b, see also Tremblay et al. 2011a, 2013a) have now successfully shown that this problem is related to the limitations of the mixing-length theory used to describe the convective energy transport in standard 1D model atmospheres calculations. These spurious $\log g$ values prevent us from obtaining reliable mass and distance estimates for DA stars in

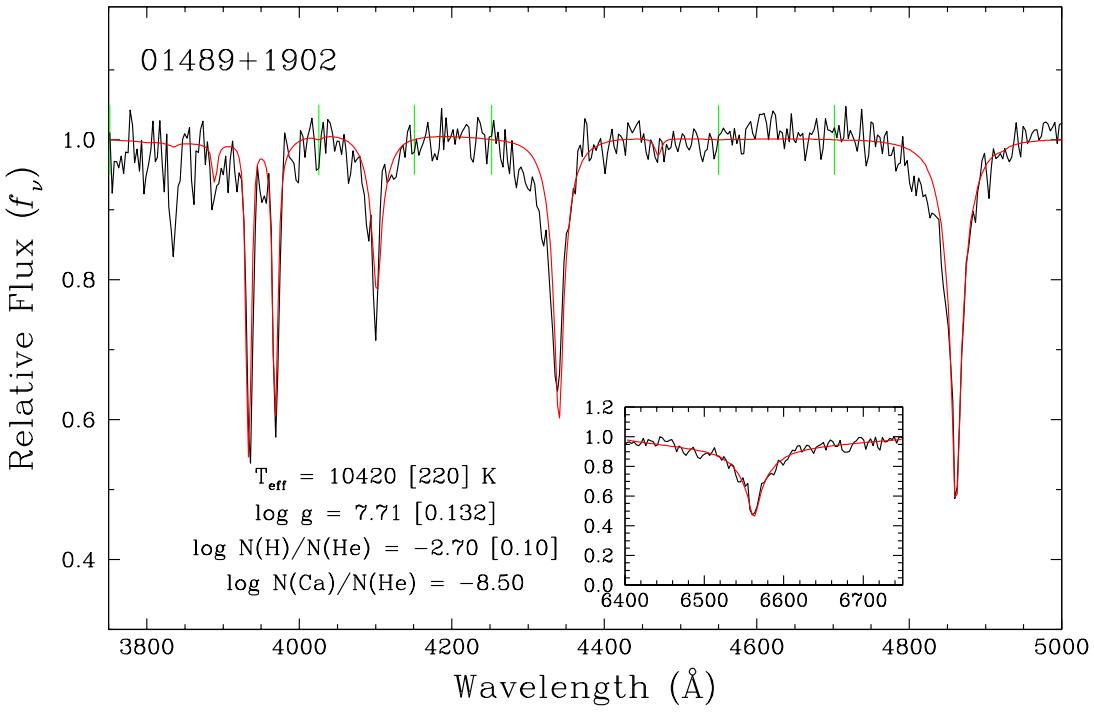

FIGURE 3.18 – Our best spectroscopic fit to the helium-rich DAZB white dwarf 01489+1902 (GD 16); the insert shows the region covering the Hα line profile.

our sample in this particular range of temperature. Indeed, those higher $\log g$ values will yield underestimated spectroscopic distances, biasing our census of white dwarfs within 40 pc. To overcome this problem, Giammichele et al. (2012) derived an empirical procedure (see their Section 5 and Figure 16) to correct the $\log g$ values based on the DA stars in the SDSS (DR4), analyzed by Tremblay et al. (2011a); this was also our approach in Paper I. Here we make use of the latest results from Tremblay et al. (2013b) who presented their first complete grid of 3D synthetic spectra for DA white dwarfs based on 3D hydrodynamical model atmospheres. In particular, they provided correction functions to be applied to both $T_{\rm eff}$ and $\log g$ measurements determined using the spectroscopic technique with model spectra calculated within the mixing-length theory — the ML2/$\alpha = 0.7$ prescription in our case. We thus apply these corrections to our sample of DA stars whose atmospheric parameters have been obtained using the spectroscopic method.

Because the distance to each white dwarf in our sample is a key issue in our study, some care must be taken to reduce the uncertainty on the distance estimates as much as possible. For stars with trigonometric parallax measurements available (134 objects), we adopt the corresponding distances directly. Out of these 134 parallax measurements, 9 have uncertainties larger than 20%, while Feige 4 and HZ 9 have uncertainties of 31% and 30%, respectively. However, even for these last two objects we prefer to use the parallax-based distances because the spectroscopic distance to Feige 4 is largely inconsistent with the parallax value (Bergeron et al. 2011), and because HZ 9 is a DA + M dwarf system whose spectral energy distribution is highly contaminated by the M dwarf, which means we only have a single data point to determine the distance from the photometric fit. For stars without parallaxes fitted using the photometric method (DC, DQ, DZ, and cool DA stars), the distance is determined from the measured solid angle $\pi(R/D)^2$ combined with the stellar radius corresponding to $\log g = 8.0 \pm 0.25$, as discussed in Section 3.4.2.1. Finally, for white dwarfs in our sample only fitted with the spectroscopic technique and without parallaxes, we fit all the available photometric data but force the spectroscopic values of $T_{\rm eff}$ and $\log g$ (and the corresponding radius) and derive the distance from the fitted solid angle (see also Limoges et al. 2013). The distance uncertainty in this case is obtained from the combination in quadrature of the error on the

spectroscopic $\log g$ and the solid angle. This approach for measuring spectroscopic distances has the advantage of using all the photometric information rather than relying on the distance modulus from a single bandpass.

Our final results for the 322 white dwarfs identified in our survey and for the 460 known white dwarfs within 40 pc of the Sun with $\delta > 0$ are presented in Tables 3.5 and 3.6, respectively. We give for each object the PM I designation if the white dwarf is a SUPERBLINK object, the spectral type, effective temperature ($T_{\rm eff}$), surface gravity ($\log g$), stellar mass ($M/M_{\odot}$), atmospheric composition (H- or He-dominated), absolute visual magnitude (M_V), luminosity ($L/L_{\odot}$), distance (D), trigonometric parallax (π) if available, white dwarf cooling time ($\log \tau$), and the method used to determine the atmospheric parameters. As discussed above, the spectroscopic solutions for both $T_{\rm eff}$ and $\log g$ for the DA stars have been corrected for the high-$\log g$ problem and these differ from the uncorrected values given in Figure 3.14.

TABLE 3.5 – Atmospheric Parameters of New White Dwarfs from SUPERBLINK

PM I	ST	$T_{\rm eff}$[a] K	log g[a]	$M/M_\odot$	Comp.	M_V	log $L/L_\odot$	D (pc)	log τ	Fit[b]	Other name
00023+6357	DC	4630 (563)	8.00 (0.25)	0.58 (0.15)	H	14.77	−4.18	26.7 (5.2)	9.85	2	
00050+4003	DZA:	8150 (549)	8.00 (0.25)	0.58 (0.15)	He	12.50	−3.20	52.2 (9.4)	9.05	2	GD 1
00056+4825	DA	6970 (105)	7.95 (0.09)	0.56 (0.05)	H	13.47	−3.43	48.4 (1.0)	9.15	1	
00074+3403	DC:	5830 (113)	8.00 (0.25)	0.57 (0.15)	He	14.23	−3.79	42.0 (5.2)	9.46	2	
00079+3947	DC	4890 (453)	8.00 (0.25)	0.58 (0.15)	H	15.16	−4.09	20.2 (3.0)	9.79	2	
00217+2640	DC	5160 (645)	8.00 (0.25)	0.58 (0.15)	H	14.67	−3.99	35.2 (6.1)	9.69	2	
00276+0542	DA	5520 (855)	8.00 (0.25)	0.58 (0.15)	H	14.65	−3.87	21.5 (3.7)	9.49	2	
00331+4742S	DA	16580 (265)	8.02 (0.05)	0.63 (0.03)	H	11.13	−1.95	55.0 (1.1)	8.17	1	
00334+2506	DA	6310 (107)	7.89 (0.16)	0.52 (0.09)	H	13.81	−3.58	42.1 (0.4)	9.22	1	
00532+3927	DA	7530 (113)	7.96 (0.08)	0.57 (0.05)	H	13.19	−3.31	55.3 (1.6)	9.08	1	
00559+5948	DC:	5840 (1061)	8.00 (0.25)	0.57 (0.15)	He	13.32	−3.78	26.2 (4.7)	9.45	2	
01043+3816	DA	16280 (257)	8.05 (0.05)	0.64 (0.03)	H	11.20	−2.00	57.7 (1.1)	8.22	1	
01088+7600	DA	6430 (128)	8.52 (0.22)	0.93 (0.14)	H	14.66	−3.93	38.0 (1.0)	9.66	1	
01216+3440	DZ	6890 (116)	8.00 (0.25)	0.58 (0.15)	He	13.66	−3.49	41.7 (0.9)	9.23	2	
01278+7328	DA	7400 (117)	8.20 (0.10)	0.72 (0.07)	H	13.61	−3.48	25.1 (1.3)	9.26	1	
01327+6635	DA	11940 (288)	8.09 (0.11)	0.66 (0.07)	H	11.80	−2.57	75.2 (2.0)	8.63	1	
01327+4604	DA	10680 (163)	7.97 (0.06)	0.59 (0.04)	H	11.91	−2.70	41.7 (0.2)	8.69	1	WD0129+458
01382+4442	DA	11200 (170)	8.12 (0.06)	0.68 (0.04)	H	11.99	−2.70	49.5 (1.1)	8.72	1	
01390+2402	DA	8710 (166)	6.88 (0.27)	0.19 (0.06)	H	11.14	−2.46	234.5 (3.5)	8.33	1	
01457+2918	DC	4740 (879)	8.00 (0.25)	0.58 (0.15)	H	15.04	−4.14	39.6 (14.2)	9.83	2	
01486+3615	DA	6480 (119)	8.68 (0.19)	1.03 (0.11)	H	14.91	−4.03	24.0 (0.6)	9.68	1	
01534+3557	DA	7330 (114)	8.32 (0.09)	0.80 (0.06)	H	13.82	−3.57	43.7 (1.0)	9.41	1	
01565+2955	DA	15270 (238)	7.99 (0.05)	0.61 (0.03)	H	11.23	−2.08	49.5 (1.0)	8.27	1	
02062+1836	DC	4230 (530)	8.00 (0.25)	0.58 (0.15)	H	15.92	−4.34	31.0 (7.8)	9.92	2	
02118+7119	DC	5150 (52)	8.00 (0.25)	0.58 (0.15)	H	14.75	−4.00	28.0 (3.2)	9.69	2	

TABLE 3.5 – Continued

PM I	ST	$T_{\rm eff}{}^a$ K	log g^a	$M/M_\odot$	Comp.	M_V	log $L/L_\odot$	D (pc)	log τ	Fit^b	Other name
02149+7746	DC	5480 (598)	8.00 (0.25)	0.57 (0.15)	He	14.32	−3.89	67.4 (10.1)	9.61	2	
02199+3520	DA	5580 (791)	8.00 (0.25)	0.58 (0.15)	H	14.28	−3.85	43.1 (8.3)	9.47	2	
02230+5544	DA	6980 (110)	8.40 (0.10)	0.85 (0.07)	H	14.14	−3.70	35.3 (1.0)	9.54	1	
02236+4816	DB	16590 (295)	8.25 (0.07)	0.75 (0.04)	He	11.44	−2.11	54.1 (2.2)	8.35	1	GD 27
02238+2055	DC	4300 (91)	8.00 (0.25)	0.58 (0.15)	H	16.02	−4.31	33.5 (3.9)	9.91	2	
02241+2325	DA	4980 (130)	8.00 (0.25)	0.58 (0.15)	H	14.97	−4.06	58.3 (7.3)	9.76	2	
02321+5211	DA	9330 (157)	8.00 (0.13)	0.60 (0.08)	H	12.43	−2.95	84.6 (1.9)	8.86	1	
02334+2125	DC	4730 (52)	8.00 (0.25)	0.58 (0.15)	H	15.15	−4.15	26.3 (3.0)	9.83	2	
02379+1638	DC	5150 (607)	8.00 (0.25)	0.57 (0.15)	He	14.63	−4.00	30.7 (5.0)	9.74	2	
02478+4138	DB	16960 (294)	8.18 (0.10)	0.70 (0.06)	He	11.27	−2.02	128.1 (3.8)	8.27	1	
02497+3307	DA	5890 (119)	8.31 (0.26)	0.79 (0.17)	H	14.72	−3.94	31.6 (0.2)	9.67	1	
02557+2106S	DA	6320 (105)	8.16 (0.15)	0.69 (0.10)	H	14.17	−3.72	46.3 (0.4)	9.45	1	
02562+4954	DA	6050 (101)	8.00 (0.25)	0.59 (0.15)	H	14.14	−3.71	41.0 (1.1)	9.34	1	
03009+5432	DA	7780 (125)	8.23 (0.10)	0.74 (0.07)	H	13.46	−3.41	43.7 (1.0)	9.23	1	
03031+2317	DA+dM	23330 (6829)	8.00 (0.25)	0.63 (0.14)	H	9.47	−1.34	43.7 (1.0)	7.50	2	
03053+2603	DA	5190 (686)	8.00 (0.25)	0.58 (0.15)	H	14.64	−3.98	45.0 (9.0)	9.67	2	
03109+6634	DC	4620 (662)	8.00 (0.25)	0.58 (0.15)	H	15.31	−4.19	36.4 (9.1)	9.86	2	
03127+2218	DA	6670 (114)	7.70 (0.16)	0.43 (0.08)	H	13.34	−3.38	55.1 (1.3)	9.06	1	
03196+3630	DZ	5770 (234)	8.00 (0.25)	0.57 (0.15)	He	14.26	−3.80	29.9 (1.5)	9.48	2	
03203+2333	DC	4510 (447)	8.00 (0.25)	0.58 (0.15)	H	15.52	−4.23	29.3 (5.4)	9.88	2	
03433+1958	DA	7150 (107)	8.47 (0.08)	0.89 (0.05)	H	14.16	−3.71	22.8 (0.7)	9.55	1	
03471+0520W	DC	7010 (81)	8.00 (0.25)	0.58 (0.15)	He	13.37	−3.46	82.0 (9.2)	9.22	2	
03473+4358	DA	13650 (316)	7.99 (0.05)	0.60 (0.03)	H	11.42	−2.27	33.9 (1.2)	8.41	1	
04010+5131W	DC	5220 (342)	8.00 (0.25)	0.58 (0.15)	H	14.57	−3.97	30.8 (4.2)	9.66	2	
04032+2520E	DA+dM	21580 (3633)	8.00 (0.25)	0.63 (0.14)	H	9.95	−1.47	97.1 (29.5)	7.68	2	

TABLE 3.5 – Continued

PM I	ST	$T_{\rm eff}{}^a$ K	log g^a	$M/M_\odot$	Comp.	M_V	log $L/L_\odot$	D (pc)	log τ	Fit^b	Other name
04032+2520W	DA	22770 (441)	8.06 (0.06)	0.67 (0.04)	H	10.63	−1.42	101.9 (2.4)	7.64	1	
04037+1459	DA	14710 (344)	8.41 (0.05)	0.87 (0.03)	H	11.95	−2.41	40.7 (0.4)	8.61	1	
04180+4211	DA	4580 (374)	8.00 (0.25)	0.58 (0.15)	H	15.17	−4.20	23.8 (3.6)	9.86	2	
04201+3233	DA	11280 (250)	8.05 (0.12)	0.63 (0.07)	H	11.86	−2.64	73.3 (2.0)	8.67	1	
04214+4607	DA	7790 (123)	7.87 (0.11)	0.52 (0.06)	H	12.94	−3.19	30.5 (1.1)	8.98	1	
04259+4614	DC	4520 (504)	8.00 (0.25)	0.58 (0.15)	H	15.44	−4.22	32.5 (7.0)	9.88	2	
04263+4820	DA+DC	4240 (325)	8.00 (0.25)	0.58 (0.15)	H	14.23	−4.34	29.0 (4.6)	9.92	2	
04294+4945	DA	8380 (153)	8.09 (0.15)	0.65 (0.09)	H	12.98	−3.19	49.4 (1.2)	9.04	1	
04308+1611	DA	8710 (134)	8.05 (0.09)	0.63 (0.05)	H	12.76	−3.10	57.8 (2.1)	8.97	1	
04334+0414	DA	5220 (596)	8.00 (0.25)	0.58 (0.15)	H	14.62	−3.97	26.5 (4.2)	9.66	2	
04339+2827	DA	13930 (331)	8.05 (0.05)	0.64 (0.03)	H	11.47	−2.27	69.0 (3.8)	8.42	1	
04343+3054	DC:	4670 (577)	8.00 (0.25)	0.58 (0.15)	H	15.28	−4.17	36.2 (7.5)	9.85	2	
04372+4524	DA	6570 (112)	8.12 (0.15)	0.66 (0.10)	H	13.96	−3.63	40.4 (1.2)	9.36	1	
04389+6351	DA+dM	13190 (640)	7.78 (0.10)	0.49 (0.05)	H	11.20	−2.22	146.0 (7.6)	8.33	1	
04523+2519	DAH	11500 (2655)	8.00 (0.25)	0.60 (0.14)	H	11.66	−2.58	43.7 (6.5)	8.62	2	
04558+3840	DA	5020 (613)	8.00 (0.25)	0.58 (0.15)	H	14.82	−4.04	32.5 (5.9)	9.75	2	
04586+6209	DA+dM	10960 (704)	8.88 (0.13)	1.14 (0.07)	H	13.40	−3.27	21.6 (0.6)	9.30	1	
04588+6410	DC	6860 (913)	8.00 (0.25)	0.58 (0.15)	He	13.37	−3.50	52.1 (11.4)	9.24	2	
05025+5401	DA	11290 (169)	8.09 (0.05)	0.65 (0.03)	H	11.92	−2.67	44.2 (1.1)	8.69	1	
05158+2839	DAH	6640 (104)	8.00 (0.25)	0.59 (0.15)	H	13.39	−3.55	35.0 (4.1)	9.24	2	
05269+4435	DC	4700 (632)	8.00 (0.25)	0.58 (0.15)	H	15.14	−4.16	37.0 (8.7)	9.84	2	
05280+4850	DA+dM	11100 (393)	8.72 (0.12)	1.05 (0.07)	H	13.04	−3.12	57.9 (1.6)	9.22	1	
05327+0624	DA	9110 (134)	8.10 (0.06)	0.66 (0.04)	H	12.67	−3.05	54.3 (3.4)	8.95	1	
05332+0925	DA	13900 (393)	8.09 (0.05)	0.66 (0.03)	H	11.53	−2.30	57.9 (1.8)	8.45	1	
05353+5715	DC	5210 (462)	8.00 (0.25)	0.57 (0.15)	He	14.66	−3.98	39.1 (5.1)	9.72	2	

TABLE 3.5 – Continued

PM I	ST	$T_{\rm eff}{}^a$ K	log g^a	$M/M_\odot$	Comp.	M_V	log $L/L_\odot$	D (pc)	log τ	Fit^b	Other name
05372+6759	DAH:	8710 (1615)	8.00 (0.25)	0.60 (0.15)	H	12.55	−3.07	51.2 (9.3)	8.93	2	
05383+4436	DA	6200 (134)	7.99 (0.25)	0.58 (0.15)	H	14.02	−3.66	43.0 (0.9)	9.31	1	
05410+3959	DA	5970 (147)	8.00 (0.25)	0.59 (0.15)	H	14.20	−3.73	44.7 (1.3)	9.36	1	
05431+3637	DAZ	6540 (101)	7.84 (0.11)	0.50 (0.06)	H	13.59	−3.48	27.2 (0.9)	9.16	1	
05462+1115	DC:	4290 (137)	8.00 (0.25)	0.57 (0.15)	He	15.84	−4.32	27.5 (3.3)	9.88	2	
05492+5747	DA+dM	16810 (416)	8.20 (0.07)	0.74 (0.04)	H	11.37	−2.04	106.9 (2.6)	8.28	1	
06018+2751	DA	13950 (718)	8.06 (0.08)	0.65 (0.05)	H	11.49	−2.28	54.8 (2.1)	8.43	1	GD 258
06019+3726	DAH	15750 (8579)	8.00 (0.25)	0.61 (0.14)	H	11.06	−2.03	122.8 (90.4)	8.23	2	
06026+0904	DA	5920 (132)	7.75 (0.29)	0.45 (0.14)	H	13.91	−3.61	40.4 (1.2)	9.21	1	
06206+3443	DA	9910 (148)	8.21 (0.07)	0.73 (0.04)	H	12.52	−2.97	62.7 (0.5)	8.92	1	
06324+2230	DA	5620 (1471)	8.00 (0.25)	0.58 (0.15)	H	14.72	−3.84	37.4 (10.3)	9.45	2	
06445+2731	DA	7020 (119)	8.69 (0.13)	1.04 (0.08)	H	14.63	−3.90	30.7 (0.3)	9.63	1	
06492+1519	DC	5050 (392)	8.00 (0.25)	0.57 (0.15)	He	14.85	−4.04	34.9 (6.3)	9.76	2	
06494+7521	DA	5450 (1044)	8.00 (0.25)	0.58 (0.15)	H	14.02	−3.89	34.4 (7.4)	9.53	2	
06506+1657	DA	5240 (661)	8.00 (0.25)	0.58 (0.15)	H	14.60	−3.96	34.2 (6.4)	9.65	2	
06513+6242	DAH	6900 (289)	8.00 (0.25)	0.59 (0.15)	H	13.30	−3.48	65.3 (12.4)	9.20	2	
06538+6355	DA	6220 (137)	8.44 (0.23)	0.87 (0.15)	H	14.67	−3.93	20.8 (0.6)	9.67	1	
06556+5920	DA+dM	12050 (490)	8.48 (0.10)	0.91 (0.06)	H	12.39	−2.80	53.1 (1.3)	8.89	1	
06577+4007	DA	6900 (118)	8.21 (0.16)	0.73 (0.10)	H	13.89	−3.60	50.3 (1.3)	9.37	1	
07029+4406	DA	10920 (161)	8.09 (0.05)	0.65 (0.03)	H	12.02	−2.72	47.4 (1.0)	8.73	1	
07087+2044	DA	5810 (117)	8.00 (0.25)	0.59 (0.15)	H	14.33	−3.78	35.2 (1.1)	9.39	1	
07241+0431	DA	5670 (120)	8.00 (0.25)	0.59 (0.15)	H	14.45	−3.83	64.2 (4.3)	9.44	1	
07270+1434	DA	5680 (89)	8.00 (0.25)	0.59 (0.15)	H	14.44	−3.82	30.5 (0.2)	9.43	1	
07300+2716W	DA	9600 (161)	8.44 (0.11)	0.88 (0.07)	H	13.02	−3.17	44.2 (0.4)	9.15	1	
07419+0136	DC	6270 (432)	8.00 (0.25)	0.57 (0.15)	He	13.79	−3.66	80.7 (18.0)	9.34	2	

TABLE 3.5 – Continued

PM I	ST	$T_{\rm eff}{}^a$ K	log g^a	$M/M_\odot$	Comp.	M_V	log $L/L_\odot$	D (pc)	log τ	Fit^b	Other name
07419+1511	DA	14400 (262)	8.01 (0.05)	0.62 (0.03)	H	11.36	−2.20	76.6 (0.6)	8.36	1	
07451+2627	DC	3620 (144)	8.00 (0.25)	0.58 (0.15)	H	16.68	−4.61	32.3 (3.8)	10.00	2	
07475+1107	DA	8060 (126)	8.82 (0.08)	1.11 (0.05)	H	14.35	−3.75	29.3 (0.3)	9.53	1	
07504+1740	DA	6900 (103)	8.01 (0.08)	0.60 (0.05)	H	13.60	−3.48	51.2 (0.4)	9.20	1	SDSSJ075026.30+1
08015+4852	DA	5280 (365)	8.00 (0.25)	0.58 (0.15)	H	14.76	−3.95	36.1 (5.3)	9.63	2	
08054+0735	DA:	5370 (45)	8.00 (0.25)	0.58 (0.15)	H	14.42	−3.92	37.0 (4.2)	9.58	2	
08068+2215	DA	5770 (91)	8.12 (0.12)	0.66 (0.08)	H	14.54	−3.87	49.0 (0.4)	9.54	1	
08082+1854	DA	5690 (126)	8.21 (0.28)	0.72 (0.18)	H	14.73	−3.94	43.8 (0.4)	9.65	1	
08126+1737	DA	16400 (241)	8.09 (0.04)	0.67 (0.03)	H	11.25	−2.02	32.7 (0.7)	8.24	1	
08152+1633	DC:	4710 (80)	8.00 (0.25)	0.58 (0.15)	H	15.23	−4.15	40.4 (4.6)	9.84	2	
08184+6606	DA+dM	12990 (1078)	8.00 (0.25)	0.61 (0.14)	H	10.57	−3.52	113.8 (51.2)	8.48	2	
08212+7120	DA	8690 (171)	7.93 (0.19)	0.56 (0.10)	H	12.60	−3.04	56.8 (1.1)	8.90	1	
08223+2023	DC	7240 (150)	8.00 (0.25)	0.58 (0.15)	He	13.12	−3.41	35.6 (4.1)	9.18	2	
08281+0942	DC	5190 (372)	8.00 (0.25)	0.57 (0.15)	He	14.59	−3.99	54.5 (9.1)	9.72	2	
08293+2539	DC	4010 (95)	8.00 (0.25)	0.58 (0.15)	H	16.58	−4.43	32.4 (3.6)	9.95	2	
08429+2409	DA	5900 (120)	8.00 (0.25)	0.59 (0.15)	H	14.26	−3.76	38.7 (0.2)	9.37	1	WD0840+243
08490+4439	DC	5990 (56)	8.00 (0.25)	0.57 (0.15)	He	14.43	−3.74	51.1 (5.7)	9.41	2	
08516+1624	DC	5580 (78)	8.00 (0.25)	0.57 (0.15)	He	14.19	−3.86	29.0 (3.3)	9.56	2	
08558+3700	DA	5620 (59)	8.00 (0.25)	0.58 (0.15)	H	14.17	−3.84	43.4 (5.0)	9.45	2	
09021+2010	DQ	5010 (34)	8.00 (0.25)	0.57 (0.15)	He	15.98	−4.05	37.6 (0.6)	9.78	2	
09026+1535	DC	4670 (36)	8.00 (0.25)	0.58 (0.15)	H	15.38	−4.17	31.6 (3.5)	9.85	2	
09027+3120	DA	9930 (143)	8.23 (0.05)	0.75 (0.03)	H	12.56	−2.98	34.1 (0.3)	8.94	1	
09033+2012	DA	7170 (113)	8.01 (0.11)	0.60 (0.06)	H	13.45	−3.42	50.8 (0.4)	9.16	1	
09106+2156	DA	5640 (90)	8.00 (0.25)	0.59 (0.15)	H	14.47	−3.83	37.5 (0.2)	9.44	1	WD0907+221
09112+1515	DC	4740 (124)	8.00 (0.25)	0.58 (0.15)	H	15.30	−4.14	50.4 (6.2)	9.83	2	

TABLE 3.5 – Continued

PM I	ST	$T_{\rm eff}{}^a$ K	log g^a	$M/M_\odot$	Comp.	M_V	log $L/L_\odot$	D (pc)	log τ	Fit^b	Other name
09122+2538	DA	6720 (105)	8.32 (0.11)	0.80 (0.07)	H	14.17	−3.72	32.5 (0.3)	9.52	1	
09127+2251	DC	4960 (69)	8.00 (0.25)	0.58 (0.15)	H	14.76	−4.06	43.9 (5.0)	9.77	2	
09192+7723	DA	9290 (164)	7.72 (0.16)	0.45 (0.08)	H	12.06	−2.81	41.6 (0.7)	8.72	1	
09222+0504	DAH	5910 (77)	8.00 (0.25)	0.59 (0.15)	H	13.74	−3.75	59.3 (7.1)	9.37	2	
09234+0559	DA	6040 (111)	8.00 (0.25)	0.59 (0.15)	H	14.15	−3.71	51.8 (0.7)	9.34	1	
09245+3120	DC	4800 (71)	8.00 (0.25)	0.58 (0.15)	H	14.66	−4.12	38.8 (4.3)	9.82	2	
09249+3613	DAH	11690 (306)	8.00 (0.25)	0.61 (0.14)	H	9.80	−2.56	237.1 (35.2)	8.60	2	
09286+1841	DA	7730 (116)	8.45 (0.07)	0.88 (0.05)	H	13.83	−3.56	35.9 (0.3)	9.45	1	
09395+4951	DA	5990 (69)	8.00 (0.25)	0.59 (0.15)	H	13.79	−3.73	43.3 (5.1)	9.35	2	
09422+0942	DA	5250 (60)	8.00 (0.25)	0.58 (0.15)	H	14.32	−3.96	46.2 (5.3)	9.64	2	
09432+5134	DC	4800 (75)	8.00 (0.25)	0.58 (0.15)	H	15.08	−4.12	41.9 (4.7)	9.82	2	
09481+2023	DC	4820 (60)	8.00 (0.25)	0.58 (0.15)	H	15.11	−4.11	35.8 (4.1)	9.81	2	
09488+1319	DA	6800 (110)	7.69 (0.13)	0.42 (0.06)	H	13.24	−3.34	66.3 (0.6)	9.04	1	
09503+1509	DC	5440 (54)	8.00 (0.25)	0.58 (0.15)	H	14.78	−3.90	38.8 (4.5)	9.53	2	
09513+1900	DC	5870 (73)	8.00 (0.25)	0.57 (0.15)	He	13.70	−3.78	51.2 (5.8)	9.45	2	WD0948+192
10042+2438	DA	11540 (177)	8.04 (0.05)	0.63 (0.03)	H	11.81	−2.60	85.0 (0.7)	8.64	1	
10118+2647	DA	5280 (121)	8.00 (0.25)	0.58 (0.15)	H	14.66	−3.95	41.6 (5.0)	9.63	2	SDSSJ101151.05+264745
10155+1850	DC	4600 (89)	8.00 (0.25)	0.58 (0.15)	H	15.38	−4.19	45.0 (5.1)	9.86	2	
10170+7619	DA	7170 (115)	8.00 (0.12)	0.59 (0.07)	H	13.43	−3.41	44.7 (1.0)	9.16	1	
10228+3904	DZ	5300 (50)	8.00 (0.25)	0.57 (0.15)	He	14.74	−3.95	37.1 (0.5)	9.68	2	
10289+1105	DA	13970 (348)	8.11 (0.05)	0.68 (0.03)	H	11.56	−2.31	63.6 (0.5)	8.46	1	
10347+2245	DZ	6510 (96)	8.00 (0.25)	0.57 (0.15)	He	13.40	−3.59	36.5 (0.7)	9.30	2	WD1032+230
10355+2126	DAH	7110 (144)	8.00 (0.25)	0.59 (0.15)	H	13.18	−3.43	54.2 (6.8)	9.16	2	
10403+1004	DC	5920 (94)	8.00 (0.25)	0.57 (0.15)	He	14.11	−3.76	39.1 (4.5)	9.43	2	
10471+3453	DA	8690 (129)	7.57 (0.08)	0.38 (0.04)	H	12.12	−2.85	73.4 (0.6)	8.73	1	

TABLE 3.5 – Continued

PM I	ST	$T_{\rm eff}$[a] K	log g[a]	$M/M_\odot$	Comp.	M_V	log $L/L_\odot$	D (pc)	log τ	Fit[b]	Other name
10502+3226	DA:	5610 (57)	8.00 (0.25)	0.58 (0.15)	H	14.02	−3.84	44.6 (5.1)	9.46	2	
10521+4050	DC	6180 (116)	8.00 (0.25)	0.57 (0.15)	He	14.26	−3.68	35.7 (4.1)	9.36	2	
10538+2425	DA	5900 (55)	8.00 (0.25)	0.59 (0.15)	H	14.36	−3.76	50.7 (5.9)	9.37	2	
10557+2111	DAH	6490 (82)	8.00 (0.25)	0.59 (0.15)	H	13.76	−3.59	63.1 (7.4)	9.26	2	
10565+2336	DA	5190 (58)	8.00 (0.25)	0.58 (0.15)	H	15.06	−3.98	42.1 (4.8)	9.67	2	
11036+1555	DA+dM	9800 (368)	7.72 (0.29)	0.45 (0.14)	H	11.85	−2.71	171.1 (5.4)	8.66	1	
11071+1446	DA	6700 (110)	8.32 (0.12)	0.80 (0.08)	H	14.18	−3.73	30.5 (0.2)	9.53	1	
11111+3848	DC	5080 (145)	8.00 (0.25)	0.57 (0.15)	He	14.64	−4.03	48.1 (6.0)	9.76	2	SDSSJ111109.10+384856
11132+2859	DA	4830 (62)	8.00 (0.25)	0.58 (0.15)	H	15.27	−4.11	34.9 (4.0)	9.81	2	WD1110+292
11144+3341	DA	8270 (133)	8.03 (0.11)	0.62 (0.07)	H	12.94	−3.18	92.5 (1.4)	9.01	1	
11210+3756	DA	9810 (145)	8.26 (0.06)	0.76 (0.04)	H	12.65	−3.02	36.5 (0.3)	8.97	1	
11222+2839	DA	5690 (56)	8.00 (0.25)	0.59 (0.15)	H	14.01	−3.82	52.7 (6.1)	9.43	2	WD1119+289
11253+2111	DC	6390 (117)	8.00 (0.25)	0.57 (0.15)	He	13.51	−3.63	41.2 (4.8)	9.32	2	
11337+6243	DA+DC	6660 (81)	8.00 (0.25)	0.59 (0.15)	H	13.41	−3.54	48.1 (5.6)	9.24	2	
11364+0802S	DA	5500 (45)	8.00 (0.25)	0.58 (0.15)	H	14.39	−3.88	47.3 (5.4)	9.50	2	
11364+0838	DA	6600 (101)	8.26 (0.10)	0.75 (0.07)	H	14.14	−3.71	49.5 (0.3)	9.49	1	
11401+0112W	DA	9800 (144)	8.12 (0.06)	0.67 (0.04)	H	12.43	−2.93	46.2 (0.4)	8.88	1	
11460+0514	DA	6770 (111)	7.68 (0.14)	0.42 (0.07)	H	13.25	−3.34	55.5 (0.5)	9.04	1	WD1143+055
11495+2353	DC	4960 (54)	8.00 (0.25)	0.58 (0.15)	H	14.51	−4.06	42.0 (4.7)	9.77	2	
11506+0343	DA	6120 (44)	8.00 (0.25)	0.59 (0.15)	H	13.66	−3.69	54.5 (6.2)	9.33	2	
11545+2422	DA	8790 (141)	8.57 (0.09)	0.96 (0.06)	H	13.57	−3.42	25.2 (0.2)	9.38	1	WD1151+246
11582+0004	DC	4410 (83)	8.00 (0.25)	0.58 (0.15)	H	15.78	−4.27	31.1 (3.5)	9.90	2	
11592+4842	DA	6080 (92)	8.60 (0.09)	0.98 (0.06)	H	15.04	−4.08	31.6 (0.2)	9.73	1	
11598+0007	DA	9640 (805)	8.00 (0.25)	0.60 (0.15)	H	12.20	−2.89	66.9 (9.5)	8.82	2	
12019+3400	DQ	6110 (84)	8.00 (0.25)	0.57 (0.15)	He	14.41	−3.70	46.4 (0.8)	9.38	2	

TABLE 3.5 – Continued

PM I	ST	$T_{\rm eff}{}^a$ K	log g^a	$M/M_\odot$	Comp.	M_V	log $L/L_\odot$	D (pc)	log τ	Fit^b	Other name
12033+2439	DB	13810 (255)	8.08 (0.14)	0.64 (0.09)	He	11.62	−2.33	104.4 (2.7)	8.49	1	
12113+0724	DA	5270 (41)	8.00 (0.25)	0.58 (0.15)	H	14.57	−3.95	24.7 (2.8)	9.63	2	WD1208+076
12145+7822	DZ	5000 (656)	8.00 (0.25)	0.58 (0.15)	H	14.88	−4.05	32.9 (6.4)	9.75	2	
12155+4630	DA	6720 (109)	8.17 (0.12)	0.70 (0.08)	H	13.94	−3.63	42.6 (0.3)	9.37	1	
12274+3150	DA	6580 (106)	7.99 (0.13)	0.58 (0.08)	H	13.77	−3.56	37.9 (0.3)	9.24	1	WD1224+321
12280+3300	DC	4630 (75)	8.00 (0.25)	0.58 (0.15)	H	15.24	−4.18	35.7 (4.1)	9.85	2	
12370+1814	DC	9860 (256)	8.00 (0.25)	0.58 (0.15)	He	12.66	−2.87	80.0 (9.4)	8.84	2	
12377+6023	DA	5300 (75)	8.00 (0.25)	0.58 (0.15)	H	14.48	−3.94	46.5 (5.4)	9.61	2	
12405+1807W	DA	5420 (46)	8.00 (0.25)	0.58 (0.15)	H	15.14	−3.90	39.0 (4.5)	9.54	2	
12425+1311W	DC	4970 (135)	8.00 (0.25)	0.58 (0.15)	H	15.38	−4.06	44.7 (5.6)	9.77	2	
12429+6542	DA	6960 (121)	8.85 (0.14)	1.12 (0.07)	H	14.95	−4.03	33.0 (0.3)	9.63	1	
12430+2057	DB	14470 (273)	7.97 (0.20)	0.57 (0.11)	He	11.34	−2.18	136.5 (3.3)	8.35	1	
12476+0646	DQpec	5000 (—)	8.00 (0.25)	0.57 (0.15)	He	15.90	−4.06	66.8 (0.6)	9.78	2	
12541+3620	DC	4790 (52)	8.00 (0.25)	0.58 (0.15)	H	15.15	−4.12	26.8 (3.0)	9.82	2	
13032+7510	DC	7550 (264)	8.00 (0.25)	0.58 (0.15)	He	13.25	−3.33	42.9 (5.4)	9.14	2	
13096+6933	DA+dM	8810 (202)	8.45 (0.17)	0.88 (0.11)	H	13.36	−3.33	70.8 (2.3)	9.28	1	
13103+1404	DA	8560 (126)	8.07 (0.07)	0.64 (0.04)	H	12.86	−3.14	49.4 (0.4)	9.00	1	WD1307+143
13108+7236	DA	7960 (129)	8.06 (0.11)	0.63 (0.07)	H	13.12	−3.26	59.4 (2.4)	9.07	1	
13176+0621	DA	5250 (60)	8.00 (0.25)	0.58 (0.15)	H	14.91	−3.96	47.6 (5.4)	9.65	2	
13246+0857	DA	8170 (128)	8.02 (0.10)	0.61 (0.06)	H	12.96	−3.19	53.7 (0.5)	9.02	1	WD1322+092
13291+2450	DC	3990 (72)	8.00 (0.25)	0.58 (0.15)	H	16.72	−4.44	38.9 (4.3)	9.96	2	
13333+2450	DC	4110 (850)	8.00 (0.25)	0.58 (0.15)	H	15.96	−4.39	50.1 (28.7)	9.94	2	
13346+0943E	DA	5140 (585)	8.00 (0.25)	0.58 (0.15)	H	15.03	−4.00	40.7 (13.9)	9.70	2	
13349+6945	DA	14420 (258)	7.98 (0.05)	0.60 (0.03)	H	11.31	−2.17	73.2 (1.5)	8.33	1	
13413+0500	DC	4180 (46)	8.00 (0.25)	0.58 (0.15)	H	16.05	−4.36	13.2 (1.5)	9.93	2	WD1336(8)+052

TABLE 3.5 – Continued

PM I	ST	$T_{\rm eff}$[a] K	log g[a]	$M/M_{\odot}$	Comp.	M_V	log $L/L_{\odot}$	D (pc)	log τ	Fit[b]	Other name
13455+4200	DC	4650 (51)	8.00 (0.25)	0.58 (0.15)	H	15.21	−4.17	23.3 (2.6)	9.85	2	
13521+1053	DA	6070 (111)	8.12 (0.21)	0.67 (0.13)	H	14.30	−3.78	32.6 (0.3)	9.47	1	
13537+1656	DA	8720 (130)	7.68 (0.08)	0.43 (0.04)	H	12.24	−2.89	74.7 (0.6)	8.77	1	
14037+0644	DC	6470 (102)	8.00 (0.25)	0.57 (0.15)	He	13.45	−3.60	51.0 (5.8)	9.30	2	WD1401+069
14064+1608	DA	6950 (132)	8.79 (0.18)	1.09 (0.10)	H	14.85	−3.99	33.8 (0.2)	9.64	1	WD1404+163
14067+3130	DC	4750 (83)	8.00 (0.25)	0.58 (0.15)	H	15.41	−4.14	37.2 (4.3)	9.83	2	
14106+0245	DAZ	5840 (90)	8.00 (0.25)	0.59 (0.15)	H	14.31	−3.77	30.6 (0.2)	9.38	1	WD1408+029
14149+4336	DA	6670 (121)	8.65 (0.16)	1.01 (0.10)	H	14.74	−3.95	33.8 (0.3)	9.66	1	
14236+3037	DA	5300 (52)	8.00 (0.25)	0.58 (0.15)	H	14.92	−3.95	40.1 (4.6)	9.62	2	
14244+6246	DA	5000 (65)	8.00 (0.25)	0.58 (0.15)	H	15.22	−4.05	45.0 (5.1)	9.75	2	
14278+0532	DA+DC	7030 (218)	8.00 (0.25)	0.59 (0.15)	H	13.57	−3.45	69.3 (8.4)	9.18	2	WD1425+057
14339+1907	DA	5020 (62)	8.00 (0.25)	0.58 (0.15)	H	15.16	−4.04	45.8 (5.2)	9.75	2	
14407+0807	DA	5670 (100)	8.00 (0.25)	0.59 (0.15)	H	14.45	−3.83	45.4 (0.7)	9.44	1	
14456+2527	DA	5190 (52)	8.00 (0.25)	0.58 (0.15)	H	14.84	−3.98	17.5 (2.0)	9.67	2	
14553+5655	DA	15140 (238)	8.09 (0.05)	0.67 (0.03)	H	11.38	−2.15	48.5 (0.4)	8.34	1	
14588+1146	DC	4810 (71)	8.00 (0.25)	0.58 (0.15)	H	15.02	−4.12	40.9 (4.6)	9.82	2	
15010+6138	DA	5820 (173)	8.04 (0.39)	0.61 (0.23)	H	14.38	−3.80	43.8 (0.3)	9.43	1	
15164+2803	DAH	7930 (197)	8.00 (0.25)	0.59 (0.15)	H	13.32	−3.23	50.5 (6.1)	9.04	2	
15167+2910	DA	13670 (435)	7.96 (0.06)	0.59 (0.03)	H	11.38	−2.26	127.7 (0.7)	8.39	1	
15206+3903	DA	8710 (129)	8.05 (0.07)	0.62 (0.04)	H	12.75	−3.10	68.0 (0.6)	8.96	1	
15263+2936	DA	5110 (109)	8.00 (0.25)	0.58 (0.15)	H	15.43	−4.01	22.4 (2.6)	9.71	2	
15342+0218	DA	8260 (126)	8.62 (0.08)	1.00 (0.05)	H	13.89	−3.57	29.8 (0.3)	9.47	1	WD1531+024
15359+2125	DA	6500 (112)	8.47 (0.16)	0.89 (0.10)	H	14.54	−3.88	37.6 (0.2)	9.64	1	
15494+4802	DC	6730 (125)	8.00 (0.25)	0.57 (0.15)	He	13.20	−3.54	52.0 (5.9)	9.26	2	WD1547+481
15589+0417	DC	6680 (117)	8.00 (0.25)	0.57 (0.15)	He	51.52	−3.55	30.3 (3.5)	9.27	2	

TABLE 3.5 – Continued

PM I	ST	$T_{\rm eff}{}^a$ K	log g^a	$M/M_\odot$	Comp.	M_V	log $L/L_\odot$	D (pc)	log τ	Fit^b	Other name
16053+5556	DA	6840 (113)	7.57 (0.14)	0.37 (0.06)	H	13.06	−3.27	64.8 (2.3)	8.98	1	
16096+4735	DA	13270 (264)	8.17 (0.06)	0.71 (0.04)	H	11.74	−2.44	87.4 (0.8)	8.56	1	
16142+1729	DQpec	5230 (182)	8.00 (0.25)	0.57 (0.15)	He	15.24	−3.98	48.5 (2.9)	9.71	2	
16171+0530	DA+dM	15000 (345)	7.92 (0.06)	0.56 (0.03)	H	11.15	−2.07	56.1 (0.6)	8.24	1	
16222+0532	DA	7690 (179)	8.20 (0.23)	0.72 (0.15)	H	13.46	−3.41	45.5 (0.4)	9.22	1	
16264+1938	DA	6300 (102)	8.32 (0.14)	0.79 (0.09)	H	14.43	−3.83	27.6 (0.2)	9.59	1	
16265+1355	DA	6820 (101)	7.97 (0.09)	0.57 (0.05)	H	13.60	−3.48	56.9 (0.5)	9.19	1	
16286+7053	DA	4790 (918)	8.00 (0.25)	0.58 (0.15)	H	15.57	−4.12	31.7 (11.1)	9.82	2	
16325+0851	DA	5730 (90)	8.00 (0.25)	0.59 (0.15)	H	14.40	−3.81	13.8 (0.1)	9.42	1	WD1630+089
16335+5231	DA	6700 (111)	8.08 (0.14)	0.64 (0.09)	H	13.82	−3.58	51.1 (0.3)	9.29	1	
16477+2636	DZ	7230 (135)	8.00 (0.25)	0.58 (0.15)	He	13.44	−3.41	52.1 (1.2)	9.18	2	
16514+6635	DZ	7920 (142)	8.00 (0.25)	0.58 (0.15)	He	12.81	−3.25	47.8 (2.1)	9.08	2	
16546+5742	DA	9340 (141)	7.82 (0.08)	0.50 (0.05)	H	12.18	−2.85	56.9 (2.1)	8.76	1	
17027+1022	DA	5080 (57)	8.00 (0.25)	0.58 (0.15)	H	14.86	−4.02	37.3 (4.2)	9.72	2	
17052+0423	DA	8450 (137)	8.37 (0.10)	0.83 (0.07)	H	13.37	−3.35	34.9 (0.7)	9.25	1	
17238+0458	DA	8480 (130)	8.16 (0.09)	0.69 (0.05)	H	13.03	−3.21	56.0 (1.1)	9.07	1	
17283+0211	DA	8050 (121)	8.17 (0.08)	0.70 (0.05)	H	13.23	−3.31	40.2 (1.0)	9.13	1	
17328+0213	DA	7230 (118)	7.97 (0.12)	0.57 (0.07)	H	13.36	−3.38	49.2 (1.1)	9.13	1	
17335+7949	DC	4970 (231)	8.00 (0.25)	0.57 (0.15)	He	14.57	−4.07	29.5 (3.6)	9.78	2	
17344+4236	DA	7370 (114)	7.47 (0.12)	0.33 (0.04)	H	12.64	−3.09	61.7 (1.4)	8.87	1	
17368+3635	DA	6820 (139)	7.46 (0.26)	0.32 (0.10)	H	12.94	−3.22	82.6 (2.6)	8.95	1	
17376+0138	DA	7450 (119)	8.11 (0.11)	0.66 (0.07)	H	13.45	−3.41	45.3 (1.0)	9.18	1	
17417+2401	DA	7150 (111)	8.38 (0.09)	0.84 (0.06)	H	14.02	−3.65	32.6 (0.9)	9.50	1	
17430+1701	DC	4720 (433)	8.00 (0.25)	0.58 (0.15)	H	15.54	−4.15	32.1 (5.5)	9.84	2	
17433+1434S	DC	10440 (234)	8.00 (0.25)	0.58 (0.15)	He	11.67	−2.77	35.7 (4.3)	8.77	2	

TABLE 3.5 – Continued

PM I	ST	$T_{\rm eff}{}^a$ K	log g^a	$M/M_\odot$	Comp.	M_V	log $L/L_\odot$	D (pc)	log τ	Fit^b	Other name
17471+2859	DC	5350 (495)	8.00 (0.25)	0.57 (0.15)	He	14.58	−3.94	37.9 (5.1)	9.66	2	
17574+1021	DZA	7880 (243)	8.00 (0.25)	0.58 (0.15)	He	13.05	−3.26	44.1 (3.3)	9.09	2	
17579+5441	DA	7680 (120)	7.97 (0.10)	0.58 (0.06)	H	13.13	−3.28	64.3 (0.6)	9.06	1	
18014+5049	DC	4990 (103)	8.00 (0.25)	0.58 (0.15)	H	14.87	−4.05	34.0 (4.0)	9.76	2	
18018+0846	DA	5930 (100)	8.00 (0.25)	0.59 (0.15)	H	14.23	−3.74	44.3 (1.5)	9.36	1	
18073+0357	DA	10410 (150)	8.09 (0.05)	0.65 (0.03)	H	12.17	−2.81	34.7 (1.3)	8.79	1	
18138+2119	DA	18200 (279)	7.95 (0.05)	0.59 (0.03)	H	10.87	−1.75	80.3 (2.7)	7.97	1	
18154+3158	DA	5020 (949)	8.00 (0.25)	0.58 (0.15)	H	15.17	−4.04	41.0 (10.8)	9.75	2	
18199+1739	DC	4820 (677)	8.00 (0.25)	0.58 (0.15)	H	15.08	−4.11	35.1 (8.0)	9.81	2	
18435+2740	DA	11060 (163)	8.10 (0.05)	0.66 (0.03)	H	12.00	−2.71	39.7 (0.9)	8.73	1	GD 381
18510+7738	DC:	5230 (49)	8.00 (0.25)	0.58 (0.15)	H	14.86	−3.97	30.3 (3.5)	9.65	2	
18572+2026	DA	5350 (1009)	8.00 (0.25)	0.58 (0.15)	H	13.72	−3.93	31.7 (7.9)	9.59	2	
19005+0020	DA	9580 (154)	8.14 (0.09)	0.68 (0.06)	H	12.54	−2.99	99.1 (6.4)	8.92	1	
19033+6035	DA	11550 (178)	8.07 (0.05)	0.65 (0.03)	H	11.84	−2.62	44.1 (0.9)	8.66	1	
19128+5343	DA	17870 (273)	8.32 (0.05)	0.81 (0.03)	H	11.45	−2.01	22.1 (0.8)	8.29	1	
19132+2949	DA	6110 (114)	8.00 (0.25)	0.59 (0.15)	H	14.09	−3.69	39.9 (1.0)	9.33	1	
19146+1428	DA	7050 (126)	8.68 (0.14)	1.03 (0.09)	H	14.59	−3.89	35.0 (4.7)	9.62	1	
19167+8044	DA	5040 (632)	8.00 (0.25)	0.58 (0.15)	H	14.83	−4.03	35.4 (7.2)	9.74	2	
19401+8348	DC	4840 (672)	8.00 (0.25)	0.58 (0.15)	H	15.08	−4.11	38.8 (8.9)	9.81	2	
19455+4650N	DAH:	4800 (398)	8.00 (0.25)	0.58 (0.15)	H	15.13	−4.12	27.5 (4.1)	9.82	2	
19493+0747	DA	9310 (134)	8.19 (0.06)	0.71 (0.04)	H	12.72	−3.07	36.2 (1.0)	8.98	1	
20062+5902	DA	13750 (263)	7.79 (0.05)	0.50 (0.03)	H	11.13	−2.15	73.8 (0.6)	8.28	1	
20069+6143	DA	5540 (91)	8.00 (0.25)	0.58 (0.15)	H	14.57	−3.87	26.2 (0.2)	9.49	1	
20223+8333	DC	5880 (713)	8.00 (0.25)	0.57 (0.15)	He	14.04	−3.77	39.3 (5.8)	9.44	2	
20235+7001	DA	7250 (134)	8.15 (0.16)	0.69 (0.10)	H	13.61	−3.48	100.4 (5.1)	9.24	1	

TABLE 3.5 – Continued

PM I	ST	$T_{\rm eff}{}^a$ K	log g^a	$M/M_\odot$	Comp.	M_V	log $L/L_\odot$	D (pc)	log τ	Fit^b	Other name
20279+0523	DA	7170 (115)	7.91 (0.12)	0.54 (0.06)	H	13.31	−3.36	56.8 (1.3)	9.10	1	
20300+0729	DC	8180 (285)	8.00 (0.25)	0.58 (0.15)	He	12.79	−3.19	42.2 (5.1)	9.05	2	
20597+5517	DC	4530 (59)	8.00 (0.25)	0.58 (0.15)	H	15.98	−4.22	22.6 (2.5)	9.87	2	
21077+0740	DA	7080 (116)	8.06 (0.12)	0.63 (0.08)	H	13.57	−3.47	35.8 (0.9)	9.20	1	
21117+0120	DA	16390 (266)	8.10 (0.05)	0.67 (0.03)	H	11.26	−2.02	63.1 (1.2)	8.24	1	
21134+0727	DA	6510 (112)	8.26 (0.15)	0.76 (0.10)	H	14.20	−3.74	24.3 (1.6)	9.51	1	
21222+0413	DA	4970 (36)	8.00 (0.25)	0.58 (0.15)	H	15.07	−4.06	21.6 (2.4)	9.77	2	WD2119+040
21384+1856	DA	12600 (258)	7.74 (0.08)	0.47 (0.04)	H	11.22	−2.27	153.2 (0.8)	8.36	1	
21420+2252	DZ	8170 (150)	8.00 (0.25)	0.58 (0.15)	He	12.88	−3.20	38.9 (0.7)	9.05	2	
21429+0805	DA	4830 (515)	8.00 (0.25)	0.58 (0.15)	H	14.74	−4.11	25.1 (4.4)	9.81	2	
21474+1127	DA	4870 (130)	8.00 (0.25)	0.58 (0.15)	H	14.54	−4.10	49.1 (6.2)	9.80	2	
21492+0415	DA	5440 (187)	8.00 (0.25)	0.58 (0.15)	H	14.28	−3.90	26.2 (3.1)	9.53	2	
21551+4103	DZA	5950 (703)	8.00 (0.25)	0.57 (0.15)	He	14.21	−3.75	37.0 (5.8)	9.42	2	
21597+2936	DA	52250 (1135)	7.65 (0.08)	0.55 (0.03)	H	8.50	+0.36	266.8 (5.7)	6.28	1	
22105+4532	DC	5110 (597)	8.00 (0.25)	0.58 (0.15)	H	14.78	−4.01	34.4 (5.8)	9.71	2	
22118+5649	DA	16880 (287)	8.11 (0.05)	0.68 (0.03)	H	11.23	−1.97	22.3 (0.9)	8.21	1	
22133+0349	DC	4190 (323)	8.00 (0.25)	0.58 (0.15)	H	14.95	−4.36	30.4 (6.5)	9.93	2	
22198+4805	DA	6400 (101)	8.23 (0.12)	0.74 (0.08)	H	14.23	−3.75	59.5 (4.0)	9.50	1	
22230+2201N	DA	19440 (387)	8.46 (0.06)	0.91 (0.04)	H	11.55	−1.96	67.3 (0.5)	8.30	1	
22230+2201S	DA	17730 (336)	8.46 (0.06)	0.91 (0.04)	H	11.71	−2.12	74.7 (1.1)	8.42	1	
22276+1753	DAZ	6750 (151)	8.28 (0.23)	0.77 (0.15)	H	14.08	−3.68	30.5 (0.7)	9.48	1	
22299+3024	DA	10630 (155)	7.72 (0.05)	0.46 (0.03)	H	11.58	−2.57	75.6 (1.6)	8.57	1	
22331+2610	DA	11810 (180)	8.05 (0.05)	0.64 (0.03)	H	11.76	−2.57	54.9 (1.3)	8.62	1	
22340+5543	DA	6830 (120)	7.55 (0.17)	0.36 (0.07)	H	13.05	−3.26	69.9 (2.3)	8.98	1	
22410+3646	DA	7350 (113)	8.20 (0.09)	0.72 (0.06)	H	13.63	−3.49	53.2 (1.3)	9.27	1	

TABLE 3.5 – Continued

PM I	ST	$T_{\rm eff}$[a] K	log g[a]	$M/M_{\odot}$	Comp.	M_V	log $L/L_{\odot}$	D (pc)	log τ	Fit[b]	Other name
22418+0432	DQpec	5000 (—)	8.00 (0.25)	0.57 (0.15)	He	14.83	−4.06	43.4 (4.3)	9.78	2	
22447+1513W	DA	5860 (104)	8.00 (0.25)	0.59 (0.15)	H	14.29	−3.77	66.3 (3.6)	9.38	1	
22497+3623	DA	5430 (826)	8.00 (0.25)	0.58 (0.15)	H	15.08	−3.90	43.7 (7.9)	9.54	2	
22595+5717	DA	5170 (1286)	8.00 (0.25)	0.58 (0.15)	H	15.34	−3.99	34.9 (14.3)	9.68	2	
23003+2204	DZ	6110 (177)	8.00 (0.25)	0.57 (0.15)	He	14.00	−3.70	44.9 (3.0)	9.38	2	
23027+4312	DA	8060 (119)	8.12 (0.07)	0.67 (0.05)	H	13.16	−3.28	57.0 (2.2)	9.10	1	
23056+4334	DC	4220 (1039)	8.00 (0.25)	0.58 (0.15)	H	15.86	−4.35	35.7 (39.3)	9.93	2	
23098+5506E	DA	5700 (86)	8.00 (0.25)	0.59 (0.15)	H	14.42	−3.82	16.2 (0.6)	9.42	1	
23160+0559	DA	15300 (256)	7.98 (0.05)	0.60 (0.03)	H	11.21	−2.07	127.9 (1.1)	8.26	1	
23162+1720	DC	4810 (61)	8.00 (0.25)	0.58 (0.15)	H	14.99	−4.12	35.2 (4.0)	9.81	2	
23186+5458	DZ	11720 (459)	8.00 (0.25)	0.59 (0.15)	He	11.78	−2.56	97.7 (3.2)	8.64	2	
23229+3358	DA+dM	14090 (574)	8.20 (0.06)	0.73 (0.04)	H	11.68	−2.35	100.6 (2.4)	8.51	1	
23234+7255	DA	7600 (117)	7.99 (0.09)	0.59 (0.05)	H	13.20	−3.31	46.6 (1.1)	9.08	1	
23243+2835	DA	7060 (118)	7.83 (0.13)	0.50 (0.07)	H	13.27	−3.35	38.6 (0.8)	9.07	1	
23283+3319	DA+dM	15040 (738)	8.72 (0.07)	1.06 (0.04)	H	12.45	−2.60	49.3 (1.2)	8.81	1	
23300+0120	DC	6230 (254)	8.00 (0.25)	0.57 (0.15)	He	13.82	−3.67	52.9 (10.5)	9.35	2	
23389+2101E	DA	5300 (636)	8.00 (0.25)	0.58 (0.15)	H	14.36	−3.94	40.4 (6.8)	9.61	2	
23390+5316	DA	6290 (105)	7.66 (0.16)	0.41 (0.08)	H	13.54	−3.46	48.8 (1.7)	9.11	1	
23462+1158	DC	5220 (285)	8.00 (0.25)	0.57 (0.15)	He	14.77	−3.98	34.0 (4.3)	9.71	2	
23475+0304	DC	4900 (47)	8.00 (0.25)	0.58 (0.15)	H	15.12	−4.08	22.7 (2.6)	9.79	2	
23478+0223	DA	5120 (48)	8.00 (0.25)	0.58 (0.15)	H	14.87	−4.01	42.7 (4.9)	9.71	2	
23489+4300	DC:	4810 (63)	8.00 (0.25)	0.58 (0.15)	H	15.12	−4.11	36.2 (4.1)	9.81	2	

(a) The correction functions of Tremblay et al. (2013b) were applied to the values of $T_{\rm eff}$ and $\log g$.

(b) Fit: 1=Spectroscopic, 2=Photometric.

TABLE 3.6 – Atmospheric Parameters of White Dwarfs within 40 pc of the Sun

PM I	ST	$T_{\rm eff}$[a] (K)	log g[a]	$M/M_\odot$	Comp.	M_V	log $L/L_\odot$	D (pc)	π (mas)	log τ	Fit[b]	WD name	Notes
00023+6357*	DC	4630 (563)	8.00 (0.25)	0.58 (0.15)	H	14.77	−4.18	26.7 (7.2)		9.85	2		
00051+7313	DB	14490 (236)	8.34 (0.12)	0.80 (0.08)	He	11.90	−2.40	34.7 (5.8)	28.8 (4.7)	8.59	1	0002+729	
00073+1230	DC	5090 (65)	8.00 (0.25)	0.57 (0.15)	He	14.62	−4.02	21.0 (3.4)		9.76	2	0004+122	
00074+3403*	DC:	5830 (113)	8.00 (0.25)	0.57 (0.15)	He	14.23	−3.79	42.0 (7.3)		9.46	2		
00079+3947*	DC	4890 (453)	8.00 (0.25)	0.58 (0.15)	H	15.16	−4.09	20.2 (4.2)		9.79	2		
00113+4240	DA	7140 (106)	8.24 (0.07)	0.75 (0.05)	H	13.80	−3.56	19.3 (0.5)		9.35	1	0008+424	
00122+5025	DAP	6420 (99)	8.15 (0.10)	0.68 (0.06)	H	14.09	−3.69	11.0 (0.4)	90.6 (3.7)	9.42	1	0009+501	
00136+0019	DA	9520 (137)	7.97 (0.05)	0.58 (0.03)	H	12.31	−2.90	30.4 (4.5)	32.9 (4.8)	8.82	1	0011+000	
	DB	18110 (288)	8.09 (0.06)	0.65 (0.04)	He	10.99	−1.86	33.3 (11.6)	30.0 (9.4)	8.12	1	0017+136	
00217+2640*	DC	5160 (645)	8.00 (0.25)	0.58 (0.15)	H	14.67	−3.99	35.2 (8.5)		9.69	2		
00222+4236	DA	5590 (782)	8.00 (0.25)	0.58 (0.15)	H	14.00	−3.85	12.9 (3.0)		9.46	2	0019+423	
00276+0542*	DA	5520 (855)	8.00 (0.25)	0.58 (0.15)	H	14.65	−3.87	21.5 (5.1)		9.49	2		
	DA	10830 (157)	8.71 (0.05)	1.05 (0.03)	H	13.10	−3.16	32.9 (4.4)	30.4 (4.0)	9.24	1	0033+016	
	DA	8850 (130)	8.45 (0.06)	0.89 (0.04)	H	13.35	−3.33	33.9 (1.6)		9.28	1	0033+771	
00413+5550E	DC	8860 (2029)	8.00 (0.25)	0.58 (0.15)	He	12.34	−3.05	20.9 (5.4)		8.96	2	0038+555	
00491+0523	DZ	6110 (144)	8.16 (0.01)	0.67 (0.01)	He	13.88	−3.80	4.3 (0.0)	232.5 (1.9)	9.55	2	0046+051	
00547+2256	DA	9540 (142)	8.55 (0.06)	0.95 (0.04)	H	13.25	−3.26	37.1 (0.9)		9.28	1	0052+226	
00559+5948*	DC:	5840 (1061)	8.00 (0.25)	0.57 (0.15)	He	13.32	−3.78	26.2 (6.5)		9.45	2		
01038+0504	DA	8560 (92)	7.69 (0.13)	0.43 (0.06)	H	12.30	−2.93	21.3 (4.6)	46.9 (3.8)	8.80	2	0101+048	
01049+2119	DA	4960 (600)	8.00 (0.25)	0.58 (0.15)	H	15.04	−4.06	40.0 (10.2)		9.77	2	0102+210A	
01049+2120	DC	4890 (497)	8.00 (0.25)	0.58 (0.15)	H	15.27	−4.09	38.8 (9.1)		9.79	2	0102+210B	
01088+7600*	DA	6430 (128)	8.52 (0.22)	0.93 (0.14)	H	14.66	−3.93	38.0 (1.4)		9.66	1		
01107+2758	DA	6260 (72)	8.00 (0.25)	0.59 (0.15)	H	13.06	−3.65	26.6 (4.4)		9.30	2	0108+277	
01180+1610	DQ	9050 (250)	8.16 (0.07)	0.68 (0.04)	He	12.91	−3.11	15.4 (0.8)	64.9 (3.0)	9.02	2	0115+159	
01243+4023	DA	5300 (112)	7.91 (0.28)	0.53 (0.16)	H	14.92	−3.90	31.2 (5.6)	32.1 (5.5)	9.50	2	0121+401	

TABLE 3.6 – Continued

PM I	ST	$T_{\rm eff}{}^a$ (K)	log g^a	$M/M_\odot$	Comp.	M_V	log $L/L_\odot$	D (pc)	π (mas)	log τ	Fit^b	WD name	Notes
01278+7328*	DA	7400 (117)	8.20 (0.10)	0.72 (0.07)	H	13.61	−3.48	25.1 (1.8)		9.26	1		
01294+1023	DA	8550 (122)	7.61 (0.05)	0.39 (0.02)	H	12.22	−2.89	35.2 (3.9)	28.4 (3.1)	8.76	1	0126+101	
	DA	7970 (114)	8.19 (0.05)	0.72 (0.03)	H	13.31	−3.34	21.2 (0.8)		9.17	1	0136+152	
01414+8334	DA	19420 (300)	8.07 (0.05)	0.66 (0.03)	H	10.93	−1.70	27.8 (1.0)		7.97	1	0134+833	
01451+3132	DA	9270 (133)	8.12 (0.05)	0.67 (0.03)	H	12.63	−3.03	35.5 (5.5)	28.2 (4.3)	8.94	1	0142+312	
01457+2918*	DC	4740 (879)	8.00 (0.25)	0.58 (0.15)	H	15.04	−4.14	39.6 (18.5)		9.83	2		
	DA	9210 (132)	8.32 (0.05)	0.80 (0.03)	H	12.97	−3.17	26.1 (0.9)		9.08	1	0143+216	
	DA	12910 (219)	8.11 (0.05)	0.67 (0.03)	H	11.69	−2.45	34.3 (1.2)		8.55	1	0145+234	
01486+3615*	DA	6480 (119)	8.68 (0.19)	1.03 (0.11)	H	14.91	−4.03	24.0 (0.8)		9.68	1		
	DA	8880 (126)	8.20 (0.05)	0.72 (0.03)	H	12.92	−3.16	16.2 (0.8)		9.04	1	0148+641	
	DA	13910 (279)	8.05 (0.05)	0.64 (0.03)	H	11.48	−2.28	15.9 (0.9)	63.0 (3.7)	8.43	1	0148+467	
01528+2553	DA	7530 (124)	7.98 (0.12)	0.58 (0.07)	H	13.22	−3.32	30.4 (1.0)		9.09	1	0150+256	
01596+1548	DC	7760 (117)	8.00 (0.25)	0.58 (0.15)	He	12.87	−3.29	38.3 (6.3)		9.11	2	0156+155	
02062+1836*	DC	4230 (530)	8.00 (0.25)	0.58 (0.15)	H	15.92	−4.34	31.0 (10.6)		9.92	2		
02087+2514	DA	21120 (316)	7.91 (0.05)	0.58 (0.02)	H	10.54	−1.46	33.3 (2.8)	30.0 (2.5)	7.63	1	0205+250	
02113+3955	DAZ	7250 (107)	7.82 (0.08)	0.49 (0.04)	H	13.16	−3.30	16.7 (1.0)	59.8 (3.5)	9.04	1	0208+396	
02118+7119*	DC	5150 (52)	8.00 (0.25)	0.58 (0.15)	H	14.75	−4.00	28.0 (4.6)		9.69	2		
02162+3951	DA	9230 (133)	8.38 (0.05)	0.84 (0.03)	H	13.06	−3.20	19.6 (0.7)		9.14	1	0213+396	
02169+4258	DA	5410 (127)	8.03 (0.13)	0.60 (0.08)	H	14.80	−3.92	19.9 (1.8)	50.2 (4.1)	9.58	2	0213+427	
02199+3520*	DA	5580 (791)	8.00 (0.25)	0.58 (0.15)	H	14.28	−3.85	43.1 (11.6)		9.47	2		
02230+5544*	DA	6980 (110)	8.40 (0.10)	0.85 (0.07)	H	14.14	−3.70	35.3 (1.4)		9.54	1		
02238+2055*	DC	4300 (91)	8.00 (0.25)	0.58 (0.15)	H	16.02	−4.31	33.5 (5.4)		9.91	2		
02258+4228W	DA	5410 (177)	8.00 (0.25)	0.58 (0.15)	H	14.70	−3.91	38.1 (1.3)		9.55	1	0222+422.2	
	DC	4530 (264)	8.00 (0.04)	0.58 (0.03)	H	15.78	−4.22	31.8 (4.4)	31.4 (0.8)	9.87	2	0222+648	
	DA	19640 (296)	7.90 (0.05)	0.57 (0.03)	H	10.65	−1.58	26.9 (0.7)		7.75	1	0227+050	

TABLE 3.6 – Continued

PM I	ST	$T_{\rm eff}{}^a$ (K)	log g^a	$M/M_\odot$	Comp.	M_V	log $L/L_\odot$	D (pc)	π (mas)	log τ	Fit^b	WD name	Notes
02316+2709	DA	4850 (107)	8.00 (0.25)	0.58 (0.15)	H	14.92	−4.10	26.2 (4.4)		9.80	2	0228+269	
02334+2125*	DC	4730 (52)	8.00 (0.25)	0.58 (0.15)	H	15.15	−4.15	26.3 (4.2)		9.83	2		
02355+5715	DA	13790 (314)	8.03 (0.05)	0.63 (0.03)	H	11.47	−2.28	28.4 (1.5)		8.43	1	0231+570	
02363+5244	DA	17760 (275)	8.38 (0.05)	0.85 (0.03)	H	11.57	−2.06	30.5 (1.1)		8.35	1	0232+525	
02379+1638*	DC	5150 (607)	8.00 (0.25)	0.57 (0.15)	He	14.63	−4.00	30.7 (7.1)		9.74	2		
02393+2609	DA	5590 (60)	8.00 (0.25)	0.58 (0.15)	H	14.48	−3.85	21.1 (3.4)		9.47	2	0236+259	
02421+1112	DAH	8510 (196)	8.00 (0.25)	0.60 (0.15)	H	12.68	−3.11	45.9 (8.0)		8.96	2	0239+109	
	DAZ	5040 (100)	8.16 (0.05)	0.68 (0.03)	H	15.28	−4.12	10.4 (1.8)	96.6 (3.1)	9.85	2	0245+541	
02497+3307*	DA	5890 (119)	8.31 (0.26)	0.79 (0.17)	H	14.72	−3.94	31.6 (0.2)		9.67	1		
02562+4954*	DA	6050 (101)	8.00 (0.25)	0.59 (0.15)	H	14.14	−3.71	41.0 (1.5)		9.34	1		
02599+0811	DAP	6740 (480)	7.96 (0.15)	0.57 (0.09)	H	13.25	−3.50	27.9 (2.9)	35.9 (3.5)	9.20	2	0257+080	
03053+2603*	DA	5190 (686)	8.00 (0.25)	0.58 (0.15)	H	14.64	−3.98	45.0 (12.5)		9.67	2		
03062+6222	DA	10990 (162)	8.11 (0.05)	0.67 (0.03)	H	12.03	−2.73	38.8 (1.4)		8.74	1	0302+621	
03109+6634*	DC	4620 (662)	8.00 (0.25)	0.58 (0.15)	H	15.31	−4.19	36.4 (12.4)		9.86	2		
03196+3630*	DZ	5770 (234)	8.00 (0.25)	0.57 (0.15)	He	14.26	−3.80	29.9 (2.1)		9.48	2		
03203+2333*	DC	4510 (447)	8.00 (0.25)	0.58 (0.15)	H	15.52	−4.23	29.3 (7.5)		9.88	2		
	DC	5170 (381)	7.89 (0.26)	0.51 (0.14)	He	14.79	−3.94	40.0 (7.5)	25.0 (3.8)	9.63	2	0324+738	
03433+1958*	DA	7150 (107)	8.47 (0.08)	0.89 (0.05)	H	14.16	−3.71	22.8 (0.9)		9.55	1		
03445+1826	DQ	6420 (108)	7.93 (0.09)	0.53 (0.05)	He	13.80	−3.58	19.0 (1.1)	52.6 (3.0)	9.26	2	0341+182	
03471+0138	DQ	4850 (76)	8.00 (0.25)	0.57 (0.15)	He	15.25	−4.11	17.9 (0.4)		9.80	2	0344+014	
03473+4358*	DA	13650 (316)	7.99 (0.05)	0.60 (0.03)	H	11.42	−2.27	33.9 (1.6)		8.41	1		
	DA	14550 (379)	8.31 (0.05)	0.81 (0.03)	H	11.80	−2.36	35.2 (0.8)		8.55	1	0352+096	
03582+4628	DA+dM	8230 (171)	7.75 (0.11)	0.46 (0.05)	H	12.57	−3.04	38.4 (1.0)		8.87	1	0354+463	1
04004+0814	DA	5450 (62)	8.03 (0.10)	0.60 (0.06)	H	14.58	−3.91	17.8 (1.4)	56.1 (3.7)	9.56	2	0357+081	
04010+5131W*	DC	5220 (342)	8.00 (0.25)	0.58 (0.15)	H	14.57	−3.97	30.8 (5.9)		9.66	2		

TABLE 3.6 – Continued

PM I	ST	$T_{\rm eff}{}^a$ (K)	log g^a	$M/M_\odot$	Comp.	M_V	log $L/L_\odot$	D (pc)	π (mas)	log τ	Fit^b	WD name	Notes
04045+2508	DA	12610 (203)	8.03 (0.05)	0.63 (0.03)	H	11.61	−2.44	27.0 (1.6)	37.0 (2.2)	8.53	1	0401+250	
04101+1802	DA	14260 (246)	7.92 (0.05)	0.57 (0.03)	H	11.25	−2.16	38.2 (9.8)	26.2 (6.3)	8.31	1	0407+179	
04102+1954	DC	4910 (760)	8.00 (0.25)	0.58 (0.15)	H	14.89	−4.08	33.2 (10.5)		9.79	2	0407+197	
04180+4211*	DA	4580 (374)	8.00 (0.25)	0.58 (0.15)	H	15.17	−4.20	23.8 (5.1)		9.86	2		
04214+4607*	DA	7790 (123)	7.87 (0.11)	0.52 (0.06)	H	12.94	−3.19	30.5 (1.5)		8.98	1		
04258+1211	DC	5900 (77)	8.00 (0.07)	0.57 (0.04)	He	14.70	−3.77	17.4 (4.5)	57.6 (2.5)	9.43	2	0423+120	
04259+4614*	DC	4520 (504)	8.00 (0.25)	0.58 (0.15)	H	15.44	−4.22	32.5 (9.6)		9.88	2		
04263+0432	DA	4720 (542)	8.00 (0.25)	0.58 (0.15)	H	15.14	−4.15	22.6 (6.4)		9.83	2	0423+044.2	
04263+4820*	DA+DC	4240 (325)	8.00 (0.25)	0.58 (0.15)	H	14.23	−4.34	29.0 (6.5)		9.92	2		
	DC	7130 (182)	8.15 (0.01)	0.67 (0.00)	He	13.71	−3.52	5.5 (1.9)	180.7 (0.8)	9.29	2	0426+588	
	DA+dM	17620 (427)	8.02 (0.06)	0.63 (0.03)	H	11.02	−1.84	50.0 (16.5)	20.0 (6.0)	8.08	1	0429+176	1
04334+0414*	DA	5220 (596)	8.00 (0.25)	0.58 (0.15)	H	14.62	−3.97	26.5 (6.0)		9.66	2		
04343+3054*	DC:	4670 (577)	8.00 (0.25)	0.58 (0.15)	H	15.28	−4.17	36.2 (10.4)		9.85	2		
	DA	5640 (84)	8.00 (0.25)	0.59 (0.15)	H	14.47	−3.83	16.6 (0.8)	60.2 (2.9)	9.45	1	0433+270	
04372+4524*	DA	6570 (112)	8.12 (0.15)	0.66 (0.10)	H	13.96	−3.63	40.4 (1.6)		9.36	1		
04404+0923	DA	6310 (97)	8.46 (0.11)	0.89 (0.07)	H	14.65	−3.92	29.2 (0.9)		9.66	1	0437+093	
04439+5106	DA	8630 (125)	8.13 (0.06)	0.68 (0.04)	H	12.92	−3.16	46.3 (11.9)	21.6 (5.2)	9.03	1	0440+510	
04523+2519*	DAH	11500 (2655)	8.00 (0.25)	0.60 (0.14)	H	11.66	−2.58	43.7 (9.2)		8.62	2		
04558+3840*	DA	5020 (613)	8.00 (0.25)	0.58 (0.15)	H	14.82	−4.04	32.5 (8.2)		9.75	2		
04573+4155	DA	14290 (255)	7.82 (0.05)	0.51 (0.03)	H	11.10	−2.10	43.5 (5.0)	23.0 (2.6)	8.24	1	0453+418	
04586+6209*	DA+dM	10960 (704)	8.88 (0.13)	1.14 (0.07)	H	13.40	−3.27	21.6 (0.9)		9.30	1		
	DBA	15640 (258)	8.09 (0.07)	0.64 (0.04)	He	11.33	−2.11	28.5 (1.4)		8.33	1	0503+147	
05140+0800	DA	6620 (106)	8.33 (0.12)	0.80 (0.08)	H	14.23	−3.75	21.5 (0.6)		9.54	1	0511+079	
05158+2839*	DAH	6640 (104)	8.00 (0.25)	0.59 (0.15)	H	13.39	−3.55	35.0 (5.8)		9.24	2		
05269+4435*	DC	4700 (632)	8.00 (0.25)	0.58 (0.15)	H	15.14	−4.16	37.0 (11.8)		9.84	2		

TABLE 3.6 – Continued

PM I	ST	$T_{\rm eff}{}^a$ (K)	log g^a	$M/M_\odot$	Comp.	M_V	log $L/L_\odot$	D (pc)	π (mas)	log τ	Fit^b	WD name	Notes
	DA	22550 (343)	9.16 (0.05)	1.26 (0.01)	H	12.67	−2.26	40.2 (1.5)		8.70	1	0525+526	
05353+5715*	DC	5210 (462)	8.00 (0.25)	0.57 (0.15)	He	14.66	−3.98	39.1 (7.2)		9.72	2		
05363+4129	DA	7600 (109)	7.97 (0.05)	0.57 (0.03)	H	13.16	−3.29	20.6 (0.7)		9.07	1	0532+414	
05431+3637*	DAZ	6540 (101)	7.84 (0.11)	0.50 (0.06)	H	13.59	−3.48	27.2 (1.3)		9.16	1		
05462+1115*	DC:	4290 (137)	8.00 (0.25)	0.57 (0.15)	He	15.84	−4.32	27.5 (4.6)		9.88	2		
05557+4650S	DA	5260 (302)	8.00 (0.25)	0.58 (0.15)	H	14.68	−3.96	30.0 (5.6)		9.64	2	0551+468	
05564+0521	DAH	5790 (134)	8.22 (0.04)	0.73 (0.03)	H	14.78	−3.92	8.0 (2.0)	125.1 (3.6)	9.63	2	0553+053	
06025+1553	DA	7110 (115)	8.48 (0.11)	0.90 (0.07)	H	14.20	−3.72	33.1 (1.1)		9.56	1	0559+158	
06026+0904*	DA	5920 (132)	7.75 (0.29)	0.45 (0.14)	H	13.91	−3.61	40.4 (1.7)		9.21	1		
06137+2050*	DA+DQ	5950 (668)	8.00 (0.25)	0.59 (0.15)	H	13.81	−3.74	40.0 (6.0)		9.36	2	GD 73	2
06153+1743	DA	26100 (389)	7.98 (0.05)	0.63 (0.03)	H	10.25	−1.13	36.1 (2.9)	27.7 (2.2)	7.23	1	0612+177	
06207+0645	DA	5990 (126)	8.52 (0.27)	0.93 (0.17)	H	14.98	−4.05	22.6 (2.1)	44.2 (4.2)	9.73	1	0618+067	
06324+2230*	DA	5620 (1471)	8.00 (0.25)	0.58 (0.15)	H	14.72	−3.84	37.4 (13.9)		9.45	2		
06364+4054	DA	7860 (120)	8.73 (0.08)	1.06 (0.04)	H	14.27	−3.73	29.7 (0.8)		9.54	1	0632+409	
	DAP	14060 (3216)	8.00 (0.25)	0.61 (0.14)	H	11.39	−2.23	48.1 (10.4)		8.38	2	0637+477	
06445+2731*	DA	7020 (119)	8.69 (0.13)	1.04 (0.08)	H	14.63	−3.90	30.7 (0.4)		9.63	1		
06473+0231	DA	7080 (103)	8.53 (0.06)	0.94 (0.04)	H	14.31	−3.77	18.5 (1.9)	54.2 (5.5)	9.58	1	0644+025	
06476+3730	DA	22140 (337)	8.09 (0.05)	0.68 (0.03)	H	10.73	−1.49	15.1 (0.5)	66.3 (2.1)	7.74	1	0644+375	
06492+1519*	DC	5050 (392)	8.00 (0.25)	0.57 (0.15)	He	14.85	−4.04	34.9 (8.8)		9.76	2		
06494+7521*	DA	5450 (1044)	8.00 (0.25)	0.58 (0.15)	H	14.02	−3.89	34.4 (10.2)		9.53	2		
06506+1657*	DA	5240 (661)	8.00 (0.25)	0.58 (0.15)	H	14.60	−3.96	34.2 (8.9)		9.65	2		
06534+6403	DA	6050 (98)	8.60 (0.15)	0.98 (0.09)	H	15.07	−4.09	33.3 (5.9)	30.0 (5.2)	9.73	1	0648+641	
06538+6355*	DA	6220 (137)	8.44 (0.23)	0.87 (0.15)	H	14.67	−3.93	20.8 (0.9)		9.67	1		
06573+0241	DC	8100 (893)	8.22 (0.21)	0.72 (0.13)	He	13.24	−3.34	38.5 (7.1)	26.0 (3.7)	9.18	2	0654+027	
07008+3157	DA	4880 (96)	8.02 (0.03)	0.59 (0.02)	H	14.67	−4.10	18.7 (2.0)	53.5 (0.9)	9.81	2	0657+320	

TABLE 3.6 – Continued

PM I	ST	$T_{\rm eff}{}^a$ (K)	log g^a	$M/M_\odot$	Comp.	M_V	log $L/L_\odot$	D (pc)	π (mas)	log τ	Fit^b	WD name	Notes
07087+2044*	DA	5810 (117)	8.00 (0.25)	0.59 (0.15)	H	14.33	−3.78	35.2 (1.5)		9.39	1		
07102+3740N	DQ	6060 (562)	7.82 (0.10)	0.47 (0.05)	He	13.43	−3.63	24.3 (1.4)	41.2 (2.4)	9.26	2	0706+377	
07180+4547	DC	8890 (158)	8.00 (0.25)	0.58 (0.15)	He	12.17	−3.05	34.1 (5.7)		8.95	2	0714+458	
07181+1229	DA	7130 (111)	7.98 (0.10)	0.58 (0.06)	H	13.43	−3.41	33.0 (1.2)		9.15	1	0715+125	
07270+1434*	DA	5680 (89)	8.00 (0.25)	0.59 (0.15)	H	14.44	−3.82	30.5 (0.3)		9.43	1		
	DA	4940 (85)	8.12 (0.02)	0.65 (0.01)	H	15.33	−4.13	11.1 (1.7)	90.0 (1.0)	9.86	2	0727+482B	
07307+4810	DA	4910 (105)	7.86 (0.02)	0.50 (0.01)	H	14.51	−4.01	11.1 (1.7)	90.0 (1.0)	9.66	2	0727+482A	
	DAP	5170 (141)	8.00 (0.25)	0.58 (0.15)	H	14.53	−3.99	18.6 (3.0)		9.68	2	0728+642	
	DA	14870 (330)	8.58 (0.05)	0.98 (0.03)	H	12.21	−2.51	35.0 (1.2)		8.72	1	0730+487	
	DQZ	7870 (433)	8.08 (0.00)	0.63 (0.00)	He	13.21	−3.31	3.5 (0.0)	285.0 (0.8)	9.13	2	0736+053	
07451+2627*	DC	3620 (144)	8.00 (0.25)	0.58 (0.15)	H	16.68	−4.61	32.3 (5.4)		10.00	2		
07474+4408W	DA	15120 (336)	8.47 (0.05)	0.91 (0.03)	H	12.00	−2.40	37.5 (0.5)		8.62	1	0743+442	
07475+1107*	DA	8060 (126)	8.82 (0.08)	1.11 (0.05)	H	14.35	−3.75	29.3 (0.4)		9.53	1		
07502+0711N	DC	4370 (92)	7.83 (0.02)	0.48 (0.01)	H	15.65	−4.20	18.3 (1.7)	54.7 (0.7)	9.80	2	0747+073.1	
07502+0711S	DC	4390 (92)	7.84 (0.02)	0.48 (0.01)	H	15.44	−4.19	18.3 (1.7)	54.7 (0.7)	9.80	2	0747+073.2	
07532+4230	DC	4620 (111)	8.00 (0.25)	0.58 (0.15)	H	15.24	−4.19	25.6 (4.4)		9.86	2	0749+426	
07534+5229	DC	6950 (148)	8.00 (0.25)	0.58 (0.15)	He	13.00	−3.48	27.5 (4.5)		9.22	2	0749+526	
07554+3621	DA	7780 (115)	8.03 (0.07)	0.61 (0.04)	H	13.17	−3.29	33.9 (5.1)	29.5 (4.3)	9.08	1	0752+365	
07560+5741	DC	9290 (171)	7.90 (0.22)	0.52 (0.12)	He	12.23	−2.92	35.2 (4.9)	28.4 (3.8)	8.83	2	0751+578	
07565+4139	DA	6750 (117)	8.05 (0.15)	0.62 (0.09)	H	13.74	−3.55	39.9 (0.5)		9.26	1	0753+417	
07599+4335	DC	6910 (307)	8.00 (0.25)	0.58 (0.15)	He	13.44	−3.49	32.5 (5.6)		9.23	2	0756+437	
08015+4852*	DA	5280 (365)	8.00 (0.25)	0.58 (0.15)	H	14.76	−3.95	36.1 (7.4)		9.63	2		
08054+0735*	DA:	5370 (45)	8.00 (0.25)	0.58 (0.15)	H	14.42	−3.92	37.0 (6.0)		9.58	2		
08059+3833	DA	5140 (69)	8.00 (0.25)	0.58 (0.15)	H	14.66	−4.00	24.2 (3.9)		9.70	2	0802+387	
08091+3527	DA	8950 (128)	8.37 (0.05)	0.83 (0.03)	H	13.15	−3.25	24.5 (0.2)		9.17	1	0805+356	

TABLE 3.6 – Continued

PM I	ST	$T_{\rm eff}{}^a$ (K)	log g^a	$M/M_\odot$	Comp.	M_V	log $L/L_\odot$	D (pc)	π (mas)	log τ	Fit^b	WD name	Notes
08097+2920	DA	6900 (99)	8.00 (0.05)	0.59 (0.03)	H	13.58	−3.48	32.7 (0.4)		9.19	1	0806+294	
08126+1737*	DA	16400 (241)	8.09 (0.04)	0.67 (0.03)	H	11.25	−2.02	32.7 (1.0)		8.24	1		
08141+4845	DC	6640 (142)	8.00 (0.25)	0.57 (0.15)	He	13.66	−3.56	18.0 (2.9)		9.28	2	0810+489	
08152+1633*	DC:	4710 (80)	8.00 (0.25)	0.58 (0.15)	H	15.23	−4.15	40.4 (6.5)		9.84	2		
08167+2137	DA	6250 (116)	8.10 (0.22)	0.65 (0.14)	H	14.13	−3.71	37.0 (0.5)		9.40	1	0813+217	
08200+3834W	DA	7750 (154)	8.27 (0.14)	0.77 (0.09)	H	7.00	−3.44	39.7 (5.8)	25.2 (2.5)	9.28	2	0816+387	
08223+2023*	DC	7240 (150)	8.00 (0.25)	0.58 (0.15)	He	13.12	−3.41	35.6 (5.8)		9.18	2		
08293+2539*	DC	4010 (95)	8.00 (0.25)	0.58 (0.15)	H	16.58	−4.43	32.4 (5.2)		9.95	2		
08306+3241	DA	7270 (106)	8.38 (0.06)	0.83 (0.04)	H	13.94	−3.62	22.3 (1.9)	44.9 (3.8)	9.47	1	0827+328	
08429+2409*	DA	5900 (120)	8.00 (0.25)	0.59 (0.15)	H	14.26	−3.76	38.7 (0.3)		9.37	1	0840+243	
08454+3801	DA	7940 (114)	8.00 (0.05)	0.59 (0.03)	H	13.04	−3.23	38.8 (0.4)		9.04	1	0842+382	
08467+3538	DZ	8580 (126)	8.00 (0.25)	0.58 (0.15)	He	12.73	−3.11	25.5 (0.5)		8.99	2	0843+358	
08491+3429	DA	7530 (111)	8.08 (0.07)	0.64 (0.04)	H	13.36	−3.37	28.7 (0.3)		9.15	1	0846+346	
08516+1624*	DC	5580 (78)	8.00 (0.25)	0.57 (0.15)	He	14.19	−3.86	29.0 (4.6)		9.56	2		
08558+3700*	DA	5620 (59)	8.00 (0.25)	0.58 (0.15)	H	14.17	−3.84	43.4 (7.1)		9.45	2		
08592+3257	DQ	10650 (166)	8.82 (0.08)	1.10 (0.04)	He	13.52	−3.28	20.5 (1.4)	48.8 (3.4)	9.29	2	0856+331	
09018+3607	DA	12080 (179)	8.16 (0.05)	0.70 (0.03)	H	11.87	−2.59	33.6 (0.4)		8.66	1	0858+363	
09021+2010*	DQ	5010 (34)	8.00 (0.25)	0.57 (0.15)	He	15.98	−4.05	37.6 (0.9)		9.78	2		
09026+1535*	DC	4670 (36)	8.00 (0.25)	0.58 (0.15)	H	15.38	−4.17	31.6 (5.0)		9.85	2		
09027+3120*	DA	9930 (143)	8.23 (0.05)	0.75 (0.03)	H	12.56	−2.98	34.1 (0.4)		8.94	1		
09055+7314	DC	5120 (609)	8.00 (0.25)	0.58 (0.15)	H	14.76	−4.01	25.9 (6.0)		9.71	2	0900+734	
09106+2156*	DA	5640 (90)	8.00 (0.25)	0.59 (0.15)	H	14.47	−3.83	37.5 (0.3)		9.44	1	0907+221	
09122+2538*	DA	6720 (105)	8.32 (0.11)	0.80 (0.07)	H	14.17	−3.72	32.5 (0.4)		9.52	1		
09127+1951	DA	5040 (45)	8.00 (0.25)	0.58 (0.15)	H	14.75	−4.03	34.0 (5.4)		9.74	2	0909+200	
09127+2251*	DC	4960 (69)	8.00 (0.25)	0.58 (0.15)	H	14.76	−4.06	43.9 (7.0)		9.77	2		

TABLE 3.6 – Continued

PM I	ST	$T_{\rm eff}{}^a$ (K)	log g^a	$M/M_\odot$	Comp.	M_V	log $L/L_\odot$	D (pc)	π (mas)	log τ	Fit^b	WD name	Notes
09159+5325	DCP	7370 (120)	8.42 (0.03)	0.85 (0.02)	He	14.05	−3.63	10.3 (0.8)	97.0 (1.9)	9.48	2	0912+536	
09166+4359	DA	8590 (123)	8.03 (0.05)	0.62 (0.03)	H	12.80	−3.12	28.9 (3.4)	34.6 (4.0)	8.97	1	0913+442	
09229+0103	DAZ	6010 (111)	8.00 (0.25)	0.59 (0.15)	H	14.17	−3.72	31.2 (0.7)		9.35	1	0920+012	
09245+3120*	DC	4800 (71)	8.00 (0.25)	0.58 (0.15)	H	14.66	−4.12	38.8 (6.1)		9.82	2		
09286+1841*	DA	7730 (116)	8.45 (0.07)	0.88 (0.05)	H	13.83	−3.56	35.9 (0.4)		9.45	1		
09336+2911	DA	8290 (121)	8.52 (0.06)	0.93 (0.04)	H	13.70	−3.49	28.1 (0.3)		9.42	1	0930+394	
09336+2911	DA	8320 (201)	8.39 (0.20)	0.84 (0.13)	H	7.46	−3.39	32.1 (6.4)		9.29	2	0930+394	
09395+4951*	DA	5990 (69)	8.00 (0.25)	0.59 (0.15)	H	13.79	−3.73	43.3 (7.1)		9.35	2		
09402+0907W	DC	5120 (115)	8.00 (0.25)	0.58 (0.15)	H	14.74	−4.01	43.1 (7.2)		9.71	2	0937+093	
09422+0942*	DA	5250 (60)	8.00 (0.25)	0.58 (0.15)	H	14.32	−3.96	46.2 (7.5)		9.64	2		
09432+5134*	DC	4800 (75)	8.00 (0.25)	0.58 (0.15)	H	15.08	−4.12	41.9 (6.7)		9.82	2		
09463+3251N	DA	6860 (119)	8.56 (0.14)	0.96 (0.09)	H	14.48	−3.85	34.2 (0.4)		9.62	1	0943+330	
	DA	13240 (285)	7.69 (0.05)	0.45 (0.02)	H	11.07	−2.16	34.2 (3.4)	29.2 (2.9)	8.27	1	0943+441	
09481+2023*	DC	4820 (60)	8.00 (0.25)	0.58 (0.15)	H	15.11	−4.11	35.8 (5.8)		9.81	2		
09487+2421	DAXP+DA	14530 (1021)	8.40 (0.11)	0.86 (0.07)	H	12.16	−2.42	40.0 (5.0)		8.61	1	0945+245	3
09502+5315	DC	8790 (253)	8.43 (0.11)	0.86 (0.07)	He	13.47	−3.33	23.0 (2.1)	43.5 (3.5)	9.27	2	0946+534	
09503+1509*	DC	5440 (54)	8.00 (0.25)	0.58 (0.15)	H	14.78	−3.90	38.8 (6.3)		9.53	2		
09578+2432	DA	8530 (122)	8.18 (0.05)	0.70 (0.03)	H	13.03	−3.21	24.4 (2.8)	40.9 (4.5)	9.07	1	0955+247	
10013+4656	DC	4440 (119)	8.00 (0.25)	0.58 (0.15)	H	15.81	−4.26	39.0 (6.8)		9.89	2	0958+471	
10024+6108	DC	4240 (119)	8.00 (0.25)	0.58 (0.15)	H	16.08	−4.34	37.6 (6.5)		9.92	2	0958+613	
	DQpecP	4020 (46)	7.93 (0.01)	0.52 (0.01)	He	15.95	−4.40	14.8 (0.5)	67.4 (0.4)	9.87	2	1008+290	
10118+2647*	DA	5280 (121)	8.00 (0.25)	0.58 (0.15)	H	14.66	−3.95	41.6 (7.0)		9.63	2		
10140+0305N	DA	5190 (143)	8.00 (0.25)	0.58 (0.15)	H	15.07	−3.98	47.8 (8.5)		9.67	2	1011+033	
10145+4226	DA	7490 (109)	8.28 (0.06)	0.77 (0.04)	H	13.68	−3.51	33.1 (0.4)		9.34	1	1011+426	
10150+0806S	DC	4630 (102)	7.95 (0.19)	0.55 (0.11)	H	15.01	−4.16	29.0 (3.4)	34.5 (3.9)	9.83	2	1012+083.2	

TABLE 3.6 – Continued

PM I	ST	$T_{\rm eff}{}^a$ (K)	log g^a	$M/M_\odot$	Comp.	M_V	log $L/L_\odot$	D (pc)	π (mas)	log τ	Fit^b	WD name	Notes
10150+0806N	DA	6530 (105)	7.89 (0.12)	0.53 (0.07)	H	13.67	−3.52	29.0 (3.4)	34.5 (3.9)	9.19	1	1012+083.1	
10155+1850*	DC	4600 (89)	8.00 (0.25)	0.58 (0.15)	H	15.38	−4.19	45.0 (7.2)		9.86	2		
10221+4612	DA	7000 (101)	8.24 (0.06)	0.75 (0.04)	H	13.88	−3.60	30.6 (0.3)		9.38	1	1022+461	
10225+4600	DA	6510 (121)	8.52 (0.17)	0.93 (0.11)	H	14.62	−3.91	27.3 (0.6)		9.65	1	1019+462	
10228+3904*	DZ	5300 (50)	8.00 (0.25)	0.57 (0.15)	He	14.74	−3.95	37.1 (0.8)		9.68	2		
10231+6327	DA	6780 (100)	7.90 (0.08)	0.54 (0.05)	H	13.53	−3.46	16.3 (1.0)	61.2 (3.6)	9.16	1	1019+637	
10291+1127	DAP	6940 (116)	8.00 (0.25)	0.59 (0.15)	H	13.30	−3.47	40.0 (6.7)		9.19	2	1026+117	
10291+0205	DA	14610 (229)	7.99 (0.05)	0.61 (0.03)	H	11.31	−2.16	38.1 (0.5)		8.32	1	1026+023	
10347+2245*	DZ	6510 (96)	8.00 (0.25)	0.57 (0.15)	He	13.40	−3.59	36.5 (1.0)		9.30	2	1032+230	
10370+7110	DC	4730 (95)	8.00 (0.25)	0.58 (0.15)	H	15.11	−4.14	19.7 (3.2)		9.83	2	1033+714	
10403+1004*	DC	5920 (94)	8.00 (0.25)	0.57 (0.15)	He	14.11	−3.76	39.1 (6.3)		9.43	2		
10418+1415	DQ	7340 (98)	7.90 (0.26)	0.52 (0.14)	He	13.65	−3.33	45.0 (8.4)	22.2 (3.5)	9.09	2	1039+145	
10480+6334	DA	5080 (57)	8.00 (0.25)	0.58 (0.15)	H	14.93	−4.02	32.3 (5.2)		9.72	2	1044+638	
10502+3226*	DA:	5610 (57)	8.00 (0.25)	0.58 (0.15)	H	14.02	−3.84	44.6 (7.2)		9.46	2		
10521+4050*	DC	6180 (116)	8.00 (0.25)	0.57 (0.15)	He	14.26	−3.68	35.7 (5.7)		9.36	2		
10547+2706	DA	23930 (366)	8.41 (0.05)	0.88 (0.03)	H	11.10	−1.56	40.1 (0.5)		7.96	1	1052+273	
10565+2336*	DA	5190 (58)	8.00 (0.25)	0.58 (0.15)	H	15.06	−3.98	42.1 (6.8)		9.67	2		
11071+1446*	DA	6700 (110)	8.32 (0.12)	0.80 (0.08)	H	14.18	−3.73	30.5 (0.3)		9.53	1		
11075+4855	DC	4460 (139)	8.00 (0.25)	0.58 (0.15)	H	16.27	−4.25	47.3 (8.5)		9.89	2	1104+491	
	DA	18780 (283)	8.08 (0.05)	0.67 (0.03)	H	11.01	−1.77	35.6 (1.2)		8.03	1	1100+602	
11087+0801	DA	7520 (108)	8.03 (0.05)	0.61 (0.03)	H	13.30	−3.35	36.4 (0.5)		9.12	1	1106+082	
11109+2026	DC	4730 (109)	8.09 (0.11)	0.64 (0.07)	H	15.38	−4.20	26.1 (2.0)	38.3 (2.7)	9.89	2	1108+207	
11111+3848*	DC	5080 (145)	8.00 (0.25)	0.57 (0.15)	He	14.64	−4.03	48.1 (8.5)		9.76	2	SSJ111109.	
11132+2859*	DA	4830 (62)	8.00 (0.25)	0.58 (0.15)	H	15.27	−4.11	34.9 (5.6)		9.81	2	1110+292	
11156+0033	DA	5210 (71)	8.00 (0.25)	0.58 (0.15)	H	14.74	−3.97	32.8 (5.4)		9.66	2	1113+008	

TABLE 3.6 – Continued

PM I	ST	$T_{\rm eff}{}^a$ (K)	log g^a	$M/M_\odot$	Comp.	M_V	log $L/L_\odot$	D (pc)	π (mas)	log τ	Fit^b	WD name	Notes
11166+0627	DA	6410 (124)	8.11 (0.20)	0.66 (0.12)	H	14.05	−3.67	34.7 (0.4)		9.38	1	1114+067	
11192+0220	DA	12400 (186)	8.08 (0.05)	0.65 (0.03)	H	11.71	−2.50	37.7 (0.4)		8.58	1	1116+026	
11210+3756*	DA	9810 (145)	8.26 (0.06)	0.76 (0.04)	H	12.65	−3.02	36.5 (0.5)		8.97	1		
11235+0701	DC	4460 (106)	8.00 (0.25)	0.58 (0.15)	H	15.84	−4.25	24.9 (4.2)		9.89	2	1120+073	
11242+2121	DA	7330 (105)	8.09 (0.06)	0.65 (0.04)	H	13.47	−3.42	13.4 (0.5)	74.5 (2.8)	9.18	1	1121+216	
11253+2111*	DC	6390 (117)	8.00 (0.25)	0.57 (0.15)	He	13.51	−3.63	41.2 (6.8)		9.32	2		
11268+5919	DA	10360 (160)	8.69 (0.07)	1.04 (0.04)	H	13.21	−3.22	24.0 (0.3)		9.28	1	1124+595	
	DA	17990 (277)	8.24 (0.05)	0.77 (0.03)	H	11.33	−1.95	35.8 (1.2)		8.23	1	1129+155	
11354+2717	DC	4250 (359)	8.00 (0.25)	0.58 (0.15)	H	15.69	−4.33	39.7 (9.6)		9.92	2	1132+275	
11364+0802S*	DA	5500 (45)	8.00 (0.25)	0.58 (0.15)	H	14.39	−3.88	47.3 (7.6)		9.50	2		
	DA	22310 (339)	8.56 (0.05)	0.98 (0.03)	H	11.50	−1.79	14.2 (2.2)	70.6 (10.9)	8.20	1	1134+300	
11457+6305	DC	5270 (58)	8.00 (0.25)	0.58 (0.15)	H	14.74	−3.95	21.3 (3.4)		9.63	2	1143+633	
11459+3149W	DA	16610 (254)	8.14 (0.05)	0.70 (0.03)	H	11.30	−2.02	31.6 (2.3)	31.6 (2.3)	8.26	1	1143+321	
	DA	15890 (265)	8.05 (0.05)	0.64 (0.03)	H	11.24	−2.04	35.7 (1.3)		8.25	1	1135+321	
11495+2353*	DC	4960 (54)	8.00 (0.25)	0.58 (0.15)	H	14.51	−4.06	42.0 (6.6)		9.77	2		
11519+0528	DA	11100 (160)	8.07 (0.05)	0.64 (0.03)	H	11.94	−2.69	40.2 (0.4)		8.70	1	1149+057	
11545+2422*	DA	8790 (141)	8.57 (0.09)	0.96 (0.06)	H	13.57	−3.42	25.2 (0.2)		9.38	1	1151+246	
11562+1315	DC	4730 (115)	8.00 (0.25)	0.58 (0.15)	H	15.66	−4.15	28.0 (4.7)		9.83	2	1153+135	
11567+1822	DC	7710 (221)	8.07 (0.16)	0.62 (0.10)	He	13.39	−3.34	29.9 (3.5)	33.5 (3.5)	9.15	2	1154+186	
11582+0004*	DC	4410 (83)	8.00 (0.25)	0.58 (0.15)	H	15.78	−4.27	31.1 (5.0)		9.90	2		
11592+4842*	DA	6080 (92)	8.60 (0.09)	0.98 (0.06)	H	15.04	−4.08	31.6 (0.2)		9.73	1		
12000+4335	DA	7730 (111)	7.82 (0.06)	0.49 (0.03)	H	12.90	−3.18	37.5 (0.4)		8.96	1	1157+438	
12113+0724*	DA	5270 (41)	8.00 (0.25)	0.58 (0.15)	H	14.57	−3.95	24.7 (4.0)		9.63	2	1208+076	
12114+5724	DA	5870 (106)	7.79 (0.25)	0.47 (0.13)	H	14.01	−3.65	20.4 (1.9)	48.9 (4.6)	9.25	1	1208+576	
12145+7822*	DZ	5000 (656)	8.00 (0.25)	0.58 (0.15)	H	14.88	−4.05	32.9 (8.9)		9.75	2		

TABLE 3.6 – Continued

PM I	ST	$T_{\rm eff}{}^a$ (K)	log g^a	$M/M_\odot$	Comp.	M_V	log $L/L_\odot$	D (pc)	π (mas)	log τ	Fit^b	WD name	Notes
	DA+dM	15460 (417)	8.07 (0.07)	0.65 (0.05)	H	11.32	−2.10	37.3 (4.0)	26.8 (2.8)	8.30	1	1213+528	1
	DC	8530 (998)	9.02 (0.12)	1.20 (0.05)	He	14.54	−3.83	31.1 (5.5)	32.2 (3.6)	9.45	2	1215+323	
12265+3513	DA	5100 (56)	8.00 (0.25)	0.58 (0.15)	H	14.59	−4.01	31.2 (5.1)		9.72	2	1224+354	
12274+3150*	DA	6580 (106)	7.99 (0.13)	0.58 (0.08)	H	13.77	−3.56	37.9 (0.5)		9.24	1	D1224+321	
12280+3300*	DC	4630 (75)	8.00 (0.25)	0.58 (0.15)	H	15.24	−4.18	35.7 (5.7)		9.85	2		
12281+0022	DA	9390 (134)	7.97 (0.05)	0.58 (0.03)	H	12.36	−2.92	33.1 (0.4)		8.83	1	1225+006	
12377+6023*	DA	5300 (75)	8.00 (0.25)	0.58 (0.15)	H	14.48	−3.94	46.5 (7.7)		9.61	2		
12392+4525	DA	6810 (118)	8.66 (0.15)	1.02 (0.09)	H	14.68	−3.93	23.5 (0.2)		9.65	1	1236+457	
12405+1807W*	DA	5420 (46)	8.00 (0.25)	0.58 (0.15)	H	15.14	−3.90	39.0 (6.3)		9.54	2		
12425+1311W*	DC	4970 (135)	8.00 (0.25)	0.58 (0.15)	H	15.38	−4.06	44.7 (7.9)		9.77	2		
12429+6542*	DA	6960 (121)	8.85 (0.14)	1.12 (0.07)	H	14.95	−4.03	33.0 (0.4)		9.63	1		
12501+5447	DC	4530 (608)	7.96 (0.03)	0.56 (0.02)	H	15.56	−4.20	25.3 (1.4)	39.5 (0.7)	9.85	2	1247+550	
12541+3620*	DC	4790 (52)	8.00 (0.25)	0.58 (0.15)	H	15.15	−4.12	26.8 (4.3)		9.82	2		
12597+2734	DA	8570 (123)	8.11 (0.05)	0.66 (0.03)	H	12.91	−3.16	34.6 (5.0)	28.9 (4.1)	9.02	1	1257+278	
13001+0328	DA	5710 (94)	8.00 (0.25)	0.59 (0.15)	H	14.41	−3.81	16.6 (1.1)	60.3 (3.8)	9.42	1	1257+037	
13003+0130	DA	5450 (68)	8.00 (0.25)	0.58 (0.15)	H	14.65	−3.90	37.4 (6.2)		9.53	2	1257+017	
13013+6713	DA	6600 (109)	8.09 (0.13)	0.64 (0.08)	H	13.89	−3.61	33.8 (0.4)		9.32	1	1259+674	
13032+7510*	DC	7550 (264)	8.00 (0.25)	0.58 (0.15)	He	13.25	−3.33	42.9 (7.6)		9.14	2		
	DC	4620 (551)	8.33 (0.16)	0.80 (0.11)	H	16.04	−4.38	35.2 (6.0)	28.4 (3.3)	9.97	2	1300+263	
	DAP	5430 (135)	8.19 (0.02)	0.71 (0.02)	H	14.93	−4.01	16.5 (0.7)	60.7 (1.0)	9.74	2	1309+853	
13129+5805	DA	10470 (152)	8.15 (0.05)	0.69 (0.03)	H	12.25	−2.84	23.2 (0.2)		8.82	1	1310+583	
13178+2157	DC	6830 (254)	8.00 (0.25)	0.59 (0.15)	H	13.68	−3.50	44.5 (7.6)		9.21	2	1315+222	
13212+4623	DA	14380 (338)	8.31 (0.05)	0.80 (0.03)	H	11.81	−2.38	33.8 (0.4)		8.56	1	1319+466	
13277+5755	DA	6790 (114)	8.03 (0.14)	0.61 (0.09)	H	13.70	−3.53	37.0 (7.9)	27.0 (5.5)	9.24	1	1325+581	
13291+2450*	DC	3990 (72)	8.00 (0.25)	0.58 (0.15)	H	16.72	−4.44	38.9 (6.1)		9.96	2		

TABLE 3.6 – Continued

PM I	ST	$T_{\rm eff}{}^a$ (K)	log g^a	$M/M_\odot$	Comp.	M_V	log $L/L_\odot$	D (pc)	π (mas)	log τ	Fit^b	WD name	Notes
13309+3029	DZ	5950 (47)	7.75 (0.28)	0.43 (0.14)	He	13.92	−3.62	29.9 (4.9)	33.4 (5.3)	9.24	2	1328+307	
13333+2450*	DC	4110 (850)	8.00 (0.25)	0.58 (0.15)	H	15.96	−4.39	50.1 (35.1)		9.94	2		
13346+0943E*	DA	5140 (585)	8.00 (0.25)	0.58 (0.15)	H	15.03	−4.00	40.7 (18.2)		9.70	2		
	DB+dM	15330 (293)	7.95 (0.17)	0.56 (0.10)	He	11.17	−2.07	35.0 (4.0)	28.6 (3.2)	8.26	1	1333+487	
13365+0340	DA	4940 (74)	7.91 (0.05)	0.53 (0.03)	H	15.04	−4.02	8.2 (1.4)	121.4 (3.4)	9.69	2	1334+039	
13388+7017	DA	21150 (320)	7.95 (0.05)	0.60 (0.03)	H	10.59	−1.48	32.8 (6.6)	30.5 (5.9)	7.66	1	1337+705	
13413+0500*	DC	4180 (46)	8.00 (0.25)	0.58 (0.15)	H	16.05	−4.36	13.2 (2.1)		9.93	2	1336+052	
13455+4200*	DC	4650 (51)	8.00 (0.25)	0.58 (0.15)	H	15.21	−4.17	23.3 (3.7)		9.85	2		
13460+5700	DA	13900 (300)	8.06 (0.05)	0.65 (0.03)	H	11.49	−2.29	25.8 (0.4)		8.43	1	1344+572	
13474+1021W	DA	6940 (102)	7.91 (0.07)	0.54 (0.04)	H	13.44	−3.42	20.0 (1.4)	49.9 (3.6)	9.13	1	1344+106	
	DA	4580 (85)	7.77 (0.05)	0.45 (0.02)	H	15.56	−4.09	12.1 (0.7)	82.9 (2.2)	9.68	2	1345+238	
13490+1155	DC	4620 (106)	8.00 (0.25)	0.58 (0.15)	H	15.30	−4.18	32.8 (5.5)		9.86	2	1346+121	
13497+2755	DA	7260 (120)	8.41 (0.12)	0.86 (0.08)	H	14.01	−3.64	29.6 (0.4)		9.50	1	1347+281	
13521+1053*	DA	6070 (111)	8.12 (0.21)	0.67 (0.13)	H	14.30	−3.78	32.6 (0.4)		9.47	1		
14037+5206	DA	7490 (118)	8.37 (0.09)	0.83 (0.06)	H	13.82	−3.56	33.7 (0.4)		9.43	1	1401+523	
14064+1608*	DA	6950 (132)	8.79 (0.18)	1.09 (0.10)	H	14.85	−3.99	33.8 (0.2)		9.64	1	1404+163	
14067+3130*	DC	4750 (83)	8.00 (0.25)	0.58 (0.15)	H	15.41	−4.14	37.2 (6.1)		9.83	2		
	DA	9910 (142)	8.03 (0.05)	0.62 (0.03)	H	12.25	−2.86	36.5 (0.5)		8.81	1	1407+425	
14104+3208	DA	19010 (286)	8.00 (0.05)	0.62 (0.03)	H	10.85	−1.70	39.5 (4.4)	25.3 (2.8)	7.93	1	1408+323	
14106+0245*	DAZ	5840 (90)	8.00 (0.25)	0.59 (0.15)	H	14.31	−3.77	30.6 (0.3)		9.38	1	1408+029	
14149+4336*	DA	6670 (121)	8.65 (0.16)	1.01 (0.10)	H	14.74	−3.95	33.8 (0.4)		9.66	1		
14236+3037*	DA	5300 (52)	8.00 (0.25)	0.58 (0.15)	H	14.92	−3.95	40.1 (6.5)		9.62	2		
14244+6246*	DA	5000 (65)	8.00 (0.25)	0.58 (0.15)	H	15.22	−4.05	45.0 (7.2)		9.75	2		
14246+0917	DA	12760 (197)	8.05 (0.05)	0.64 (0.03)	H	11.62	−2.43	38.6 (0.4)		8.53	1	1422+095	
14339+1907*	DA	5020 (62)	8.00 (0.25)	0.58 (0.15)	H	15.16	−4.04	45.8 (7.3)		9.75	2		

TABLE 3.6 – Continued

PM I	ST	$T_{\rm eff}{}^a$ (K)	log g^a	$M/M_\odot$	Comp.	M_V	log $L/L_\odot$	D (pc)	π (mas)	log τ	Fit^b	WD name	Notes
14367+4332	DC	4710 (110)	8.00 (0.25)	0.58 (0.15)	H	15.40	−4.15	26.4 (4.4)		9.84	2	1434+437	
14456+2527*	DA	5190 (52)	8.00 (0.25)	0.58 (0.15)	H	14.84	−3.98	17.5 (2.8)		9.67	2		
14581+2937	DA	7290 (105)	7.90 (0.06)	0.54 (0.03)	H	13.24	−3.33	34.6 (5.0)	28.9 (4.1)	9.08	1	1455+298	
14588+1146*	DC	4810 (71)	8.00 (0.25)	0.58 (0.15)	H	15.02	−4.12	40.9 (6.5)		9.82	2		
15096+6332	DA	10380 (148)	7.96 (0.05)	0.58 (0.03)	H	11.99	−2.74	35.5 (0.9)		8.72	1	1508+637	
15111+4048	DA	8650 (126)	8.19 (0.06)	0.71 (0.04)	H	13.00	−3.19	34.7 (0.4)		9.06	1	1509+409	
15114+3204	DA	14550 (272)	8.11 (0.05)	0.68 (0.03)	H	11.49	−2.23	47.8 (10.1)	20.9 (4.2)	8.41	1	1509+322	
15257+5629	DC	5520 (71)	8.00 (0.25)	0.58 (0.15)	H	14.32	−3.87	28.8 (4.8)		9.49	2	1524+566	
15263+2936*	DA	5110 (109)	8.00 (0.25)	0.58 (0.15)	H	15.43	−4.01	22.4 (3.7)		9.71	2		
15342+0218*	DA	8260 (126)	8.62 (0.08)	1.00 (0.05)	H	13.89	−3.57	29.8 (0.4)		9.47	1	1531+024	
15348+4649	DC	4410 (106)	8.00 (0.25)	0.58 (0.15)	H	16.01	−4.27	29.8 (5.0)		9.90	2	1533+469	
15350+1247	DZ	5180 (19)	8.00 (0.25)	0.57 (0.15)	He	14.85	−3.99	16.9 (0.2)		9.73	2	1532+129	
15359+2125*	DA	6500 (112)	8.47 (0.16)	0.89 (0.10)	H	14.54	−3.88	37.6 (0.3)		9.64	1		
15377+6501	DA	9660 (141)	7.98 (0.06)	0.59 (0.03)	H	12.27	−2.88	31.1 (0.4)		8.81	1	1537+651	
15405+3308N	DA	8780 (125)	8.15 (0.05)	0.69 (0.03)	H	12.89	−3.15	27.5 (0.3)		9.03	1	1538+333	
15425+2329	DA	6250 (113)	8.82 (0.18)	1.11 (0.10)	H	15.33	−4.20	19.6 (0.2)		9.70	1	1540+236	
15524+1810	DA	14810 (295)	8.37 (0.05)	0.84 (0.03)	H	11.86	−2.37	40.5 (1.0)		8.57	1	1550+183	
15555+5025	DA	6190 (105)	7.62 (0.19)	0.39 (0.08)	H	13.56	−3.47	40.2 (0.5)		9.10	1	1554+505	
15589+0417*	DC	6680 (117)	8.00 (0.25)	0.57 (0.15)	He	51.52	−3.55	30.3 (4.9)		9.27	2		
16012+5316	DA	6680 (102)	8.04 (0.09)	0.61 (0.05)	H	13.77	−3.56	36.1 (0.5)		9.26	1	1559+534	
16013+3648	DA	11240 (162)	8.00 (0.05)	0.60 (0.03)	H	11.81	−2.62	33.1 (3.7)	30.2 (3.3)	8.65	1	1559+369	
16048+0055	DC	4810 (115)	8.00 (0.25)	0.58 (0.15)	H	15.56	−4.11	30.8 (5.1)		9.81	2	1602+010	
16072+3423	DA	5790 (70)	8.00 (0.25)	0.59 (0.15)	H	13.91	−3.79	36.4 (6.0)		9.40	2	1605+345	
16083+4205	DA	13070 (214)	7.87 (0.05)	0.53 (0.03)	H	11.33	−2.28	45.0 (7.3)	22.2 (3.5)	8.39	1	1606+422	
16114+1322	DA	9230 (132)	8.48 (0.05)	0.90 (0.03)	H	13.23	−3.27	18.3 (1.6)	54.5 (4.7)	9.25	1	1609+135	

TABLE 3.6 – Continued

PM I	ST	$T_{\rm eff}{}^a$ (K)	log g^a	$M/M_\odot$	Comp.	M_V	log $L/L_\odot$	D (pc)	π (mas)	log τ	Fit^b	WD name	Notes
16264+1938*	DA	6300 (102)	8.32 (0.14)	0.79 (0.09)	H	14.43	−3.83	27.6 (0.3)		9.59	1		
16278+0912	DA	7130 (134)	8.60 (0.16)	0.98 (0.10)	H	14.40	−3.81	23.4 (2.1)	42.8 (3.7)	9.60	1	1625+093	
16284+3646	DZA	8020 (156)	7.98 (0.05)	0.56 (0.03)	He	13.01	−3.22	15.9 (0.5)	62.7 (2.0)	9.05	2	1626+368	
16286+7053*	DA	4790 (918)	8.00 (0.25)	0.58 (0.15)	H	15.57	−4.12	31.7 (14.4)		9.82	2		
16325+0851*	DA	5730 (90)	8.00 (0.25)	0.59 (0.15)	H	14.40	−3.81	13.8 (0.1)		9.42	1	1630+089	
16343+5710	DQpec	6200 (105)	8.12 (0.05)	0.65 (0.03)	He	14.19	−3.74	14.4 (0.6)	69.2 (2.5)	9.48	2	1633+572	
	DA	10030 (142)	7.79 (0.05)	0.48 (0.02)	H	11.86	−2.70	19.0 (0.8)		8.66	1	1632+177	
16350+4317	DAZ	6560 (112)	7.93 (0.15)	0.55 (0.08)	H	13.69	−3.53	15.1 (0.7)	66.2 (3.0)	9.20	1	1633+433	
16394+3325	DA	10180 (146)	8.03 (0.05)	0.62 (0.03)	H	12.15	−2.81	28.6 (2.6)	35.0 (3.2)	8.78	1	1637+335	
16409+5341	DAH	7410 (99)	8.06 (0.11)	0.62 (0.07)	He	13.81	−3.40	21.1 (2.1)	47.4 (3.5)	9.19	2	1639+537	
16416+1512	DA	7450 (110)	8.49 (0.07)	0.91 (0.04)	H	14.04	−3.65	21.5 (0.6)		9.51	1	1639+153	
16473+3228	DB	25250 (370)	7.92 (0.05)	0.57 (0.03)	He	10.33	−1.17	36.6 (4.5)	27.3 (3.3)	7.33	1	1645+325	
16484+5903	DA	12570 (197)	8.31 (0.05)	0.80 (0.03)	H	12.02	−2.61	12.2 (0.6)	81.9 (4.6)	8.72	1	1647+591	
16547+3829	DAZ	5940 (101)	8.00 (0.25)	0.59 (0.15)	H	14.23	−3.74	32.3 (0.4)		9.36	1	1653+385	
16571+2126	DA	9240 (132)	8.02 (0.05)	0.61 (0.03)	H	12.50	−2.98	23.3 (1.7)	43.0 (3.1)	8.88	1	1655+215	
16595+4425	DA	5690 (123)	8.09 (0.33)	0.64 (0.20)	H	14.55	−3.87	28.0 (0.3)		9.52	1	1658+445	
17027+1022*	DA	5080 (57)	8.00 (0.25)	0.58 (0.15)	H	14.86	−4.02	37.3 (6.0)		9.72	2		
17052+0423*	DA	8450 (137)	8.37 (0.10)	0.83 (0.07)	H	13.37	−3.35	34.9 (1.0)		9.25	1		
17081+0257	DZ	6650 (153)	8.21 (0.14)	0.70 (0.09)	He	13.89	−3.68	17.5 (1.7)	57.0 (5.4)	9.45	2	1705+030	
17131+6931	DA	15880 (239)	7.99 (0.05)	0.61 (0.03)	H	11.16	−2.01	27.7 (3.2)	36.1 (4.0)	8.21	1	1713+695	
17148+3918	DAP	7010 (123)	8.00 (0.25)	0.59 (0.15)	H	13.75	−3.45	38.2 (6.4)		9.18	2	1713+393	
17185+0156N	DA	13550 (345)	7.91 (0.05)	0.56 (0.03)	H	11.33	−2.24	35.6 (3.3)	28.1 (2.6)	8.37	1	1716+020	
17283+0211*	DA	8050 (121)	8.17 (0.08)	0.70 (0.05)	H	13.23	−3.31	40.2 (1.5)		9.13	1		
17335+7949*	DC	4970 (231)	8.00 (0.25)	0.57 (0.15)	He	14.57	−4.07	29.5 (5.1)		9.78	2		
17417+2401*	DA	7150 (111)	8.38 (0.09)	0.84 (0.06)	H	14.02	−3.65	32.6 (1.3)		9.50	1		

TABLE 3.6 – Continued

PM I	ST	$T_{\rm eff}{}^a$ (K)	log g^a	$M/M_\odot$	Comp.	M_V	log $L/L_\odot$	D (pc)	π (mas)	log τ	Fit^b	WD name	Notes
17428+4338	DA	5480 (118)	8.00 (0.25)	0.58 (0.15)	H	14.15	−3.88	31.8 (5.3)		9.51	2	1741+436	
17430+1701*	DC	4720 (433)	8.00 (0.25)	0.58 (0.15)	H	15.54	−4.15	32.1 (7.7)		9.84	2		
17433+1434S*	DC	10440 (234)	8.00 (0.25)	0.58 (0.15)	He	11.67	−2.77	35.7 (6.1)		8.77	2		
17471+2859*	DC	5350 (495)	8.00 (0.25)	0.57 (0.15)	He	14.58	−3.94	37.9 (7.1)		9.66	2		
17481+7052	DXP	5260 (64)	8.20 (0.02)	0.70 (0.01)	He	15.20	−4.08	6.1 (1.5)	164.7 (2.4)	9.79	2	1748+708	
17484+4503	DC	8750 (284)	8.00 (0.25)	0.58 (0.15)	He	12.64	−3.08	37.4 (6.3)		8.97	2	1747+450	
17498+8246	DA	7230 (106)	7.89 (0.07)	0.53 (0.04)	H	13.26	−3.34	15.6 (0.7)	63.9 (2.9)	9.08	1	1756+827	
17570+4052	DC	5920 (67)	8.00 (0.25)	0.59 (0.15)	H	13.91	−3.75	38.7 (6.4)		9.37	2	1755+408	
17583+1417	DA	5400 (238)	8.00 (0.25)	0.58 (0.15)	H	14.88	−3.91	22.8 (4.1)		9.55	2	1756+143	
18014+5049*	DC	4990 (103)	8.00 (0.25)	0.58 (0.15)	H	14.87	−4.05	34.0 (5.6)		9.76	2		
18073+0357*	DA	10410 (150)	8.09 (0.05)	0.65 (0.03)	H	12.17	−2.81	34.7 (1.8)		8.79	1		
18154+3158*	DA	5020 (949)	8.00 (0.25)	0.58 (0.15)	H	15.17	−4.04	41.0 (14.6)		9.75	2		
18161+2454	DAP	6920 (115)	8.00 (0.25)	0.59 (0.15)	H	13.60	−3.48	46.7 (8.0)		9.19	2	1814+248	
18171+1328	DA	5190 (203)	8.12 (0.03)	0.66 (0.02)	H	15.13	−4.05	14.2 (2.3)	70.3 (1.2)	9.79	2	1814+134	
18199+1739*	DC	4820 (677)	8.00 (0.25)	0.58 (0.15)	H	15.08	−4.11	35.1 (11.0)		9.81	2		
18205+1239	DAH	7590 (998)	7.52 (0.38)	0.35 (0.14)	H	12.37	−3.06	40.8 (0.0)	24.5 (5.5)	8.86	2	1818+126	
18213+6101	DA	4880 (49)	7.93 (0.09)	0.54 (0.05)	H	15.07	−4.05	12.8 (2.3)	78.2 (4.1)	9.74	2	1820+609	
18303+5447	DXP	6210 (101)	8.44 (0.11)	0.86 (0.07)	He	14.25	−3.94	15.0 (2.6)	66.8 (5.6)	9.68	2	1829+547	
18434+0420	DA	8900 (127)	8.21 (0.05)	0.73 (0.03)	H	12.92	−3.15	25.0 (2.1)	40.0 (3.4)	9.04	1	1840+042	
18435+2740*	DA	11060 (163)	8.10 (0.05)	0.66 (0.03)	H	12.00	−2.71	39.7 (1.3)		8.73	1	GD 381	
18510+7738*	DC:	5230 (49)	8.00 (0.25)	0.58 (0.15)	H	14.86	−3.97	30.3 (5.0)		9.65	2		
18572+2026*	DA	5350 (1009)	8.00 (0.25)	0.58 (0.15)	H	13.72	−3.93	31.7 (10.6)		9.59	2		
18575+3357	DA	12300 (186)	8.31 (0.05)	0.80 (0.03)	H	12.07	−2.65	32.8 (4.8)	30.5 (4.4)	8.74	1	1855+338	
18576+5330	DC	5570 (546)	8.00 (0.25)	0.58 (0.15)	H	14.37	−3.86	31.8 (6.3)		9.47	2	1856+534	
19001+7039	DAP	11880 (744)	8.54 (0.04)	0.93 (0.02)	He	12.69	−2.88	13.0 (2.3)	77.0 (2.3)	8.96	2	1900+705	

TABLE 3.6 – Continued

PM I	ST	$T_{\rm eff}{}^a$ (K)	log g^a	$M/M_\odot$	Comp.	M_V	log $L/L_\odot$	D (pc)	π (mas)	log τ	Fit^b	WD name	Notes
19128+5343*	DA	17870 (273)	8.32 (0.05)	0.81 (0.03)	H	11.45	−2.01	22.1 (1.1)		8.29	1		
19132+2949*	DA	6110 (114)	8.00 (0.25)	0.59 (0.15)	H	14.09	−3.69	39.9 (1.4)		9.33	1		
19136+1336	DA	13770 (337)	7.98 (0.05)	0.60 (0.03)	H	11.39	−2.26	34.4 (1.2)		8.39	1	1911+135	
19146+1428*	DA	7050 (126)	8.68 (0.14)	1.03 (0.09)	H	14.59	−3.89	35.0 (6.6)	28.6 (5.2)	9.62	1		4
19167+8044*	DA	5040 (632)	8.00 (0.25)	0.58 (0.15)	H	14.83	−4.03	35.4 (0.0)		9.74	2		
19189+3843	DC	6410 (163)	8.25 (0.06)	0.73 (0.04)	He	14.27	−3.77	11.7 (2.3)	85.5 (3.4)	9.54	2	1917+386	
	DA	15340 (245)	8.23 (0.05)	0.75 (0.03)	H	11.58	−2.22	19.8 (2.2)	50.5 (5.5)	8.43	1	1919+145	
19372+2743	DA	12490 (187)	8.03 (0.05)	0.62 (0.03)	H	11.63	−2.45	18.0 (0.9)	55.7 (2.9)	8.54	1	1935+276	
19384+3253	DA	22120 (341)	7.93 (0.05)	0.59 (0.03)	H	10.49	−1.39	34.8 (2.9)	28.7 (2.4)	7.55	1	1936+327	
19401+8348*	DC	4840 (672)	8.00 (0.25)	0.58 (0.15)	H	15.08	−4.11	38.8 (12.1)		9.81	2		
19455+4650N*	DAH:	4800 (398)	8.00 (0.25)	0.58 (0.15)	H	15.13	−4.12	27.5 (5.8)		9.82	2		
19455+1627	DA	20370 (310)	7.94 (0.05)	0.59 (0.03)	H	10.65	−1.54	42.2 (4.8)	23.7 (2.7)	7.74	1	1943+163	
19493+0747*	DA	9310 (134)	8.19 (0.06)	0.71 (0.04)	H	12.72	−3.07	36.2 (1.3)		8.98	1		
20069+6143*	DA	5540 (91)	8.00 (0.25)	0.58 (0.15)	H	14.57	−3.87	26.2 (0.2)		9.49	1		
20123+3113	DBP	15900 (2465)	8.77 (0.09)	1.07 (0.05)	He	12.59	−2.54	28.8 (3.2)	34.7 (2.7)	8.79	2	2010+310	
20139+0642	DC	6620 (133)	8.19 (0.06)	0.70 (0.04)	He	13.32	−3.68	22.4 (2.4)	44.7 (1.9)	9.45	2	2011+065	
20223+8333*	DC	5880 (713)	8.00 (0.25)	0.57 (0.15)	He	14.04	−3.77	39.3 (8.2)		9.44	2		
20300+0729*	DC	8180 (285)	8.00 (0.25)	0.58 (0.15)	He	12.79	−3.19	42.2 (7.2)		9.05	2		
20343+2503	DA	20500 (307)	8.03 (0.05)	0.64 (0.03)	H	10.77	−1.58	14.3 (0.5)	69.9 (2.7)	7.82	1	2032+248	
20491+3728	DA	14600 (282)	8.32 (0.05)	0.81 (0.03)	H	11.81	−2.36	17.3 (0.0)	57.8 (0.0)	8.55	1	2047+372	
20503+2630	DC	4940 (69)	7.11 (0.15)	0.20 (0.04)	H	13.31	−3.64	20.1 (2.6)	49.8 (3.4)	9.21	2	2048+263	
20597+5517*	DC	4530 (59)	8.00 (0.25)	0.58 (0.15)	H	15.98	−4.22	22.6 (3.6)		9.87	2		
21005+5051	DA	9680 (139)	8.05 (0.05)	0.63 (0.03)	H	12.37	−2.91	37.5 (1.4)		8.85	1	2058+506	
	DQ	9800 (4381)	8.01 (0.19)	0.59 (0.11)	He	7.30	−2.88	34.5 (6.0)	29.0 (3.5)	8.85	2	2059+316	
21020+1912	DA	6920 (108)	8.45 (0.10)	0.88 (0.06)	H	14.25	−3.75	38.3 (6.6)	26.1 (4.4)	9.57	1	2059+190	

TABLE 3.6 – Continued

PM I	ST	$T_{\rm eff}{}^a$ (K)	log g^a	$M/M_\odot$	Comp.	M_V	log $L/L_\odot$	D (pc)	π (mas)	log τ	Fit^b	WD name	Notes
21022+2457	DA	6290 (107)	8.56 (0.16)	0.95 (0.10)	H	14.82	−3.99	27.7 (3.2)	36.1 (4.2)	9.69	1	2059+247	
21077+0740*	DA	7080 (116)	8.06 (0.12)	0.63 (0.08)	H	13.57	−3.47	35.8 (1.3)		9.20	1		
21134+0727*	DA	6510 (112)	8.26 (0.15)	0.76 (0.10)	H	14.20	−3.74	24.3 (2.2)	41.1 (3.8)	9.51	1		4
21137+2621	DA	8530 (123)	8.15 (0.06)	0.69 (0.04)	H	13.00	−3.20	31.8 (3.8)	31.4 (3.7)	9.06	1	2111+261	
21189+5412	DA	14590 (238)	7.92 (0.05)	0.57 (0.03)	H	11.21	−2.12	19.7 (2.9)	50.7 (7.4)	8.28	1	2117+539	
21207+5819	DA	8090 (119)	8.03 (0.06)	0.61 (0.04)	H	13.01	−3.22	39.5 (1.4)		9.04	1	2119+581	
21222+0413*	DA	4970 (36)	8.00 (0.25)	0.58 (0.15)	H	15.07	−4.06	21.6 (3.4)		9.77	2	2119+040	
21264+5513	DA	13920 (271)	8.53 (0.05)	0.94 (0.03)	H	12.22	−2.59	36.0 (3.9)	27.8 (3.0)	8.76	1	2124+550	
21269+7338	DA	15950 (234)	7.97 (0.04)	0.60 (0.03)	H	11.13	−1.99	21.2 (1.1)	47.1 (2.4)	8.19	1	2126+734	
21337+8303	DA	17780 (264)	7.99 (0.05)	0.61 (0.03)	H	10.96	−1.81	26.0 (3.1)	38.4 (4.5)	8.03	1	2136+828	
21387+2309	DA	10130 (147)	7.93 (0.05)	0.56 (0.03)	H	12.03	−2.77	42.0 (5.5)	23.8 (3.1)	8.73	1	2136+229	
21420+2252*	DZ	8170 (150)	8.00 (0.25)	0.58 (0.15)	He	12.88	−3.20	38.9 (1.0)		9.05	2		
21426+2059	DQ	8220 (198)	7.82 (0.06)	0.47 (0.04)	He	12.75	−3.09	12.5 (0.5)	79.9 (3.2)	8.91	2	2140+207	
21429+0805*	DA	4830 (515)	8.00 (0.25)	0.58 (0.15)	H	14.74	−4.11	25.1 (6.2)		9.81	2		
21492+0415*	DA	5440 (187)	8.00 (0.25)	0.58 (0.15)	H	14.28	−3.90	26.2 (4.4)		9.53	2		
21499+2816	DB	11920 (237)	8.00 (0.14)	0.59 (0.09)	He	11.85	−2.54	35.3 (3.8)	28.3 (3.0)	8.62	1	2147+280	
21524+0223	DA	18200 (265)	8.01 (0.04)	0.63 (0.03)	H	10.95	−1.78	24.5 (1.5)	40.8 (2.5)	8.02	1	2149+021	
21551+4103*	DZA	5950 (703)	8.00 (0.25)	0.57 (0.15)	He	14.21	−3.75	37.0 (7.9)		9.42	2		
22097+1429	DA	7570 (110)	8.19 (0.06)	0.71 (0.04)	H	13.50	−3.43	25.5 (2.9)	39.2 (4.4)	9.22	1	2207+142	
22105+4532*	DC	5110 (597)	8.00 (0.25)	0.58 (0.15)	H	14.78	−4.01	34.4 (8.1)		9.71	2		
22118+5649*	DA	16880 (287)	8.11 (0.05)	0.68 (0.03)	H	11.23	−1.97	22.3 (1.2)		8.21	1		
22133+0349*	DC	4190 (323)	8.00 (0.25)	0.58 (0.15)	H	14.95	−4.36	30.4 (8.9)		9.93	2		
22141+3727	DC	6220 (115)	8.00 (0.25)	0.57 (0.15)	He	13.70	−3.67	39.0 (6.4)		9.35	2	2211+372	
22177+3707	DC	4990 (226)	8.00 (0.25)	0.58 (0.15)	H	14.99	−4.05	23.6 (4.4)		9.76	2	2215+368	
22188+4839	DA	5650 (85)	8.00 (0.25)	0.59 (0.15)	H	14.47	−3.83	26.2 (1.0)		9.44	1	2216+484	

TABLE 3.6 – Continued

PM I	ST	$T_{\rm eff}{}^a$ (K)	log g^a	$M/M_\odot$	Comp.	M_V	log $L/L_\odot$	D (pc)	π (mas)	log τ	Fit^b	WD name	Notes
22194+2122	DC	4600 (355)	8.00 (0.25)	0.58 (0.15)	H	15.62	−4.19	32.0 (7.3)		9.86	2	2217+211	
22225+1221	DC	4260 (132)	8.00 (0.25)	0.58 (0.15)	H	15.48	−4.33	36.3 (6.4)		9.92	2	2220+121	
22276+1753*	DAZ	6750 (151)	8.28 (0.23)	0.77 (0.15)	H	14.08	−3.68	30.5 (0.9)		9.48	1		
22309+1523	DA	4820 (478)	8.00 (0.25)	0.58 (0.15)	H	15.30	−4.11	32.8 (7.8)		9.81	2	2228+151	
22418+0432*	DQpec	5000 (—)	8.00 (0.25)	0.57 (0.15)	He	14.83	−4.06	43.4 (6.0)		9.78	2		
22419+1332	DA	6050 (73)	8.00 (0.25)	0.59 (0.15)	H	14.14	−3.71	42.3 (7.0)		9.34	2	2239+132	
22490+2236	DA	10470 (151)	8.66 (0.05)	1.02 (0.03)	H	13.13	−3.18	19.0 (1.5)	52.5 (4.1)	9.25	1	2246+223	
22497+3623*	DA	5430 (826)	8.00 (0.25)	0.58 (0.15)	H	15.08	−3.90	43.7 (11.0)		9.54	2		
22513+2939	DA	5640 (127)	7.58 (0.16)	0.37 (0.07)	H	13.67	−3.62	20.9 (2.4)	47.8 (4.2)	9.18	2	2248+293	
22536+8130	DC:	5200 (652)	8.00 (0.25)	0.58 (0.15)	H	14.49	−3.98	27.7 (7.4)		9.67	2	2253+812	
22541+1323	DC	4330 (117)	8.00 (0.25)	0.58 (0.15)	H	15.71	−4.30	41.1 (7.1)		9.91	2	2251+131	
22595+5717*	DA	5170 (1286)	8.00 (0.25)	0.58 (0.15)	H	15.34	−3.99	34.9 (18.2)		9.68	2		
	DA	9880 (145)	8.17 (0.06)	0.70 (0.04)	H	12.48	−2.95	36.7 (1.9)		8.90	1	2258+406	
23056+4334*	DC	4220 (1039)	8.00 (0.25)	0.58 (0.15)	H	15.86	−4.35	35.7 (44.5)		9.93	2		
23082+2414	DC	4760 (105)	8.00 (0.25)	0.58 (0.15)	H	15.15	−4.14	35.1 (5.8)		9.83	2	2305+239	
23098+5506E*	DA	5700 (86)	8.00 (0.25)	0.59 (0.15)	H	14.42	−3.82	16.2 (0.9)		9.42	1		
23121+1310	DA	5110 (113)	8.00 (0.25)	0.58 (0.15)	H	14.65	−4.01	29.8 (5.0)		9.71	2	2309+129	
23162+1720*	DC	4810 (61)	8.00 (0.25)	0.58 (0.15)	H	14.99	−4.12	35.2 (5.6)		9.81	2		
23220+0946E	DC:	4490 (356)	8.00 (0.25)	0.58 (0.15)	H	15.47	−4.24	46.7 (11.6)		9.88	2	2319+095	
23243+2835*	DA	7060 (118)	7.83 (0.13)	0.50 (0.07)	H	13.27	−3.35	38.6 (1.1)		9.07	1		
23253+1403	DA	5080 (58)	7.49 (0.08)	0.32 (0.03)	H	13.95	−3.77	22.3 (1.8)	44.9 (2.0)	9.30	2	2322+137	
23259+2552	DA	5940 (111)	8.00 (0.25)	0.59 (0.15)	H	14.23	−3.74	35.8 (1.2)		9.36	1	2323+256	
23261+1600	DC	9980 (356)	8.00 (0.25)	0.58 (0.15)	He	11.90	−2.85	35.5 (6.0)		8.82	2	2323+157.1	
23287+0514	DA	12020 (183)	8.13 (0.05)	0.69 (0.03)	H	11.84	−2.58	13.6 (0.8)	73.4 (4.0)	8.65	1	2326+049	
23315+4101	DA	16560 (257)	8.02 (0.05)	0.63 (0.03)	H	11.13	−1.95	34.1 (8.2)	29.3 (6.7)	8.17	1	2329+407	

TABLE 3.6 – Continued

PM I	ST	$T_{\rm eff}{}^a$ (K)	log g^a	$M/M_\odot$	Comp.	M_V	log $L/L_\odot$	D (pc)	π (mas)	log τ	Fit^b	WD name	Notes
23320+2658	DAH	9540 (896)	8.03 (0.28)	0.62 (0.16)	H	12.17	−2.93	38.6 (7.5)	25.9 (4.7)	8.85	2	2329+267	
23389+2101E*	DA	5300 (636)	8.00 (0.25)	0.58 (0.15)	H	14.36	−3.94	40.4 (9.5)		9.61	2		
	DA	13030 (199)	8.01 (0.05)	0.62 (0.03)	H	11.54	−2.37	17.6 (0.6)	56.8 (1.8)	8.48	1	2341+322	
23462+1158*	DC	5220 (285)	8.00 (0.25)	0.57 (0.15)	He	14.77	−3.98	34.0 (6.0)		9.71	2		
23475+0304*	DC	4900 (47)	8.00 (0.25)	0.58 (0.15)	H	15.12	−4.08	22.7 (3.6)		9.79	2		
23478+0223*	DA	5120 (48)	8.00 (0.25)	0.58 (0.15)	H	14.87	−4.01	42.7 (6.9)		9.71	2		
23489+4300*	DC:	4810 (63)	8.00 (0.25)	0.58 (0.15)	H	15.12	−4.11	36.2 (5.9)		9.81	2		
23499+2934	DA	5850 (143)	7.86 (0.14)	0.51 (0.08)	H	14.19	−3.69	21.5 (2.6)	46.5 (4.1)	9.29	2	2347+292	
23532+2051	DA	7390 (152)	8.00 (0.25)	0.59 (0.15)	H	13.10	−3.36	44.9 (7.7)		9.12	2	2350+205	
23549+4027	DQ	7200 (723)	7.65 (0.25)	0.39 (0.11)	He	12.84	−3.24	25.8 (3.8)	38.7 (5.6)	8.98	2	2352+401	

(a) The correction functions of Tremblay et al. (2013b) were applied to the values of $T_{\rm eff}$ and $\log g$.

(b) Fit: 1=Spectroscopic, 2=Photometric.

(1) Gianninas et al. (2011);

(2) D from Vennes & Kawka (2012);

(3) DXP+DA: $T_{\rm eff}$, $\log g$ and D come from Liebert et al. (1993) and belong to the DA component. The values given in Liebert et al. (1993) for the companion are $T_{\rm eff} = (16,000 \pm 2000)$ K and $\log g = 8.5 \pm 0.2$.;

(4) parallax from Dahn et al. (1982).

3.5 Physical Properties of the 40 pc Sample

The atmospheric parameters of white dwarfs within 40 pc of the Sun given in Table 3.6 represent the end result of our large spectroscopic survey undertaken in 2009, and the foundation of the homogeneous study of the local white dwarf population presented below. Although not yet complete, this sample of 460 white dwarfs should be relatively free of kinematic bias, allowing us to draw a picture of the local white dwarf population (in the northern hemisphere) to a distance twice as large as the 20 pc sample analyzed by Holberg et al. (2008), Giammichele et al. (2012), and their predecessors. We provide in the following a detailed analysis of the physical properties of this sample, but we first attempt to evaluate the completeness of the sample in order to better understand its limitations.

3.5.1 Completeness of the 40 pc Sample

We compile 460 white dwarfs within 40 pc — to within the distance uncertainties — among which 173 are new identifications. Only 144 of these stars have trigonometric parallax measurements, however, and additional measurements in the near future (e.g. by the Gaia mission) will most likely add or remove stars from this sample. Until then, we can still evaluate the completeness of the 40 pc sample by calculating the cumulative number of stars as a function of distance. The results are displayed in Figure 3.19 where the cumulative number of stars in our sample is compared to the expected number of white dwarfs assuming a space density of 4.8×10^{-3} pc^{-3}, which corresponds to the value derived from the smaller 13 pc sample, which is however believed to be complete (Holberg et al. 2008). The expected number of stars is also divided by a factor of two since our survey is restricted to the northern hemisphere. Also shown for comparison is the expected number of stars for the whole celestial sphere.

We first notice that within 20 pc, the cumulative number of stars appears to exceed the expected number of white dwarfs. However, out of the 68 stars within 20 pc in our sample, 4 are new identifications, among which only 2 are actually fitted with the spectroscopic method allowing for more robust distance measurements, while for the other 2 objects, the distances are only estimated from the photometric method under the assumption of $\log g = 8$. If we take into account the formal uncertainties in our distance measurements, the number of new identifications within 20 pc increases to 14, but here again, a robust distance estimate is available only for 2 stars. Nevertheless, these results suggest that the 20 pc sample is most likely complete, with a density consistent with the 13 pc sample - this will be confirmed when more trigonometric parallaxes become available.

Similarly, we find 120 white dwarfs within 25 pc (possibly up to 162 if we consider the

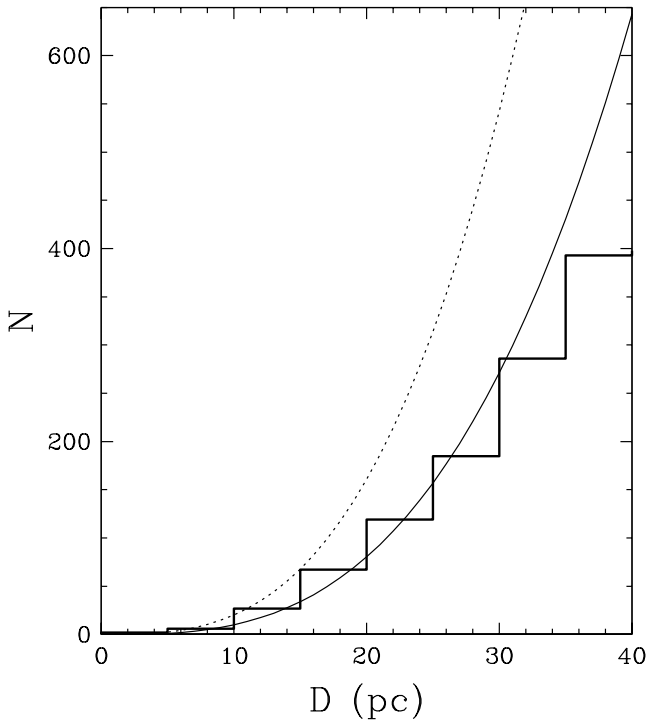

FIGURE 3.19 – Cumulative number of stars as a function of distance, for our northern hemisphere census. The solid line represents the expected number of white dwarfs in one hemisphere, assuming an average space density of 4.8×10^{-3} pc^{-3}, while the dotted line represents the expected number of white dwarfs on the whole celestial sphere.

distance uncertainties), whereas Sion et al. (2014) report a total of 224 white dwarfs for the same volume but in both hemispheres. Sion et al. (2014) estimate the completeness of their sample at 65%, which implies an expected number of white dwarfs around ∼172 in the northern hemisphere only. Hence, we are slightly below this number even if we allow for distance uncertainties. At 30 pc, the cumulative number of stars in Figure 3.19 becomes significantly less than expected (assuming that the space density of the 13 pc sample is valid everywhere) which suggests that our sample is significantly incomplete beyond this range.

By taking only the subsample of 396 stars with $D < 40$ pc from Table 3.6, we derive a space density of 3.01×10^{-3} pc^{-3}, with an upper estimate of 3.48×10^{-3} pc^{-3} if we take into account the distance uncertainties, which correspond to 63% to 73% of the density of the 13 pc sample (4.8×10^{-3} pc^{-3}). Our upper estimate is thus very close to the 77% completeness value estimated in Paper I for the present efficiency of our survey in detecting white dwarfs using reduced proper motion diagrams. However, as mentioned in Section 3.3.2, ∼330 high-priority objects still remain to be observed out of our larger list of 1180 white dwarf candidates. Results from Paper I suggested that our discovery rate dropped to 54% when stars that did not meet our best selection criteria (but with distance estimates less than 30 pc) were observed spectroscopically. Therefore, even if only 50% of the remaining 330 high-priority candidates are confirmed as white dwarfs within 40 pc of the Sun, the number of such stars could rise to more than 600, which is the expected number of objects in Figure 3.19 based on the space density at 13 pc.

We must also consider the various sources of incompleteness in our survey that can prevent the identification of all white dwarfs within 40 pc of the Sun, especially those associated with our use of the SUPERBLINK catalog as the primary source of candidates. First, our selection excludes stars fainter than $V = 19$ since the rate of spurious detection in SUPERBLINK increases significantly at fainter magnitudes. Stars are also excluded if they have non-standard magnitudes for a white dwarf, a good example of which are Sirius-like systems, which are completely overlooked in our selected sample. In Sirius-like systems, as opposed to binary systems where the companion is an M dwarf, the flux is completely dominated by the main sequence star. In the 20 pc sample of Giammichele et al. (2012), there are 7 Sirius-like systems,

all of which are in the southern hemisphere, with the exception of Procyon B (0736+053), while in Holberg et al. (2013), there are 6 Sirius-like systems with $D < 40$ pc in the northern hemisphere only. As expected, none of these were recovered by our selection criteria. We note, however, that 5 of these 6 systems were included in our analysis afterward; 0911+023 at 34.8 pc was let aside, however, since it is unresolved with a B star. The Sirius-like systems thus represent 3% of the white dwarf population within 25 pc, and we may expect that ∼13 of these systems are missed in the 40 pc sample. In Table 3.4, 5 other stars were missed because of their inaccurate colors, or because of a mismatch with SDSS and/or 2MASS magnitudes.

Some white dwarfs were also missed simply because they are not in the SUBERBLINK catalog to begin with. Stars with proper motions < 40 mas yr^{-1} would of course not be part of our selection, but there are other cases where stars might be missing from the catalog. To be included in SUPERBLINK, a star must either be a TYCHO-2 or Hipparcos catalog stars, or it must be detected as a high proper motion stars on the digitized POSS I and II plates. As discussed by Lépine & Shara (2005), SUPERBLINK is less efficient at recovering stars with bright saturated cores on those plates, leaving some bright stars out. Thus we note that 3 of the 4 WD + M dwarf systems known to be within 40 pc were missed, in particular HZ 9, Case 1, and GD 325, which are all brighter than $V = 13$ at I_N. In Table 3.4, 16 very bright white dwarfs could also not be found in the published version of the SUPERBLINK catalog of Lépine & Shara (2005), and are thus also missing from our candidate list.

Finally, some stars can also be overlooked because of missing or inaccurate tabulated photometry in SUPERBLINK, most often due to faulty optical magnitudes from the USNO-B1.0 catalog counterpart. Because our selection criteria and distance estimates are based on empirical V magnitudes derived from USNO-B1.0 magnitudes, the estimated distances can be severely affected if the B_J, R_F, and I_N are inaccurate by more than the adopted 0.5 mag value. We actually identified 2 known white dwarfs that were not recovered in the USNO-B1.0 catalog, and 11 white dwarfs were also excluded from our candidate list because we estimated a distance larger than 55 pc. All in all, about 3% of the stars in Table 3.4 are missed in this manner.

Taking into account all the sources of incompleteness, we estimate that, to the best of our

knowledge, some 50 white dwarfs have probably been overlooked by our survey, for a ratio of missed-to-found of 17%, a value consistent with the apparent 77% efficiency of our survey at detecting white dwarfs, as discussed above. With these limitations in mind, we provide a detailed statistical analysis of our sample knowing that ∼30% of the white dwarfs might still be missing from our sample. Nevertheless, even if our 40 pc sample cannot be analyzed as thoroughly as the 20 pc sample, the small number statistics problem inherent to the 20 pc sample discussed by Giammichele et al. (2012) has been significantly improved.

3.5.2 Kinematics of the 40 pc Sample

Before interpreting the global properties of the 40 pc sample, we must first verify if the sample is relatively free of kinematic bias, which we do by examining its velocity-space distribution. The velocity components (U, V, W) are determined from the photometric distances (or trigonometric parallaxes when available) and proper motions for each star. Since radial velocities are not available for most of the stars in our sample, we assume $V_{\rm rad} = 0$, but in order to obtain an unbiased representation of the motion of the stars in our sample despite this approximation, we use the method described in Lépine et al. (2013). We first evaluate the (X, Y, Z) positions of the stars in the Galactic reference frame and then we use the fact that $U \propto \frac{X}{D} V_{rad}$, $V \propto \frac{Y}{D} V_{rad}$ and $W \propto \frac{Z}{D} V_{rad}$ to obtain the (U, V, W) velocity components. However, if $|X| > |Y|$ and $|X| > |Z|$, then the position vector as well as the radial velocity vector mainly points toward the X direction, so the radial velocity mainly contributes to the U component of velocity, but its contribution to the V and W components of velocity is small. Then, the $V_{rad} = 0$ approximation is valid to obtain *estimates* for the velocity components V and W, but not for U. Likewise, stars with the largest $\pm Y$ components (or $\pm Z$ components) are good tracers of the velocity dispersion in U and W (or U and V), even if their radial velocities are not known. We can then estimate in this manner at least two velocity components for each star, and the component that depends the most on the radial velocity is excluded from any representation or statistical calculation.

Our results are displayed in Figure 3.20. For reasons outlined in the previous paragraph,

each star appears in a single panel only. The mean values of the velocity components are

$$\langle U \rangle = -9.82,\ \sigma_U = 41.00 \text{ km s}^{-1}$$

$$\langle V \rangle = -26.58,\ \sigma_V = 29.46 \text{ km s}^{-1}$$

$$\langle W \rangle = -8.26,\ \sigma_V = 17.37 \text{ km s}^{-1}$$

which happen to be in relative agreement with those reported by Fuchs et al. (2009) for stars

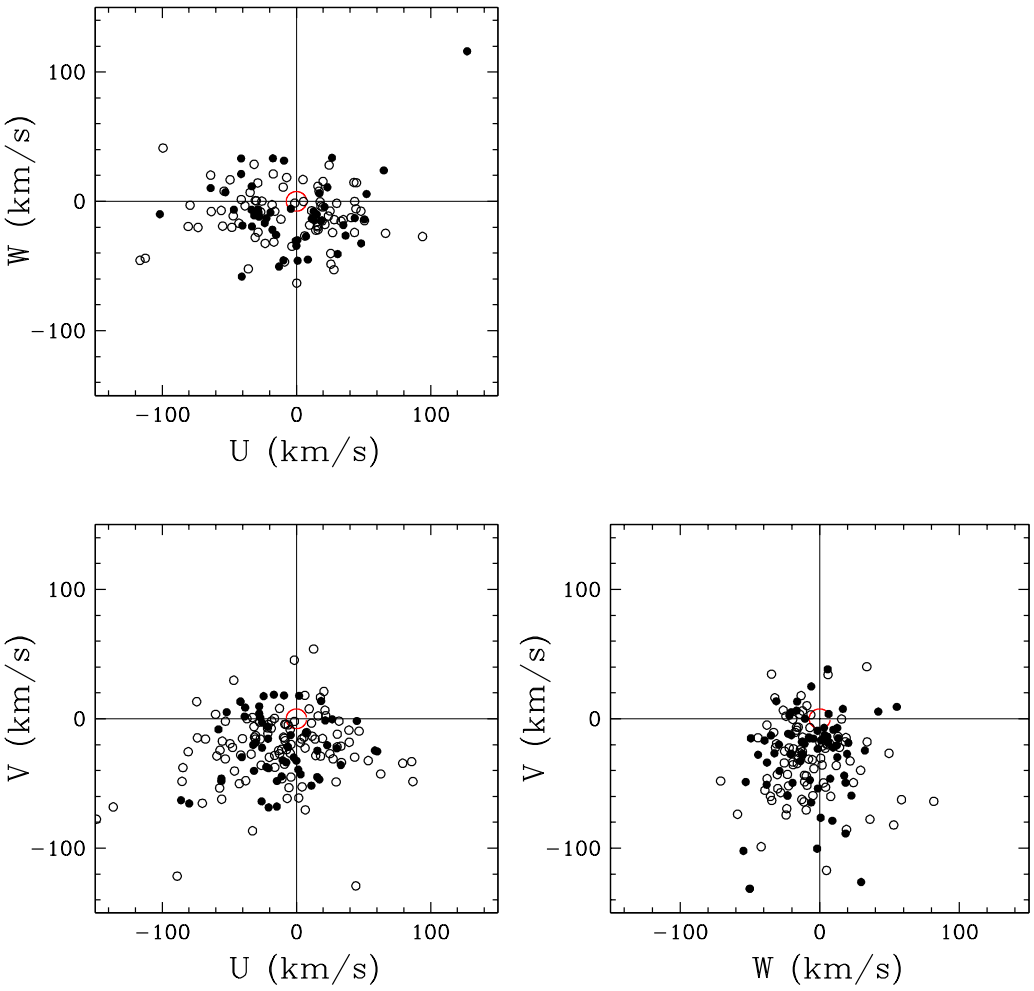

FIGURE 3.20 – Velocity-space projections for the white dwarfs within 40 pc of the Sun. Velocities are calculated assuming $V_{\rm rad} = 0$, and using only the projections having the smallest contribution to $V_{\rm rad}$. Each star is thus displayed in one panel only. The new white dwarf identifications are plotted with solid circles, while those already known in the literature are shown with by open circles; the red circles at $(0, 0)$ indicate our limit of detection.

in the SDSS belonging to the thin disk: $\langle U \rangle = -8.6$ and $\sigma_U = 32.4$ km s^{-1}, $\langle V \rangle = -20.0$ and $\sigma_V = 23.0$ km s^{-1}, and $\langle W \rangle = -7.1$ and $\sigma_V = 18.1$ km s^{-1}. If we consider only the new white dwarf identifications (shown as solid circles in Figure 3.20), the space velocities we derive are of the same order, $\langle U \rangle = -8.09$ and $\sigma_U = 34.27$ km s^{-1}, $\langle V \rangle = -23.98$ and $\sigma_V = 27.87$ km s^{-1}, and $\langle W \rangle = -6.85$ and $\sigma_V = 19.31$ km s^{-1}, but we still notice the presence of "holes" in the distribution of new white dwarfs near $(U, W) = (0, 0)$ and $(U, V) = (0, 0)$ when compared to the velocity distribution of known white dwarfs. The red circle in each panel of Figure 3.20 represents the presumed kinematic limit of our survey due to the $\mu > 0\farcs04$ yr^{-1} proper motion limit and $D < 40$ pc distance range, which corresponds to a transverse motion $v_T = 4.74\,\mu D = 7.6$ km s^{-1}. In *Hipparcos*, 2.3% of the stars fainter than $V \sim 9$ with $\delta > 0$ and $\pi > 0\farcs25$ yr^{-1} ($D < 40$ pc) have $\mu > 0\farcs04$ yr^{-1}, implying that we are only missing ∼11 white dwarfs within 40 pc because of the presumed kinematic limit of our survey. We also notice that the holes are larger than our presumed limit of detection, implying that some low-velocity white dwarfs are probably still hiding in our list of candidates, awaiting spectroscopic confirmation.

We find no white dwarfs in our 40 pc sample that appear reliably old enough to belong to the halo population of old stars. This is consistent with the Sion et al. (2014) study of the 25 pc sample, where no definite halo white dwarf was found either. Our only possible halo candidates are the two DC stars cool enough to be very old, however we cannot be certain of their age because we assumed $\log g = 8.0$ by default for these stars, and an accurate cooling age can only be obtained when the stellar mass is known. Another possible candidate is the star 19401+8348, seen in the upper right corner of the (U, W) diagram in Figure 3.20, which has relatively high velocity components compared to the other stars in the diagram. This object is a DC star with $T_{\rm eff} \sim 4800$ K and a distance of $D = 38.8 \pm 12$ pc, for which we also assumed $\log g = 8.0$, which means its cooling age remains uncertain. Even if we extend our search to stars with $D > 40$ pc (not shown in Figure 3.20), we do not find any white dwarf that would reliably appear old enough to be a member of the halo population. This is however not inconsistent with the single-point luminosity function of Fontaine et al. (2001) based on the two halo white dwarfs 2316−064 and 1022+009, from which we estimate $n(L) = 10^{-5.39}$

pc^{-3} M_{bol}^{-1} at $\log L/L_{\odot} \sim -4.09$ (T_{eff} ∼5000 K), which predicts the existence of only a single halo white dwarf within 40 pc of the Sun in this particular luminosity range.

3.5.3 Mass Distribution

The mass distribution for the white dwarfs in Table 3.6 with $D \lesssim 40$ pc is displayed in Figure 3.21 as a function of effective temperature. Only those with a measured mass are shown here (254 out of 460 objects from Table 3.6); the objects with an assumed value of $\log g = 8$ are shown at the bottom of the figure. These include the coolest DA stars with weak hydrogen lines analyzed spectroscopically, most of the magnetic white dwarfs, and all non-DA stars analyzed photometrically but without trigonometric parallax measurements. Since most of our new identifications do not have trigonometric parallaxes available yet, the number of cool helium-rich white dwarfs with mass measurements is rather small in this figure; compare for instance with the mass distribution displayed in Figure 21 of Bergeron et al. (2001), which includes all cool white dwarfs with trigonometric parallax measurements available at that time. There, 54 out of 150 white dwarfs (or 36%) had helium-rich atmospheres, compared to 38 out 255 (or 15%) in Figure 3.21. In fact, most cool helium-atmosphere white dwarfs with mass determinations come from the 20 pc sample. The situation will of course change significantly when the Gaia mission is completed.

The mass distribution for the same subset of white dwarfs, and for all effective temperatures, is displayed in Figure 3.22, where the separate contributions of hydrogen- and helium-rich stars are also shown. This distribution can be contrasted with that shown in Figure 21 of Giammichele et al. (2012) for the 20 pc sample. Here again we see that the helium-atmosphere white dwarfs in the 40 pc sample are significantly undersampled in the cumulative mass distribution. The relative number of helium- to hydrogen-rich objects in our sample is small, but we observe that the median masses and mass dispersions of both subsamples are generally comparable. The *mean mass* of the hydrogen-rich sample, however, is nearly 0.04 $M_{\odot}$ larger than the helium-rich counterpart. This is mostly due to the prominent high-mass tail observed in the distribution of hydrogen-atmosphere white dwarfs. To better illustrate this feature, we contrast in Figure 3.23 the mass distribution of the 40 pc sample with that of the 20 pc

sample from Giammichele et al. (2012), which is based on both spectroscopic and photometric mass measurements, and with the spectroscopic mass distributions of DA stars from the SDSS (Tremblay et al. 2011a) and from the WD catalog (Gianninas et al. 2011). The excess of high mass white dwarfs in the 40 pc sample is quite obvious, a result that strongly suggests we are successfully recovering the high-mass, less luminous white dwarfs, which are often missed in magnitude-limited surveys (see, e.g., Liebert et al. 2005 in the case of the PG survey, and in particular their discussion of Figure 13). This excess of massive white dwarfs seems to be related to the population of low temperature white dwarfs apparent in Figure 3.21, between roughly $T_{\rm eff} = 6000$ K and 7000 K. These are all DA stars for which the atmospheric para-

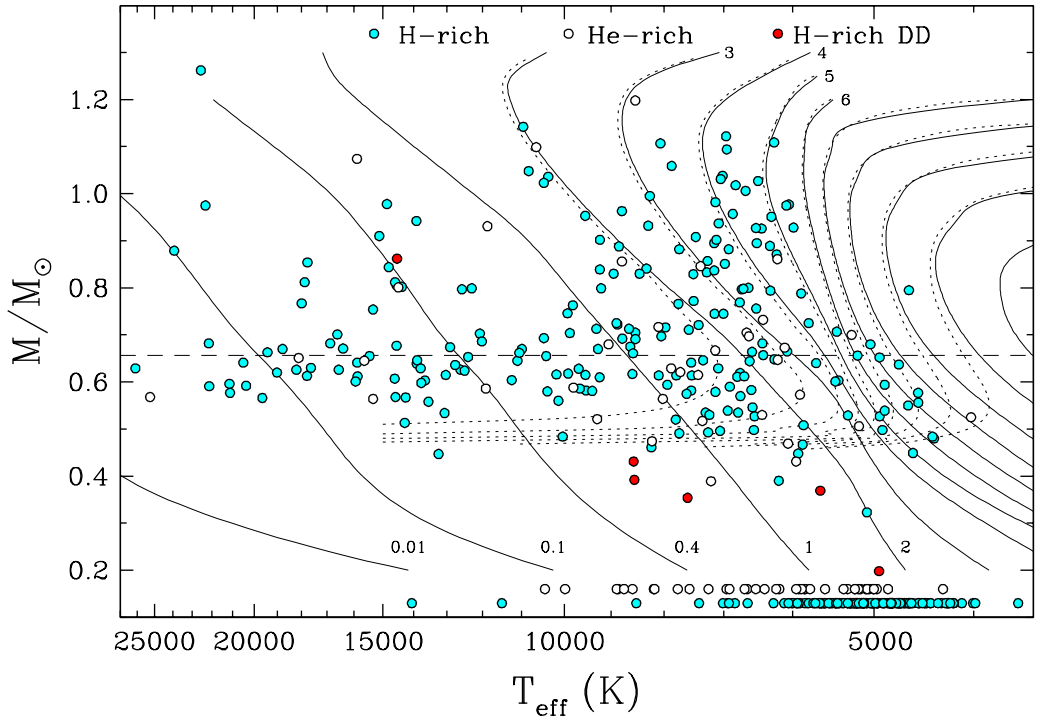

FIGURE 3.21 – Mass as a function of effective temperature for the 254 white dwarfs in the 40 pc sample with mass determinations; the 204 white dwarfs fitted with an assumed $\log g = 8.0$ value are displayed at the bottom the figure. Also shown are theoretical isochrones for our C/O core evolutionary models with thick hydrogen layers labeled in Gyr; solid lines correspond to white dwarf cooling ages only, while the dotted lines also include the main sequence lifetime. The dashed line represents a 0.655 $M_{\odot}$ sequence, which corresponds to the median mass of our sample.

meters — and in particular $\log g$ and thus M — have been determined spectroscopically. It is thus legitimate to question the validity of the spectroscopic masses in this particular range of temperature. As discussed in Tremblay et al. (2010) — see in particular their Figure 14 (panel b) and Section 5.1 — the strength of the hydrogen lines in this temperature regime is particularly sensitive to the *neutral particle interactions* in the description of the occupation probability formalism, and a slight change in the hard sphere radius in this case may result in significantly lower $\log g$ values. Indeed, Bergeron et al. (1991) found that a direct implementation of the Hummer-Mihalas occupation probability formalism yields $\log g$ values that are too low in the regime where non-ideal effects become dominated by neutral interactions ($T_{\rm eff} \lesssim 8000$ K), a problem that could be overcome by simply dividing the hydrogen radius

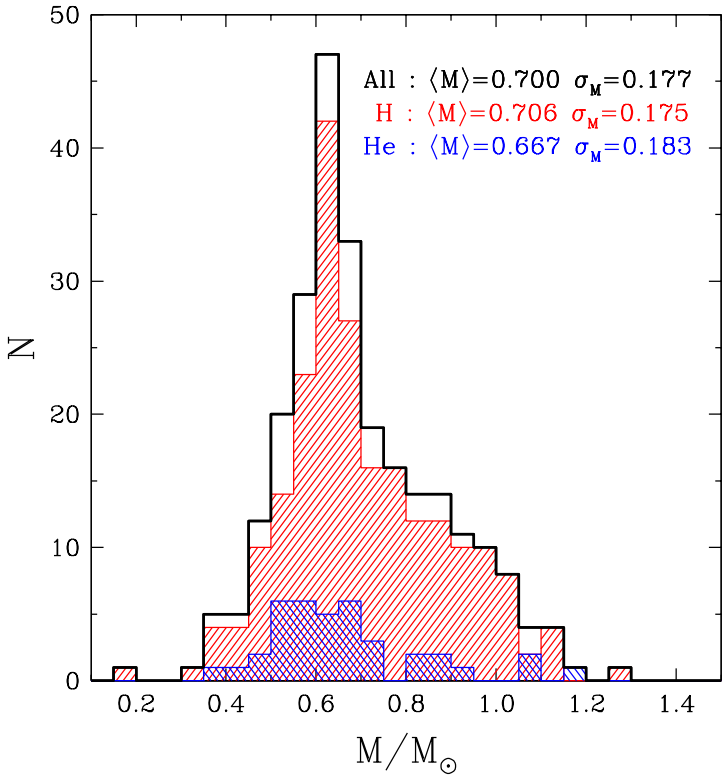

FIGURE 3.22 – Mass distribution for the white dwarfs in our sample that have mass determinations. The thick solid line histogram shows the distribution for the 255 stars with $D < 40$, while the red and blue shaded histograms correspond, respectively, to the subsamples of 217 hydrogen- and 38 helium-atmosphere white dwarfs. The corresponding mean values and standard deviations are given in the figure.

by a factor of two to reduce the non-ideal effects for the higher lines of the Balmer series (this is the factor actually used in our models). At the same time, we also notice in Figure 3.21 that the mass distribution near $\sim$0.6 $M_{\odot}$ in the same temperature range, and below, appears perfectly normal, suggesting that the model spectra are properly calibrated. Hence the high mass tail observed in Figure 3.22 might be real after all. Clearly, a detailed comparison of mass measurements derived from spectroscopy and *precise* trigonometric parallaxes in this range of temperature should shed some light on this result. Finally, we also note in Figure 3.21 an abrupt cutoff of massive white dwarfs below $\sim$6000 K, but this is certainly due to the fact that cooler objects would appear as DC stars (or weak DA stars) whose masses can only be determined from the photometric method using trigonometric parallax measurements, which are currently unavailable. Hence it is possible that this high mass tail extends to even lower temperatures.

Also superposed on the mass distribution shown in Figure 3.21 are the theoretical isochrones for our C/O core evolutionary models with thick hydrogen layers, as well as the corresponding isochrones with the main sequence (MS) lifetime taken into account; here we assume for simplicity (see Wood 1992) $t_{\rm MS} = 10(M_{\rm MS}/M_{\odot})^{-2.5}$ Gyr and $M_{\rm MS}/M_{\odot} = 8\ln[(M_{\rm WD}/M_{\odot})/0.4]$. In the 20 pc sample of Giammichele et al. (2012), the 5 stars older than 8 Gyr (among which the oldest is 9.5 Gyr old) are all located in the southern hemisphere, and they are thus not included in our sample. The oldest white dwarf in Figure 3.21 is only $\sim$8 Gyr old, although we see that there are plenty of objects without mass determinations that may be significantly older. The isochrones that include the MS lifetime reveal that white dwarfs with $M \lesssim 0.48$ $M_{\odot}$ cannot have C/O cores, and yet have been formed from single star evolution within the lifetime of the Galaxy. Some, and probably all, of the low-mass white dwarfs in Figure 3.21 must be unresolved double degenerate binaries with helium cores, i.e. the result of common envelope evolution. The known double degenerate systems are identified in Figure 3.21. Three of these low-mass white dwarfs (with $\delta > 0$), 0101+048, 2048+263, and 2248+293, have already been discussed in Giammichele et al. (2012), while we identify here (with $M < 0.45$ $M_{\odot}$) 01294+1023 (0126+101, DD, Bergeron et al. 2001), 13309+3029 (1328+307, DZ), 15555+5025 (1554+505), 18205+1239 (1818+126, DD, Berge-

ron et al. 2001), 23253+1403 (2322+137), and 23549+4027 (2352+401, DQ). Not surprisingly, all of these were already known in the literature since these objects, with their large radii and high luminosities, can easily be detected in most surveys.

The mean mass of the 40 pc sample (with mass determinations) is $\langle M \rangle = 0.700\ M_{\odot}$ with a standard deviation of $\sigma_M = 0.177\ M_{\odot}$ (Figure 3.22). These values are significantly larger than those reported by Giammichele et al. (2012) for the 20 pc sample, $\langle M \rangle = 0.650\ M_{\odot}$ and $\sigma_M = 0.161\ M_{\odot}$. Our higher mean mass is actually due to the hydrogen-rich white dwarfs in the 40 pc sample, with $\langle M_{\rm H} \rangle = 0.706\ M_{\odot}$, while Giammichele et al. obtained $\langle M_{\rm H} \rangle = 0.650\ M_{\odot}$. However, the mean masses for the helium-atmosphere white dwarfs are quite comparable, $\langle M_{\rm He} \rangle = 0.667\ M_{\odot}$ and $0.660\ M_{\odot}$, respectively, which also compare really well with the mean mass for DB stars determined spectroscopically by Bergeron et al. (2011), $\langle M_{\rm H} \rangle = 0.671\ M_{\odot}$.

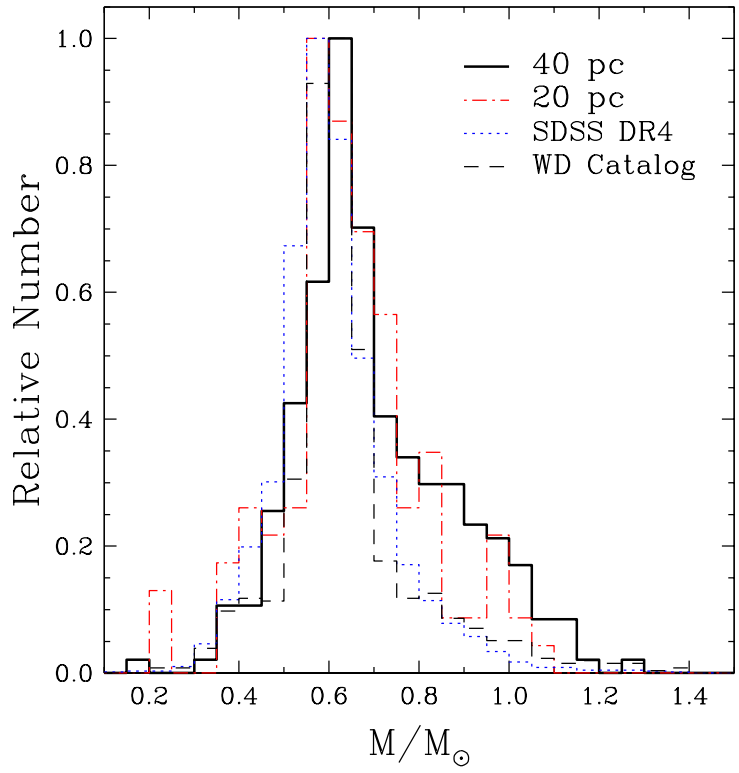

FIGURE 3.23 – Mass distribution for the white dwarfs in the 40 pc sample with mass determinations, compared with the mass distribution for the 20 pc sample (Giammichele et al. 2012), for the DA stars in the SDSS DR4 (Tremblay et al. 2011a), and for the DA stars in the WD Catalog (Gianninas et al. 2011).

As mentioned above, the mass distribution of the 40 pc sample also peaks at larger mass values than the 20 pc sample, although it is comparable to the peak value obtained by Gianninas et al. (2011) for the DA stars in the WD catalog of McCook & Sion, also reproduced in Figure 3.22.

3.5.4 Evolution of the Surface Composition

Since the photometric data set for the 40 pc sample is not as accurate as that of the 20 pc sample, it is not yet possible to study the evolution of the surface composition as a function of temperature in as much detail as in Bergeron et al. (1997, 2001), for instance (see also Bergeron et al. 2013). Also, since trigonometric parallax measurements are not available for most of the new white dwarfs identified in the 40 pc sample, stellar masses cannot be determined for these objects either. It is still possible, however, to examine the spectral evolution of the white dwarfs in our sample by ignoring this second parameter, and by remembering that our temperature scale remains somewhat uncertain for some stars, in particular those that have only USNO-B1.0 photographic magnitudes available. The distribution of the main spectral types (DA, DC, DQ, DB, and DZ) as a function of effective temperature is displayed in Figure 3.24; the only 2 white dwarfs missing from this figure are the DXP stars 17481+7052 (1748+708, G240-72) and 18303+5447 (1829+547, G227-35). We can see that, as expected, the local sample is dominated by cool white dwarfs (see also Figure 3.21), with the typical rise in the number of cool DA and DC stars — the dominant spectral types here — expected at the faint end of the luminosity function. We notice that the sudden drop in the number of DA stars below $T_{\rm eff}$ $\sim$5000 K is largely compensated by the significant increase in the number of DC stars in the same temperature range, which suggests that several of these DC stars probably have hydrogen-rich atmospheres. Many of them might even reveal the presence of Hα when observed at even larger signal-to-noise ratios using 4 to 10-m class telescopes, as demonstrated for instance by Greenstein (1986) or Bergeron et al. (1997).

While no DB stars were reported in the 20 pc sample studied by Giammichele et al. (2012), the 40 pc sample now includes 7 DB stars — 00051+7313 (0002+729), Feige 4 (0017+136), KUV 05034+1445 (0503+147), GD 325 (1333+487), 16473+3228 (WD 1645+325), 20123+2338

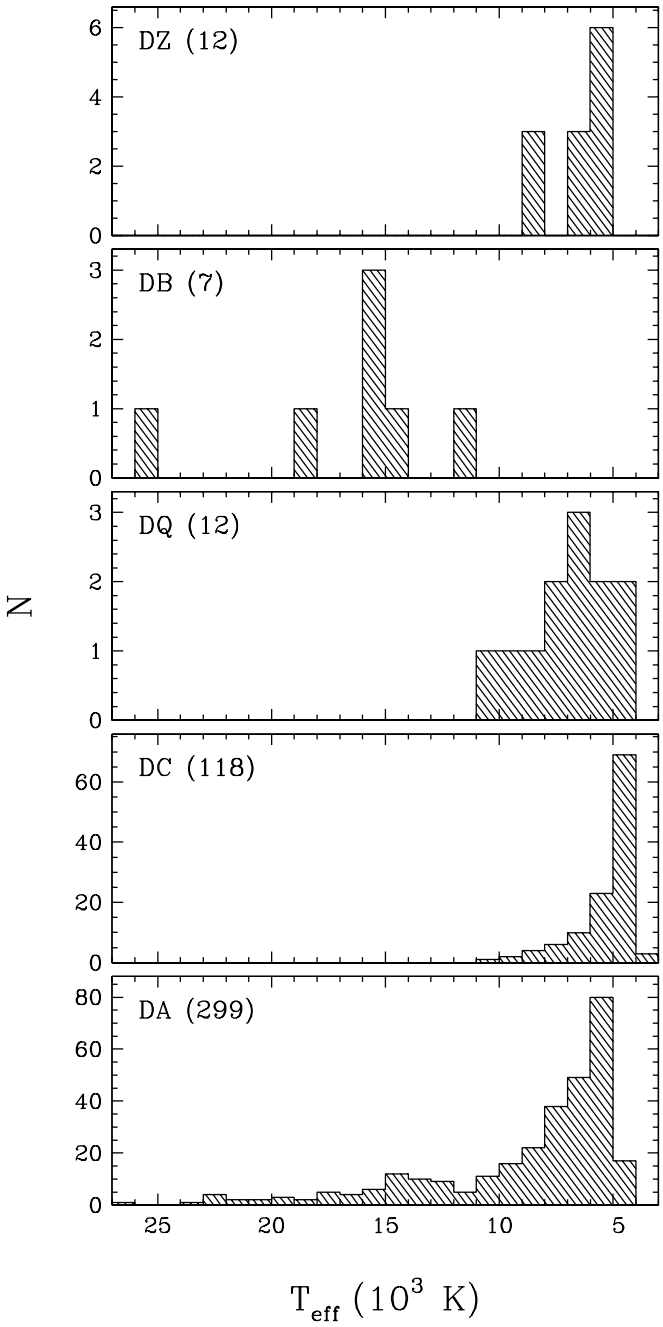

FIGURE 3.24 – Distribution of the various spectral types for the white dwarfs in the 40 pc sample as a function of effective temperature. The number of stars of each spectral type is indicated in the panels.

(2010+310) and 21499+2816 (2147+280) — and none of these correspond to new detections. DQ and DZ stars are rather rare in our sample, representing only 6% of all white dwarfs below $T_{\rm eff}$ $\sim$12,000 K, but still 40% of all helium-atmosphere white dwarfs in the $6000 - 12,000$ K temperature range (the spectral type alone below 6000 K is not sufficient to infer the chemical composition). While it is difficult to misclassify a DQ star in our sample, in particular at low temperatures where the C_2 Swan bands are usually the strongest, a significant number of DZ stars might still be present among the 118 cool DC stars in our sample due to the lack of appropriate spectral coverage, resolution, or signal-to-noise ratio of our spectroscopic observations.

As discussed in the Introduction, it is now believed that most, if not all, cool DC stars with $T_{\rm eff} \lesssim 5000$ K probably have hydrogen-rich atmospheres, a result based on a reanalysis of the existing photometry with model atmospheres that include the red wing opacity from Lyα (this excludes DQ and strong DZ stars in the same temperature range, which obviously have helium-dominated atmospheres). We have 4 white dwarfs below 5000 K in Figure 3.21 with helium atmospheres, 2 of which are known in the literature and only one with trigonometric parallax, and thus mass measurements. For some of these objects, we do not even have a spectrum near Hα, and in some other cases the photometry is clearly suspicious, in particular at JHK. Hence for all 4 stars, the pure hydrogen solution would be equally acceptable. We thus reaffirm the conclusion first made by Kowalski & Saumon (2006), and supported by Giammichele et al. (2012), that most cool DC stars probably have hydrogen atmospheres.

One of the most puzzling results of our analysis is displayed in Figure 3.25 where we show in the left panel the total number of stars as a function of effective temperature per bin size of 2000 K, as well as the individual contribution of the hydrogen-atmosphere white dwarfs, while we show in the right panel the ratio of helium-atmosphere white dwarfs to the total number of stars. As mentioned in the previous paragraph, the results below $T_{\rm eff} = 5000$ K should be considered with caution. The results above this temperature, however, are fairly robust since most solutions are constrained by the presence or absence of Hα when the photometric method is used, or in the case of hotter DA stars, the atmospheric parameters have been obtained from the spectroscopic method. Above 15,000 K, the fraction of helium-atmosphere white dwarfs

is around 20%, in excellent agreement with the fraction of DB stars found in the PG survey, as determined by Bergeron et al. (2011). In the $13,000 - 15,000$ K temperature range, this fraction drops to only 5%, although the total number of helium-rich stars in this temperature bin is admittedly small (see left panel). Below 13,000 K, the fraction of helium-atmosphere white dwarfs gradually increases towards lower temperatures, and keeps increasing to a ratio around $\sim$25% in the $7000 - 9000$ K temperature range. Even though this trend is entirely consistent with the results reported by Giammichele et al. (2012, see their Figure 20) for the 20 pc sample, the fraction of helium-atmosphere white dwarfs reaches a much higher value around 40% in the 20 pc sample. To better understand this discrepancy, we show in Figure 3.26 similar results as those displayed in Figure 3.25 but only for temperatures in the range $7000 < T_{\rm eff} < 9000$ K and this time as *a function of distance*. Below 20 pc, we recover the

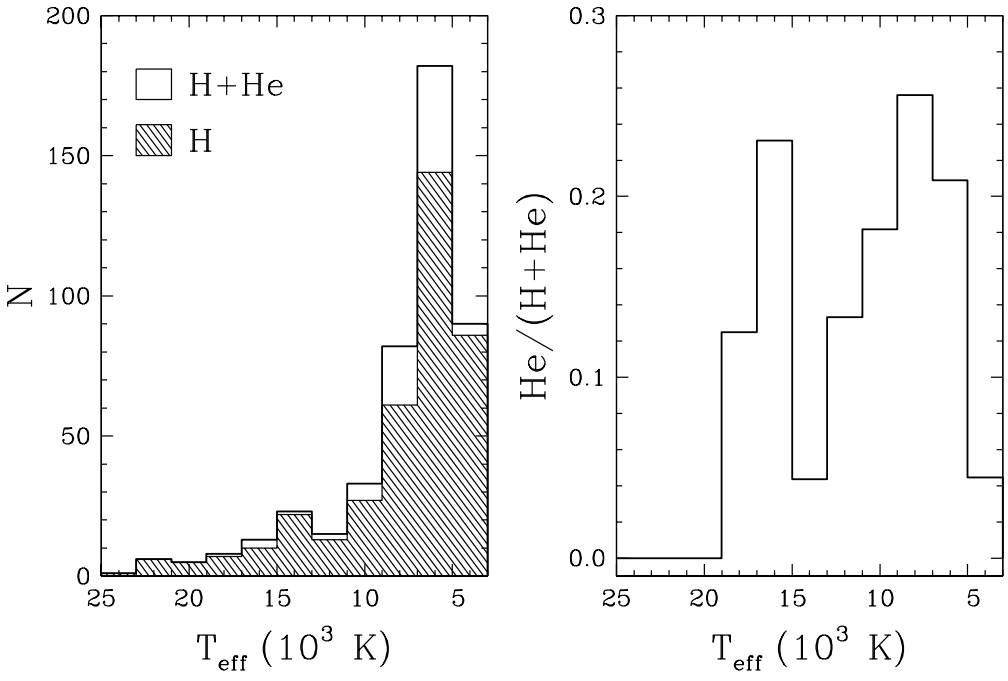

FIGURE 3.25 – Left panel: total number of white dwarfs (solid-line histogram) and hydrogen-atmosphere white dwarfs (hatched histogram) as a function of effective temperature. Right panel: ratio of helium-atmosphere white dwarfs to the total number of stars as a function of effective temperature.

results of Giammichele et al. (2012) almost perfectly, but beyond this distance, the fraction of helium-atmosphere white dwarfs drops abruptly. By looking at the results shown in the left panel of Figure 3.26, we can see that the 20 pc sample probably suffers from small number statistics, and that these statistics become more significant at larger distances. Otherwise, we cannot think of a single bias in our survey that would produce such a trend, either in favor of DA stars beyond 20 pc, or against non-DA stars. We thus believe that the peak value near 40% reported by Giammichele et al. was overestimated.

In Giammichele et al. (see also Tremblay & Bergeron 2008), the increase in the fraction of helium-atmosphere white dwarfs at lower temperatures was interpreted as the result of convective mixing, where the thin convective hydrogen atmosphere is mixed with the deeper and more massive helium convection zone. Since the fraction of helium-atmosphere white

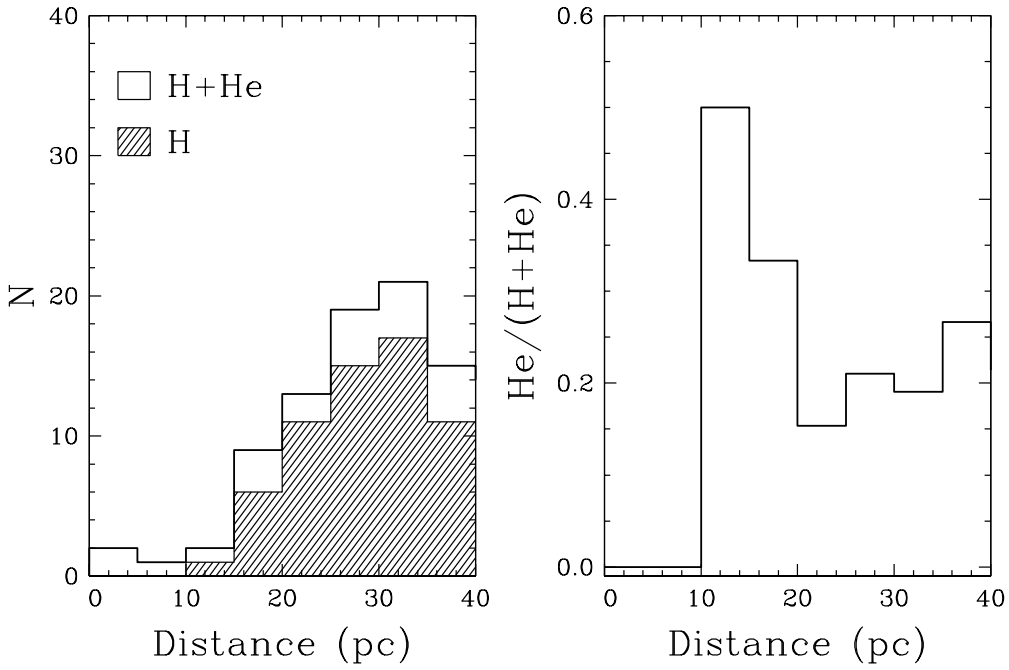

FIGURE 3.26 – Left panel: total number of white dwarfs in the 7000 − 9000 K temperature bin (solid-line histogram) and hydrogen-atmosphere white dwarfs (hatched histogram) as a function distance. Right panel: ratio of helium-atmosphere white dwarfs to the total number of stars in the same temperature bin as a function of distance.

dwarfs at low temperatures in our sample is now consistent with that of DB stars at higher temperatures (here and in the PG sample), there appears to be little evidence that convective mixing ever occurs in cool DA stars, at least in the temperature range considered here. This in turn implies that DA stars have fairly thick hydrogen layers of the order of $M_{\rm H}/M_{\rm tot} \sim 10^{-6}$ (see Figure 1 of Tremblay & Bergeron 2008). This revised conclusion is a direct consequence of our analysis of a more statistically significant, volume-limited sample.

Finally, as discussed in the Introduction, Bergeron et al. (1997, 2001) suggested the presence of a non-DA gap (or deficiency) between $T_{\rm eff}$ ∼5000 K and 6000 K where most stars appear to have hydrogen-rich compositions, while helium-atmosphere white dwarfs exist above and below this temperature range (see also Bergeron et al. 2013). While we have indeed very few (∼3) helium-atmosphere white dwarfs in Figure 3.21 with a mass determination in this particular range of temperature, our sample still contains a significant number of such helium-rich stars without mass determinations. However, as mentioned before, the photometric data for most of these objects are not accurate enough to pinpoint their temperature with sufficient precision, and we will thus refrain from further interpreting the presence or absence of this non-DA gap in our sample at this stage.

3.5.5 Luminosity Function

As discussed in the Introduction, one of the major goals of our spectroscopic survey is to provide an improved determination of the cool end of the white dwarf luminosity function (WDLF), as statistically complete as possible, which can then be compared to those obtained from magnitude-limited surveys, from large photometric and spectroscopic surveys like the SDSS, or from the volume-limited sample of white dwarfs within 20 pc of the Sun. The WDLF is a measure of the number of stars per pc^3 per unit of bolometric magnitude, which can be obtained in our case using the bolometric magnitude of each white dwarf within 40 pc of the Sun and with $\delta > 0$ derived from the spectroscopic or photometric results provided in Table 3.6. The bolometric magnitudes can be obtained from the luminosity of each star given in the table ($\log L/L_{\odot}$) and the simple relation $M_{\rm bol} = -2.5 \log L/L_{\odot} + M_{\rm bol}^{\odot}$, where $M_{\rm bol}^{\odot} = 4.75$ is the bolometric magnitude of the Sun. We present here an *observed luminosity function*, in the

sense that we do not attempt to apply any correction due to the incompleteness of our survey. Each object in the sample is then simply added to the appropriate bolometric magnitude bin, and the overall results are divided by the volume defined by a 40 pc half-sphere. Since the WDLF requires a proper account of the number of individual stars in each magnitude bin, the confirmed and suspected double degenerate binary systems are counted as two stars. Also, in order to obtain the most accurate mass density as possible, we deconvolve the individual masses of each system by using the procedure described in Section 6.4 of Giammichele et al. (2012). Doing so, our luminosity function now includes a total of 460 individual white dwarfs. The luminosity function for the white dwarfs within 40 pc of the Sun is presented in Figure 3.27 (the approximate temperature scale for a 0.6 $M_{\odot}$ evolutionary sequence is shown at the top of the figure). Our results are also compared with those obtained by Giammichele et al. (2012) for the 20 pc sample, by Harris et al. (2006) for white dwarfs in the SDSS, and by Bergeron et al. (2011) for the DA and DB stars in the PG survey. Also superposed in the figure are theoretical luminosity functions from Fontaine et al. (2001) for a total age of 10, 11, and 12 Gyr, normalized to our own observational results between $M_{\rm bol} = 12 - 14$. These were obtained, as explained in Fontaine et al. (2001), with a constant star formation rate (SFR), a classic Salpeter initial mass function (IMF, $\phi = M^{-2.35}$), an initial-to-final mass relation (IFR) given by $M_{\rm WD} = 0.4\, e^{0.125M}$, and a main sequence lifetime law given by $t_{\rm MS} = 10M^{-2.5}$ Gyr (M and $M_{\rm WD}$ are in solar units).

If the SFR is constant, we expect a monotonous rise of the luminosity function, as shown by the theoretical curves. Alternatively, bursts in star formation would show up as bumps in the luminosity function. Our WDLF displayed Figure 3.27 shows a definite bump near $M_{\rm bol} \sim$10. A similar bump was also observed in the WDLF determined by Giammichele et al. (2012, see their Figure 22) for the 20 pc sample, but this peculiar result was attributed by the authors to small number statistics. Here we have more than tripled the number of stars in the magnitude bins of interest, and the result now appears to be statistically significant. The first two points at $M_{\rm bol} = 8$ and 9 have error bars that are still large enough to be consistent with the theoretical expectations, but the points at $M_{\rm bol} = 10$ and 11 are solid determinations. This particular feature in the WDLF can also be observed *directly* in Figure 3.25 and in

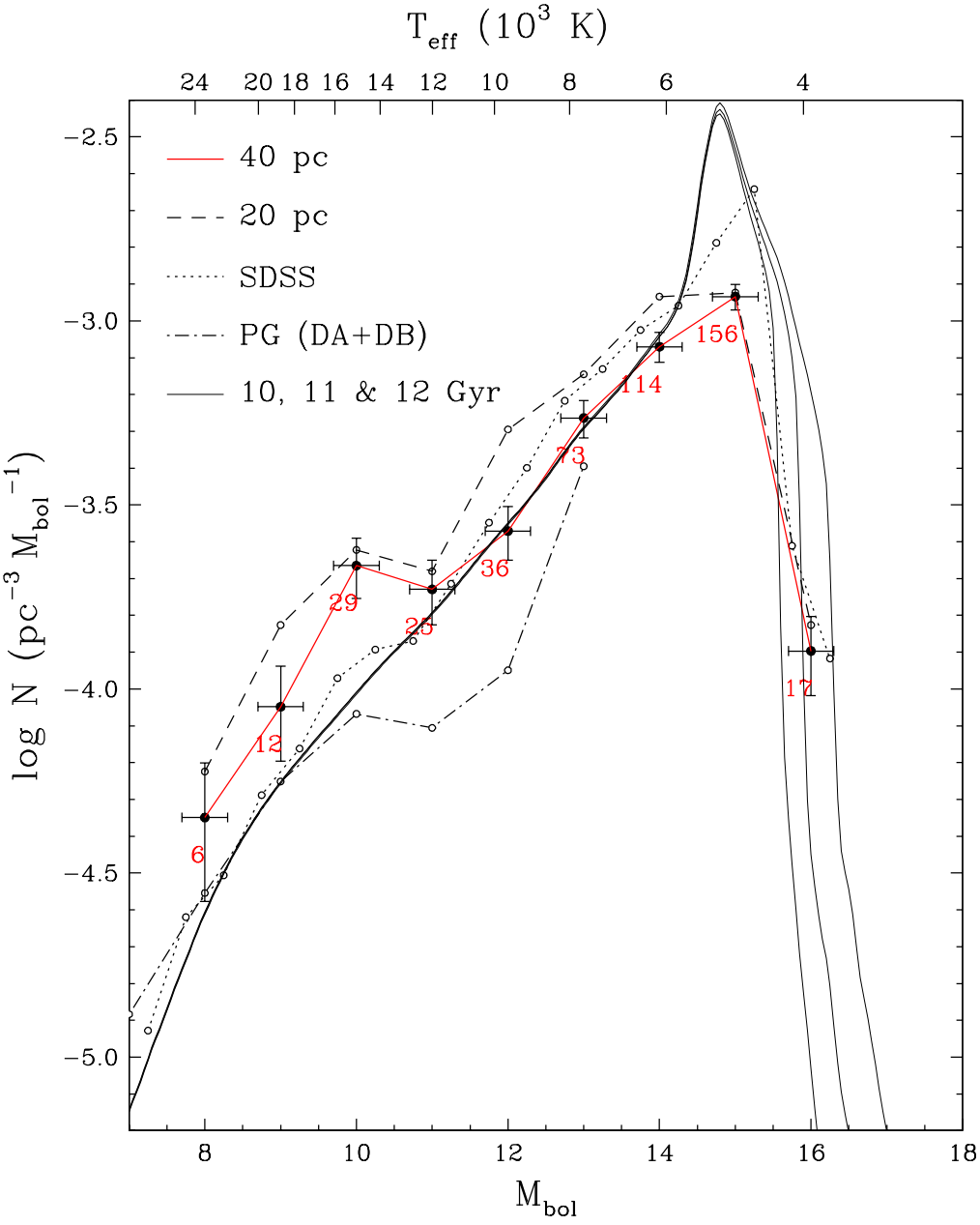

FIGURE 3.27 – Luminosity function for our sample of white dwarfs within 40 pc of the Sun as a function of $M_{\rm bol}$ (red line), compared to the luminosity functions obtained by Giammichele et al. (2012) for the 20 pc sample, by Harris et al. (2006) for white dwarfs in the SDSS, and by Bergeron et al. (2011) for the DA and DB stars in the PG survey; the number of stars in each magnitude bin is given for the 40 pc sample only. The approximate temperature scale for a $M = 0.6\ M_{\odot}$ sequence is shown at the top of the figure. Also shown are theoretical luminosity functions from Fontaine et al. (2001) for a total age of 10, 11, and 12 Gyr.

the left panel of Figure 3.21 and could be explain by a sudden burst of star formation in a recent past. An alternative explanation would be that the luminosity function for $M_V > 10$ is still very incomplete. Indeed, the drop in the space density near $M_{\rm bol} = 11$ is also observed in the luminosity function of the PG sample, precisely in the region where the PG survey becomes incomplete. However, the number of stars missing in our survey would have to be enormous (Figure 3.27 uses a logarithmic scale), an unlikely possibility given our estimate of the completeness of this survey. In Giammichele et al. (2012), this drop in the number of stars near $T_{\rm eff}$ $\sim$14,000 K was also tentatively explained by the inaccurate treatment of convective energy transport in the models, since this corresponds to the temperature where the atmospheres of DA stars become convective. However, since we applied here the appropriate 3D to 1D hydrodynamical corrections from Tremblay et al. (2013b), this explanation can be ruled out. We are thus left with a puzzling result.

As expected, the WDLF displayed in Figure 3.27 shows that our survey samples the cool end of the luminosity function really well, with a significant number of stars in each magnitude bin, as opposed to the color-excess PG survey for instance. Our derived space density is somewhat lower than that obtained by Harris et al. (2006) for white dwarfs in the SDSS, but again, our results have not been corrected for incompleteness. At the same time, there are significant corrections applied to the SDSS sample in this particular range of luminosities, all of which remain extremely uncertain. Note also that the number of stars in the fainter magnitude bins of our WDLF must be considered with caution, since for most cool white dwarfs in our sample, we had to assume a value of $\log g = 8.0$ due to the lack of trigonometric parallax measurements. Hence a change in $\log g$ values could shift some stars from one bin to the other. As a matter of fact, the mean mass of our sample is actually closer to 0.7 $M_{\odot}$ rather than the 0.6 $M_{\odot}$ assumed here for those stars. A larger average mass would imply smaller radii and lower luminosities, thus shifting the stars to fainter magnitude bins in Figure 3.27. Precise parallax measurements, like those that will become available from the Gaia mission, will be required to improve the shape of the WDLF at low luminosities, in particular since only the last magnitude bin is sensitive to the age of the galactic disk. Despite these uncertainties, we can still conclude that our results are consistent with an age of the

galactic disk around 11 Gyr.

Finally, by integrating the WDLF over all magnitude bins, it is possible to obtain a measure of the *total space density* of white dwarfs in our sample, which in turn can be used to evaluate the completeness of our survey. Holberg et al. (2008) obtained for the 13 pc sample, believed to be complete, a space density of $(4.8 \pm 0.5) \times 10^{-3}$ pc^{-3} and a mass density of $(3.2 \pm 0.3) \times 10^{-3}$ $M_{\odot}$ pc^{-3}. Using these numbers as a reference point, Giammichele et al. (2012) concluded that the 20 pc sample was 90% complete. For the 40 pc sample, we derive a space density of 3.47×10^{-3} pc^{-3} and a corresponding mass density of 2.27×10^{-3} $M_{\odot}$ pc^{-3}, which would imply that the 40 pc sample is 72.5% complete, in agreement with our other estimates above.

3.6 Concluding Remarks

Our spectroscopic survey of white dwarfs within 40 pc of the Sun is near completion, but there is still a significant amount of work to be done. First of all, we have a few high-priority targets in our sample, some of which are bright enough to be observed with 2-m class telescopes, while some faint targets around $V \sim$19 will require large aperture telescopes, such as Gemini North or South. Among the brightest objects which could not be observed because of uncooperative weather, several candidates with $D < 30$ pc remain on our target list, as well as 5 Giclas objects: 01309+5321 (GD 278), 02011+1212 (GD 21), 07544+6611 (GD 454), 14065+7418 (GD 492), and 22022+3848 (GD 399). Also, the southern hemisphere should eventually be dealt with, but it is not clear how much effort should be put into this given the work of Sayres et al. (2012) for declinations close to $\delta = 0$, as well as the SOAR + SMARTS Southern White Dwarf SURVEY (SSSWDS) of Subasavage et al. (2009), which uncovered 100 new white dwarfs. The current homogeneity of white dwarf surveys within 20 pc of the Sun in both hemispheres is about to be extended to 25 pc in a near future, but eventually to larger distances. The ultimate confirmation of the white dwarfs identified in our survey as members of the 40 pc sample will of course come from precise trigonometric parallaxes from the Gaia mission. In addition to adding or removing stars from the 40 pc sample, these measurements will also help to better define the faint end of the luminosity function revealed by our survey.

Acknowledgements

We would like to thank the director and staff of Steward Observatory, Kitt Peak National Observatory, and the Observatoire du Mont-Mégantic for the use of their facilities, as well as the Director and staff of Gemini North and South Observatories for the remote observing. We would also like to thank P. Dufour for making his DQ and DZ models available to us, G. Fontaine for the theoretical luminosity functions, and S.R. Kulkarni and M.H. van Kerkwijk for allowing us to use their spectrum of SDSS 1257+5428. This work was supported in part by the NSERC Canada and by the Fund FRQ-NT (Québec). S.L. was supported in this research by NSF grants AST 06-07757 and AST 09-08419. S.L also acknowledges support from the *GALEX* Guest Investigator program under NASA grant NNX09AF88G. This research made use of the SIMBAD database and the VizieR catalog access tool, operated at CDS, Strasbourg, France, and also made use of data products from the Two Micron All Sky Survey, which is a joint project of the University of Massachusetts and the Infrared Processing and Analysis Center/California Institute of Technology, funded by the National Aeronautics and Space Administration and the National Science Foundation.

Bibliographie

Adelman-McCarthy, J. K., Agüeros, M. A., Allam, S. S., et al. 2008, ApJS, 175, 297

Badenes, C., Mullally, F., Thompson, S. E., & Lupton, R. H. 2009, ApJ, 707, 971

Beauchamp, A., Wesemael, F., & Bergeron, P. 1997, ApJS, 108, 559

Bergeron, P., Dufour, P., & Giammichele, N. 2013, in Astronomical Society of the Pacific Conference Series, Vol. 469, 18th European White Dwarf Workshop., ed. Krzesiń, J. ski, G. Stachowski, P. Moskalik, & K. Bajan, 127

Bergeron, P., Leggett, S. K., & Ruiz, M. T. 2001, ApJS, 133, 413

Bergeron, P., Ruiz, M. T., & Leggett, S. K. 1997, ApJS, 108, 339

Bergeron, P., Saffer, R., & Liebert, J. 1992, ApJ, 394, 228

Bergeron, P., Saumon, D., & Wesemael, F. 1995, ApJ, 443, 764

Bergeron, P., Wesemael, F., Dufour, P., Beauchamp, A., Hunter, C., Saffer, R. A., Gianninas, A., Ruiz, M. T., Limoges, M.-M., Dufour, P., Fontaine, G., & Liebert, J. 2011, ApJ, 737, 28

Bergeron, P., Wesemael, F., & Fontaine, G. 1991, ApJ, 367, 253

Bohlin, R. C. & Gilliland, R. L. 2004, AJ, 127, 3508

Chen, E. Y. & Hansen, B. M. S. 2011, MNRAS, 413, 2827

—. 2012, ApJ, 753, L16

Cohen, M., Wheaton, W. A., & Megeath, S. T. 2003, AJ, 126, 1090

Dahn, C. C., Harrington, R. S., Riepe, B. Y., Christy, J. W., Guetter, H. H., Kallarakal, V. V., Miranian, M., Walker, R. L., Vrba, F. J., Hewitt, A. V., Durham, W. S., & Ables, H. D. 1982, AJ, 87, 419

Dufour, P., Bergeron, P., & Fontaine, G. 2005, ApJ, 627, 404

Dufour, P., Bergeron, P., Liebert, J., Harris, H. C., Knapp, G. R., Anderson, S. F., Hall, P. B., Strauss, M. A., Collinge, M. J., & Edwards, M. C. 2007, ApJ, 663, 1291

Fontaine, G., Brassard, P., & Bergeron, P. 2001, PASP, 113, 409

Fuchs, B., Dettbarn, C., Rix, H.-W., Beers, T. C., Bizyaev, D., Brewington, H., Jahreiß, H., Klement, R., Malanushenko, E., Malanushenko, V., Oravetz, D., Pan, K., Simmons, A., & Snedden, S. 2009, AJ, 137, 4149

Fukugita, M., Ichikawa, T., Gunn, J. E., Doi, M., Shimasaku, K., & Schneider, D. P. 1996, AJ, 111, 1748

Giammichele, N., Bergeron, P., & Dufour, P. 2012, ApJS, 199, 29

Gianninas, A., Bergeron, P., & Ruiz, M. T. 2011, ApJ, 743, 138

Giclas, H. L., Burnham, Jr., R., & Thomas, N. G. 1980, Lowell Observatory Bulletin, 8, 157

Gil de Paz, A., Boissier, S., Madore, B. F., Seibert, M., Joe, Y. H., Boselli, A., Wyder, T. K., Thilker, D., Bianchi, L., Rey, S.-C., Rich, R. M., Barlow, T. A., Conrow, T., Forster, K., Friedman, P. G., Martin, D. C., Morrissey, P., Neff, S. G., Schiminovich, D., Small, T., Donas, J., Heckman, T. M., Lee, Y.-W., Milliard, B., Szalay, A. S., & Yi, S. 2009, VizieR Online Data Catalog, 217, 30185

Green, R., Schmidt, M., & Liebert, J. 1986, ApJS, 61, 305

—. 1986, ApJ, 304, 334

Harris, H. C., Munn, J. A., Kilic, M., Liebert, J., Williams, K. A., von Hippel, T., Levine, S. E., Monet, D. G., Eisenstein, D. J., Kleinman, S. J., Metcalfe, T. S., Nitta, A., Winget, D. E., Brinkmann, J., Fukugita, M., Knapp, G. R., Lupton, R. H., Smith, J. A., & Schneider, D. P. 2006, AJ, 131, 571

Høg, E., Fabricius, C., Makarov, V. V., Urban, S., Corbin, T., Wycoff, G., Bastian, U., Schwekendiek, P., & Wicenec, A. 2000, A&A, 355, L27

Holberg, J. B. & Bergeron, P. 2006, AJ, 132, 1221

Holberg, J. B., Oswalt, T. D., Sion, E. M., Barstow, M. A., & Burleigh, M. R. 2013, MNRAS, 435, 2077

Holberg, J. B., Sion, E. M., Oswalt, T., McCook, G. P., Foran, S., & Subasavage, J. P. 2008, AJ, 135, 1225

Holberg, J. B., Sion, E. M., & Oswalt, T. D. 2011, in Bulletin of the American Astronomical Society, Vol. 43, American Astronomical Society Meeting Abstracts no.217, no.341.02

Hummer, D. G. & Mihalas, D. 1988, ApJ, 331, 794

Kawka, A. & Vennes, S. 2006, ApJ, 643, 402

Kepler, S. O., Kleinman, S. J., Nitta, A., Koester, D., Castanheira, B. G., Giovannini, O., Costa, A. F. M., & Althaus, L. 2007, MNRAS, 375, 1315

Kilic, M., Leggett, S. K., Tremblay, P.-E., von Hippel, T., Bergeron, P., Harris, H. C., Munn, J. A., Williams, K. A., Gates, E., & Farihi, J. 2010, ApJS, 190, 77

Kilic, M., Munn, J. A., Harris, H. C., Liebert, J., von Hippel, T., Williams, K. A., Metcalfe, T. S., Winget, D. E., & Levine, S. E. 2006, AJ, 131, 582

Kilic, M., Thorstensen, J. R., Kowalski, P. M., & Andrews, J. 2012, MNRAS, 423, L132

Koester, D., Napiwotzki, R., Christlieb, N., Drechsel, H., Hagen, H.-J., Heber, U., Homeier, D., Karl, C., Leibundgut, B., Moehler, S., Nelemans, G., Pauli, E.-M., Reimers, D., Renzini, A., & Yungelson, L. 2001, A&A, 378, 556

Koester, D., Napiwotzki, R., Voss, B., Homeier, D., & Reimers, D. 2005, A&A, 439, 317

Koester, D., Voss, B., Napiwotzki, R., Christlieb, N., Homeier, D., Lisker, T., Reimers, D., & Heber, U. 2009, A&A, 505, 441

Kondo, M., Noguchi, T., & Maehara, H. 1984, Annals of the Tokyo Astronomical Observatory, 20, 130

Kowalski, P. M. 2010, A&A, 519, L8

Kowalski, P. M. & Saumon, D. 2006, ApJ, 651, L137

Kulkarni, S. R. & van Kerkwijk, M. H. 2010, ApJ, 719, 1123

Leggett, S. K., Ruiz, M. T., & Bergeron, P. 1998, ApJ, 497, 294

Lépine, S. & Gaidos, E. 2011, AJ, 142, 138

Lépine, S., Hilton, E. J., Mann, A. W., Wilde, M., Rojas-Ayala, B., Cruz, K. L., & Gaidos, E. 2013, AJ, 145, 102

Lépine, S. & Shara, M. M. 2005, AJ, 129, 1483

Lépine, S., Shara, M. M., & Rich, R. M. 2002, AJ, 124, 1190

Liebert, J., Bergeron, P., & Holberg, J. 2005, ApJS, 156, 47

Liebert, J., Bergeron, P., & Saffer, R. A. 1991, in NATO ASIC Proc. 336: White Dwarfs, ed. G. Vauclair & E. Sion, 409

Liebert, J., Bergeron, P., & Saffer, R. A. 1991, in NATO ASIC Proc. 336: White Dwarfs, ed. G. Vauclair & E. Sion, 409

Liebert, J., Bergeron, P., Schmidt, G. D., & Saffer, R. A. 1993, ApJ, 418, 426

Limoges, M.-M., Bergeron, P., & Lépine, S. 2010, in American Institute of Physics Conference Series, Vol. 1273, American Institute of Physics Conference Series, ed. K. Werner & T. Rauch, 193–196

Limoges, M.-M., Lépine, S., & Bergeron, P. 2013, AJ, 145, 136

Marsh, T. R., Gänsicke, B. T., Steeghs, D., Southworth, J., Koester, D., Harris, V., & Merry, L. 2011, ApJ, 736, 95

McCook, G. P. & Sion, E. M. 1999, ApJS, 121, 1

—. 2006, VizieR Online Data Catalog, 3235, 0

Monet, D. G., Levine, S. E., Canzian, B., Ables, H. D., Bird, A. R., Dahn, C. C., Guetter, H. H., Harris, H. C., Henden, A. A., Leggett, S. K., Levison, H. F., Luginbuhl, C. B., Martini, J., Monet, A. K. B., Munn, J. A., Pier, J. R., Rhodes, A. R., Riepe, B., Sell, S., Stone, R. C., Vrba, F. J., Walker, R. L., Westerhout, G., Brucato, R. J., Reid, I. N., Schoening, W., Hartley, M., Read, M. A., & Tritton, S. B. 2003, AJ, 125, 984

Morrissey, P. & GALEX Science Team. 2004, in Bulletin of the American Astronomical Society, Vol. 36, American Astronomical Society Meeting Abstracts, 1385

Press, W. H., Flannery, B. P., & Teukolsky, S. A. 1986, Numerical recipes. The art of scientific computing, ed. Press, W. H., Flannery, B. P., & Teukolsky, S. A.

Rebassa-Mansergas, A., Gänsicke, B. T., Schreiber, M. R., Koester, D., & Rodríguez-Gil, P. 2010, MNRAS, 402, 620

Sayres, C., Subasavage, J. P., Bergeron, P., Dufour, P., Davenport, J. R. A., AlSayyad, Y., & Tofflemire, B. M. 2012, AJ, 143, 103

Schilbach, E. & Röser, S. 2012, A&A, 537, A129

Sion, E. M., Holberg, J. B., Oswalt, T. D., McCook, G. P., Wasatonic, R., & Myszka, J. 2014, ArXiv e-prints

Skrutskie, M. F., Cutri, R. M., Stiening, R., Weinberg, M. D., Schneider, S., Carpenter, J. M., Beichman, C., Capps, R., Chester, T., Elias, J., Huchra, J., Liebert, J., Lonsdale, C., Monet, D. G., Price, S., Seitzer, P., Jarrett, T., Kirkpatrick, J. D., Gizis, J. E., Howard, E., Evans,

T., Fowler, J., Fullmer, L., Hurt, R., Light, R., Kopan, E. L., Marsh, K. A., McCallon, H. L., Tam, R., Van Dyk, S., & Wheelock, S. 2006, AJ, 131, 1163

Subasavage, J. P., Jao, W.-C., Henry, T. J., Bergeron, P., Dufour, P., Ianna, P. A., Costa, E., & Méndez, R. A. 2009, AJ, 137, 4547

Tonry, J. L., Stubbs, C. W., Kilic, M., Flewelling, H. A., Deacon, N. R., Chornock, R., Berger, E., Burgett, W. S., Chambers, K. C., Kaiser, N., Kudritzki, R.-P., Hodapp, K. W., Magnier, E. A., Morgan, J. S., Price, P. A., & Wainscoat, R. J. 2012, ApJ, 745, 42

Tremblay, P.-E. & Bergeron, P. 2008, ApJ, 672, 1144

—. 2009, ApJ, 696, 1755

Tremblay, P.-E., Bergeron, P., & Gianninas, A. 2011, ApJ, 730, 128

Tremblay, P.-E., Bergeron, P., Kalirai, J. S., & Gianninas, A. 2010, ApJ, 712, 1345

Tremblay, P.-E., Ludwig, H.-G., Steffen, M., & Freytag, B. 2013a, A&A, 552, A13

—. 2013b, A&A, 559, A104

Tremblay, P.-E., Schilbach, E., Röser, S., Jordan, S., Ludwig, H.-G., & Goldman, B. 2012, A&A, 547, A99

Vennes, S. 1992, ApJ, 390, 590

Vennes, S. & Kawka, A. 2012, ApJ, 745, L12

Vennes, S., Kawka, A., & Németh, P. 2011, MNRAS, 413, 2545

Voss, B., Koester, D., Napiwotzki, R., Christlieb, N., & Reimers, D. 2007, A&A, 470, 1079

Wood, M. A. 1992, ApJ, 386, 539

Woodley, K. A., Goldsbury, R., Kalirai, J. S., Richer, H. B., Tremblay, P.-E., Anderson, J., Bergeron, P., Dotter, A., Esteves, L., Fahlman, G. G., Hansen, B. M. S., Heyl, J., Hurley, J., Rich, R. M., Shara, M. M., & Stetson, P. B. 2012, AJ, 143, 50

Chapitre 4

Conclusion

4.1 Résumé

Cette thèse rapporte les résultats de notre relevé spectroscopique d'étoiles naines blanches à moins de 40 pc du Soleil, et l'échantillon ainsi assemblé est, à ce jour, le plus complet qui existe jusqu'à une telle distance. De plus, 322 naines blanches ont été identifiées grâce à ce relevé, toutes distances confondues. Ce relevé spectroscopique a été rendu possible grâce au catalogue d'étoiles à grands mouvements propres de Lépine-Shara, appelé SUPERBLINK, du nom du logiciel comparateur d'images qui a permis l'extraction des coordonnées, des magnitudes photographiques et des mouvements propres des plaques photographiques des relevés POSS. Notre étude a débuté après que SUPERBLINK fut comparé aux catalogues *GALEX*, 2MASS et SDSS, nous permettant de profiter de ces informations photométriques supplémentaires afin d'extraire les naines blanches de l'hémisphère nord des quelques 2 millions d'étoiles de SUPERBLINK.

Nous avons donc calculé des mouvements propres réduits pour toutes les étoiles du catalogue SUPERBLINK, où les naines blanches connues nous ont aidé à déterminer les critères à appliquer afin d'identifier les candidates naines blanches. Ensuite, grâce aux relations couleur-magnitudes théoriques de Holberg & Bergeron (2006), nous avons pu assigner des magnitudes absolues à nos candidates naines blanches qui, couplées avec les magnitudes apparentes, nous ont permis d'estimer les distances de nos candidates naines blanches, et de nous concentrer

sur celles qui se trouvaient à moins de 40 pc (ou 55 pc si l'on prend en compte les incertitudes). Nous avons ensuite décidé d'appliquer un critère en couleur pour les étoiles les plus brillantes qui nous a permis de réduire la contamination par les étoiles brillantes de la séquence principale.

Nous avons confirmé le statut de naine blanche pour 322 étoiles, grâce à 15 missions d'observations en spectroscopie et 6 télescopes différents, soit ceux de 2.3 m de l'Observatoire Steward, les télescopes de 2.1 m et de 4 m du NOAO, tous trois à Tucson, en Arizona, les télescopes Gemini Nord (Hawaii) et Sud (Chili) de 8 m chacun, et finalement, avec l'Observatoire du Mont-Mégantic et son télescope de 1.6 m. Nos observations totalisent 70 nuits, sans compter les données obtenues à distances grâce aux observatoires Gemini.

Des 322 nouvelles naines blanches identifiées, 173 se trouvent à moins de 40 pc du Soleil. Les distances ont pu être déterminées d'après les paramètres atmosphériques que nous avons obtenus en procédant à l'ajustement de chaque spectre et de chaque distribution d'énergie avec des modèles d'atmosphère sophistiqués. En plus des nouvelles étoiles naines blanches, nous avons analysé de la même manière chaque naine blanche connue située à moins de $\sim$ 40 pc du Soleil.

Nous avons ainsi assemblé un échantillon de 460 naines blanches, toutes analysées de manière homogène, et dont les solutions obtenues les placent à moins de 40 pc du Soleil. Bien que cet échantillon soit moins complet que celui des naines blanches à l'intérieur de 20 pc, il est en revanche moins soumis aux incertitudes de petit nombre et il est libre de biais cinématique. Il nous a ainsi permis de dresser le premier portrait des étoiles naines blanches de notre environnement local jusqu'à 40 pc du Soleil.

4.2 Retombées et projets de recherche potentiels

Dans cette étude, nous avons doublé la distance à laquelle il existe un échantillon d'étoiles naines blanches dont les propriétés peuvent être étudiées de manière homogène. L'échantillon est complet à 70%, ce qui représente un travail de défrichage majeur en ce qui concerne la recherche de naines blanches dans le voisinage solaire. Nous avons de même montré que certaines des naines blanches que nous avons confirmées étaient considérées comme des candidates

depuis plusieurs dizaines d'années.

Tel qu'anticipé au début de cette étude, le catalogue SUPERBLINK a réellement un fort potentiel de détection de nouvelles naines blanches, surtout lorsque les coordonnées, mouvements propres et magnitudes qu'il contient sont couplés aux magnitudes provenant de relevés tels que *GALEX*, SDSS et 2MASS. Nous avons jeté les bases d'une méthode qui permettra à ceux qui le désireront d'entamer la recherche de naines blanches du voisinage solaire pour les étoiles de l'hémisphère sud.

Notre méthode peut également être utilisée pour identifier des naines blanches dans une petite portion du ciel, dans le cadre d'un relevé profond limité par la magnitude. En plus des objets froids trouvés par les relevés limités par le volume, cet échantillon contiendrait des naines blanches très chaudes, visibles jusqu'à plus grande distance. Un tel relevé permettrait d'identifier plus de DA chaudes, de DB chaudes, et aurait le potentiel de trouver des étoiles DO et des DAO, qui sont totalement absentes de notre relevé. Les jeunes naines blanches chaudes comme les DO, les DA et les DAO nous permettent d'étudier directement la formation des naines blanches. Certaines sont encore au centre d'une nébuleuse planétaire, et leur observation dans l'UV montre une quantité impressionnante de métaux. Les études comme celle de Gianninas et al. (2010) ont permis de les modéliser avec plus de précision, mais les théoriciens pourraient tirer profit d'un plus grand nombre de naines blanches chaudes connues.

De plus, sans chercher plus loin, notre échantillon de naines blanches à lui seul a le potentiel de fournir du travail pour plusieurs projets de recherche. En effet, grâce aux modèles d'atmosphère sophistiqués développés au fil des ans, la modélisation des naines blanches se fait avec une précision quasi inégalée dans les autres domaines de l'astrophysique stellaire. Par contre, ici, la précision des résultats obtenus est limitée par la qualité des données, puisque d'une part, toutes les étoiles de notre échantillon ne bénéficient pas de données photométriques de la même précision. L'obtention de photométrie de type $ugriz$ et JHK_S, lorsque ces données sont manquantes ou manquent de précision (ce qui n'est pas rare pour les magnitudes K_s de 2MASS), permettrait d'améliorer significativement nos estimés de température et de distance qui sont basés sur les distributions d'énergie. De telles mesures pourraient être réalisées à l'Observatoire du Mont-Mégantic, avec l'instrument CPAPIR en photométrie infrarouge (dont

JHK_S), et avec le futur instrument PESTO développé sous la supervision du professeur David Lafrenière de l'Université de Montréal, en lumière visible à l'aide de filtres $griz$.

D'autre part, il reste encore dans notre échantillon des spectres à faible signal sur bruit, obtenus pour fins de classification spectrale. Généralement, un rapport signal sur bruit de $S/N = 50$ est idéal pour l'utilisation de la méthode spectroscopique, alors que pour différencier une naine blanche d'une étoile de la séquence principale, $S/N = 25$ est souvent suffisant. Or, tel que démontré par Gianninas et al. (2005), l'augmentation du rapport signal sur bruit a un impact important sur la précision des paramètres atmosphériques qui sont dérivés par ajustement des raies spectrales. Ces paramètres déterminent, par exemple, l'appartenance d'une étoile à la bande d'instabilité des ZZ Ceti. En effet, nous avons identifié 9 naines blanches qui se trouvent dans la bande d'instabilité des ZZ Ceti, et seule une courbe de lumière obtenue par photométrie rapide permet de confirmer que ces étoiles varient. Par contre, des paramètres atmosphériques qui manquent de précision peuvent nous induire en erreur sur l'emplacement d'une étoile par rapport à la bande d'instabilité, et ainsi gaspiller du temps de télescope.

Nous fournissons finalement à la communauté des étoiles pour lesquelles il vaudra la peine d'obtenir des mesures de parallaxes, puisque pour les naines blanches, ces programmes favorisent les objets les plus près du Soleil. Dans un futur très rapproché, la sonde Gaia de l'Agence spatiale européenne, actuellement au point L2 de Lagrange à 1.5 millions de kilomètres de la Terre et en phase de calibration, commencera à mesurer les positions de plus d'un milliard d'étoiles de notre Galaxie. Ses données permettront de mesurer avec une précision inégalée l'astrométrie d'un nombre record d'objets. Grâce à Gaia, la cadence de détection et la mesure des distances des étoiles naines blanches s'accéléreront, et les astronomes, ayant des parallaxes pour toutes les naines blanches les plus proches, pourront enfin mesurer le rayon de toutes les étoiles naines blanches froides. Bientôt, nous aurons un portrait complet de la population des naines blanches les plus près du Soleil, et nous pourrons alors tester la relation masse-rayon théorique, déterminer la composition exacte du coeur des naines blanches, nous pencher sur la relation masse initiale-masse finale des naines blanches, et enfin déterminer l'incidence et la fraction de masse de ces minuscules cadavres stellaires à travers notre Galaxie.

Bibliographie

Adelman-McCarthy, J. K., Agüeros, M. A., Allam, S. S., et al. 2008, ApJS, 175, 297

Badenes, C., Mullally, F., Thompson, S. E., & Lupton, R. H. 2009, ApJ, 707, 971

Beauchamp, A., Wesemael, F., & Bergeron, P. 1997, ApJS, 108, 559

Bergeron, P., Dufour, P., & Giammichele, N. 2013, in Astronomical Society of the Pacific Conference Series, Vol. 469, 18th European White Dwarf Workshop., ed. Krzesiń, J. ski, G. Stachowski, P. Moskalik, & K. Bajan, 127

Bergeron, P., Leggett, S. K., & Ruiz, M. T. 2001, ApJS, 133, 413

Bergeron, P., Ruiz, M. T., & Leggett, S. K. 1997, ApJS, 108, 339

Bergeron, P., Saffer, R., & Liebert, J. 1992, ApJ, 394, 228

Bergeron, P., Saumon, D., & Wesemael, F. 1995, ApJ, 443, 764

Bergeron, P., Wesemael, F., Dufour, P., Beauchamp, A., Hunter, C., Saffer, R. A., Gianninas, A., Ruiz, M. T., Limoges, M.-M., Dufour, P., Fontaine, G., & Liebert, J. 2011, ApJ, 737, 28

Bergeron, P., Wesemael, F., & Fontaine, G. 1991, ApJ, 367, 253

Bohlin, R. C. & Gilliland, R. L. 2004, AJ, 127, 3508

Burleigh, M. R., Barstow, M. A., & Fleming, T. A. 1997, MNRAS, 287, 381

Carollo, D., Bucciarelli, B., Hodgkin, S. T., Lattanzi, M. G., McLean, B., Morbidelli, R., Smart, R. L., Spagna, A., & Terranegra, L. 2006, A&A, 448, 579

Chen, E. Y. & Hansen, B. M. S. 2011, MNRAS, 413, 2827

—. 2012, ApJ, 753, L16

Cohen, M., Wheaton, W. A., & Megeath, S. T. 2003, AJ, 126, 1090

Cutri, R. M., Skrutskie, M. F., van Dyk, S., Beichman, C. A., Carpenter, J. M., Chester, T., Cambresy, L., Evans, T., Fowler, J., Gizis, J., Howard, E., Huchra, J., Jarrett, T., Kopan, E. L., Kirkpatrick, J. D., Light, R. M., Marsh, K. A., McCallon, H., Schneider, S., Stiening, R., Sykes, M., Weinberg, M., Wheaton, W. A., Wheelock, S., & Zacarias, N. 2003, VizieR Online Data Catalog, 2246, 0

Dahn, C. C., Harrington, R. S., Kallarakal, V. V., Guetter, H. H., Luginbuhl, C. B., Riepe, B. Y., Walker, R. L., Pier, J. R., Vrba, F. J., Monet, D. G., & Ables, H. D. 1988, AJ, 95, 237

Dahn, C. C., Harrington, R. S., Riepe, B. Y., Christy, J. W., Guetter, H. H., Kallarakal, V. V., Miranian, M., Walker, R. L., Vrba, F. J., Hewitt, A. V., Durham, W. S., & Ables, H. D. 1982, AJ, 87, 419

Darling, G. 1994, PhD thesis, Dartmouth College

DeGennaro, S., von Hippel, T., Winget, D. E., Kepler, S. O., Nitta, A., Koester, D., & Althaus, L. 2008, AJ, 135, 1

Dufour, P., Bergeron, P., & Fontaine, G. 2005, ApJ, 627, 404

Dufour, P., Bergeron, P., Liebert, J., Harris, H. C., Knapp, G. R., Anderson, S. F., Hall, P. B., Strauss, M. A., Collinge, M. J., & Edwards, M. C. 2007, ApJ, 663, 1291

Eggen, O. J. & Greenstein, J. L. 1965, ApJ, 142, 925

Eisenstein, D. J., Liebert, J., Harris, H. C., Kleinman, S. J., Nitta, A., Silvestri, N., Anderson, S. A., Barentine, J. C., Brewington, H. J., Brinkmann, J., Harvanek, M., Krzesiński, J., Neilsen, Jr., E. H., Long, D., Schneider, D. P., & Snedden, S. A. 2006, ApJS, 167, 40

Farihi, J. 2004, ApJ, 610, 1013

Farihi, J., Becklin, E. E., & Zuckerman, B. 2005, ApJS, 161, 394

Fleming, T., Liebert, J., & Green, R. 1986, ApJ, 308, 176

Fontaine, G., Brassard, P., & Bergeron, P. 2001, PASP, 113, 409

Fuchs, B., Dettbarn, C., Rix, H.-W., Beers, T. C., Bizyaev, D., Brewington, H., Jahreiß, H., Klement, R., Malanushenko, E., Malanushenko, V., Oravetz, D., Pan, K., Simmons, A., & Snedden, S. 2009, AJ, 137, 4149

Fukugita, M., Ichikawa, T., Gunn, J. E., Doi, M., Shimasaku, K., & Schneider, D. P. 1996, AJ, 111, 1748

Giammichele, N., Bergeron, P., & Dufour, P. 2012, ApJS, 199, 29

Gianninas, A., Bergeron, P., Dupuis, J., & Ruiz, M. T. 2010, ApJ, 720, 581

Gianninas, A., Bergeron, P., & Fontaine, G. 2005, ApJ, 631, 1100

Gianninas, A., Bergeron, P., & Fontaine, G. 2007, in Astronomical Society of the Pacific Conference Series, Vol. 372, 15th European Workshop on White Dwarfs, ed. R. Napiwotzki & M. R. Burleigh, 577

Gianninas, A., Bergeron, P., & Ruiz, M. T. 2011, ApJ, 743, 138

Giclas, H. L. 1971, in IAU Symposium, Vol. 42, White Dwarfs, ed. W. J. Luyten, 24

Giclas, H. L., Burnham, Jr., R., & Thomas, N. G. 1978, Lowell Observatory Bulletin, 8, 89

—. 1980, Lowell Observatory Bulletin, 8, 157

Gil de Paz, A., Boissier, S., Madore, B. F., Seibert, M., Joe, Y. H., Boselli, A., Wyder, T. K., Thilker, D., Bianchi, L., Rey, S.-C., Rich, R. M., Barlow, T. A., Conrow, T., Forster, K., Friedman, P. G., Martin, D. C., Morrissey, P., Neff, S. G., Schiminovich, D., Small, T., Donas, J., Heckman, T. M., Lee, Y.-W., Milliard, B., Szalay, A. S., & Yi, S. 2009, VizieR Online Data Catalog, 217, 30185

Gliese, W. & Jahreiss, H. 1991, NASA STI/Recon Technical Report A, 92, 33932

Green, R., Schmidt, M., & Liebert, J. 1986, ApJS, 61, 305

Greenstein, J. L. 1969, ApJ, 158, 281

—. 1976, ApJ, 207, L119

—. 1984, ApJ, 276, 602

—. 1986, ApJ, 304, 334

Harris, H. C., Munn, J. A., Kilic, M., Liebert, J., Williams, K. A., von Hippel, T., Levine, S. E., Monet, D. G., Eisenstein, D. J., Kleinman, S. J., Metcalfe, T. S., Nitta, A., Winget, D. E., Brinkmann, J., Fukugita, M., Knapp, G. R., Lupton, R. H., Smith, J. A., & Schneider, D. P. 2006, AJ, 131, 571

Henry, T. J., Ianna, P. A., Kirkpatrick, J. D., & Jahreiss, H. 1997, AJ, 114, 388

Høg, E., Fabricius, C., Makarov, V. V., Urban, S., Corbin, T., Wycoff, G., Bastian, U., Schwekendiek, P., & Wicenec, A. 2000, A&A, 355, L27

Holberg, J. B. & Bergeron, P. 2006, AJ, 132, 1221

Holberg, J. B., Oswalt, T. D., & Sion, E. M. 2002, ApJ, 571, 512

Holberg, J. B., Oswalt, T. D., Sion, E. M., Barstow, M. A., & Burleigh, M. R. 2013, MNRAS, 435, 2077

Holberg, J. B., Sion, E. M., Oswalt, T., McCook, G. P., Foran, S., & Subasavage, J. P. 2008, AJ, 135, 1225

Holberg, J. B., Sion, E. M., & Oswalt, T. D. 2011, in Bulletin of the American Astronomical Society, Vol. 43, American Astronomical Society Meeting Abstracts no.217, no.341.02

Hummer, D. G. & Mihalas, D. 1988, ApJ, 331, 794

Jahreiss, H. 1987, Mem. Soc. Astron. Italiana, 58, 53

Kawka, A. & Vennes, S. 2006, ApJ, 643, 402

Kawka, A., Vennes, S., Schmidt, G. D., Wickramasinghe, D. T., & Koch, R. 2007, ApJ, 654, 499

Kawka, A., Vennes, S., & Thorstensen, J. R. 2004, AJ, 127, 1702

Kepler, S. O., Kleinman, S. J., Nitta, A., Koester, D., Castanheira, B. G., Giovannini, O., Costa, A. F. M., & Althaus, L. 2007, MNRAS, 375, 1315

Kilic, M., Leggett, S. K., Tremblay, P.-E., von Hippel, T., Bergeron, P., Harris, H. C., Munn, J. A., Williams, K. A., Gates, E., & Farihi, J. 2010, ApJS, 190, 77

Kilic, M., Munn, J. A., Harris, H. C., Liebert, J., von Hippel, T., Williams, K. A., Metcalfe, T. S., Winget, D. E., & Levine, S. E. 2006, AJ, 131, 582

Kilic, M., Thorstensen, J. R., Kowalski, P. M., & Andrews, J. 2012, MNRAS, 423, L132

Kleinman, S. J., Harris, H. C., Eisenstein, D. J., Liebert, J., Nitta, A., Krzesiński, J., Munn, J. A., Dahn, C. C., Hawley, S. L., Pier, J. R., Schmidt, G., Silvestri, N. M., Smith, J. A., Szkody, P., Strauss, M. A., Knapp, G. R., Collinge, M. J., Mukadam, A. S., Koester, D., Uomoto, A., Schlegel, D. J., Anderson, S. F., Brinkmann, J., Lamb, D. Q., Schneider, D. P., & York, D. G. 2004, ApJ, 607, 426

Knox, R. A., Hawkins, M. R. S., & Hambly, N. C. 1999, MNRAS, 306, 736

Koester, D. & Knist, S. 2006, A&A, 454, 951

Koester, D., Napiwotzki, R., Christlieb, N., Drechsel, H., Hagen, H.-J., Heber, U., Homeier, D., Karl, C., Leibundgut, B., Moehler, S., Nelemans, G., Pauli, E.-M., Reimers, D., Renzini, A., & Yungelson, L. 2001, A&A, 378, 556

Koester, D., Napiwotzki, R., Voss, B., Homeier, D., & Reimers, D. 2005, A&A, 439, 317

Koester, D., Voss, B., Napiwotzki, R., Christlieb, N., Homeier, D., Lisker, T., Reimers, D., & Heber, U. 2009, A&A, 505, 441

Kondo, M., Noguchi, T., & Maehara, H. 1984, Annals of the Tokyo Astronomical Observatory, 20, 130

Kowalski, P. M. 2010, A&A, 519, L8

Kowalski, P. M. & Saumon, D. 2006, ApJ, 651, L137

Kulkarni, S. R. & van Kerkwijk, M. H. 2010, ApJ, 719, 1123

Lanning, H. H. 1973, PASP, 85, 70

Lanning, H. H. & Lépine, S. 2006, PASP, 118, 1639

Leggett, S. K., Ruiz, M. T., & Bergeron, P. 1998, ApJ, 497, 294

Lépine, S., Bergeron, P., & Lanning, H. H. 2011, AJ, 141, 96

Lépine, S. & Gaidos, E. 2011, AJ, 142, 138

Lépine, S., Hilton, E. J., Mann, A. W., Wilde, M., Rojas-Ayala, B., Cruz, K. L., & Gaidos, E. 2013, AJ, 145, 102

Lépine, S. & Shara, M. M. 2005, AJ, 129, 1483

Lépine, S., Shara, M. M., & Rich, R. M. 2002, AJ, 124, 1190

Liebert, J., Bergeron, P., & Holberg, J. 2005, ApJS, 156, 47

Liebert, J., Bergeron, P., & Saffer, R. A. 1991, in NATO ASIC Proc. 336: White Dwarfs, ed. G. Vauclair & E. Sion, 409

Liebert, J., Bergeron, P., Schmidt, G. D., & Saffer, R. A. 1993, ApJ, 418, 426

Liebert, J., Dahn, C. C., & Monet, D. G. 1988, ApJ, 332, 891

Limoges, M.-M., Bergeron, P., & Lépine, S. 2010, in American Institute of Physics Conference Series, Vol. 1273, American Institute of Physics Conference Series, ed. K. Werner & T. Rauch, 193–196

Limoges, M.-M., Lépine, S., & Bergeron, P. 2013, AJ, 145, 136

Luyten, W. J. 1979a, LHS catalogue. A catalogue of stars with proper motions exceeding 0”5 annually, ed. n. e. Minneapolis: University of Minnesota, 1979

—. 1979b, New Luyten Catalogue of Stars with Proper Motions Larger than Two Tenths of an Arcsecond, ed. Luyten, W. J.

Marsh, T. R., Gänsicke, B. T., Steeghs, D., Southworth, J., Koester, D., Harris, V., & Merry, L. 2011, ApJ, 736, 95

McCook, G. P. & Sion, E. M. 1987, ApJS, 65, 603

—. 1999, ApJS, 121, 1

—. 2006, VizieR Online Data Catalog, 3235, 0

McLean, B. J., Greene, G. R., Lattanzi, M. G., & Pirenne, B. 2000, in Astronomical Society of the Pacific Conference Series, Vol. 216, Astronomical Data Analysis Software and Systems IX, ed. N. Manset, C. Veillet, & D. Crabtree, 145

Monet, D. G., Levine, S. E., Canzian, B., Ables, H. D., Bird, A. R., Dahn, C. C., Guetter, H. H., Harris, H. C., Henden, A. A., Leggett, S. K., Levison, H. F., Luginbuhl, C. B., Martini, J., Monet, A. K. B., Munn, J. A., Pier, J. R., Rhodes, A. R., Riepe, B., Sell, S., Stone, R. C., Vrba, F. J., Walker, R. L., Westerhout, G., Brucato, R. J., Reid, I. N., Schoening, W., Hartley, M., Read, M. A., & Tritton, S. B. 2003, AJ, 125, 984

Morrissey, P. & GALEX Science Team. 2004, in Bulletin of the American Astronomical Society, Vol. 36, American Astronomical Society Meeting Abstracts, 1385

Noguchi, T., Maehara, H., & Kondo, M. 1980, Annals of the Tokyo Astronomical Observatory, 18, 55

Oppenheimer, B. R., Hambly, N. C., Digby, A. P., Hodgkin, S. T., & Saumon, D. 2001, Science, 292, 698

Oswalt, T. D., Smith, J. A., Wood, M. A., & Hintzen, P. 1996, Nature, 382, 692

Padmanabhan, N., Schlegel, D. J., Finkbeiner, D. P., Barentine, J. C., Blanton, M. R., Brewington, H. J., Gunn, J. E., Harvanek, M., Hogg, D. W., Ivezić, Ž., Johnston, D., Kent, S. M., Kleinman, S. J., Knapp, G. R., Krzesinski, J., Long, D., Neilsen, Jr., E. H., Nitta,

A., Loomis, C., Lupton, R. H., Roweis, S., Snedden, S. A., Strauss, M. A., & Tucker, D. L. 2008, ApJ, 674, 1217

Press, W. H., Flannery, B. P., & Teukolsky, S. A. 1986, Numerical recipes. The art of scientific computing, ed. Press, W. H., Flannery, B. P., & Teukolsky, S. A.

Rebassa-Mansergas, A., Gänsicke, B. T., Schreiber, M. R., Koester, D., & Rodríguez-Gil, P. 2010, MNRAS, 402, 620

Reis, W., Corradi, W., de Avillez, M. A., & Santos, F. P. 2011, ApJ, 734, 8

Salim, S. & Gould, A. 2003, ApJ, 582, 1011

Sayres, C., Subasavage, J. P., Bergeron, P., Dufour, P., Davenport, J. R. A., AlSayyad, Y., & Tofflemire, B. M. 2012, AJ, 143, 103

Schilbach, E. & Röser, S. 2012, A&A, 537, A129

Sion, E. M., Holberg, J. B., Oswalt, T. D., McCook, G. P., & Wasatonic, R. 2009, AJ, 138, 1681

Sion, E. M., Holberg, J. B., Oswalt, T. D., McCook, G. P., Wasatonic, R., & Myszka, J. 2014, ArXiv e-prints

Skrutskie, M. F., Cutri, R. M., Stiening, R., Weinberg, M. D., Schneider, S., Carpenter, J. M., Beichman, C., Capps, R., Chester, T., Elias, J., Huchra, J., Liebert, J., Lonsdale, C., Monet, D. G., Price, S., Seitzer, P., Jarrett, T., Kirkpatrick, J. D., Gizis, J. E., Howard, E., Evans, T., Fowler, J., Fullmer, L., Hurt, R., Light, R., Kopan, E. L., Marsh, K. A., McCallon, H. L., Tam, R., Van Dyk, S., & Wheelock, S. 2006, AJ, 131, 1163

Subasavage, J. P., Henry, T. J., Bergeron, P., Dufour, P., & Hambly, N. C. 2008, AJ, 136, 899

Subasavage, J. P., Henry, T. J., Bergeron, P., Dufour, P., Hambly, N. C., & Beaulieu, T. D. 2007, AJ, 134, 252

Subasavage, J. P., Jao, W.-C., Henry, T. J., Bergeron, P., Dufour, P., Ianna, P. A., Costa, E., & Méndez, R. A. 2009, AJ, 137, 4547

Tat, H. H. & Terzian, Y. 1999, PASP, 111, 1258

Tonry, J. L., Stubbs, C. W., Kilic, M., Flewelling, H. A., Deacon, N. R., Chornock, R., Berger, E., Burgett, W. S., Chambers, K. C., Kaiser, N., Kudritzki, R.-P., Hodapp, K. W., Magnier, E. A., Morgan, J. S., Price, P. A., & Wainscoat, R. J. 2012, ApJ, 745, 42

Tremblay, P.-E. & Bergeron, P. 2008, ApJ, 672, 1144

—. 2009, ApJ, 696, 1755

Tremblay, P.-E., Bergeron, P., & Gianninas, A. 2011a, ApJ, 730, 128

Tremblay, P.-E., Bergeron, P., Kalirai, J. S., & Gianninas, A. 2010, ApJ, 712, 1345

Tremblay, P.-E., Ludwig, H.-G., Steffen, M., Bergeron, P., & Freytag, B. 2011b, A&A, 531, L19

Tremblay, P.-E., Ludwig, H.-G., Steffen, M., & Freytag, B. 2013a, A&A, 552, A13

—. 2013b, A&A, 559, A104

Tremblay, P.-E., Schilbach, E., Röser, S., Jordan, S., Ludwig, H.-G., & Goldman, B. 2012, A&A, 547, A99

van Altena, W. F., Lee, J. T., & Hoffleit, E. D. 1995, The general catalogue of trigonometric [stellar] parallaxes

van Leeuwen, F. 2007, A&A, 474, 653

Vennes, S. 1992, ApJ, 390, 590

Vennes, S. & Kawka, A. 2003, ApJ, 586, L95

—. 2012, ApJ, 745, L12

Vennes, S., Kawka, A., & Németh, P. 2011, MNRAS, 410, 2095

Vennes, S., Smith, R. J., Boyle, B. J., Croom, S. M., Kawka, A., Shanks, T., Miller, L., & Loaring, N. 2002, MNRAS, 335, 673

Voss, B., Koester, D., Napiwotzki, R., Christlieb, N., & Reimers, D. 2007, A&A, 470, 1079

Winget, D. E., Hansen, C. J., Liebert, J., van Horn, H. M., Fontaine, G., Nather, R. E., Kepler, S. O., & Lamb, D. Q. 1987, ApJ, 315, L77

Wood, M. A. 1992, ApJ, 386, 539

Woodley, K. A., Goldsbury, R., Kalirai, J. S., Richer, H. B., Tremblay, P.-E., Anderson, J., Bergeron, P., Dotter, A., Esteves, L., Fahlman, G. G., Hansen, B. M. S., Heyl, J., Hurley, J., Rich, R. M., Shara, M. M., & Stetson, P. B. 2012, AJ, 143, 50

York, D. G., Adelman, J., Anderson, Jr., J. E., Anderson, S. F., et al. 2000, AJ, 120, 1579

Annexe A

Solutions pour les nouvelles étoiles DA et DC

Nous présentons ici l'ensemble de nos solutions pour les étoiles DA et DC présentées au Chapitre 3, puisqu'en vertu des contraintes d'espace pour la publication dans l'*Astrophysical Journal* (ApJ), ces figures sont présentées de façon électronique et ne figurent donc pas dans le corps du texte. La première figure montre les solutions obtenues lors de l'ajustement de la distribution d'énergie des étoiles, et la seconde figure présente les solutions pour l'ajustement des spectres avec des modèles d'atmosphère.

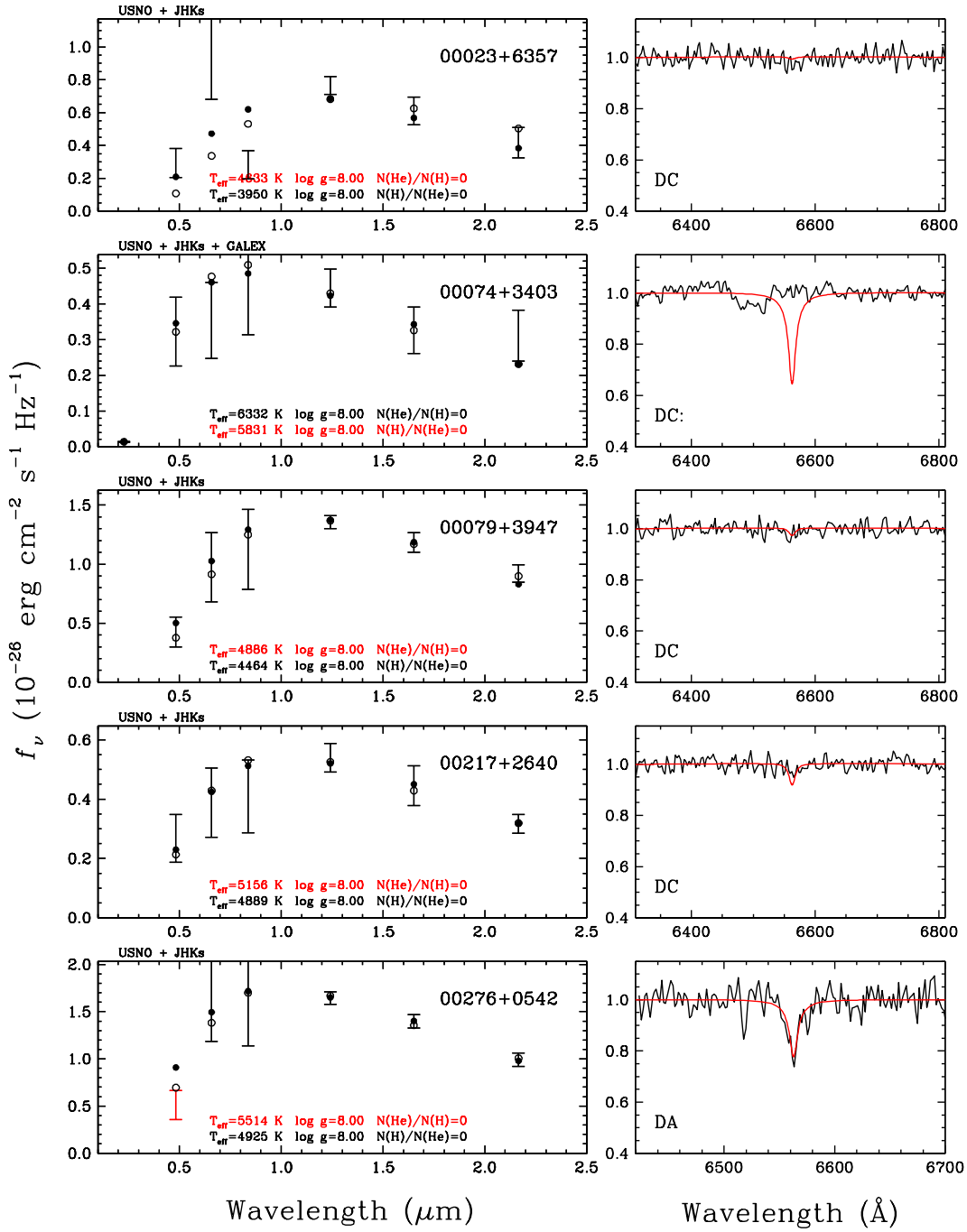

FIGURE A.1 – (a) Solutions photométriques pour les étoiles DA et DC identifiées par notre relevé, et présentées au Chapitre 3. Les données sont représentées par les barres d'erreur, alors que les solutions pour les étoiles à atmosphère d'hydrogène sont représentées par des cercles pleins, et les solutions pour les étoiles à atmosphère d'hélium avec des cercles vides. La solution adoptée est indiquée en rouge, et le panneau de droite montre le spectre observé normalisé, ainsi que le profil synthétique correspondant à la solution pour une atmosphère riche en hydrogène (en rouge).

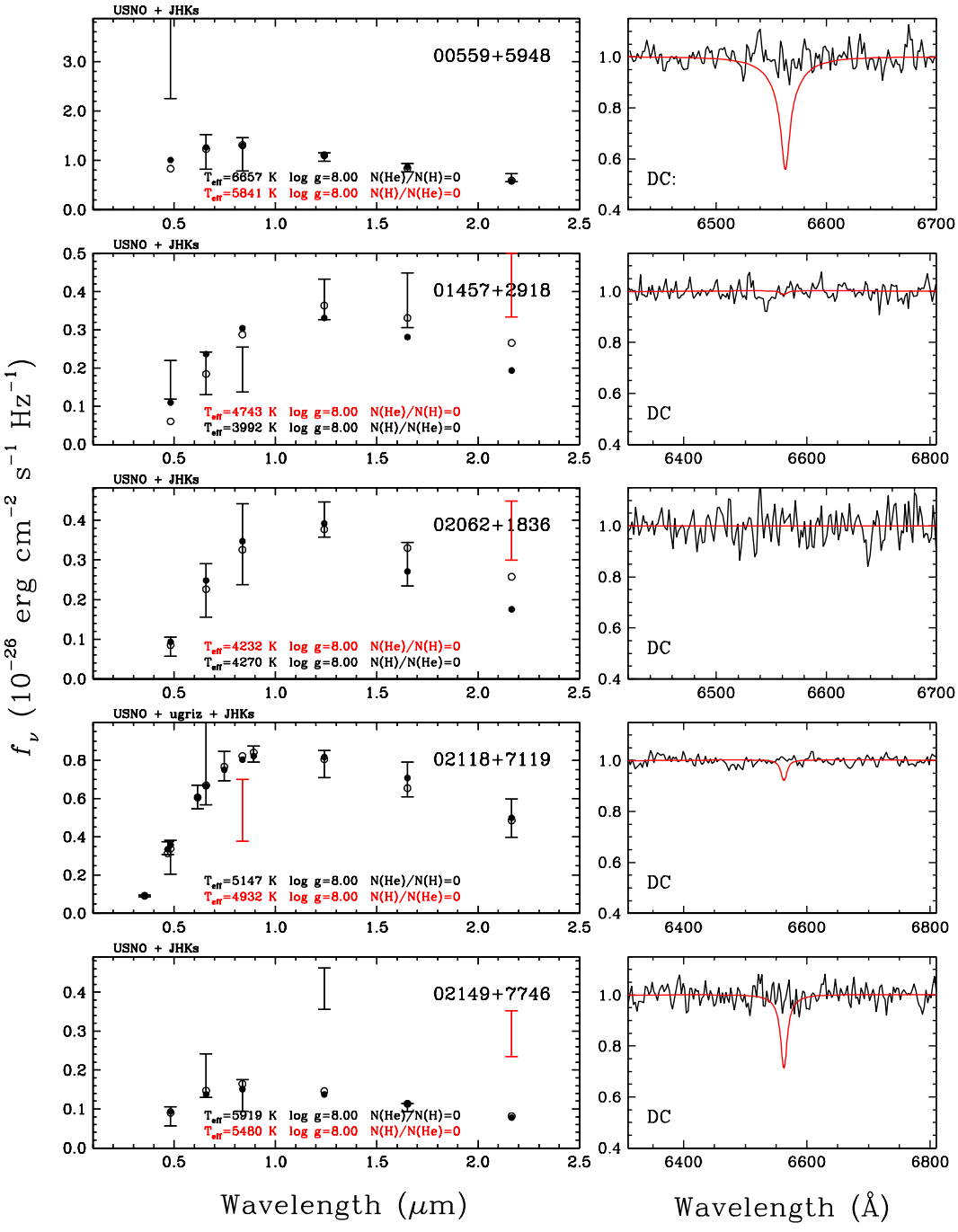

FIGURE A.1 – (b) - suite.

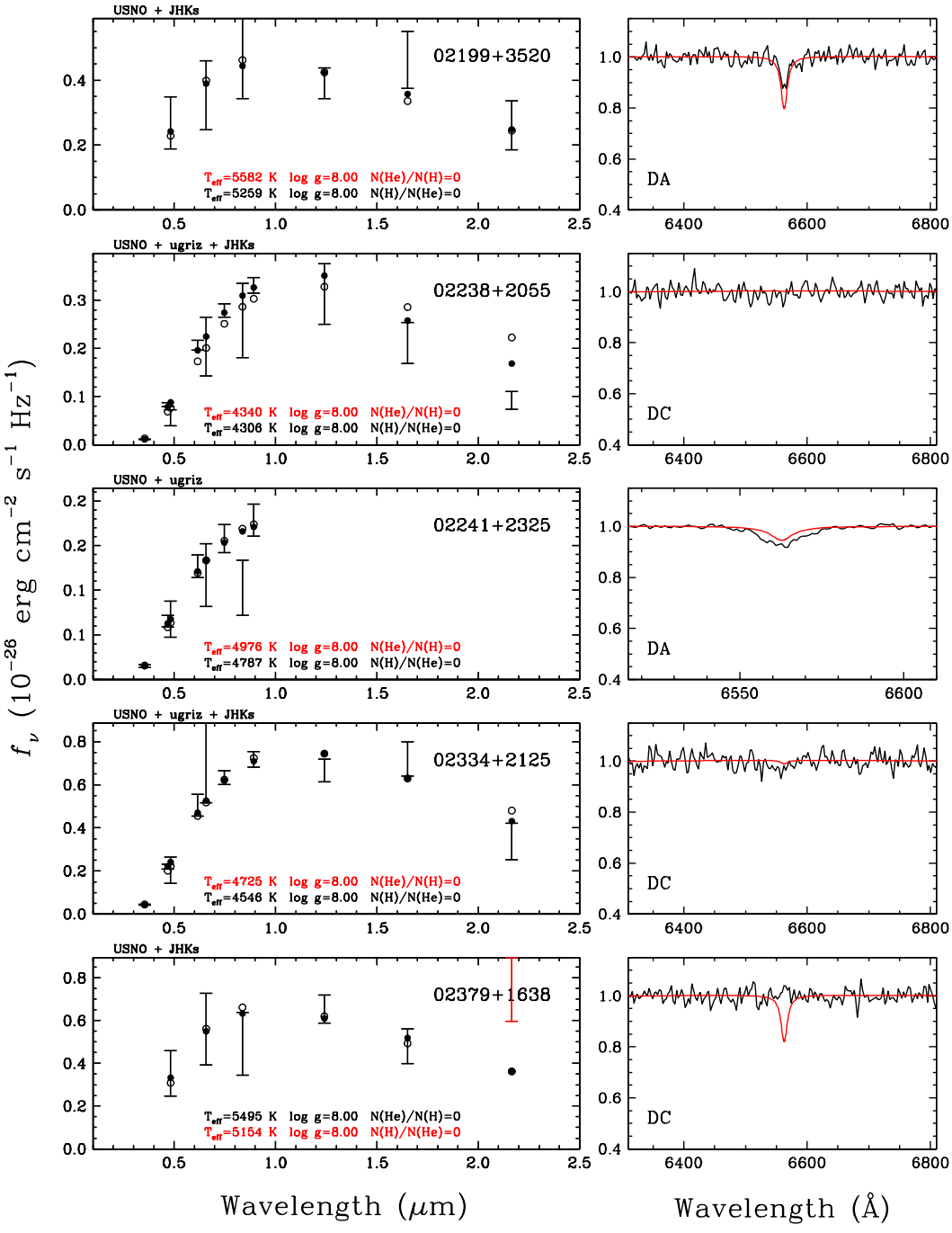

FIGURE A.1 – (c) - suite.

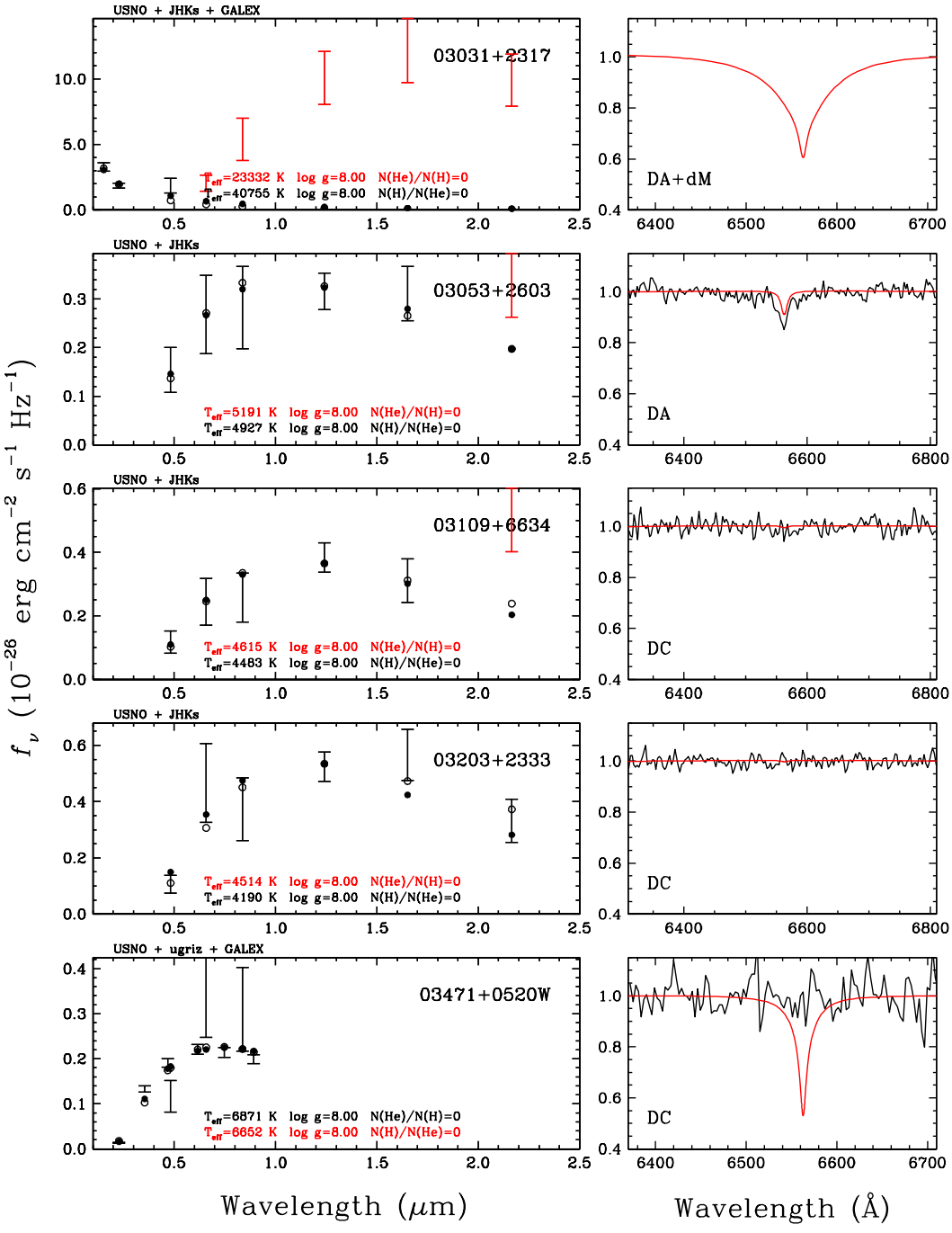

FIGURE A.1 – (d) - suite.

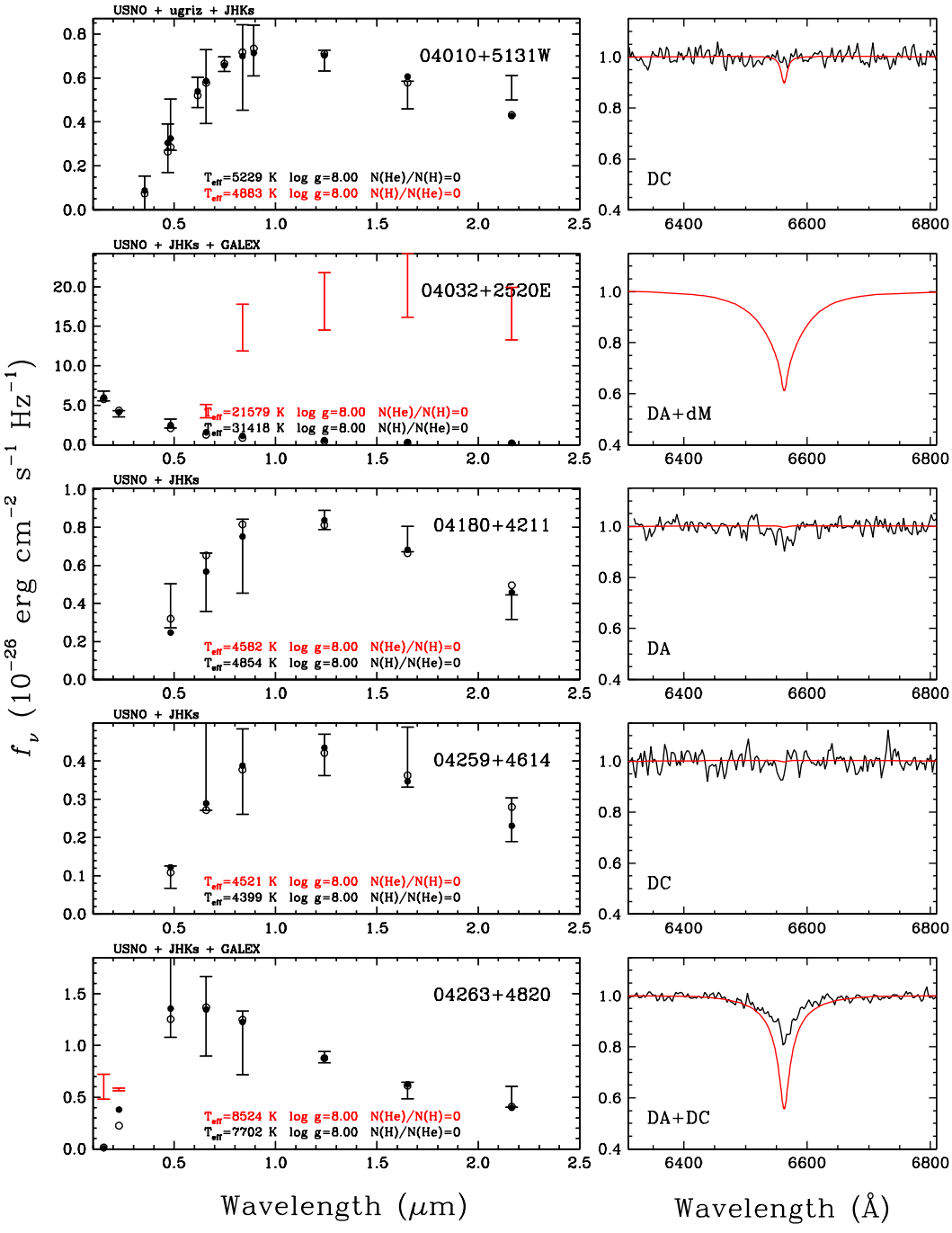

FIGURE A.1 – (e) - suite.

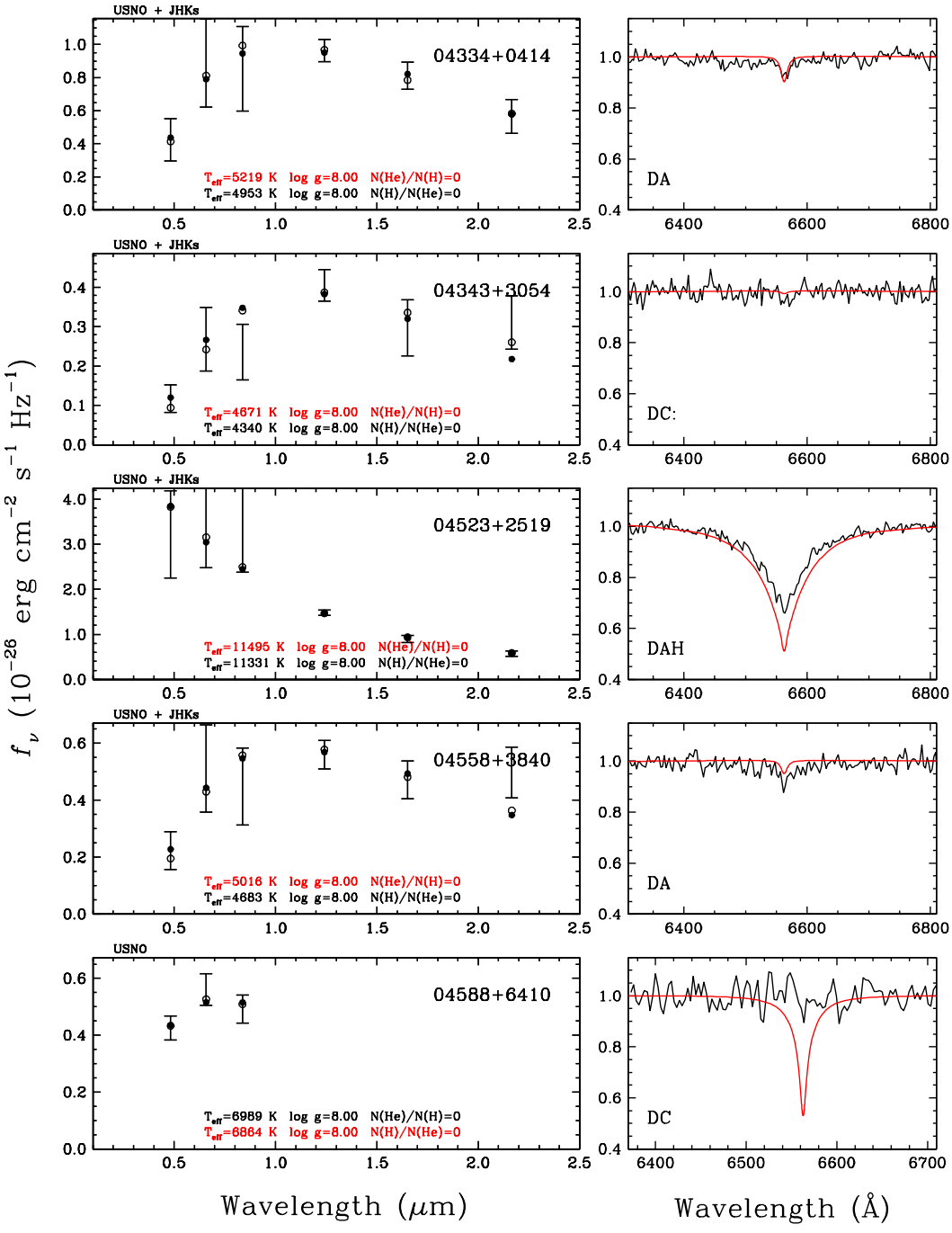

FIGURE A.1 – (f) - suite.

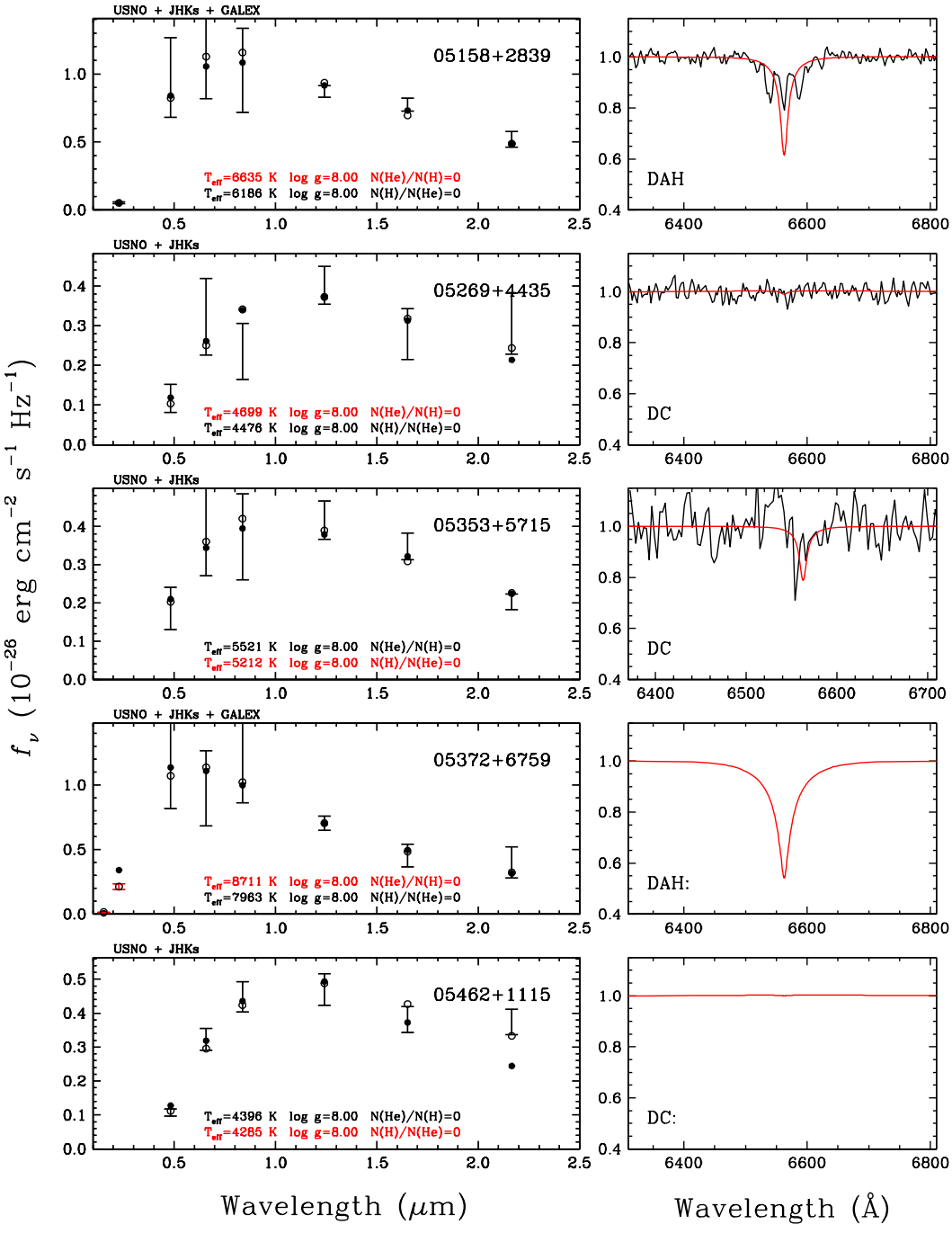

FIGURE A.1 – (g) - suite.

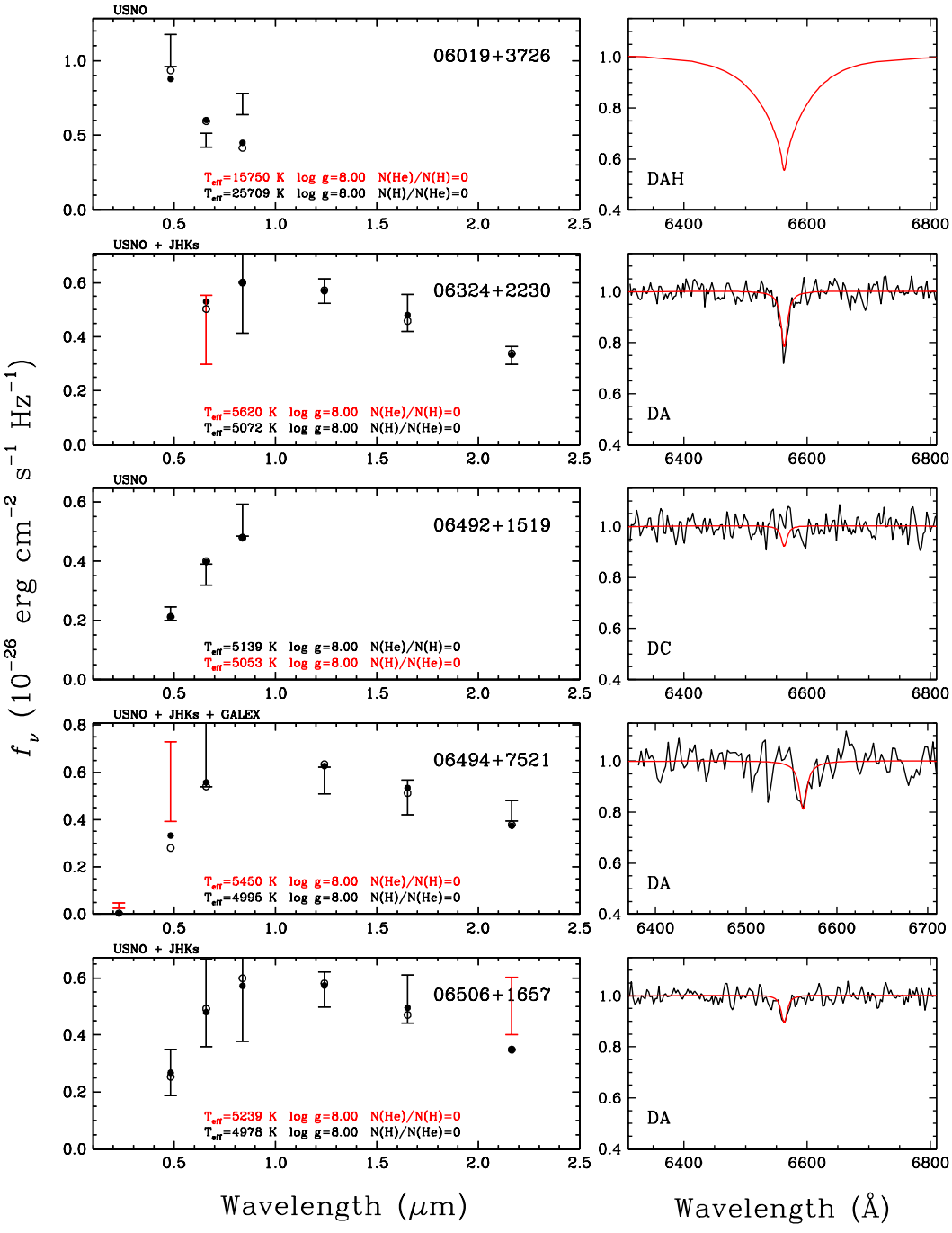

FIGURE A.1 – (h) - suite.

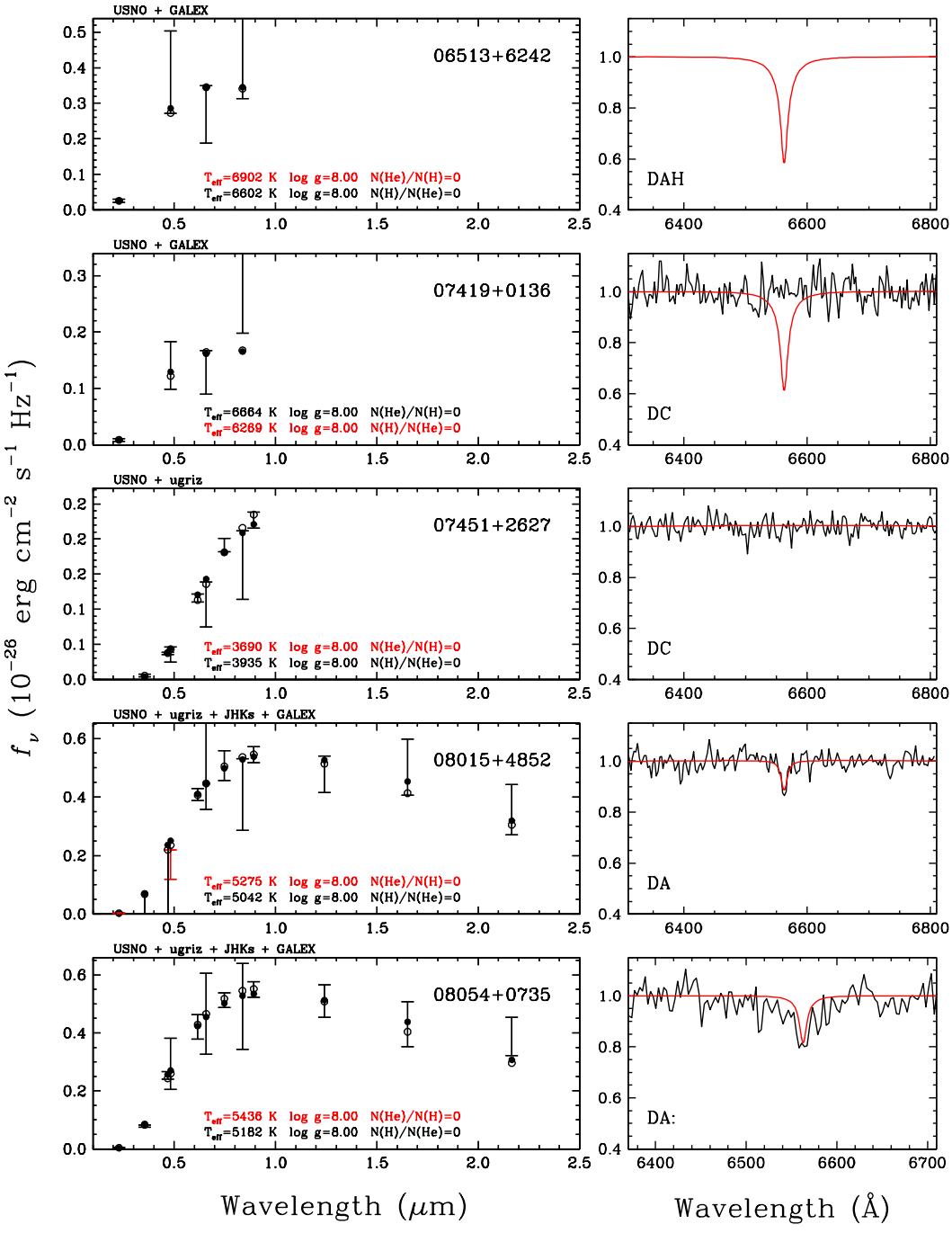

FIGURE A.1 – (i) - suite.

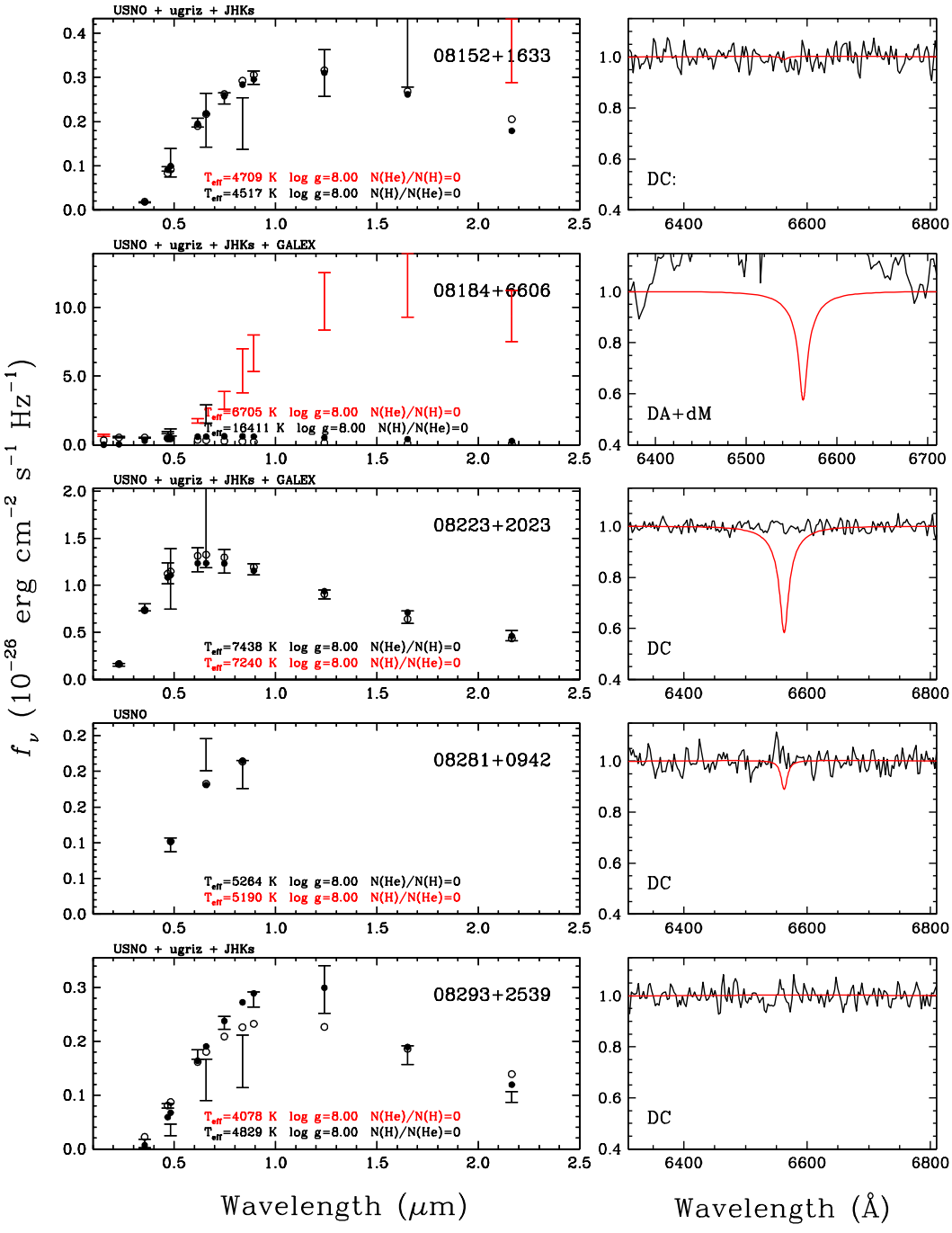

FIGURE A.1 – (j) - suite.

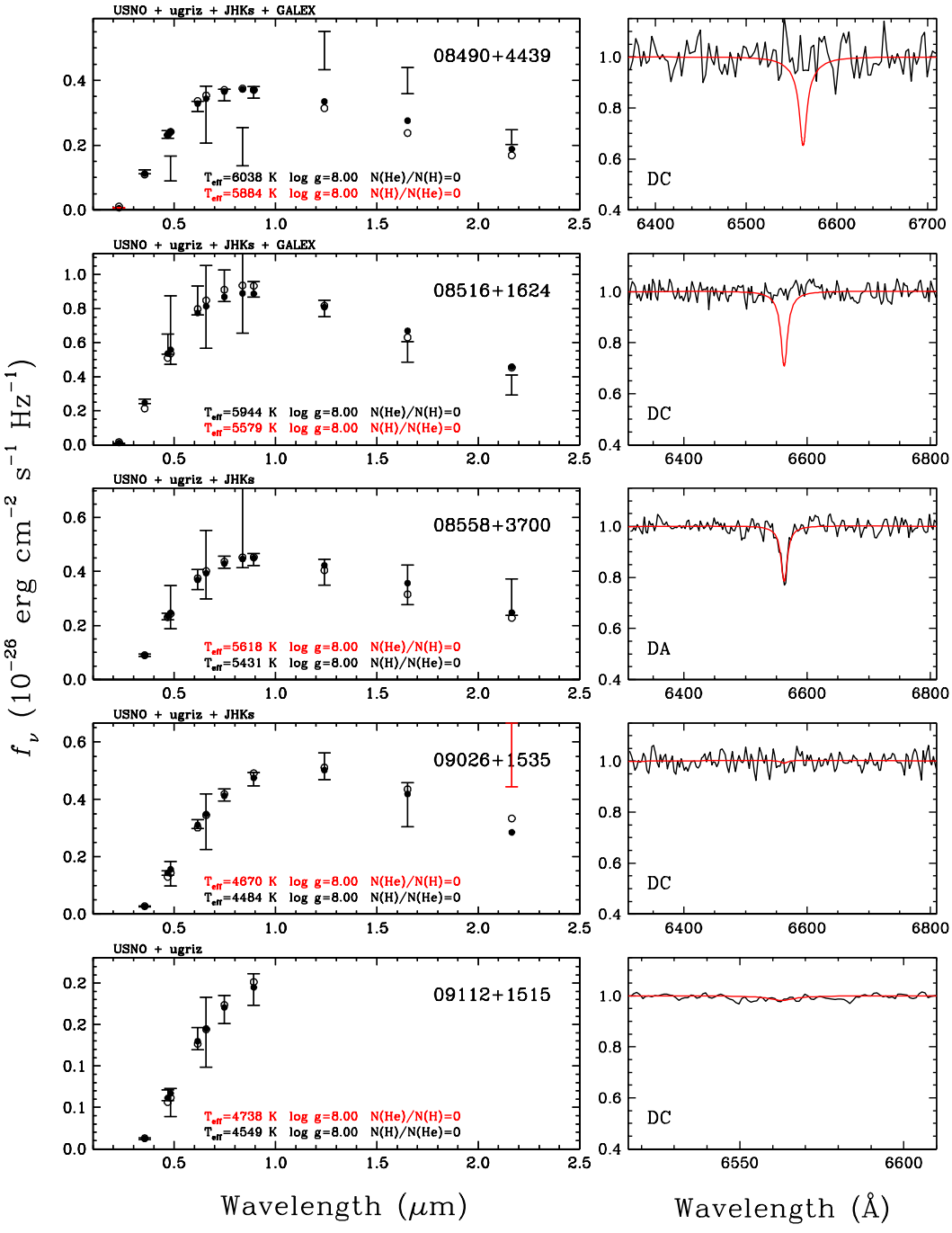

FIGURE A.1 – (k) - suite.

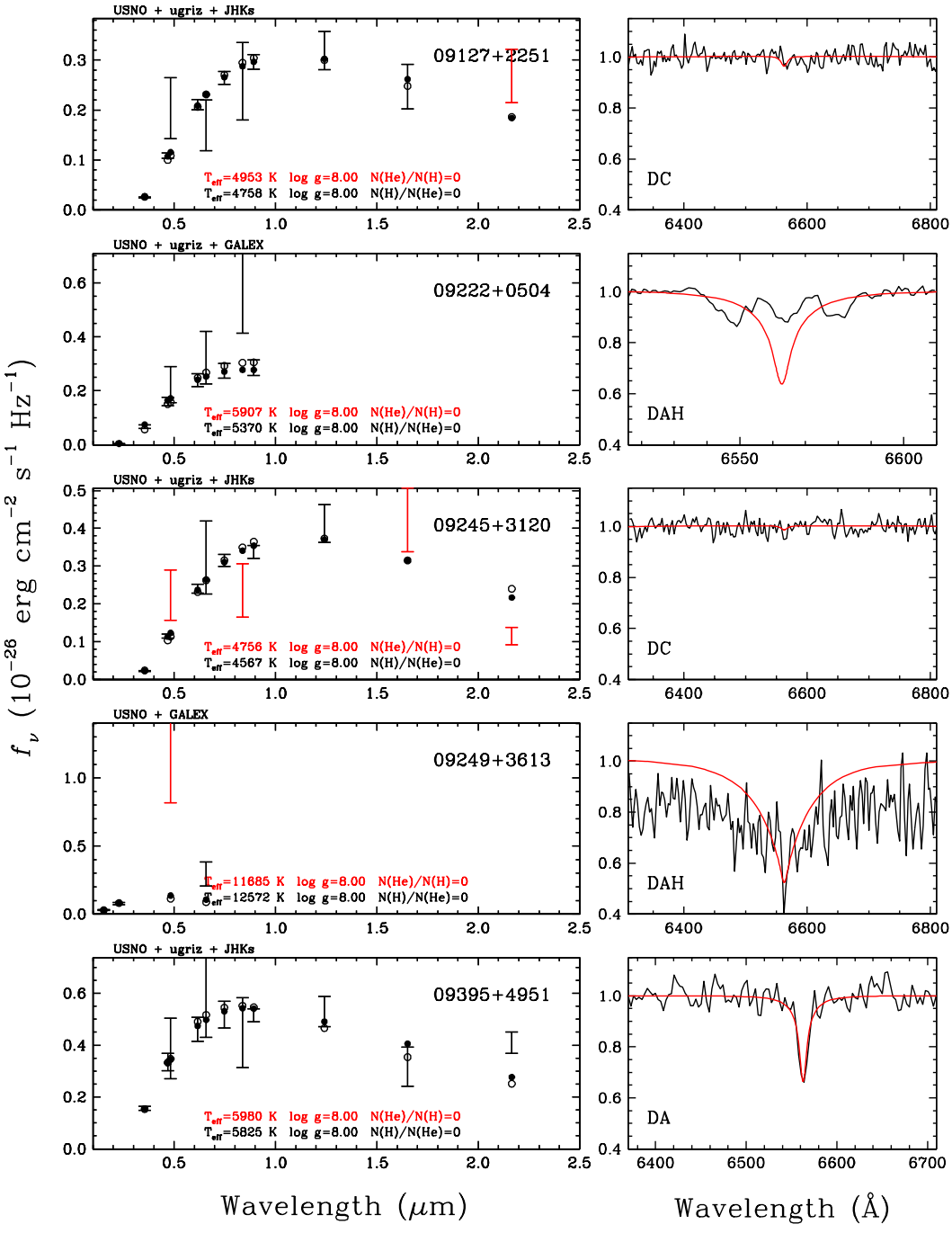

FIGURE A.1 – (l) - suite.

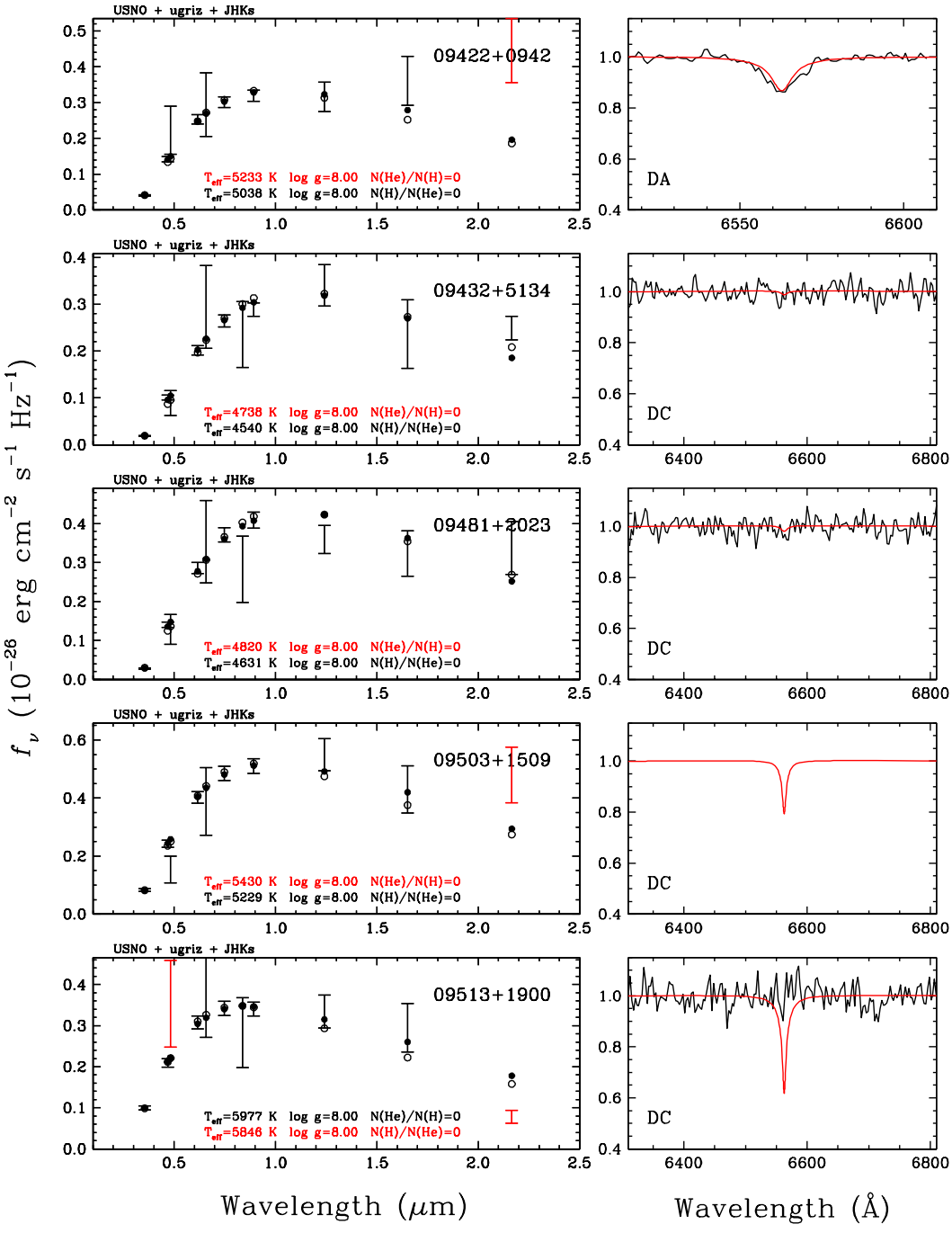

FIGURE A.1 – (m) - suite.

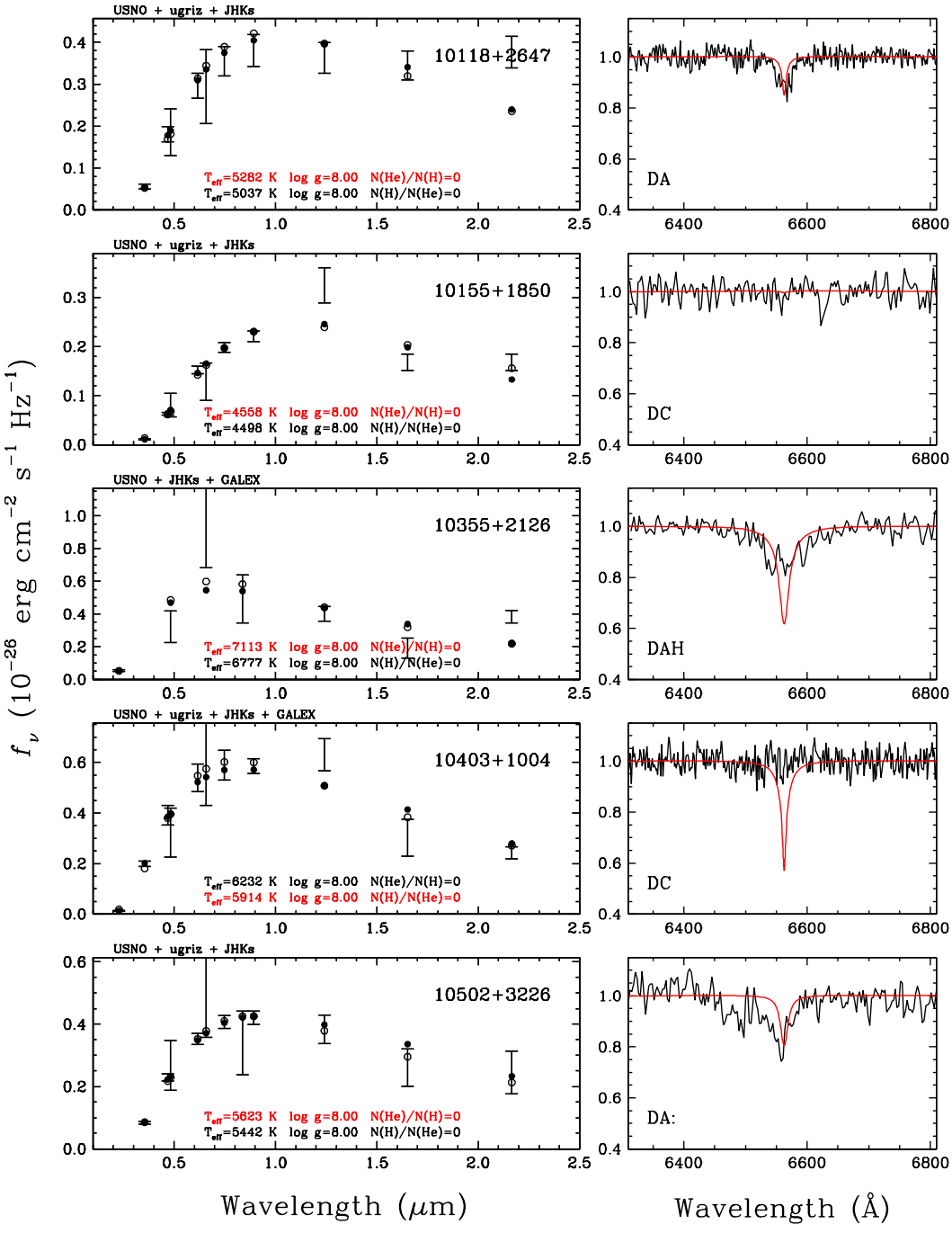

FIGURE A.1 – (n) - suite.

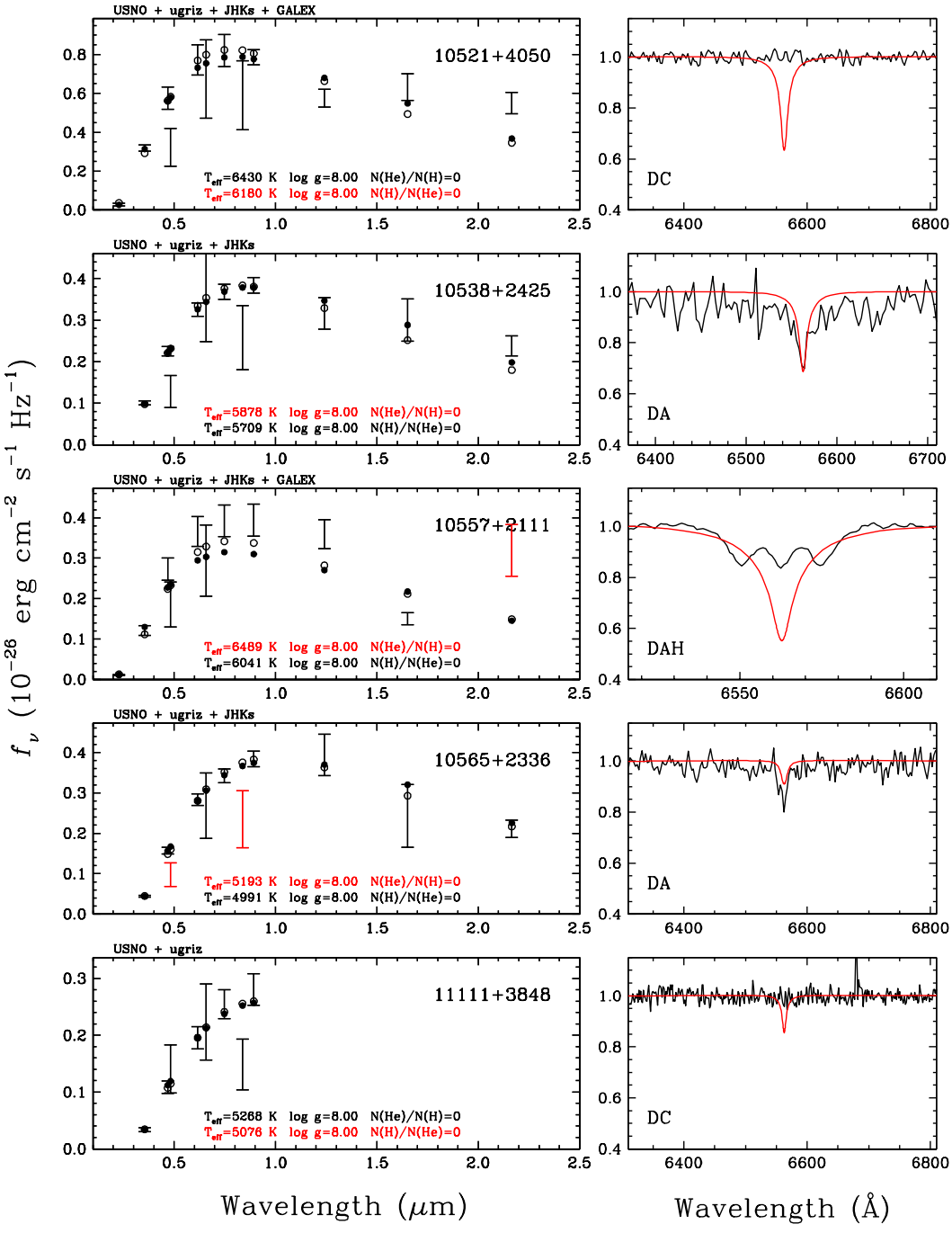

FIGURE A.1 – (o) - suite.

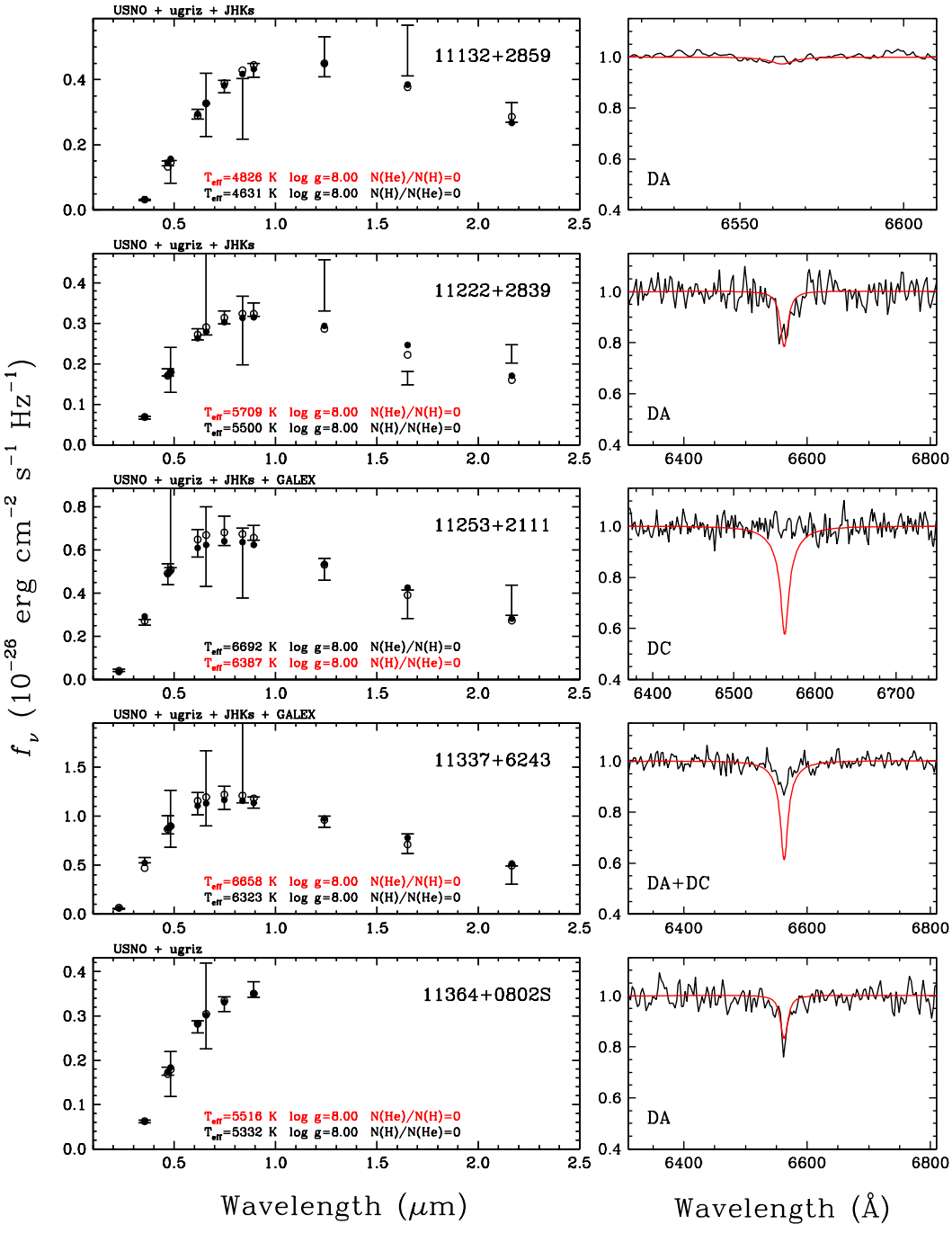

FIGURE A.1 – (p) - suite.

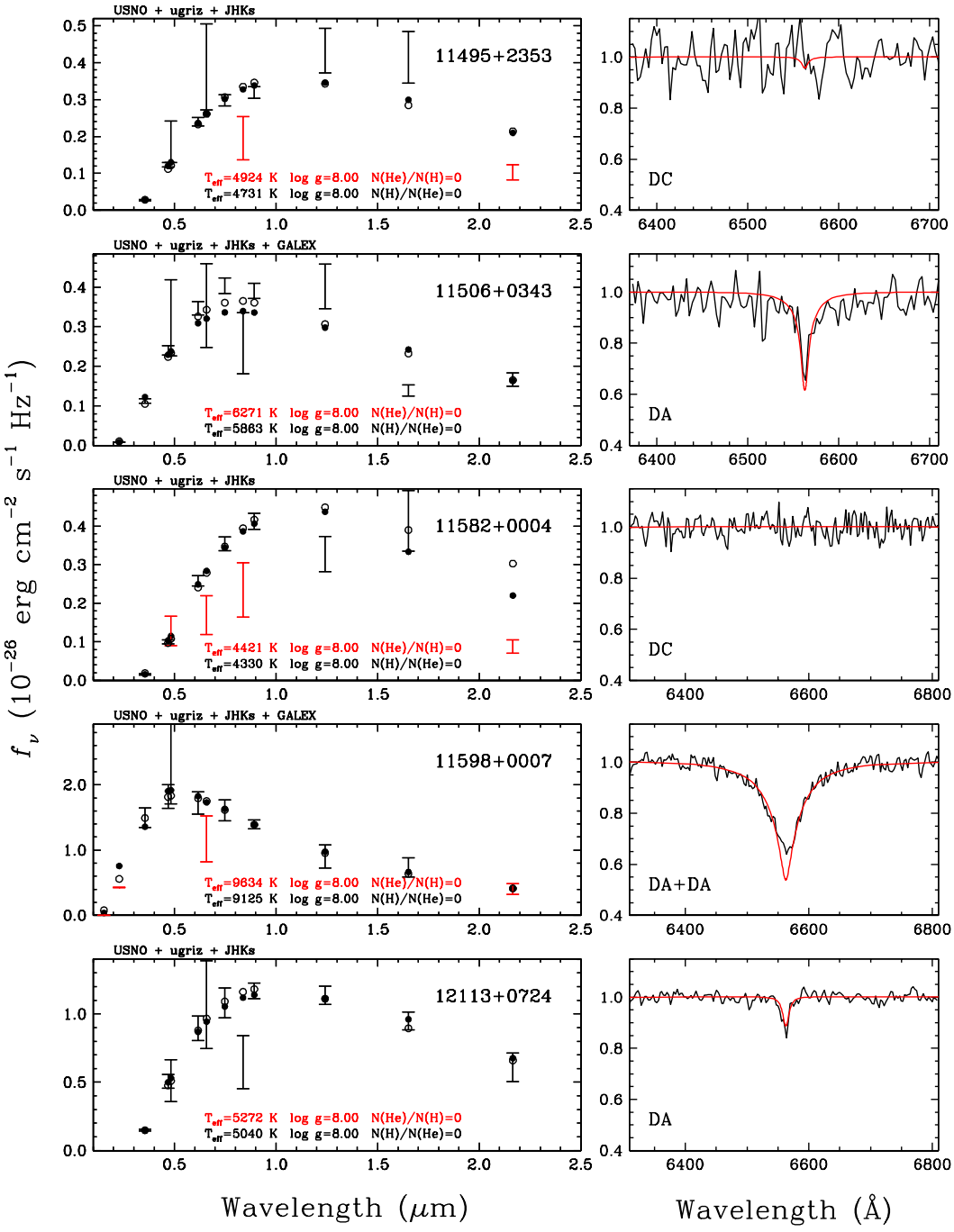

FIGURE A.1 – (q) - suite.

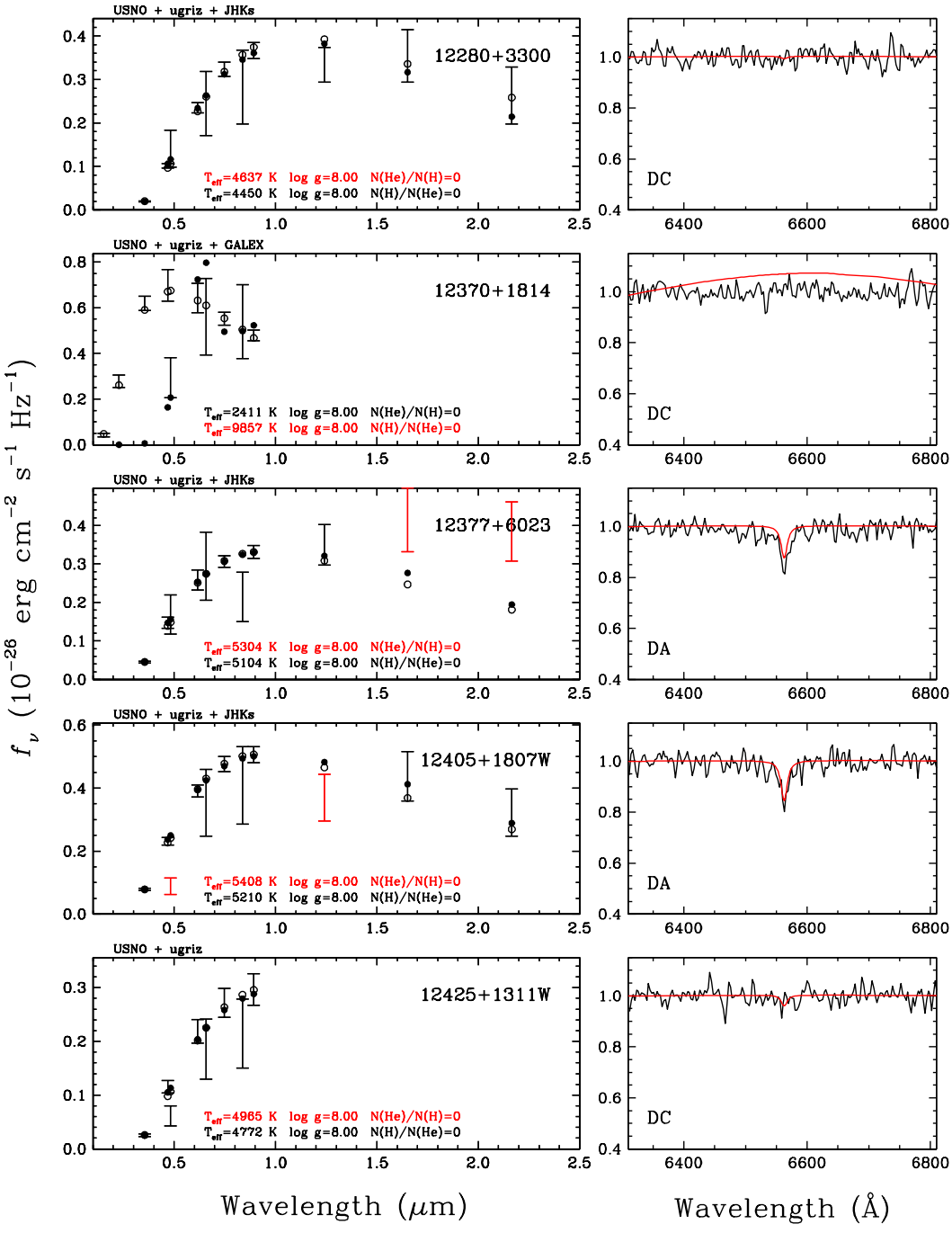

FIGURE A.1 – (r) - suite.

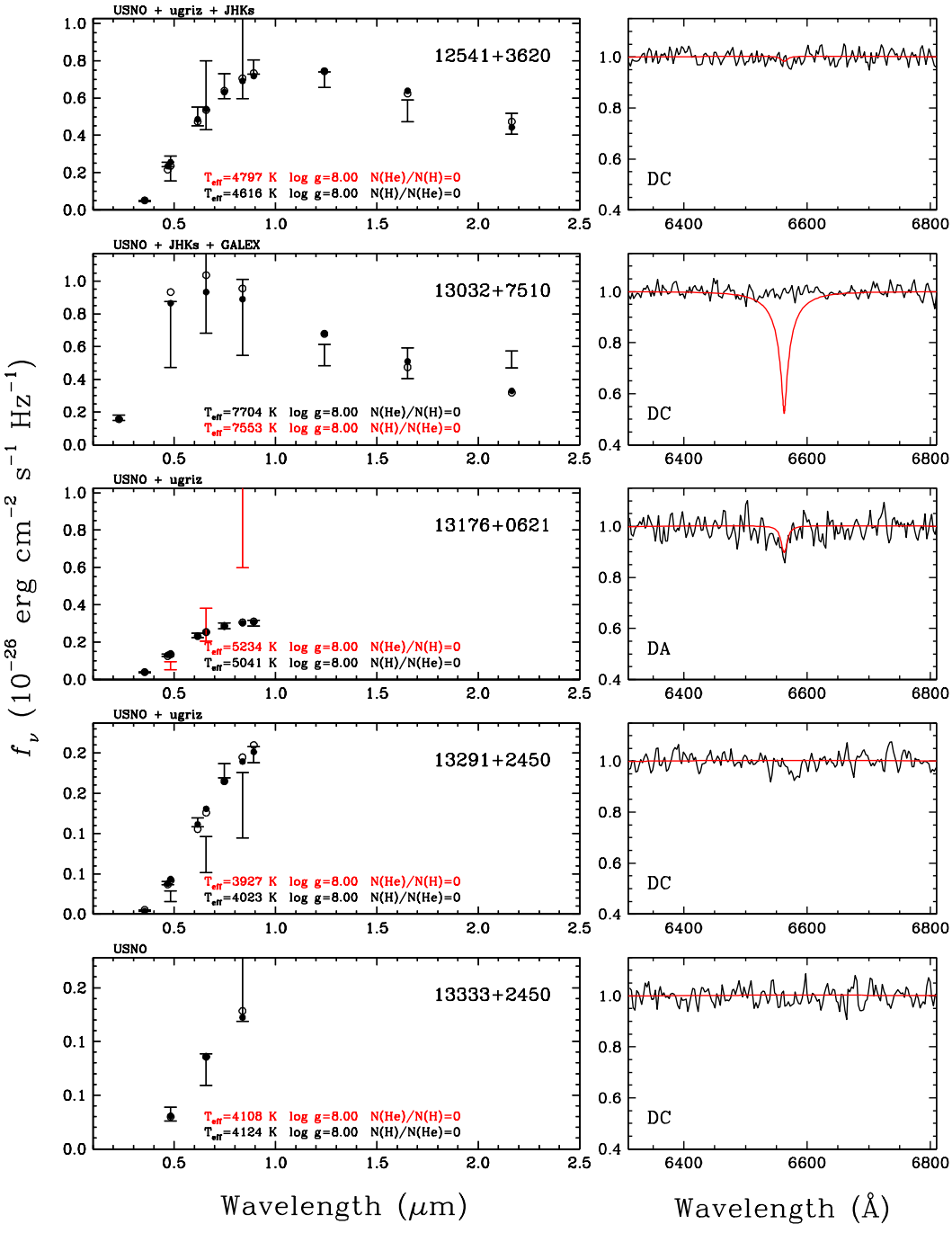

FIGURE A.1 – (s) - suite.

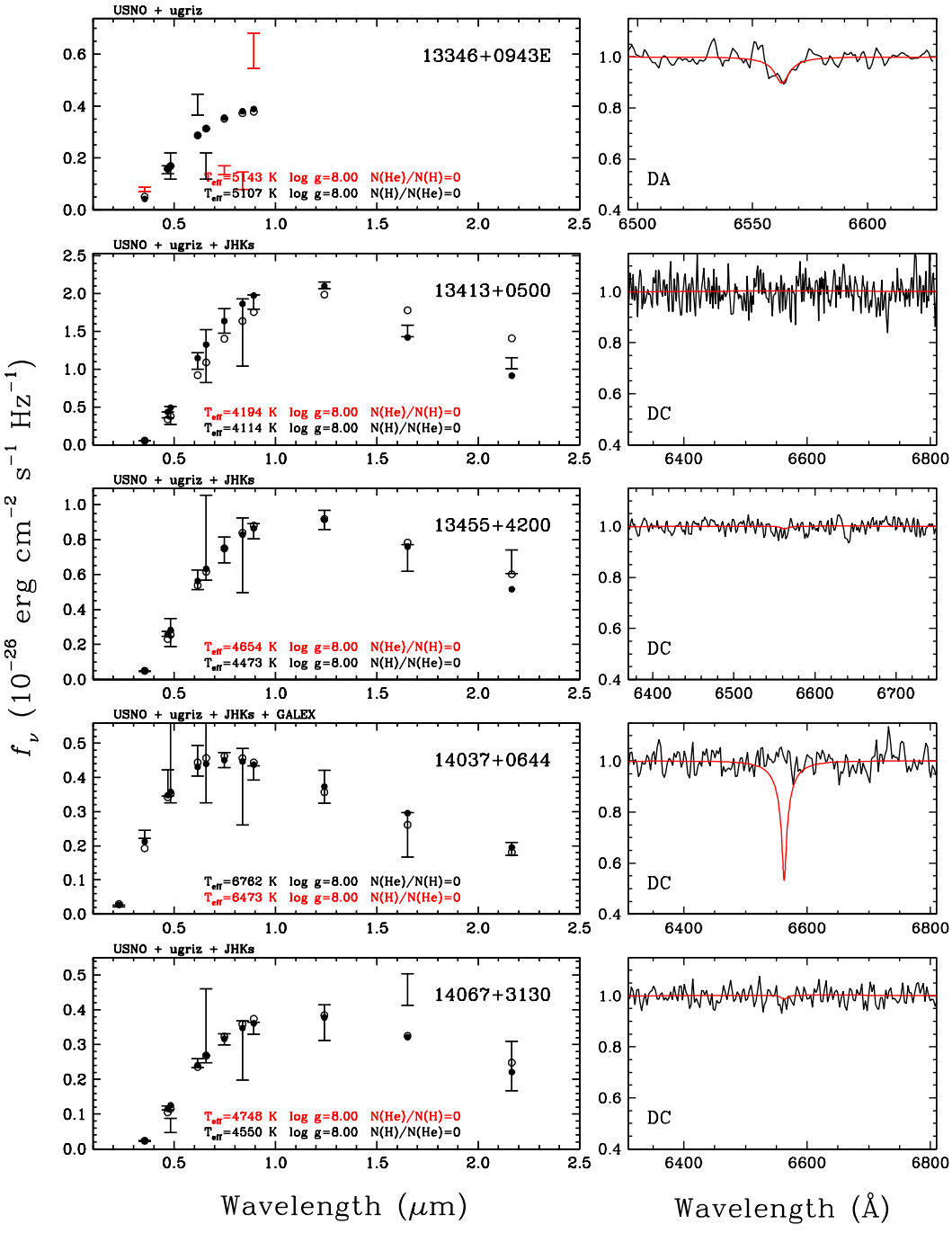

FIGURE A.1 – (t) - suite.

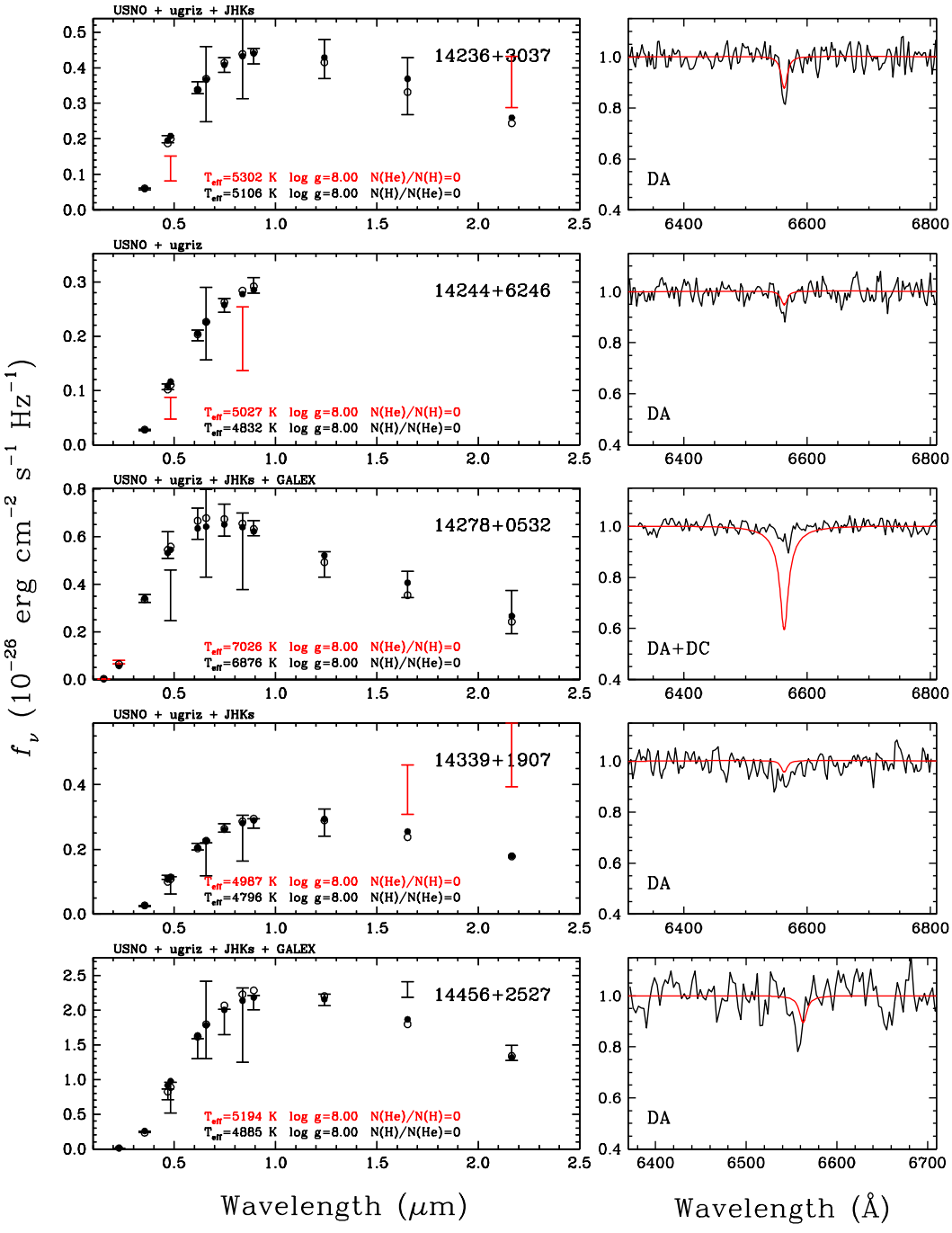

FIGURE A.1 – (u) - suite.

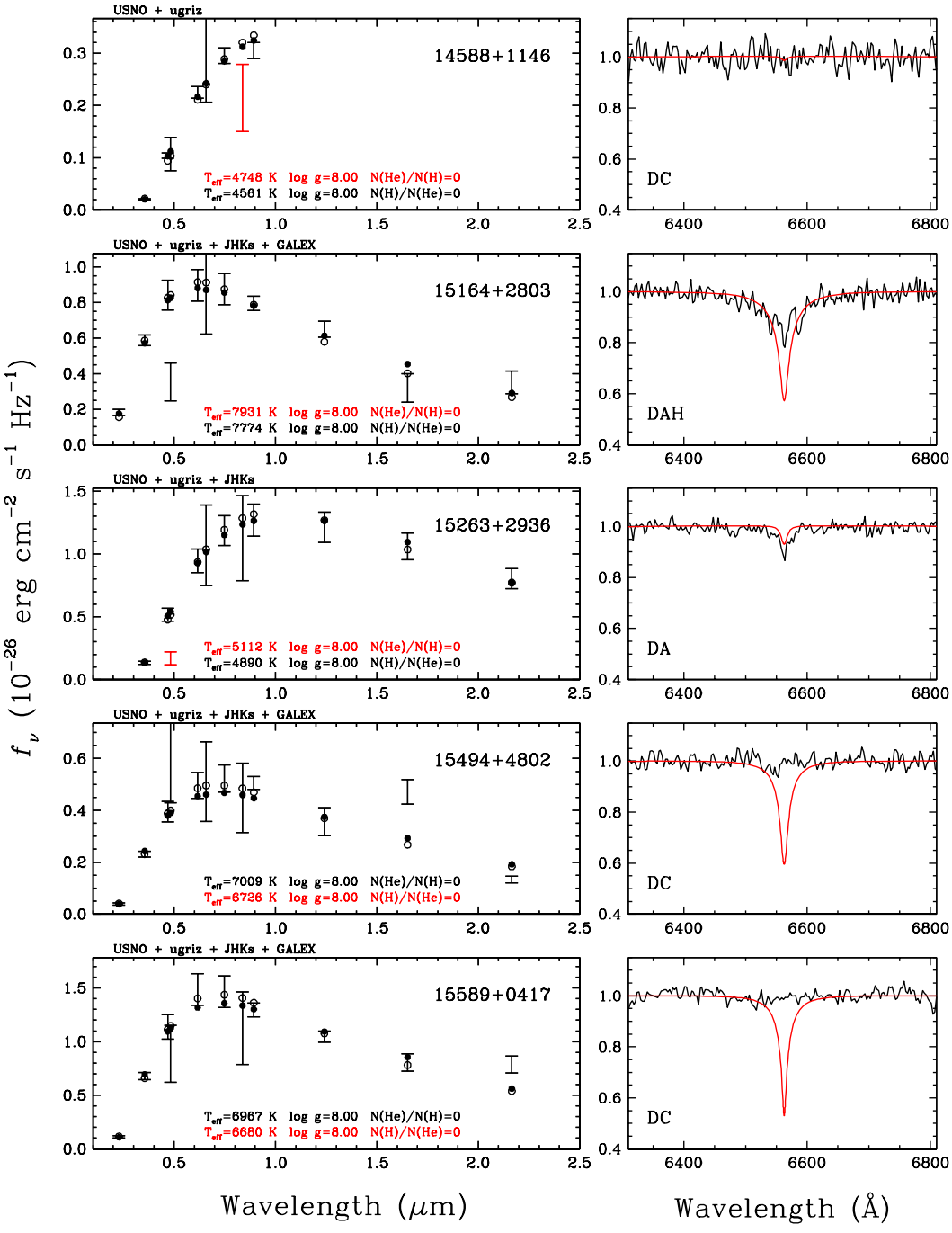

FIGURE A.1 – (v) - suite.

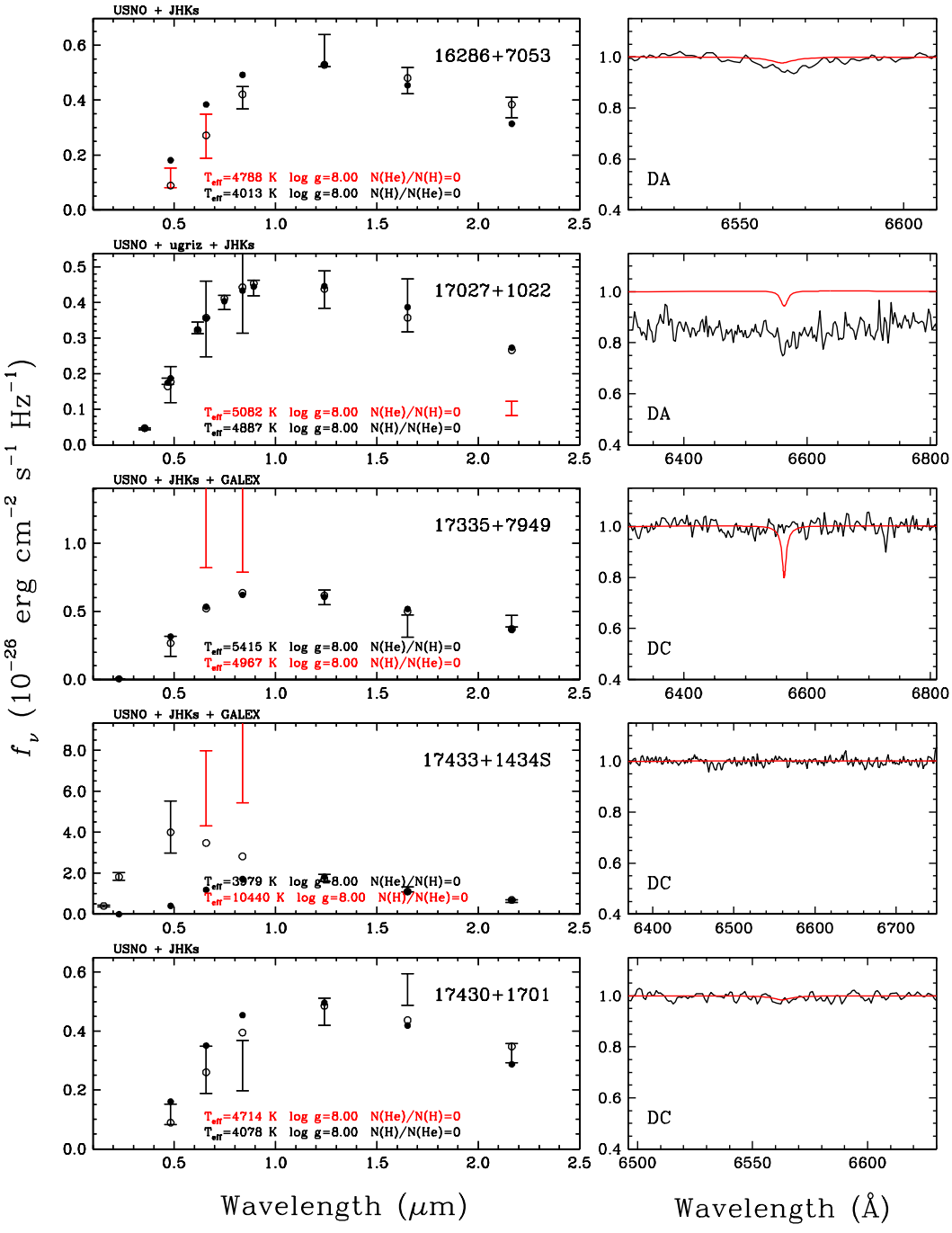

FIGURE A.1 – (w) - suite.

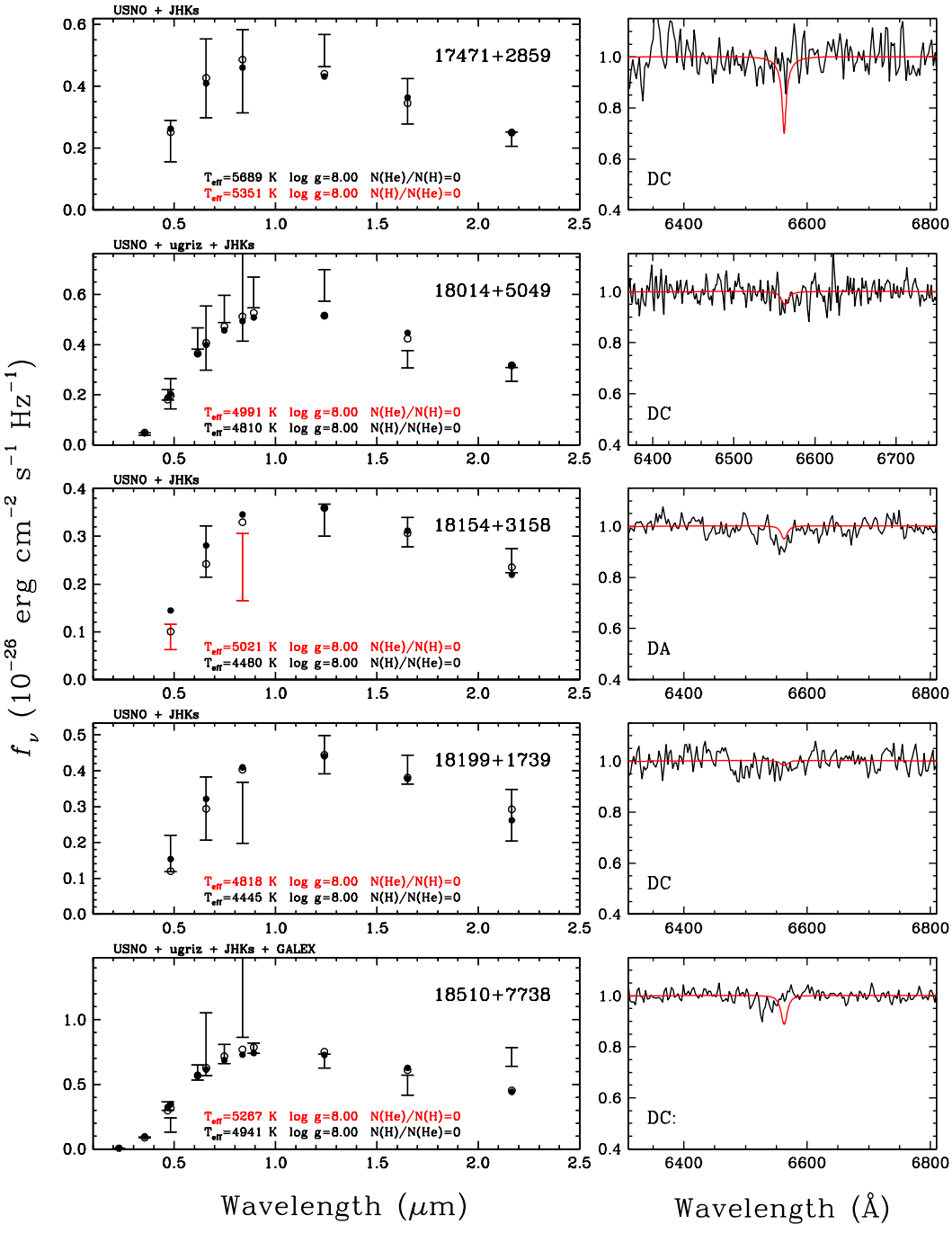

FIGURE A.1 – (x) - suite.

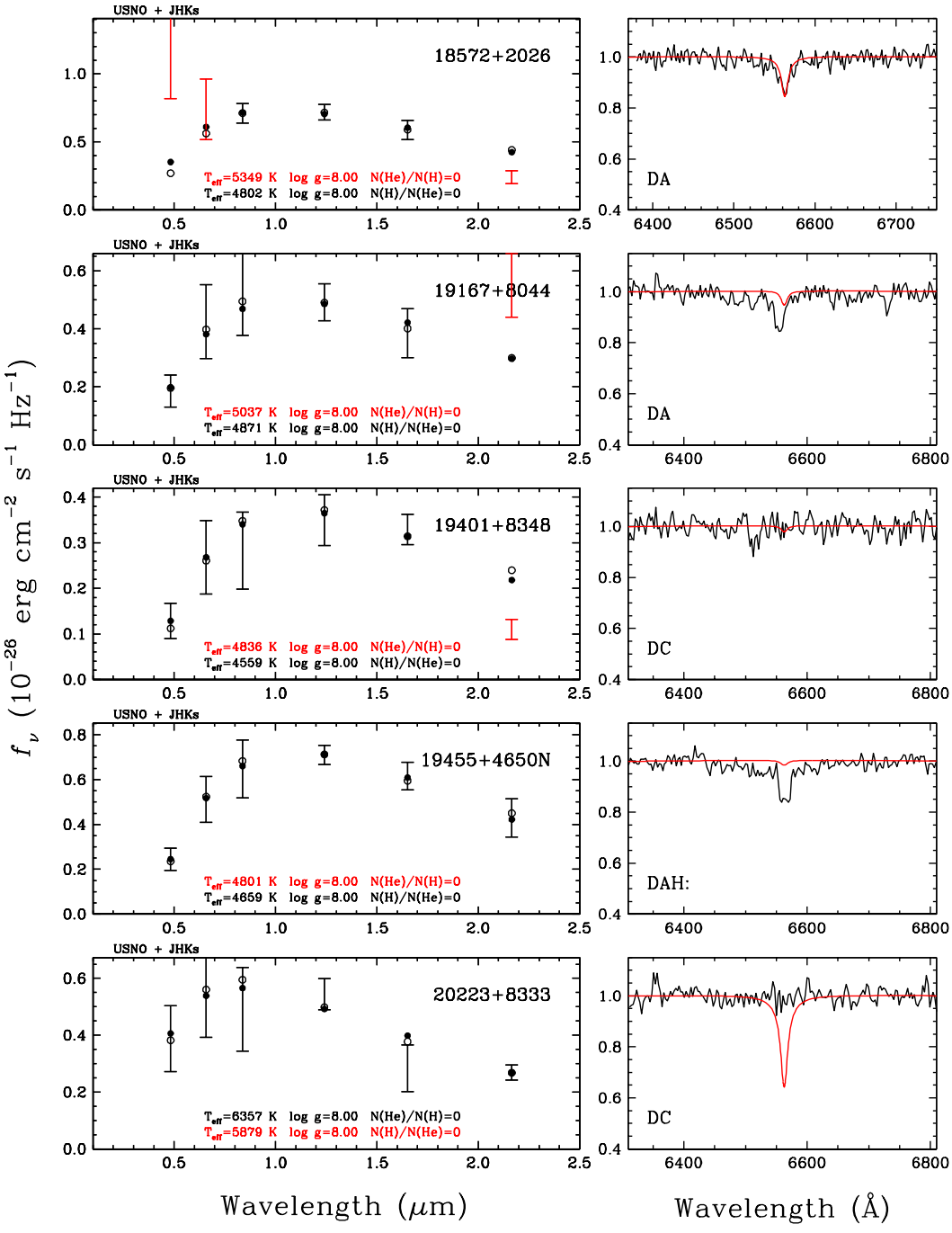

FIGURE A.1 – (y) - suite.

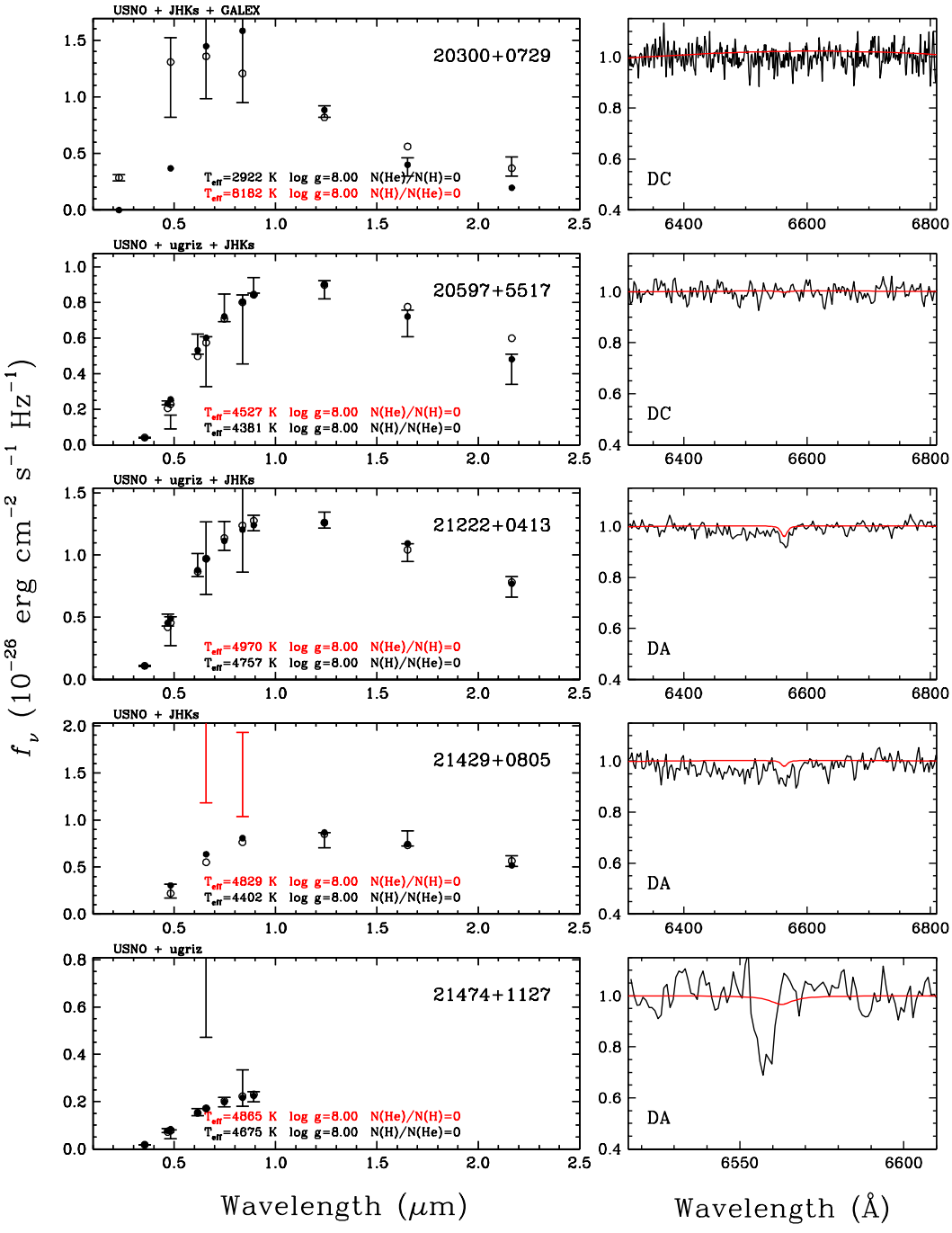

FIGURE A.1 – (z) - suite.

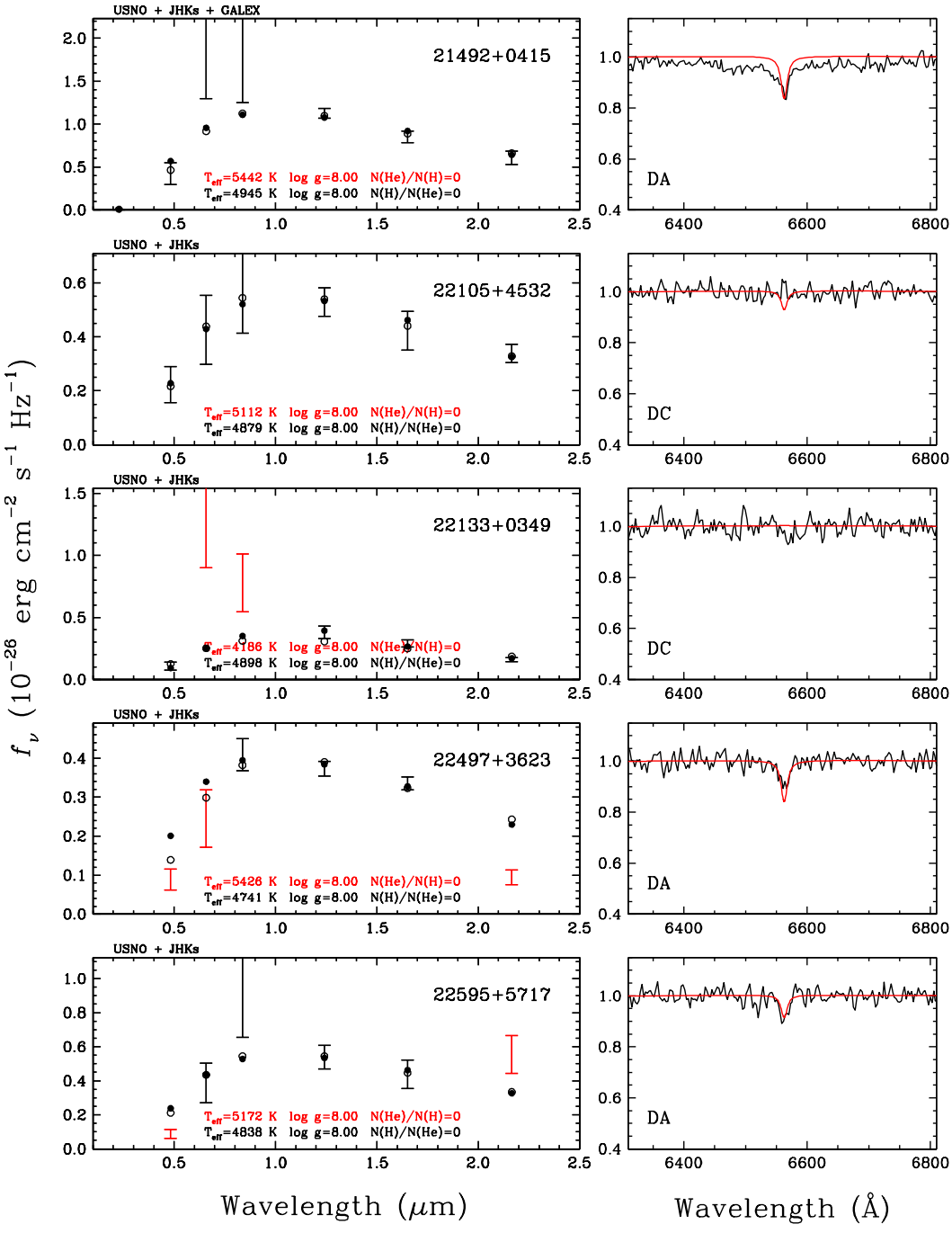

FIGURE A.1 – (A) - suite.

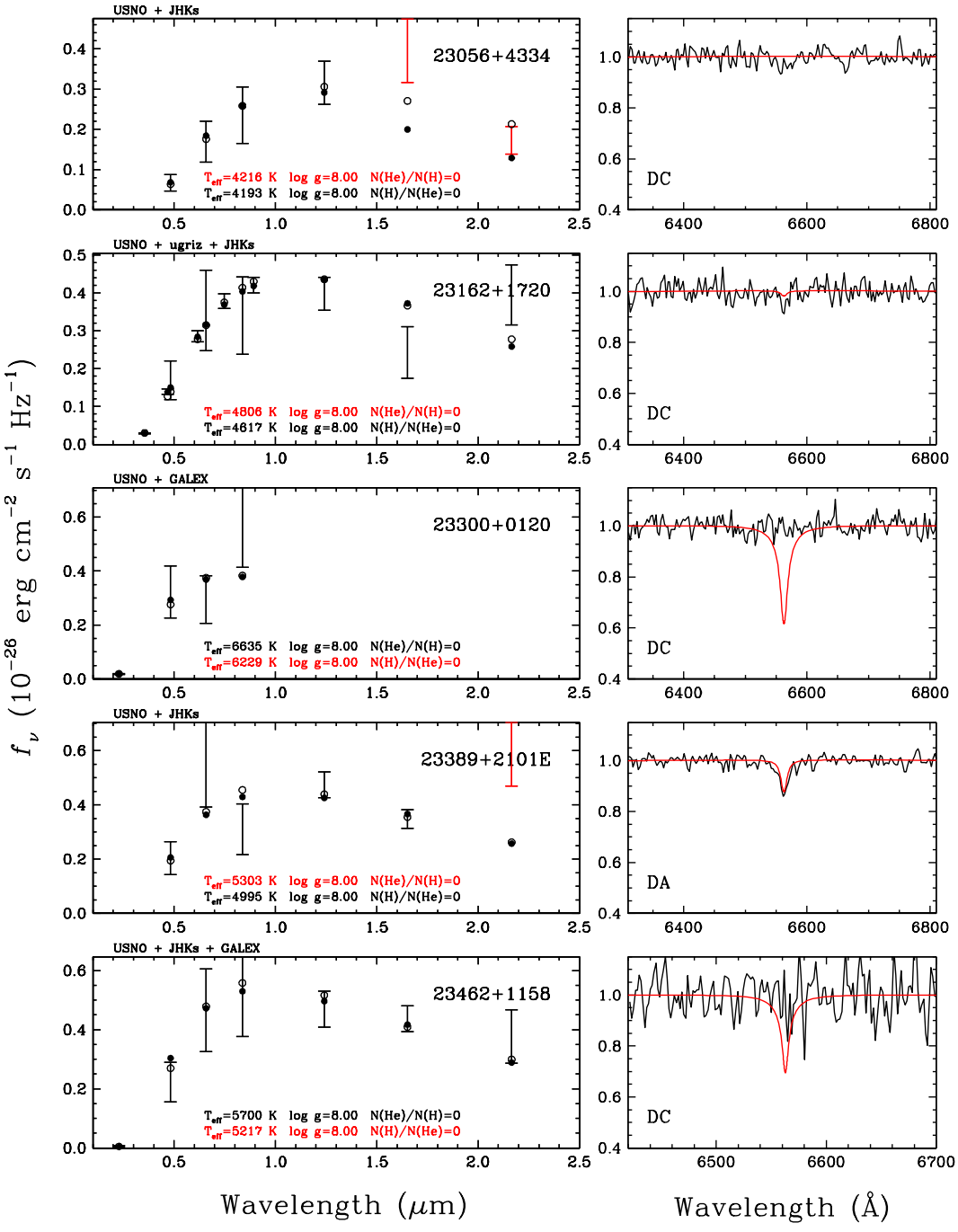

FIGURE A.1 – (B) - suite.

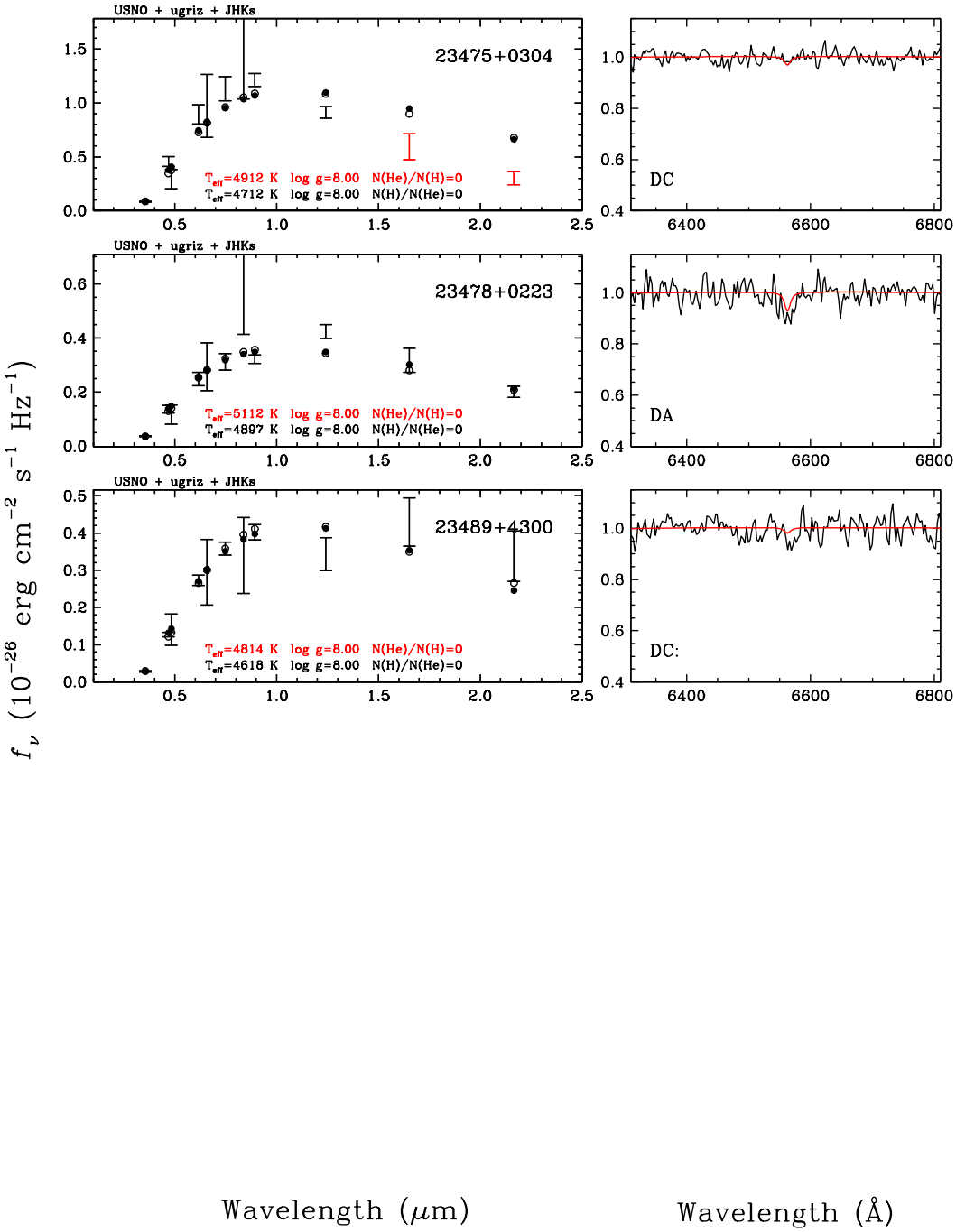

FIGURE A.1 – (C) - suite.

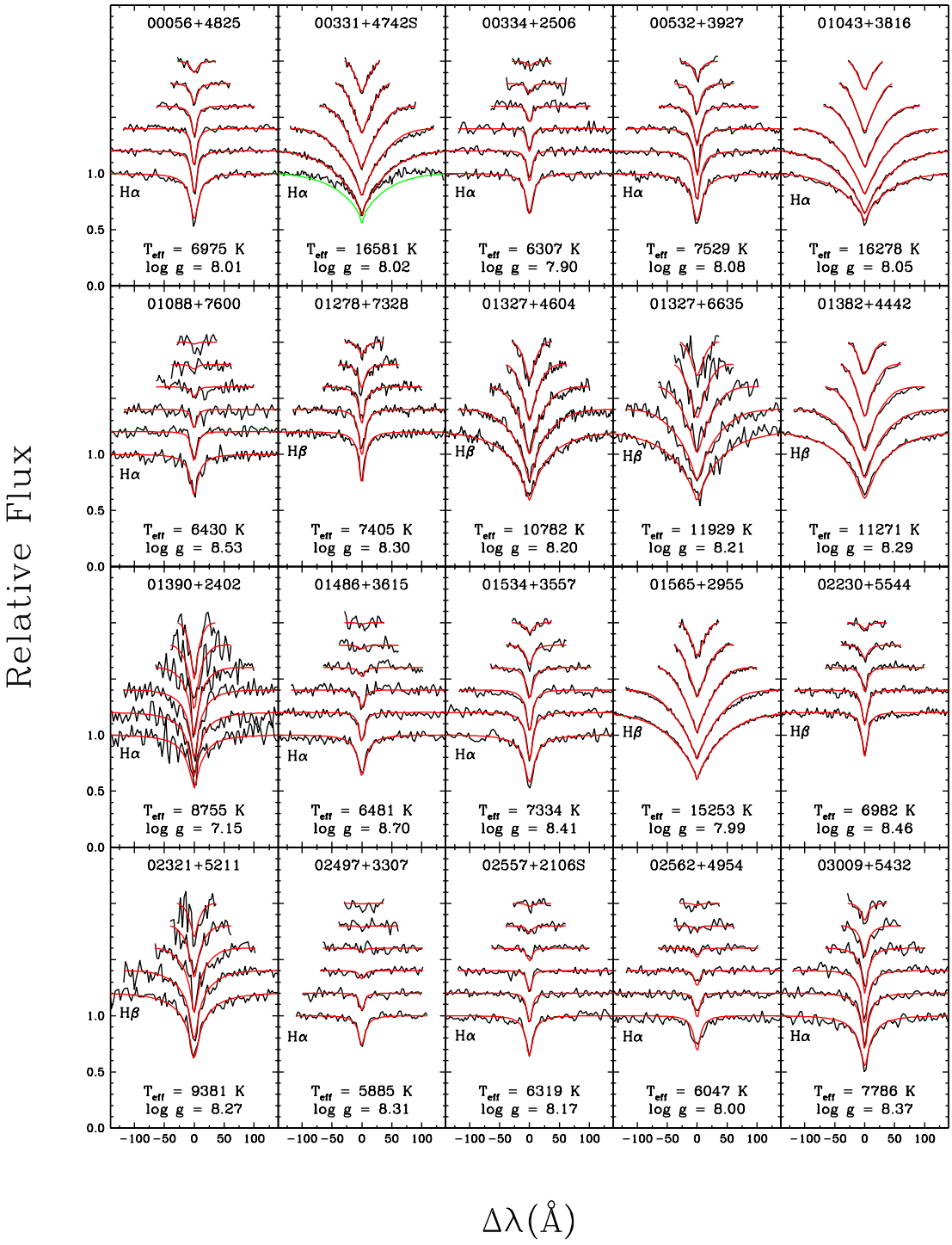

FIGURE A.2 – (a) Solutions spectroscopiques pour les étoiles DA identifiées par notre relevé, et présentées au Chapitre 3. Les profils tracés vont de Hα (si disponible) ou Hβ jusqu'à H8, et sont décalés verticalement d'un facteur de 0.2. Les profils tracés en vert sont ignorés lors de l'ajustement avec les modèles.

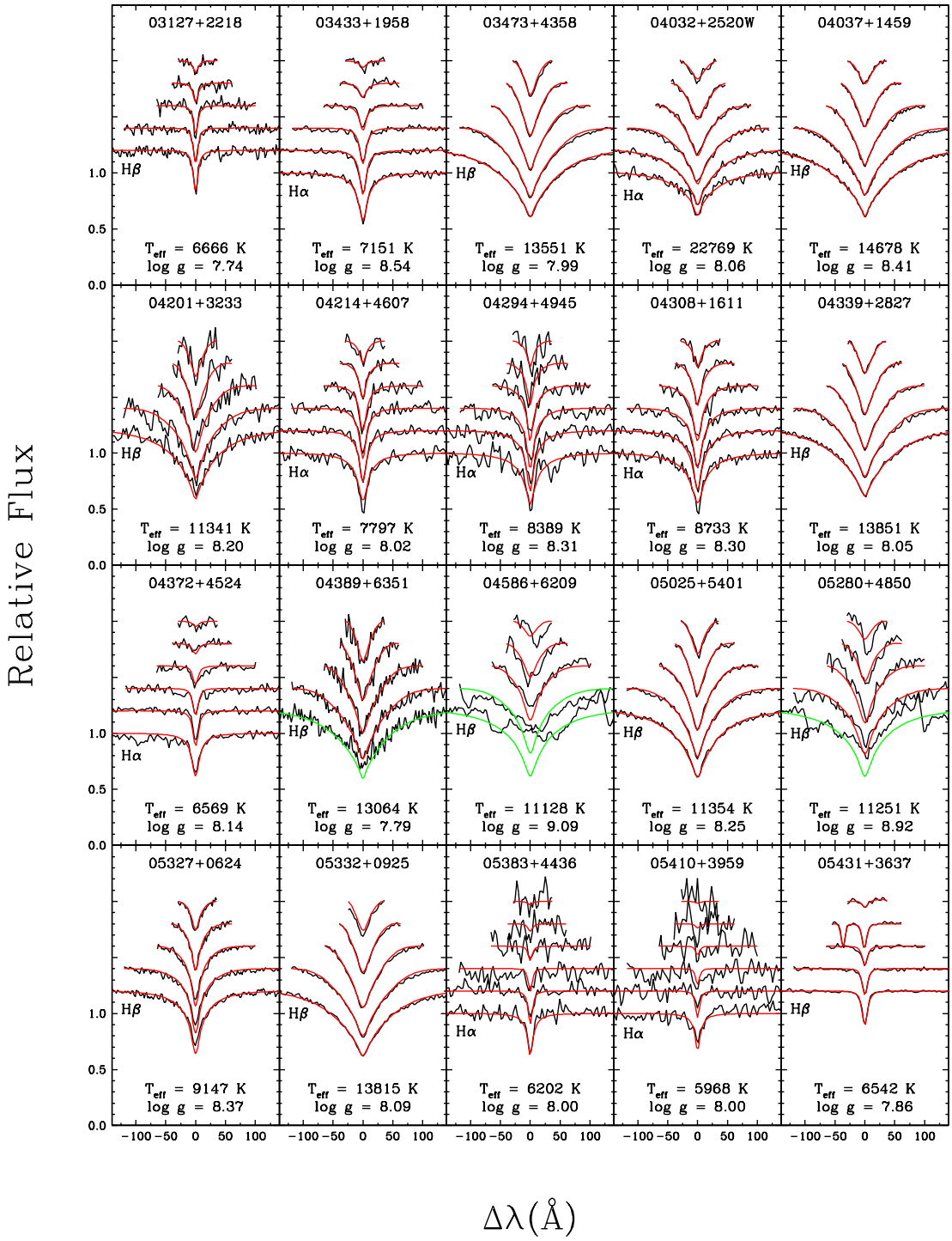

FIGURE A.2 – (b) - suite.

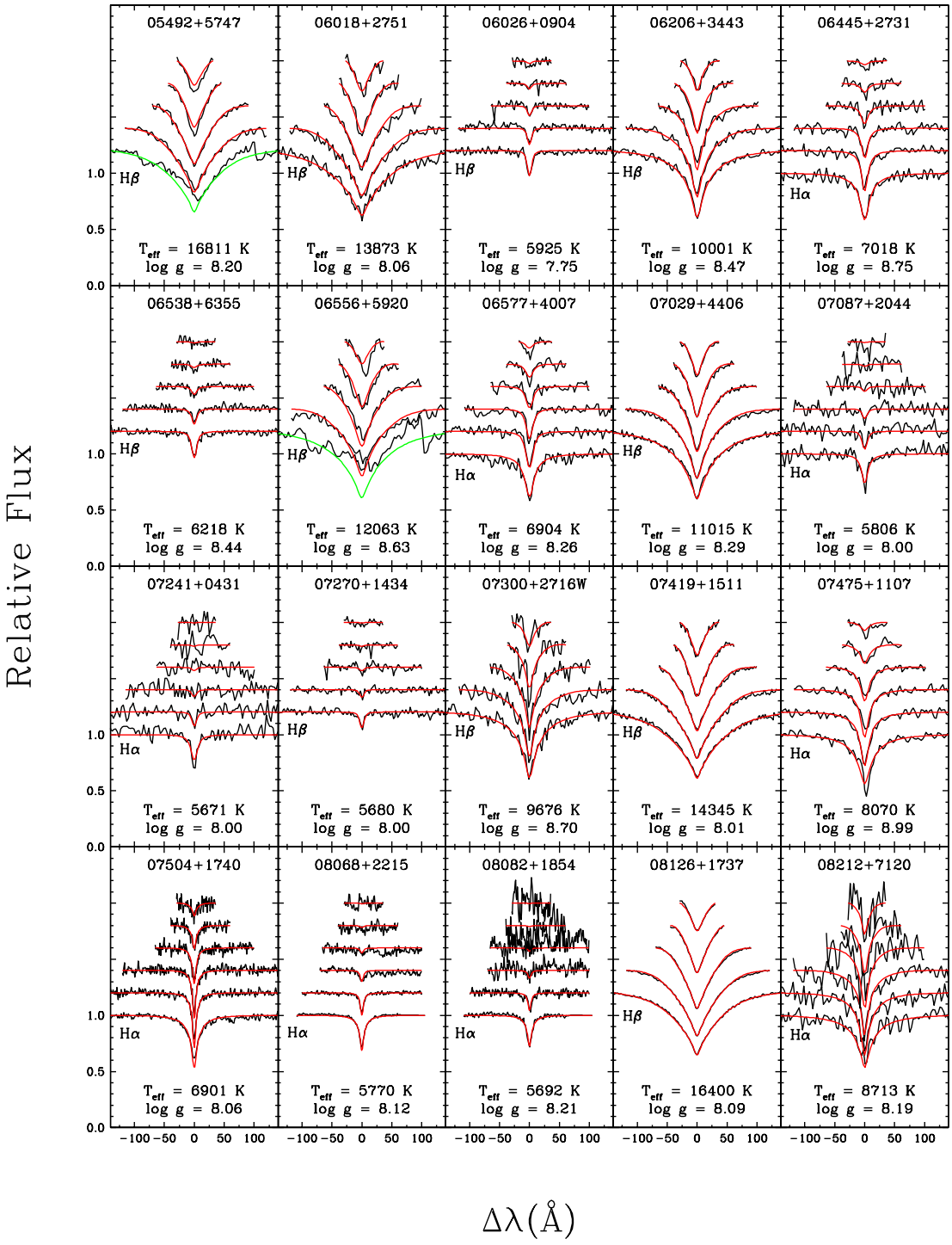

FIGURE A.2 – (c) - suite.

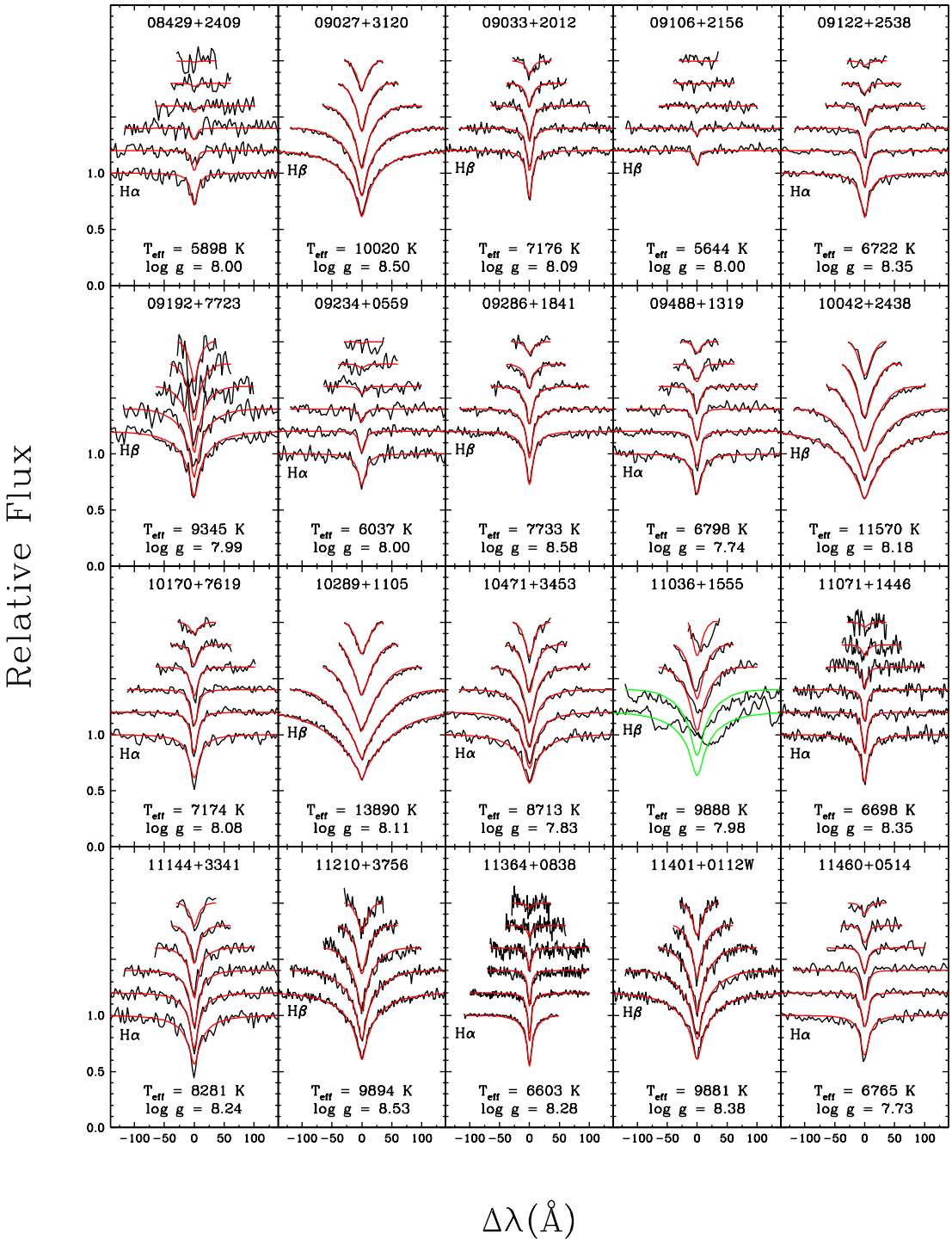

FIGURE A.2 – (d) - suite.

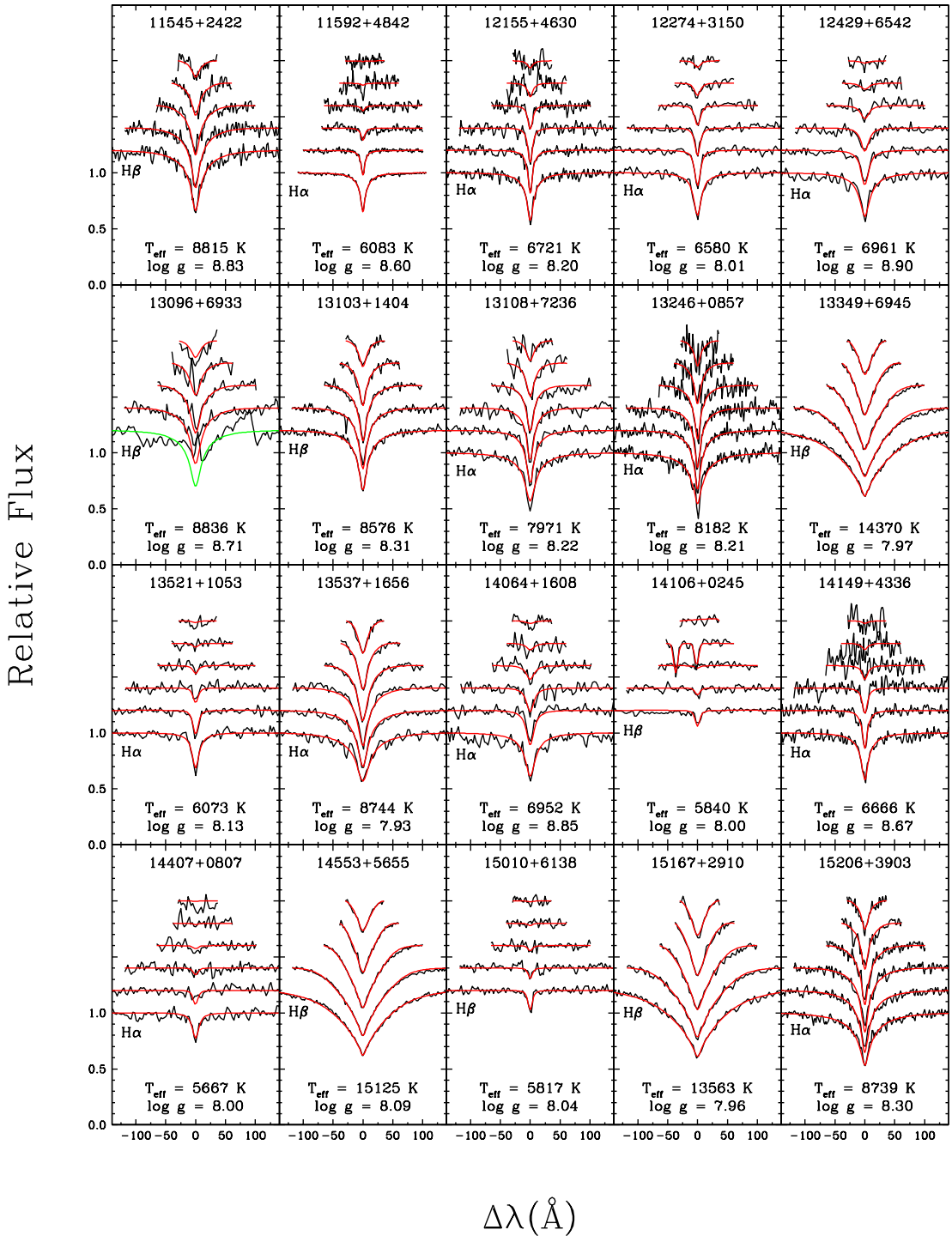

FIGURE A.2 – (e) - suite.

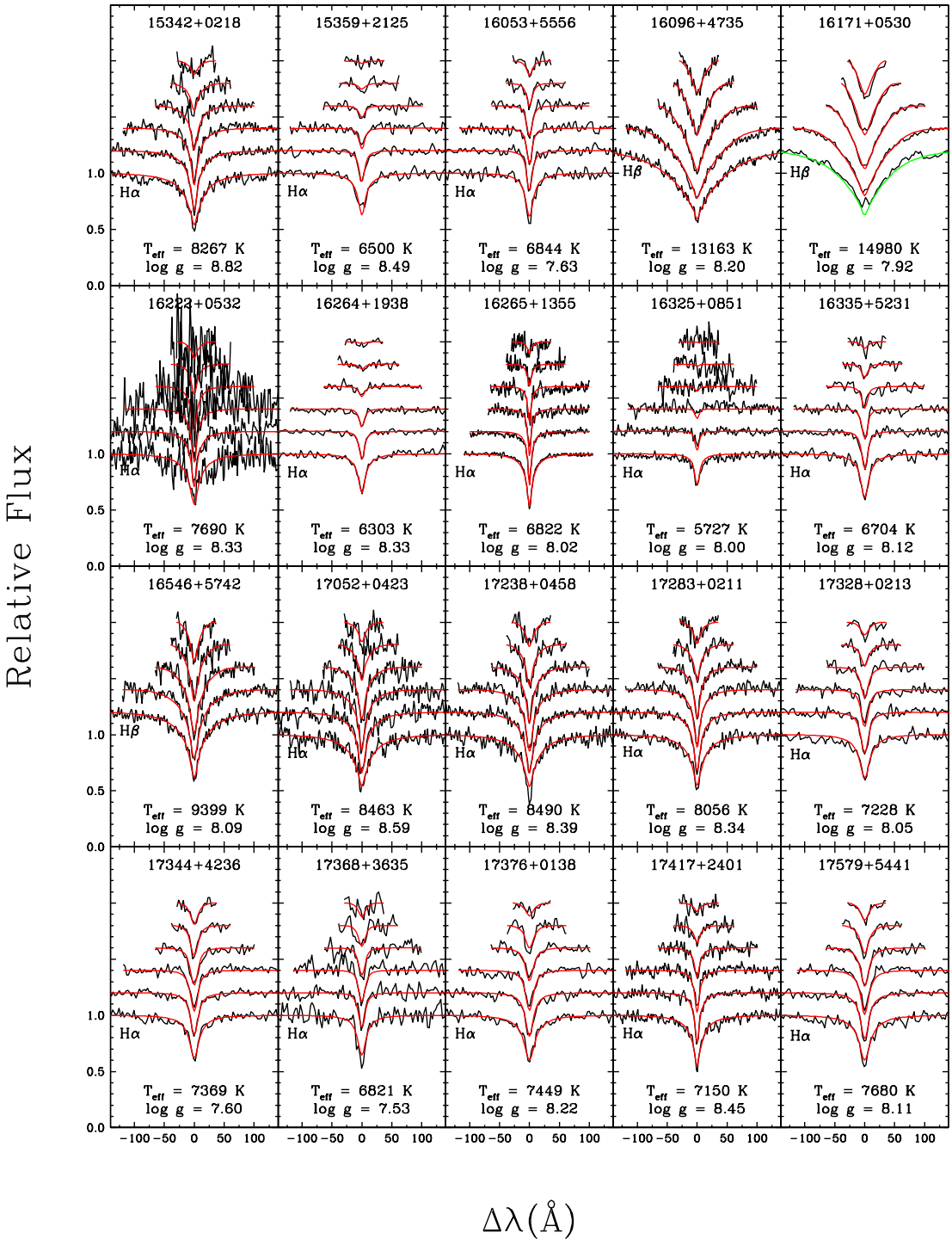

FIGURE A.2 – (f) - suite.

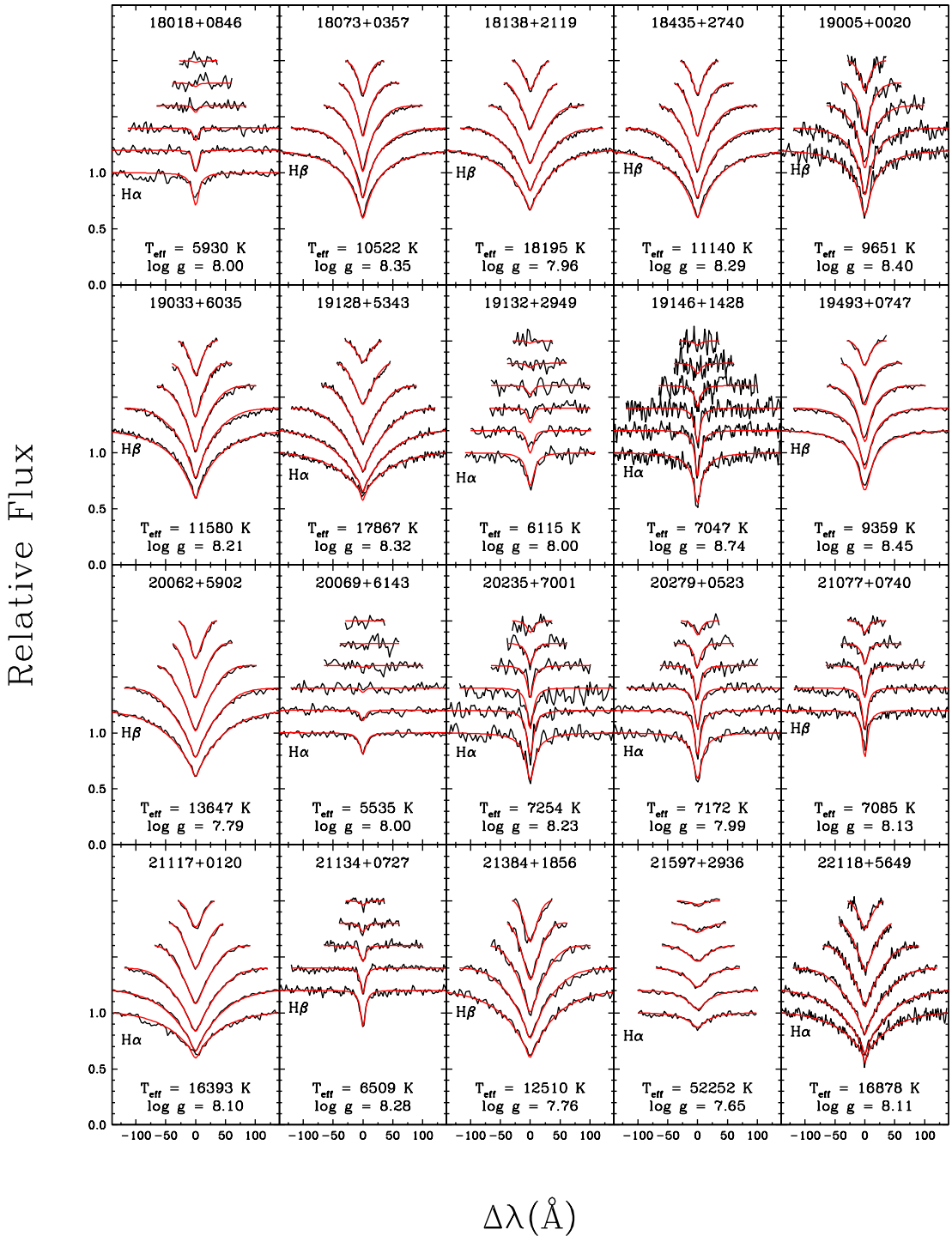

FIGURE A.2 – (g) - suite.

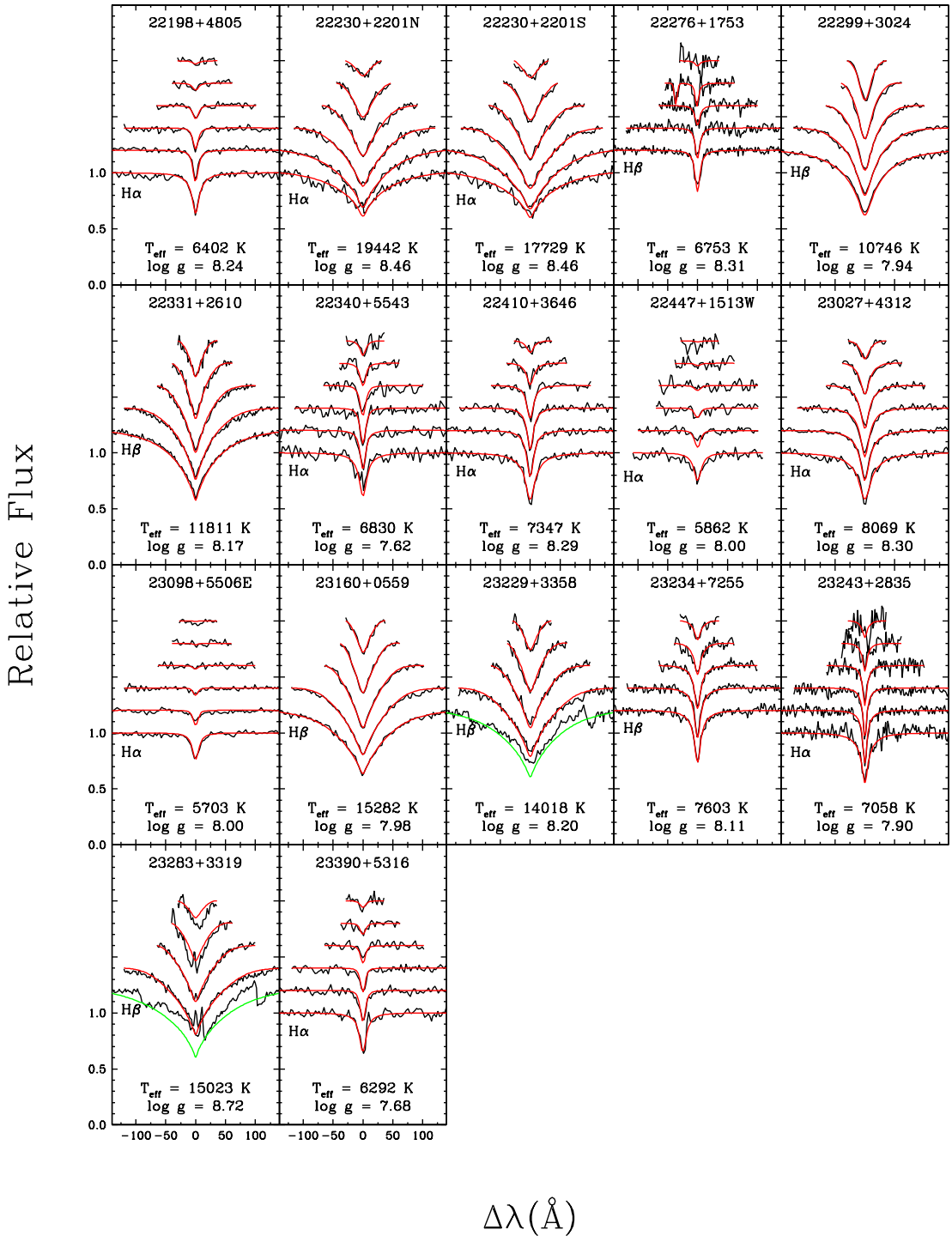

FIGURE A.2 – (h) - suite.

Annexe B

Deux nouvelles étoiles naines blanches de type ZZ Ceti

Les étoiles ZZ Ceti sont des naines blanches DA dont la luminosité varie de manière périodique. Lorsque l'étoile atteint des température entre $\sim$ 11 000 $-$ 13 000 K (voir Figure B.1), la formation d'une zone d'ionisation partielle de l'hydrogène (produisant une forte opacité) se forme à une profondeur propice à l'excitation des modes normaux de vibration de l'étoile. L'amplitude de ces modes de vibration est alors amplifiée par effet de résonance, et les variations de luminosité résultantes sont observables depuis la Terre. Ce phénomène porte le nom de mécanisme κ.

La bande d'instabilité des étoiles ZZ Ceti a été étudiée par Gianninas et al. (2007), qui en définirent les limites de manière empirique. Dans Gianninas et al. (2011), les frontières ont par la suite subit une modification de quelques centaines de Kelvins grâce à l'amélioration des modèles d'atmosphère et à leur grand échantillon de naines blanches DA. Jusqu'à maintenant, les résultats montrent que la bande d'instabilité est pure, et donc toutes les étoiles dont les paramètres atmosphériques les situent à l'intérieur de cette bande d'instabilité devraient être variables. Si c'est le cas, il est donc possible de prédire la variabilité d'une étoile en connaissant ses paramètres atmosphériques.

Une bande d'instabilité pure signifie également que toutes les étoiles naines blanches avec une atmosphère d'hydrogène passeraient par cette phase lors de leur refroidissement. Si, par

contre, une étoile dans la bande d'instabilité montre une courbe de lumière constante, alors soit les paramètres atmosphériques sont erronés, soit la bande d'instabilité est impure. Il est donc impératif d'obtenir des courbes de lumière pour chaque étoile se trouvant dans la bande d'instabilité.

Parmi notre échantillon de 322 naines blanches identifiées par notre relevé spectroscopique, 9 étoiles se trouvent dans la bande d'instabilité des ZZ Ceti. Ces étoiles sont représentées dans la Figure B.1 par des carrés. Pour trois de ces candidates et une autre qui ne se trouve maintenant plus dans la bande d'instabilité, nous avons obtenu des observations en photométrie rapide au télescope de 1.6 m du Mont Bigelow, en collaboration avec Elizabeth Green de l'Université d'Arizona. La première candidate observée, 04263+4820 (WD0458+620), est

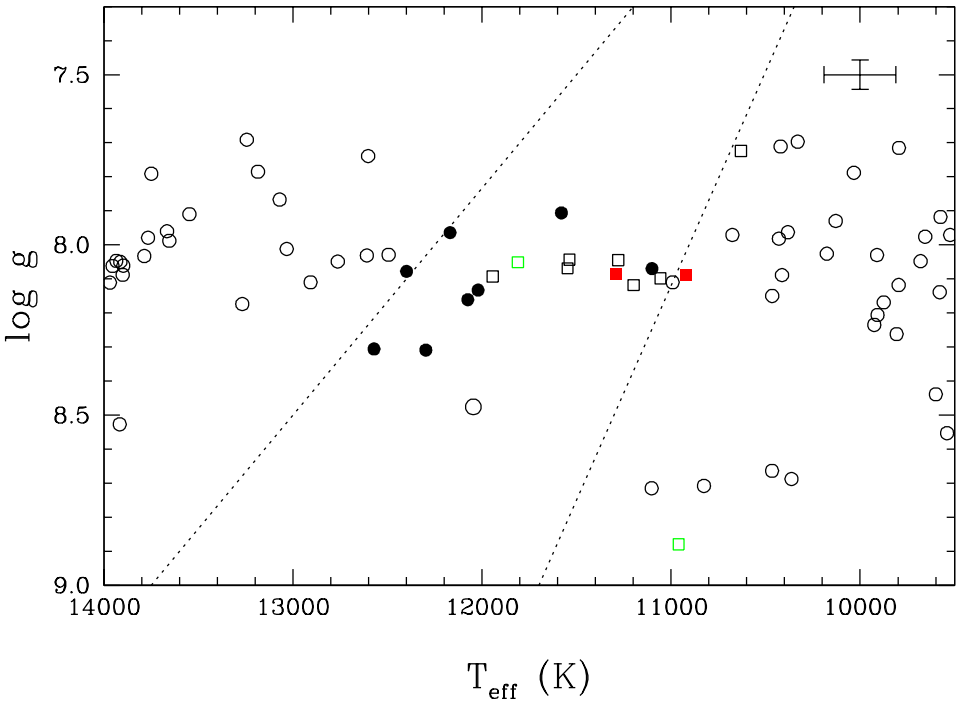

FIGURE B.1 – Logarithme de la gravité de surface en fonction de la température effective, où la bande d'instabilité empirique des ZZ Ceti se trouve entre les traits pointillés. Les cercles pleins indiquent les naines blanches connues de notre échantillon pour lesquelles des variations de luminosité ont été observées, tandis que les carrés représentent les nouvelles candidates ZZ Ceti. Les carrés verts représentent les deux naines blanches qui ne montrent pas de variation de luminosité et les carrés rouges montrent les nouvelles étoiles ZZ Ceti confirmées par photométrie rapide.

représentée en vert dans le bas de la Figure B.1, et elle ne montre pas de variation de lumière. L'étoile est en fait une DA+dM, qui rend la mesure des paramètres atmosphériques plus difficile en raison de la contamination par l'étoile M. Par contre, la courbe de lumière pour cette étoile montre une augmentation ponctuelle (voir Figure B.2) qui peut être attribuée à une phase d'activité du compagnon. Un tel phénomène fut rarement observé en photométrie rapide pour un système DA+dM. Une courbe de lumière constante fut également obtenue pour 22331+2610 (WD2233+261), bien que les paramètres atmosphériques la placent au coeur de la bande d'instabilité.

Deux autres étoiles ont été observées en photométrie rapide pour le moment, et ces étoiles

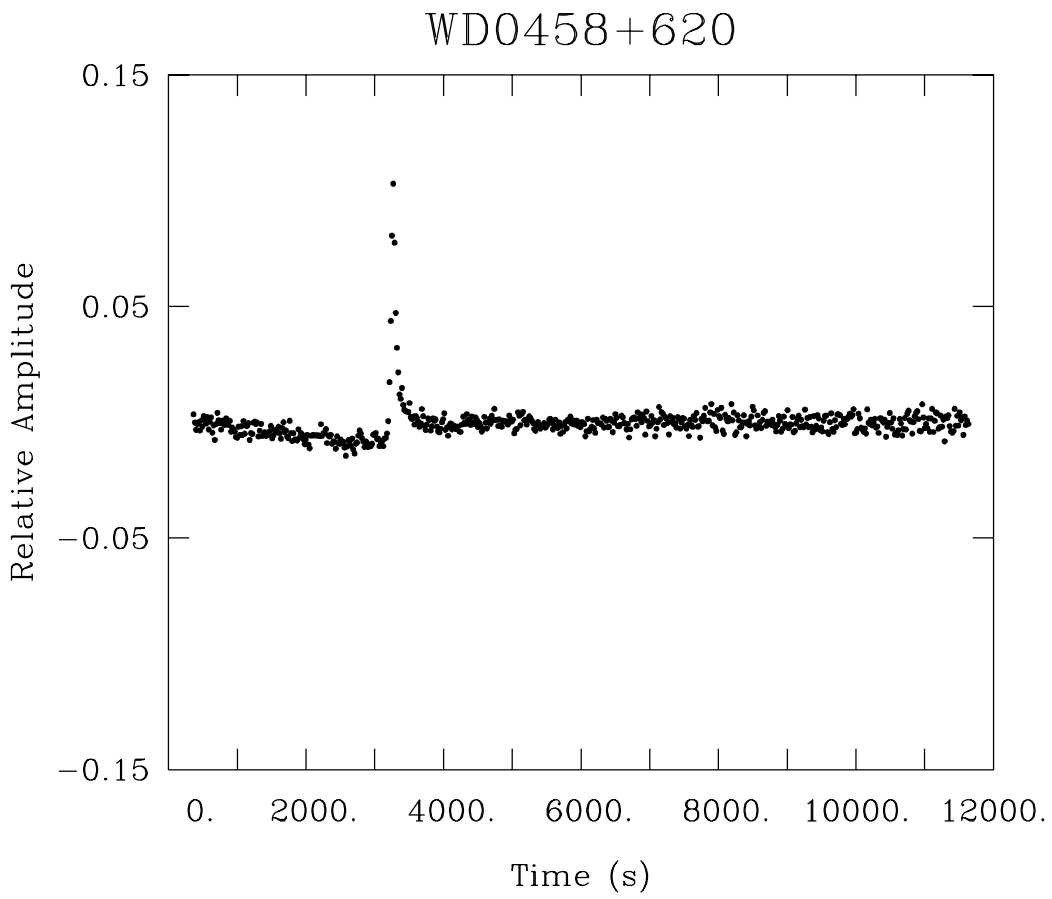

FIGURE B.2 – Courbe de lumière du système DA+dM 04263+4820 (WD0458+620) où une éruption à la surface du compagnon semble être la cause de l'augmentation ponctuelle de luminosité.

TABLE B.1 – Observations en photométrie rapide des candidates ZZ Ceti avec la combinaison Mont4K/Kuiper

Nom	$T_{\rm eff}$ (K)	Log g	Durée (hr)	Bande passante (mHz)	Limite (4σ)	Période dominante (s)	Amplitude (%)
WD0502+540	11395	8.24	9.18	0−5	0.41	873.6	1.27
WD0702+440	11002	8.29	15.05	0−10	0.07	1366.4	0.10
WD2233+261	12016	8.16	9.82	0−10	0.07	NOV	...
WD0458+620	?	?	9.16	0−10	0.07	flare!	...

sont représentées par des carrés rouges. Il s'agit de 05025+5401 (renommée WD0502+540 dans les figures) et de 07029+4406 (WD0702+440), et leur courbe de lumière montre bel et bien des variations périodiques. Les courbes de lumière sont présentées à la Figure B.3, et les périodes sont disponibles dans le tableau B.1 avec les limites de détection à 4σ au-dessus du bruit moyen ainsi que les amplitudes des pics s'il y a détection. Finalement, les transformées de Fourier pour les trois étoiles qui n'ont pas de compagnon ainsi que les périodes des modes indépendants de pulsation sont montrées à la Figure B.4.

Pour la publication qui suivra, nous devrons obtenir de nouveaux paramètres atmosphériques pour 22331+2610 afin de déterminer si l'étoile devrait bel et bien se trouver dans la bande d'instabilité suite à l'observation d'une courbe de lumière constante. Il faudra également obtenir les courbes de lumière pour les 6 autres candidates ZZ Ceti et obtenir plus de données pour les deux nouvelles étoiles variables afin d'augmenter le rapport signal sur bruit. Nous pourrons ainsi identifier un plus grand nombre de périodes de pulsation et parfaire notre modélisation de la structure de ces nouvelles étoiles ZZ Ceti.

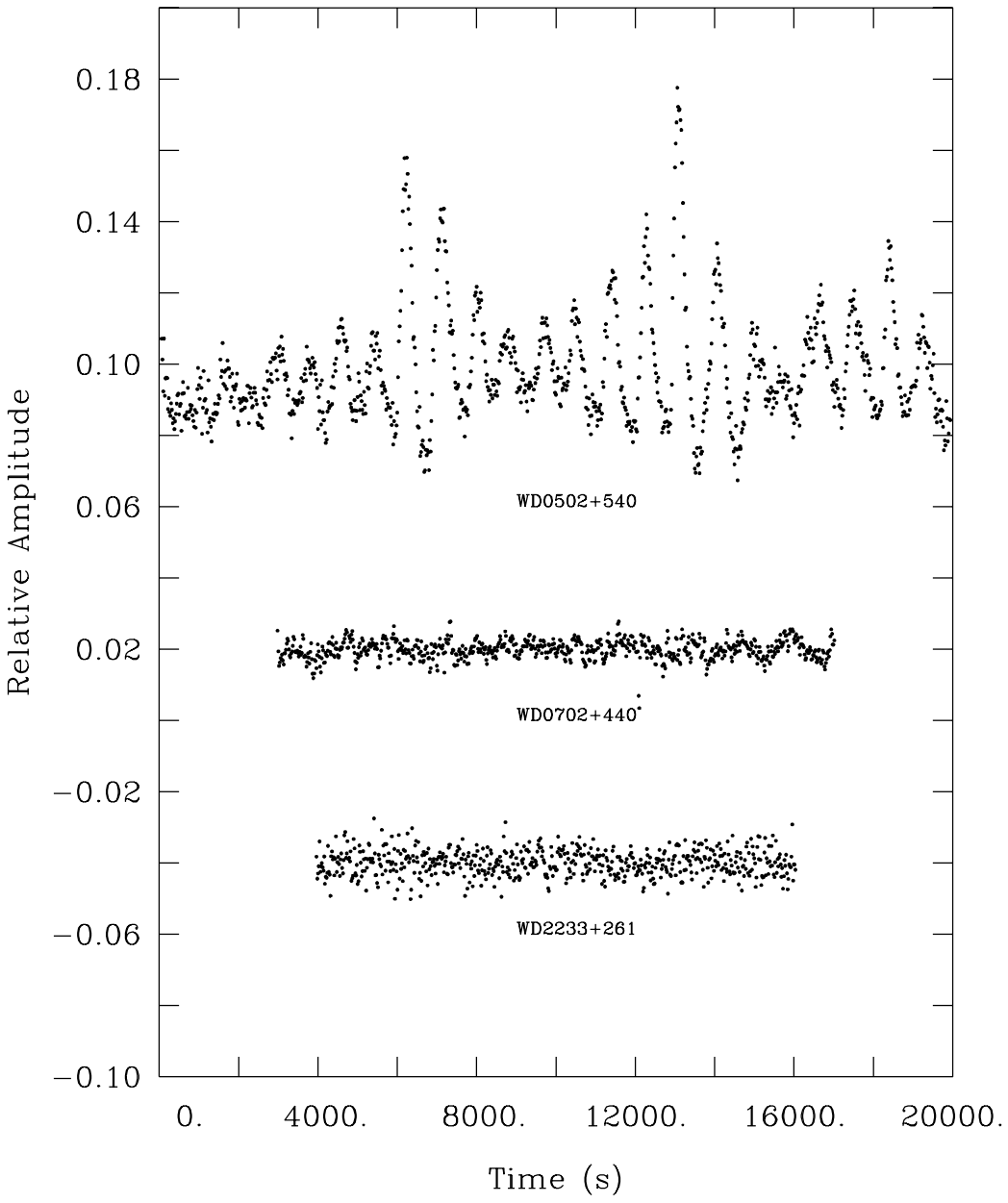

FIGURE B.3 – Courbes de lumière pour les candidates ZZ Ceti observées en photométrie rapide avec le télescope Kuiper du Mont Bigelow (Arizona) à l'aide de la caméra CCD Mont4K.

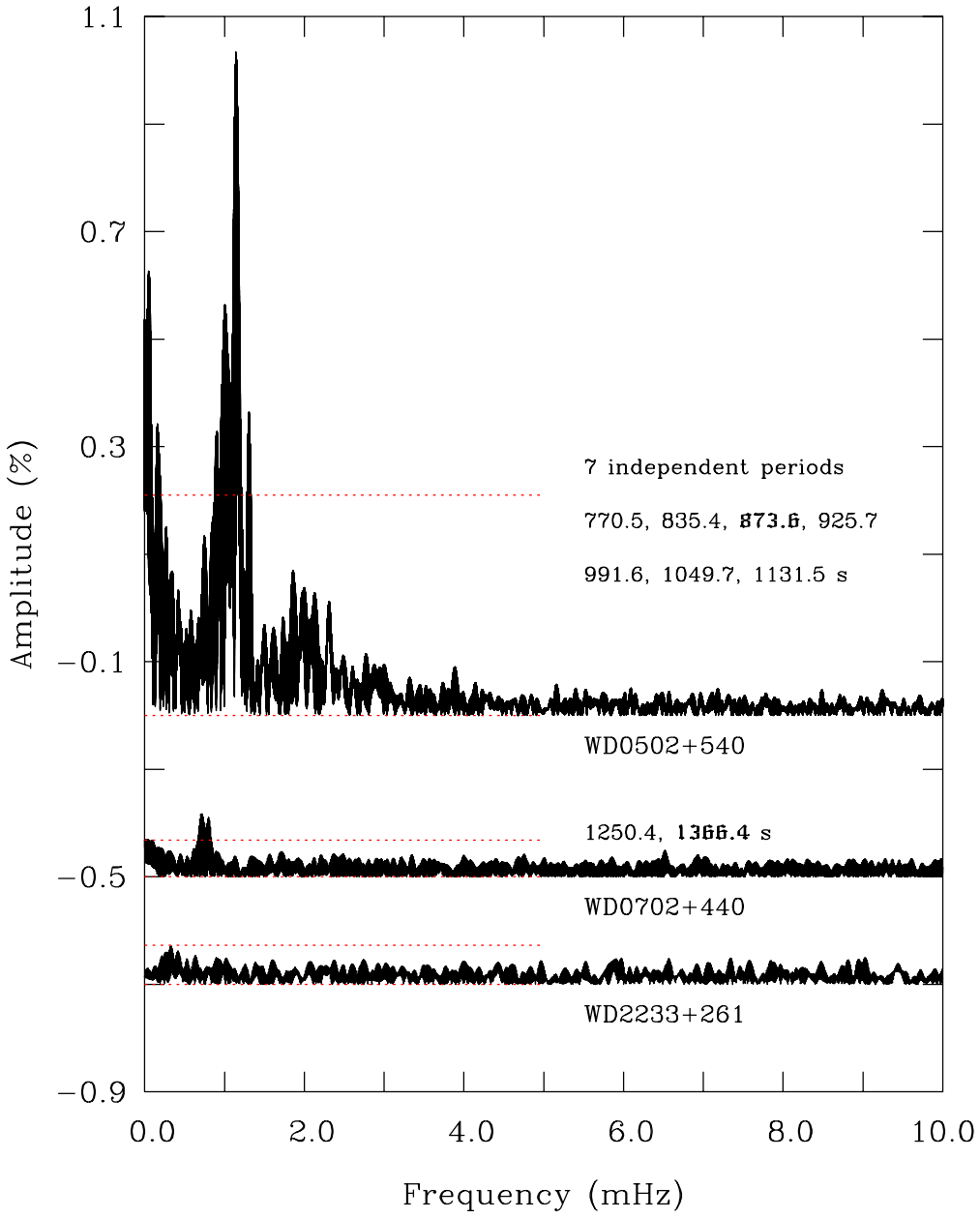

FIGURE B.4 – Transformées de Fourier pour les courbes de lumière de 3 des candidates ZZ Ceti observées en photométrie rapide. Les résultats préliminaires de l'extraction des fréquences sont montrés sur la figure sous la forme d'une liste de périodes pour les modes indépendants de pulsation détectés pour chaque étoile. La ligne rouge indique le seuil de détection des fréquences, qui correspond à 4 fois le bruit moyen.